PREMIER REFERENCE SOURCE

Geotechnical Applications for Earthquake Engineering

Research Advancements

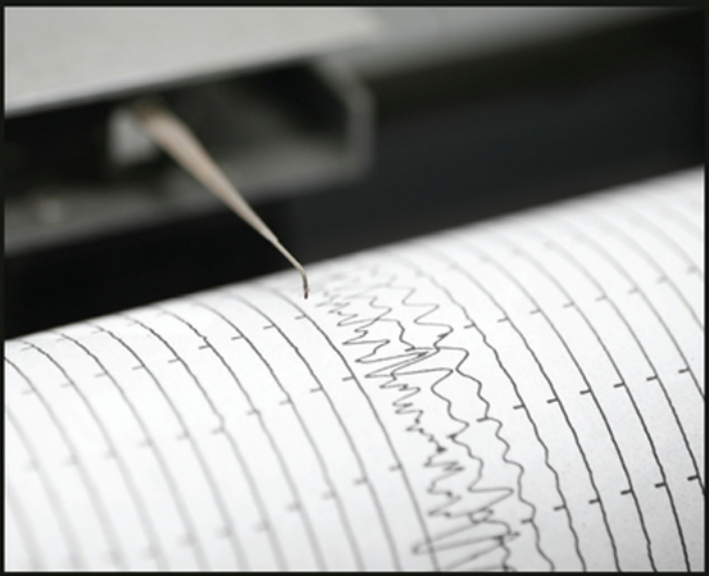

T.G. Sitharam

Geotechnical Applications for Earthquake Engineering:

Research Advancements

T.G. Sitharam
Indian Institute of Science, India

Information Science
REFERENCE

Managing Director: Lindsay Johnston
Senior Editorial Director: Heather A. Probst
Book Production Manager: Sean Woznicki
Development Manager: Joel Gamon
Acquisitions Editor: Erika Gallagher
Typesetter: Nicole Sparano
Cover Design: Nick Newcomer, Lisandro Gonzalez

Published in the United States of America by
Information Science Reference (an imprint of IGI Global)
701 E. Chocolate Avenue
Hershey PA 17033
Tel: 717-533-8845
Fax: 717-533-8661
E-mail: cust@igi-global.com
Web site: http://www.igi-global.com

Library of Congress Cataloging-in-Publication Data

Geotechnical applications for earthquake engineering: research advancements / T.G. Sitharam, editor.
p. cm.
Includes bibliographical references and index.
Summary: “This book has collected chapters from experts from around the world in a variety of applications, frameworks, and methodologies in earthquake engineering, and presents this valuable research in a form that serves as a handy reference and research guide to practitioners and academics alike”--Provided by publisher.
ISBN 978-1-4666-0915-0 (hardcover) -- ISBN 978-1-4666-0916-7 (ebook) -- ISBN 978-1-4666-0917-4 (print & perpetual access) 1. Soil mechanics. 2. Engineering geology. 3. Earthquake engineering. I. Sitharam, T. G., 1961-
TA710.G445 2012
624.1’762--dc23

2012000027

British Cataloguing in Publication Data
A Cataloguing in Publication record for this book is available from the British Library.

Editorial Advisory Board

Table of Contents

Detailed Table of Contents

Using additional dynamic parameters in the pseudo-static method like shear wave and primary wave velocities of soil, phase change in the shear and primary waves, and soil amplification for seismic accelerations, one can benefit from another useful tool called pseudo-dynamic method to solve the problem of earth pressures. In this study, the pseudo-dynamic method is used to compute the seismic passive earth pressures on a rigid gravity retaining wall by considering both the planar failure and composite failure (log-spiral and planar) mechanisms. To validate the present formulation, passive earth pressure computed by the present method are compared with those given by other authors. Seismic passive earth pressure coefficients are provided in tabular form for different parameters. The sliding and rotational displacements are also computed and results of the comparative study showed that the assumption of planar failure mechanism for rough soil-wall interfaces significantly overestimates passive earth pressure and underestimate the sliding and rotational displacements.

Knowledge of cyclic load induced pore pressure generation, post-liquefaction dissipation and volumetric densification characteristics of sands, silty sands, and silts are important for the analysis of performance of loose saturated granular deposits in seismic areas. This article presents results from an experimental study of these characteristics for such soils containing 0 to 100% non-plastic silt. Pore pressure generation characteristics are studied using undrained cyclic triaxial tests. Pre- and post-liquefaction compressibility and coefficient of consolidation, and post-liquefaction volumetric densification characteristics are determined from consolidation data prior to cyclic tests and pore pressure dissipation tests following undrained cyclic tests. Effects of fines content on these characteristics compared to those of clean sands are examined in the context of intergranular void ratio and intergranular contact density concepts.

Soil liquefaction following strong earthquakes causes extensive damage to civil engineering structures. Foundations of buildings, bridges etc can suffer excessive rotation/settlement due to liquefaction. Many of the recent earthquakes bear testimony for such damage. In this article a hypothesis that "Superstructure stiffness can determine the type of liquefaction-induced failure mechanism suffered by the foundations" is proposed. As a rider to this hypothesis, it will be argued that liquefaction will cause failure of a foundation system in a mode of failure that offers least resistance. Evidence will be offered in terms of field observations during the 921 Ji-Ji earthquake in 1999 in Taiwan and Bhuj earthquake of 2001 in India. Dynamic centrifuge test data and finite element analyses results are presented to illustrate the traditional failure mechanisms.

Behaviour of geotechnical material is very complex. Most of the theoretical frame work to understand the behaviour of geotechnical materials under different loading conditions depends on the strong background of the basic civil engineering subjects and advanced mathematics. However, it is fact that the complete behaviour of geotechnical material cannot be traced within theoretical framework. Recently, computational models based on Finite Element Method (FEM) are used to understand the behaviour of geotechnical problems. FEM models are quite complex and is of little interest to undergraduate students. A simple computational tool developed using Discrete Element Method (DEM) to simulate the laboratory experiments will be cutting edge research for geotechnical earthquake engineering education. This article summarizes the potential of DEM to simulate the cyclic triaxial behaviour of granular materials under complex loading conditions. It is shown that DEM is capable of simulating the cyclic behavior of granular materials (e.g. undrained, liquefaction and post liquefaction) similar to the laboratory experiments.

In this paper the compressive strength/elastic modulus of the jointed rock mass was estimated as a function of intact rock strength/modulus and joint factor. The joint factor reflects the combined effect of joint frequency, joint inclination and joint strength. Therefore, having known the intact rock properties and the joint factor, jointed rock properties can be estimated. The test results indicated that the rock mass strength decreases with an increase in the joint frequency and a sharp transition was observed from brittle to ductile behaviour with an increase in the number of joints. It was also found that the rocks with planar anisotropy exhibit the highest strength in the direction perpendicular to the anisotropy and the lowest at an inclination of 30o-45o in jointed samples. The anisotropy of the specimen influences the dynamic elastic modulus more than the static elastic modulus. The results were also compared well with the published works of different authors for different type of rocks.

Section 2

Blasting is the most common method of rock excavation technique in mining and civil construction and infrastructure projects. Rock blasting produces seismic waves similar to those produced by earthquakes, but with relatively high frequency and low amplitude. General blast induced damage was extensively studied by researchers globally, but the studies on damage due to repeated blast vibrations is not yet reported, quantitatively, on underground openings. This paper deals with the research work carried on the effect of repeated dynamic loading imparted on the jointed rock mass from subsequent blasts in the vicinity, on the jointed rock mass at Lohari Nag Pala Hydroelectric Power Construction Project. The

blast induced damage was monitored by borehole extensometers, borehole camera inspection surveys and triaxial geophones installed at three test sites of different joint orientations at the Main Access Tunnel of power house. The study reveals that there was extra damage of 60%, exclusively due to repeated blast vibrations. The results of the study indicate that repeated dynamic loading, resulted in damage even at 33% of the conventional damage threshold vibrations (Vc) in case of favorable joint orientations and 23% of Vc in case of unfavorable joints. The paper concludes in quantification of effect of repeated blast loading and the orientation of joints on the extension of damage zone in jointed rock mass of underground excavations.

This paper examines stope design approaches employed at a metal mining operation in Canada for extraction of transverse primary, transverse secondary, and longitudinal stopes. Variations in stope and slot design, blast design, and blast vibration attenuation are presented in detail. It is shown that the type of blasthole stoping technique employed varies according to stope sequence and ore zone width. Within this range of stopes, blasting design practices have been standardized in terms of drillhole diameter, powder factor, and the type and pattern of the explosives used.

The globally followed common vibration predictor model includes distance from source to vibration monitoring location and quantity of explosive charge per delay without giving much consideration to blast design parameters. Though there are qualitative assertions on the influence of burden on the vibration intensity by many researchers, no work on quantification of influence of burden has been reported. This paper deals with the development of a predictor model incorporating burden deviations in the existing predictor equation. The influence of burden on the vibration was viewed from the angle of detonation and rock fracturing during blasting. The new predictor equation is based on existing models developed by other researchers on the influence of burden on the blasthole pressure and vibration intensity as well as on some logical assumptions. The influence of burden on vibration was examined in two independent phases of blasting, and the net effect was calculated by adding the influence in both the phases. The study provides a quantitative explanation for the common observations of increased vibration levels produced by the blast rounds with excess burden and/or misfired shots.

The dynamic tensile strength plays a pivotal role in rock fragmentation affecting the overall economics under the present 'Mine to Mill Concept'. In this paper, a modified SHPB technique and Brazilian test method is presented to test the dynamic tensile strength of coal, shale and sandstone rock samples col-

lected from three opencast mines of Coal India Limited and is compared with the static strength value. The dynamic tensile strength of coal and rock is much higher than static strength and tensile strength of coal and rock samples increase with loading rate. The result shows that the dynamic strength of the coal sample is 1.5 times higher than static strength and the dynamic strength of the sandstone sample is 3 times higher than the static strength.

An approach for simulation of rock fracturing as a result of engineering blasting is presented in this paper. The approach uses element elimination technique within the framework of finite element method to capture the physics of engineering blasting. The approach does not require pre-placement of fracture paths which is the severe drawback of the other existing methodologies and approaches. Results of plane stress modelling for isotropic brittle rock behaviour are presented in this paper and these results are in good agreement with the existing knowledge base. The authors also review the existing approaches of numerical modelling to compare the efficacy of the element elimination technique. It is anticipated that the further developments with this approach can prove to be good experimental tool to improve engineering blasting operations.

During the process of excavation, blasting can induce cracking inside the surrounding rock. Considering the effects of material properties and loading conditions, a rock blasting excavation model with two successive excavation steps was developed through the use of AUTODYN code. Four kinds of equation of state (EOS), linear, shock, JWL, and compaction were applied to the materials employed in this numerical model. A modified principal stress failure criterion was applied to determining material statuses, and TNT explosive and a relatively homogeneous igneous rock, diorite, were used in this numerical model. By using this numerical model, rock fracturing process during blasting excavation was simulated, and rock fracturing process during two successive excavations is presented.

Blasting with longer advance per round leaves an impact both visible (in the form of overbreak) and invisible (cracks) in the surrounding rockmass, however, a number of controlled-blasting techniques, that is line drilling, pre-splitting, and smooth blasting, have been developed to minimise this problem. These techniques require additional drilling, controlled charging, and detonation, and thus, are not preferred in regular development activities. Investigations have been carried out in five different horizontal development drivages of metal mines to assess the blasting impact using burn cut and arrive at the blast-induced rock damage (BIRD) model. Vibration monitoring close to the blast was carried out

using accelerometers for the first time in India to develop vibration predictors and overbreak threshold levels for individual sites. This paper reports the development of the overbreak predictive model (BIRD) for burn cut blasting in hard rock drivages by combining the relevant rock, blast design, and explosive parameters. A multivariate statistical model has been developed and validated and the same can find ready application in tunnels and mines for exercising suitable engineering controls both in blast design and explosive selection for reduced basting impacts.

Preface

This book deals with geotechnical earthquake engineering and prediction and assessment of blast induced vibrations along with assessment and mitigation methods. The damage due to earthquakes and blasting are caused mainly due to the vibrations caused by waves. But there are differences in the types of vibrations in both the cases. In the case of earthquake, the frequency of waves will be less and its amplitude will be more. However for the vibration created during blasting, the frequency will be high and the amplitude will be lower. Moreover, the duration of vibration due to earthquakes will last longer than that due to blasting. This book examines the effects of vibrations (due to earthquake and blasting) on both soils and jointed rock mass.

The soil is a granular material, whereas the jointed rock mass consists of interlocking angular blocks separated by surfaces of discontinuity. This books deals with the effects of vibration in both these materials. The damages, which occur due to earthquake vibration, can be reduced using mitigation steps. The effective seismic hazard mitigation steps include identification of vulnerable seismic sources, evaluation of source, path characteristics, assessment of induced effects (like site amplification, liquefaction, landslides, etc.), and designing the structures for the estimated forces. The material properties of soil and rocks depend on the strain level, and in most of the cases, the variation will be nonlinear. Two of the important parameters, which will depend on the strain rate and which need to be evaluated accurately are the shear modulus and the damping. These two parameters depend heavily on the strain rate and are showing a nonlinear variation with strain. The same is the case with the pore pressure development in saturated soils.

This book is divided into fourteen chapters in two sections. The first section consists of seven chapters in the field of Geotechnical Earthquake Engineering and the second section consists of seven chapters dealing with various aspects of blast induced vibrations. The various chapters in section 1 discuss probabilistic seismic hazard analysis, site effects, seismic microzonation, liquefaction studies, cyclic triaxial test, model experiments, analysis of super structure stiffness and retaining walls, and static and dynamic modulus of jointed rocks. Section 2 of this book covers the topics of simulation of rock fracturing in blasting, blasting in tunnels, blast damage prediction, blast and impact assessment using dynamic tensile test, blast vibration prediction, damage due to repeated blast vibrations, blast induced vibration in long hole open stoping, and static and dynamic elastic modulus of jointed rock mass.

Section 1, Geotechnical Earthquake Engineering (GEE), involves multidisciplinary research. This area of research involves aspects of geology, seismology, geotechnical engineering, risk analysis, et cetera. The ultimate goal in the area of GEE is to assess seismic hazard and reduce the risk to acceptable limits. The earthquake damage is mainly caused due to the ground shaking and regional subsidence. The secondary effects of earthquake damage are due to liquefaction, landslides, tsunami, et cetera. The local

site conditions will influence the frequency content, duration and amplitude of the ground motion. The geometry and material properties of the subsurface soil and the properties of the input motion will have significant influence on the site amplification. The severe effects of site amplification were observed during Niigata, Mexico, San Francisco, and Bhuj earthquakes. There has been considerable development in the field of Geotechnical Earthquake Engineering in the recent years. Still more research need to be undertaken in the area of liquefaction, site response, ground failure, and collapse of geotechnical structures. The geotechnical aspect of seismic hazard assessment involves evaluation of liquefaction potential, landslide hazard, site response, and site amplification. The outcome of the GEE study needs to be used for seismic hazard mitigation – in the form of settlement assessment for a particular site, selection of appropriate type of foundation, slope stabilization, ground improvement, et cetera.

The first chapter deals with the evaluation of surface level peak ground acceleration values based on NEHRP site classification scheme. The seismic hazard was evaluated using a probabilistic seismic hazard analysis (PSHA) using logic tree approach. The methods to develop uniform hazard response spectrum for a particular location are discussed in this chapter. The second chapter describes the development of site specific ground motion parameters for a seismically vulnerable site. The seismic hazard was assessed based on deterministic seismic hazard assessment method. A synthetic acceleration time history was developed using deconvolution analysis method. The third chapter discusses details of the study to evaluate the seismic passive earth pressure on a rigid gravity wall based on pseudo-dynamic methods. A comparison of results obtained from the present study is done with the results obtained from other methods. The fourth chapter presents the details of pore pressure development, dissipation, and volumetric densification characteristic of sands. The results obtained from an experimental study with varying percentage of non plastic fines are discussed in this chapter. The fifth chapter presents the details of how the super structure stiffness can determine the type of liquefaction induced foundation failure. This chapter discusses the results obtained for dynamic centrifuge test result and FEM analysis to compare the foundation failure mechanism. The sixth chapter discusses the methods to simulate laboratory experiments using discrete element modelling (DEM). This chapter highlights the capabilities of simulating cyclic behaviour of granular soil using DEM. The seventh chapter gives the details of the evaluation of compressive strength/elastic modulus of jointed rock mass as a function of intact rock strength/modulus and joint factor. The details of the comparison of the results obtained from this method with the published works are also included in this chapter.

Section two concerns the use of explosives in a controlled manner to remove or excavate hard material like rocks is termed as blasting. Blasting is one of the most commonly used and economical technique for rock excavation. There has been lots of development in the area of blasting, but still, many issues related to the safety and stability need to be addressed. The structural damage due to the blast induced vibration and the human annoyance due to air blasting are common problem due to surface blasting. Blasting involves: detonation of explosives, fracture initiation and extension, rock throw and fragmentation, generation of vibration, air blast, noise, heat, and rock projectiles. Numerical modelling has emerged as one of the important area to model and understand some of the complex mechanics of blasting. The modelling of rock blasting requires proper understanding of rock properties, explosive properties, and blast design parameters. The vibration produced due to blasting is similar to that produced during earthquakes, but with high frequency and low amplitude values. It has been estimated that around 80% of the energy produced during blasting is lost in the form of vibration, air blast, and noise. Lots of research is going in the field of blasting to reduce the ill effects of the energy lost during blasting.

The eighth chapter deals with the effects of repeated dynamic loading (due to blasting) on joined rock mass. The blast induced damage was monitored using various techniques, and it was found that 60% of the damage was caused due to the repeated dynamic loading. The ninth chapter examines the various aspects of stope and slot design, blast design, and blast vibration attenuation. A detailed examination of various stope design used in metal extraction in Canada is also presented in this chapter. The tenth chapter deals with the details of development of a predictor model incorporating burden deviations in the existing predictor equations. A quantitative explanation of the increased vibration level produced by the blast rounds with excess burden is presented in this chapter. The eleventh chapter describes the development of modified SHPB technique and Brazilian test method to test the tensile strength of coal, shale, and sandstone samples. A comparison of the results obtained for dynamic and static strength of sandstone samples are presented in this chapter. The twelfth chapter discusses about an approach to simulate the rock fracturing as a result of engineering blasting. A review of existing model to compare the efficacy of element elimination technique is also presented in this chapter. The thirteenth chapter gives the details of development of rock blasting excavation model with two successive excavation steps. The details of simulation of rock fracturing process during blasting excavation are presented in this chapter. The fourteenth chapter deals with the development of overbreak predictive model (BIRD) for burn cut blasting in hard rock. To validate this new model, a multivariate statistical model was developed and this model can be applied in tunnels and mines for blast design and explosive selection.

This book is on the Advances in Geotechnical Earthquake Engineering series, which encompasses all the invited chapters from eminent academicians, practitioners, and researchers, which are published in the *International Journal of Geotechnical Earthquake Engineering* (IJGEE) Vol. 1 and 2 in the year 2010. *The International Journal of Geotechnical Earthquake Engineering* (IJGEE) contains enhanced research on the role of geotechnical engineering in soil dynamics, engineering seismology, disaster mitigation, and earthquake engineering. With international articles written by leading authors, this book, "Earthquake and Blast Induced vibrations: Research Advancements," provides the latest findings and industry solutions for all those involved in fields of earthquake and blasting vibrations. The efforts of all the authors, reviewers, and their contributions are gratefully acknowledged.

I also thank the entire editorial board of International Geotechnical earthquake engineering published by IGI Global and their contributions are gratefully acknowledged. Further, I also thank the managing director Lindsay Johnston and Senior Editorial Director, Heather A. Probst and their entire team for their kind cooperation and help in bringing out this book.

T.G. Sitharam
Indian Institute of Science, India

Section 1

Chapter 1
Evaluation of Peak Ground Acceleration and Response Spectra Considering the Local Site Effects:
A Probabilistic Logic Tree Approach

T. G. Sitharam
Indian Institute of Science, India

K. S. Vipin
Indian Institute of Science, India

ABSTRACT

The local site effects play an important role in the evaluation of seismic hazard. The proper evaluation of the local site effects will help in evaluating the amplification factors for different locations. This article deals with the evaluation of peak ground acceleration and response spectra based on the local site effects for the study area. The seismic hazard analysis was done based on a probabilistic logic tree approach and the peak horizontal acceleration (PHA) values at the bed rock level were evaluated. Different methods of site classification have been reviewed in the present work. The surface level peak ground acceleration (PGA) values were evaluated for the entire study area for four different site classes based on NEHRP site classification. The uniform hazard response spectrum (UHRS) has been developed for the city of Bangalore and the details are presented in this work.

DOI: 10.4018/978-1-4666-0915-0.ch001

1. INTRODUCTION

The modification to the seismic waves when it passes from the bed rock to the surface of earth through the overlying soil is termed as the site effects. This depends on the local site conditions and this is one of the major factors which will increase the destruction caused by the earthquakes. When the seismic waves travel through the overlying soil to the ground surface, it may get amplified or de-amplified, and this is known as site effects. The amplification factor at a site is the ratio of the intensity measure (*IM*, in the present study it is taken as peak horizontal acceleration [PHA]) for a given site condition to that of the reference site (at bed rock). The amplification factors can be determined using two approaches – based on the observed intensity measures and theoretical approach. The first method compares the *IM* for various site conditions with that of a reference site condition for determining the amplification factors. The theoretical analysis methods will be useful in extending the amplification factor models to the site conditions which are poorly represented in empirical data sets (Annie and Stewart, 2006). The frequency of ground motion, which will be influenced by the site condition, depends on the thickness of the over lying soil deposit also. If the thickness of the soil deposit is small then the amplification will occur for the waves with higher frequency and vice versa. The amplification factors can be evaluated using the observational studies. This method can be divided into two types – using a reference site and without using a reference site.

The three important factors which will affect the ground motion are the source, path and the site characteristics. The identification and removal of these effects is the greatest challenge in evaluating the site response. The simplest method to evaluate the site response is to divide the response spectrum obtained at the site with that of the bed rock (reference site). If the recording in the rock is at a close distance to the soil site, then the three governing factors, which will affect the ground motion, will be the same for both the soil site and the rock. However when the reference site and the site under consideration (soil site) are not near by, then the influence of source, path and the site characteristics will be different for these two sites. More over the geometric spreading of the seismic waves will also need to be accounted (Borcherdt & Glassmoyer, 1994; Borcherdt, 1996; Hartzell et al. 2000; Borcherdt 2002). To evaluate the source and site terms simultaneously, a generalized inversion scheme developed by Andrews (1986) can be applied. In the generalized inversion technique a relatively large dataset can be used (Stewart et al., 2003) but the nonlinear response of sedimentary deposits cannot be predicted accurately when the weak motion data are dominating the input data.

Another method of site response, which does not depend on the reference site, is based on horizontal to vertical spectral ratio (HVSR). In this method the horizontal component of the response spectra is normalized using the vertical component of the spectra for the site under consideration. This method can be applied for both the noise recordings (Nakamura, 1989; Field and Jacob, 1993) and the earthquake recordings.

The probabilistic seismic hazard analysis (PSHA) will give the likelihood of exceedance of various ground motion levels for a given return period (Cornell, 1968). The attenuation relationships used to predict the ground acceleration levels will give the acceleration values at the bed rock level. These values may change considerably when the surface level peak ground acceleration (PGA) values are evaluated. It has been found that the basins and sediment filled valleys are also having significant effect on earthquake ground motion. Researchers like Field (2000), Lee and Anderson (2000) and Steidl (2000) proposed methods for modifying the attenuation relations for predicting the peak ground acceleration (PGA) and spectral acceleration values at the ground surface level. Stewart et al. (2003) has developed empirical amplification factors for active tectonic regions. They have developed separate sets of amplifica-

tion factors for different site classes, which were identified using different methods. Even though these amplification factors were developed for active tectonic regions, the same can be applied to other tectonic regions after further studies (Stewart et al., 2003).

2. DIFFERENT SITE CLASSIFICATION SCHEMES

The methods which are commonly adopted to classify the sites can be broadly divided into the following categories.

Based on surface geology: The criteria for this type of classifications are based on the geologic age of the sediments. The different site classes as per geologic site classification are given in Table 1

Based on geotechnical data: One of the early works in site classification based on geotechnical data was done by Seed and Idriss (1982). The classification scheme recommended by them is given below:

i. Rock sites
ii. Stiff soil sites (< 60 m deep)
iii. Deep cohesionless soil sites (> 75 m deep)
iv. Sites underlain by soft to medium stiff clays

One of the main factors which differentiate this classification system from other systems is the incorporation of the sediment depth.

The three important methods used for geotechnical site classifications are based on (i) Standard penetration test (SPT) (ii) Cone penetration test (iii) Average shear wave velocity in the top 30 m (V_s^{30}). Of these, the oldest and the most widely used method of site classification is based on SPT values. There are many correlations available for evaluating different soil parameters based on the SPT values. The site classification schemes available based on the standard penetration test (SPT) values are given in Table 2.

Table 1. Site classification based on surface geology.

Age	Depositional Environment	Sediment Texture
Holocene	Fan alluvium	coarse
Pleistocene	Valley alluvium	Fine
	Lacustrine/marine	mixed
	Aeolian	
	Artificial Fill	
Tertiary		
Mesozoic + Igneous		

Table 2. Soil classification based on SPT N values

Soil Type	N Values
Very Loose	0 – 4
Loose	4 – 10
Medium dense	10 – 30
Dense	30 – 50
Very Dense	> 50

Now a days the CPT test is also widely being used for the evaluation of site classification. The soil classification schemes based on CPT values are given in Table 3.

Recently most of codes specify the site classification based on the average shear wave velocity values. The amplification of shear waves mainly depends on the density and the shear wave velocity of the overlying soil layer. Since the variation in density of soil is comparatively less, the amplification depends heavily on the shear wave velocity near the earth surface. There are two methods to denote the near surface shear wave velocity (V_s) – depth corresponding to one quarter wave length of the period of interest and the average shear wave velocity in the top 30 m. The main disadvantage with quarter wavelength V_s is that the depths associated with this will be very deep. Hence the classification based on V_s^{30} is being used more commonly now a days. This classification is based on the average shear wave velocity in the top 30 m (100 ft) soil. It is calculated using the equation

$$V_s^{30} = \frac{30}{\sum_{i=1}^{N}\left(\frac{d_i}{v_i}\right)} \quad (1)$$

Where d_i is the thickness of the i^{th} soil layer in metres and v_i is the shear wave velocity for the i^{th} layer; N – no. of layers in the top 30 m soil strata which will be considered in evaluating V_s^{30} values. Borcherdt (1994) proposed a site classification scheme based on V_s^{30} values and a similar scheme was adopted by the National Earthquake Hazard Reduction Program (NEHRP) also. The NEHRP site classification scheme is presented in Table 4.

Eurocode-8(2003) has also classified the site based on V_s^{30}, standard penetration test (SPT) values and cone penetration test (CPT) values.

Table 3. Soil classification based on CPT values (Lunne et al., 1997)

Soil Type	Cone Resistance q_c (MPa)
Soft clay and mud	< 1
Moderately compact clay	1 - 5
Silt and loose sand	≤ 5
Compact to stiff clay and compact silt	> 5
Moderately compact sand and gravel	5 – 12
Compact to very compact gravel	> 12

Table 4. Site classification as per NEHRP scheme. (BSSC, 2001)

NEHRP Site Category	Description	V_s^{30}
A	Hard rock	> 1500 m/s
B	Firm and hard rock	760 – 1500 m/s
C	Dense soil, soft rock	360 – 760 m/s
D	Stiff soil	180 – 360 m/s
E	Soft clays	< 180 m/s
F	Special study soils, e.g. liquefiable soils, sensitive clays, organic soils, soft clays > 36 m thick	

Table 5. Site classification as per Eurocode – 8 (Eurocode-8, 2003)

Ground Type	Description of stratigraphic profile	Parameters		
		V_s^{30}	SPT	C_U (KPa)
A	Rock or other rock-like geological formation, including at most 5 m of weaker material at the surface.	> 800		
B	Deposits of very dense sand, gravel, or very stiff clay, at least several tens of metres in thickness, characterised by a gradual increase of mechanical properties with depth.	360 – 800	> 50	> 250
C	Deep deposits of dense or medium dense sand, gravel or stiff clay with thickness from several tens to many hundreds of metres.	180 – 360	15 - 50	70 - 250
D	Deposits of loose-to-medium cohesion less soil (with or without some soft cohesive layers), or of predominantly soft-to-firm cohesive soil.	< 180	< 15	< 70
E	A soil profile consisting of a surface alluvium layer with vs values of type C or D and thickness varying between about 5 m and 20 m, underlain by stiffer material with vs > 800 m/s.			
S1	Deposits consisting, or containing a layer at least 10 m thick, of soft clays/silts with a high plasticity index (PI > 40) and high water content	< 100 (indicative)		10 - 20
S2	Deposits of liquefiable soils, of sensitive clays, or any other soil profile not included in types A – E or S1			

The classification given by Eurocode-8 is given in Table 5.

In many locations the rock depth will be shallow (less than 30 m) and hence the evaluation of V_s^{30} value will not be possible. In those cases, extrapolation of available V_s values has to be done to evaluate the V_s^{30}. One of the methods for this was proposed by Boore (2004). He has suggested different models to extrapolate the shear wave velocities, for depths less than 30 m, to get the V_s^{30} value. The first method is extrapolation based on constant velocity. In this model it is assumed that the velocity remains constant from the deepest velocity measurement to the 30 m.

$$V_S^{30} = \frac{30}{tt(d) + (30 - d) / V_{eff}} \tag{2}$$

Where *tt(d)* is the travel time to depth *d* and $V_{eff} = V_s(d)$, $V_s(d)$ is the timed average velocity to a depth of *d*. Even though this method is simple, it is found to under estimate the V_s^{30} values, since in most of the soils the shear wave velocity is found to increase with depth.

Another relation proposed by Boore (2004) was based on a power law relation, the V_s^{30} value can be estimated as:

$$\log V_s^{30} = a + b \log \overline{V_S}(d) \tag{3}$$

Where $\overline{V_S}(d)$ is the velocity at a depth of *d* m (30 < d >10). The values of the regression coefficients *a* and *b* can be obtained from Boore (2004). The extrapolation of V_S values can also be done based on the velocity statistics (Boore, 2004)

Where $P(\xi > V_{eff} / V_s(d))$ is the probability of exceedance of $V_{eff}/V_s(d)$. Readers can refer to Boore (2004) for more details on this analysis.

A modified site classification system based on geotechnical data was proposed by Rodriguez-Marek et al. (2001). In this system the stiffness of soil was also taken into account for the site classification. The new system is presented in Table 6.

The main advantage of this system is that it correlates the V_s^{30} values with the geotechnical and surface geological features.

3. SEISMIC CHARACTERISTICS OF THE STUDY AREA

In this article, as an example, the study area selected is South India, between latitude 8° N - 20° N and longitude 72° E – 88° E (Figure 1). Study area is a part of the peninsular Indian continental shield region, which is one of the oldest Archaean shield regions in the world. Seismic study area covers about 300 km from the boundary of study area (Regulatory Guide 1.165(1997)) and this is shown in Figure 1. Even though the peninsular Indian shield is characterized by several prominent geological and geophysical features, it can be divided into three major tectonic segments: Western Dharwar craton (WDC), Eastern Dharwar craton (EDC) and Southern Granulite terrain (SGT) (Agrawal and Pandey, 2004).

The earthquake catalogue was compiled by collecting the earthquake data from the seismic study area (Regulatory guide, 1997). The final earthquake catalogue, which was used for this study, was having data till December 2006. The hazard analysis requires the earthquake data in the same magnitude scale. Since moment magnitude scale is the most advanced and the most commonly used magnitude scale for the scientific applications, this magnitude scale was used in this analysis. After removing all the dependent events like fore shocks and after shocks from the catalogue, the catalogue contains about 1955 events, out of which 673 events were having magnitude 4 and above. Usually the earthquakes with magnitude less than 4 may not cause any damage to the structures. Hence only those events with $M_W >= 4$ were used in this study. Moreover, by adopting such a criterion the rock blats (if any) can also be filtered out from the catalogue.

4. DELINEATION OF SEISMIC SOURCE ZONES

For a large area like south India, there will be spatial variations in the earthquake occurrence pattern. To properly map the earthquake recurrence rate and to evaluate the maximum expected magnitude, it is better to divide the study area into different seismic source zones. The previous seismic source zoning of the study area was done by Seeber et al. (1999) based on the regional geology. In the present

Table 6. Classification based on geotechnical features (Rodriguez-Marek et al., 2001)

Site	Description	Comments
A	Hard rock	Crystalline bedrock; $V_s^{30} \geq 1500$ m/s
B	Competent bed rock	$V_s^{30} > 600$ m/s or < 6 m of soil. Most unweathered California rock cases
C1	Weathered rock	$V_s^{30} \sim 300$ m/s increasing to > 600 m/s, weathering zone > 6 m and < 30 m
C2	Shallow stiff soil	Soil depth > 6 m and < 30 m
C3	Intermediate depth stiff soil	Soil depth > 30 m and < 60 m
D1	Deep stiff Holocene soil	Soil depth > 60 m and < 200 m
D2	Deep stiff Pleistocene soil	Soil depth > 60 m and < 200 m
D3	Very deep stiff soil	Soil depth > 200 m
E1	Medium thickness soft clay	Thickness of soft clay layer 3 – 12 m
E2	Deep soft clay	Thickness of soft clay layer > 12 m
F	Potentially liquefiable sand	Holocene loose sand with high water table, $Z_w \leq 6$ m

Figure 1. Map showing the location of selected study area in India.

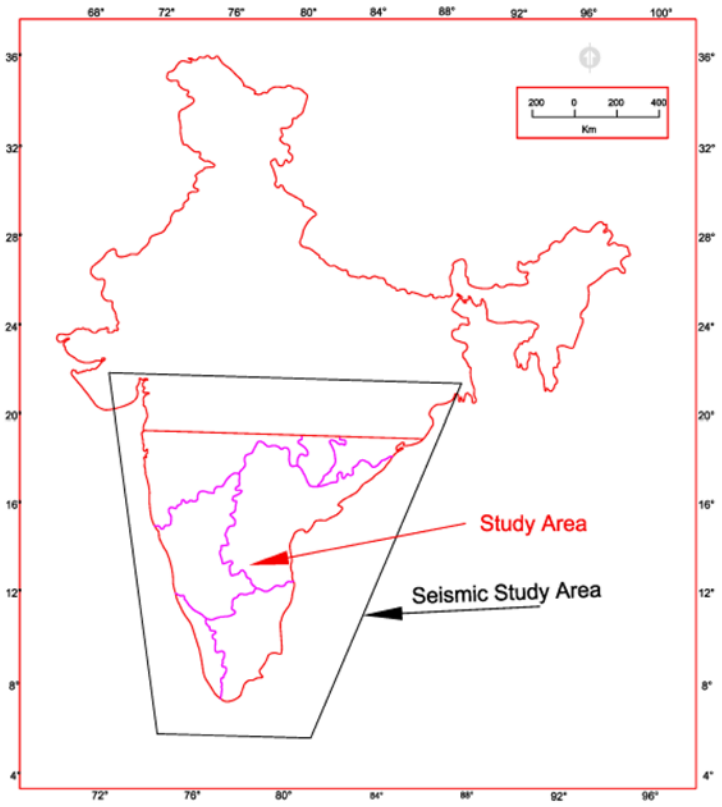

study the zoning was done based on the variation of seismicity parameters. The seismic source zones used in this study are shown in Figure 2. However apart from using different source zones, a single source zone, by considering the entire study area as a single zone, was also considered. This single source zone model was given a lesser weightage in the logic tree approach while evaluating the seismic hazard.

5. SELECTION OF SEISMIC SOURCES

The two types of seismic sources used in the study were the linear sources and areal sources. Based on the analysis of remote sensing images and geological explorations, Geological Society of India (GSI) has published maps showing the details of faults in and around India (SEISAT, 2000). From this atlas, the seismic sources which were associated with earthquakes of magnitude 4 and above were selected. These sources are presented in Figure 3.

If the seismic source is spread over an area, then it may not be appropriate to model it as a linear source. To overcome this limitation areal sources, sources which are spread over an area, were also considered in this study. The smoothed historic seismicity approach suggested by Frankel (1995) was adopted for smoothing the areal seismic sources. For the evaluation of seismic hazard, spatially smoothed areal sources, identified based on earthquakes of magnitude 4 and above were used.

Figure 2. Seismic source zones identified in the study area.

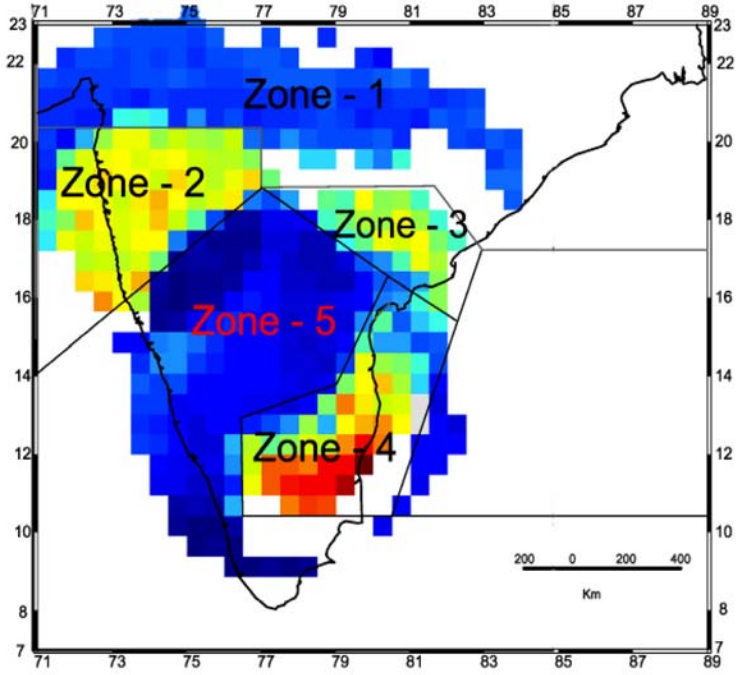

Figure 3. Active faults identified in the study area.

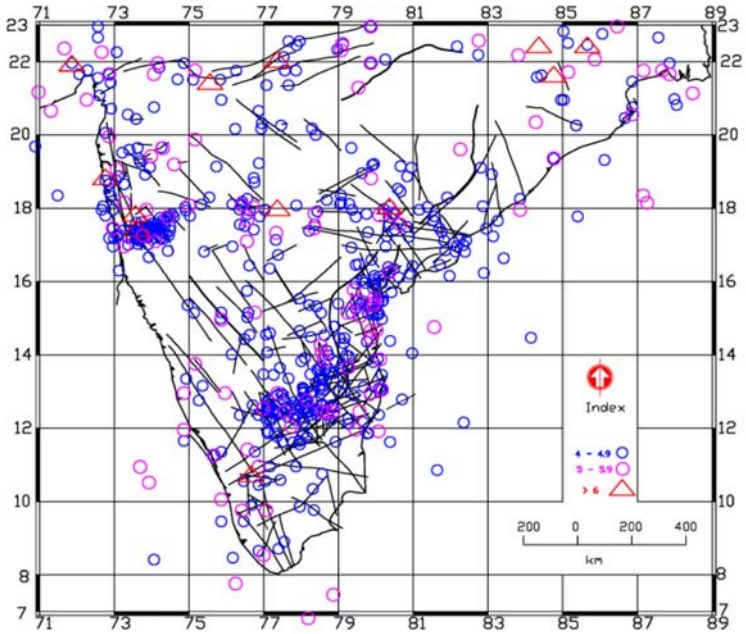

6. MODELING THE ATTENUATION CHARACTERISTICS OF THE REGION

The prediction of earthquake acceleration at a site is one of the most important as well as a difficult step in the seismic hazard evaluation. Almost all the attenuation relations will give the acceleration at the bed rock level and site effects are not considered. At present there is only one attenuation relation available for the study area, the one developed by Raghu Kanth and Iyengar (2007). After studying the ground motion attenuation of the Bhuj earthquake, Cramer and Kumar (2003) suggested that the ground motion attenuation in Eastern & Northern America (ENA) and the peninsular India are comparable. Hence two attenuation relations developed for ENA, Atkinson and Boore (2006) and Toro et al. (1997) were also considered in this study. The regional attenuation developed for the study area was given highest weightage in the logic tree. All the three attenuation relations described above will give the acceleration values at bed rock level.

7. SEISMIC HAZARD EVALUATION BASED ON PROBABILISTIC LOGIC TREE APPROACH

There are two different methods for quantifying the seismic hazard – based on deterministic approach and probabilistic approach. The deterministic seismic hazard analysis (DSHA) does not consider the uncertainties involved in the earthquake occurrence process like the recurrence rate, magnitude uncertainty, attenuation characteristics of seismic waves etc. and gives the worst scenario of ground acceleration. Probabilistic seismic hazard analysis (PSHA) incorporates the uncertainties involved in the earthquake occurrence process. Since the uncertainty in earthquake occurrence is fully accounted in this method, this method is being widely followed for the evaluation of seismic hazard. The PSHA method adopted in this study is similar to the one adopted by Raghu Kanth and Iyengar (2006), Anbazhagan *et al.* (2009) and Vipin *et al.* (2009).

The mean annual rate of exceedance of ground motion parameter, Z, with respect to z for an earthquake of magnitude m occurring at a distance of r can be evaluated using the following equation.

$$\nu(z) = \sum_{n=1}^{N} N_n(m_0) \int_{m=m^0}^{m^u} f_n(m) \left[\int_{r=0}^{\infty} f_n(r \mid m) P(Z > z \mid m, r) dr \right] dm \quad (5)$$

Where $N_n(m_0)$ is the frequency of earthquakes on a seismic source n, having a magnitude higher than a minimum magnitude m^0; $f_n(m)$ is the probability density function for a minimum magnitude of m^0 and a maximum magnitude of m^u; $f_n(r|m)$ is the conditional probability density function for the occurrence of an earthquake of magnitude m at a distance r from the site for a seismic source n; $P(Z>z|m, r)$ is the probability at which the ground motion parameter Z exceeds a predefined value of z, when an earthquake of magnitude m occurs at a distance of r from the site. Thus the function $\nu(z)$ incorporates the uncertainty in time, size and location of future earthquakes and uncertainty in the level of ground motion they produce at the site.

While evaluating the seismic hazard two types of uncertainties are encountered: epistemic and aleatory. The aleatory uncertainty involved in the spectral acceleration prediction models are given by the standard deviation of the residual error. In most of the attenuation relationships this standard error is assumed to follow a log-normal distribution (Frank *et al.*, 2005). The technique adopted in PSHA to reduce the epistemic uncertainty is through the adoption of logic tree approach (Budnitz et al., 1997; Stepp et al., 2001; Bommer et al., 2005). In logic tree approach appropriate weightage is given to each method adopted in the study. In this approach the sum of the weightage factor for all the branches at each node should be equal to unity. The main advantage of using logic tree

approach in PSHA is that it can consider multiple attenuation and source models in the evaluation of PHA and hence it can reduce the epistemic uncertainty. The logic tree model adopted for this study along with the weightage for each branch is given in Figure 4. In the present study the PHA values were evaluated using 12 different methods (3 attenuation laws x 2 types of sources x 2 types of source zones). The weightage for each of these methods were obtained by multiplying the weightage factors for the respective logic tree branches, which were used in the calculation of that particular PHA value. The final PHA value is calculated by multiplying the PHA values obtained from each branch of the logic tree with the respective weightage and then adding them together.

For calculating the seismic hazard values, the entire study area was divided into grids of size 0.1° x 0.1° (about 10000 grid cells) and the hazard values at the centre of each grid points were calculated by considering all the seismic sources and earthquake events with in a radius of 300 km. For this purpose a set of new programs were developed in MATLAB and the entire analysis were carried out using these programs.

Atkinson and Boore (2006) had proposed a method to evaluate the amplification factors based on empirical studies of ground motion data. The evaluation of PGA values for south India was done using the method proposed by Raghu Kanth and Iyengar (2007). The amplification factors can be evaluated based on the following equation.

$$\ln F_s = a_1 y_{br} + a_2 + \ln \delta_s \quad (6)$$

Where a_1 and a_2 are regression coefficients, y_{br} is the spectral acceleration at rock level and δ_s is the error term. The values of the regression coefficients a_1 and a_2 will vary for different site classes and for different time periods. These values were derived based on the statistical simulation of ground motions. For NEHRP site classes A to D, ten random samples of soil profiles were considered in evaluating the amplification factors. The values of a_1, a_2 and δ_s for different site classes for evaluating the PGA values are given in Table 7.

The value of spectral acceleration for different site classes can be obtained from:

$$y_s = y_{br} F_s \quad (7)$$

Where F_s is the amplification factor y_s is the spectral acceleration at the ground surface for a given site class.

8. RESULTS AND DISCUSSIONS

The peak horizontal acceleration (PHA) at bed rock level was evaluated based on probabilistic method for a probability of exceedance (PE) of 10% in 50 years (this corresponds to a return periods of 475 years). The contour curves showing the variation of rock level PHA values for 10% PE in 50 years are shown in Figure 5. There are variations of PHA values obtained in the present study when compared to the values given in the seismic design code of India (BIS-1893, 2002). The Koyna, Bangalore and Ongole regions are showing PHA values higher than what is specified in the BIS-1893(2002). For some regions near the southern tip of the study area (parts of Kerala and Tamilnadu), the PHA values obtained

Table 7. Amplification factors used in evaluating PGA values for different site classes in peninsular India (Raghu Kanth and Iyengar, 2007)

Site Class	a_1	a_2	ln(δ_s)
A	0.00	0.36	0.03
B	0.00	0.49	0.08
C	-0.89	0.66	0.23
D	-2.61	0.80	0.36

Figure 4. Different models used in the logic tree method.

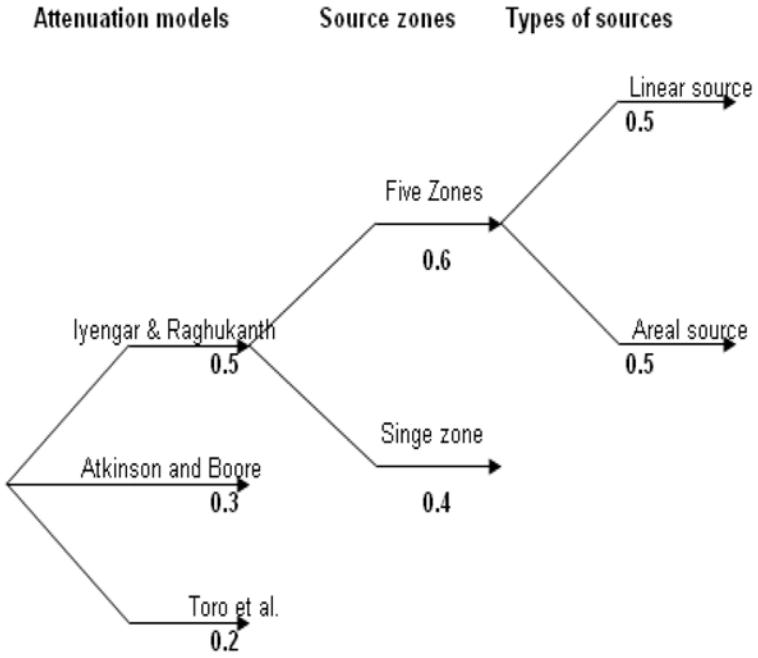

in this study are less than the specified values in BIS-1893(2002).

In the previous sections the different site classes and the classification methods are discussed in detail. In the present study the surface level peak ground acceleration (PGA) values were evaluated based on the NEHRP site classes (BSSC, 2001) for site classes A, B, C and D. It was done based on the amplification factor equations suggested by Raghu Kanth and Iyengar (2007) for the south India. Since the study area is very vast it is impossible to determine from the field tests the site classes for the entire study area. Hence the ground level PGA values were determined for four site classes (A to D) for which the amplification equations are available from south India (Raghu Kanth and Iyengar, 2007). The uniform hazard response spectrum (UHRS) for Bangalore for a PE of 10% in 50 years is shown in Figure 6. The results clearly show the variation of predominant frequency as well as the spectral acceleration with change in soil types. For Bangalore, the period of oscillation corresponding to maximum Sa varies from 0.05 seconds at bedrock level to 0.2 seconds at ground surface for site class D.

The PGA values at ground surface level were evaluated for south India for 10% PE in 50 years for four NEHRP site classes, A - D, and are shown in Figures 7, 8, 9, 10. These results clearly show the effect of amplification due to overlying soil column. The rock level PHA values (Figure 5) show that for majority of the study area the PHA value at bed rock was less than 0.15 g. However when the site effects were also considered for site class C and D, there was considerable increase in PGA values for majority of the study area. The amplification for higher PHA values were more for site classes A and B and the amplification for lower values of PHA were more in site classes C and D. A geotechnical site investigation will indicate the site class (based on V_s^{30}) at the desired location and depending on the site class to which the site belongs, the PGA at ground surface can

Figure 5. Variation of PHA values at rock level for 10% probability of Exceedance in 50 years.

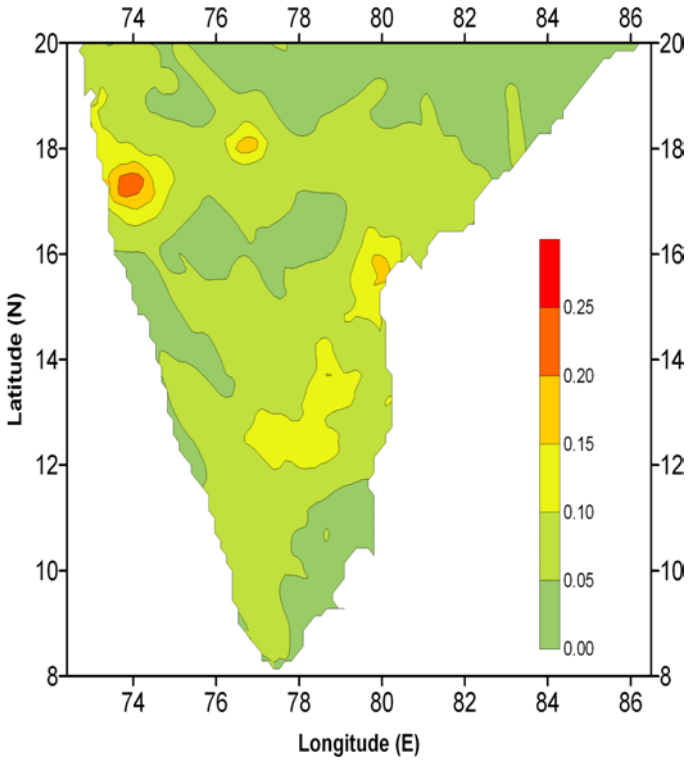

Figure 6. UHRS for Bangalore with 10% probability of exceedance in 50 years.

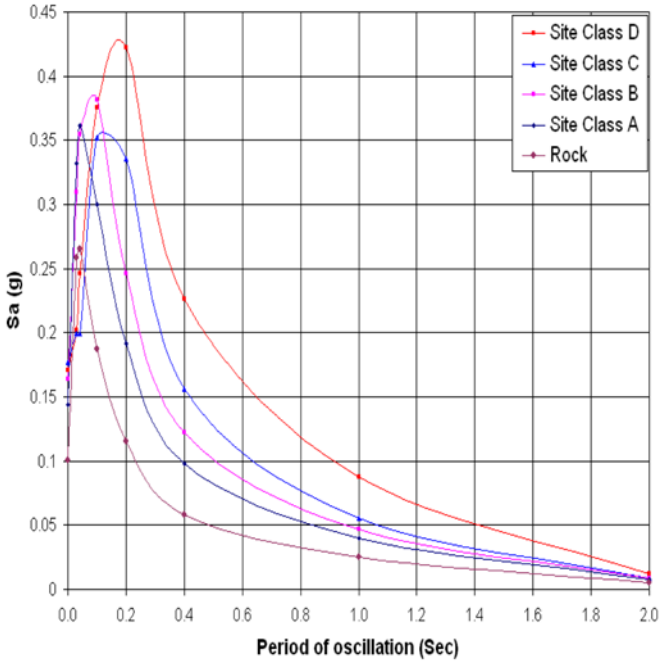

Figure 7. Spatial variation of PGA values with 10% probability of exceedance in 50 years for site class A.

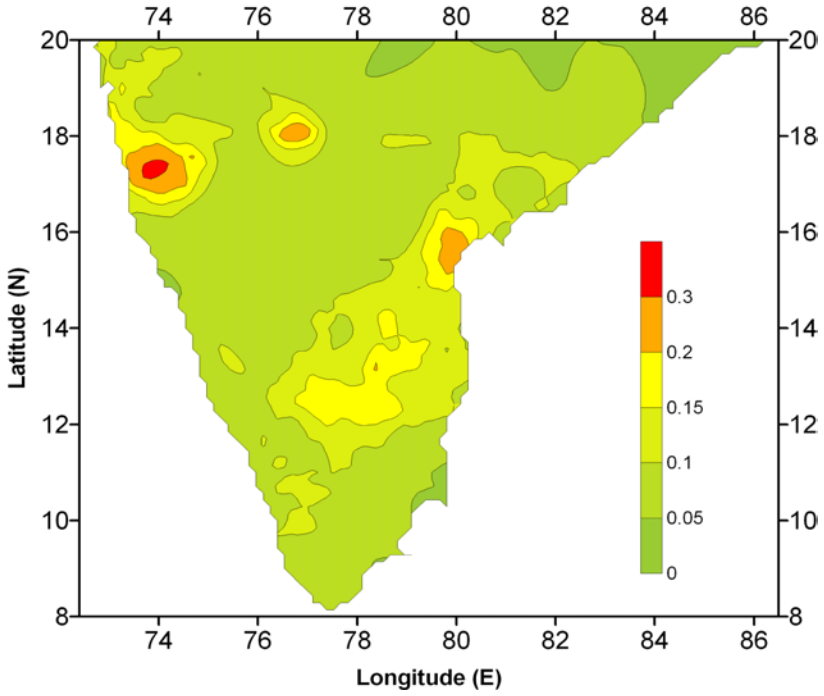

Figure 8. Spatial variation of PGA values with 10% probability of exceedance in 50 years for site class B.

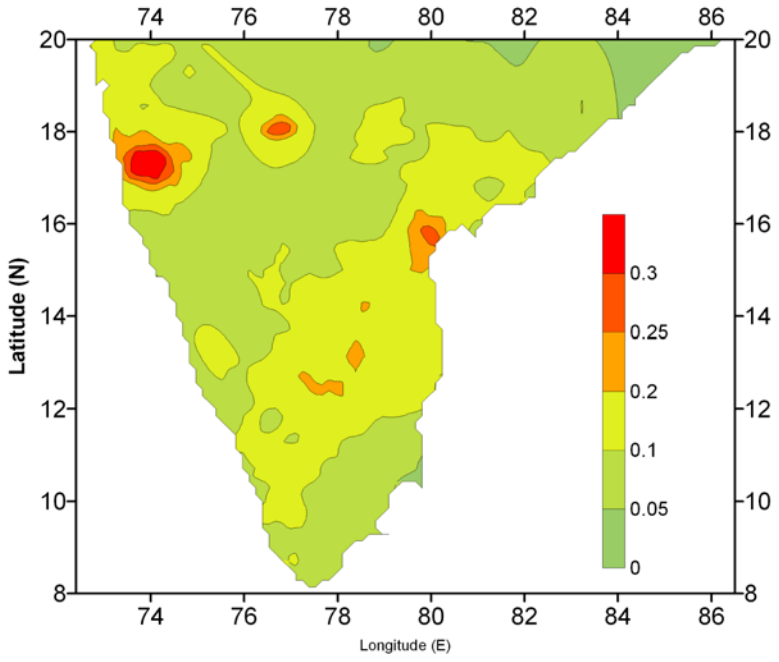

Figure 9. Spatial variation of PGA values with 10% probability of exceedance in 50 years for site class C.

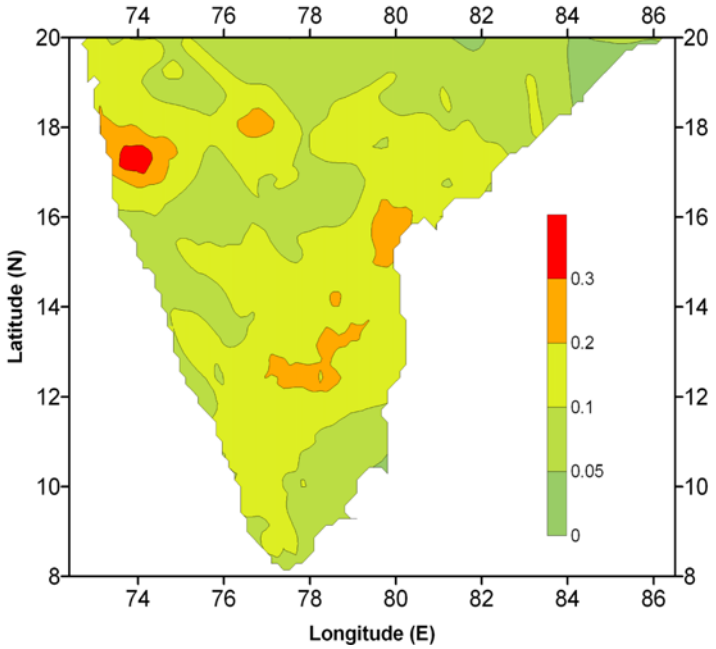

Figure 10. Spatial variation of PGA values with 10% probability of exceedance in 50 years for site class D.

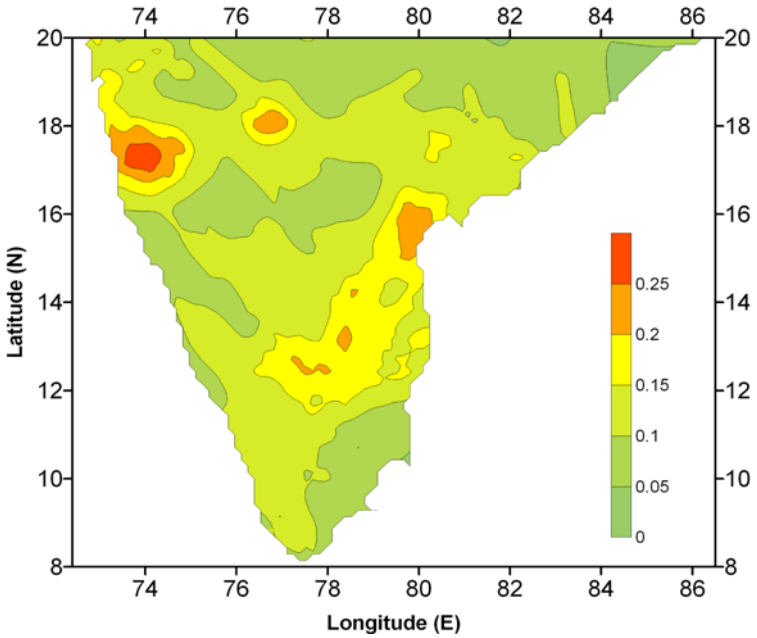

be obtained from the respective figures. However for many locations the V_s^{30} values may not be available, for those locations the site classification can be done based on the local geology and then the NEHRP site class can be determined. Thus it provides a very simple and comprehensive method to obtain the PGA value at ground surface for a vast study area like south India.

9. CONCLUSION

The evaluation of surface level PGA values and response spectra is of very high importance in the engineering design. In this article an attempt has been made to critically evaluate the different methods available for the site classification and recommends the one based on V_s^{30}. The seismic hazard of south India was evaluated based on the probabilistic logic tree approach by considering different source models and attenuation models. The logic tree approach will help in reducing the epistemic uncertainties in the different attenuation models and this will also help in getting a better hazard estimate. The PHA values obtained for some of the regions had shown significant difference from the values specified in the BIS-1893(2002). The surface level PGA values were evaluated for the entire study area for four NEHRP site classes by considering the local site effects.

REFERENCES

Agrawal, P. K., & Pandey, O. P. (2004). Unusual lithospheric structure and evolutionary pattern of the cratonic segments of the South Indian shield. *Earth, Planets, and Space*, *56*, 139–150.

Anbazhagan, P., Vinod, J. S., & Sitharam, T. G. (2009). Probabilistic seismic hazard Analysis for Bangalore. *JNat. Haz.*, *48*, 145–166. doi:10.1007/s11069-008-9253-3

Andrews, D. J. (1986). Objective determination of source parameters and similarity of earthquakes of different size in Earthquake Source Mechanics. In S. Das, J. Boatwright, & C.H. Scholz (Eds.), *American Geophysical Union* (pp. 259-268). Washington D.C.

Annie, O. K., & Stewart, J. P. (2006). Evaluation of the Effectiveness of Theoretical 1D Amplification Factors for Earthquake Ground-Motion Prediction. *Bulletin of the Seismological Society of America*, *96*(4A), 1422–1436. doi:10.1785/0120040196

Atkinson, G. M., & Boore, D. M. (2006). Earthquake Ground-Motion Prediction Equations for Eastern North America. *Bulletin of the Seismological Society of America*, *96*(6), 2181–2205. doi:10.1785/0120050245

BIS-1893. (2002). Indian Standard Criteria for Earthquake Resistant Design of Structures, Part 1 - General Provisions and Buildings. *Bureau of Indian Standards*, New Delhi.

Bommer, J., Scherbaum, F., Bungum, H., Cotton, F., Sabetta, F., & Abrahamson, N. A. (2005). On the use of logic trees for ground-motion prediction equations in seismic hazard analysis. *Bulletin of the Seismological Society of America*, *95*, 377–389. doi:10.1785/0120040073

Boore, D. M. (2004). Estimating Vs(30) (or NEHRP Site Classes) from Shallow Velocity Models (Depths < 30 m). *Bulletin of the Seismological Society of America*, *94*(2), 591–597. doi:10.1785/0120030105

Borcherdt, R. D. (1994). Estimates of site-dependent response spectra for design (methodology and justification). *Eqrthqk. Spect.*, *10*(4), 617–653. doi:10.1193/1.1585791

Borcherdt, R. D. (1996). Preliminary amplification estimates inferred from strong ground motion recordings of the Northridge earthquake of January 17, 1994. In *Proc. Int. Workshop on Site Response Subjected to Strong Ground Motion* (Vol. 1), Port and Harbor Research Institute, Yokosuka, Japan.

Borcherdt, R. D. (2002). Empirical evidence for acceleration-dependent amplification factors. *Bulletin of the Seismological Society of America*, *92*, 761–782. doi:10.1785/0120010170

Borcherdt, R. D., & Glassmoyer, G. (1994). Influences of local geology on strong and weak ground motions recorded in the San Francisco Bay region and their implications for site-specific building-code provisions The Loma Prieta, California Earthquake of October 17, 1989-Strong Ground Motion. *U.S. Geol. Surv. Profess. Pap., 1551- A*, A77-A108

BSSC. (2001). NEHRP recommended provisions for seismic regulations for new buildings and other structures 2000 edition, part 1: Provisions. *Report no. FEMA 368, Building seismic safety council for the federal emergency management agency*, Washington, D.C., USA.

Budnitz, R. J., Apostolakis, G., Boore, D. M., Cluff, L. S., Coppersmith, K. J., Cornell, C. A., & Morris, P. A. (1997). Recommendations for probabilistic seismic hazard analysis: guidance on uncertainty and use of experts. *U.S. Nuclear Regulatory Commission Report* NUREG/CR- 6372.

Cornell, C. A. (1968). Engineering seismic risk analysis. *Bulletin of the Seismological Society of America*, *58*, 1583–1606.

Cramer, C. H., & Kumar, A. (2003). 2001 Bhuj, India, earthquake engineering seismoscope recordings and Eastern North America ground motion attenuation relations. *Bulletin of the Seismological Society of America*, *93*, 1390–1394. doi:10.1785/0120020194

Eurocode-8 (2005) BS-EN 1998-1, Design of structures for earthquake resistance – part 1: General rules, seismic actions and rules for buildings. *European committee for standardization*, Brussels.

Field, E. H. (2000). A modified ground motion attenuation relationship for southern California that accounts for detailed site classification and a basin depth effect. *Bulletin of the Seismological Society of America*, *90*, S209–S221. doi:10.1785/0120000507

Field, E. H., & Jacob, K. H. (1993). The theoretical response of sedimentary layers to ambient seismic noise. *Geophysical Research Letters*, *20*, 2925–2928. doi:10.1029/93GL03054

Frank, S., Bommer, J. J., Bungum, H., Cotton, F., & Abrahamson, N. A. (2005). Composite Ground-Motion Models and Logic Trees: Methodology, Sensitivities, and Uncertainties. *Bulletin of the Seismological Society of America*, *95*(5), 1575–1593. doi:10.1785/0120040229

Frankel, A. (1995). Mapping seismic hazard in the Central Eastern United States. *Seismological Research Letters*, *66*(4), 8–21.

Hartzell, S. A., Carver, D., Cranswick, E., & Frankel, A. (2000). Variability of site response in Seattle, Washington. *Bulletin of the Seismological Society of America*, *90*, 1237–1250. doi:10.1785/0120000022

Lee, Y., & Anderson, J. G. (2000). A custom southern California ground motion relationship based on analysis of residuals. *Bulletin of the Seismological Society of America*, *90*, S170–S187. doi:10.1785/0120000509

Lunne, T., Robertson, P. K., & Powell, J. J. M. (1997). Cone Penetration Testing in Geotechnical Practice. *Blackie Academic & Professional,* London.

Nakamura, Y. (1989). A method for dynamic characteristics estimation of subsurface using microtremor on the ground surface. *Quarterly Report of the Railway Technical Research Institute*, *30*(1), 25–33.

Raghu Kanth, S. T. G., & Iyengar, R. N. (2006). Seismic hazard estimation for Mumbai city. *Current Science*, *91*(11), 1486–1494.

Raghu Kanth, S. T. G., & Iyengar, R. N. (2007). Estimation of Seismic Spectral Acceleration in Peninsular India. *Journal of Earth System Science*, *116*(3), 199–214. doi:10.1007/s12040-007-0020-8

Regulatory Guide 1.165 (1997). *Identification and characterization of seismic sources and determination of safe shutdown earthquake ground motion*. Published by U.S. Nuclear Regulatory Commission.

Rodriguez-Marek, A., Bray, J. D., & Abrahamson, N. A. (2001). An empirical geotechnical seismic site response procedure. *Earthquake Spectra*, *17*(1), 65–87. doi:10.1193/1.1586167

Seeber, L., Armbruster, J. G., & Jacob, K. H. (1999). Probabilistic Assessment of Seismic Hazard for Maharashtra, *Govt. of Maharashtra*. Unpublished Report.

Seed, H. B., & Idriss, I. M. (1982). *Ground motions and soil liquefaction during earthquakes" Monograph Series* (Vol. 5). Earthquake Engineering Research Institute.

SEISAT. (2000). Seismotectonic Atlas of India. published by *Geological Survey of India*.

Steidl, J. H. (2000). Site response in southern California for probabilistic seismic hazard analysis. *Bulletin of the Seismological Society of America*, *90*, S149–S169. doi:10.1785/0120000504

Stepp, J. C., Wong, I., Whitney, J., Quittemeyer, R., Abrahamson, N., & Toro, G. (2001). Yucca Mountain PSHA Project Members, Probabilistic seismic hazard analyses for ground motions and fault displacements at Yucca Mountain, Nevada. *Earthquake Spectra*, *17*, 113–151. doi:10.1193/1.1586169

Stewart, J. P., Liu, A. H., & Choi, Y. (2003). Amplification Factors for Spectral Acceleration in Tectonically Active Regions. *Bulletin of the Seismological Society of America*, *93*(1), 332–352. doi:10.1785/0120020049

Toro, G. N., Abrahamson, N., & Schneider, J. (1997). Model of strong ground motions from earthquakes in central and eastern North America: Best estimates and uncertainties. *Seismological Research Letters*, *68*, 41–57.

Vipin, K. S., Anbazhagan, P., & Sitharam, T. G. (2009). Estimation of peak ground acceleration and spectral acceleration for South India with local site effects: probabilistic approach. *Natural Hazards and Earth System Sciences*, *9*, 865–878.

This work was previously published in International Journal of Geotechnical Earthquake Engineering, Volume 1, Issue 1, edited by T.G. Sitharam, pp. 25-41, copyright 2010 by IGI Publishing (an imprint of IGI Global).

Chapter 2
A Site Specific Study on Evaluation of Design Ground Motion Parameters

A. Boominathan
Indian Institute of Technology Madras, India

S. Krishna Kumar
Indian Institute of Technology Madras, India

ABSTRACT

Design ground motions are usually developed by one of the two approaches: site-specific analyses or from provisions of building codes. Although contemporary codes do consider approximately the site effects, they provide more conservative estimates. Hence it is preferred to carry out site specific analysis which involves both the seismic hazard analysis and ground response analysis. This article presents a site specific analysis for a seismically vulnerable site near Ahmedabad, Gujarat. The seismic hazard analysis was carried out by DSHA approach considering seismicity and seismotectonics within 250km radius. The site is predominantly characterized by deep stiff sandy clay deposits. Extensive shear wave velocity measurement by cross hole test is used for site classification and ground response analysis. The ground response analysis was carried out by equivalent linear approach using SHAKE2000. It is found that the deep stiff soil site considered is found to amplify the ground motion. The site specific response spectra obtained from RRS analysis is compared with the codal provision which reveals high spectral acceleration in site specific spectra for mid period range.

DOI: 10.4018/978-1-4666-0915-0.ch002

INTRODUCTION

Earthquakes are one of the most devastating natural hazards that cause great loss of life and livelihood. Seismic waves generated at the earthquake source propagate through different geological formation until they reach the surface at a specific site. The path of the seismic waves in the upper geological formation strongly influences their characteristics producing varying effect on the ground surface motion. Thus the ground motion parameters at a particular site are influenced by the source, travel path and site characteristics. The influence of local soil conditions on the ground response has been recognized for many years and its significance was felt during 1985 Mexican earthquake. There can be significant differences in local site conditions such as variations in geological formations, thickness and properties of soil and rock layers, depth of bedrock and water table, surface and underground topography. These variations would have significant effects on the characteristics: amplitude, frequency content and duration of strong ground motion at the surface (Carlos et al., 2006). The extent of the influence depends on the geometry and material properties of the subsurface materials, site topography and on the characteristics of the input motion. The significance of the local site effect on the earthquake-resistant design must be accounted for by the development of site specific design ground motions i.e. motions that reflect the levels of strong motion amplitude, frequency content and duration of a structure or facility at a particular site. Hence site specific design ground motion estimation shall include both seismic hazard analysis and ground response analysis. Seismic hazard analysis can be carried out by deterministic or probabilistic based methods considering the seismicity and seismotectonics of the region. Ground response analyses are commonly carried out by equivalent linear approach to predict the design ground motion parameters including PGA and design response spectra at the surface level. This article presents evaluation of site specific design ground motion parameters for a seismically vulnerable site near Ahmedabad, Gujarat by conducting a detailed seismic hazard analysis and ground response analysis.

SIGNIFICANCE OF SITE-SPECIFIC ANALYSIS

The characteristics of the design ground motion at a particular site are influenced by the location of the site relative to potential seismic sources, the seismicity of those sources, and nature of rupture at the source, travel path effects, and the importance of the structure or facility for which the ground motion is to be used. Design ground motions are usually developed in one of two approaches: from site-specific analyses or from the provisions of building codes and standards. Although contemporary codes do consider site effects, they usually do so by lumping groups of similar soil profiles together so that their provisions apply to broad ranges of soil conditions within which the local conditions of a particular site are expected to fall. Because of this, the design ground motions developed from code provisions are usually more conservative (i.e. correspond to stronger levels of shaking) than those developed from site-specific analyses. The UBC adopts two basic approaches: static approach which considers the effects of ground motions represented by static lateral forces and dynamic approach in which ground motion is characterized by a design response spectrum. These approaches are based on developed hazard maps and provide zone factors that reflect to an extent the local site conditions. However these maps do not consider local variations at the site in developing the ground motion parameters, deeming it necessary to perform site specific ground response analysis for vulnerable sites and critical structures.

Site specific design ground motions reflect the detailed effects of the subsurface conditions at the sites of interest. The process involves develop-

ment of site-specific ground motions by seismic hazard analysis and ground response analysis. The seismic hazard analysis will produce a set of ground motion parameters that may or may not correspond to the conditions at the site of interest. Seismic hazard analyses are based on a set of attenuation equations which usually correspond to a fairly narrow range of subsurface conditions. If the site of interest is located on a similar profile the parameters developed shall be taken as ground motion parameter. If not, the parameters developed should be suitably modified for the effects of local site conditions. The parameters can be modified by analytical or empirical approach. The former involves deconvolution and conventional ground response analysis (Kramer, 1996).

A site specific analysis for evaluation of design ground motion parameters of a particular site comprises of the following aspects

1. Site characterization based on geological, geophysical and geotechnical investigation
2. Site classification using the shear wave velocity profile
3. Seismic hazard analysis which involves collection of seismicity and seismotectonic of the region, selection of predictive relationship to arrive at controlling earthquake with PGA
4. Ground response analysis
5. Evaluation of design ground motion parameters including development of site specific design response spectra.

The overall process flow of site specific response analysis based on DSHA approach adopted in the present study is presented in Figure 1.

SITE DESCRIPTION

The site considered in the present study is located about 12km from Ahmedabad in the state of Gujarat (India). The site lies in the western coastal region of India which has experienced several major earthquakes, including the disastrous Bhuj earthquake, 2001 (Mw = 7.7). Severe damages were observed on multistory buildings located in close proximity to the Sabarmati river area in Ahmedabad during 2001 Bhuj Earthquake (Sitharam and GovindaRaju, 2004). The site is categorized under Zone III as per Indian seismic code (IS 1893-2002). The site is situated in the Sabarmati River basin where the overburden thickness is reported as high as 300-500 m. Various types of high raised buildings are proposed in the site which spreads over 500 acres of land. The seismic vulnerability of the region and presence of deep soil necessitates performing site specific ground response analysis to arrive design ground motion parameters for design of various important buildings.

SITE CHARACTERIZATION

Site characterization is the initial phase of the site specific ground response analysis involves acquiring, processing and interpretation of qualitative and quantitative information of the site such as geological, geotechnical, seismic and seismotectonic details to evaluate the hazard based on level of site response. The scope of site characterization varies from simple to complex depending upon several major factors including

1. Importance of the structure and the degree of the risk
2. Regional seismicity (the degree of hazard) and adequacy of available data
3. Physiographic conditions (mountains, coastline, plains, etc.)
4. Regional and local geology (hazards, rock type and structure, soil types, and ground water characteristics)

One of the major problems in geotechnical engineering is the risk of encountering unexpected

Figure 1. Process flow for site specific response analysis based on DSHA approach

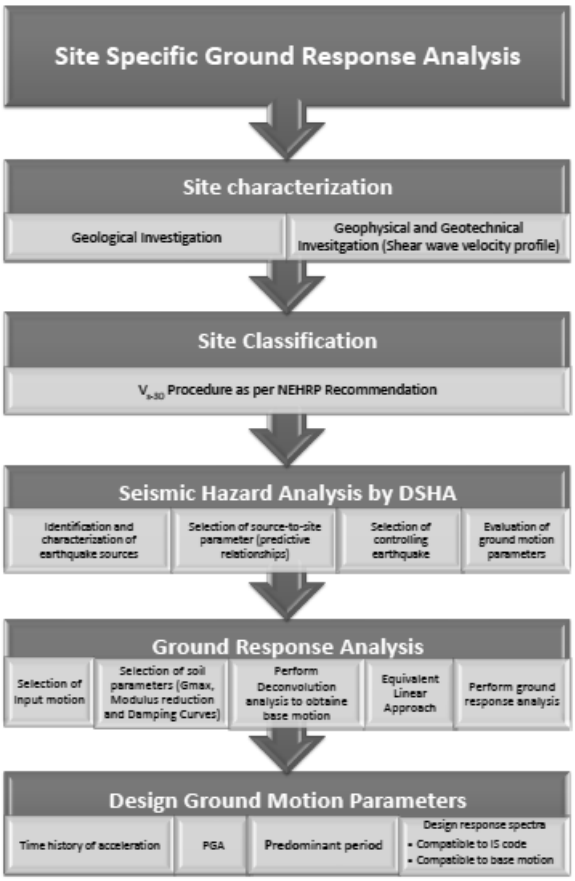

geological conditions such as sudden variation in the soil profile, rock strata, failure plane and faults in the rock, etc. Failure to anticipate such conditions generally is due to inadequate geological understanding of the site and may lead to issues concerning design and performance of critical and important structures. Hence it is very important that rigorous geological and geophysical analyses accompany extensive geotechnical investigation to understand the behavior of the site to seismic loads (Boominathan, 2004).

Geology

The geological study of the site involves identification of important natural factors such as physiography (mountain ranges, rift, basins, plains, river valleys, coastal regions, etc.) and local geological conditions (geological formations, rock types, faults, fold, lineaments, and terrain variations) that affect the response of the site. Information on physiography is obtained from topographic maps and remote sensing imageries. The physiography of the site has a direct relationship in most cases to the geological hazards, with respect to seismic response and attenuation. The geological formations at the site provide an insight to overall response of site to seismic loading. Numerous methods like radiometric dating are employed to date the geological formations. Terrain analysis and field reconnaissance provide detailed geological data of the surface conditions (Hunt, 2005). Detailed

geological studies found abundant in literature provides sufficient data to envisage the likely response of site to seismic excitation.

The study region located on the Sabarmati River basin is characterized by quaternary soil deposit with Mesozoic rocks over thrusting them (Rastogi, 2001). It is located within the Cambay rift flanked by the east and the west Cambay faults. The Cambay rift basin in northwestern India is one of the pre-continental rifts that originated between the early Jurassic and Tertiary, after the breakup of Gondwanaland. The basin is presently covered by thick layers of Quaternary and Tertiary sediments, occurred during the Cenozoic period (Biswas, 1987). Refraction and deep seismic sounding (DSS) studies established the thickness of the Quaternary and Tertiary sediments in most parts of the basin to vary between 3000 and 5500m (Kaila et al, 1981, 1990). The top 300-500 m is characterized by quaternary deposits (Tewari et al., 1995; Rastogi et al., 2001).

Geophysical and Geotechnical Investigation

Geophysical and geotechnical site investigation in seismically active regions should include gathering of information about the physical nature of the site and its environment that will allow adequate evaluation of seismic hazard. The scope of the investigation depends on the seismicity of the area and nature of the site as well as the proposed or existing construction. In addition to the effects of local soil conditions upon the severity of ground motion, investigation should cover possible earthquake danger from geological or other consequential hazards such as fault displacement, subsidence, liquefaction, landslides, mudflows, etc (Boominathan, 2004).

The Standard Penetration Test (SPT) was conducted to a depth of about 60 to 80 m at 150 locations in the site. The water table is found to be at a depth of 30 m below the ground level. The top 2.5 to 4.0 m layer is clayey sand (SC) with SPT 'N' value varying from 30 to 40. Silty sand (SM) and clays of intermediate plasticity (CI) are also observed in the top layer at certain locations. It is followed by a 25 m thick sandy clay layer with high SPT 'N' value varying from 60 to 100. A very thick clay layer with sand gravel mixtures is encountered 30 m below the ground level which extends to the borehole termination depth of 60 m. The SPT 'N' value in this layer is significantly greater than 100. The laboratory tests conducted on soil samples collected at this layer reveals plasticity index values of above 30. The unconfined compressive strength of this layer varies from 360 to 380 kPa, indicating hard consistency of the clay. The consolidation test carried out on the above soil samples shows low compression index values less than 0.06 confirming the presence of hard clay stratum. In general the soil strata at the site have a very high strength and stiffness, although rock formations are not encountered within the depth of investigation. A typical bore log of the site is presented in Figure 2.

Field tests which are most commonly employed in geotechnical earthquake engineering can be grouped into those that measure low-strain properties and those that measure properties at intermediate to high strains. Low-strain field tests typically induce seismic waves in the soil and seek to measure the velocities at which these waves propagate. Due to low strain amplitudes the measured shear wave velocity (V_s) along with soil density (ρ) is used to compute low-strain shear modulus.

$$G_{max} = \rho \, V_s^2 \qquad (1)$$

The shear wave velocity measurement in the field can be carried out either using borings or without borings. Seismic reflection and seismic refraction are staples of conventional geophysical exploration and can provide information on subsurface layer thickness and velocities of propagating waves without need for soil borings.

Figure 2. Typical borelog of the site

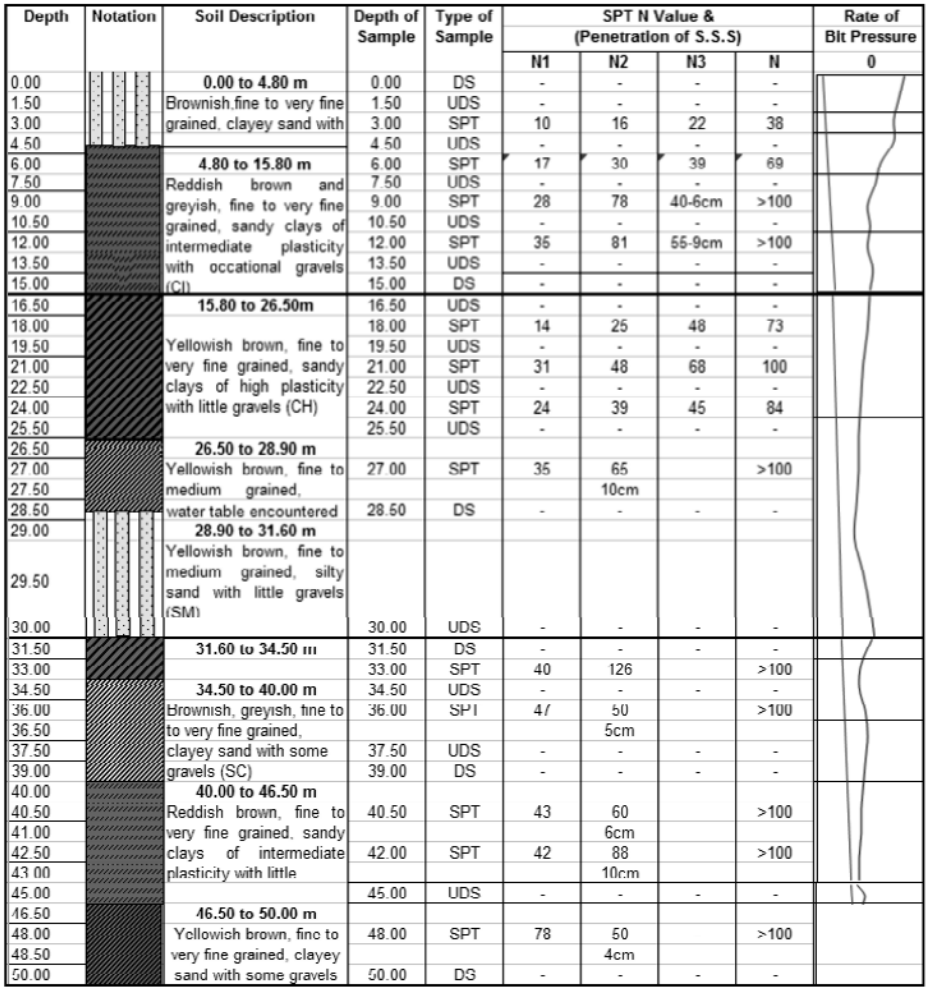

Depth	Soil Description	Depth of Sample	Type of Sample	SPT N Value & (Penetration of S.S.S)				Rate of Bit Pressure
				N1	N2	N3	N	0
0.00	**0.00 to 4.80 m**	0.00	DS	-	-	-	-	
1.50	Brownish,fine to very fine	1.50	UDS	-	-	-	-	
3.00	grained, clayey sand with	3.00	SPT	10	16	22	38	
4.50		4.50	UDS	-	-	-	-	
6.00	**4.80 to 15.80 m**	6.00	SPT	17	30	39	69	
7.50	Reddish brown and	7.50	UDS	-	-	-	-	
9.00	greyish, fine to very fine	9.00	SPT	28	78	40-6cm	>100	
10.50	grained, sandy clays of	10.50	UDS	-	-	-	-	
12.00	intermediate plasticity	12.00	SPT	35	81	55-9cm	>100	
13.50	with occational gravels	13.50	UDS	-	-	-	-	
15.00	(CI)	15.00	DS	-	-	-	-	
16.50	**15.80 to 26.50m**	16.50	UDS	-	-	-	-	
18.00		18.00	SPT	14	25	48	73	
19.50	Yellowish brown, fine to	19.50	UDS	-	-	-	-	
21.00	very fine grained, sandy	21.00	SPT	31	48	68	100	
22.50	clays of high plasticity	22.50	UDS	-	-	-	-	
24.00	with little gravels (CH)	24.00	SPT	24	39	45	84	
25.50		25.50	UDS	-	-	-	-	
26.50	**26.50 to 28.90 m**							
27.00	Yellowish brown, fine to	27.00	SPT	35	65		>100	
27.50	medium grained,				10cm			
28.50	water table encountered	28.50	DS	-	-	-	-	
29.00	**28.90 to 31.60 m**							
29.50	Yellowish brown, fine to medium grained, silty sand with little gravels (SM)							
30.00		30.00	UDS	-	-	-	-	
31.50	**31.60 to 34.50 m**	31.50	DS	-	-	-	-	
33.00		33.00	SPT	40	126		>100	
34.50	**34.50 to 40.00 m**	34.50	UDS	-	-	-	-	
36.00	Brownish, greyish, fine to	36.00	SPT	47	50		>100	
36.50	to very fine grained,				5cm			
37.50	clayey sand with some	37.50	UDS	-	-	-	-	
39.00	gravels (SC)	39.00	DS	-	-	-	-	
40.00	**40.00 to 46.50 m**							
40.50	Reddish brown, fine to	40.50	SPT	43	60		>100	
41.00	very fine grained, sandy				6cm			
42.50	clays of intermediate	42.00	SPT	42	88		>100	
43.00	plasticity with little				10cm			
45.00		45.00	UDS	-	-	-	-	
46.50	**46.50 to 50.00 m**							
48.00	Yellowish brown, fine to	48.00	SPT	78	50		>100	
48.50	very fine grained, clayey				4cm			
50.00	sand with some gravels	50.00	DS	-	-	-	-	

However these techniques fall short in detecting soft layers below stiff layers (Kramer and Stewart, 2004). A relatively new technique that can be used to determine subsurface thickness and wave propagation velocities without necessity of borings is the Multi Channel Analysis of Surface Waves (MASW) test (Nazarian and Stokoe, 1983; Suto, 2007). In this test series of vertical receivers are place on the ground in line with an impact source. The output of the receivers are recorded and transformed into the frequency domain. The phase angles between the recoded responses are used to compute an apparent travel time of the surface waves. The surface wave phase velocity is computed as a function of frequency by knowing the distance between the source and the receiver. MASW profiling also provides the stiffness of the underlying soil which is the variation of phase velocity with frequency. MASW test is becoming increasingly popular in India with its wide usage in microzonation (Sitharam et al., 2007; Hanumantharao & Ramana, 2008; Uma Maheshwari et.al., 2008; Neelima Satyam & Rao, 2009). However the MASW test is not effective in deep soil sites.

Low-strain tests that require borings include down-hole test, up-hole test, cross hole test and suspension logger test. Among these methods, cross-hole test is widely used to measure the

shear wave velocity profile particularly at deep soil sites. The cross-hole test makes use of more than one bore hole. A vibratory source is placed in one boring and the receiver is placed at the same depth in each of the other bore holes. An impulsive disturbance is applied at the source and the travel times to each of the receivers is measured. The wave propagation velocity is measure by knowing the distance between the source and the receiver. The cross-hole test is the best method to measure the shear wave velocity of the strata at any depth and it can detect the low velocity layers and it is widely used in earthquake engineering application. Therefore in the present deep soil site cross hole test was performed to measure the shear wave velocity.

Cross hole test was performed at 28 locations in the site as per ASTM standard 4428 M-84. The test was conducted using three 150 mm size boreholes: a source borehole and two receiver boreholes each spaced 3.0 m apart. The receiver bore holes drilled were cased with a PVC pipe of 150 mm diameter and the gap between the casing and the receiver bore hole was filled with fine sand slurry to establish good contact between the surrounding soil medium and the casing. In the present investigation, blows of SPT hammer in the source bore hole were used to generate seismic waves. The P and S-waves generated at seismic source are gathered by a borehole-pick which essentially consists of acceleration transducer, pneumatic packer assembly, pneumatic pump and control. The seismic wave signals were acquired and recorded using a HBM make multi-channel Digital carrier frequency amplifier system with data acquisition system and CATMAN Professional software installed in Laptop. The cross hole tests were performed at the site at an interval of 1.5 m up to a depth of 60.0 m. The typical wave traces obtained from the cross hole test is presented in Figure 3a. Figure 3b shows a typical variation P-wave and S-wave velocity with depth.

Maximum shear modulus of soil (G_{max}) is the fundamental property of the soil in geotechnical earthquake engineering application. The most reliable methods to determine the maximum shear modulus of soil are those conducted in the field. This is because the laboratory soil testing of undisturbed soil samples is often subjected to errors due to sample disturbance. Even if the disturbance is minor in advanced technique of sampling, time and expense may be substantial. Hence in the present study shear wave velocity obtained from the cross hole test is utilized to compute the maximum shear modulus of the soil using the formula discussed earlier.

SITE CLASSIFICATION

Site classification can be carried out by different schemes: based on average shear wave velocity in the upper 30 m, V_{s-30}, surface geology and geotechnical data are available to represent the generic response of the site to seismic excitations (Kramer & Stewart, 2004). The V_{s-30} scheme (Borcherdt, 1994) is the most widely used site classification procedure in modern practice. Hence, in the present study the site classification is carried out based on V_{s-30} approach. The average shear wave velocity for the upper 30 m is determined by using the following formula (Lew, 2001).

$$V_{s-30} = \frac{\sum_{i=1}^{n} d_i}{\sum_{i=1}^{n} \frac{d_i}{v_{si}}}$$

where: d_i = Thickness of Layer *i* in m

V_{si} = Shear wave velocity in Layer *i* in (m/s)

The average shear wave velocity for the upper 30m computed using the cross-hole test data. The average shear wave velocity in the top 30m for most of the locations varies between 400m/s to 600m/s and is classified as C class site as per

Figure 3. (a)Typical wave trace obtained from the cross hole test (b)Typical variation of P-wave and S-wave velocity in the study area

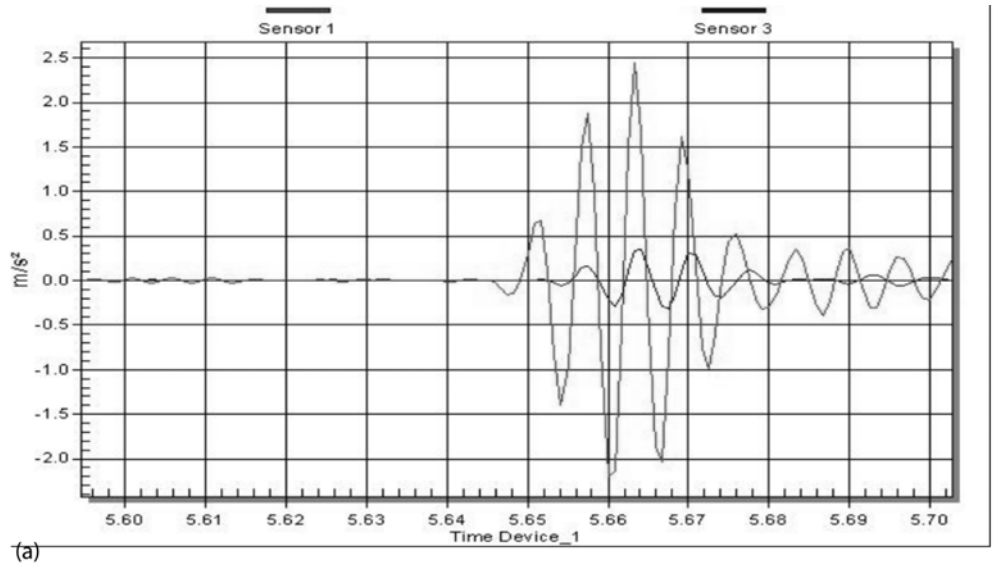

(a)

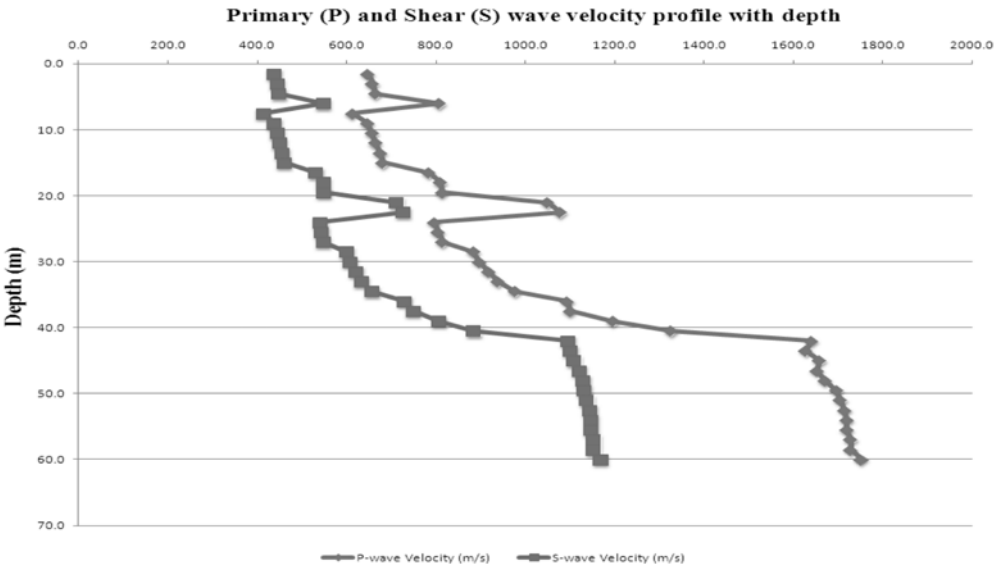

(b)

NEHRP (BSSC, 2001) classification. Only very few locations the average shear wave velocity in the top 30m exceeds 750m/s and hence are classified as B class site. The above site classifications are used in the seismic hazard analysis to consider approximately the site effects.

SEISMIC HAZARD ANALYSIS

Seismic hazard analyses involve the quantitative estimation of ground shaking hazards at a particular site. To evaluate the seismic hazard for a particular site or region all possible sources of seismic activity must be identified and their potential for generating future strong motion evaluated. Seismic hazards may be analyzed deterministically, as when a particular earthquake scenario is assumed or probabilistically, in which certain uncertainties are considered explicitly (Kramer, 1996). The earthquake ground motions that ultimately are selected for engineering design depend mainly on the criticality of a site or structure and the engineering analyses that are to be performed (Krinitzsky, 2002).

In the past 20 to 30 years the use of probabilistic concepts has allowed uncertainties in the size, location and rate of recurrence of earthquakes and in the variation of ground motion characteristics with earthquake size and location to be explicitly considered in the evaluation of seismic hazards. Probabilistic seismic hazard analysis (PSHA) provides a frame-work in which these uncertainties can be identified, quantified, and combined in a rational manner to provide a more complete picture of seismic hazard. The proper performance of a PSHA requires careful attention to the problems of source characterization and ground motion parameter prediction and to the mechanics of the probability computations.

Deterministic Seismic Hazard Analysis (DSHA) analysis is simple and more prevalent methods of hazard analysis in geotechnical earthquake engineering. DSHA involves the development of a particular seismic scenario upon which a ground motion hazard evaluation is based. The scenario consists of the postulated occurrence of an earthquake of a specified size occurring at a specified location. DSHA is more logical, more transparent, and more appropriate for requirements in engineering design. DSHA should be considered as the basis for design of critical construction. DSHA identifies individual faults with their estimated MCEs affecting a site and gives site-specific hazard estimates from the earthquake potential of each fault (Krinitzsky, 2003). Hence in the present study seismic hazard analysis is carried out by deterministic approach. The deterministic based seismic hazard analyses were also performed for microzonation of various cities in India (Sitharam et al., 2007; Boominathan et al., 2008)

Deterministic seismic hazard analysis involves the following steps (Reiter, 1990) which are discussed in detail in the succeeding sections.

- Identification and characterization of all earthquake sources capable of producing significant ground motion at the site.
- Selection of source to site distance parameter for each source zone.
- Estimation of PGA for all earthquake sources considered using appropriate attenuation equation
- Selection of the controlling earthquake, which is expected to produce the maximum PGA.

Identification and Characterization of Earthquake sources

Seismicity and Seismotectonics

Historical seismicity of the study region is pivotal in site specific ground response analysis. Details of historical seismic activities are made available through catalogs of earthquake provided by USGS Earthquake Hazards Program, IMD, GSI and other reliable agencies. Seismic susceptibility of the area can be assessed with the help of the seismicity data on the occurrence of past earthquakes and seismotectonic details that describes the tectonic features of the site. Seismological information and seismotectonic features are pro-

Figure 4. Base map of the study region

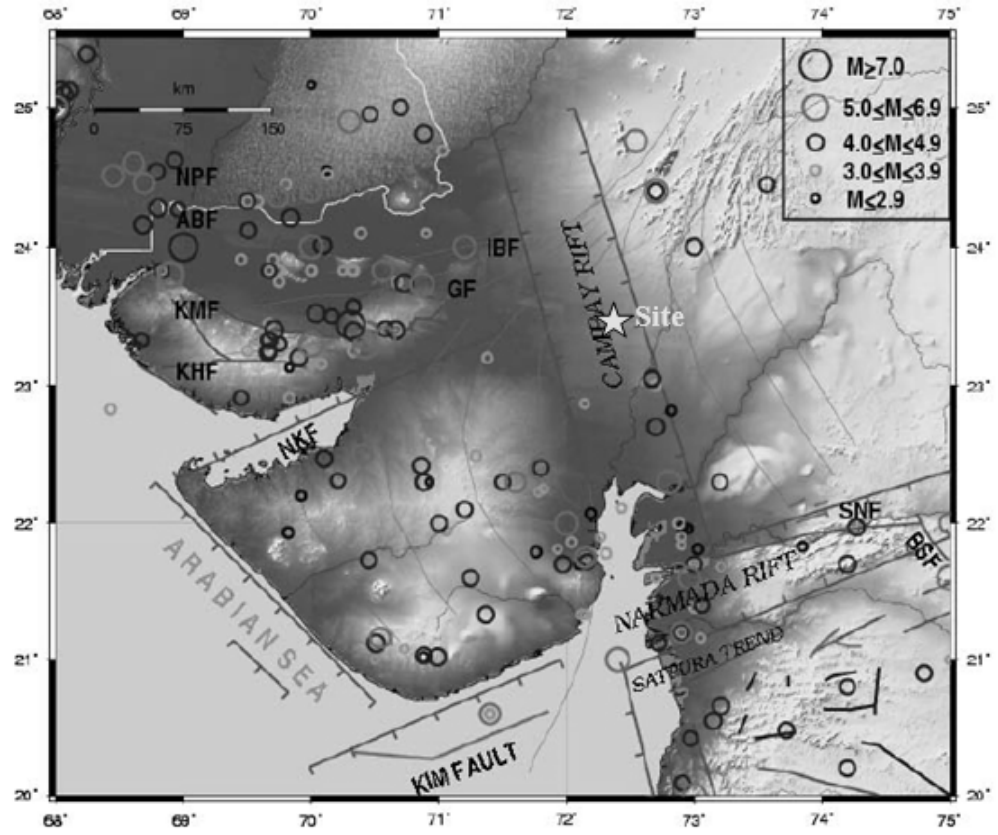

vided by Seismotectonic Atlas or shall be obtained from terrain analysis employing remote sensing imageries to locate fault structures, length and to identify capable faults. Seismicity data are alone not sufficient for the purpose of identification and characterization of earthquake sources and are to be supplemented by historical and instrumental seismicity data.

In the present study the details of the faults and lineaments that lie within 250 km radius of the study area were collected from the seismotectonic atlas of India (GSI 2000). The mere presence of fault however does not indicate the likelihood of future earthquakes. Hence it is required to identify the *capable faults* which are capable of generating strong motion. Thirteen earthquake sources were identified within 250kms from the study region. The identified sources are shown in base map which is developed using the Geographic Information System (GIS) tool Arc GIS 9.2 (Figure 4).

The earthquake data from 1668 to 2008 were collected from various sources such as IMD, USGS, GSI, ISR, ISC, and GERI which includes details on time of occurrence, location, depth, magnitude and intensity. These earthquake details were mapped onto the faults based on the location and depth of the earthquake and the length of the fault as shown in Figure 4. This information is utilized while assigning the maximum magnitude for each fault source by considering the seismicity around the particular fault source. The maximum magnitude for a particular seismic source was taken as the largest observed past magnitude plus 0.5 (Kijko and Graham, 1998; Sokolov et

al., 2001). In the present study the source to site distance is selected as the shortest epicentral distance from the sources to the site.

Controlling Earthquake

The earthquake that is expected to produce the strongest level of shaking is the controlling earthquake, generally expressed in terms of some ground motion parameter, at the site. The selection is made by comparing the levels of shaking produced by different earthquake sources identified in the earthquake source characterization phase. The controlling earthquake is described in terms of the size (magnitude) and distance from the site.

The peak ground acceleration is the most commonly used parameter to evaluate the effect of ground shaking due to different earthquakes identified. The peak ground acceleration at the ground surface is obtained using attenuation equations or predictive relationships. Predictive relationships, which express a particular ground motion parameter in terms of the quantities that affect it most strongly, are used to estimate ground motion parameters. A large number of useful attenuation relationships for different geographic and tectonic environments are available to predict the ground motion parameters (Campbell, 1981; Boore et al., 1983; Frankel et al., 1996). The predictive relationship that characterize the source, travel path and that idealizes the site condition should be chosen from the available relationships. The predictive equations shall be checked with the recorded PGA value at or near the site.

It is observed that the crustal intra-plate relation of Frankel et al. (1996) yields ground motions similar to the strong ground motion data recorded from the 2001 earthquake at large distances (Cramer and Wheeler, 2001). Hence in the present study, the PGA value is estimated based on the predictive relationship proposed by Frankel et al (1996). The crustal intra-plate relation developed is for the site condition specified as the boundary between NEHRP classes B and C, having an average shear-wave velocity of 760 m/second in the top 30 m. The study area considered also have an average shear wave velocity of about 800m/second in the top 30m, justifying the use of Frankel attenuation relation. It is also observed that the PGA of 0.1g at Ahmedabad recorded by seismogram located at the ground floor of regional passport office during Bhuj 2001 earthquake (Hazarika and Boominathan, 2009) compares well with the predictive relation proposed by Frankel having a PGA of 0.14g for magnitude of 7.7. As the Cambay rift region is more susceptible to shallow focus earthquakes, a focal depth of 15km was adopted. The Frankel predictive relationship was adopted to obtain the PGA at the surface. The earthquake that is expected to produce the strongest level of shaking is referred as the controlling earthquake and is obtained by plotting the variation of peak ground acceleration with distance for different sources. The details of the estimation of PGA for all the sources are presented in Table 1. It can be found from Table 1 that the East Cambay fault located at a distance of about 20.5 km from the site for the magnitude of 6.2 causes the maximum PGA of 0.46g and hence it is identified as the controlling earthquake source.

SITE SPECIFIC GROUND RESPONSE ANALYSIS

Local site effects profoundly influence all of the important characteristics: amplitude, frequency content, and duration of strong ground motion. The extent of the influence depends on the geometry and material properties of the subsurface materials, onsite topography and on the characteristics of the input ground motion. Site response analysis includes 1-D ground response effects, basin effects and topographic effects. Ground response analysis is performed either using 1D models or nonlinear models. Most ground response analysis models solve for one dimensional wave propagation problems. Nonlinear behavior of the soil can

Table 1. Estimation of PGA

S. No	Name of the Fault	Moment Magnitude (M_w)	Distance from site (km)	PGA (g)
1	East Cambay Fault	6.2	20.51	0.460
2	West Cambay Fault	5.1	15.72	0.110
3	West Coast Lineament	5.5	100.30	0.030
4	Island Belt Fault	6.1	130.00	0.024
5	Katrot Bhuj Fault	6.5	236.50	0.016
6	Kutch Mainland Fault	8.3	169.50	0.140
7	North Kaitwar Fault	4.9	95.00	0.007
8	Chambal Jamnagar Lineament	6.2	100.00	0.027
9	Kim Fault	4.3	292.00	---
10	Son Narmada Fault	5.1	207.50	0.003
11	Tapti North Fault	6.2	230.75	0.006
12	Paldi Fault	5.9	141.50	0.016
13	Allah Bund Fault	5.6	255.00	0.004

be approximated by an equivalent linear characterization of dynamic properties (Seed and Idriss, 1970). The most widely used computer program for 1-D ground response analysis utilizing this model is currently SHAKE91 (Idriss and Sun, 1992), which is a modified version of the program SHAKE (Schnabel et al., 1972). The program uses an equivalent linear, total stress analysis procedure to compute the response of a 1-D, horizontally layered viscoelastic system subjected to vertically propagating shear waves. The program uses the exact continuum solution to the wave equation adapted for use with transient motions through the Fast Fourier Transform algorithm. The equivalent linear method models the nonlinear variation of soil shear moduli and damping as a function of shear strain. The hysteretic stress-strain behavior of soils under symmetrical cyclic loading is represented by an equivalent modulus, G, corresponding to the secant modulus through the endpoints of the hysteresis loop and equivalent linear damping ratio, β, which is proportional to the energy loss from a single cycle of shear deformation. For a given soil layer, G and β are assumed to be constant with time during the earthquake shaking. An iterative procedure, based on linear dynamic analysis, is performed to find the shear moduli and damping ratios corresponding to the computed shear strains.

Nonlinear models solve the one-dimensional wave equation by direct numerical integration in the time domain. A variety of material models are used, which range from relatively simple cyclic stress-strain relationships to advanced constitutive models incorporating yield surfaces, hardening laws and flow rules (Wang, 1990). Nonlinear methods can be formulated in terms of effective stresses to allow modeling of the generation, redistribution and eventual dissipation of excess pore pressure during and after earthquake shaking, whereas equivalent linear methods can only perform total stress analysis. Cyclic nonlinear models generally consist of a backbone curve and rules that describe unload-reload behavior, pore-pressure generation and cyclic modulus degradation. DYNA1D, SUMDES, SPECTRA and AMPLE are some of the nonlinear analysis program which includes advanced constitutive models. Nonlinear multi-dimensional ground

response analyses are sometimes preferred for critical structures.

Equivalent linear analyses are more efficient than non linear analyses when the input motion can be characterized with acceptable accuracy (Kramer, 1996). Hence in the present study equivalent linear approach is adopted to perform one dimensional ground response analysis using the software SHAKE2000.

Input Motion

Earthquake response of structures and their foundations is an outcome of the complex interaction between the random input ground motion and the continuously changing dynamic characteristics of the system subjected to the ground motion. The site specific ground response analysis involves the determination of input acceleration time history characterized by amplitude, frequency and duration content. The time history of the ground motions can be obtained by two approaches: use of natural strong motion earthquake data and artificial ground motion generation. The ideal procedure for the selection of strong motions for use in analysis is to obtain records generated in conditions that are identical to those of the seismic design scenario. Bolt (1978) showed that if all the characteristics of the design earthquake could be matched to those of a previous earthquake, the probability of the characteristics of the record matching would be unity. Hence in the present study, the input acceleration time history is obtained by scaling the acceleration time history of a previously recorded natural earthquake which has magnitude, distance and local site characteristics that are similar to those of seismic scenario at the site. The bracketed duration was estimated based on the magnitude and the epicentral distance from the causative fault as 18s (Chang and Krinitzsky, 1977). The accelerogram of 1999 Chi-Chi earthquake with a similar site conditions was scaled to a required PGA of 0.46g as estimated from the DSHA and it represents the required surface acceleration time history (Figure 5). The Fourier spectrum for the adopted input motion is plotted in Figure 6 and it shows the predominant frequency of 2Hz.

Deconvolution Analysis

Deconvolution is the process of obtaining the bedrock motion from a known free surface motion. The average shear wave velocity variation at the site was used to characterize the strata for deconvolution analysis. The deconvolution analysis was carried out for the surface acceleration time history using SHAKE2000 to obtain the base motion at a depth of 60m. The obtained time history at the base level is shown in Figure 7 and its Fourier spectra is shown in Figure 8. It is evident from Figures 7 and 8 that the deconvolution resulted in decrease in the PGA value to 0.3 g as well as shift in the predominant frequency from 2 to 0.6 Hz. The deconvoluted accelerogram is used as input at the base level for further site specific ground response analysis.

Input Soil Data

The overall soil profile of 60 m thickness is divided into layers of 1.5 m thick is considered. Each layer is characterized by the unit weight of soil obtained from SPT data and shear wave velocity obtained from the seismic cross hole test data. A typical input soil data used in SHAKE analysis is presented in Figure 9. The water table is taken to be at a depth of 30 m below the ground level.

The nonlinear behavior of soil, reduction in stiffness and increase in the damping with increase in the shear strain, is accounted by selecting the standard modulus reduction and damping curves. In the present study, the standard modulus reduction and damping curves proposed by Sun et al (1988) are selected based on the soil characteristics and confining pressure which is depicted in Figure 10.

Figure 5. Input acceleration time history obtained from DSHA

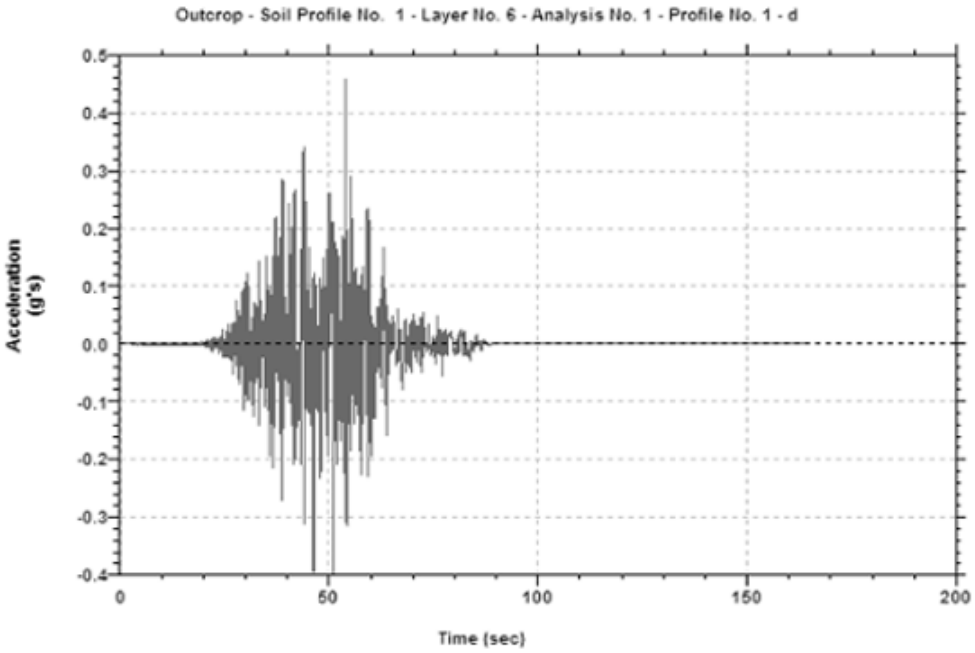

Figure 6. Fourier response spectrum for input acceleration time history

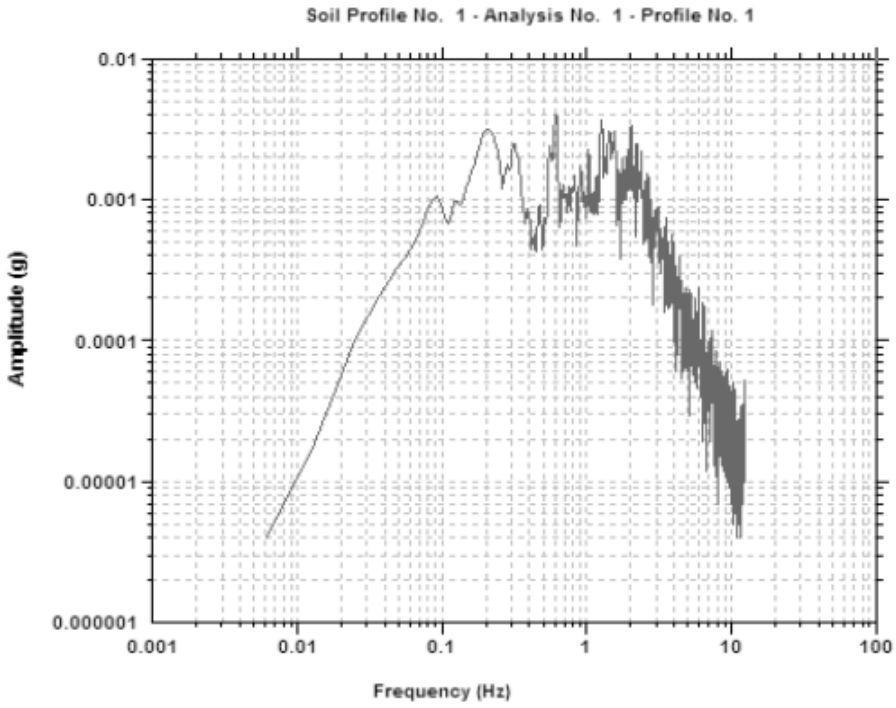

Figure 7. Acceleration time history at the base obtained from deconvolution analysis

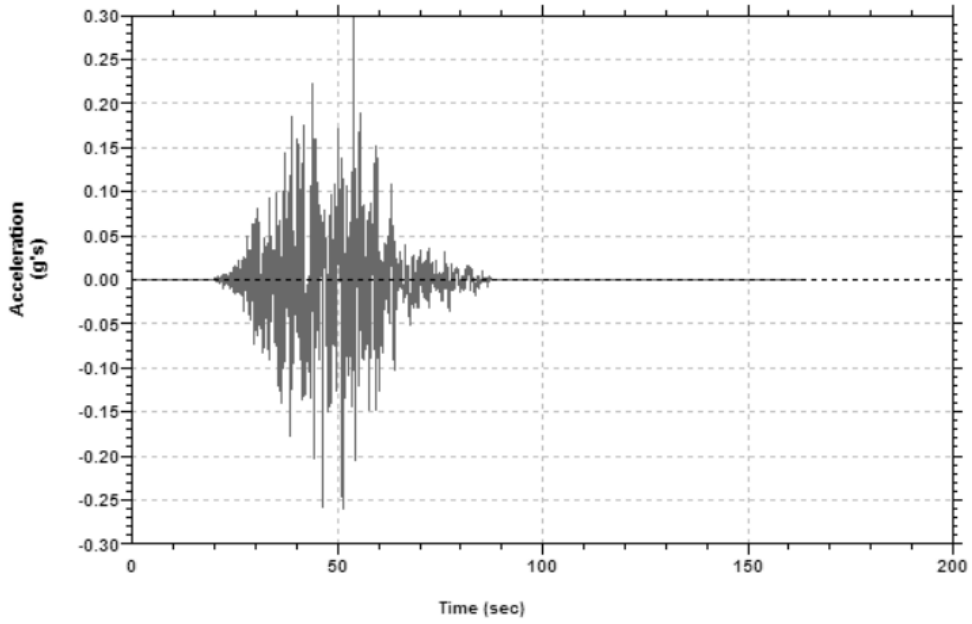

Figure 8. Fourier response spectrum for base motion obtained from deconvolution analysis

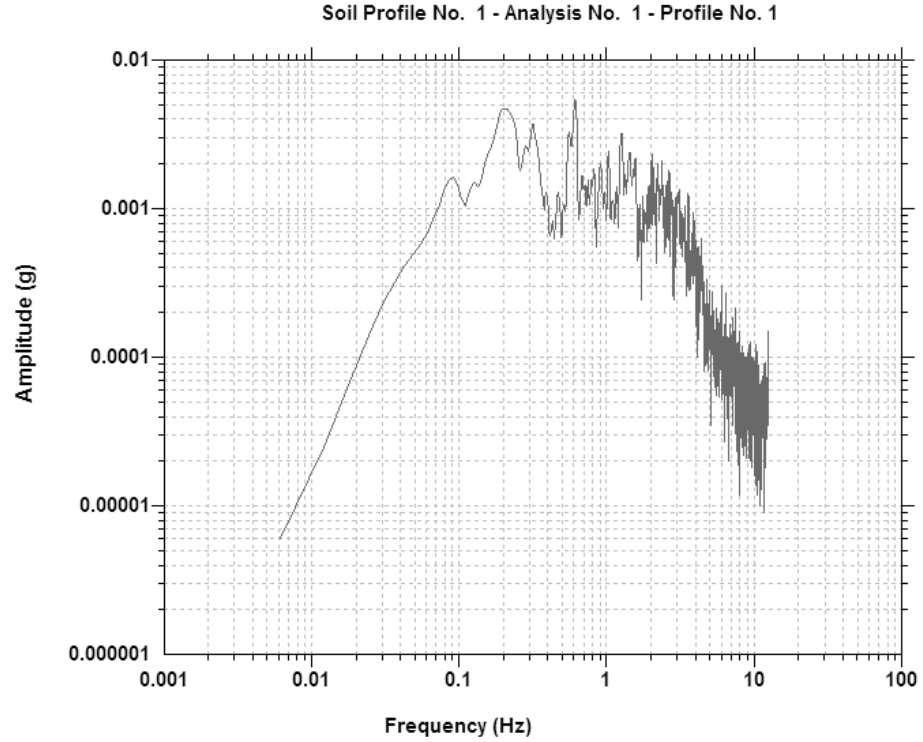

Figure 9. (a)Unit weight, Shear wave velocity and shear modulus variation with depth for typical soil profile for C class site (b)Unit weight, Shear wave velocity and shear modulus variation with depth for typical soil profile for B class site

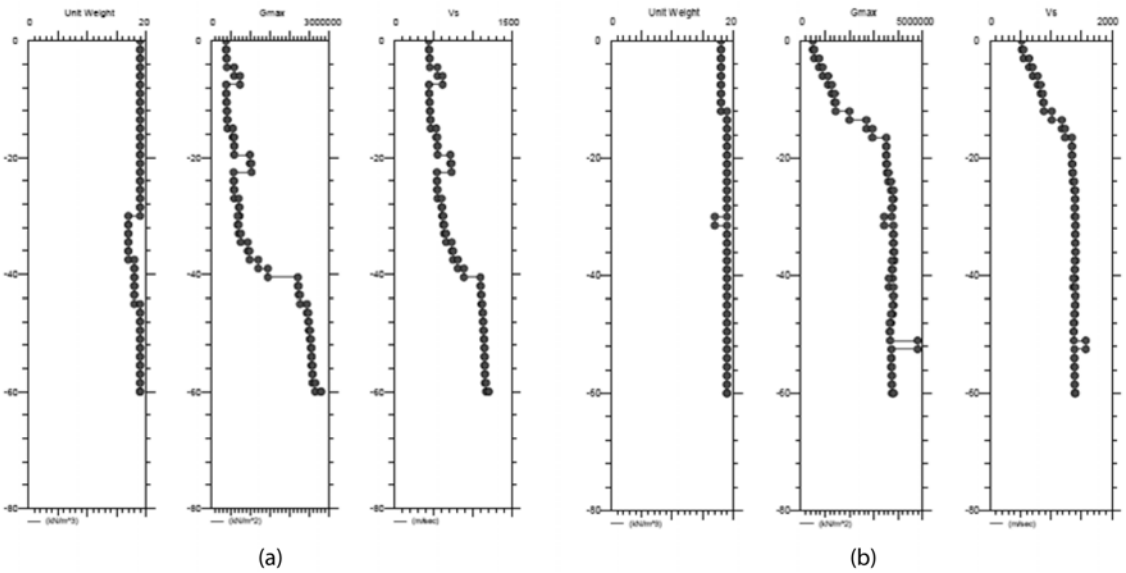

Design Ground Motion Parameters

History of Surface Acceleration

The surface acceleration time history obtained from the ground response analysis for two typical sites C class site and B class site are presented in Figures 11a and 11b respectively. It can be noticed from Figure 11 that the surface peak ground acceleration for C class and B class site is 0.53 g and 0.31g respectively. It is evident that the C class site amplifies the ground motion in comparison to the input ground motion with PGA of 0.3 g. However the B class site does not amplify the input motion due to the presence of a thick hard sandy clay deposits characterized by very high shear wave velocity.

Predominant frequency

The Fourier spectra for the surface motion obtained from the ground response analysis for site class C and B are presented in Figures 12a and 12b respectively. It is evident from the figures that the frequency content of surface motion is found to be distributed between 0.6 to 2.0 Hz for both class sites. However C class site exhibits a shift in the predominant frequency to the lower frequency of 1.7 Hz in comparison to the base motion frequency of 2.0 Hz, but the predominant frequency remains unaltered in B class site category.

Site Specific Response Spectra

The design response spectra i.e. the spectral acceleration versus the period of structure obtained from the surface time history of acceleration for 5, 10 and 20% damping for both class sites are presented in Figure 13. It can be observed from the figure that the peak spectral acceleration for 5% damping in C and B class sites are 2.6 g and 1.3 g respectively. However the peak spectral acceleration occurs practically at the same period of about 0.6 s for both site classes.

The design response spectrum is also obtained by the Ratio of Response Spectral (RRS) analysis

Figure 10. (a)Modulus reduction curve for ground response analysis (b)Damping curve for ground response analysis

(a)

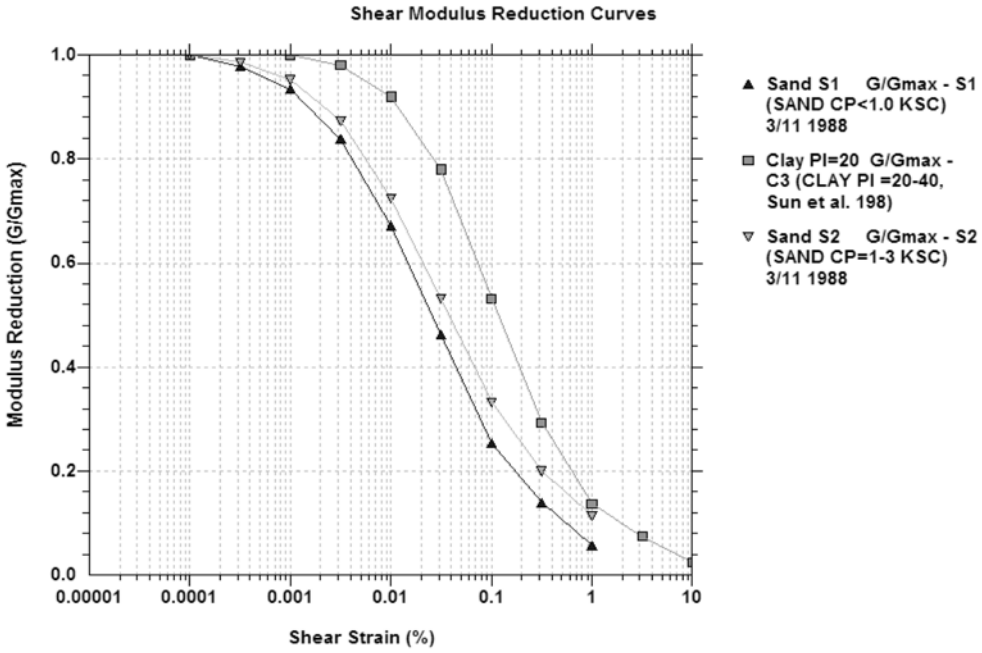

(b)

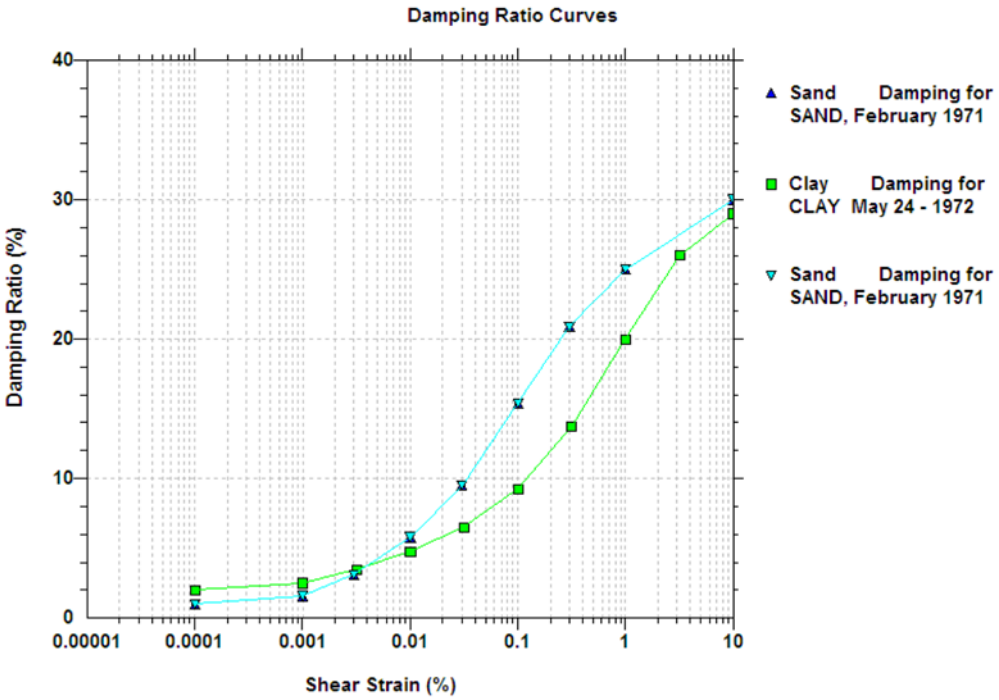

Figure 11. (a)Acceleration time history obtained at the surface for C class site (b)Acceleration time history obtained at the surface for B class site

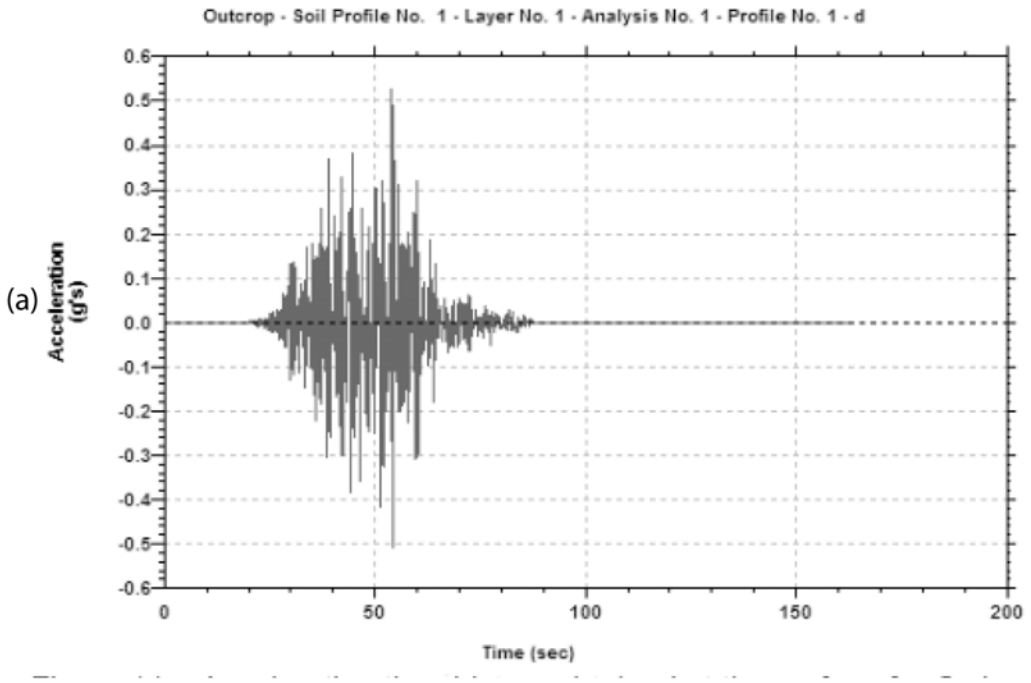

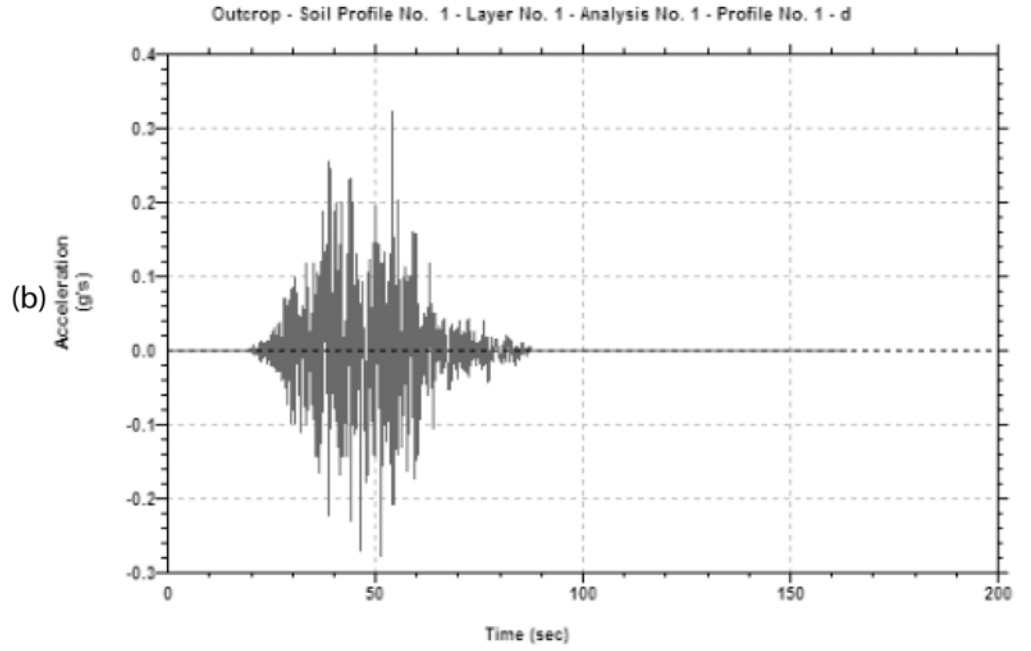

Figure 12. (a)Fourier spectrum for surface motion for C class site (b)Fourier spectrum for surface motion for B class site

(a)

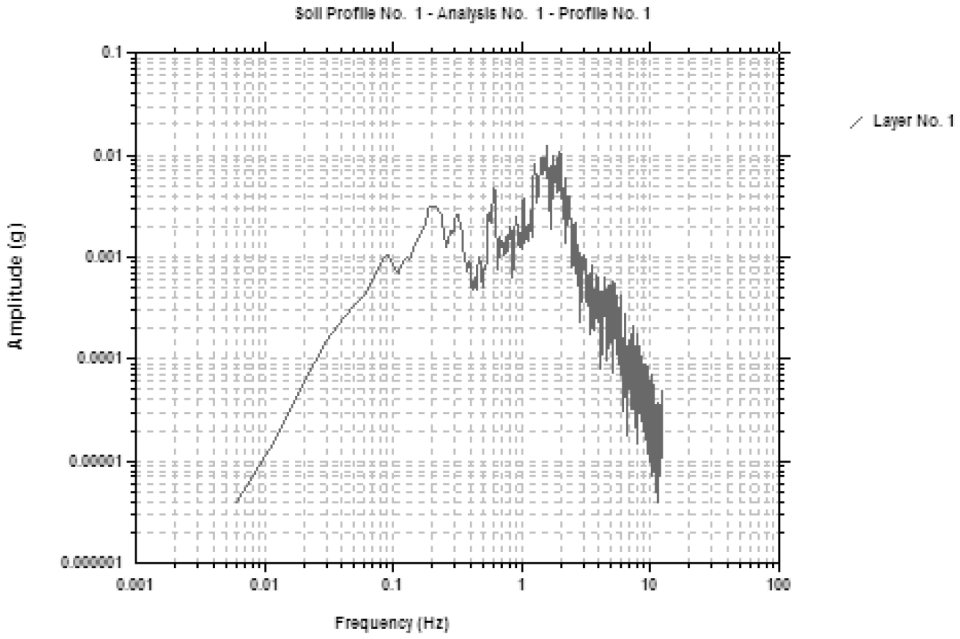

(b)

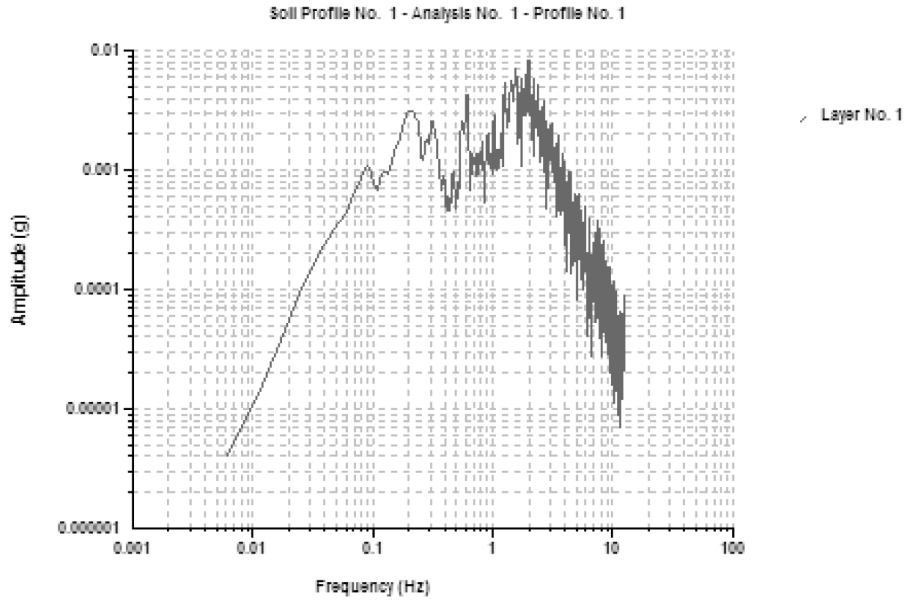

Figure 13. (a)Response spectrum at surface for C class site (b)Response spectrum at surface for B class site

(a)

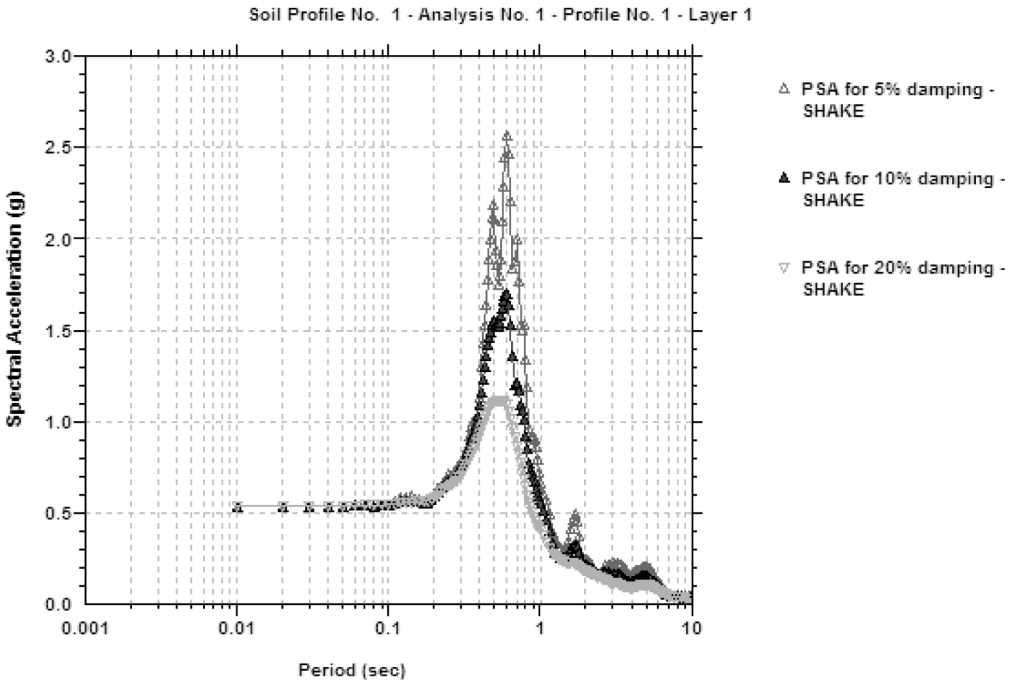

(b)

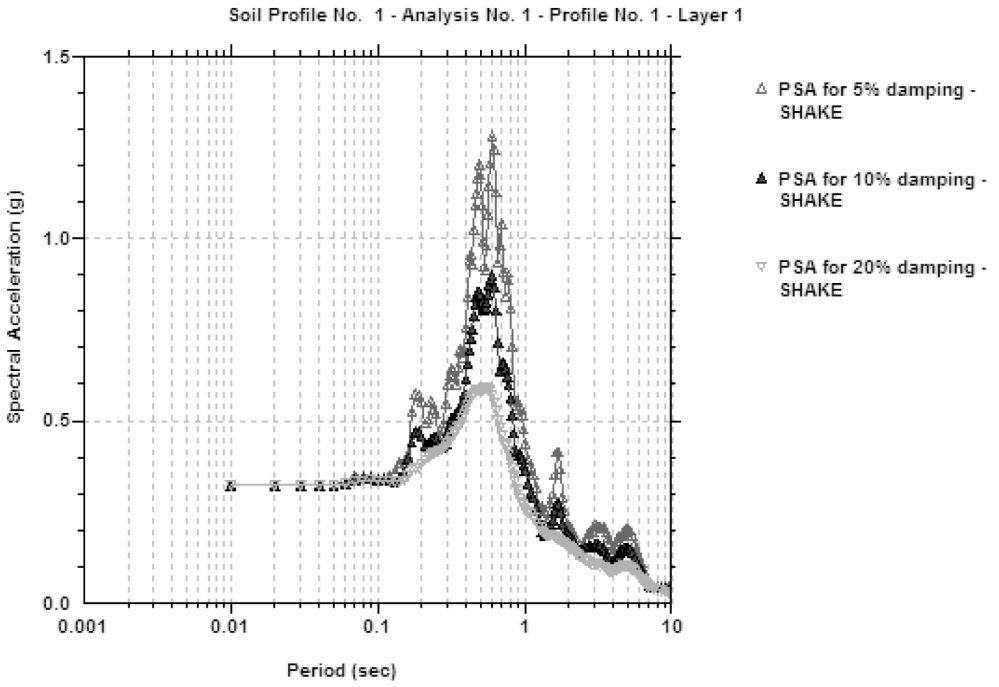

Figure 14. Ratio of Response Spectra (RRS) mean curves considering response spectra of all sites

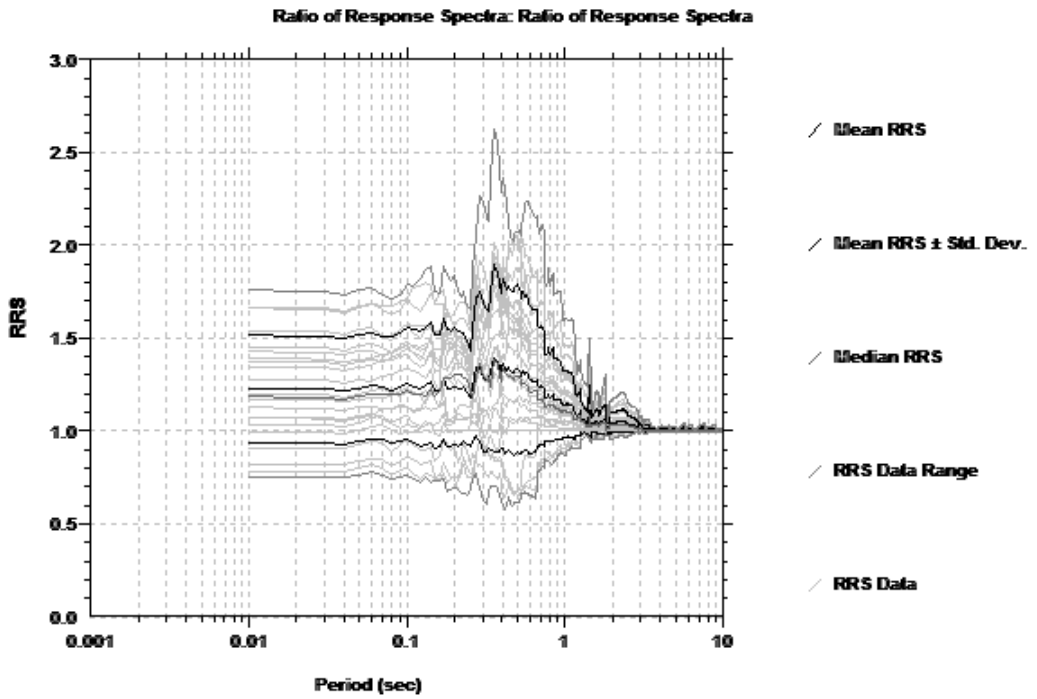

method. The RRS analysis involves obtaining the spectral acceleration for the surface and the base motion, then dividing the surface spectrum by the base spectrum for each period. In the present case the surface spectra obtained from the ground response analysis covering the entire site is utilized to obtain the Ratio of the Response Spectra (RRS) curves. The RRS curves obtained from the ground response analysis is shown in Figure 14. The mean and the median values of RRS curves are multiplied with the base spectrum to arrive the site specific spectra. The base spectrum in this case considered by the following two types:

1. The response spectra of the base motion obtained from the present study.
2. IS 1893-2002 design response spectra.

The site specific spectra arrived from the RRS analysis considering the response spectra of the base motion obtained from the present study is shown in Figure 15. It can be found from the figure that the maximum spectral acceleration is about 1.8 g at the range of period of 0.4 to 0.6 s.

The site specific spectra arrived from the RRS analysis considering the response spectra specified in IS 1893-2002, i.e., site specific spectra compatible to IS design spectra is shown in Figure 16. The IS design spectra for Type I soil is also shown in Figure 16. It can be noticed from the figure that the spectral ratio (Sa/g) at the short and mid period ranges up to about 0.6s is 20% higher than the IS spectral ratio values.

SUMMARY AND CONCLUSION

A Site specific evaluation of design ground motion parameters for a seismically vulnerable site located 12 km from Ahmedabad (Gujarat) was carried out involving both seismic hazard analysis and ground response analysis. The seismic hazard

Figure 15. Response spectrum compatible to the base ground motion obtained from the present study

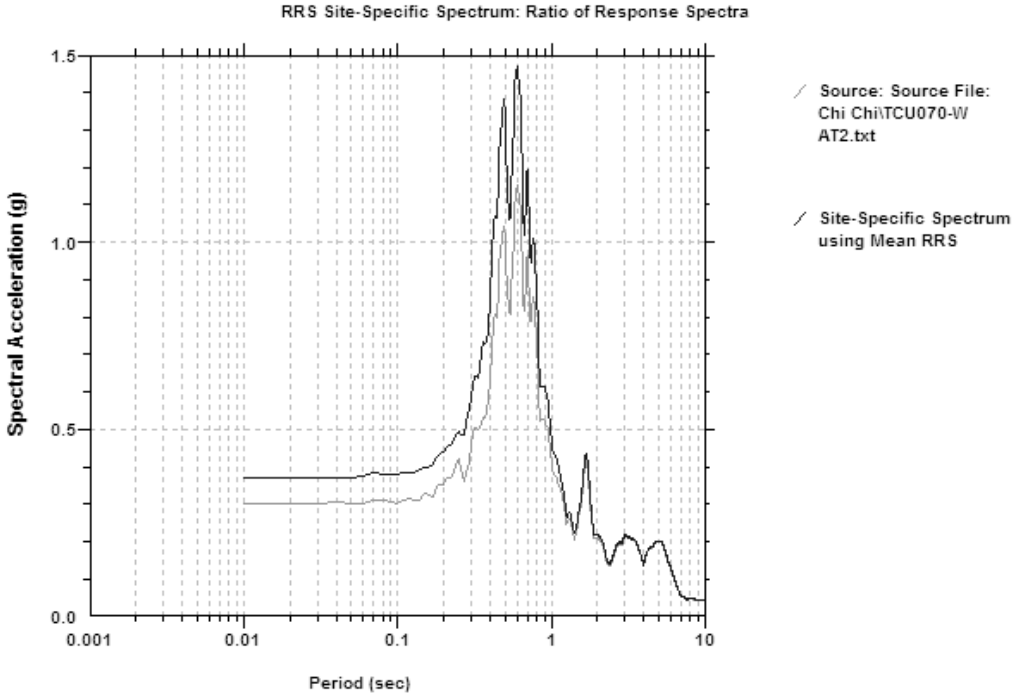

Figure 16. Normalized site specific response spectra compatible to IS 1893- 2002 design spectra

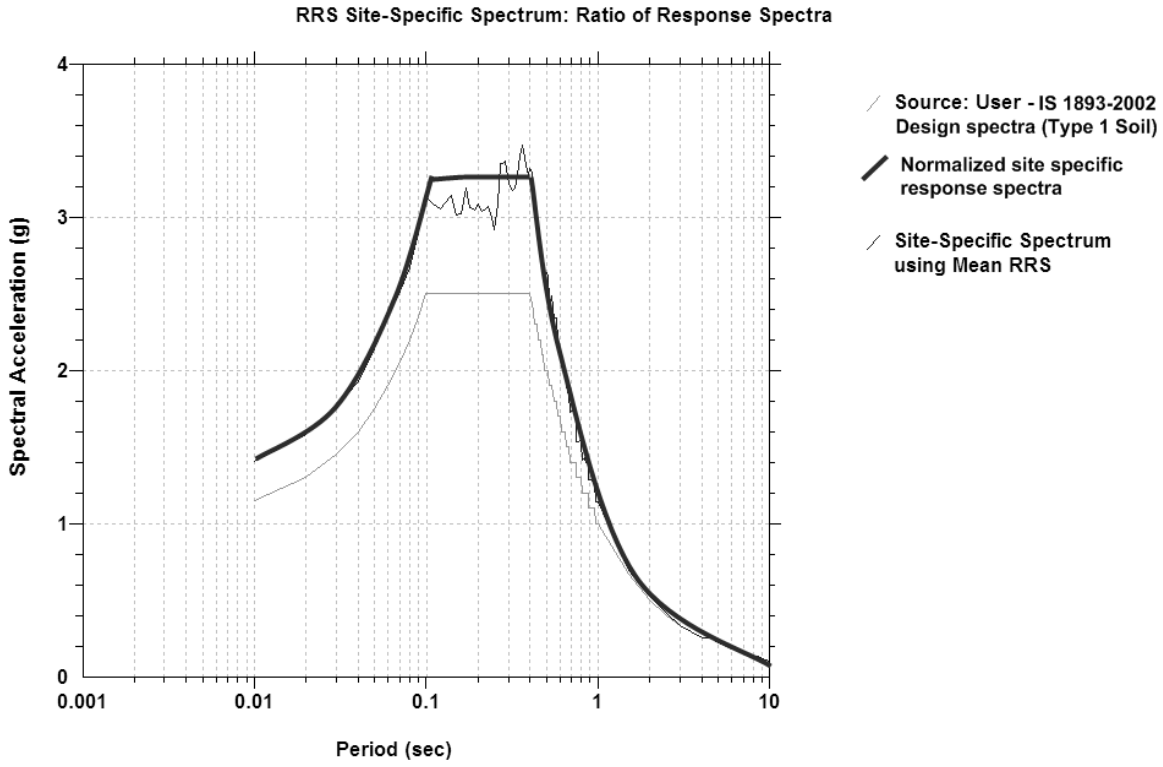

analysis was performed by DSHA approach considering the seismicity and seismotectonic details for 250 km radius from the site using Frankel et al., (1996) predictive relationship. It is found that the East Cambay fault with moment magnitude of 6.2 is the controlling source that causes surface PGA of 0.46 g at the site.

The acceleration time history at the surface for the site considered is obtained from the recorded ground motion data considering similar magnitude, distance and frequency content of the controlling earthquake. The 1999 Chi-Chi earthquake accelerogram is adopted and is scaled to the required PGA. Deconvolution analysis was performed to obtain the acceleration time history at base (60m depth).

Based on the extensive shear wave velocity measurement carried out at the site by cross hole test, most locations in the site are classified as C class except a few locations as B class as per NEHRP classification.

The site specific ground response analysis performed by equivalent linear approach shows amplification for C class site with PGA of 0.53 g, whereas B class site don't amplify the ground motion. The predominant frequency for C class site shifted from 2Hz to 1.7Hz whereas B class site did not alter the frequency content.

The site specific elastic design spectra was developed compatible to Indian standard IS 1893-2002 design spectra (Type 1 soil) by RRS analysis and it indicates that the spectral ratio (Sa/g) at the short and mid period ranges up to about 0.6s is 20% higher than the IS spectral ratio values.

It is evident from the present site specific study that the deep very stiff soil sites also can significantly amplify the ground motion and hence it is important to conduct site specific study even for stiff soil sites.

REFERENCES

ASTM standard D 4428-M (2007). *Standard test methods for seismic cross hole testing*. ASTM International, West Conshohocken, PA, 2003, DOI: 10.1520/D4428_D4428M-07.

Biswas, S. K. (1987). Regional tectonic framework, structure and evolution of western marginal basins of India. *Tectonophysics*, *135*, 305–327. doi:10.1016/0040-1951(87)90115-6

Boominathan, A. (2004). Seismic site characterization for nuclear structures and power plants. *Current Science*, *87*(10), 1388–1397.

Boominathan, A., Dodagoudar, G. R., Suganthi, A., & Uma Maheshwari, R. (2008). Seismic hazard assessment of Chennai city considering local site effects. *Journal of Earth System Science*, *117*(S2), 853–863. doi:10.1007/s12040-008-0072-4

Boore, D. M. (1983). Stochastic simulation of high-frequency ground motions based on seismological models of the radiated spectra. *Bulletin of the Seismological Society of America*, *237*(6), 68–78.

Borcherdt, R. D. (1994). Estimates of site-dependent response spectra for design (methodology and justification). *Earthquake Spectra*, *10*, 617–653. doi:10.1193/1.1585791

BSSC. (2001). BSSC, *NEHRP recommended provisions for seismic regulations for new buildings and other structures 2000 edition, part 1: Provisions*. Report no. FEMA 368, Building seismic safety council for the federal emergency management agency, Washington, D.C., USA (2001).

Campbell, K. W. (1981). Near source attenuation of peak horizontal acceleration. *Bulletin of the Seismological Society of America*, *71*, 2039–2070.

Carlos, S. O., Antoni, R., & Xavier, G. (2006). *Assessing and managing earthquake risk.* Springer.

Chang, F.K., & Krinitzsky, E.L. (1977). *Duration, spectral content and predominant period of strong motion earthquake records from Western United States.* Miscellaneous paper 5-73-1, U.S. Army Corps Engineers Waterways Experiment Station Vicksburg, Missipppi.

Cramer, C.H., & Wheeler, R.L. (2001). The 2001 Gujarat, India earthquake and seismic hazard in central and Eastern North America. *Abstract in Seismological Research Letters, 72*, 396.

Frankel, A., Mueller, C., Barnhard, T., Perkins, D., Leyendecker, E. V., & Dickman, N. (1996). National seismic hazard maps: documentation June 1996. *U.S. Geological Survey Open-file Report*, 96–532.

GSI. (2000). *Seismotechnic Atlas of India*. New Delhi: Geology Society of India.

Hanumantharao, C., & Ramana, G. V. (2008). Dynamic soil properties for microzonation of Delhi India. *Journal of Earth System Science*, *117*(S2), 719–730. doi:10.1007/s12040-008-0066-2

Hazarika, H., & Boominathan, A. (2009, June15-18). Liquefaction and ground failures during the 2001 Bhuj Earthquake India. In *Proceedings of International Conference on Performance-Based Design in Earthquake Geotechnical Engineering from case history to practice*, Tokyo, Japan, Chapter 13, (in CD ROM).

Hunt, R. E. (2005). *Geotechnical Investigation Handbook* (2nd ed.). Boca Raton, FL: Taylor & Francis.

Idriss, I. M., & Sun, J. I. (1992). *SHAKE91: A computer program for conducting equivalent linear seismic response analyses of horizontally layered soil deposits*. Center for Geotechnical Modeling, Department of Civil and Environmental Engineering, University of California, Davis, 130.

IS 1893 (Part 1). 2002 *Indian Standard Criteria for Earthquake Resistant Design of structures: Part 1 General Provisions and Buildings* (5th Revision).

Kaila, K. L., Krishna, V. G., & Mall, D. M. (1981). Crustal structure along Mehmedabad-Billimora profile in the Cambay basin, India, from deep seismic sounding. *Tectonophysics*, *76*, 99–130. doi:10.1016/0040-1951(81)90255-9

Kaila, K. L., Tewari, H. C., Krishna, V. G., Dixit, M. M., Sarkar, D., & Reddy, M. S. (1990). Deep seismic sounding studies in the north Cambay and Sanchor basins, India. *Geophysical Journal International*, *103*, 621–637. doi:10.1111/j.1365-246X.1990.tb05676.x

Kijko, A., & Graham, G. (1998). Parametric-historic procedure for probabilistic seismic hazard analysis, Part I: Estimation of maximum regional magnitude Mmax. *Pure and Applied Geophysics*, *152*, 413–442. doi:10.1007/s000240050161

Kramer, S. L. (1996). *Geotechnical Earthquake Engineering*. Prentice-Hall, Inc.

Kramer, S. L., & Stewart, J. P. (2004). *Geotechnical aspects of seismic hazards; In Earthquake Engineering from Engineering Seismology to Performance Based Engineering.* CRC press.

Krinitzsky, E. L. (2002). How to obtain earthquake ground motions for engineering design. *Engineering Geology*, *65*, 1–16. doi:10.1016/S0013-7952(01)00098-9

Krinitzsky, E. L. (2003). How to combine deterministic and probabilistic methods for assessing earthquake hazards. *Engineering Geology*, *70*, 157–163. doi:10.1016/S0013-7952(02)00269-7

Lew (2001). *The Seismic Design Handbook.* Kluwer academic publishers.

Nazarian, S., & Stokoe, K.H. (1983). *Use of spectral analysis of surface waves for determination of moduli and thicknesses of pavement systems*. Transportation Research Record No. 954.

Neelima Satyam, D., & Rao, K. S. (2009). Dynamic site characterization in Delhi region using MASW testing. *International Journal of Earth Sciences and Engineering*, *2*(1), 32–42.

Petersen, M. D., Rastogi, B. K., Schweig, E. S., Harmsen, S. C., & Gomberg, J. S. (2004). *Sensitivity analysis of seismic hazard for the northwestern portion of the state of Gujarat, India.*

Rastogi, B. K. (2001). Ground deformation study of Mw 7.7 Bhuj earthquake of 2001. *Episodes*, *24*, 160–165.

Reiter, L. (1990). *Earthquake hazard analysis – Issues and Insights*. New York: Columbia University Press.

Schnabel, P. M., Lysmer, J., & Seed, H. B. (1972). *SHAKE: A computer program for earthquake response analysis of horizontally layered sites*. Report No. EERC 72/12, Earthquake Engineering Research Centre, University of California, Berkley.

Seed, H. B., & Idriss, I. M. (1970). *Soil modules and damping factors for dynamic response analyses*. Report EERC 70–10, Earthquake Engineering Research Center, University of California, Berkeley.

SHAKE. 2000 (2000). *A computer program for conducting equivalent-linear seismic response analyses for horizontally layered soil deposits*. A modified PC version of the original SHAKE program published in 1972 by Schnabel, Lysmer and Seed (modifications made by Idriss IM, Sum JI). EERI, University of California, Berkley.

Sitharam, T.G., & GovindaRaju, L. (2004). Geotechnical aspects and ground response studies in Bhuj earthquake, India. *Geotechnical and Geological Engineering*, *22*, 439–455. doi:10.1023/B:GEGE.0000025045.90576.d3

Sitharam, T.G., & Anbazhagan, P. (2007). Seismic hazard analysis for Bangalore region. *Journal of natural hazards, 40*, 261-278.

Sokolov, Y. V., Loh, C. H., & Wen, K. L. (2001). Empirical models for site- and region-dependent ground motion parameters in the Taepei area: A unified approach. *Earthquake Spectra*, *17*(2), 313–332. doi:10.1193/1.1586177

Sun, J. I., Golesorkhi, R., & Seed, H. B. (1988). *Dynamic moduli and damping ratios for cohesive soils*. EERC 88-15, University of California, Berkeley.

Suto, K. (2007). Multichannel analysis of surface waves (MASW) for investigation of ground competence: an introduction in Engineering Advances in Earthworks. In *Proceedings of the Sydney Chapter 2007 Symposium* (pp. 71-81). Australian Geomechanics Society.

Tewari, H. C., Dixit, M. M., Sarkar, D., & Kaila, K. L. (1991). A crustal density model across Cambay basin, India and its relationship with the Aravallis. *Tectonophysics*, *194*, 123. doi:10.1016/0040-1951(91)90276-X

Uma Maheshwari, R., Boominathan, A., & Dodagoudar, G. R. (2008). Development of empirical correltation between shear wave velocity and standard penetration resistance in soils of Chennai. In *Proceedings of 14th World Conference on Earthquake Engineering*, Beijing, Paper No: 04-01-0090.

Wang, W. (1990). *Bounding surface hypoplasticity model for granular soils and its applications*. University of California, Davis.

This work was previously published in International Journal of Geotechnical Earthquake Engineering, Volume 1, Issue 1, edited by T.G. Sitharam, pp. 1-24, copyright 2010 by IGI Publishing (an imprint of IGI Global).

Chapter 3
Analysis of Passive Earth Pressure and Displacements of Retaining Walls Using Pseudo-Dynamic Approach

B. Munwar Basha
Indian Institute of Science, India

G. L. Sivakumar
BabuIndian Institute of Science, India

ABSTRACT

Using additional dynamic parameters in the pseudo-static method like shear wave and primary wave velocities of soil, phase change in the shear and primary waves, and soil amplification for seismic accelerations, one can benefit from another useful tool called pseudo-dynamic method to solve the problem of earth pressures. In this study, the pseudo-dynamic method is used to compute the seismic passive earth pressures on a rigid gravity retaining wall by considering both the planar failure and composite failure (log-spiral and planar) mechanisms. To validate the present formulation, passive earth pressure computed by the present method are compared with those given by other authors. Seismic passive earth pressure coefficients are provided in tabular form for different parameters. The sliding and rotational displacements are also computed and results of the comparative study showed that the assumption of planar failure mechanism for rough soil-wall interfaces significantly overestimates passive earth pressure and underestimate the sliding and rotational displacements.

DOI: 10.4018/978-1-4666-0915-0.ch003

INTRODUCTION

Gravity retaining walls are one of the most important structures which would suffer disastrous damages during earthquakes. Siddle et al. (2005) reported that during the October 23, 2004 Chuetsu earthquake, several residential developments constructed on reclaimed land in Nagaoka city, Niigata Prefecture, experienced damages to houses and roads due to seismically-induced failure of artificial fill slopes. Post-earthquake field reconnaissance surveys revealed that many fill slope failures were caused by the excessive seismic displacements of the gravity retaining walls supporting the fill material. Housner and Thiel (1995) indicated that excessive wall displacements are undesirable. Due to earthquakes, the permanent tilting of retaining wall can be either outward or inward, depending on the active or passive state of earth pressure that is dominant. In this article, the evaluation of inward movement of wall is discussed. Due to integral connection of wall with the superstructure, gravity walls attempt to move towards the backfill which compress the backfill and hence, it is of practical significance to assess the seismic passive earth pressure acting on the retaining walls and the associated displacements.

The calculation of passive earth pressure is very important as the permanent displacements of gravity walls (like base sliding and rotation) are governed by the passive earth pressure. In design practice, such wall needs to be proportioned to resist the earth loading for safety against base sliding and rotation in earthquakes. Design methods based on displacements are desirable for defining the comprehensive seismic performance and are required in the context of performance based design in earthquake geotechnical engineering. For gravity wall, typical failure modes during earthquakes are due to excessive deformation such as sliding and tilting. Therefore it is necessary to develop a seismic design approach of gravity walls considering earthquake forces, and control the damage within an acceptable extent.

The seismic effects are generally considered as pseudo-static forces to be added to the other static forces. A detailed review of the literature regarding the computation of passive earth pressure using planar failure, composite failure mechanism and experimental investigations are presented in the following sections. In addition, the review of the literature for the computation of earthquake-induced displacements is also presented.

Studies Pertaining to Static Passive Earth Pressures

In Coulomb's theory, it is assumed that the failure surface in the backfill is planar. However Terzaghi et al. (1996), Kumar and Subba Rao (1997) and Zhu and Qian (2000) indicated that the assumption of planar rupture surface seriously overestimates the passive pressures for higher wall friction angles. Terzaghi et al. (1996) reported that due to the influence of wall friction, the surface of the sliding in the backfill consists of a curved lower part and a straight upper part. They have also reported that for smooth walls, the rupture surface is planar and for values of the wall friction angle greater than one third of friction angle of the backfill, only curved rupture surfaces should be assumed in the analysis for the passive case.

Studies Pertaining to Pseudo-Static Passive Earth Pressures

The conventional method for the calculation of seismic passive earth pressure is the Mononobe and Okabe method (Kramer, 2003). Morrison and Ebeling (1995) reported that the Mononobe and Okabe equation assumes a planar failure surface, which is not the most critical mode of failure for determining the passive failure load. Soubra (2000), Kumar (2001), Soubra and Macuh (2002) and Subba Rao and Choudhury (2005) used

the pseudo static method along with the curved rupture surfaces for the computation of passive earth pressures. However, all these methods have the similar type of limitations as observed in Mononobe–Okabe method of analysis.

Studies Pertaining to Experimental Investigations

Duncan and Mokwa (2001) reported the experimental results and concluded that the logarithmic spiral earth pressure theory provides more accurate estimates of passive pressures for conditions where the interface friction angle is more than about 40% of the friction angle of the backfill. Fang et al. (2002) presented the results of experimental investigation on the passive earth pressure on retaining walls and concluded that for low wall friction angles, Coulomb and Terzaghi theories were found to be in good agreement with the experimental ultimate thrusts.

Studies Pertaining to Pseudo-Dynamic Methods

In the pseudo-static method, the dynamic nature of earthquake loading is considered in a very approximate way. The approach did not consider the actual dynamic effect with variation of time and propagation of shear and primary wave velocities through the medium. Steedman and Zeng (1990) computed the seismic active earth pressure coefficients by considering the phase difference due to finite shear wave propagation behind a retaining wall using a pseudo-dynamic method. Again Zeng and Steedman (1993) compared the theoretical results with centrifuge model test results to validate the pseudo-dynamic method. Further Choudhury and Nimbalkar (2005) studied the case of passive earth pressure behind a retaining wall by a pseudo-dynamic method considering horizontal and vertical seismic acceleration and finite shear and primary wave propagations using planar failure surface. Nimbalkar and Choudhury (2008) reported a study to obtain the values of the seismic earth pressures behind a rigid retaining wall by pseudo-dynamic approach by considering both the soil amplification and the effects of phase difference in body waves. Basha and Babu (2008) and Basha (2009) proposed an approach for computing seismic passive earth pressure coefficients using composite failure surface (log-spiral and planar) based on the pseudo-dynamic method.

Studies Pertaining to Estimation of Permanent Displacements

A rigid sliding block procedure was proposed by Newmark (1965) and his procedure is still the basis of most numerical techniques used to calculate earthquake-induced sliding displacements in practice. The seismic stability of gravity-type soil retaining walls situated on competent, flat ground was studied by Seed and Whitman (1970). The permanent displacement of the sliding mass may be calculated by integrating the relative velocity during slippage as a function of time (Franklin and Chang, 1977; Makdisi and Seed, 1978). A pioneering study on the seismic displacement of soil retaining walls was performed by Richards and Elms (1979) using a pseudo-static method. The importance of the amplification of the response of soil retaining walls was emphasized by Nadim and Whitman (1983) using a finite element method and performed calculations on the seismic displacement of the retaining wall.

Zeng and Steedman (2000) developed an analytical procedure to determine the sliding and rotational response of gravity walls subjected to pseudo-static loads considering wall under active condition. However, the study did not consider the influence of vertical seismic excitation.

Choudhury and Nimbalkar (2007) extended the work of Zeng and Steedman (2000) for the retaining wall under passive condition considering vertical seismic excitation and presented the results of rotational displacements of rigid retaining walls using planar failure mechanism. Basha

and Babu (2009) also presented a formulation for the calculation of sliding component of response of gravity retaining walls using pseudo-dynamic method considering the composite curved rupture surface for the design of gravity walls.

OBJECTIVES OF THE PRESENT STUDY

The review of the literature in the above sections indicates that the computation of magnitudes of passive earth pressure, sliding displacements and rotational displacements of gravity walls by considering the dynamic nature of earthquake loading using composite failure mechanism has received little attention. The primary objective of this research effort is to study the influence of the assumption of failure mechanisms (planar and composite) on the magnitudes of permanent sliding and rotational displacements for rough soil wall interfaces. The novelty of the present contribution lies in the minimization of nonlinear passive resistance by using improved Nelder-Mead simplex method. The critical failure surface has been located by estimating the subtended angle of logarithmic spiral and the angle of the rupture plane with the ground surface. The design values of the seismic passive earth pressures behind a rigid retaining wall are provided in the tabular and graphical forms. The following sections present the approach developed for the computation of permanent sliding and rotational displacements.

ASSESSMENT OF PASSIVE EARTH PRESSURE

Consider a rigid gravity retaining wall of height, H supporting horizontal cohesionless backfill and the developing failure surface can be represented by a logarithmic spiral and a straight line as shown in Figure 1 Logarithmic spiral portion of the failure surface (GJ) is governed by height of the retaining wall (H_1G) and the location of centre of the logarithmic spiral arc (A). The logarithmic spiral starts at the initial radius AG joins the conjugate failure surface of wedge MNJ. AJ lies on a final radius of the logarithmic spiral zone that passes through the center of the logarithmic spiral arc (A). As a result, the location of the center of the log-spiral curve (A) can be accurately defined based on the subtended angle ' θ_1 ' as shown in Figure 2. The usage of sinusoidal motions instead of full time-history earthquake records is justified in the study presented by Basha and Babu (2009). The authors reported that a few cycles of sinusoidal motions, which are likely to induce peak accelerations that are similar to those induced by earthquake records for a wide range of maximum accelerations and predominant frequencies, can be used in the analyses.

The formulation of pseudo-dynamic analysis, which considers a finite shear wave velocity, can be developed by assuming that the shear modulus G is constant with depth. The present analysis considers both shear wave velocity $v_s = \sqrt{G/\rho}$ and primary wave velocity, $v_p = \sqrt{\frac{G(2-2\nu)}{\rho(1-2\nu)}}$, where ρ and ν are the density and Poisson's ratio of soil medium. The analysis includes a period of lateral shaking (T), which can be expressed as $T = 2\pi/\omega$. For a sinusoidal base shaking subjected to linearly varied horizontal and vertical earthquake accelerations with amplitude of $\left(1+\frac{H-z}{H}(f-1)\right)k_h g$ and $\left(1+\frac{H-z}{H}(f-1)\right)k_v g$ respectively, where ' g ' is the acceleration due to gravity; the acceleration at any depth ' z ' below the ground surface and time ' t ' with soil amplification factor (f) can be expressed as:

Figure 1. Movement of gravity wall towards the backfill and composite curved rupture surface

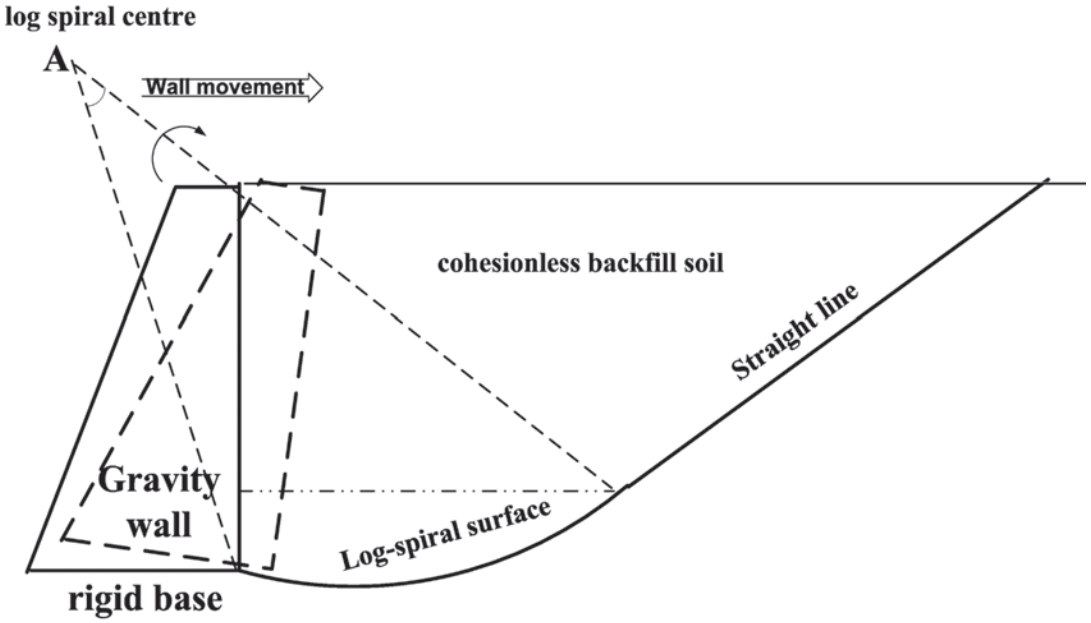

$$a_h(z,t) = \left(1 + \frac{H-z}{H}(f-1)\right) k_h g \sin\omega\left(t - \frac{H-z}{v_s}\right) \tag{1}$$

Figure 2. Geometry of the curved failure surface and phase change between the base and ground surface

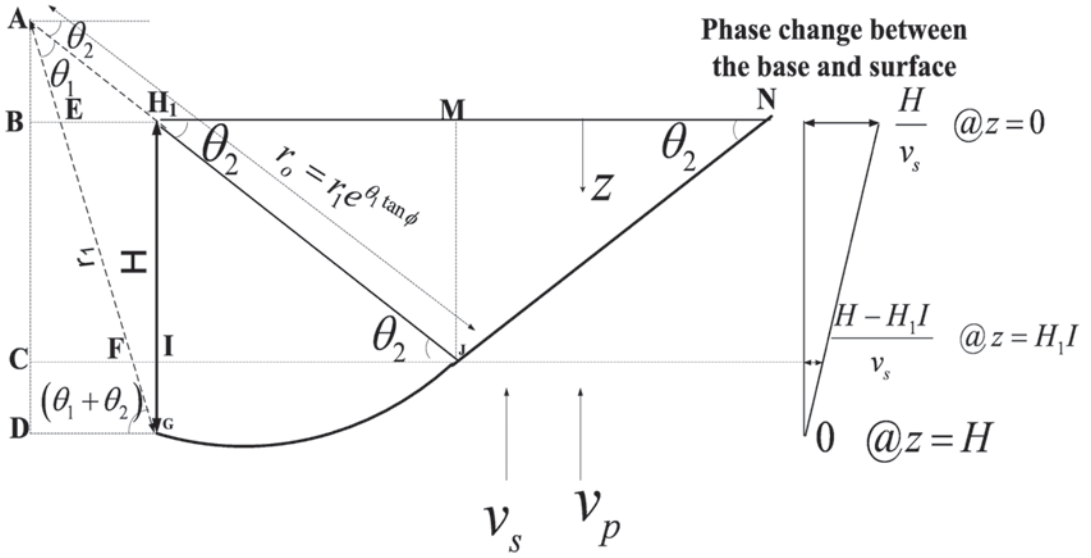

$$a_v(z,t) = \left(1 + \frac{H-z}{H}(f-1)\right) k_v g \sin\omega\left(t - \frac{H-z}{v_p}\right) \tag{2}$$

Inertial Forces Acting on H_1GJ and H_1NJ

Basha and Babu (2009) derived expressions for total horizontal and vertical inertial forces acting on the part of logarithmic spiral H_1GJ, which can be written as follows:

$$Q_{h\_H_1GJ} = Q_{h\_H_1IJ} + Q_{h\_IGJ} \tag{3}$$

The total vertical inertial force acting on H_1GJ is

$$Q_{v\_H_1GJ} = Q_{v\_H_1IJ} + Q_{v\_IGJ} \tag{4}$$

where $Q_{h\_H_1IJ}$, $Q_{v\_H_1IJ}$, Q_{h_IGJ} and Q_{v_IGJ} are horizontal and vertical inertial forces acting on H_1IJ and IGJ respectively. The horizontal inertial force acting on the wedge H_1IJ can be written as follows:

$$\frac{Q_{h\_H_1IJ}(t)}{0.5\gamma H^2} = 2k_h \cot\theta_2 \left\{ \begin{array}{l} f\left[\left(\frac{1}{2\pi}\frac{\lambda}{H}\right)^2 \{\sin 2\pi\xi_1 - \sin 2\pi\xi_2\} - \left(\frac{1}{2\pi}\frac{\lambda}{H}\right)(hi)\cos 2\pi\xi_1\right] \\ +(1-f)\left[-\left(\frac{1}{2\pi}\frac{\lambda}{H}\right)(hi)^2 \cos 2\pi\xi_1 + \left(\frac{1}{2\pi}\frac{\lambda}{H}\right)^2 2(hi)\sin 2\pi\xi_1\right] \\ \quad +2\left(\frac{1}{2\pi}\frac{\lambda}{H}\right)^3 (\cos 2\pi\xi_1 - \cos 2\pi\xi_2) \end{array} \right\} \tag{5}$$

where $\xi_1 = \left(\frac{t}{T} - \frac{H}{\lambda}(1-hi)\right)$, $\xi_2 = \left(\frac{t}{T} - \frac{H}{\lambda}\right)$, $H_1I = r_o \sin\theta_2 \left[1 - e^{-\theta_1 \tan\phi}\frac{\cos(\theta_1+\theta_2)}{\cos\theta_2}\right]$, , $H = \left(\frac{\sin\theta_1}{\cos\theta_2}\right) r_1$, r_1 = initial radius of the log-spiral wedge (AGJ), r_o = final radius of the log-spiral wedge (AGJ), θ_1 = subtended angle of log-spiral wedge (AGJ), H_1NJ = the angle of the failure plane (JN) with the horizontal ground surface, IGJ = unit weight of the backfill soil, H_1IJ = friction angle of the backfill soil, H_1NJ = time, H_1GJ = period of lateral shaking ($= 2\pi/\omega$), $\lambda = Tv_s$ is the wavelength of the vertically propagating shear wave and ω = angular frequency of the base shaking. The vertical inertial force acting on the wedge H_1IJ can be written as follows:

$$\frac{Q_{v\_H_1IJ}(t)}{0.5\gamma H^2} = 2k_v \cot\theta_2 \left\{ \begin{array}{l} f\left[\left(\frac{1}{2\pi}\frac{\eta}{H}\right)^2 \{\sin 2\pi\xi_3 - \sin 2\pi\xi_4\} - \left(\frac{1}{2\pi}\frac{\eta}{H}\right)(hi)\cos 2\pi\xi_3\right] \\ +(1-f)\left[-\left(\frac{1}{2\pi}\frac{\eta}{H}\right)(hi)^2 \cos 2\pi\xi_3 + \left(\frac{1}{2\pi}\frac{\eta}{H}\right)^2 2(hi)\sin 2\pi\xi_3\right] \\ \quad +2\left(\frac{1}{2\pi}\frac{\eta}{H}\right)^3 (\cos 2\pi\xi_3 - \cos 2\pi\xi_4) \end{array} \right\} \tag{6}$$

where $\xi_3 = \left(\frac{t}{T} - \frac{H}{\eta}(1-hi)\right)$, $\xi_4 = \left(\frac{t}{T} - \frac{H}{\eta}\right)$ and $\eta = Tv_p$ is the wavelength of the vertically propagating primary wave through the backfill.

The horizontal inertia force acing on wedge, IGJ is given by,

$$Q_{h\_IGJ}(t) = \int_{H_1I}^{GI} m(\theta_r)\, a_h(\theta_r, t)\, d\theta \tag{7}$$

The vertical inertia force acing on wedge, IGJ is given by

$$Q_{v\_IGJ}(t) = \int_{H_1I}^{GI} m(\theta_r)\, a_v(\theta_r, t)\, d\theta \tag{8}$$

where $a_h(\theta_r, t)$ is horizontal acceleration in the wedge IGJ, $a_v(\theta_r, t)$ is the vertical acceleration in the wedge IGJ, $m(\theta_r)$ is the mass of elemental strip in the wedge IGJ, θ_r = angle of the radial line of elemental strip with final radius of the log-spiral wedge. The horizontal inertial force acting on the wedge H_1NJ is given by,

Figure 3. Pseudo-dynamic forces acting on H_1GJ and H_1NJ

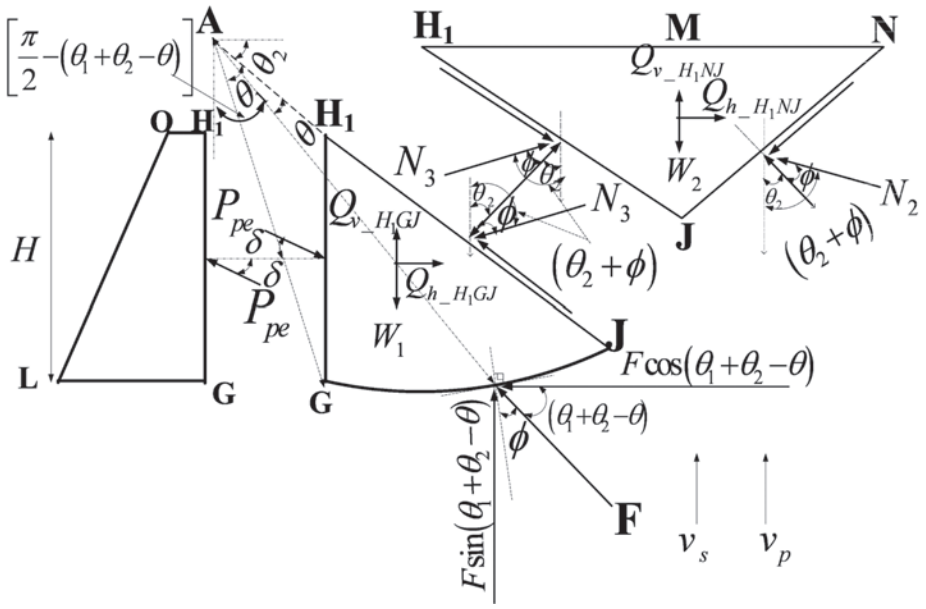

$$\frac{Q_{h\_H_1NJ}(t)}{0.5\gamma H^2} = 4k_h \tan\theta_2 \left\{ \begin{array}{l} \left(\frac{1}{2\pi}\frac{\lambda}{H}\right)^2 \left(\sin 2\pi\xi_2 - \sin 2\pi\xi_1\right) + \left(\frac{1}{2\pi}\frac{\lambda}{H}\right)(hi)\cos 2\pi\xi_2 \\ +(1-f)\left[-2hi\left(\frac{1}{2\pi}\frac{\lambda}{H}\right)^2 \sin 2\pi\xi_1 + 2\left(\frac{1}{2\pi}\frac{\lambda}{H}\right)^3 \left[\cos 2\pi\xi_2 - \cos 2\pi\xi_1\right]\right] \end{array} \right\} \tag{9}$$

The vertical inertial force acting on the wedge H_1NJ can be written as follows:

$$\frac{Q_{v\_H_1NJ}(t)}{0.5\gamma H^2} = 4k_v \tan\theta_2 \left\{ \begin{array}{l} \left(\frac{1}{2\pi}\frac{\eta}{H}\right)^2 \left(\sin 2\pi\xi_4 - \sin 2\pi\xi_3\right) + \left(\frac{1}{2\pi}\frac{\eta}{H}\right)(hi)\cos 2\pi\xi_4 \\ +(1-f)\left[-2hi\left(\frac{1}{2\pi}\frac{\eta}{H}\right)^2 \sin 2\pi\xi_3 + 2\left(\frac{1}{2\pi}\frac{\eta}{H}\right)^3 \left[\cos 2\pi\xi_4 - \cos 2\pi\xi_3\right]\right] \end{array} \right\} \tag{10}$$

The seismic passive earth pressure ($P_{pe}(t)$) can be obtained by resolving the forces on portions, H_1GJ and H_1NJ horizontally and vertically (Refer free body diagram shown in Figure 3), and considering the equilibrium of the forces and hence it can be expressed as follows:

$$P_{pe}(t) = \frac{\left\{ \begin{array}{l} \left[0.5\left(W_2 - Q_{v\_H_1NJ}\right)\tan(\theta_2+\phi) - 0.5Q_{h\_H_1NJ}\right]\left[\cot(\theta_2+\phi)\cot(\theta_1/2+\theta_2)+1\right] \\ +\left(W_1 - Q_{v\_H_1GJ}\right)\cot(\theta_1/2+\theta_2) - Q_{h\_H_1GJ} \end{array} \right\}}{\left[\cos\delta - \sin\delta\cot(\theta_1/2+\theta_2)\right]} \tag{11}$$

where W_1 = weight of the log-spiral portion ' H_1GJ ' and W_2 = weight of the triangular wedge, H_1NJ . The location of the critical failure surface to detect the minimum passive earth pressure (P_{pe}) can be determined using the following optimization routine.

$$\text{Find } \theta_1,\ \theta_2 \text{ and } \frac{t}{T} \text{ which } \left\{ \text{minimize } P_{pe} \text{ subjected to } \left\{ \begin{array}{l} 0^o < \theta_1 < 90^o \\ 0^o < \theta_2 < 90^o \\ t/T > 0 \end{array} \right. \right. \tag{12}$$

Seismic passive earth pressure coefficient (K_{pe}) can be computed as

$$K_{pe} = \frac{P_{pe}}{0.5\gamma H^2} \tag{13}$$

Figure 4 shows the details of the computation of subtended angle of logarithmic spiral (θ_1) and the angle of the rupture plane with the ground surface (θ_2), t/T ratio and seismic passive earth pressure coefficient (K_{pe}) for typical values of $\phi = 30^o$, $\delta = \phi/2$, $H/\lambda = 0.3$, $H/\eta = 0.16$,

Figure 4. Convergence of θ_1, θ_2 and t / T ratio in the optimization routine for $\phi = 30^o, \delta = \phi / 2$, $H / \lambda = 0.3$, $H / \eta = 0.16$, $k_h = 0.1$ and $k_v = k_h / 2$.

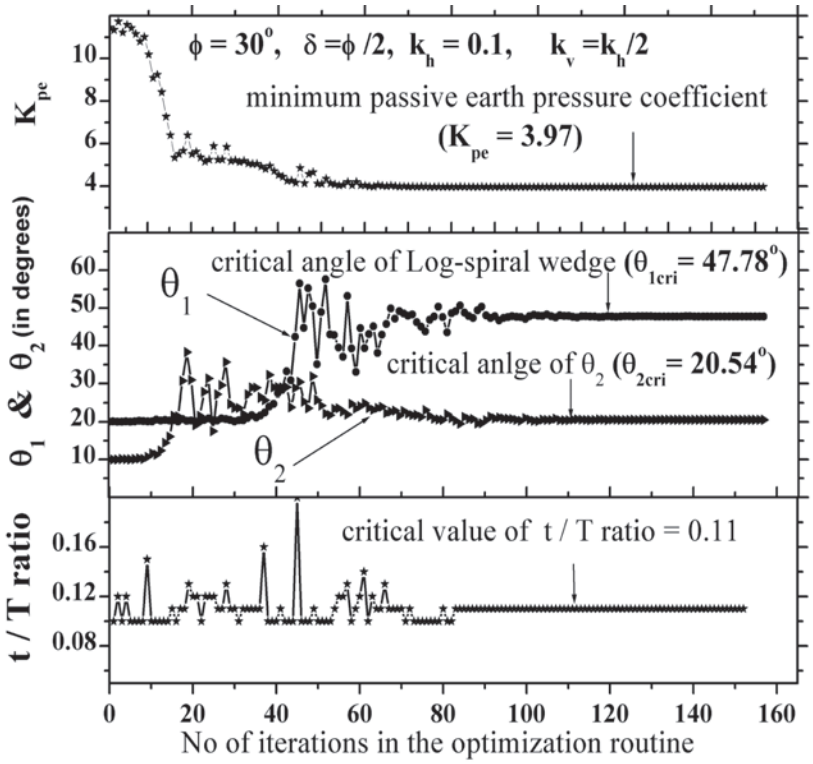

$k_h = 0.1$, $k_v = k_h / 2$ and for each iteration during the optimization. It can be noted from Figure 4 that after 100 iterations, K_{pe} converges to 3.97 for critical angles $\theta_{1cri} = 47.78^o$ and $\theta_{2cri} = 20.58^o$, and $t / T = 0.11$. In the following section, the results of the study are compared with the studies in literature and the influence of various parameters on the seismic stability of gravity walls is discussed.

Determination of Point of Application of Seismic Passive Earth Pressure

Choudhury and Nimbalkar (2005) computed the seismic passive earth pressure distribution using pseudo-dynamic approach. The total seismic passive earth pressure (P_{pe}) can be defined as

$$P_{pe} = P_p + P_{pd} \tag{14}$$

P_p = pressure acting on the retaining wall due to vertical weight of the failure portion ' H_1GN ' can be written as $0.5\gamma H^2 K_p$ and P_{pd} = pressure acting on the wall due to horizontal and vertical inertia of the failure portion ' H_1GN '.

Seismic passive earth pressure distribution can be obtained by differentiating the total passive earth pressure with respect to the depth of the wall is given by,

$$p_{pe}(t) = \frac{\partial P_{pe}(t)}{\partial z} = p_p + p_{pd} \tag{15}$$

The point of application of $P_{pe}(h)$ can be computed by estimating the point of application

of $P_{pd}(H_d)$ above the base by taking moments about the base of the wall as shown below:

$$H_d = \frac{M_d(z=H)}{P_{pd}\cos\delta} = \int_0^H \frac{p_{pd}\cos\delta(H-z)}{P_{pd}\cos\delta} \qquad (16)$$

ESTIMATION OF SLIDING DISPLACEMENTS

A rigid gravity wall is considered as resting on a rigid-perfectly plastic interface as shown in Figure 5. When the wall base is subjected to earthquake shaking, horizontal and vertical inertial forces influence both the driving and resisting forces, leading to potential situations in which the driving forces at least temporarily exceed the resisting forces. Such situations will lead to relative motion between the block and the plane. In this study, the term 'critical state' means the state at which the sliding starts to occur and the acceleration corresponding to this state is the critical acceleration. When the wall is subjected to accelerations greater than the critical acceleration, the wall will move relative to the base. The critical acceleration to be used in the computation is evaluated as the value to yield a dynamic safety factor equal to unity against base sliding failure. Dynamic factor of safety against sliding (FSS_{dyn}) is given by,

$$FSS_{dyn} = \frac{\text{Resisting force } (\mathrm{F_b})}{\text{driving force } (\mathrm{F_d})} \qquad (17)$$

The following equation represents the resisting force (F_b) as shown in Figure 5

$$F_b = N_b \tan\phi_b = \left[W_\omega - P_{pe}\sin\delta - Q_{vw\_H_1GLO}(t)\right]\tan\phi_b \qquad (18)$$

Figure 5. Sliding of gravity retaining wall towards the backfill.

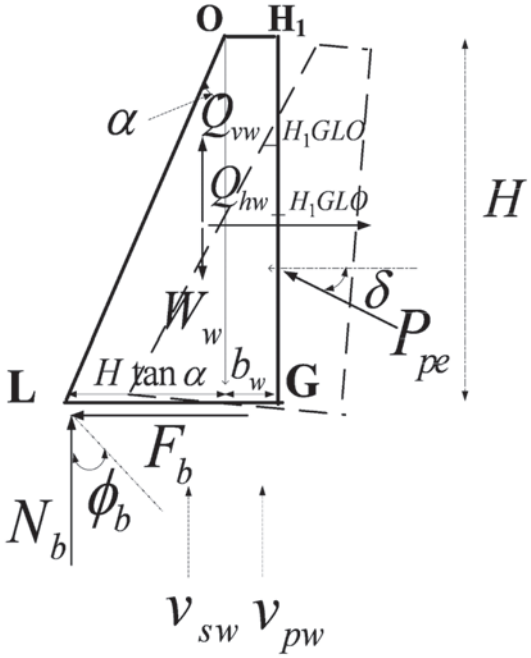

where $N_b = W_w - P_{pe}\sin\delta - Q_{vw\_H_1GLO}(t)$ is the normal force at the base and W_w is the weight of the wall can be written as

$$W_w = \frac{1}{2}\gamma_w H\left[2b_w + H\tan\alpha\right] \tag{19}$$

the driving force is given by

$$F_d = Q_{hw\_H_1GLO}(t) - P_{pe}\cos\delta \tag{20}$$

the term FSS_{dyn} can be written as

$$FSS_{dyn} = \frac{\left[W_\omega - P_{pe}\sin\delta - Q_{vw\_H_1GLO}(t)\right]\tan\phi_b}{Q_{hw\_H_1GLO}(t) - P_{pe}\cos\delta} \tag{21}$$

By considering the horizontal force equilibrium of wall, we can write the following equation.

$$\left[W_\omega - P_{pe}\sin\delta - Q_{vw\_H_1GLO}(t)\right]\tan\phi_b + P_{pe}\cos\delta = Q_{hw\_H_1GLO}(t) \tag{22}$$

where ϕ_b is the interface friction angle between the wall base and foundation. Refer to appendix for the expressions of inertial forces acting on the wall, $Q_{hw\_H_1GLO}(t)$ and $Q_{vw\_H_1GLO}(t)$ (Basha and Babu, 2009). Critical seismic acceleration coefficient for sliding (k_{cs}) can be found by rearranging the above Eq. (22) as follows:

$$k_{cs} = \frac{P_{pe}\cos\delta + \left[W_w - P_{pe}\sin\delta\right]\tan\phi_b}{\left[\dfrac{Q_{hw\_H_1GLO}(t)}{k_h} + \dfrac{Q_{vw\_H_1GLO}(t)}{k_h}\tan\phi_b\right]} \tag{23}$$

Using Newmark's sliding block approach, for a given harmonic ground acceleration time history and a known value of k_{cs}, the sliding displacement (S) can be calculated by double integrating the relative acceleration $(k_h - k_{cs})g$ of the block as follows:

$$S = \int_0^t\int_0^t (k_h - k_{cs})\, g\ dt \tag{24}$$

ESTIMATION OF ROTATIONAL DISPLACEMENTS

In order to perform the double integration of the acceleration history, it is necessary to know the limiting acceleration value for which the factor of safety drops below one. In this section, the equations of motion for rotation are presented to calculate the tilting displacements as explained in the following sections. The coordinates of the centre of gravity of the wall with respect to the heel point 'G' (x_c, y_c) are shown in Figure 6. For the stability against rotation about the heel point, the resisting moment around the heel point ('G') due to available passive resistance and weight of gravity wall should be more than the disturbing moment around the heel point ('G') due to horizontal and vertical seismic inertial forces. Dynamic factor of safety against rotation (FSR_{dyn}) is given by,

$$FSR_{dyn} = \frac{\text{Resisting moment } (\mathrm{M_r})}{\text{Disturbing moment } (\mathrm{M_d})} \tag{25}$$

The following equation represents the resisting moment about the point 'G' as shown in Figure 6.

$$M_r = \left[W_w - Q_{vw\_H_1GLO}(t)\right]x_c \tag{26}$$

the disturbing moment about the point 'G' as shown in Figure 6 is given by

$$M_d = Q_{hw\_H_1GLO}(t)\, y_c - \left(P_{pe}\cos\delta\right)h \tag{27}$$

the dynamic factor of safety against rotation (FSR_{dyn}) can be written as,

$$FSR_{dyn} = \frac{\left[W_w - Q_{vw\_H_1GLO}(t)\right]x_c}{\left[Q_{hw\_H_1GLO}(t)\,y_c - \left(P_{pe}\cos\delta\right)h\right]} \qquad (28)$$

The following equation represents the moment equilibrium about point 'G'

$$Q_{hw\_H_1GLO}(t)\,y_c - \left(P_{pe}\cos\delta\right)h = \left[W_w - Q_{vw\_H_1GLO}(t)\right]x_c \qquad (29)$$

Again, from Eq. (28) sum of moments about point 'G' can be written as,

$$\sum M_O = Q_{hw\_H_1GLO}(t)\,y_c - \left(P_{pe}\cos\delta\right)h - \left[W_w - Q_{vw\_H_1GLO}(t)\right]x_c \qquad (30)$$

The equation of motion about the point 'G' can be expressed as follows:

$$\sum M_o = y_c\frac{W_w}{g}a_c(x) + x_c\frac{W_w}{g}a_c(y) + I_c\Omega \qquad (31)$$

where M_o = moment about heel point 'G', $a_c(x)$ = acceleration of the centroid in x-direction, $a_c(y)$ = acceleration of the centroid in y-direction, g = acceleration due to gravity, I_c = polar moment of inertia of the wall about the centroid. Ω = angular acceleration. The acceleration at the centroid of the wall can be expresses as follows:

$$a_c = -a_g + \Omega r_c - \Psi^2 r_c \qquad (32)$$

where a_g = ground acceleration, r_c = radial distance between the heel and centroid of wall and Ψ = angular velocity. The horizontal and vertical seismic accelerations at the centroid (a_c) are

$$a_c(x) = -a_g + \Omega y_c + \Psi^2 x_c \qquad (33)$$

$$a_c(y) = \Omega x_c - \Psi^2 y_c \qquad (34)$$

Figure 6. Forces and accelerations on gravity wall with rotation during base shaking.

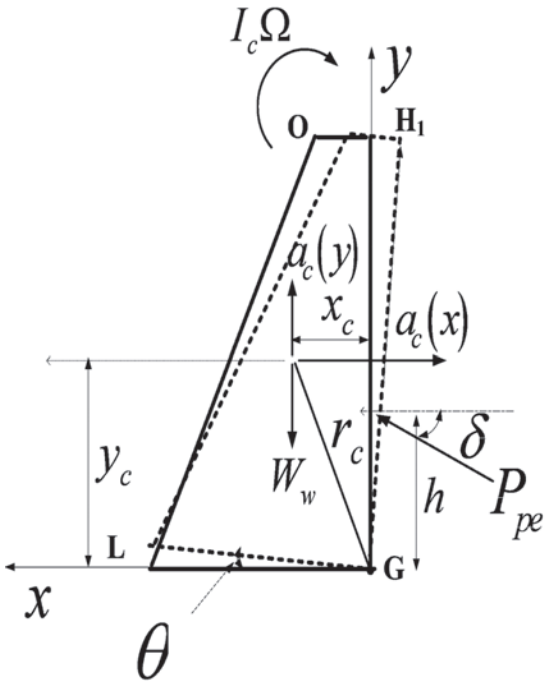

Substituting the above equations for $a_c(x)$ and $a_c(y)$ into Eq. (31), we get

$$\sum M_o = \frac{W_w}{g} r_c^2 \Omega - \frac{W_w}{g} a_g y_c + I_c \Omega \tag{35}$$

Equating (30) and (35), and after some simplification, the final equation for Ω can be obtained as follows:

$$\Omega = \frac{\left[Q_{vw\_H_1GLO}(t)x_c + Q_{hw\_H_1GLO}(t)y_c - (P_{pe}\cos\delta)h - W_w x_c + W_w y_c k_h\right]}{\left[I_c + (W_w / g) r_c^2\right]} \tag{36}$$

Rotational displacement of the wall is expected to take place only when angular acceleration (Ω) exceeds the threshold acceleration for rotation (k_{cr}). Once rotation commences, it is assumed to continue at a constant acceleration equal to k_{cr} until the relative velocity between the rotating mass and base become zero.

Angular velocity (Ψ) can be expressed as

$$\Psi = \int_o^t \Omega \; dt \tag{37}$$

rotational displacement (θ) is calculated by

$$\theta = \int_o^t \Psi \; dt \tag{38}$$

The total rotational displacement is the summation of individual rotations during the entire earthquake motion.

RESULTS AND DISCUSSION

Range of Parameters Considered for the Present Study

The range of parameters for presenting the results are as follows: ϕ = 20 - 45°, δ / ϕ = 0.0 - 1.0, k_h = 0.0 to 0.6, k_v / k_h = 0.0 – 1.0, f = 1.0 - 2.0, $b = b_w / H = 0.2$, α = 15°, duration of earthquake, t = 0.5 sec and period of sinusoidal acceleration, T = 0.3 sec. The phase change, H / λ and H / η are dimensionless parameters a typical value of H / λ = 0.3 is chosen for the analysis. The ratio of v_p / v_s is 1.87 (Kramer, 2003). Therefore a magnitude of H / η = 0.16 satisfies this relationship. Typical values of H / φ = 0.012 and H / κ = 0.0077 are chosen in the present study. The influence of various parameters on the critical failure surface, seismic passive earth pressure and sliding and rotational displacement is discussed in the following sections.

Influence of ϕ and δ on Critical Failure Surface

Table 1 shows the effect of soil friction angle (ϕ) and soil-wall interface friction angle (δ) on critical failure surface which is governed by the critical angles of logarithmic spiral (θ_{1cri}), the rupture plane with the ground surface (θ_{2cri}) and t / T ratio for typical values of k_h = 0.1, k_v = 0.05, H / λ = 0.3, H / η = 0.16 and f = 1.0. It can be found from Table 1 that for constant ratio of δ / ϕ, as the friction angle (ϕ) increases from 20 – 45°, the magnitudes of θ_{1cri}, θ_{2cri} and t / T ratio decreases significantly and consequently the magnitude of seismic passive earth pressure coefficient (K_{pe}) increases considerably. This is because as the magnitude of ϕ increases, the rupture plane also becomes flatter and hence the critical failure surface extends laterally away from the backfill. In addition, the values of θ_{1cri}, θ_{2cri}, t / T ratio and K_{pe} show significant increase with increase in δ / ϕ ratio from 0.0 – 1.0. This behavior is attributed to increased shear resistance at the interface between the soil and wall.

Table 1. The angles of critical failure surface (θ_{1cri} and θ_{2cri}), time ratio (t / T) and minimum value of K_{pe} for $k_h = 0.1$ and $k_v / k_h = 0.5$

θ_{1cri}, θ_{2cri}, t / T ratio and K_{pe} for $k_h = 0.1$ and $k_v / k_h = 0.5$												
$\frac{\delta}{\phi}$	$\phi = 20^o$				$\phi = 25^o$				$\phi = 30^o$			
	θ_{1cri} (in °)	θ_{2cri} (in °)	$\frac{t}{T}$	K_{pe}	θ_{1cri} (in °)	θ_{2cri} (in °)	$\frac{t}{T}$	K_{pe}	θ_{1cri} (in °)	θ_{2cri} (in °)	$\frac{t}{T}$	K_{pe}
0.0	43.57	16.90	0.45	1.80	41.14	15.69	0.25	2.21	38.14	14.47	0.15	2.60
0.2	46.30	18.84	0.56	1.88	44.81	17.96	0.36	2.38	42.84	17.07	0.26	3.06
0.4	48.25	20.53	1.10	2.06	47.48	19.95	0.90	2.70	46.41	19.35	0.80	3.62
0.6	49.61	22.23	1.80	2.27	49.31	22.04	1.60	3.09	52.81	19.12	1.50	3.75
0.8	50.47	24.13	1.90	2.52	54.27	24.63	1.70	3.34	53.05	22.91	1.60	4.62
1.0	55.18	26.93	2.90	2.31	57.71	25.18	2.70	3.63	53.07	26.92	2.60	5.82
	$\phi = 35^o$				$\phi = 40^o$				$\phi = 45^o$			
0.0	34.70	13.29	0.10	3.34	30.93	12.19	0.10	4.12	26.92	11.20	0.10	5.32
0.2	40.44	16.18	0.21	4.02	37.71	15.33	0.11	5.42	34.78	14.52	0.10	7.58
0.4	45.07	18.75	0.76	5.03	43.54	18.16	0.66	7.31	42.00	17.57	0.56	11.24
0.6	51.13	19.83	1.46	5.68	47.99	21.42	1.36	10.21	49.67	20.07	1.26	16.07
0.8	52.53	23.77	1.56	7.55	52.87	24.25	1.46	13.47	-	-	-	-
1.0	53.38	28.23	2.55	10.39	-	-	-	-	-	-	-	-

Planar Failure Mechanism versus Composite Failure Mechanism

Table 2 shows a comparison of K_{pe} values obtained using composite failure surface and the values obtained by employing the Coulomb planar failure surface for $k_h = 0.0$, $k_v = 0.0$, $\phi = 20\text{-}45^o$ and $\delta / \phi = 0.0 - 1.0$.

It can be noted from Table 2 that the values of K_{pe} predicted by employing the composite failure mechanism are lower than the planar failure mechanism reported in Kramer (2003) for the case of $\delta \geq 0.4\phi$; and the difference increases for higher values of δ / ϕ. Similar observations can also found in the results presented in Tables 3, 4 and 5. As the value of δ approaches ϕ, the error in the value of K_p computed with the assumption of planar failure surface becomes very large. It can be concluded that the present pseudo-dynamic method considering composite failure mechanism gives the minimum seismic passive resistance than the assumption of planar failure mechanism that is the best estimate for the design of gravity walls under passive conditions. Similar to the observation of previous investigators, it confirms that, the planar failure surface is not the appropriate failure mechanism to predict passive resistance

Table 2. Passive earth pressure coefficients (K_{pe}) for $k_h = 0.0$, $k_v / k_h = 0.0$, $\delta / \phi = 0.0 - 1.0$ and $\phi = 20^o - 45^o$.

K_{pe} for $k_h = 0.0$ and $k_v / k_h = 0.0$												
$\frac{\delta}{\phi}$	$\phi = 20^o$		$\phi = 25^o$		$\phi = 30^o$		$\phi = 35^o$		$\phi = 40^o$		$\phi = 45^o$	
	Coulomb	Composite failure	Coulomb	Composite failure	Coulomb	Composite failure	Coulomb	Composite failure	Coulomb	Composite failure	Coulomb	Composite failure
0.0	2.04	2.04	2.46	2.46	3.00	3.00	3.69	3.69	4.64	4.64	5.83	5.83
0.1	2.14	2.10	2.64	2.58	3.29	3.22	4.16	4.08	5.37	5.29	7.11	7.04
0.2	2.26	2.19	2.83	2.73	3.62	3.48	4.73	4.53	6.35	6.06	8.87	8.41
0.3	2.37	2.28	3.05	2.90	4.00	3.77	5.42	5.04	7.63	6.99	11.38	10.14
0.4	2.50	2.38	3.29	3.09	4.45	4.10	6.27	5.64	9.36	8.11	15.18	12.36
0.5	2.64	2.49	3.55	3.29	4.98	4.48	7.36	6.35	11.77	9.50	21.38	15.27
0.6	2.78	2.61	3.86	3.51	5.61	4.90	8.77	7.18	15.32	11.22	32.59	19.15
0.7	2.94	2.74	4.20	3.76	6.38	5.39	10.66	8.18	20.88	13.40	56.36	24.40
0.8	3.12	2.87	4.60	4.03	7.33	5.95	13.28	9.38	30.36	16.19	-	-
0.9	3.31	3.02	5.06	4.34	8.54	6.60	17.09	10.84	48.75	19.80	-	-
1.0	3.53	3.18	5.60	4.67	10.10	7.34	22.97	12.61	-	-	-	-

when surface of gravity walls are in rough condition.

Pseudo-Dynamic Passive Earth Pressure Coefficients (K_{pe})

The pseudo-dynamic passive earth pressure coefficients (K_{pe}) are computed using planar failure (using the expression for K_{pe} reported in Nimbalkar and Choudhury, 2008) and composite failure mechanisms and presented in Tables 3, 4 and 5 for $\phi = 20 - 45^o$, $\delta / \phi = 0.0 - 1.0$, $k_h = 0.1$, 0.2 and 0.3 $k_v / k_h = 0.0 - 1.0$ and $f = 1.0$. The following soil friction angles are considered in order to avoid the shear fluidization of the backfill soil (Richards et al. 1990).

$$\phi > \tan^{-1}\left(\frac{fk_h}{1 - fk_v}\right) \tag{39}$$

The influence of seismic parameters on the magnitude of seismic passive resistance, sliding and rotational displacements is discussed in the following sections.

Influence of k_h and k_v on Passive Resistance

The results presented in Tables 3, 4 and 5 shows the effect of horizontal seismic acceleration coefficient (k_h) and vertical seismic acceleration coefficient (k_v) (expressed in terms of k_h as 0, 0.5 k_h and k_h)on the magnitude of seismic passive earth pressure. It can be noted that as the magnitudes of k_h and k_v / k_h ratio increase, seismic

Table 3. Seismic passive earth pressure coefficients (K_{pe}) for k_h = 0.1, 0.2 and 0.3, k_v / k_h = 0.0, δ / ϕ = 0.0 – 1.0, ϕ = 20° – 45° and f = 1.0

K_{pe} for k_h = 0.1 and k_v / k_h = 0.0												
$\frac{\delta}{\phi}$	ϕ = 20°		ϕ = 25°		ϕ = 30°		ϕ = 35°		ϕ = 40°		ϕ = 45°	
	Planar failure	Composite failure	Planar failure	Com-posite failure	Planar failure	Compos-ite failure	Planar failure	Compos-ite failure	Planar failure	Composite failure	Planar failure	Composite failure
0.0	1.90	1.89	2.32	2.30	2.84	2.80	3.51	3.49	4.40	4.39	5.61	5.60
0.2	2.08	1.99	2.64	2.51	3.39	3.23	4.46	4.24	6.02	5.73	8.44	8.01
0.4	2.29	2.18	3.03	2.85	4.13	3.83	5.86	5.32	8.78	7.71	14.32	11.86
0.6	2.53	2.40	3.53	3.27	5.16	3.99	8.11	6.04	14.24	10.77	30.41	17.03
0.8	2.81	2.66	4.17	3.22	6.69	5.65	12.17	8.03	27.93	14.28	-	-
1.0	3.15	2.47	5.04	3.79	9.12	6.19	20.83	11.03	-	-	-	-
k_h = 0.2 and k_v / k_h = 0.0												
0.0	1.75	1.74	2.16	2.03	2.67	2.65	3.33	3.32	4.20	4.22	5.38	5.36
0.2	1.89	1.70	2.43	2.21	3.15	2.91	4.18	3.90	5.68	5.36	8.01	7.57
0.4	2.06	1.89	2.76	2.56	3.80	3.53	5.43	4.96	8.20	7.28	13.44	11.33
0.6	2.25	2.12	3.18	2.99	4.70	4.28	7.45	4.38	13.15	7.81	28.22	14.73
0.8	2.47	2.42	3.72	1.74	6.03	3.26	11.05	6.19	25.47	12.16	-	-
1.0	2.75	2.72	4.45	2.15	8.13	4.42	18.67	9.21	-	-	-	-
k_h = 0.3 and k_v / k_h = 0.0												
0.0	1.56	1.52	1.97	1.92	2.48	2.42	3.13	3.00	3.98	3.87	5.14	5.10
0.2	1.66	1.35	2.20	1.85	2.90	2.52	3.88	3.48	5.33	4.88	7.58	7.05
0.4	1.78	1.50	2.47	2.13	3.45	3.05	4.99	4.46	7.60	6.75	12.56	10.74
0.6	1.92	1.69	2.81	2.50	4.22	3.78	6.76	5.97	12.04	8.19	26.01	11.58
0.8	2.08	1.91	3.24	2.99	5.35	4.25	9.90	6.81	23.01	9.73	-	-
1.0	2.28	2.05	3.83	3.24	7.11	4.80	16.49	7.87	-	-	-	-

passive resistance significantly decreases. These results are expected, as the horizontal and vertical earthquake accelerations develop the inertial forces within the backfill.

As an illustration from Table 3, for typical value of ϕ = 30°, δ / ϕ = 1.0, k_v / k_h = 0.0, the magnitude of K_{pe} computed using composite failure mechanism drastically reduces from 6.19 to 4.80, when k_h value changes from 0.1 to 0.3. Similarly, for ϕ = 30°, δ / ϕ = 1.0, k_h = 0.3, the value of K_{pe} reduces from 4.80 (Table 3) to 2.36 (Table 5). It is clear from the discussion that the effect of k_v can not be neglected for the seismic design.

Table 4. Seismic passive earth pressure coefficients (K_{pe}) for k_h = 0.1, 0.2 and 0.3, k_v = 0.5, δ / ϕ = 0.0 – 1.0, ϕ = 20° – 45° and f = 1.0

K_{pe} for k_h = 0.1 and k_v / k_h = 0.5												
$\frac{\delta}{\phi}$	ϕ = 20°		ϕ = 25°		ϕ = 30°		ϕ = 35°		ϕ = 40°		ϕ = 45°	
	Planar failure	Composite failure	Planar failure	Composite failure	Planar failure	Composite failure	Planar failure	Composite failure	Planar failure	Composite failure	Planar failure	Composite failure
0.0	1.81	1.80	2.21	2.21	2.71	2.60	3.35	3.34	4.20	4.12	5.35	5.32
0.2	1.99	1.88	2.52	2.38	3.24	3.06	4.25	4.02	5.74	5.42	8.05	7.58
0.4	2.18	2.06	2.89	2.70	3.94	3.62	5.58	5.03	8.37	7.31	13.65	11.24
0.6	2.41	2.27	3.36	3.09	4.92	3.75	7.73	5.68	13.57	10.21	28.98	16.07
0.8	2.68	2.52	3.97	3.34	6.37	4.62	11.60	7.55	26.61	13.47	-	-
1.0	3.00	2.31	4.80	3.63	8.69	5.82	19.84	10.39	-		-	-
k_h = 0.2 and k_v / k_h = 0.5												
0.0	1.57	1.52	1.94	1.88	2.40	2.34	3.00	2.94	3.79	3.75	4.86	4.76
0.2	1.69	1.56	2.18	1.92	2.84	2.54	3.76	3.43	5.12	4.73	7.23	6.72
0.4	1.84	1.62	2.48	2.22	3.41	3.08	4.88	4.39	7.38	6.46	12.10	10.08
0.6	2.00	1.82	2.85	2.63	4.22	3.78	6.68	5.03	11.81	6.56	25.37	12.76
0.8	2.20	2.06	3.33	2.80	5.40	4.15	9.90	5.76	22.84	10.48	-	-
1.0	2.44	2.39	3.97	3.05	7.26	4.64	16.69	7.88	-	-	-	-
k_h = 0.3 and k_v / k_h = 0.5												
0.0	1.26	1.20	1.64	1.53	2.08	2.05	2.63	2.41	3.36	3.16	4.36	4.30
0.2	1.33	1.29	1.81	1.40	2.42	2.21	3.25	2.76	4.48	3.94	6.39	5.75
0.4	1.42	1.39	2.02	1.62	2.86	2.38	4.16	3.55	6.37	5.45	10.55	8.79
0.6	1.52	1.48	2.29	1.91	3.48	2.96	5.61	4.73	10.03	6.48	21.74	8.36
0.8	1.63	1.57	2.63	2.28	4.38	3.12	8.17	5.30	19.05	7.62	-	-
1.0	1.77	1.67	3.08	2.35	5.79	3.41	13.51	6.07	-	-	-	-

Influence of Amplification Factor (*f*) on K_{pe}

Figure 7 shows the variation of the seismic passive earth pressure coefficients (K_{pe}) computed using planar and composite failure mechanisms with amplification factors (f) for k_h = 0.1, 0.2 and 0.3 and for typical values of ϕ = 30°, δ / ϕ = 0.5, H / λ = 0.3, H / η = 0.16 and k_v = 0.5 k_h. It can be noted from Figure 7 that for the case of k_h =

Table 5. Seismic passive earth pressure coefficients (K_{pe}) for k_h = 0.1, 0.2 and 0.3, k_v / k_h = 1.0, δ / ϕ = 0.0 – 1.0, ϕ = 20° – 45° and f = 1.0

K_{pe} **for** k_h **= 0.1 and** k_v / k_h **= 1.0**												
$\frac{\delta}{\phi}$	ϕ = 20°		ϕ = 25°		ϕ = 30°		ϕ = 35°		ϕ = 40°		ϕ = 45°	
	Planar failure	Com-posite failure	Planar failure	Com-posite failure	Planar failure	Com-posite failure	Planar failure	Com-posite failure	Planar failure	Com-posite failure	Planar failure	Com-posite failure
0.0	1.72	1.70	2.09	2.05	2.57	2.45	3.17	3.07	3.98	3.89	5.07	5.02
0.2	1.88	1.77	2.38	2.24	3.07	2.88	4.03	3.79	5.44	5.12	7.63	7.16
0.4	2.07	1.94	2.74	2.54	3.73	3.42	5.29	4.75	7.93	6.90	12.94	10.63
0.6	2.28	2.14	3.18	2.92	4.66	3.50	7.33	5.32	12.86	9.65	27.46	15.11
0.8	2.53	2.37	3.76	3.16	6.04	4.32	10.98	7.08	25.21	12.65	-	-
1.0	2.84	2.14	4.54	3.45	8.23	5.45	18.79	9.76	-	-	-	-
k_h = 0.2 and k_v / k_h = 1.0												
0.0	1.37	1.20	1.70	1.62	2.12	2.08	2.65	2.56	3.35	3.33	4.30	4.26
0.2	1.48	1.22	1.91	1.72	2.50	2.17	3.31	2.95	4.52	4.10	6.39	5.86
0.4	1.60	1.36	2.17	1.88	3.00	2.63	4.30	3.79	6.50	5.64	10.68	8.83
0.6	1.74	1.52	2.49	2.20	3.69	3.28	5.87	4.33	10.39	6.67	22.33	10.57
0.8	1.91	1.73	2.90	2.33	4.72	3.55	8.67	4.94	20.03	8.54	-	-
1.0	2.11	1.98	3.45	2.51	6.33	3.96	14.58	6.51	-	-	-	-
k_h = 0.3 and k_v / k_h = 1.0												
0.0	0.85	0.81	1.27	1.24	1.64	1.59	2.10	2.01	2.70	2.65	3.52	3.49
0.2	0.88	0.83	1.39	1.30	1.89	1.61	2.58	2.05	3.58	2.99	5.13	4.45
0.4	0.92	0.85	1.54	1.35	2.22	1.71	3.27	2.64	5.04	4.15	8.40	6.82
0.6	0.97	0.87	1.72	1.40	2.68	2.13	4.37	3.53	7.88	4.77	17.17	8.25
0.8	1.02	0.89	1.95	1.46	3.35	2.19	6.31	3.84	14.83	5.51	-	-
1.0	1.09	0.91	2.27	1.51	4.38	2.36	10.33	4.35	-	-	-	-

0.1, the passive resistance marginally reduces with increase in the amplification factor (f) and the rate of decrease is more for k_h = 0.2 and 0.3. The influence of soil amplification can be of practical significance if the horizontal acceleration is greater than 0.1. Thus, the results presented reveal the importance of the amplification factor in the seismic design of gravity walls.

Figure 7. Influence of seismic acceleration coefficient (k_h) and amplification factor (f) on seismic passive earth pressure coefficient (K_{pe}).

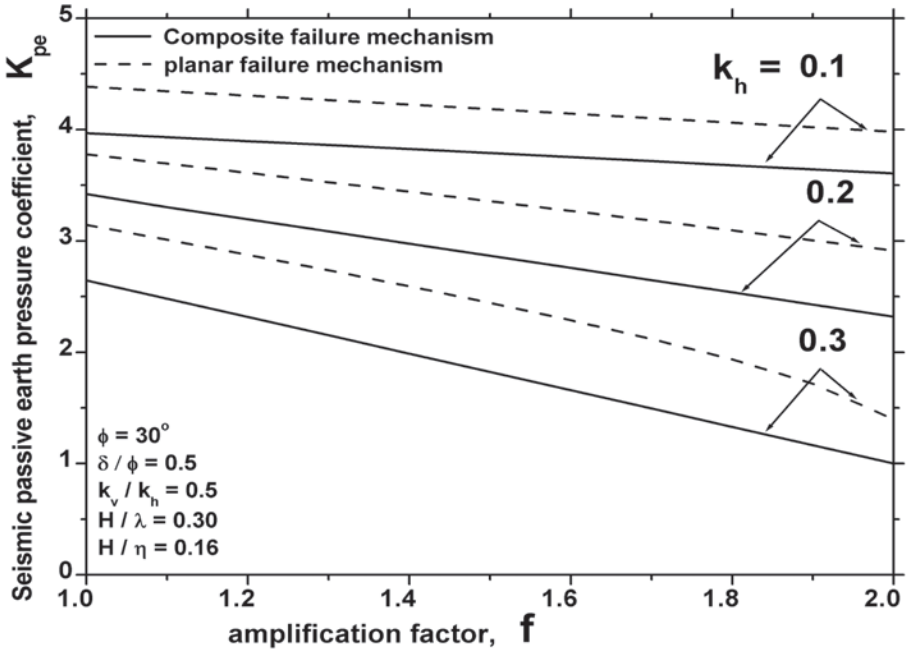

Influence of Assumption of Failure Mechanism on the Permanent Displacements

The results of sliding and rotational displacements of gravity walls subjected to oscillatory nature of earthquake loading by considering composite curved rupture surface and planar failure surface are presented in Figures 8 and 9 for $f = 1.4$, $\phi = 25 - 40^o$, $b_w / H = 0.2$, $\alpha = 15^o$, $\delta = \phi / 2$ and $k_v = 0.5k_h$. For the sake of estimation of sliding and rotational displacements using planar failure mechanism, the expression for K_{pe} reported in Nimbalkar and Choudhury (2008) is used in the present study. It can be noted from Figures 8 and 9 that the sliding and rotational displacements computed using planar failure mechanism are underestimated. It can also be noticed from Figures 8 and 9 that the critical seismic acceleration coefficients for sliding (k_{cs}) and rotation (k_{cr}) computed using planar failure mechanism are overestimated. This is due to the fact that, pseudo-dynamic method considering composite failure mechanism gives lower seismic passive resistance than the value obtained using assumption of planar failure mechanism.

For example, it can be found in Figure 8 that the assumption of planar failure surface overestimates the critical acceleration values ($k_{cs}g$) to the extent of 11.52% for $\phi = 30^o$. In addition, for a constant value of $k_h = 0.46$ and $\phi = 30^o$, planar failure mechanism predicts the magnitude of sliding displacement (S) value as 10 cm, whereas composite failure mechanism predicts S value as 70 cm, the difference reaches as high as 85.71%. It may be noted in Figure 9 that the assumption of planar failure surface overestimates the value of k_{cr} and difference reaches as high as 34.48% for $\phi = 30^o$, and further for a constant value of $k_h = 0.40$, planar failure mechanism predicts a rotational displacement (θ) of 2.0^o, whereas compos-

Figure 8. Comparison of sliding displacements (S) estimated using planar and composite failure mechanisms for different k_h and ϕ values.

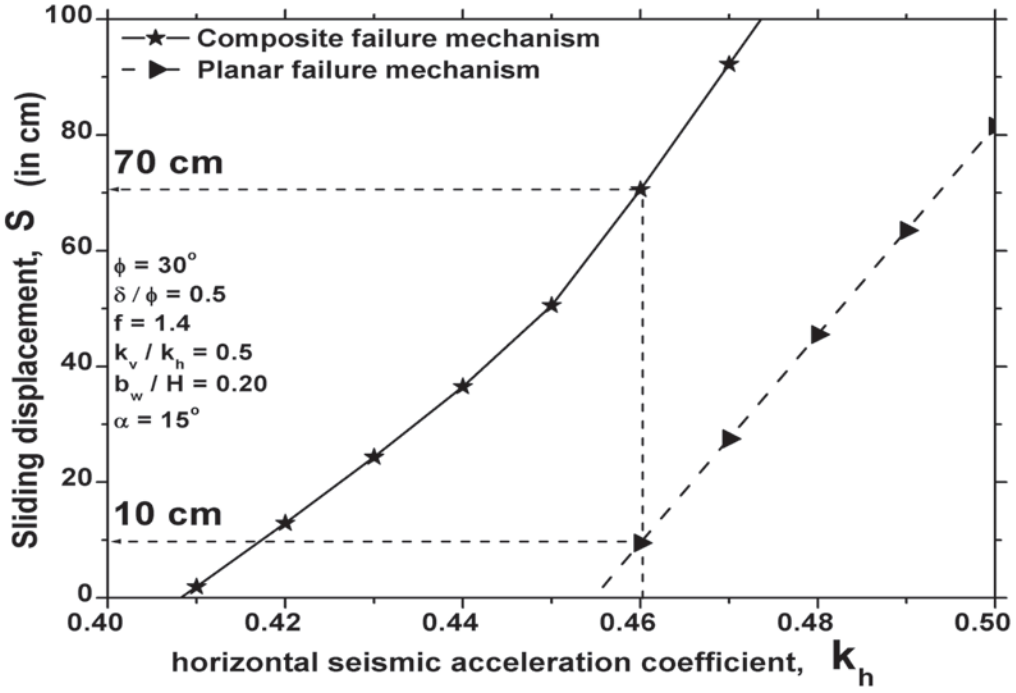

Figure 9. Comparison of rotational displacements (θ) estimated using planar and composite failure mechanisms for different k_h and ϕ values.

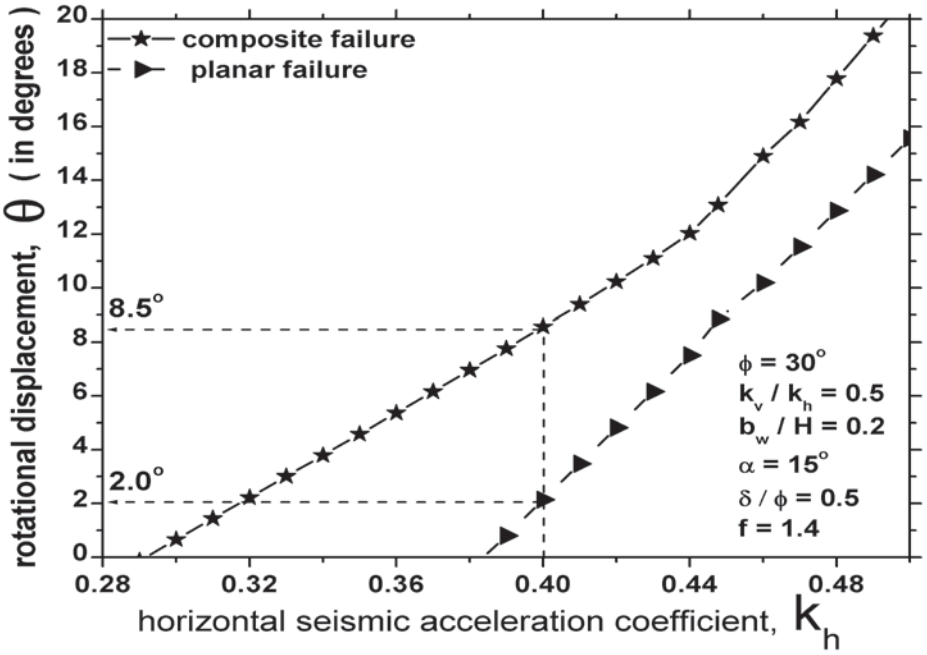

ite failure mechanism predicts θ value as 8.5°, and the difference is high as 76.47%.

CONCLUSION

The study provides a comparative study of formulations for the computation of seismic passive earth pressure coefficients considering the effect of time, soil amplification and phase difference in both shear and primary waves propagating through the backfill behind the gravity retaining wall, using the planar as well as composite curved rupture surface for the design of gravity walls. The following major conclusions can be made from the present study.

1. It is shown that planar failure mechanism overestimates the passive earth pressure for rough soil wall interfaces (i.e. $\delta \geq 0.4\phi$).
2. It is observed that with the increase in values of soil friction angle (ϕ) and soil-wall interface friction angle (δ), the passive resistance increases significantly and the stability of gravity walls reduces with the increase in values of horizontal and vertical seismic accelerations.
3. The influence of soil amplification on the stability of wall is marginal for k_h value is less than 0.1 and its influence can be of practical significance for k_h value is greater than 0.1.
4. For $\phi = 30^o$ and $\delta = 15^o$, the assumption of planar failure mechanism overestimates the critical seismic acceleration values for sliding and rotation by 11.52 and 34.48% respectively, and further it underestimates the sliding and rotational displacements to the extent of 85.71 and 76.47% respectively. Accordingly the error in the estimation can be magnified as magnitude of δ approaches ϕ ; hence the planar failure mechanism is not the appropriate one to predict the passive resistance for rough soil-wall interfaces. Hence the selection of appropriate failure mechanism for estimation of passive pressures, critical accelerations, sliding and rotational displacements significantly influences the design decisions concerning stability of retaining walls.

REFERENCES

Basha, B. M. (2009). *Optimum design of retaining structures under static and seismic loading: A reliability based approach.* Unpublished doctoral dissertation, Indian Institute of Science, Bangaluru, Karnataka, India.

Basha, B. M., & Babu, G. L. S. (2008). Seismic passive earth pressure coefficients by pseudo-dynamic method using composite failure mechanism. *In Geosustainability and Geohazard Mitigation, ASCE Geotechnical Special Publication, 178*, 343 - 350.

Basha, B. M., & Babu, G. L. S. (2009). Computation of sliding displacements of bridge abutments by pseudo-dynamic method. *Soil Dynamics and Earthquake Engineering*, *29*(1), 103–120. doi:10.1016/j.soildyn.2008.01.006

Choudhury, D., & Nimbalkar, S. (2005). Seismic passive resistance by pseudo-dynamic method. *Geotechnique*, *55*(9), 699–702. doi:10.1680/geot.2005.55.9.699

Choudhury, D., & Nimbalkar, S. (2007). Seismic rotational displacement of gravity walls by pseudo-dynamic method: passive case. *Soil Dynamics and Earthquake Engineering*, *27*, 242–249. doi:10.1016/j.soildyn.2006.06.009

Duncan, J. M., & Mokwa, R. L. (2001). Passive earth pressures: theories and tests. *Journal of Geotechnical and Geoenvironmental Engineering*, *127*(3), 248–257. doi:10.1061/(ASCE)1090-0241(2001)127:3(248)

Fang, Y. S., Chen, T. J., & Wu, B. F. (1994). Passive earth pressures with various wall movements. *Journal of Geotechnical Engineering*, *120*(8), 1307–1323. doi:10.1061/(ASCE)0733-9410(1994)120:8(1307)

Housner, G. W., & Theil, C. C. (1995). The continuing challenge: report on the performance of the state bridges in the Northridge earthquake. *Earthquake Spectra*, *11*(4), 569–615. doi:10.1193/1.1585829

Kramer, S. L. (2003). *Geotechnical earthquake engineering*. Upper Saddle River, NJ: Prentice Hall.

Kumar, J. (2001). Seismic passive earth pressure coefficients for sands. *Canadian Geotechnical Journal*, *38*, 876–881. doi:10.1139/cgj-38-4-876

Kumar, J., & Subba Rao, K. S. (1997). Passive pressure coefficients, critical failure surface and its kinematic admissibility. *Geotechnique*, *47*(1), 185–192. doi:10.1680/geot.1997.47.1.185

Makdisi, F. I., & Seed, H. B. (1978). Simplified procedure for estimating dam and embankment earthquake induced deformations. *Journal of Geotechnical Engineering*, *104*(7), 1427–1434.

Morrison, E. E., & Ebeling, R. M. (1995). Limit equilibrium computation of dynamic passive earth pressure. *Canadian Geotechnical Journal*, *32*, 481–487.

Nadim, F., & Whitman, R. V. (1983). Seismically induced movement of retaining walls. *Journal of Geotechnical Engineering*, *109*(7), 915–931. doi:10.1061/(ASCE)0733-9410(1983)109:7(915)

Newmark, N. M. (1965). Effects of earthquakes on dams and embankments. *Geotechnique*, *15*(2), 139–160. doi:10.1680/geot.1965.15.2.139

Nimbalkar, S. S., & Choudhury, D. (2008). Effects of body waves and soil amplification on seismic earth pressures. *Journal of Earthquake and Tsunami*, *2*(1), 33–52. doi:10.1142/S1793431108000256

Richards, R., & Elms, D. G. (1979). Seismic behavior of gravity retaining walls. *Journal of the Geotechnical Engineering Division*, *105*(4), 449–464.

Richards, R., Elms, D. G., & Budhu, M. (1990). Dynamic fluidization of soils. *Journal of Geotechnical Engineering*, *116*(5), 740–759. doi:10.1061/(ASCE)0733-9410(1990)116:5(740)

Seed, H. B., & Whitman, R. V. (1970). Design of earth retaining structures for dynamic loads. *Lateral stresses in the ground and design of earth retaining structures, ASCE*, New York, (pp. 103–147).

Sidle, R. C., Kamai, T., & Trandafir, A. C. (2005). Evaluating landslide damage during the 2004 Chuetsu earthquake, Niigata, Japan. *Eos, Transactions, American Geophysical Union*, *86*(13), 133–136. doi:10.1029/2005EO130001

Soubra, A. H. (2000). Static and seismic passive earth pressure coefficients on rigid retaining structures. *Canadian Geotechnical Journal*, *37*, 463–478. doi:10.1139/cgj-37-2-463

Soubra, A. H., & Macuh, B. (2002). Active and passive earth pressure coefficients by a kinematical approach. In *Proceedings of Institution of Civil Engineers*. *Geotechnical Engineering*, *155*(2), 119–131.

Steedman, R. S., & Zeng, X. (1990). The influence of phase on the calculation of pseudo-static earth pressure on a retaining wall. *Geotechnique*, *40*(1), 103–112. doi:10.1680/geot.1990.40.1.103

Subba Rao, K. S., & Choudhury, D. (2005). Seismic passive earth pressures in soils. *Journal of Geotechnical and Geoenvironmental Engineering*, *131*(1), 131–135. doi:10.1061/(ASCE)1090-0241(2005)131:1(131)

Terzaghi, K., Peck, R. B., & Mesri, G. (1996). *Soil mechanics in engineering practice* (3rd ed). New York: John Wiley and Sons.

Zeng, X., & Steedman, R. S. (1993). On the behavior of quay walls in earthquakes. *Geotechnique*, *43*(3), 417–431. doi:10.1680/geot.1993.43.3.417

Zeng, X., & Steedman, R. S. (2000). Rotating block method for seismic displacement of gravity walls. *Journal of Geotechnical and Geoenvironmental Engineering*, *126*(8), 709–717. doi:10.1061/(ASCE)1090-0241(2000)126:8(709)

Zhu, D. Y., & Qian, Q. (2000). Determination of passive earth pressure coefficients by the method of triangular slices. *Canadian Geotechnical Journal*, *37*, 485–491. doi:10.1139/cgj-37-2-485

APPENDIX

Inertial Forces Acting on Gravity Wall (H_1GLO)

The inertial forces acting on the wall (H_1GLO) (Basha and Babu, 2009) can be expressed as follows: The horizontal inertial force acting on the wedge H_1GLO can be written as

$$\frac{Q_{hw\_H_1GLO}(t)}{0.5\gamma H^2} = 2\frac{\gamma_w}{\gamma}k_h\left\{\begin{array}{l} -\frac{1}{2\pi}\frac{\varphi}{H}\left(\frac{b_w}{H}f + c_1 - c_2\right)\cos 2\pi\left(\frac{t}{T}\right) + \frac{b_w}{H}f\frac{1}{2\pi}\frac{\varphi}{H}\cos 2\pi\xi_5 \\ +\left(c_1 - 2c_2\right)\left(\frac{1}{2\pi}\frac{\varphi}{H}\right)^2\sin 2\pi\left(\frac{t}{T}\right) - c_1\left(\frac{1}{2\pi}\frac{\varphi}{H}\right)^2\sin 2\pi\xi_5 \\ -2c_2\left(\frac{1}{2\pi}\frac{\varphi}{H}\right)^3\cos 2\pi\left(\frac{t}{T}\right) + 2c_2\left(\frac{1}{2\pi}\frac{\varphi}{H}\right)^3\cos 2\pi\xi_5 \end{array}\right\} \quad (40)$$

where $\xi_5 = \left(\frac{t}{T} - \frac{H}{\varphi}\right)$, $c_1 = f\tan\alpha - (f-1)(b_w / H)$, $c_2 = (f-1)\tan\alpha$, $\varphi = Tv_{sw}$ is the wavelength of the vertically propagating shear wave through the wall, v_{sw} is the shear wave velocity propagating through the wall material, γ_w = unit weight of concrete and b_w = top width of the gravity wall, α = angle of the front face of the gravity wall with the vertical. The vertical inertial force acting on the gravity wall H_1GLO can be written as follows:

$$\frac{Q_{vw\_H_1GLO}(t)}{0.5\gamma H^2} = 2\frac{\gamma_w}{\gamma}k_v\left\{\begin{array}{l} -\frac{1}{2\pi}\frac{\kappa}{H}\left(\frac{b_w}{H}f + c_1 - c_2\right)\cos 2\pi\left(\frac{t}{T}\right) + \frac{b_w}{H}f\frac{1}{2\pi}\frac{\kappa}{H}\cos 2\pi\xi_6 \\ +\left(c_1 - 2c_2\right)\left(\frac{1}{2\pi}\frac{\kappa}{H}\right)^2\sin 2\pi\left(\frac{t}{T}\right) - c_1\left(\frac{1}{2\pi}\frac{\kappa}{H}\right)^2\sin 2\pi\xi_6 \\ -2c_2\left(\frac{1}{2\pi}\frac{\kappa}{H}\right)^3\cos 2\pi\left(\frac{t}{T}\right) + 2c_2\left(\frac{1}{2\pi}\frac{\kappa}{H}\right)^3\cos 2\pi\xi_6 \end{array}\right\} \quad (41)$$

where $\xi_6 = \left(\frac{t}{T} - \frac{H}{\kappa}\right)$, $\kappa = Tv_{pw}$ is the wavelength of the vertically propagating primary wave through the wall and v_{pw} is the primary wave velocity propagating through the wall.

This work was previously published in International Journal of Geotechnical Earthquake Engineering, Volume 1, Issue 1, edited by T.G. Sitharam, pp. 88-109, copyright 2010 by IGI Publishing (an imprint of IGI Global).

Chapter 4
Cyclic Pore Pressure Generation, Dissipation and Densification in Granular Mixes

S. Thevanayagam
University at Buffalo, SUNY, NY, USA

T. Shenthan
Advanced Earth Sciences Inc., CA, USA

ABSTRACT

Knowledge of cyclic load induced pore pressure generation, post-liquefaction dissipation and volumetric densification characteristics of sands, silty sands, and silts are important for the analysis of performance of loose saturated granular deposits in seismic areas. This article presents results from an experimental study of these characteristics for such soils containing 0 to 100% non-plastic silt. Pore pressure generation characteristics are studied using undrained cyclic triaxial tests. Pre- and post-liquefaction compressibility and coefficient of consolidation, and post-liquefaction volumetric densification characteristics are determined from consolidation data prior to cyclic tests and pore pressure dissipation tests following undrained cyclic tests. Effects of fines content on these characteristics compared to those of clean sands are examined in the context of intergranular void ratio and intergranular contact density concepts.

INTRODUCTION

Soil liquefaction and its post-liquefaction response have been of great interest in geotechnical engineering for more than three decades. Liquefaction induced failures include landslides, sand boils, cracks, excessive ground settlements, lateral spreading, and foundation failures. Pore water pressure builds up in loose saturated soil deposits due to cyclic shearing. At the same time, dissipation and redistribution of this shear induced pressure take place at a rate depending on the hydraulic conductivity and volume compressibility characteristics of the soil deposit and drainage

DOI: 10.4018/978-1-4666-0915-0.ch004

conditions. When the rate of pore pressure generation and build up is significant, a non-plastic soil temporarily loses a large portion of its strength, which may lead to liquefaction and breakdown of the soil structure. Pore pressure dissipation will usually be accompanied by rearrangement of particles, reconsolidation and a reduction in volume of voids, hence settlement of ground surface. Current knowledge on pore pressure generation and post-liquefaction dissipation and volume change characteristics of granular soils rely primarily on data from clean sands (Ishihara & Yoshimine, 1992; Lee & Albaisa, 1974; Pyke et al., 1975; Silver & Seed, 1971a,b; Seed et al., 1976; Tatsuoka et al., 1984; Tokimatsu & Seed, 1984, 1987; Yoshimi et al., 1975). However, recent earthquake case histories indicate that sites containing a significant percentage of fine grains, mostly non-plastic, also liquefy due to seismic loading (Seed et al. 1983, Youd et al. 2001). Only a limited amount of research information is available for silty soils. Therefore, not surprisingly, evaluation of liquefaction characteristics of silty soils has recently attracted attention of researchers. Recently there has been advances in the understanding of the effects of silt content on monotonic and cyclic strength and liquefaction resistance of silty soils and to a lesser extent on post-liquefaction response of silty soils (Andrews & Martin 2000, Chang 1990, Georgiannou et al. 1990, 1991, Ishihara 1993, Koester 1994, Pitman et al. 1994, Shenthan 2001, Singh 1994, Thevanayagam et al. 2001, Thevanayagam and Martin 2002, Thevanayagam et al. 2002, Thevanayagam et al. 2007a-b, Vaid 1994, Yamamuro & Lade 1998). Data on post-liquefaction characteristics of such soils are scarce.

This article presents results from an experimental study of pre- and post-liquefaction characteristics of non-plastic sand-silt mixes at silt contents from 0% to 100% by weight, and three natural non-plastic silts. Undrained cyclic triaxial tests followed by dissipation of cyclic-induced pore pressures were carried out in order to determine pore pressure generation, pre- and post-liquefaction compressibility, pre- and post-liquefaction coefficient of consolidation, and post-liquefaction densification characteristics of these soils. Findings from this study are summarized. The influence of silt content on these characteristics is examined in the context of intergranular void ratio and intergranular contact density concepts (Vaid 1994, Thevanayagam et al. 2002, Thevanayagam 2007a).

EXPERIMENTAL PROGRAM

Materials

The experiments in this study involved several granular mixes prepared by mixing Ottawa Silica Sand (OS-F55, US Silica Company, Illinois) with a non-plastic silt (crushed silica fines Sil-co-Sil #40) at silt contents of (a) 0%, (b) 15%, (c) 25%, (d) 40%, (e) 60%, and (f) 100% fines by dry weight. The dry soils were mixed thoroughly until there was no obvious color difference. A limited number of tests were also conducted on three remolded natural silts from New Jersey; Los Angeles, CA; and San Fernando, CA, USA. Figure 1 shows the gradation data. Table 1 summarizes the index properties of the Ottawa sand-silt mixtures and the three natural silts. The New Jersey silt was non-plastic sandy silt, and the Los Angeles, CA silt was also non-plastic sandy silt or very low plasticity material classified as ML according to USCS classification. The San Fernando, CA silt was classified as ML-CL, a low plasticity silt material.

Specimen Preparation

The experiments were conducted on relatively large cylindrical specimens of 155 mm in height and 75 mm in diameter prepared using Moist Tamping Method. Each specimen was prepared at a different final void ratio. A known weight of

Figure 1. Gradation

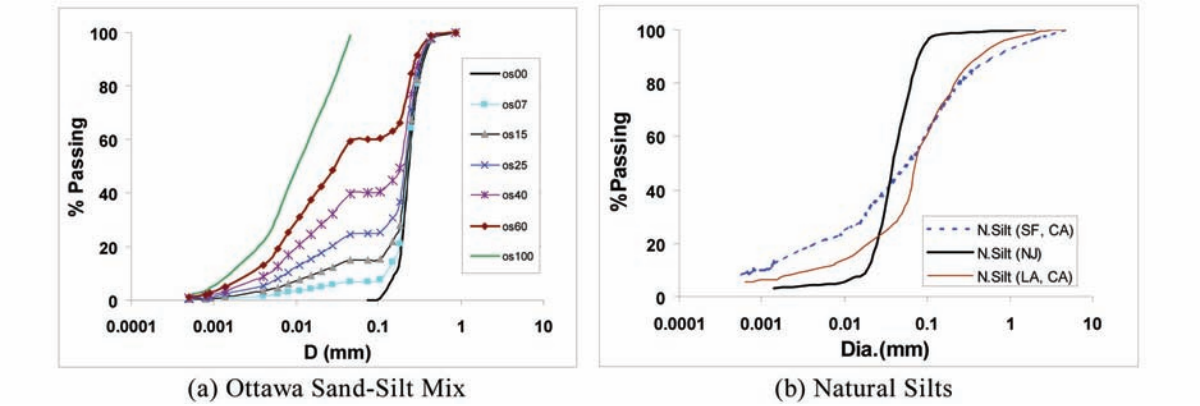

(a) Ottawa Sand-Silt Mix (b) Natural Silts

Table 1. Index properties

	Ottawa Sand / Silt Ratio by weight						Natural Silt		
Property	**100/0 (Clean Sand)**	**85/15**	**75/25**	**60/40**	**40/60**	**0/100 (Silt)**	**Newark NJ**	**San Fernando CA**	**Los Angeles CA**
G_s	2.65	—				2.65	—		
e_{min}	0.608	0.428	0.309	0.33	0.413	0.627	—		
e_{max}	0.79	0.75	0.86	1.07	1.35	2.10	—		
D_{10} (mm)	0.16	0.018	0.0085	0.005	0.0027	0.0015	0.02	0.0009	0.004
D_{30} (mm)	0.22	0.19	0.15	0.025	0.01	0.006	0.03	0.017	0.047
D_{50} (mm)	0.25	0.235	0.23	0.185	0.0285	0.01	0.04	0.06	0.07
D_{60} (mm)	0.27	0.245	0.24	0.22	0.07	0.015	0.05	0.095	0.1
C_u	1.69	13.61	28.24	46.81	25.93	10.00	2.5	105	25
C_c	1.12	8.19	11.03	0.60	0.53	1.60	0.9	3.4	5.5
% < 75μm	0	15	25	40	60	100	89	54	53
% < 2μm	0	2	4	5	8	11	3	15	8
LL	—	—		—			24	28	39
PI	—	—		—			1	8	7
USCS	SP	SM		ML			ML	CL-ML	ML

Note: e_{min} = minimum void ratios (ASTM D1557), e_{max} = maximum void ratios (ASTM D4254 method C). LL = liquid limit (ASTM D4318), PI = plasticity index (ASTM D4318 method B), $C_u = D_{60} / D_{10}$, and $C_c = D_{30}^2 / (D_{10}D_{60})$.

dry solids required to reach the target void ratio was weighed and mixed thoroughly with water at a water content of about 5%. The soil was divided into four equal portions. Each portion was poured into a mold mounted on a triaxial cell, and tamped gently using a wooden rod until the height corresponding to the target void ratio was achieved. The specimen was then percolated with CO_2 and saturated with deaired water using back pressure saturation. The back pressure was increased gradually while maintaining the effective confining pressure at 15 to 20 kPa. This process was continued until the B ($=\Delta u/\Delta\sigma_c$) factor exceeded 0.95. Following saturation, the

specimens were consolidated to a final effective isotropic consolidation stress of 100 kPa before cyclic loading.

In each stage, the amount of water flowing into or out of the specimen was recorded. The void ratio at every stage of consolidation stress and the final void ratio at the end of consolidation of the specimen were calculated using the dry weight of the solids, specific gravity of solids, and net volume of water introduced into the specimen at the corresponding stage. Following the consolidation phase, a small amount of water was removed from the triaxial cell surrounding the soil specimen while the cell pressure was maintained the same as the value at the end of consolidation. This was done to make room for cyclic movement of the axial loading piston into and out of the triaxial cell during the cyclic loading phase without adversely affecting the cell pressure.

Experiments

Undrained cyclic triaxial tests were conducted using an automated apparatus (GEOCOMP Inc., MA) at a constant cyclic stress ratio ($CSR=\Delta\sigma_l/2\sigma_c'$) of 0.2 at a frequency of 0.2 Hz. For safety purposes, the maximum axial strain allowable was set at 8%. All specimens had an initial effective isotropic confining stress of 100 kPa. The axial displacement, cell pressure, and sample pore water pressure were monitored using a built-in data acquisition system. Once the specimen liquefied, cyclic loading phase was terminated.

Post-liquefaction pore pressure dissipation tests were initiated immediately following the end of cyclic loading phase. The bottom end of the specimen was connected to a pressure controlled volume measuring burette. The top end of the specimen was connected to a pore pressure transducer with no drainage allowed from this end. This setup simulated a one-way drainage condition. The dissipation tests were done in three stages. In the first stage the pressure in the burette was set at a value such that the post-consolidation effective stress in the specimen was 25kPa. In the second and third stages, the burette pressure was set at values such that the post-consolidation effective stresses were 50 and 100 kPa, respectively, at the end of each stage. The time histories of pore pressure at the top-end of the specimen and outflow volume of the water exiting from the bottom of the specimen were recorded in each stage. The duration of each stage varied from 16 sec to more than 3 hours, depending on the soil and silt content of the specimen.

RESULTS

Pore Pressure Generation

Figures 2a-h shows cyclic shear induced pore pressure ratio r_u (= shear induced pore pressure $\Delta u/\sigma_c'$) versus normalized number of cycles N/N_l, where N=number of cycles applied and N_l=number of cycles to reach liquefaction, for a number of specimens at different silt contents. The specimen notations are as follows: 25-408 = Ottawa sand/silt mix at 25% silt content and e=0.408; and NS(NJ)-785 = Natural silt from New Jersey at e=0.785. Also shown in these figures are the best-fit envelope curves for clean sands proposed by Seed et al. (1976) and the envelope curves proposed by El Hosri et al. (1984) for clayey silt with plasticity index of 8 to 15.

Ottawa Sand-Silt Mix: The data for clean sand and non-plastic silty sand up to 25% silt content (Figures 2a-c) follow the envelope for clean sand reported by Seed at al. (1976). They agree with the results reported by others (Guo and Prakash 1999, 2000). The data for Ottawa sand-silt mixtures at intermediate silt contents of 40 and 60% (Figures 2d-e) fall above the Seed et al. envelope for clean sand and indicate a faster pore pressure generation initially and a slower rate with further cyclic loading. The data for 100% silt (sil-co-sil #40) follows the upper bound Seed et al. envelope (Figures 2f).

Figure 2. Pore pressure generation

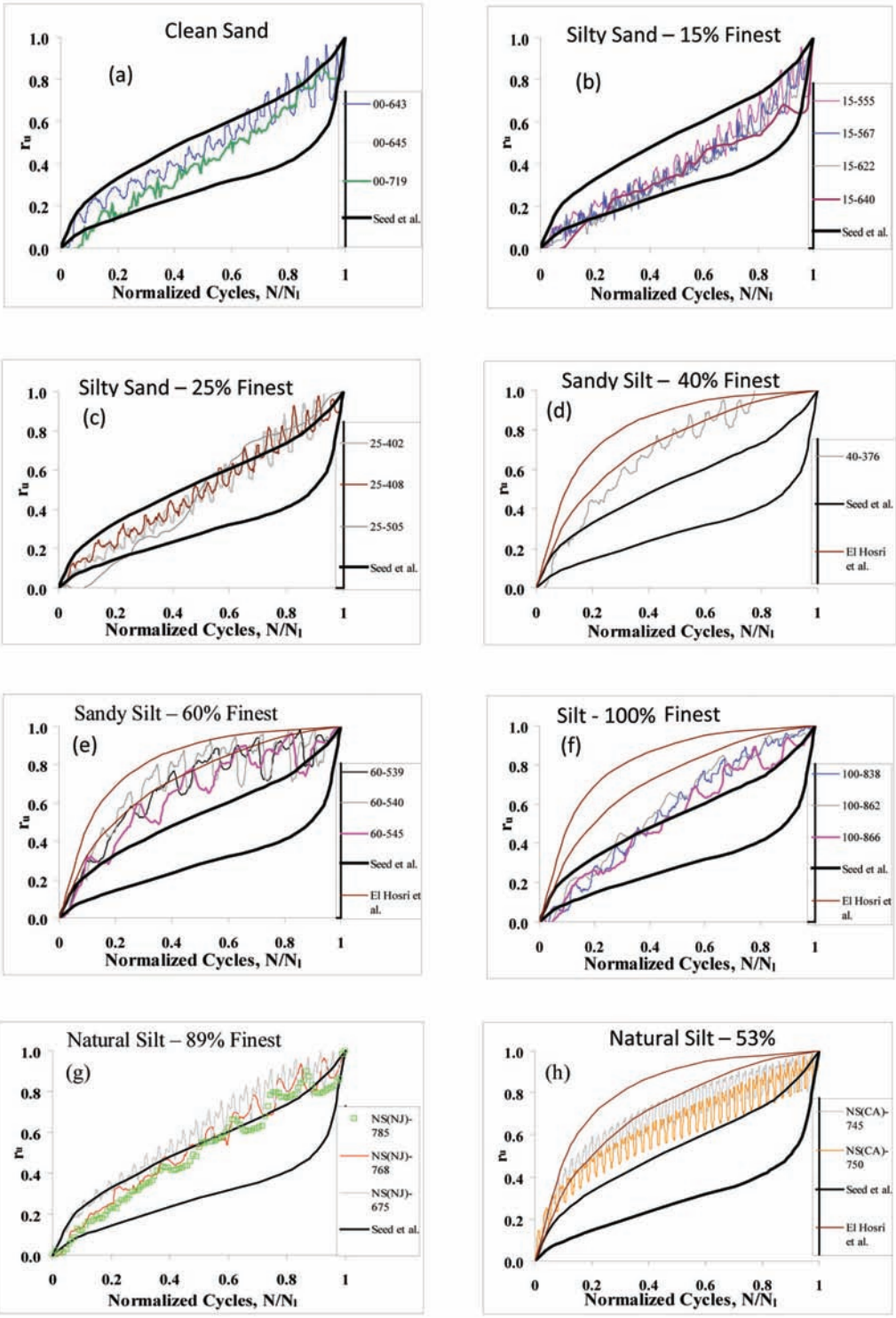

Figure 3. Pre- and post-liquefaction e versus σ'$_3$

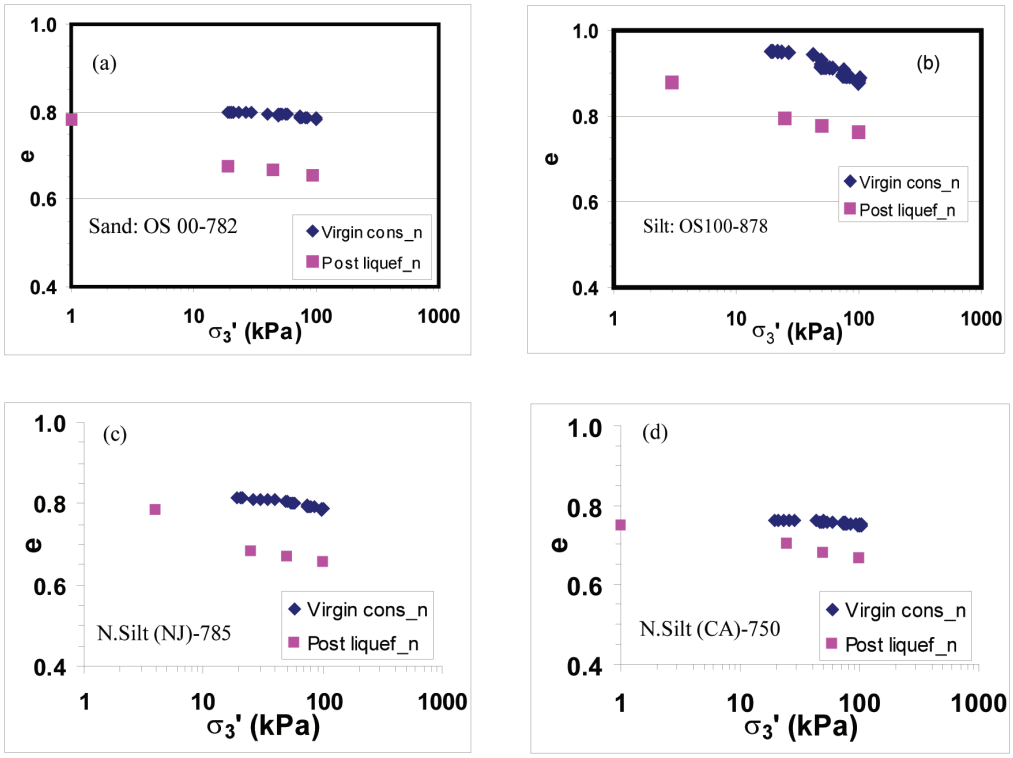

Natural Silts: The non-plastic natural silt from New Jersey with a high silt content of 89% behaved similar to that of sil-co-sil #40 silt (Figure 2g). The natural silt from Los Angeles, CA with fines content of 53% and 8% particles smaller than 2μm with plasticity index of 7% showed a pore pressure response similar to that of non-plastic Ottawa sand silt mixtures at 40 to 60% silt content. The silt from San Fernando, CA had a fines content of 54% and 15% particles smaller than 2μm with plasticity index of 8%. It reached a high level of 5% of double amplitude axial strain in 9 cycles, but the pore pressure ratio did not build up beyond 65% (Shenthan 2001). No further tests were done on this soil.

Compressibility

Effect of Liquefaction: Pre-liquefaction virgin consolidation path (e vs. σ_3') during initial consolidation of the specimens up to initiation of undrained cyclic loading and post-liquefaction consolidation path after termination of cyclic loading and opening of the drainage valves were determined from pore pressure and volume change data obtained during each stage of the tests. Figures 3a-d show the data for clean Ottawa sand, 100% sil-co-sil#40 silt, and two natural silts (NJ and Los Angeles, CA), at 89% and 53% silt contents, respectively. The data refer to one specimen for each soil. The last three digits in the text inside each figure refer to the void ratio of the specimen. For clean Ottawa sand, Figure 3a refers to a specimen initially prepared and cyclically loaded at e=0.782. The blue data points correspond to initial compression path prior to cyclic loading and the pink data points refer to post-liquefaction pore pressure dissipation and reconsolidation path. The post-liquefaction consolidation line is nearly parallel to the virgin consolidation line for all soils. This indicates that

during liquefaction and subsequent shear strain accumulation the soil skeleton is remolded. Post-liquefaction soil behaves like a freshly deposited soil during subsequent reconsolidation. The post-liquefaction compression line follows a new virgin consolidation line differing from a typical unload-reload recompression line that would be expected if the specimen is simply unloaded and reloaded with drainage. The same trend has been reported by Tatsuoka et al. (1984) for clean sand. The present study indicates that non-plastic silty soils also follow this trend.

Effect of Confining Stress: Figures 4a-b show pre- and post-liquefaction volume compressibility data (m_v) for non-plastic Ottawa sand-silt mixes and a natural silt (NJ). Compressibility values of silt and silty sand are of the same order of magnitude as that of sands at the same effective stress. The post-liquefaction compressibility values are slightly smaller than the pre-liquefaction virgin compressibility values. The values are significantly stress-dependent. At the confining stress of about 100 kPa, a reasonable value for the compressibility can be in the order of 0.1 $(MPa)^{-1}$. However, it increases by more than an order of magnitude to more than 1 $(MPa)^{-1}$ with a reduction in confining stress to 10 kPa. These ranges may differ for silty soils of other minerals or prepared by other sample preparation methods.

Effect of Silt Content: The data in Figures 4a-b also shows that there is some difference between m_v values depending on the silt content and void ratio. Figures 5a-b shows the m_v values for a few specimens corresponding to an effective stress range from 50 to 100 kPa. Typically compressibility would decrease with a decrease in void ratio for the same soil. In Figure 5a, some specimens of silty sands at smaller void ratios than clean Ottawa sand specimens appear to have larger compressibility than that for clean sand. Some sandy silt specimens at very small void ratios appear to have similar compressibility as 100% silt. This apparent anomaly is due to the inability of the global void ratio to represent the intergrain contact density of silty soils compared to clean sand. Compressibility, like other mechanical deformation characteristics and strength, is dependent on soil skeleton structure and intergrain contact density of the soil. This limitation could be alleviated by analyzing the data using the intergranular void ratio concepts and intergrain contact density concepts (Thevanayagam et al. 2002, Thevanayagam 2007a).

Figures 6a-b show the same data after splitting the data for Ottawa sand-silt mixes into two parts, one for sands and silty sands up to 25% silt content, and the other for sandy silts with silt content above 25%, and plotted against the equivalent intergranular and interfine void ratios $(e_c)_{eq}$ and $(e_f)_{eq}$ (Thevanayagam et al. 2002), respectively:

$$(e_c)_{eq} = \frac{e + (1-b)fc}{1-(1-b)fc} \tag{1}$$

$$(e_f)_{eq} = \left[\frac{e}{fc + \dfrac{(1-fc)}{R_d^m}}\right] \tag{2}$$

where e = global void ratio, fc = FC/100, FC = (silt) fines content in percentage, and b and m are coefficients that depend on gradation characteristics (Thevanayagam 2007a), $R_d = D_{50}/d_{50}$, D_{50} = 50% passing diameter of sand portion, and d_{50} = 50% passing diameter of fines portion.

When plotted against $(e_c)_{eq}$ and $(e_f)_{eq}$, each data set for m_v falls in a narrow band in Figures 6a and b, respectively. Presence of silt grains appears to slightly increase the compressibility of the soil. It is also interesting to note that the above respective equivalent intergranular void ratios have also been found to correlate well with the number of mechanical properties of soils including cyclic strength, shear wave velocity, shear modulus, and undrained shear strength of granular mixes (Kanagalingam & Thevanayagam 2006, Ni et

Figure 4. Pre and post-liquefaction volume compressibility

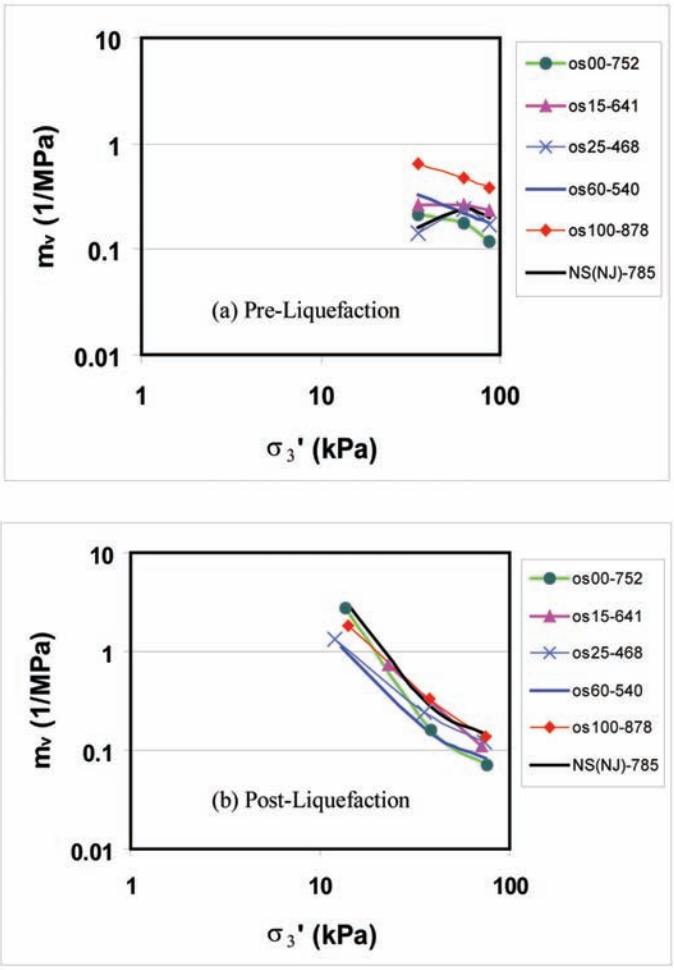

Figure 5. Effect of fines content and void ratio on m_v (σ'_3=50 to 100 kPa)

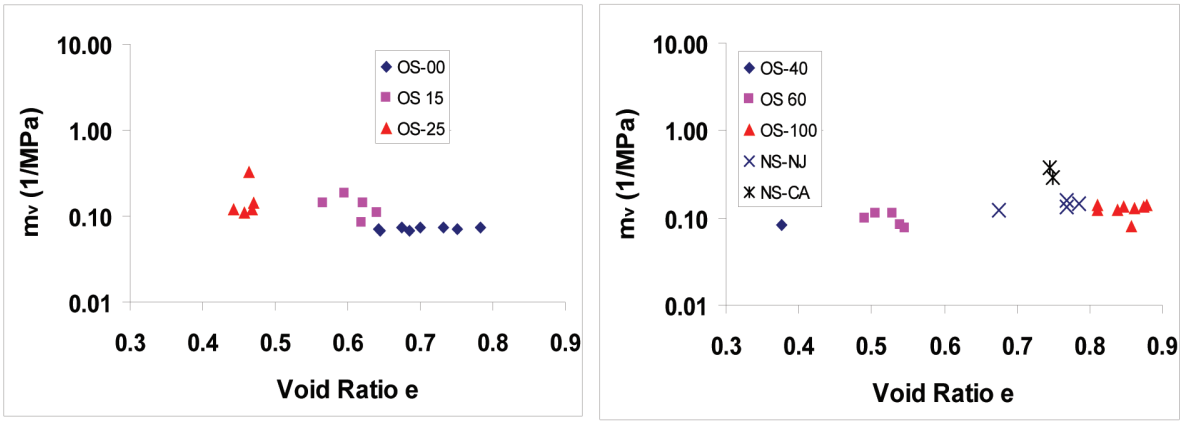

(a) FC=0~25%

(b) FC>25%

Figure 6. Effect of fines content and $(e_c)_{eq}$ and $(e_f)_{eq}$ on m_v (Ottawa sand silt – Mixes; σ'_3=50 to 100 kPa)

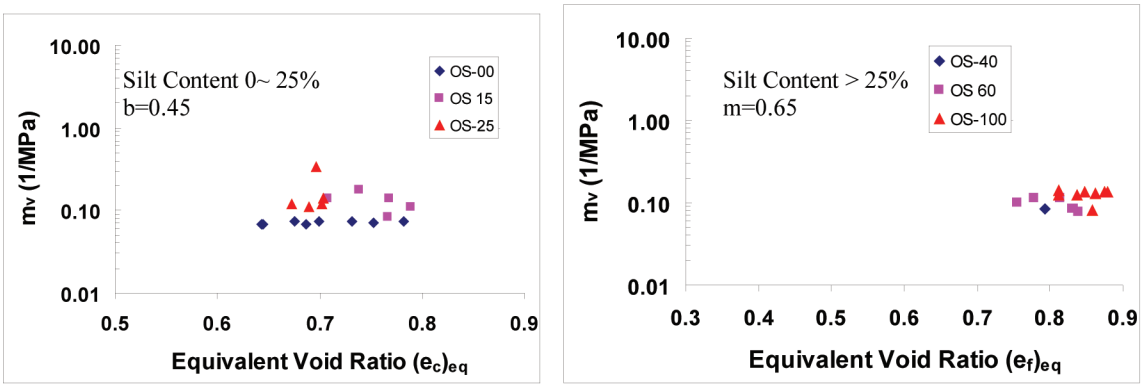

(a) FC=0~25% (b) FC>25%

al. 2004, Thevanayagam 2000, Thevanayagam et al. 2000, Thevanayagam 2007a-b,, Yang et al. 2006) for sands and silty sands, and sandy silts and silts, respectively.

Coefficient of Consolidation

Pre-liquefaction coefficient of consolidation (c_v) values for each specimen were calculated based on measured hydraulic conductivity (k) and volume compressibility (m_v) data for *virgin loading* shown in Figure 4a. Post-liquefaction c_v values were back-calculated using time histories of pore pressure dissipation and volume change measurements obtained during post-liquefaction dissipation tests for each incremental change in effective stresses. Back-calculations of c_v were done by fitting the measured pore pressure vs. elapsed time data at the closed-end of the specimen to the theoretical solution for pore pressure at that end based on Terzaghi's one dimensional consolidation theory (Coduto 1999), given by

$$u = \Delta\sigma \sum_{m=0}^{\infty} \{ \frac{4}{(2m+1)\pi} \sin[\frac{(2m+1)\pi}{2} \frac{Z_{dr}}{H_{dr}}] e^{-[\frac{(2m+1)^2 \pi^2}{4} T_v]} \} \quad (3)$$

where H_{dr} = length of longest drainage path, T_v = time factor, u = excess pore pressure, Z_{dr} = nearest distance to the drainage end, and $\Delta\sigma$ = change in total stress. Similarly, volume change versus elapsed time data was also used to back calculate c_v using Terzaghi's one dimensional consolidation theory.

Figures 7a-b show a typical comparison of the measured and theoretical dissipation data plots based on pore pressure dissipation and volume change versus time data, respectively, for a 100% silt specimen (os100-838) at void ratio of 0.838. The theoretical back-calculated value for c_v for these numerical simulations is shown in each figure. In both cases, the back-calculated c_v values are 0.2 cm^2/s and 0.15 cm^2/s in close agreement with each other. Figures 7c-d show another typical comparison of the measured and theoretical curves for the corresponding back-calculated c_v for sand and New Jersey silt, respectively. The data in these figures correspond to post-liquefaction dissipation test during a period where the effective stress in the specimen increases from 25 to 50 kPa. The c_v values were also dependent on the effective stress range and they were different for each specimen. Silt content and hydraulic conductivity k of each specimen also influenced the c_v values.

Effect of Liquefaction: Figures 8a-b show the pre- and post-liquefaction c_v values as a function of effective confining stress for a number of specimens at different silt contents. For the same

Figure 7. Back-calculation of c_v

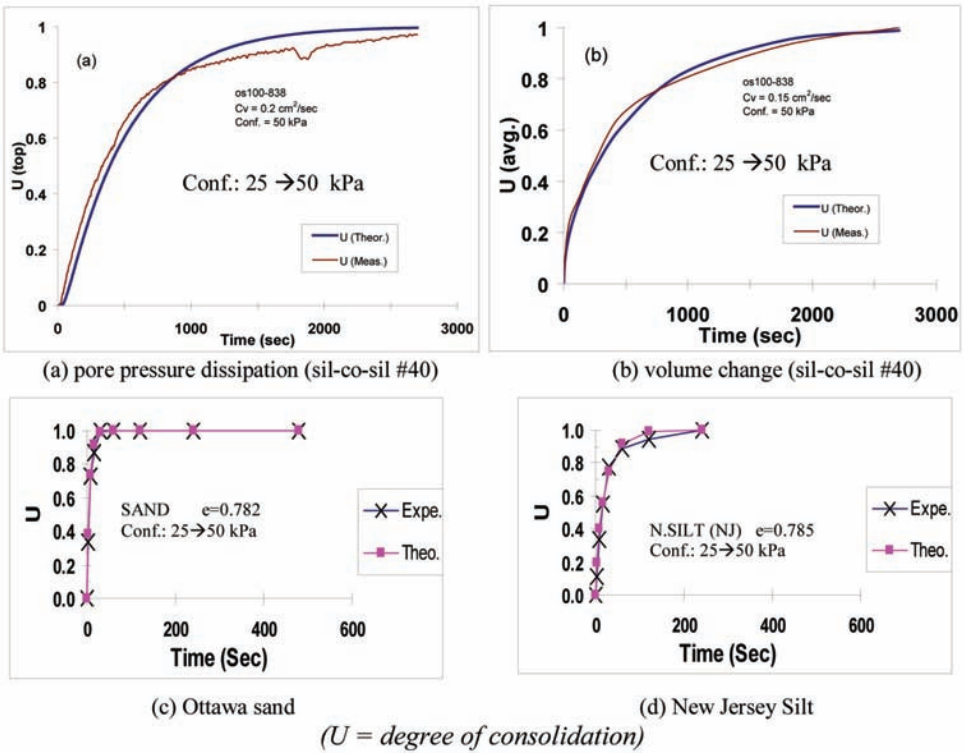

(a) pore pressure dissipation (sil-co-sil #40)

(b) volume change (sil-co-sil #40)

(c) Ottawa sand

(d) New Jersey Silt

(U = degree of consolidation)

specimen, at the same effective confining stress, the pre-liquefaction c_v values for consolidation along virgin loading and post-liquefaction c_v values are not significantly different except for differences due to changes in void ratio and associated changes in permeability and m_v. The reason for this is the same as that identified in the prior discussion pertaining to m_v. The soil is completely remolded following liquefaction and it behaves as a freshly deposited soil. Any changes in k and m_v during this process affect the post-liquefaction c_v values. However these post-liquefaction c_v values are far from the very high values expected for specimens that would simply be unloaded and reloaded with drainage.

None of the specimens in the present test series was subjected to cyclic stress-induced pore pressure dissipation and drainage tests before liquefaction occurred. Hence no direct data is available to determine the relevant values for c_v for soils that may not reach liquefaction. Complete remolding of the soil structure may not occur for specimens not reaching high r_u values. Therefore the post-cyclic loading m_v values for such cases may be smaller than that post-liquefaction m_v values. The corresponding c_v values may be higher than the c_v values for fully liquefied soils. It is thought that the c_v values for soils experiencing small pore pressure ratios would be similar to the c_v value corresponding drained unloading/reloading recompression line. However, this remains to be verified. Development of a relationship for c_v values as a function of maximum r_u values reached during cyclic loading would be useful.

For the same soil, c_v at an effective confining stress of 10 kPa is more than one order of magnitude smaller compared to its value at 100 kPa (Figures 8a-b). This indicates the need to use confining stress dependent c_v values for post-liquefaction dissipation analyses.

Figure 8. Coefficient of consolidation

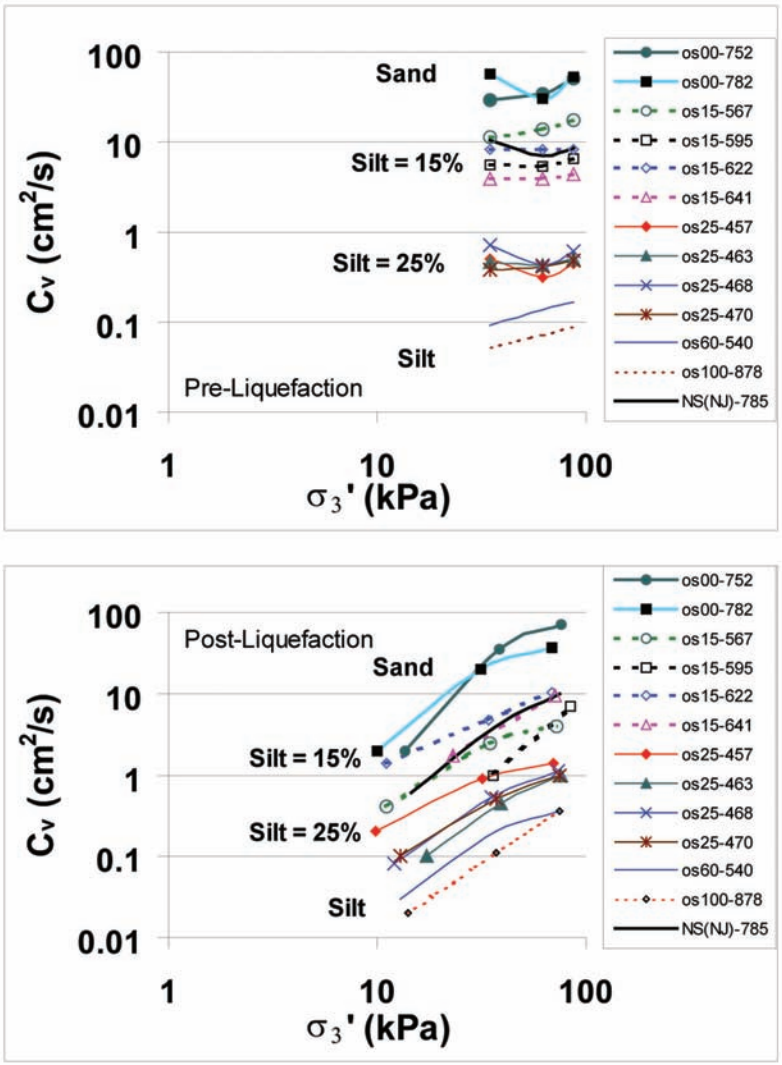

Effect of Silt Content: Silt content has a significant influence on c_v. At the same confining stress, the c_v values are smaller for silty soils by more than one to two orders of magnitude compared to sand (Figure 8). Figure 9 illustrates this more clearly. It shows the change in normalized coefficient of consolidation $(c_v)/(c_v)_0$ for Ottawa sand silt mixes, where, $(c_v)_0$ is the coefficient of consolidation value for clean Ottawa sand, and c_v=coefficient of consolidation of Ottawa sand-silt soil mixes tested in this study.

Silt content affects the c_v values through its influence on m_v and hydraulic conductivity k. For the same sand-silt mix at different proportions of silt content, m_v appears to be influenced by equivalent intergranular void ratios (Figure 6a-b). Hydraulic conductivity is affected by both void ratio and silt content. Silt content has a significant effect on k than the influence of void ratio on k. Hydraulic conductivity of the soil specimens in this study ranged from 0.6 to 1.3×10^{-3} cm/s for the clean sand, 9×10^{-5} cm/s for 15% silt content,

Figure 9. Normalized c_v – Ottawa sand – Silt mix specimens

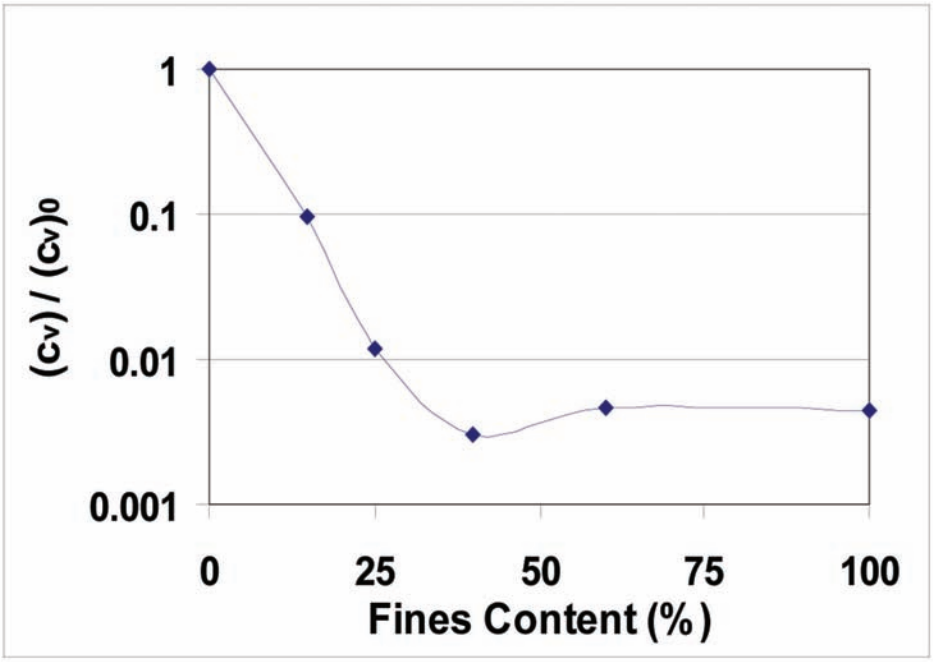

0.6 to 1.2x10^{-5} cm/s for 25% silt content, and 3 to 5x10^{-6} cm/s for 60% and 100% silt contents, a nearly three orders of magnitude change from clean sand to 100% silt. The c_v values in Figures 8 and 9 decrease in the same manner as hydraulic conductivity, with smaller influences by m_v. An interesting observation from Figure 9 is that the change in c_v somewhat stabilizes once the silt content exceeds about 35%. The reason for this is that as the silt content exceeds a threshold value in the vicinity of about 25 to 30%, the voids are completely filled by the silt. Any further filling of the voids does not have a significant influence in reducing the hydraulic conductivity as much as the first instance of filling the empty voids. Beyond this transition silt content, the permeability and compressibility of the silt influences the c_v with a diminishing influence by the sand grains with further increase in silt content.

Figures 10a-b show a comparison of the post-liquefaction dissipation data for a clean sand and 100% silt specimen, respectively. The m_v values for these two specimens (Figs. 5a-b) are not too different from one another. Figures 10a-b highlight the influence of silt content on hydraulic conductivity and c_v on dissipation times for these two soils. Increasing silt content decreases the hydraulic conductivity significantly and causes significant reduction in c_v and a significant increase in dissipation time. These findings have significant influence on understanding of and the analysis of post-liquefaction performance of liquefiable sites containing different amounts of silt content, as well as understanding and designing suitable ground improvement/densification techniques to mitigate liquefaction in silty soils compared to clean sands (Nashed et al. 2009). This also has a significant influence on understanding the response of silty soils to in situ CPT or SPT penetration resistance testing and their use in field liquefaction screening (Thevanayagam & Martin 2002, Thevanayagam & Ecemis 2008).

Natural Silt: The c_v values for the natural silt NS(NJ) at 89% silt content in Figures 8a-b are

Figure 10. Comparison of dissipation times for sand and silt

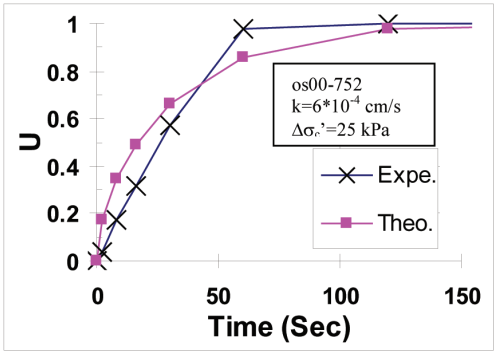

(a) Ottawa Sand

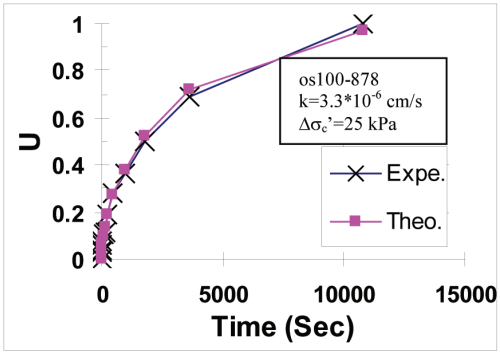

(b) Sil-co-sil#40

significantly higher than those for 100% silt (sil-co-sil #40). But the m_v values (Figure 4) for these two soils are not very different. The difference in c_v for these two soils appears to stem from the difference in grain sizes and hydraulic conductivities for these two silts. Grain size (d_{50}) for the natural silt is about 38µm versus 10µm for sil-co-sil #40. Hydraulic conductivity values are of the order of $2x10^{-4}$ cm/s for the natural silt versus 3 to $5x10^{-6}$ cm/s for sil-co-sil #40. This difference in hydraulic conductivities is reflected in the c_v values for these two silts.

Post-Liquefaction Volumetric Strain

Determination of post-liquefaction ground settlement and volumetric strain is an important aspect in performance evaluation of liquefiable soil sites. At present, there is only limited data available on this subject (Ishihara & Yoshimine, 1992; Lee & Albaisa, 1974; Pyke et al., 1975; Silver & Seed, 1971a,b; Tatsuoka et al., 1984; Tokimatsu & Seed; 1984, 1987; Yoshimi et al., 1975). The data are primarily limited to clean sands. The data from the current study sheds further light on this subject.

Clean Sand: The available post-liquefaction reconsolidation volumetric strain vs. relative density data for clean sands in the literature is summarized in Figures 11a-b (Ishihara & Yoshimine, 1992, Soydemir, 1994, Tatsuoka et al., 1984, Tokimatsu & Seed 1984, 1987). The volumetric strain is also affected by the maximum shear strain amplitude induced by cyclic loading. It increases with cyclic strain amplitude and reaches an asymptotic value at a strain level of 10 to 15%. The maximum shear strain reached for each specimen in the current study is 12%. Figure 11c shows a comparison of the results for clean sand from the current study with the data from the literature shown in Figures 11a-b. The current data for clean sands fall in the range reported in the literature for the appropriate shear strain amplitude levels.

Effect of Silt Content: Figure 12a shows the post-liquefaction volumetric strain data for all of the soils tested in this study. There is no single relationship for volumetric compression against void ratio for all soils. Figures 12b-c show the data after splitting the data for Ottawa sand-silt mixes into two parts, one for sands and silty sands up to 25% silt content, and the other for sandy silts with silt content above 25%, and plotted against the equivalent intergranular and interfine void ratios $(e_c)_{eq}$ and $(e_f)_{eq}$, respectively. Each data set falls in a narrow band.

Figure 13a shows the volumetric strain vs. relative density D_r for clean sand, silty sands, and sandy silts. Similar to equivalent void ratios $(e_c)_{eq}$ and $(e_f)_{eq}$, a set of equivalent relative densities

Figure 11. Post-Liquefaction volumetric strain and cyclic strain level (Clean Sands)

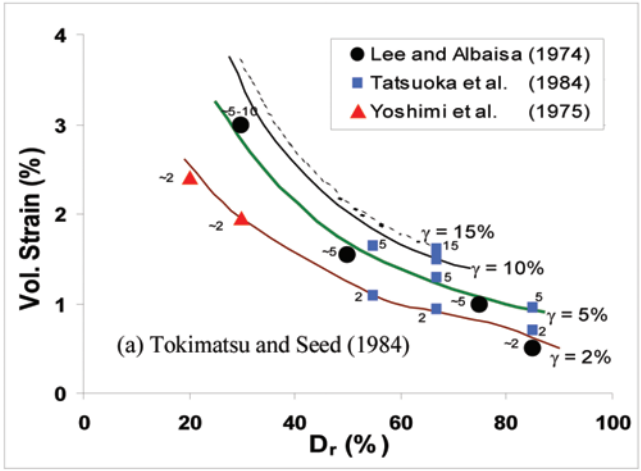

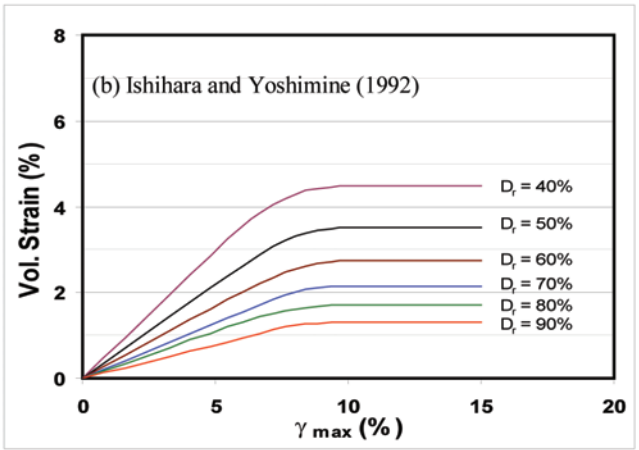

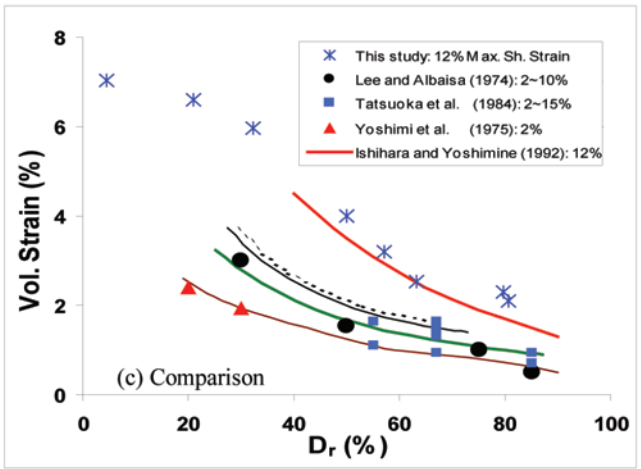

Figure 12. Post-liquefaction volumetric strain

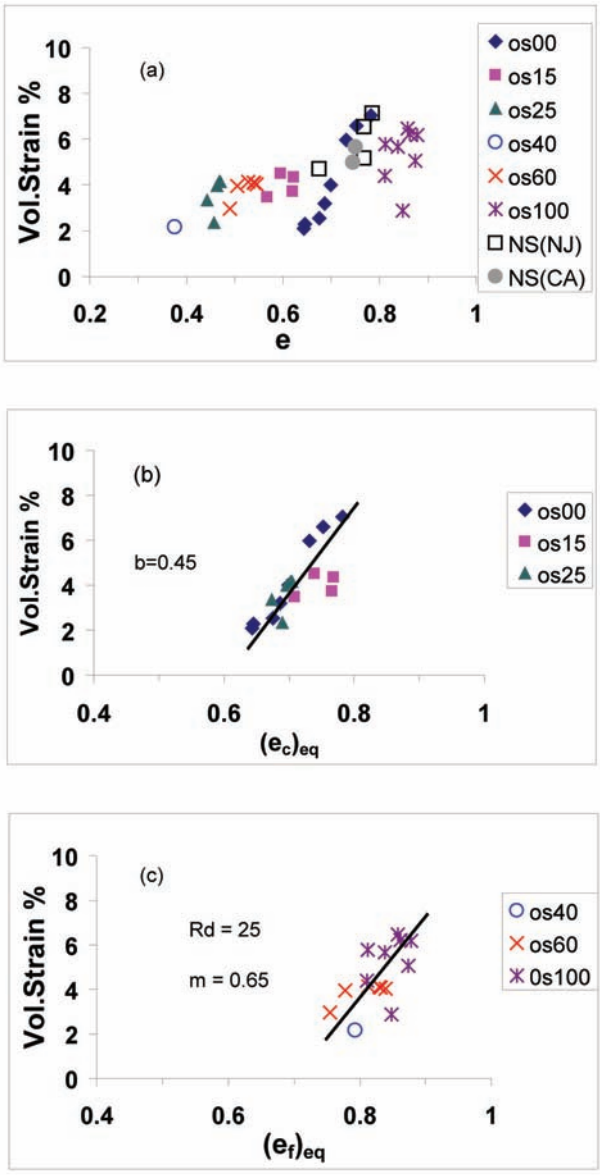

$(D_{rc})_{eq}$ and $(D_{rf})_{eq}$, can also be defined (Thevanayagam 2007a-b):

$$(D_{rc})_{eq} = \left[\frac{(e_{\max,HS} - (e_c)_{eq})}{(e_{\max,.HS} - e_{\min,HC})}\right] \text{ for FC<FC}_{th} \qquad (4)$$

$$(D_{rf})_{eq} = \left[\frac{(e_{\max,HF} - (e_f)_{eq})}{(e_{\max,.HF} - e_{\min,HF})}\right] \text{ for FC>FC}_{th} \qquad (5)$$

where, $e_{max,HS}$ and $e_{min,HS}$ are maximum and minimum void ratios of clean sand, respectively; $e_{max,HF}$ and $e_{min,HF}$ are maximum and minimum void ratios

Figure 13. Volumetric strain of sand and sandy silts

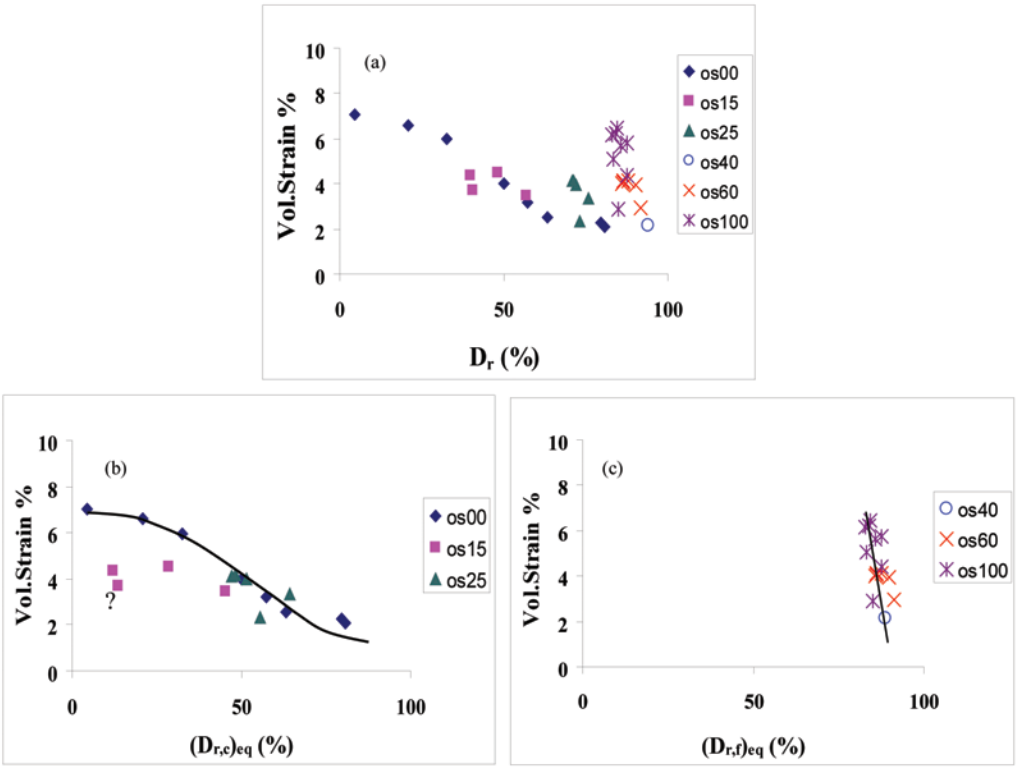

of pure fines respectively; and FC_{th} is a transition fines content.

Figure 13b shows the volumetric strain data against $(D_{rc})_{eq}$ for sand and silty sand at silt content up to 25%. The data in Figure 13b falls in a narrow band, similar to the Figure 12b. These results combined with Figure 11c indicate that post-liquefaction volumetric strain in silty sands follows the same trend as shown in Figure 11c for clean sands, when combined together using equivalent relative density $(D_{rc})_{eq}$. The data for soils at silt content higher than 25% is shown in Figure 13c against $(D_{rf})_{eq}$.

CONCLUSION

A comprehensive laboratory experimental study on pore pressure generation, post-liquefaction dissipation and densification characteristics of granular mixes containing 0 to 100% silt content is presented.

Liquefaction process of granular mixes containing non-plastic silts leading to significant shear strain amplitudes appears to cause a complete remolding of the soil structure. Post-liquefaction reconsolidation and associated volume compressibility is similar to that of a virgin consolidated specimen of that soil at the same stress level. Post-liquefaction compressibility is highly stress-dependent.

Silt content does influence the compressibility of the soil. However, at the same equivalent intergranular void ratio $(e_c)_{eq}$, a clean sand and granular mix containing the same host sand and silt have similar volume compressibility. At the same equivalent interfine void ratio $(e_f)_{eq}$, a sandy silt has similar volume compressibility as the host silt.

Post-liquefaction coefficient of consolidation of a soil is similar to that of a freshly deposited soil at the same void ratio. It is highly influenced by silt content. The influence of silt content on c_v is significant through its effect on hydraulic conductivity than through its effect on volume compressibility. Both parameters influence c_v. It is also highly stress-dependent.

The post-liquefaction volumetric strain data for clean sand from this study falls in the range of data for clean sands available in the literature. Silt content also affects the post-liquefaction volumetric strain response. However, at the same equivalent intergranular void ratio $(e_c)_{eq}$, a clean sand and granular mix containing the same host sand and non-plastic silt have similar post-liquefaction volumetric strain response. At the same equivalent interfine void ratio $(e_f)_{eq}$, a sandy silt has similar post-liquefaction volumetric strain response as the host silt. Equivalent relative density may be a useful parameter to collectively characterize the post-liquefaction compressibility and volumetric strain response of silty sands with clean sands.

ACKNOWLEDGMENT

Financial support for this research was provided by MCEER Highway project at University at Buffalo, sponsored by the FHWA. The authors wish to thank Geoffrey R. Martin, J. Liang, T. Kanagalingam, and R. Nashed for their creative and valuable contributions toward this research.

REFERENCES

Andrews, D. C. A., & Martin, G. R. (2000). Criteria for liquefaction of silty soils. In *Proceedings of the 12th WCEE 2000 Conferance*, Auckland, NZ.

Chang, N. Y. (1990). *Influence of fines content and plasticity on earthquake-induced soil liquefaction*. contract No. DACW3988-C-0078, US Army WES, MS.

Coduto, D. P. (1999). *Geotechnical*. Upper Saddle River, NJ: Prentice Hall, Inc.

El Hosri, M. S., Biarez, J., & Hicher, P. Y. (1984). Liquefaction characteristics of silty clay. In *Proceedings of the 8th World Conference Earthquake Eng.* (Vol. 3) (pp. 277-84), San Francisco, CA.

Georgiannou, V. N., Burland, J. B., & Hight, D. W. (1990). The undrained behaviour of clayey sands in triaxial compression and extension. *Geotechnique*, *40*(3), 431–449. doi:10.1680/geot.1990.40.3.431

Georgiannou, V. N., Hight, D. W., & Burland, J. B. (1991). Undrained behaviour of natural and model clayey sands. *Soil and Foundation*, *31*(3), 17–29.

Guo, T., & Prakash, S. (1999). Liquefaction of silts and silt-clay mixtures. *J. Geotech. Eng. Div., ASCE, 125*(8), 706-10.

Guo, T., & Prakash, S. (2000). Liquefaction of silt-clay mixtures. In *Proceedings of the 12th World Conferance Earthq. Eng.*, New Zealand.

Ishihara, K. (1993). Liquefaction and flow failure during earthquakes. *Geotechnique*, *43*(3), 351–41. doi:10.1680/geot.1993.43.3.351

Ishihara, K., & Yoshimine, M. (1992, March). Evaluation of settlements in sand deposits following liquefaction during earthquakes. *Soil and Foundation*, *32*(1), 173–188.

Kanagalingam, T., & Thevanayagam, S. (2006). Energy dissipation and liquefaction assessment in sands and silty soils. ASCE. In D. J. DeGroot et al. (Eds.), *Geotechnical Engineering in the Information Age*, I0-7844-0803-3.

Koester, J. P. (1994). The influence of fines type and conent on cyclic strength. In Proceedings of the ASCE Conv., Atlanta. *Geotech. Spec. Pub. 44*, 17-32.

Lee, K.L., & Albaisa, A. (1974). Earthquake induced settlements in saturated sands. *J. Geotech. Eng. Div., ASCE, 100*(4), 387-406.

Nashed, R., Thevanayagam, S., & Martin, G. R. (2009). Densification and Liquefaction Mitigation of Saturated Silty Soils by Dynamic Compaction – Design. *Ground Improvement Journal*, Institute of Civil Engineers, UK.

Ni, Q., Tan, T. S., Dasari, G. R., & Hight, D. W. (2004). Contribution of fines to the compressive strength of mixed soils. *Geotechnique*, *54*(9), 561–569.

Pitman, T. D., Robertson, P. K., & Sego, D. C. (1994). Influence of fines on the collapse of loose sands. *Canadian Geotechnical Journal*, *31*, 728–739. doi:10.1139/t94-084

Pyke, R., Seed, H. B., & Chan, C. K. (1975). Settlement of sands under multi directional shaking. *Journal of the Geotechnical Engineering Division*, *101*(4), 379–397.

Seed, H.B., Idriss, I.M., & Arango, I. (1983). Evaluation of liquefaction potential using field performance data. *J. Geot.. Eng. Div., ASCE, 109*(3), 458-482.

Seed, H.B, Martin, P.P., & Lysmer, J. (1976). Pore water pressure change during soil liquefaction. *J. Geotech. Eng. Div., ASCE, 102*(4), 323-346.

Shenthan, T. (2001). *Factors affecting liquefaction mitigation in silty soils using stone columns.* MS Thesis, Department of Civi, Structural and Environ. Eng., University at Buffalo, NY, USA.

Silver, M. L., & Seed, H. B. (1971a). Deformation characteristics of sands under cyclic loading. *Journal of the Soil Mechanics and Foundations Division*, *97*(SM8), 1081–1098.

Silver, M. L., & Seed, H. B. (1971b). Volume changes in sands during cyclic loading. *Journal of the Soil Mechanics and Foundations Division*, *97*(SM9), 1171–1182.

Singh, S. (1994). Liquefaction characteristics of silts. Ground failures under seismic conditions. In S. Prakash & P. Dakoulas (Eds.), *Proceedings ASCE Convention, GSP. 44, ASCE,* (pp. 105-116).

Soydemir, C. (1994, October). Earthquake-induced settlements in silty sands for New England seismicity. Ground failures under seismic conditions. In S. Prakash & P. Dakoulas (Eds.), *Proceedings of the ASCE Convention, GSP. 44, ASCE* (pp. 77-90), Atlanta, GA.

Tatsuoka, F., Sasaki, T., & Yamada, S. (1984). Settlement in saturated sand induced by cyclic undrained simple shear. In Proc. 8th World Conf. Earthq. Eng., San Francisco, CA, V3, 95-102.

Thevanayagam, S. (2000). Liquefaction potential and undrained fragility of silty soils. In the *Proceedings of the12th World Conf. Earthq. Eng*., New Zealand.

Thevanayagam, S. (2007a). Intergrain contact density indices for granular mixes I - Framework. J. *Earthquake Engineering and Engineering Vibrations*, *6*(2), 123–134. doi:10.1007/s11803-007-0705-7

Thevanayagam, S. (2007b). Intergrain contact density indices for granular mixes- II: Liquefaction resistance. *J. Earthquake Engineering and Engineering Vibrations*, *6*(2), 135–146. doi:10.1007/s11803-007-0706-6

Thevanayagam, S., & Ecemis, N. (2008). Effects of permeability on liquefaction resistance and cone resistance. *ASCE Geotechnical Special Publication 181, Geotechnical Earthquake Engineering and Soil Dynamics* (p. 11).

Thevanayagam, S., Fiorillo, M., & Liang, J. (2000). Effect of non-plastic fines on undrained cyclic strength of silty sands. In R.Y.S. Pak & J. Yamamura (Eds.), *ASCE Geotech Spec. Publ. 107*, (pp. 77-91).

Thevanayagam, S., Liang, J., & Shenthan, T. (2000). Contact index and liquefaction potential of silty and gravely soils. In the *Proceedings of the 14th ASCE Eng. Mech. Conference,* Austin, Texas.

Thevanayagam, S., & Martin, G. R. (2002). Liquefaction in silty soils: screening and remediation issues. *J. Soil Dyn. & Eq. Eng.*, *22*, 1035–1042. doi:10.1016/S0267-7261(02)00128-8

Thevanayagam, S., Martin, G. R., Shenthan, T., & Liang, J. (2001). Post-liquefaction pore pressure dissipation and densification in silty soils. In *Proceedings of the 4th Intl. Conf. Soil Dynamics & Earthq. Eng.,* San Diego, CA.

Thevanayagam, S., Shenthan, T., Mohan, S., & Liang, J. (2002). Undrained fragility of sands, silty sands and silt. *ASCE. Journal of Geotechnical and Geoenvironmental Engineering*, *128*(10), 849–859. doi:10.1061/(ASCE)1090-0241(2002)128:10(849)

Tokimatsu, K., & Seed, H. B. (1984). *Simplified procedures for the evaluation of settlements in sands due to earthquake shaking*. Report No. UCB/EERC-84/16, Univ. of Calif., Berkeley, CA.

Tokimatsu, K., & Seed, H.B. (1987). Evaluation of settlements in sands due to earthquake shaking. *J. Geotech. Eng. Div., ASCE, 113*(8), 861-78.

Vaid, Y. P. (1994). Liquefaction of silty soils. *ASCE Conv. Geotech. Spec. Publ.*, *44*, 1–16.

Yamamuro, J.A., & Lade, P.V. (1998). Steady-state concepts and static liquefaction of silty sands. *J. Geotech. and Geoenv. Engrg. Div., ASCE, 124*(9), 868-877.

Yang, S. L., Sandven, R., & Grande, L. (2006). Instability of sand–silt mixtures. *Soil Dynamics and Earthquake Engineering*, *26*(2-4), 183–190. doi:10.1016/j.soildyn.2004.11.027

Yoshimi, Y., Kuwabara, F., & Tokimatsu, K. (1975). One-dimensional volume change characteristics of sands under low confining stresses. *Soil and Foundation*, *15*(3), 51–60.

Youd, T. L., Idriss, I. M., Andrus, R. D., Arango, I., Castro, G., & Christian, J. T. (2001). Liquefaction Resistance of Soils: Summary Report from the 1996 NCEER and 1998 NCEER/NSF Workshops on Evaluation of Liquefaction Resistance of Soils. *ASCE J. of Geotech. and Geoenv. Eng.*, *127*(10), 817–833. doi:10.1061/(ASCE)1090-0241(2001)127:10(817)

This work was previously published in International Journal of Geotechnical Earthquake Engineering, Volume 1, Issue 1, edited by T.G. Sitharam, pp. 42-61, copyright 2010 by IGI Publishing (an imprint of IGI Global).

Chapter 5
Effect of Superstructure Stiffness on Liquefaction-Induced Failure Mechanisms

S.P.G. Madabhushi
University of Cambridge, UK

S.K. Haigh
University of Cambridge, UK

ABSTRACT

Soil liquefaction following strong earthquakes causes extensive damage to civil engineering structures. Foundations of buildings, bridges etc can suffer excessive rotation/settlement due to liquefaction. Many of the recent earthquakes bear testimony for such damage. In this article a hypothesis that "Superstructure stiffness can determine the type of liquefaction-induced failure mechanism suffered by the foundations" is proposed. As a rider to this hypothesis, it will be argued that liquefaction will cause failure of a foundation system in a mode of failure that offers least resistance. Evidence will be offered in terms of field observations during the 921 Ji-Ji earthquake in 1999 in Taiwan and Bhuj earthquake of 2001 in India. Dynamic centrifuge test data and finite element analyses results are presented to illustrate the traditional failure mechanisms.

INTRODUCTION

Soil liquefaction plays a major role in the damage suffered by many a civil engineering structures. This is illustrated by many of the recent earthquakes including the Kobe earthquake of 1995 in Japan, the Kocaeli earthquake in Turkey and the 921 Ji-Ji earthquake in Taiwan during 1999 and Bhuj earthquake of 2001 in India. In these earthquakes many examples of failures have been observed, for example settlement and/or rotation of structures owing to foundation liquefaction, bowing out of quay walls owing to liquefaction

DOI: 10.4018/978-1-4666-0915-0.ch005

of the backfill, excessive settlement and damage of pile foundations etc.

It is well known that soil liquefaction occurs in loose, saturated sand or silt layers. The cyclic shear stresses generated by the earthquake loading will cause the excess pore pressures rise over and above the hydrostatic pore pressures. The degree of liquefaction is often measured by the excess pore pressure ratio r_u defined as;

$$r_u = \frac{u_{excess}}{\sigma'_{vo}} \quad (1)$$

While this factor is easy to visualise in the case of free-field sites, its estimation is more involved when liquefaction below foundations of existing structures is being considered primarily as it involves the calculation of initial effective stress σ'_{vo}. The range of r_u varies from 0 to 1 i.e. no excess pore pressures generated to full liquefaction condition. When the value of r_u reaches 1, the foundations of buildings, bridges and other civil engineering structures would suffer excessive settlements and/or rotations.

The main emphasis of this article will be on the failure mechanisms suffered by the foundations when full liquefaction is reached. It will be argued that the superstructure stiffness has a role to play in determining the actual failure mechanism by which the foundation will fail. This aspect is important in understanding the failure mechanisms suffered by foundations in past earthquakes and in attempts to carryout liquefaction resistant designing of future structures.

BEHAVIOUR OF LIQUEFIED SOILS

There has been a significant amount of research on the liquefaction behaviour of loose, saturated sands and silts for about 40 years since the 1964 Niigata and Alaskan earthquakes. Ishihara (1993) identified the Phase Transformation Line (PTL) in the q-p′ space, which demarcates the contractile and dilatant behaviour of sands. A similar concept was also proposed by Luong and Sidaner (1981) who proposed the concept of a 'Characteristic State Line' with sub-characteristic and sur-characteristic regions to identify the contractile and dilatant behaviour of sands. At Cambridge, Schofield (1981) proposed the Critical State Line (CSL) concept. When the stress path of a loose sand sample reaches the CSL by suffering softening owing to excess pore pressure generation (due to contractile behaviour), its behaviour will become dilatant. All these concepts capture the cyclic triaxial sample behaviour in which loose sand exhibits contractile behaviour until the CSL is reached after which point it starts to dilate.

LIQUEFACTION DURING RECENT EARTHQUAKES

Liquefaction has been observed in many of the recent major earthquakes. In this article, examples from the Kocaeli earthquake in Turkey and the 921 Ji-Ji earthquake in Taiwan in 1999 and the Bhuj earthquake in India in 2001 will be considered.

Liquefaction played a major role in damage suffered by buildings during the Kocaeli earthquake, Free et al. (2003). Liquefaction was observed at several locations during the 921 Ji-Ji earthquake, Madabhushi (2007). The Taichung harbour witnessed excessive settlements of backfill behind quay walls. Similarly liquefaction and liquefaction induced lateral spreading was observed at several bridge sites.

Widespread liquefaction was observed during the Bhuj earthquake of 2001, Madabhushi et al. (2005). Sand boils were observed at several locations in the Rann of Kachchh. Moderate to severe damage was recorded to quay walls at Navalakhi port, rotation of Harbour Master Tower at Kandla port, damage to piles supporting wharfs,

settlement of railway lines and cracks and lateral spreading of earth dam slopes. In this article, one particular bridge site that was studied following this earthquake will be considered in detail.

Field Observations of Building Foundation Failures

The Adapazari district suffered extensive liquefaction induced damage during the Kocaeli earthquake of 1999 in Turkey. In Figures 1 and 2 examples of liquefaction damage are presented. Both buildings had shallow foundations. It is interesting to note that in both these examples, the structural damage to the buildings was small, albeit the buildings are no longer functional or repairable. In Figure 1 the foundations have suffered a punch type failure. The foundation soil has liquefied and the building suffered extensive vertical settlement. In Figure 2 the foundations have suffered rotational failure allowing the building on the top to rotate.

Considering the above two examples, it would be useful to be able to predict the vulnerability of the foundations to either type of failure before the earthquake event occurs. This is particularly true if retrofit measures are being planned to remediate the foundations against liquefaction induced failure. In this regard it is helpful to contemplate whether the building shape, stiffness and inertial mass have a role to play in the type of failure mechanism, once the foundation soil liquefies. For example, a building that is top heavy or has high centre of gravity may be more vulnerable to rotational failure while a short structure is more vulnerable to punch type failure.

Field Observations of Bridge Foundation Failures

Liquefaction induced damage has been observed at several bridge sites during recent earthquakes. One example was recorded during the 921 Ji-Ji earthquake at a bridge site near Nantou city in Taiwan. In Figure 3 a view of the bridge is pre-

Figure 1. Punch failure of foundations

Figure 2. Rotational failure of foundations

Figure 3. A bridge site that suffered liquefaction induced lateral spreading during 921 Ji-Ji earthquake

sented. The site showed clear signs of liquefaction induced lateral spreading. The left hand side abutment has rotated clockwise while the bridge piers showed an anti-clockwise rotation. A new bridge was being constructed at this site at the time of the earthquake. The new bridge piers were supported on deep pile foundations. Although lateral spreading of the non-liquefied crust that overlaid the deeper, liquefied layers occurred, the new bridge piers were able to resist the additional horizontal loads, Madabhushi et al. (2009).

A more interesting case of a bridge site near the towns of Bachau and Vondh, was recorded during the Bhuj earthquake of 2001 in India. This site had four bridges crossing a small river. Two of the bridges are for railway, one an old arch bridge and the other a plate girder bridge, each with 7 spans. The other two were highway bridges, one older bridge was under use at the time of the earthquake and a new bridge that was being constructed at that time. A recent satellite image of the bridge site is presented in Figure 4 showing the two railway bridges to the North (highlighted at the top of the figure). In this figure it can be seen that the older highway bridge no longer exists and the new four lane highway bridge seen towards the South (bottom of the figure) is fully operational. The bridges are oriented approximately in the East-West direction. In this article only the two railway bridges shown in Figure 5 will be considered.

The bridge site exhibited evidence of extensive soil liquefaction in the form of sand boils at the foundations piers supporting of all the bridges. These sand boils are clearly visible in Figure 6 taken soon after the earthquake event. Although no explicit measurements of pore water pressures were made, the presence of such extensive sand boils may be considered as evidence of wide spread liquefaction at the bridge site. Given this, the distress exhibited by the plate girder bridge and the arch bridge following the Bhuj earthquake will be considered in some detail in later sections of this article.

DYNAMIC CENTRIFUGE TESTS

An extensive research program was undertaken at Cambridge University to investigate the response of bridge foundations to soil liquefaction. A main component of this research was to conduct dynamic centrifuge tests on saturated sand deposits on which model bridge pier foundations were placed.

Figure 4. A satellite image of the bridge site

Figure 5. A view of the two railway bridges

Figure 6. Liquefaction induced sand boils at the bridge site

Coelho et al. (2007) investigated the behaviour of sandy soils of different relative density subjected to earthquake loading in dynamic centrifuge tests. Soil layers of 18m thickness at three different relative densities (50%, 60% and 80%) were subjected to sinusoidal earthquake loading of about 0.15g. The excess pore pressures recorded near

Figure 7. Earthquake-induced excess-pore-pressure generation in level sand beds (Coelho et al, 2007). (a) RD = 50% (b) RD = 80%

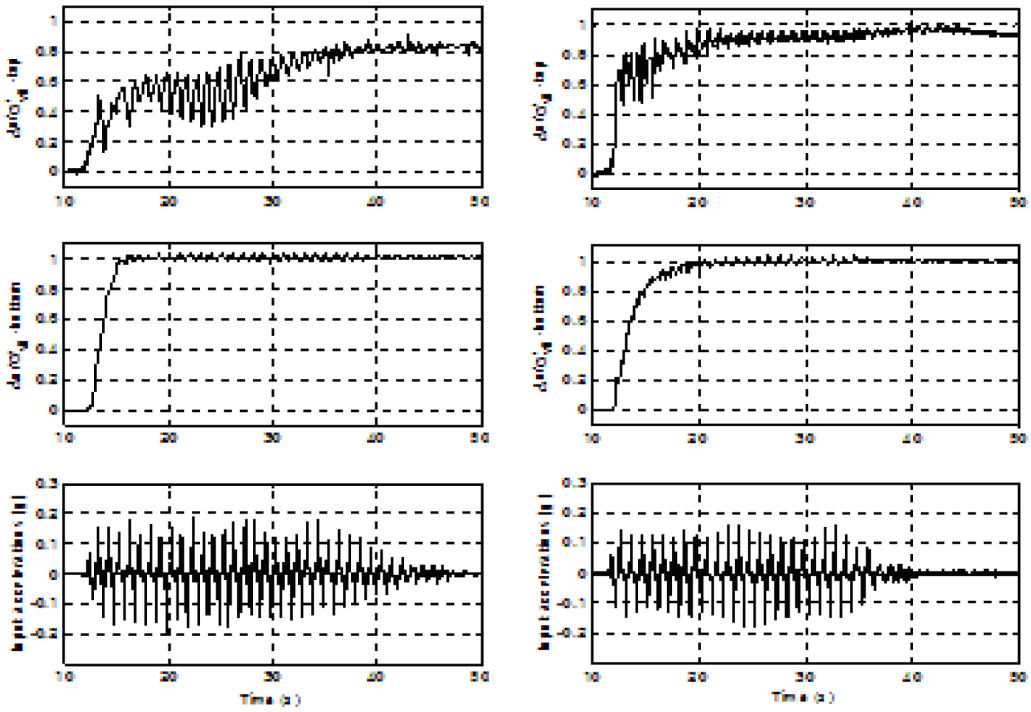

the surface and at the base of the level sand beds for two relative densities are shown in Figure 7, along with the input motion. It was concluded based on this study that uniform sand deposits at any of these relative densities reached the full liquefaction condition (i.e. $r_u = 1$). The only difference is that the denser deposits show a slightly slower rate of excess pore pressure generation compared to looser deposits which liquefy in the first few cycles of shaking.

However, when bridge foundations are present on identical soil beds, the foundations on denser deposits suffered much smaller settlements. The model bridge piers applied a bearing pressure of 100 kPa during the centrifuge test. The vertical settlements suffered by the bridge foundation are presented in Figure 8 along with the respective input motions applied. In this figure it can be seen that the foundation on a saturated loose sand layer (RD = 50%) suffered a settlement of about 0.55m at prototype scale while the foundation on a saturated dense sand layer (RD = 80%) suffered a settlement of only 0.1m. Clearly the settlement of the foundation is much smaller for the dense sand case.

FINITE ELEMENT ANALYSES

The same boundary value problem of the bridge foundation tested in the dynamic centrifuge tests was also analysed using SWANDYNE, Chan (1988). DIANA-SWANDYNE-II (Dynamic Interaction and Nonlinear Analysis-SWANsea DYNamic version II), or simply SWANDYNE, is a two-dimensional FE code created to perform static, consolidation and dynamic analysis in Geomechanics. The code uses a full effective stress-based framework to properly model the dynamic behaviour of saturated soil. The solid and pore-

Figure 8. Settlement of bridge foundations

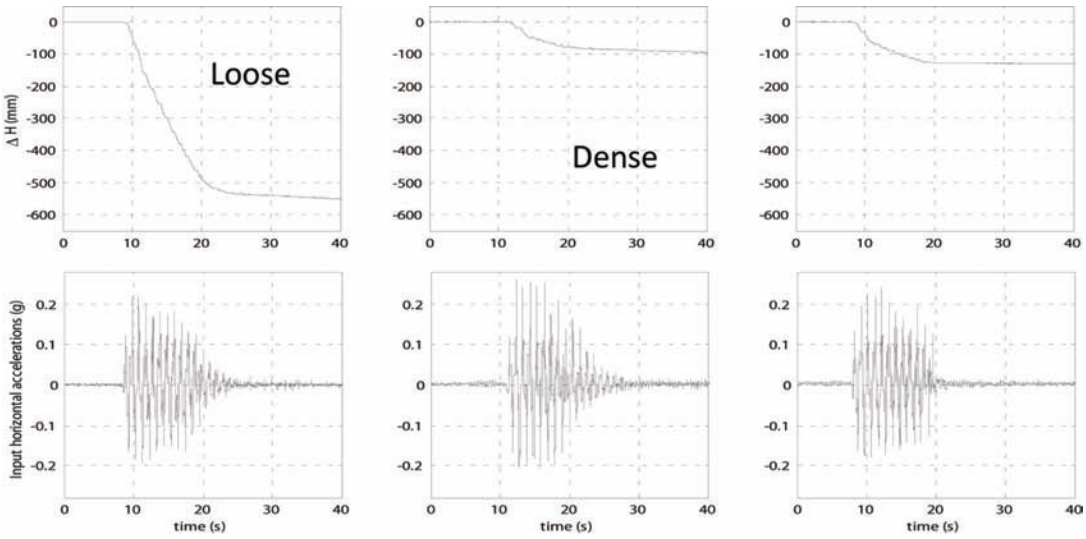

fluid dynamic interaction is established through a simplified form of the fully-coupled large-strain equations, termed dynamic u-p formulation. Integration is performed using the Generalized Newmark Single-Step integration scheme.

The performance of SWANDYNE, employing P-Z-III as the soil model, when carrying out liquefaction analysis has been satisfactorily validated by simulating the dynamic behaviour of different centrifuge experiments (Madabhushi and Zeng, 1998, 2006, 2007). The value of SWANDYNE was particularly demonstrated when modelling centrifuge experiments performed in VELACS project, Madabhushi and Zeng (1993).

The constitutive model parameters for PZ-III model were calibrated using the centrifuge test data from the loose, level sand bed test series shown in Figure 7. All the FE analysis results reported in this article are for an 18m deep, loose sand layer and are presented at prototype scale. In Figure 9 the FE discretisation used in these analyses is presented. A series of FE analyses were carried out for different bearing pressures applied by the bridge foundation on to the foundation soil for a sinusoidal input motion of 0.1g. In Figure 10, the time histories obtained from the FE analyses for 0 kPa, 40 kPa and 80 kPa bearing pressures are presented. In this figure it can be seen that the acceleration of the footing reduces dramatically after the first few cycles of shaking. The excess pore pressures build up quickly and reach full liquefaction level. For the case of higher bearing pressures, the excess pore pressures show a drop after about 20 s of shaking. This is due to the monotonic shear developing in the foundation soil as the footing settles into the liquefied soil. The monotonic shear will invoke a dilatant behaviour in the liquefied soil as the stress path crosses the PTL or CSL lines described earlier. This is manifested as a drop in excess pore pressure. The PZ-III soil model is able to capture this behaviour very well. Similarly the footing settlements increase with increased bearing pressure i.e. about 1.8m for 40 kPa bearing pressure and about 2.1m for 80 kPa bearing pressure. These are much larger than for the case of no footing (0 kPa) which suffers only a settlement of 0.2m due to contraction of the soil.

In Figure 11, the excess pore pressure ratio r_u contours 20 s into the earthquake shaking are presented for the three bearing pressures, namely 0, 40 and 80 kPa. The deformed mesh is also overlaid onto to the contours. In this figure it can

Figure 9. FE discretisation

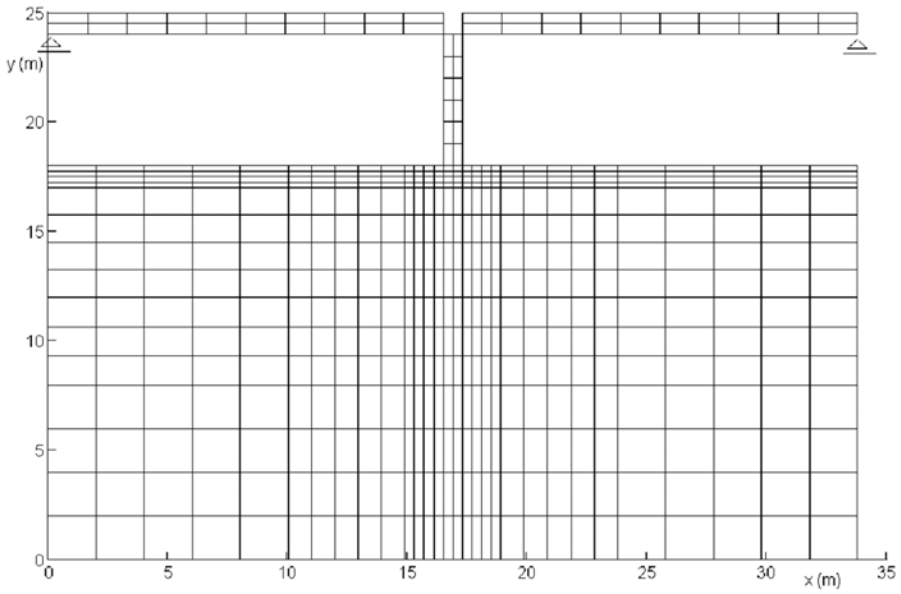

be seen that, for no footing case, the whole soil bed is fully liquefied. For the case of 40 kPa bearing pressure, the r_u contours indicate that a zone of dilation develops underneath the footing, indicated by the darker contours (refer to gray scale on the side colour bar). This zone of dilation extends much deeper for the case of 80 kPa bearing pressure. It is logical that the heavier footing should mobilise shear to a deeper level and this aspect is well captured by the FE analysis.

The nodal displacement information obtained during the FE analysis can be used to create plots of the displacement vectors. Such images can be plotted between any two instants. In Figure 12, the displacement vectors are plotted comparing the post earthquake positions to pre earthquake positions of all nodes in the FE mesh. As before, these are done for the three bearing pressures i.e. 0, 40 and 80 kPa. For the no footing case (0 kPa) the displacement vectors suggest that the soil settles vertically except at the boundaries, where some lateral movement is detected. In the presence of the footing, the displacement vectors show the movement of the soil from below the footing outwards into the free-field. These displacement vectors increases in magnitude for the case of heavier footing (80 kPa) compared to the lighter footing (40 kPa) as seen in Figure 12.

The centrifuge test results and subsequent FE analyses show that it is possible to investigate the soil behaviour during liquefaction and make reasonable predictions of the settlements suffered by the foundations of bridges. In the next section of the article, the Bachau-Vondh railway bridges will be considered in the immediate aftermath of the Bhuj earthquake of 2001. It will be argued that the super-structure stiffness has an important role to play in how the soil-structure system behaves, once the foundations suffer liquefaction.

ROTATION OF A PLATE GIRDER BRIDGE

The foundation soil at the site of the plate girder bridge showed signs of liquefaction, as indicated by the sand boils seen in Figure 6. The plate girder bridge introduced earlier, suffered some rotation

Figure 10. Time series comparison for different footing pressures (a) footing pressure = 0 kPa (b) footing pressure = 40 kPa (c) footing pressure = 80 kPa

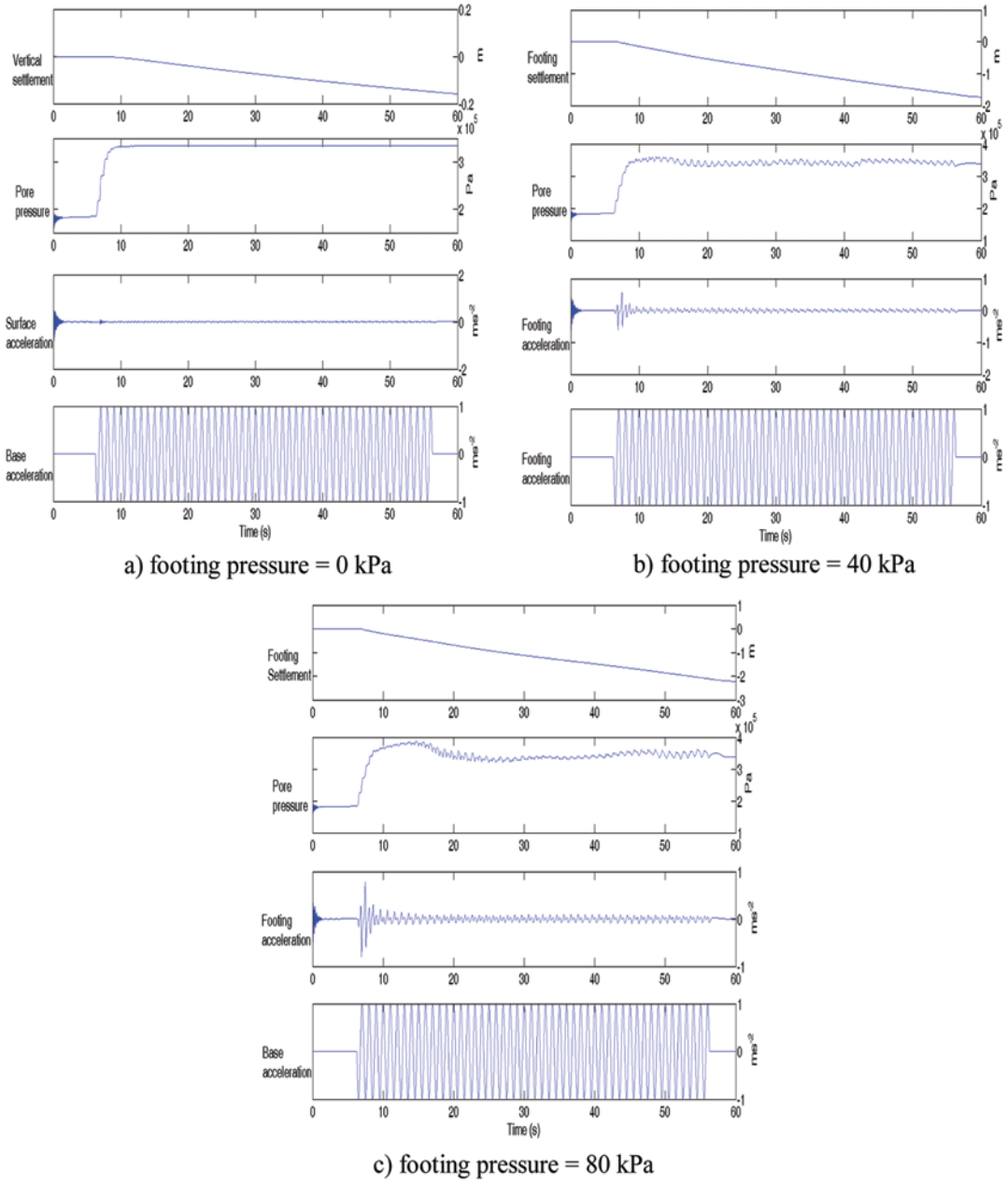

a) footing pressure = 0 kPa

b) footing pressure = 40 kPa

c) footing pressure = 80 kPa

about the longitudinal axis. This can be seen by observing the position of successive piers as seen in Figure 13 as recorded during the post earthquake visit, Madabhushi et al. (2005). The amount of rotation is relatively small. In order to understand this behaviour, the plate girder bridge is considered in some detail. The elevation and cross-sectional views of this bridge are presented in Figure 14,

Figure 11. Excess pore pressure contours for different footing pressures (a) footing pressure = 0 kPa (b) footing pressure = 40 kPa (c) footing pressure = 80 kPaFigure 9. FE discretisation

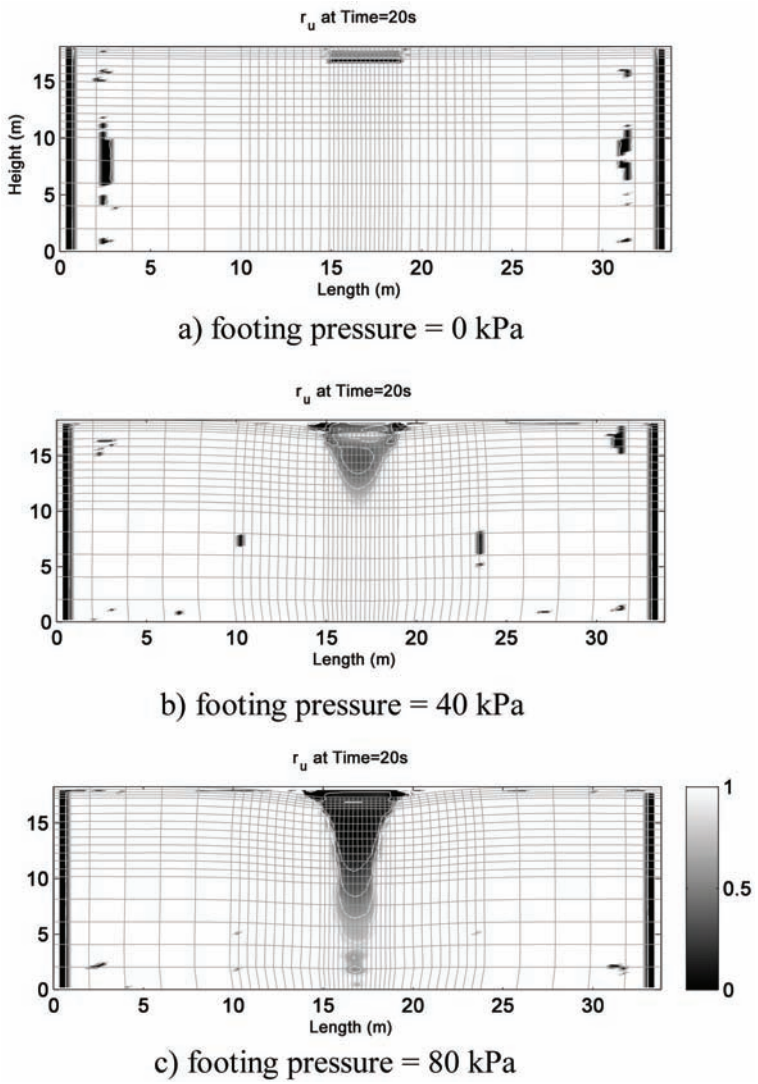

along with approximate dimensions. The bridge has 7 spans, each 7.2m long with the total length of the bridge being 50.4m. The decks carrying the broad gauge railway (1.676m between rails) are formed from two I-sections each approximately 533 × 210 × 122 made from 21.3 mm thick steel plate. The moment of inertia I_{yy} = 3388 cm^4 and the cross-sectional area of each I-section is 155 cm^2. The Young's modulus of steel may be taken as 210 GPa.

In Figure 13 the piers show relative rotation about the longitudinal axis of the bridge, i.e. about the cross-section of the pier shown in Figure 14a. The piers did not suffer any rotation about the shorter section shown as elevation in Figure 14c, which would have offered much smaller resistance to rotation once the foundation soil has suffered

Figure 12. Displacement vectors showing the soil displacements at the end of the earthquake loading (a) footing pressure = 0 kPa (b) footing pressure = 40 kPa (c) footing pressure = 80 kPa

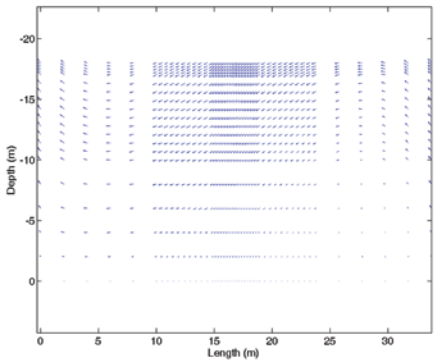

a) footing pressure = 0 kPa

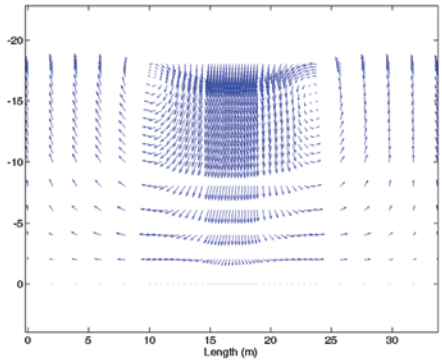

b) footing pressure = 40 kPa

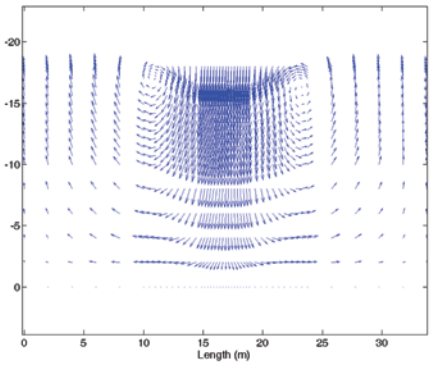

c) footing pressure = 80 kPa

liquefaction. The reason for this is that when the foundation tries to rotate in this direction, the axial stiffness of the bridge deck resists the rotation. The axial stiffness *EA* of the I-sections is quite high. This is particularly true given the short span lengths that prevent any out of plane buckling. When the piers try to rotate about the cross-section, the bridge deck suffers bending. If all the piers try to rotate then the bridge deck can only prevent this with its lateral bending stiffness.

Assuming that the two I-sections act in unison, i.e. that they are tied together by the cross-bracing and the sleepers, the lateral bending stiffness can be estimated as follows:

Figure 13. Rotation of the piers

Moment of Inertia

$$I = 2I_{yy} + Ay^2 = 2 \times 3388 + 155 \times \left(\frac{1.676 \times 100}{2}\right)^2 \text{ cm}^4 \quad (2)$$

$I = 0.0109$ m^4

Flexural stiffness

$$EI = 210 \times 10^9 \times 0.0109 = 2.3 \times 10^9 \text{ Nm}^2 \quad (3)$$

Lateral bending stiffness

$$K_{plate} = \frac{384EI}{5L^4} = \frac{384 \times 2.3 \times 10^9}{5 \times 50.4^4} = 27375.8 \text{ N/m} \quad (4)$$

So, the lateral stiffness can be taken as 27.4 kN/m.

This simple calculation assumes the loading imposed on the bridge deck is uniformly distributed. Better estimates can be made by assuming that concentrate loads act laterally on the deck at each of the pier locations.

Figure 14. The crown of the arch repaired by resin-injection

The lateral bending stiffness of the plate girder bridge is quite small in comparison to the axial stiffness ($2 \times EA$ = 3.255 GNm^2) or the Euler buckling load of each span. So when the piers try to rotate about their cross-sectional axis, the superstructure i.e. bridge deck offers least resistance.

SPREADING OF AN ARCH BRIDGE

The arch bridge supporting the second railway line is next to the plate girder bridge as seen in Figures 4 and 5. This is also a 7 seven span bridge and the span lengths match the plate girder bridge. The foundations of arch bridge also suffered liquefaction. However, the arch bridge expresses a totally different type of distress as shown in Figures 15 and 16. In these figures it can be seen that the arch suffered cracking at its crown and at the join with support piers. This type of damage can result by the settlement of the pier relative to the abutment. Once the piers suffer differential settlement, the arch accommodates these by opening cracks at the crown and at the supports. The soil movement that

Figure 15. Cracks at thrust lines on support piers repaired by resin-injection

allows the pier foundations may be as indicated by soil displacement vectors obtained from the FE analysis shown in Figure 12.

It is interesting to consider why the piers of the arch bridge did not show any rotation but rather chose to suffer settlements, once the foundation soil has liquefied. The cross-section and elevation of the arch bridge along with approximate dimensions are presented in Figure 14b and d. The lateral bending stiffness of the arch bridge can be computed following similar procedure as

Figure 16. Approximate sections of the two bridges (a) Cross-section of the plate girder bridge (b) Cross-section of the arch bridge (c) Sectional view of the plate girder bridge (d) Sectional view of the arch bridge

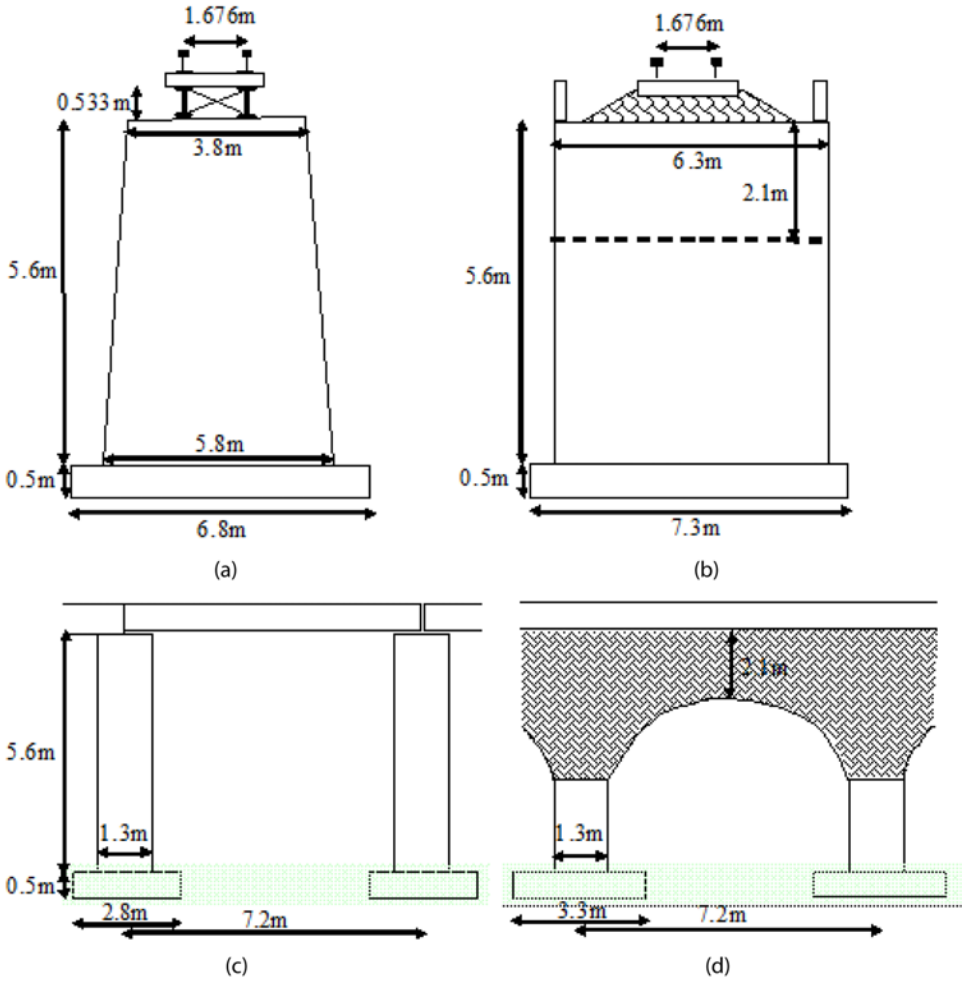

before. In these calculations it is necessary to assume that the end thrust from the abutments will keep the masonry forming the arch in compression along all sections. Also the cross-section of the arch shown in Figure 14b is transformed into a smaller section that is 2.1 m deep × 6.3 m wide, to allow for the reduction in cross-section of the arch as one moves from the supports to the crown. This is a conservative assumption. Similarly, the Young's modulus of stone is taken as 20 GPa, (Ashby, 1992).

Moment of Inertia

$$I = \frac{1}{12} bd^3 = \frac{1}{12} \times 2.1 \times 6.3^3 = 43.8 \text{ m}^4 \quad (5)$$

Flexural stiffness

$$EI = 20 \times 10^9 \times 43.8 = 876 \times 10^9 \text{ Nm}^2 \quad (6)$$

Lateral bending stiffness

$$K_{arch} = \frac{384EI}{5L^4} = \frac{384 \times 876 \times 10^9}{5 \times 50.4^4 \times 1000} = 10426.7 \text{ kN/m} \quad (7)$$

So, the lateral stiffness of the arch bridge is 380 times larger than that of the plate girder bridge. When the foundation soil liquefies, the arch bridge will resist any attempt by the piers to rotate about the longitudinal axis of the bridge. However, when the piers settle into the foundation soil, the arch can suffer cracks at crown and supports as seen in Figs.15 and 16.

These calculations of bending stiffness are rather simple, but sufficient to illustrate that the super structural stiffness of the bridge influences the failure mechanism suffered by the foundation. A corollary to this statement, that may have more significant impact on liquefaction behaviour, is that once the foundations suffer liquefaction, the superstructure will try to fail in a mode that offers least resistance. For the plate girder bridge this may be rotation of piers while for arch bridge this may be the settlement of piers. It is therefore necessary to understand all the possible failure mechanisms so that the liquefaction resistant design may attempt to prevent each of these failure modes.

CONCLUSION

Soil liquefaction results in extensive damage to a wide variety of civil engineering structures. Foundations may suffer severe settlement and/or rotation. In this article examples of foundation failures that were observed during many recent earthquakes are presented. In particular the case two railway bridges at the Bachau-Vondh bridge site is considered in detail. Recent research findings firstly based on dynamic centrifuge tests on bridge foundations are presented that indicate significant excess pore pressures being generated in both loose and dense sands. However, it was shown that the settlements suffered by the bridge foundations on denser deposits were significantly smaller than those on loose deposits. Finite element analyses were carried out that are based on soil models calibrated against the dynamic centrifuge test data. It was shown that the finite element analyses were able to capture some of the key issues of soil dilation below the foundations. Finally the deformation mechanisms that were exhibited by the plate girder and arch bridges were considered in detail. It was argued that the deformation of the foundations is influenced by the superstructure stiffness.

REFERENCES

Ashby, M. F. (1992). *Materials selection in mechanical design.* London: Pergamon Press.

Chan, A. H. C. (1988). *User manual for DIANA SWANDYNE-II*. Department of civil engineering, University of Glasgow, UK.

Coelho, P.A.L.F., Haigh, S.K., Madabhushi, S.P.G., & O'Brien, A.S. (2007). Post-earthquake behaviour of footings when using densification as a liquefaction resistance measure. *Ground Improvement Journal – Special Issue on Ground Improvement techniques, 11*(1), 45-53.

Free, M., May, R., & Teymur, B. (2003). Geological and Geotechnical Aspects, The Kocaeli, Turkey Earthquake of 17 August 1999. In D'Ayala & Free (Ed.), *A field report by EEFIT* (pp. 81-121). London, UK: Institute of Structural Engineers.

Ishihara, K. (1993). Liquefaction and flow failure during earthquakes. *Geotechnique*, *43*(3), 351–415. doi:10.1680/geot.1993.43.3.351

Luong, M. P., & Sidaner, J. F. (1981). Undrained behaviour of cohesionless soils under cyclic and transient loading. In *Proceedings of the Int. Conf. Rec. Advances in Geotechnical Earthquake engineering and soil dynamics* (Vol. 1.) (pp. 215-220), St Louis, MI.

Madabhushi, S. P. G. (2007). Geotechnical Aspects of the 921 Ji-Ji earthquake of Taiwan. *EEFIT Report* (pp. 14-38). London, UK: Institution of Structural Engineers.

Madabhushi, S. P. G., Knappett, J. A., & Haigh, S. K. (2009). *Design of pile foundations in liquefiable soils*. Imperial College Press. ISBN 978-1-84816-362-1.

Madabhushi, S. P. G., Patel, D., & Haigh, S. K. (2005). Geotechnical Aspects of the Bhuj Earthquake. *EEFIT Report*. London, UK, Institution of Structural Engineers. ISBN 0901297 372.

Madabhushi, S. P. G., & Zeng, X. (1993). An analysis of the seismic behaviour of quay walls. In K. Arulanandan & R.F. Scott (Ed.), *Proceedings Verification of Liquefaction Analyses by Centrifuge studies*, (VELACS), (Vol. 2), Davis, California.

Madabhushi, S. P. G., & Zeng, X. (1998). Behaviour of gravity quay walls subjected to earthquake loading. Part II: Numerical Modelling. *Journal of Geotechnical Engineering*. *American Society of Civil Eng.*, *124*(5), 418–428.

Madabhushi, S. P. G., & Zeng, X. (2006). Seismic Response of Flexible Cantilever Retaining Walls with Dry Backfill, *Geomechanics and Geoengineering*. *International Journal (Toronto, Ont.)*, *1*(4), 275–290.

Madabhushi, S. P. G., & Zeng, X. (2007). Simulating Seismic Response of Cantilever Retaining Walls with Saturated Backfill. *ASCE Journal of Geotechnical and GeoEnv. Engineering*, *133*(5), 539–549.

Schofield, A. N. (1981), Dynamic and earthquake geotechnical modelling, *Proc. Int. Conf. Rec. Advances in Geotechnical Earthquake engineering and soil dynamics*, St Louis, Vol.3., pp 1081-1100.

This work was previously published in International Journal of Geotechnical Earthquake Engineering, Volume 1, Issue 1, edited by T.G. Sitharam, pp. 70-87, copyright 2010 by IGI Publishing (an imprint of IGI Global).

Chapter 6
DEM Simulations in Geotechnical Earthquake Engineering Education

J. S. Vinod
University of Wollongong, Australia

ABSTRACT

Behaviour of geotechnical material is very complex. Most of the theoretical frame work to understand the behaviour of geotechnical materials under different loading conditions depends on the strong background of the basic civil engineering subjects and advanced mathematics. However, it is fact that the complete behaviour of geotechnical material cannot be traced within theoretical framework. Recently, computational models based on Finite Element Method (FEM) are used to understand the behaviour of geotechnical problems. FEM models are quite complex and is of little interest to undergraduate students. A simple computational tool developed using Discrete Element Method (DEM) to simulate the laboratory experiments will be cutting edge research for geotechnical earthquake engineering education. This article summarizes the potential of DEM to simulate the cyclic triaxial behaviour of granular materials under complex loading conditions. It is shown that DEM is capable of simulating the cyclic behavior of granular materials (e.g. undrained, liquefaction and post liquefaction) similar to the laboratory experiments.

DOI: 10.4018/978-1-4666-0915-0.ch006

INTRODUCTION

Geotechnical Earthquake Engineering is a branch of civil engineering which deals with soil, rock and underground water and their relation to the design, construction and operation of engineering projects during dynamic loading. Sound knowledge in engineering mechanics, mechanics of solids, vibrations and fluid mechanics is a pre- requisite to this branch of civil engineering. However, the behaviour of geotechnical material is often complex and theoretical background developed with the aid of advanced mathematics is not sufficient to understand its true nature. In addition, most of the students have difficulty in bridging the results of the laboratory experiments to the theoretical component. Many students would not grasp the underlying mechanics involved in the different laboratory experiments. This may be partially due to the fact that the students during the lectures learn theories and methods for the design, while the lab testing focuses on studying the response of small elements or samples.

In the recent past, several researches have been carried out to improve the geotechnical engineering education through educational websites and internet based virtual labs (Budhu, 2002, Arduino et al. 2002, Elgamal et al. 2005). Such learning environment greatly facilitates the (1) efficient use of time and resources, (2) flexibility in accessing information, and (3) convenience of self-paced learning with the aid of physical models (Soh and Gupta 2000). Nowadays, computational modeling using Finite Element Method (FEM) is widely adopted to understand the behaviour of complex geotechnical problems. For undergraduate program this FEM modeling is of little interest due to the complexity of common computational models that make use of the Finite Element Method. In addition, these students usually lack the background that is required to implement such methods. A viable solution is to introduce relatively simpler numerical tool such as Discrete Element Method (DEM) to simulate the basic laboratory experiments. DEM models the soil as a collection of discrete particles (Figure 1) rather than continuum (Sitharam et al., 2005). Moreover, DEM model treats individual particles separately and the particle movements are captured by Newton's second laws motion.

Figure 1. (a) 2 D view of initially generated assembly without overlaps (Sitharam et al, 2005) (b) 3 D view of initially generated assembly without overlaps (Sitharam et al, 2005)

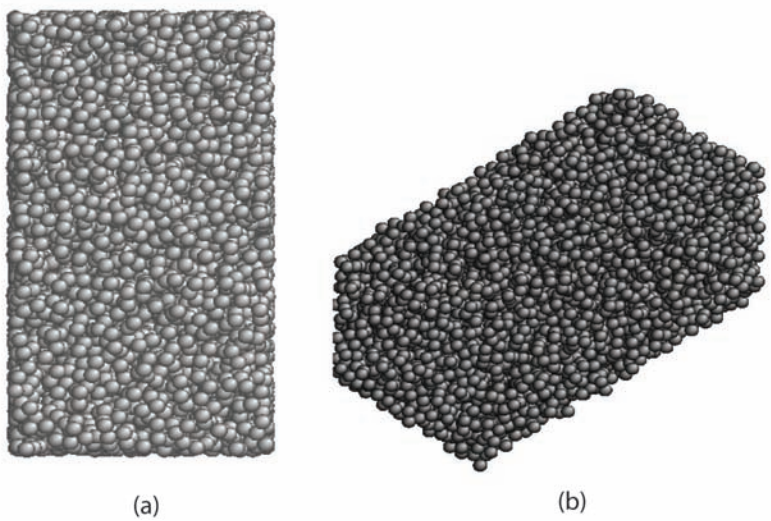

The contact force developed between the particles is computed using simple spring, dashpot model. The advantage of using DEM-based models is that the underlying physics are clearly resolved and the models are inherently discontinuous and heterogeneous (EL Shamy, 2006). Recently, DEM has been implemented in education at the graduate level (You, 2005) and has emerged as a powerful illustrative tool (Lobo-Guerrero and Vallejo 2006). This article highlights the potential of DEM to simulate the cyclic triaxial test, one of the most widely used equipment in geotechnical earthquake engineering.

Discrete Element Method

Discrete element method is pioneered by Cundall and Strack (1979), which employs an explicit finite difference scheme and can handle particles of different shape. The discrete numerical simulation predicts the overall behaviour of the assembly due to cumulative effect of all particle to particle interactions in the assembly. This method is based on the strict modeling of the granular media at the grain scale level. The advantage with this method is that it has flexibility in facilitating the isolation of the effects and influences of the loading configurations, particle parameters such as size distribution, shape, roughness and physical properties in relation to the mechanical behaviour of the assembly. The discrete numerical simulation has been used to have an insight into the micromechanical behaviour of the granular assembly to facilitate the development of a micromechanical based constitutive model for granular materials. The fundamental idea of DEM is that each particle is modeled as an element obeying Newton's second law of motion. Equilibrium contact forces and displacements are found in a stressed assembly of particles through a series of calculations tracing the movement of each particle. The movement of each particle is tracked by solving a set of Newton's equation of motion. A contact force generates when the elements overlap and the magnitude of contact force is determined by the force-displacement law. Coulomb's friction law is adopted for the relative slippage between elements. A suitable damping in the form of Rayleigh damping is incorporated to dissipate the kinetic energy generated. The resultant force vector on each element is the vectorial sum of contact forces. The law of motion is applied to each sphere during the time step. The particle accelerations, velocities and displacements are obtained by integrating the law of motion and are assumed to be constant over a time step. During the next time step, new set of contact forces on a sphere particle is obtained from force-displacement law and the cycle of calculation will continue. Force boundary conditions, displacement boundary conditions and gravitational loads can be applied on the system. A typical calculation cyclic is shown in Figure 2. In DEM, internal stresses and contact behavior can be captured efficiently, and sample reproducibility is guaranteed. The major advantage is the wealth of micromechanical and statistical information that can be generated by the DEM simulations along with the macroscopic response.

Undrained Behaviour of Granular Materials

The undrained behavior of isotropically consolidated saturated sand during monotonic loading is characterized by development of the excess pore water pressure which, in turn, leads to different forms of undrained (liquefaction) responses. Such behavior featuring a positive build up in excess porewater pressure yields a contractive response. The growth of the excess porewater pressure continues until reaching a stable value corresponding to the lowest value of undrained resistance of the sand, known as its steady state strength. Moreover, the sand shows continuous large deformation under constant effective confining pressure, constant shear stress, and constant rate of shear strain. Such behavior of sand is known as complete liquefaction (Kramer, 1995). However, liquefied

Figure 2. A typical calculation cycle (Vinod, 2006)

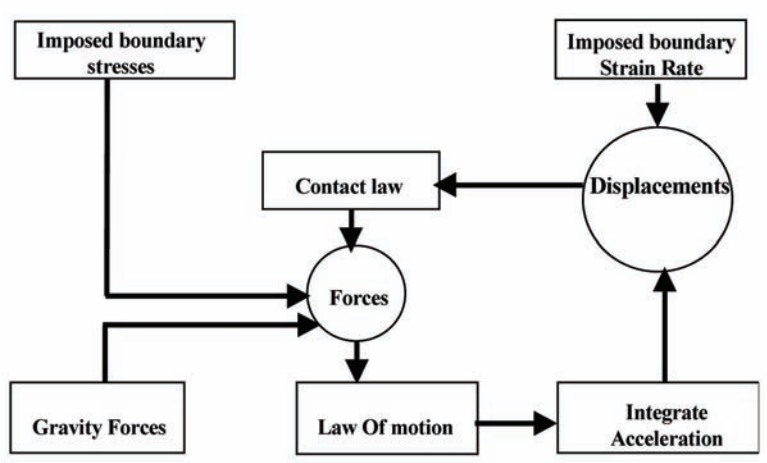

sands may exhibit a large increase followed by a decrease in the excess pore water pressure which results in dilative response. Such behavior is a consequence of the higher relative density of the sand. Figure 3 shows a typical undrained DEM simulation results in the form of stress ratio (q/p) and excess pore pressure increment (δu) with axial strain for a confining pressure of 50 kPa. Excess pore pressure has been computed from the difference between undrained (effective) and drained (total) stress path during shear deformation. The undrained tests (constant volume test) are carried out keeping the volume of the sample constant during shearing. Similar attempt has also been done to carry out undrained tests using DEM (Sitharam et al., 2002 and Sitharam, 2003). The trends of numerical results match closely with undrained experimental test results on real sands (Sitharam & Vinod, 2009).

Cyclic Behaviour of Granular Materials

Liquefaction is more likely to occur in cyclic loading than during static loading. During cyclic loading (e.g. earthquake loading) almost all saturated soil will develop positive pore water pressure due to contractive response of sand at small strains. Sitharam and Vinod (2008) carried out extensive DEM simulations to capture the liquefaction behaviour of granular materials using DEM during strain controlled cyclic loading condition. Due to the constant application of cyclic loading, there is a gradual and steady decrease in mean principal and deviator stress which finally goes to zero (Figure 4). This steady decrease in the deviator stress is due to the development of the excess pore water pressure during cyclic loading in undrained conditions. In addition, Figure 5 shows the plot of deviator stress, *(q)* versus deviatoric strain, which shows a steady decrease in deviator stress with repeated application of cyclic strain amplitudes.

The variation of pore water pressure ratio ($U = u_{max}/\sigma_3$) with number of cycles is presented in Figure 6. Also presented in this figure the variation of, micromechanical parameter, average coordination number with number of cycles. The average coordination number, $\gamma = M/N$, of the assembly is defined as the ratio of total number of contact points (M) within the assembly volume (V) to the total number of particles (N) in the assembly. Sitharam and Vinod (2008) reported that the pore water pressure slowly builds up with number of cycles due to the application of cyclic

Figure 3. Plot of stress ratio and excess pore pressure increment for a confining pressure of 50 kPa (Sitharam & Vinod, 2009)

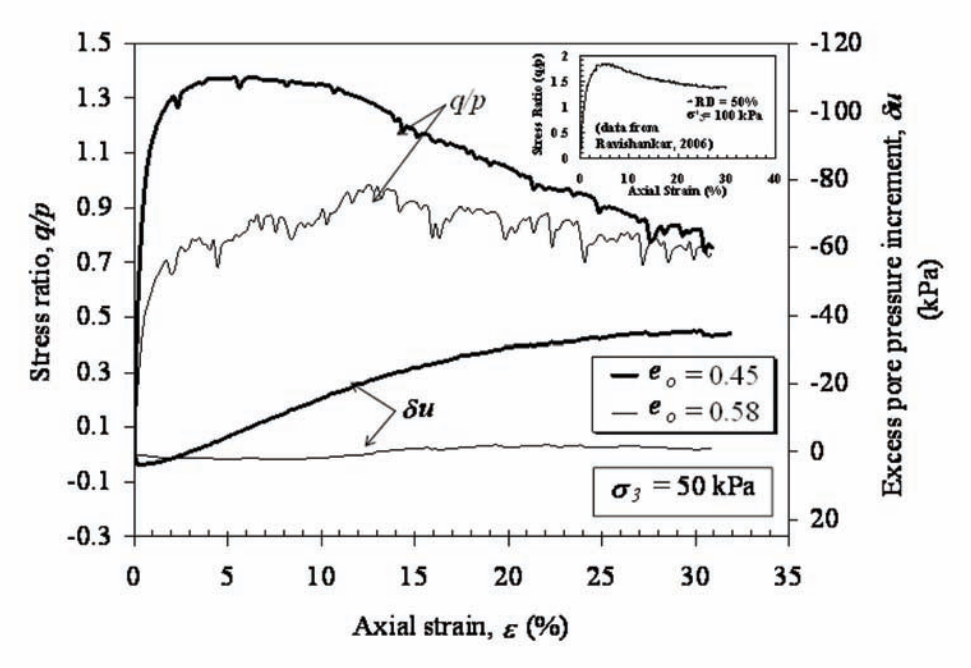

Figure 4. Plot of deviator stress with mean p for a confining pressure of 25 kPa (Sitharam & Vinod, 2008)

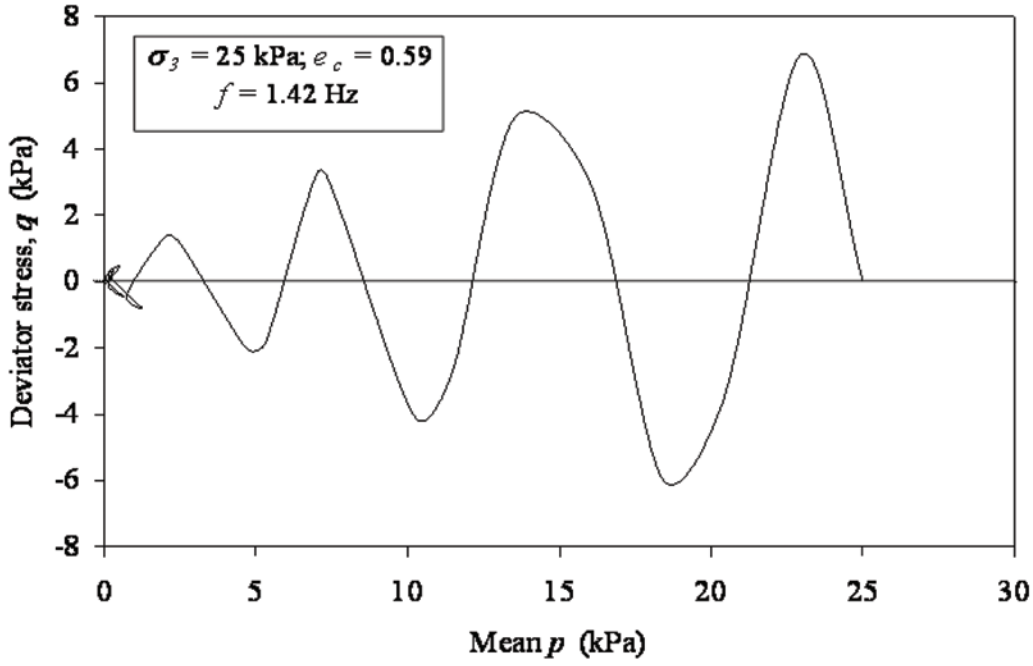

Figure 5. Plot of deviator stress with deviatoric strain at a confining pressure of 25 kPa (Sitharam & Vinod, 2008)

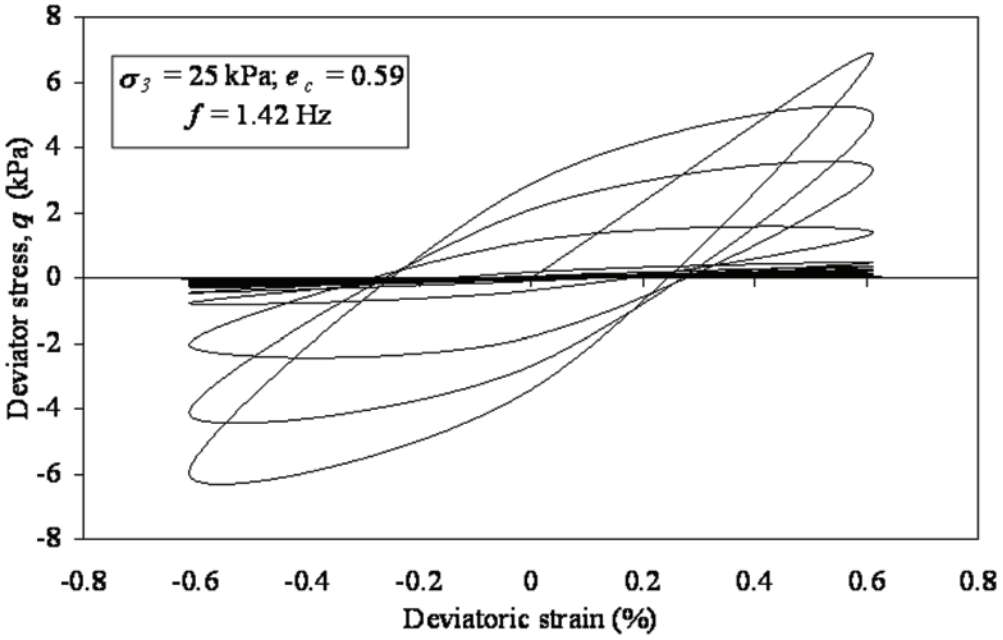

strain amplitude (Figure 6). This of course has a major influence on the particle to particle contacts. As expected, a steady decrease in the average coordination number with increase in the increase in the number of cycles can be observed, which in turn decreases the effective stress. Moreover, a sudden collapse in the assembly beyond a value of average coordination number equal to 3 can be observed, which again corresponds to a pore pressure ratio of 1. This steady decrease in average coordination number is attributed to the development of pore pressure during constant cyclic strain application on the sample in undrained condition. This process of strength reduction (effective stress approaching to zero) due to the application of cyclic loading and this is termed as liquefaction.

Figure 7 presents the results of an average coordination number with deviator stress for a confining pressure of 25 kPa. As observed from the figure, there is a reduction in the deviator stress and average coordination number with successive number of cycles. This reduction in the deviator stress is due to the development of excess pore water pressure, which there by reduces the number of contacts in the assembly. Decrease in the number of contacts per particle can be observed both on the compression and extension loading stage. Reduction in average coordination number and deviator stress is observed up to a value of average coordination number equal to 3. There after the assembly is seen not with standing any stresses and the internal structure collapses undergoing liquefaction.

These numerical simulation results highlight the potential of DEM to simulate the realistic behaviour of undrained cyclic response of granular media and have simulated the liquefaction behaviour of granular media very well.

Figure 6. Plot of average coordination number with number of cycles at a confining pressure of 25 kPa (Sitharam & Vinod, 2008)

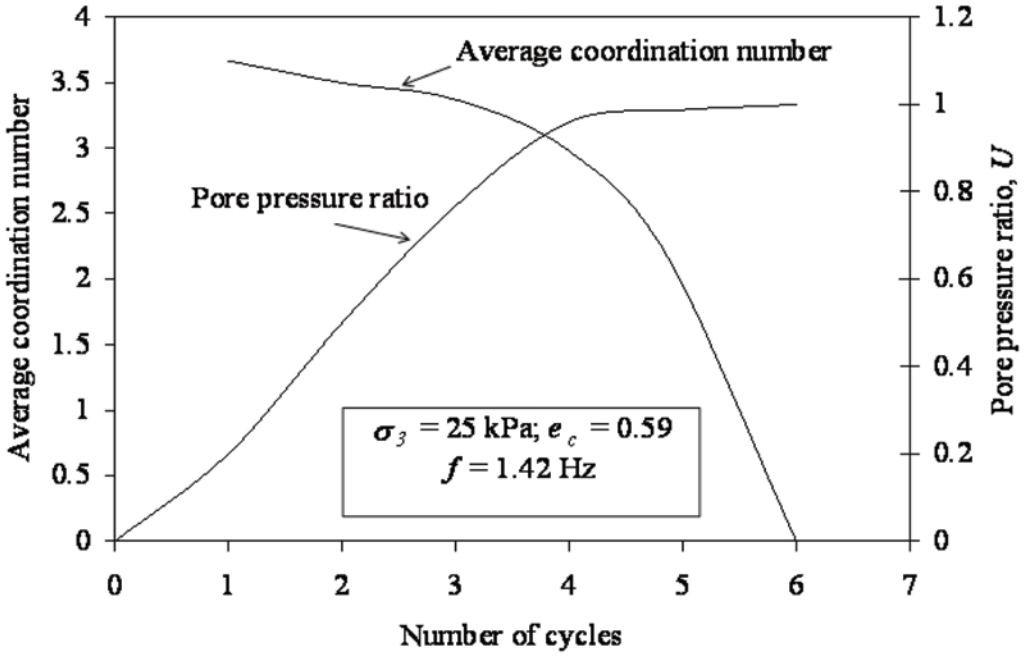

Figure 7. Variation of average coordination number with deviator stress at a confining pressure of 25 kPa (Sitharam & Vinod, 2008)

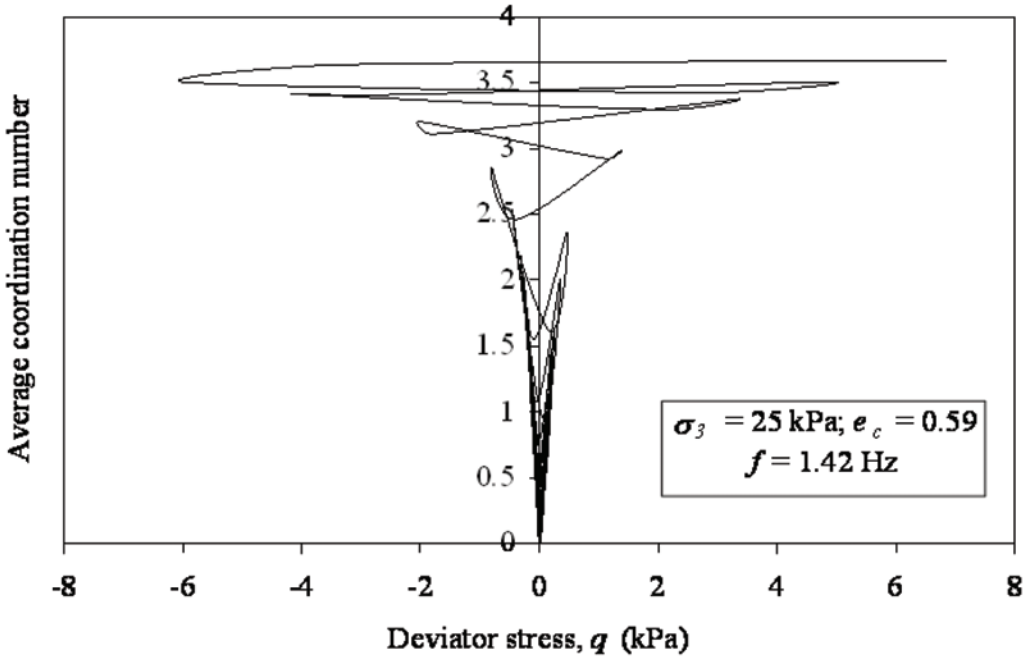

Figure 8. Post liquefaction undrained monotonic response with and without drainage after liquefaction: Variation of deviator stress with Mean p

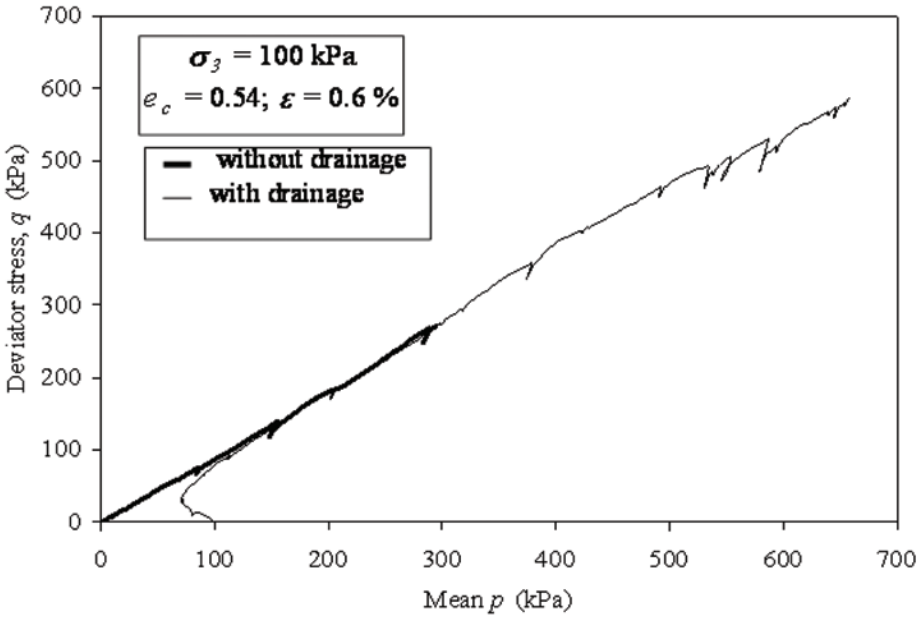

Post - Liquefaction Behaviour of Granular Materials

The vital information required for the evaluation of earthquake induced settlements is the stress-strain response of post-liquefied sands. Moreover, the assessment of post earthquake undrained stress-strain behaviour will allow the designer to predict the potential resistance of liquefied sand, to sustain monotonically increasing post earthquake loading. So far, undrained laboratory experiments on representative sand samples are the only way to assess the post liquefaction undrained stress-strain response. Sitharam et al., (2009) reported the results of laboratory and DEM simulations on an assembly of granular materials to study the influence of different parameters such as amplitudes of axial strain, confining pressure, and density on the post liquefaction undrained monotonic behaviour of granular materials with and with- out drainage after liquefaction. In addition, DEM simulations have been carried out on an assembly of spheres to simulate post liquefaction behaviour. The simulations were very similar to the experiments with an objective to understand the behaviour of monotonic strength of liquefied samples from the grain scale. A typical DEM simulation result capturing the post liquefaction undrained monotonic behaviour with and with drainage after liquefaction is presented in Figure 8. It has been presented that the DEM simulations have captured qualitatively all the features of the post liquefaction undrained monotonic response in a manner similar to that of the experiments (Sitharam et al., 2009).

CONCLUSION

This article explores the potential of discrete element method in simulating the cyclic triaxial behaviour of granular materials. The use of this

tool motivates the students to understand the underlying mechanism during cyclic loading and associated soil response. Implementation of these numerical experiments can vary from being just in the form of a visual presentation by the instructor to an assignment given to students where they are asked to conduct the simulation. A more advanced utilization of DEM-based simulations may be further implemented for advanced courses in earthquake geotechnical engineering. In future, DEM tool can be effectively expanded to simulate several other dynamic tests such as cyclic simple shear test, torsional shear tests, wave propagation studies etc.

REFERENCES

Arduino, P., Miller, G. R., & Ogurinde, A. (2002). Live modeling of 1-D wave propagation in layered soil media. *Computer Applications in Engineering Education*, *9*(4), 248–258. doi:10.1002/cae.10003

Budhu, M. (2002). Virtual laboratories for engineering education. In *Proceedings of the International Conferance on Engineering Education* (CD-ROM), Manchester, U.K., International Network for Engineering Education and Research (INEER), Arlington, Va.

Chantawarungal, K. (1993). *Numerical simulations of three dimensional granular assemblies*. Ph.D. thesis, University of waterloo, waterloo, Ontario, Canada.

Cundall, P. A., & Strack, O. D. L. (1979). A discrete numerical model for granular assemblies. *Geotechnique*, *29*(1), 47–65. doi:10.1680/geot.1979.29.1.47

Elgamal, A., Fraser, M., & McMartin, F. (2005). On-line educational shake table experiments. *Journal of Professional Issues in Engineering Education and Practice*, *131*(1), 41–49. doi:10.1061/(ASCE)1052-3928(2005)131:1(41)

Kramer, S. L. (1996) *Geotechnical earthquake engineering*. New York: Prentice Hall.

Lobo-Guerrero, S., & Vallejo, L. E. (2006, February 26-March 1). DEM as an educational tool in geotechnical engineering. In *Proceedinhgs of the Geocongress 2006*, Atlanta, GA.

EL Shamy, U. (2006). DEM Based computational Lab for Geotechnical Engineering Education. *GeoDenver*, GSP 166.

Sitharam, T. G. (2003). Discrete element modeling of cyclic behaviour of granular materials. *Geotechnical and Geological Engineering*, *21*, 297–329. doi:10.1023/B:GEGE.0000006036.00597.0b

Sitharam, T. G., Dinesh, S. V., & Shimizu, N. (2002). Micromechanical modeling of monotonic shear behaviour of granular media using three dimensional DEM. *International Journal for Numerical and Analytical Methods in Geomechanics*, *26*, 1167–1189. doi:10.1002/nag.240

Sitharam, T. G., & Vinod, J. S. (2008). Numerical simulation of liquefaction and pore pressure generation in granular materials using DEM. *International Journal of Geotechnical Engineering*, *2*(2), 103–113. doi:10.3328/IJGE.2008.02.02.103-113

Sitharam, T. G., & Vinod, J. S. (2009). Critical state behaviour of Granular materials from isotropic compression and rebound paths: DEM simulations. *Granular Matter*, *11*(1), 33–42. doi:10.1007/s10035-008-0113-3

Sitharam, T. G., Vinod, J. S., & Ravishankar, B. V. (2009). Post liquefaction undrained monotonic behaviour of sands: Experiments and DEM simulations. *Geotechnique*.

Sitharam, T. G., Vinod, J. S., & Rothenburg, L. (2005). *Shear behavior of glass beads, International conference micromechanics of granular media. Powder and Grains* (pp. 257-260), University of Stuttgart, Germany.

Soh, C. K., & Gupta, A. (2000). Intelligent interactive tutoring system engineering mechanics. *Journal of Professional Issues in Engineering Education and Practice*, *126*(4), 166–173. doi:10.1061/(ASCE)1052-3928(2000)126:4(166)

Vinod, J. S. (2006). *Liquefaction and dynamic properties of granular materials: A DEM approach*. Ph.D. thesis, submitted to Indian Institute of science, Bangalore, India

You, Z. (2005, June 1-3). Introduction to discrete element method - a numerical method to engineering graduate students. In *Proceedings of the McMat2005, Joint ASME/ASCE/SES Conference on Mechanics and Materials*, Baton Rouge, LA.

This work was previously published in International Journal of Geotechnical Earthquake Engineering, Volume 1, Issue 1, edited by T.G. Sitharam, pp. 61-69, copyright 2010 by IGI Publishing (an imprint of IGI Global).

Chapter 7
Static and Dynamic Elastic Modulus of Jointed Rock Mass: Influence of Joint Frequency, Joint Inclination and Joint Factor

T. G. Sitharam
Indian Institute of Science, India

M. Ramulu
Central Mining Research Institute, India

V. B. Maji
Indian Institute of Technology, India

ABSTRACT

In this paper the compressive strength/elastic modulus of the jointed rock mass was estimated as a function of intact rock strength/modulus and joint factor. The joint factor reflects the combined effect of joint frequency, joint inclination and joint strength. Therefore, having known the intact rock properties and the joint factor, jointed rock properties can be estimated. The test results indicated that the rock mass strength decreases with an increase in the joint frequency and a sharp transition was observed from brittle to ductile behaviour with an increase in the number of joints. It was also found that the rocks with planar anisotropy exhibit the highest strength in the direction perpendicular to the anisotropy and the lowest at an inclination of 30^o-45^o in jointed samples. The anisotropy of the specimen influences the dynamic elastic modulus more than the static elastic modulus. The results were also compared well with the published works of different authors for different type of rocks.

DOI: 10.4018/978-1-4666-0915-0.ch007

1. INTRODUCTION

The behaviour of rock mass is largely influenced by the in-situ anisotropy and is different from other engineering materials. The assessment of the strength and deformation of rocks is essential for engineering design and analysis. The deformation modulus of a rock mass is an important input parameter in analysis of rock mass behaviour. Field tests to determine this parameter directly are time consuming and expensive. Therefore, several authors (references) have proposed empirical relations for estimating the rock mass deformation modulus on the basis of classification schemes. There are two elastic moduli, namely, static and dynamic. According to Ciccitti and Mulargia (2004) the values of the static modulus, in general, are 5-10% lower than those of dynamic moduli. The dynamic modulus of elasticity is very important when dealing with the problems like blasting.

The paper presents the study on the strength and deformation characteristics of jointed rock by conducting laboratory tests on cylindrical specimens of plaster of Paris (POP) by introducing artificial joints, under static and dynamic conditions. Cylindrical specimens of POP mixed with Portland cement to simulate rock of higher strength (wall strength) were also tested. The study aims to understand the effect of important joint properties namely joint frequency, joint strength and joint inclination on the static and dynamic responses of jointed rock mass. The specimens having one to four joints at inclinations varying from 0^o to 90^o were tested under unconfined conditions. The laboratory results were presented as stress-strain plots and were examined to understand the effect of joint frequency and joint inclination on the strength and deformation behaviour of jointed rock mass. The objective of this paper is to derive the compressive strength/elastic modulus of the jointed rock mass as a function of intact rock strength/modulus and joint factor. The joint factor reflects the combined effect of joint frequency, joint inclination and joint strength. Therefore, having known the intact rock properties and the joint factor, jointed rock properties can be estimated.

Similar studies were carried out by Brown and Trollope (1970), Brown (1970), Einstein and Hirschfeld (1973), Yaji (1984), Arora (1987), Singh and Dev (1988) and Sharma (1989) and Roy (1993) which covers a wide range of data on rocks and rock like materials namely POP, different kinds of sandstone, granite and gypsum plaster with parallel and unparallel joints with different joint fabric at different confining pressures. Another objective of the paper is to compare the results of the study with the published works in this regard.

2. MODEL MATERIAL

Laboratory tests were conducted on cylindrical specimen of Plaster of Paris (POP). Because of the ease of casting, flexibility, quick hardening and low cost, POP was selected as a model material. The behaviour of hardened POP is similar to the behaviour of a soft rock. Specimens of 38mm in diameter and 76mm in height were prepared for uniaxial and triaxial compression tests, conducted at different confining pressures. Tests to determine the composition and texture of POP X-ray diffraction study has been done. X-Ray diffraction shows that POP used here contains mostly bassanite ($CaSO_4 0.5H_20$) and gypsum ($CaSO_4 2H_20$).

3. EXPERIMENTAL INVESTIGATION

3.1 Specimen Preparation

Molded cylindrical specimens of 76mm height and 38mm diameter were prepared using POP by pouring the plaster mix into casting moulds of 38mm diameter ensuring that no air bubbles were entrapped in the specimens. These specimens attained constant weight in about 10-12 days when

Table 1. Physical and engineering properties of POP

Properties	Values
Density, kg/m ^{3} (Unit weight, kN/ m^3)	933 9.3
Uniaxial compressive strength, MPa	2.21
Tangent modulus (E_t), GPa	0.3
Poisson's ratio (υ)	0.26
Tensile strength, MPa	0.30
Angle of internal friction (φ)	31^o

kept for drying in room temperature and normal humidity conditions.

The physical and engineering properties of the specimens (Table 1) were determined as per the ISRM specifications. The physical and engineering properties of POP are given in Table 1. The, tensile strength of rocks, which is usually 8-12% of the uniaxial compressive strength, was found to be 13.5% of the uniaxial compressive strength. The tangent modulus was calculated at 50% failure stress considering tests at three confining stresses 200, 400 and 600 kPa. The corresponding c and φ value were calculated using the Mohr failure envelope. The Poisson's ratio (υ) was calculated by the ratio of average lateral strain with the longitudinal strain considering 50% of failure stress.

Anisotropy was introduced into the intact specimens by developing a number of rough joints at various inclinations mainly 0^o, 30^o, 50^o, 70^o and 90^o using a special device fabricated locally, which is shown in Figure 1. The device has a triangular indent to create notch on the specimen at different inclination and then breaking the specimen along that notch to create rough joints at desired inclinations. The equipment is similar the point load test apparatus, consists of two conical blunt edges with an included angle of 45^o. Each edge is 8cm long. The lower edge is fixed to a round base plate where as upper edge is mounted on a rectangular plate and has free movement with respect the lower edge along the guide rods fixed to the base plate. To develop the joint at desired inclination the specimen was first suitably notched with marking gauge and then positioned in between the two edges along the notching. To break the specimen along the created notch, load was applied slowly by rotating the handle of the loading apparatus.

The maximum number of joints created was four for 90^o, three at 70^o, two at 50^o inclinations and only one for 30^o and 0^o joint inclinations. The complete joint configuration for the testing program is given in Figure 2. The photograph of POP specimens with horizontal and vertical joints and the same of POP-cement mix specimens with various joints are shown in Figure 3 and Figure 4.

3.2 Uniaxial Testing of POP Samples

The uniaxial compressive strength of all the POP specimens were determined under unconfined conditions, using a 5 tonne capacity loading frame as per ISRM (1977) and IS 9143 (1979).

3.3 Ultrasonic Testing of POP Samples for Dynamic Modulus of Elasticity

Ultrasonic methods, which have been used to detect flaws in metals and concrete, was used to estimate crack depths in rocks. Due to the inhomogeneous nature of the rock, only a few rock types such as rock salt and basalt are suited for flaw detection. This is because of the fact that acoustic velocity in a single material may vary over a large range due to the grain size and density variation (Koltonski & Malecki, 1958). The in-situ values of the velocity also vary because of the pressure effect. In general, attenuation is so high that only frequencies below 500 kHz can be considered for ultrasonic testing (Krautkrammer & Krautkrammer, 1993). A "Telesonic" instrument (Roop Telesonics-India) was used to measure V_p and V_s of POP samples. The instrument consists of

Figure 1. Creating joints in the POP specimen

Figure 2. Joint configurations studied on POP specimens

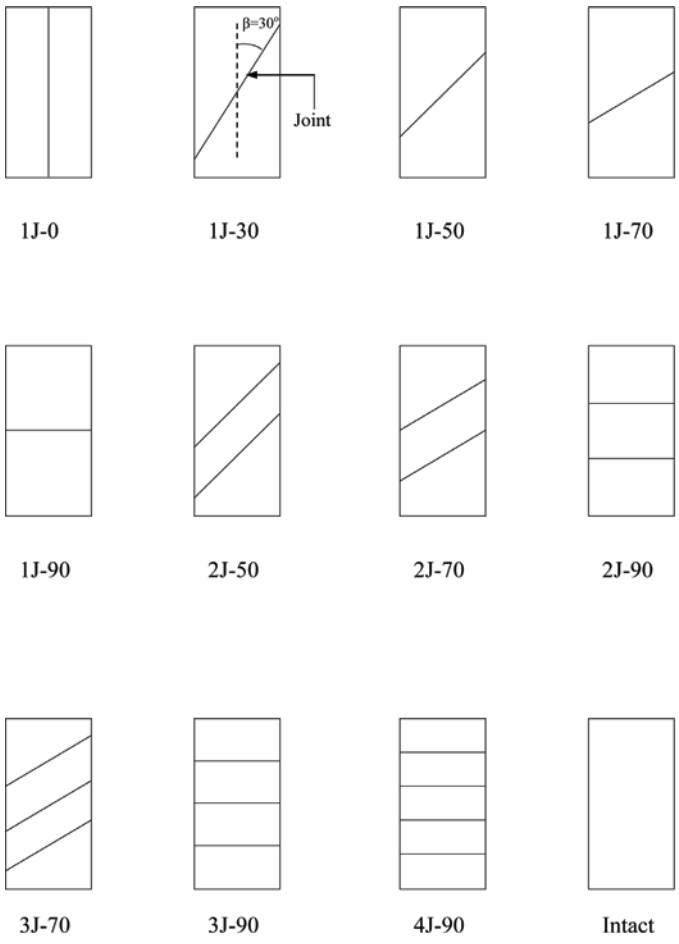

Note: 1J-30 indicates one joint at β =30°

Figure 3. POP specimens with marks representing the position of joints

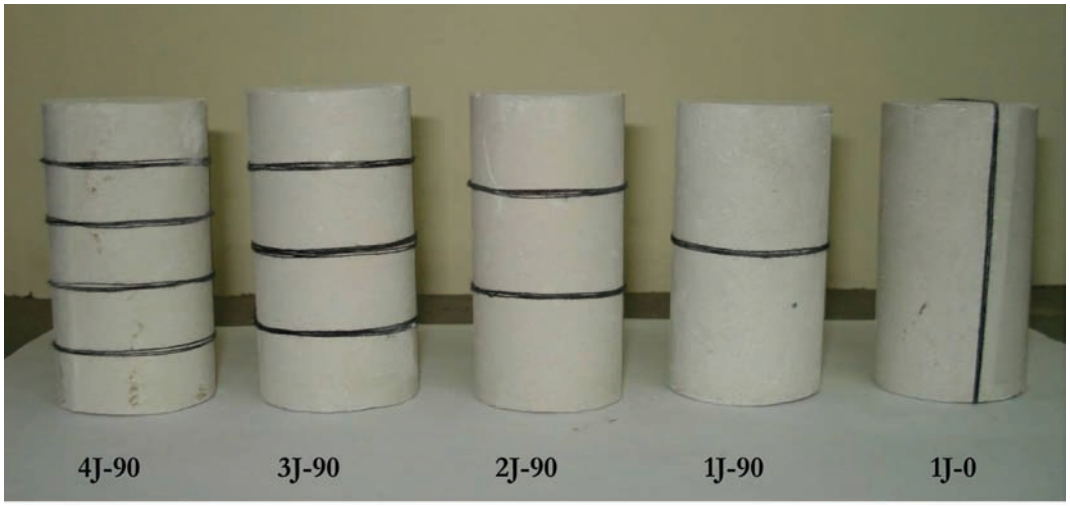

Figure 4. POP-cement mix specimens with marks representing the position of joints

a double probe (separate transmitter and receiver combination) which can be moved separately on the surface. The frequency range of the transducer is between 1 and 1000 kHz. The technique uses the indirect method of recording travel time of ultrasonic waves across a crack. The principle behind the technique is that a sound wave travels from a transducer to a receiver along the shortest

Figures 5. Measurement of V_p of POP specimen

path. The instrument was checked for calibration by measuring V_p and V_s of a standard specimen. The V_p and V_s were measured for the entire POP and POP-cement mix specimens with various joint sets. The measurement of V_p and V_s of POP and POP-cement mix samples is shown in Figure 5 and Figure 6, respectively.

4. TEST RESULTS AND DISCUSSION

4.1 Effect of Joint Frequency

The joint frequency is the number of joints per meter length and had significant influence in the strength of rock mass. For a laboratory specimen of 78mm height with a single joint, the joint frequency will be 13 which represent the possible number of joints in 1000mm length. As the joint frequency increases the strength of rock mass decreases and is true for all uniaxial conditions. Figure 7 shows clearly the effect of number of joints on strength and deformation behaviour of POP specimen under unconfined condition. The strength decreases drastically and further the strain at failure increases. It can be seen that, as the joint frequency increases, the ductile nature of the specimen is more pronounced and a transition between brittle to ductile behaviour is observed from intact to specimen with three joints (Figure 7). The reduction in the strength for one joint at $\beta=90^o$ i.e., 13 joints per meter, is around 10% (Figure 7). The reduction is around 30% and 40% for 26 joints and 39 joints per meter respectively. Although the strength decreases with an increase in the number of joints, failure modes are almost similar for a specific inclination and the crack propagation usually interrupted due to the presence of discontinuity. Similar observation was reported by Arora (1987) and the reduction of strength was around 7% for 10 joints per meter

Figures 6. Measurement of V_s of POP-cement mix specimen

Figure 7. Stress-strain curves for POP specimen with different number of joints at 90^o joint inclination tested in unconfined condition

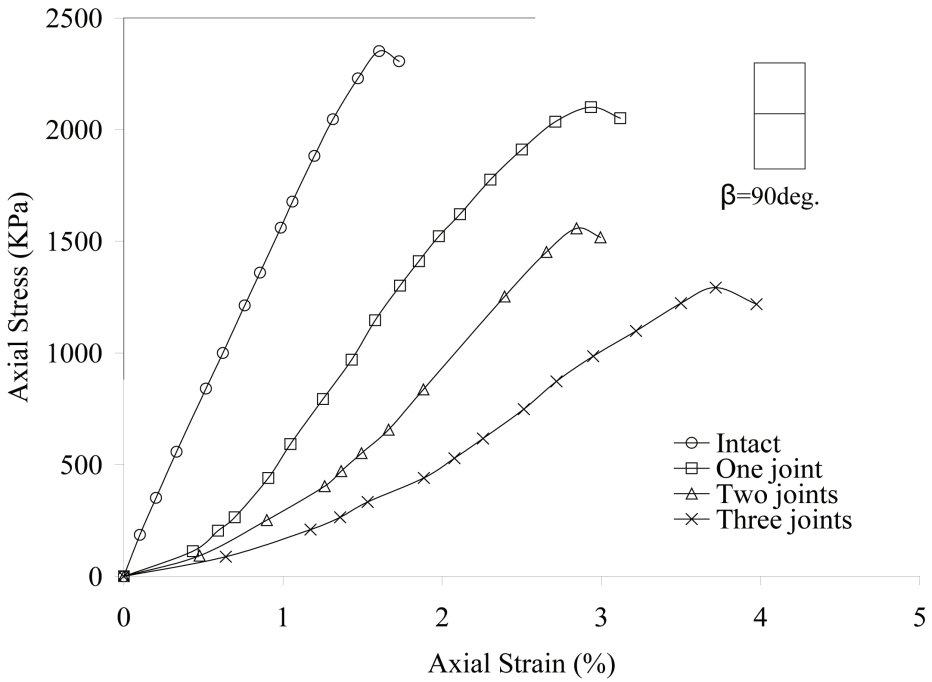

Figure 8. Variation of compressive strength ratio with joint frequency for specimen of POP with joints at different inclination

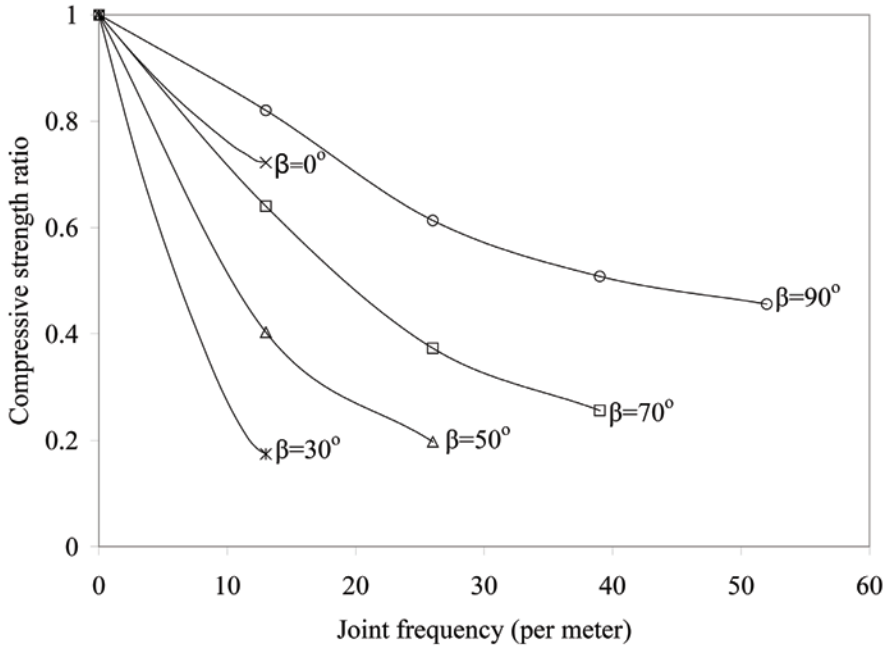

whereas for 100 joints per meter the corresponding reduction was around 50%.

In the present laboratory study the reduction is around 30% and 40% for 26 joints and 39 joints per meter respectively and can be seen in Figure 7. It is observed that, although the strength decreases with increase in the number of joints, failure modes are almost similar for a specific inclination and propagation of cracks usually interrupted due to the presence of discontinuity.

The effect of frequency and orientation of joints is clearly depicted in Figure 8. This figure shows the variation of compressive strength ratio with joint frequency for jointed rock specimen at five different inclinations 0^0, 30^0, 50^0, 70^0, 90^0 and clearly shows the reduction of strength with the increase with the number of joints. The maximum reduction of strength is observed for the specimen with 30^0 joint inclination. The observed reduction in strength for single joint at $\beta=30^0$ is relatively greater than the reduction due to two joints at $\beta=50^0$, three joints at $\beta=70^0$ and four joints at $\beta=90^0$. Rock mass strength decreases with the increase in joint frequency and it is observed that a sharp transition from brittle to ductile behaviour with increase of number in joints. Figure 9 shows the stress-strain curves for POP specimen with one, two and three joints at 70^0 inclination tested at confining pressure of 600 kPa.

4.2 Effect of Joint Inclination

Joint inclination has a very significant influence on the strength behaviour of jointed rock mass (Figure 8). It has observed that the jointed rocks exhibit a minimum value of strength when the joints are oriented at $\beta=30\text{-}40^0$. Figure 9 shows the variation of compressive strength ratio of POP specimen versus inclination of a single joint. The shape shown in the Figure 9 resembles U-type

Figure 9. Variation of compressive strength ratio of POP specimen with orientation of a single joint

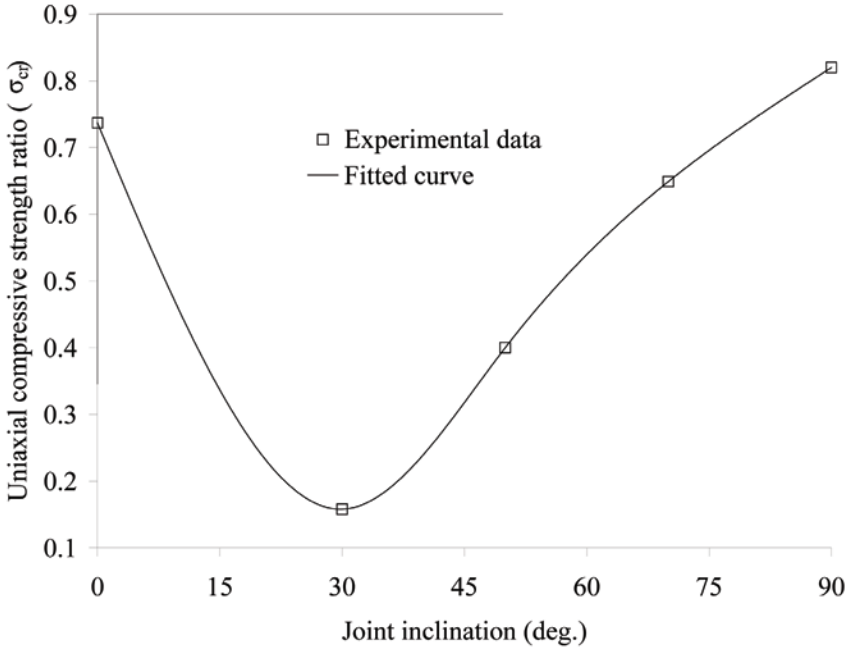

which is predominant in soft rocks with parallel set of cleavage or weak planes as the source of their anisotropy (Ramamurthy & Arora, 1994). As expected, the maximum uniaxial compressive strength was observed for $\beta=90^{o}$ and the minimum $\beta=30^{0}$.

4.3 POP with Cement Mix

POP mixed with 10% Portland cement by weight was also used to prepare cylindrical specimens to have relatively higher uniaxial compressive strength and to represent higher wall strength, in case of jointed specimens. A total of 110 gm mixture was taken containing 11 gm Portland cement and was thoroughly dry mixed with a stirrer. This POP with cement mix was then mixed with specific quantity of water (always kept constant for every sample) to cast cylindrical specimens with split moulds similar to POP without cement mix specimens. These specimens of POP with cement mix with relatively higher strength have a uniaxial compressive strength close to 4000 kPa as against a value of 2400 kPa for POP specimens as shown in Figure 10, which shows the stress-strain curves for POP with cement mix specimen with different number of joints at 90^{o} joint inclination. Figure 11 shows the stress-strain curves for POP with cement mix specimen with different number of joints at 70^{o} joint inclination. Figure 12 shows the stress-strain curves for POP with cement mix specimen with different number of joints at 50^{o} joint inclination.

In all the cases, with increase in the joint frequency, there is a decrease in the strength. Figure 13 shows the failed cylindrical specimens of POP with different number joints at 90^{o} inclination, after the test. As can be seen, mostly horizontal cracks were formed similar to the POP specimen without cement mix, but with a more pronounced brittle nature due to the addition of cement. In

Figure 10. Stress-strain curves for POP with cement mix specimen with different number of joints at 90^o joint inclination tested

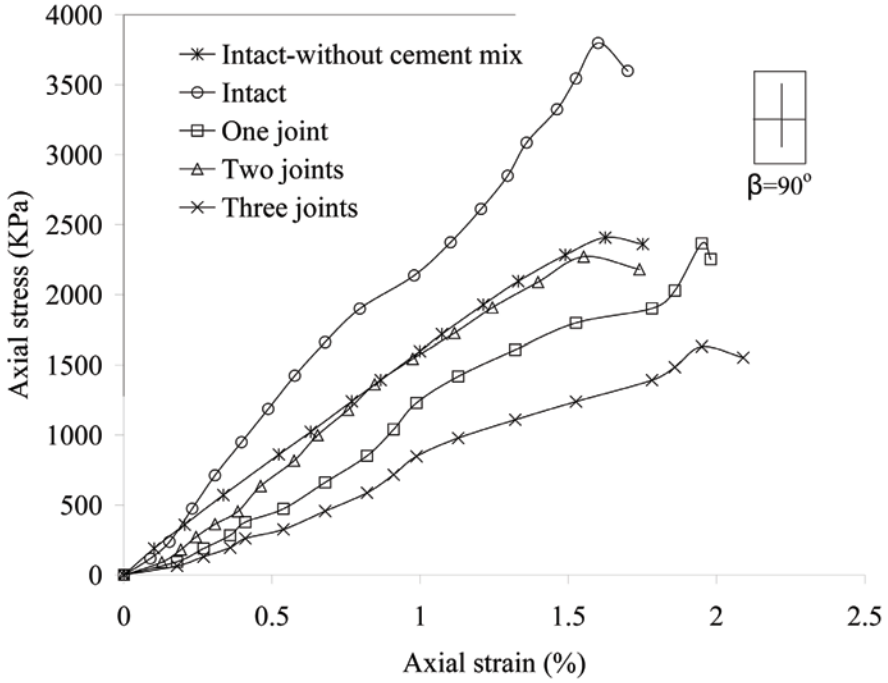

Figure 11. Stress-strain curves for POP with cement mix specimen with different number of joints at 70^o joint inclination

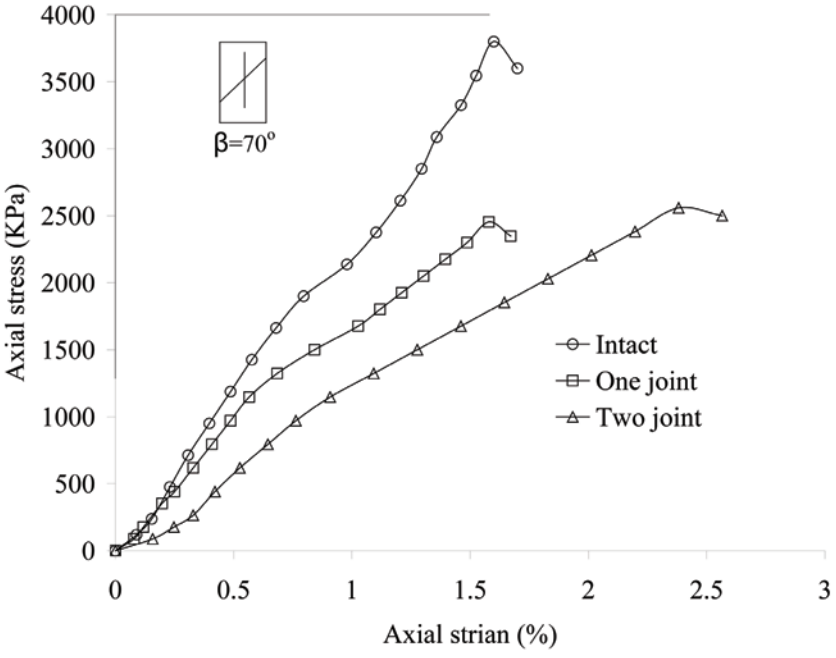

Figure 12. Stress-strain curves for POP with cement mix specimen with different number of joints at 50^o joint inclination

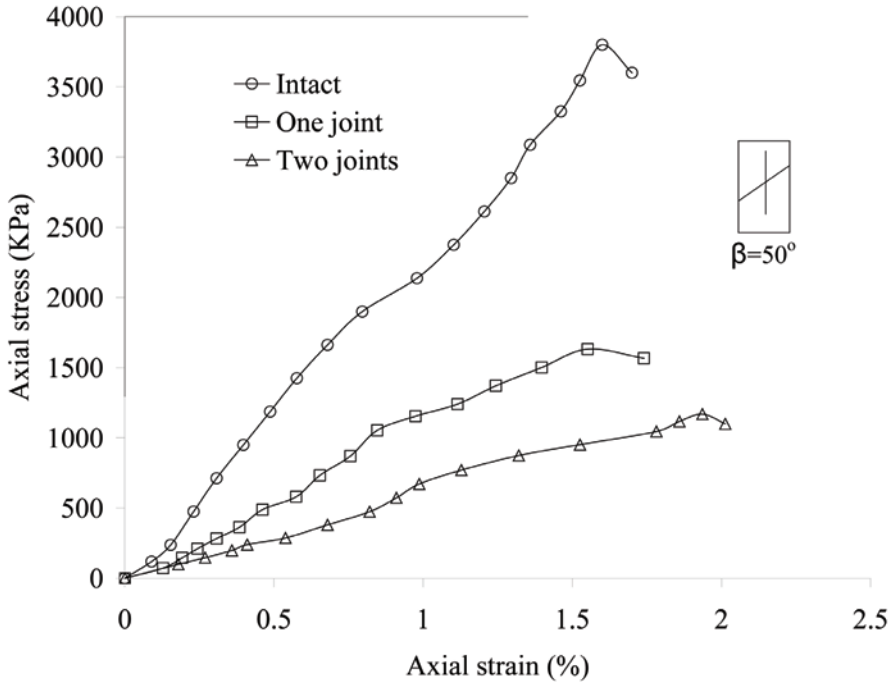

Figure 13. Failed cylindrical specimens of POP with cement mix

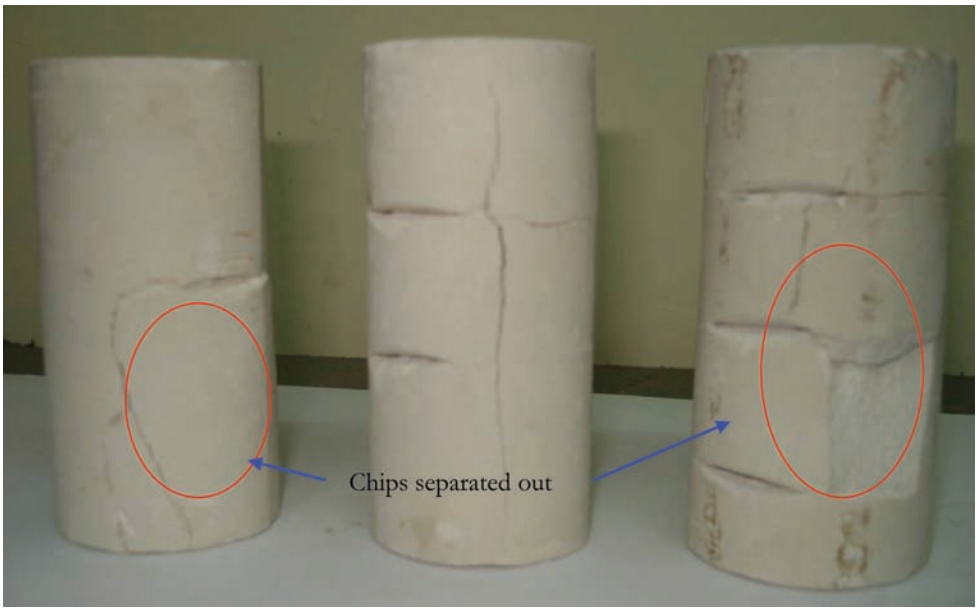

Table 2. Values of V_p and V_s for POP samples

S.No.	Sample/Inclination	P-wave Velocity, m/s	S-wave Velocity, m/s	Vp/Vs	Dynamic elasticity modulus, GPa
1	Intact	2133.33	1047.12	2.04	3.38
2	1J-0^0	1958.33	885.96	2.21	2.54
3	1J-30^0	1948.96	810.81	2.40	0.95
4	1J-50^0	1923.08	745.65	2.58	2.16
5	1J-70^0	1896.91	722.14	2.63	2.70
6	1J-90^0	1867.47	687.87	2.71	0.51
7	2J-50^0	1740.89	648.57	2.68	0.97
8	2J-70^0	1697.42	616.62	2.75	1.45
9	2J-90^0	1679.84	609.40	2.76	0.49
10	3J-70^0	1518.03	514.89	2.95	1.05
11	3J-90^0	1490.07	498.87	2.99	0.68
12	4J-90^0	1396.05	476.00	2.93	0.64

Table 3. Values of V_p and V_s for POP-cement mix samples

S.No.	Sample/Inclination	P-wave Velocity, m/s	S-wave Velocity, m/s	Vp/ Vs	Dynamic elasticity modulus, GPa
1	Intact	2898.3	1317.4	2.2	4.13
2	1J-0^0	2723.3	1237.9	2.2	2.64
3	1J-50^0	2714.0	1233.6	2.2	1.20
4	1J-70^0	2588.1	1125.3	2.3	3.30
5	1J-90^0	2561.9	1164.5	2.2	3.55
6	2J-50^0	2454.5	981.8	2.5	0.54
7	2J-70^0	2327.9	931.2	2.5	1.45
8	2J-90^0	2284.4	913.8	2.5	3.10
9	2J-90^0	2045.7	794.9	2.6	0.58
10	3J-90^0	1932.8	732.7	2.6	1.16

Figure 13, small chips of the specimens usually seen to be separated out from the parent specimens.

4.4 Determination of Dynamic Modulus of Elasticity

The dynamic modulus of elasticity of POP and POP-cement mix samples was found by determination of seismic velocity of samples, viz. P-wave velocity and S-wave velocity. The values of V_p, V_s and dynamic modulus of elasticity for both POP and POP-cement mix samples are given in Table 2 and Table 3 respectively. The equation (Eqn. 1) provided by Barton (1991) was used for calculation of dynamic modulus of elasticity.

$$E_d = V_s^2 \rho \frac{3(V_p / V_s)^2 - 4}{(V_p / V_s)^2 - 1} \quad (1)$$

where,

ρ – density of sample material (Table 1).

Figure 14. The experimental values of uniaxial compressive strength ratio versus joint factor along with a fitted curve

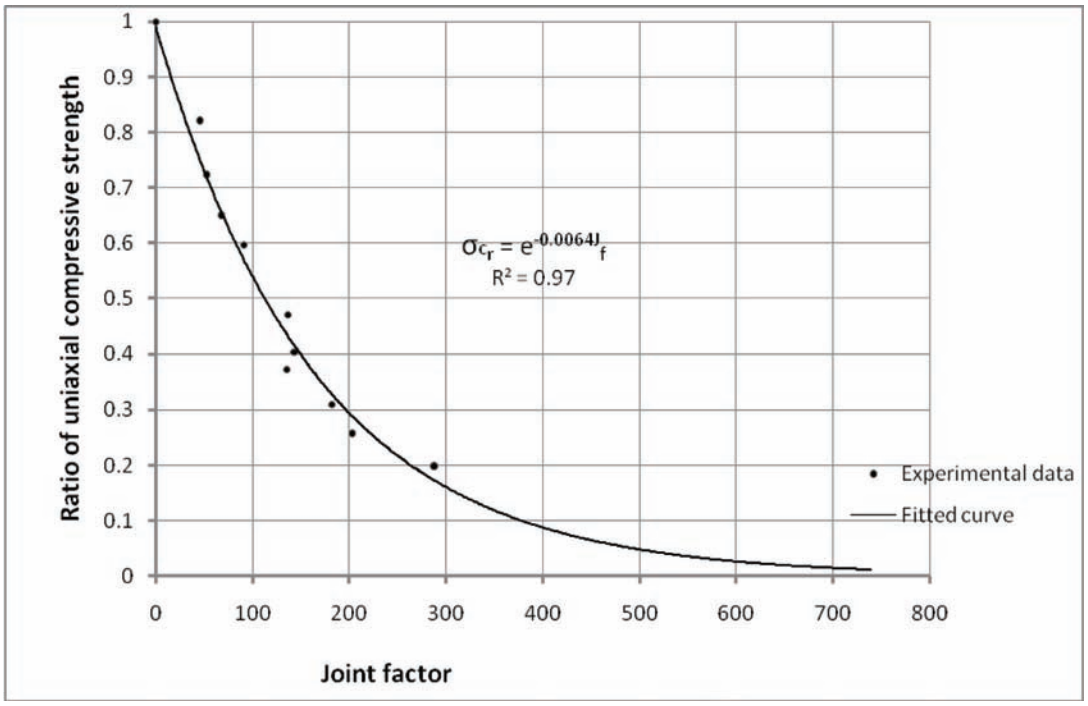

5. UNIAXIAL COMPRESSIVE STRENGTH/ELASTIC MODULUS OF JOINTED ROCKS

It is attempted to evaluate uniaxial compressive strength (UCS) and elastic modulus of rock mass as a function of UCS or elastic modulus of intact rock and joint factor. Figure 14 shows the variation of σ_{cr} (the ratio of UCS of jointed rock to the intact rock) with joint factor (J_f) for tested material. The term joint factor (J_f), introduced by Ramamurthy (1993), which reflects the combined effect of joint frequency, joint inclination and joint roughness (or wall strength) and is expressed as:

$$J_f = \frac{J_n}{n.r} \qquad (2)$$

where,

J_n = is the number of joints/m.
n= is the joint inclination parameter dependent on the joint orientation
r= roughness parameter which depends upon the joint condition

Joint factor for a jointed rock specimen can be calculated using equation (2) after calculating the joint frequency, inclination parameter from the corresponding joint inclination and joint strength parameter as discussed by Ramamurthy and Arora (1994). The calculated joint factor values for different tested POP specimens without any addition of cement, along with the corresponding value of uniaxial compressive strength ratio and ratio of elastic modulus are given in Table 4. An exponential curve was fitted to show a relation between compressive strength ratio (σ_{cr}) and joint factor (see Figure 14):

Table 4. Calculated joint factor values with corresponding uniaxial compressive strength ratio and ratio of elastic modulus for POP specimens

J_n		n	r	J_f	σ_{cr}	E_{sr}	E_{dr}
Intact	0	0.00	0.3	0.00	1.000	1.000	1.00
1J-0^0	13	0.82	0.3	52.84	0.722	0.787	0.75
1J-30^0	13	0.056	0.3	766.00	0.174	0.191	0.28
1J-50^0	13	0.3	0.3	144.44	0.403	0.325	0.64
1J-70^0	13	0.64	0.3	67.71	0.649	0.55	0.80
1J-90^0	13	0.95	0.3	45.61	0.820	0.926	0.15
2J-50^0	26	0.3	0.3	288.88	0.197	0.069	0.29
2J-70^0	26	0.64	0.3	135.40	0.373	0.403	0.43
2J-90^0	26	0.95	0.3	91.23	0.497	0.365	0.14
3J-70^0	39	0.64	0.3	203.12	0.256	0.12	0.31
3J-90^0	39	0.95	0.3	136.84	0.471	0.293	0.20
4J-90^0	52	0.95	0.3	182.45	0.310	0.216	0.19

σ_{cr} -Compressive strength ratio; E_{sr} -Ratio of static elastic modulus;
E_{dr} Ratio of dynamic elastic modulus

$$\sigma_{cr} = \frac{\sigma_{cj}}{\sigma_{ci}} = e^{-0.0064 J_f} \quad (3)$$

where, σ_{cr} is the ratio of UCS of jointed rock (σ_{cj}) to the intact rock (σ_{ci}). Similar exponential relations were established when the ratio of static elastic modulus (E_{sr}) was plotted against the corresponding joint factor (see Figure 15). For unconfined case the expression is as shown below:

$$E_{sr} = \frac{E_j}{E_i} = e^{-0.0086 J_f} \quad (4)$$

where, E_{sr} is the ratio of static elastic modulus of jointed rock (E_j) to the intact rock elastic modulus (E_i).

Another exponential relations was established when the ratio of dynamic elastic modulus (E_{dr}) was plotted against the corresponding joint factor (Figure 16). For unconfined condition, the expression is as shown below,

$$E_{dr} = \frac{E_j}{E_i} = e^{-0.0075 J_f} \quad (5)$$

where, E_{dr} is the ratio of dynamic elastic modulus of jointed rock (E_j) to the dynamic elastic modulus (E_i) of intact rock.

With the help of these equations the uniaxial compressive strength/elastic modulus of jointed rocks can be determined for known values of joint factor and uniaxial compressive strength/elastic modulus of intact rock. It is observed that the ratios of both static and dynamic elastic modulus decreases with an increase in the joint factor under unconfinement. The test results of POP and the POP-cement mix specimens are given in Table 5. Figure 14 shows the experimental values of uniaxial compressive strength ratio versus joint factor along with a fitted curve.

The plots of ratio of elastic modulus with the joint factor derived from the experimental data, for unconfined, are shown in Figure 15. The plots of ratio of dynamic elastic modulus with the joint factor are shown in Figure 16, which shows the variation of experimental values of uniaxial compressive strength ratio with joint factor for POP-

Figure 15. Ratio of static elastic modulus versus joint factor

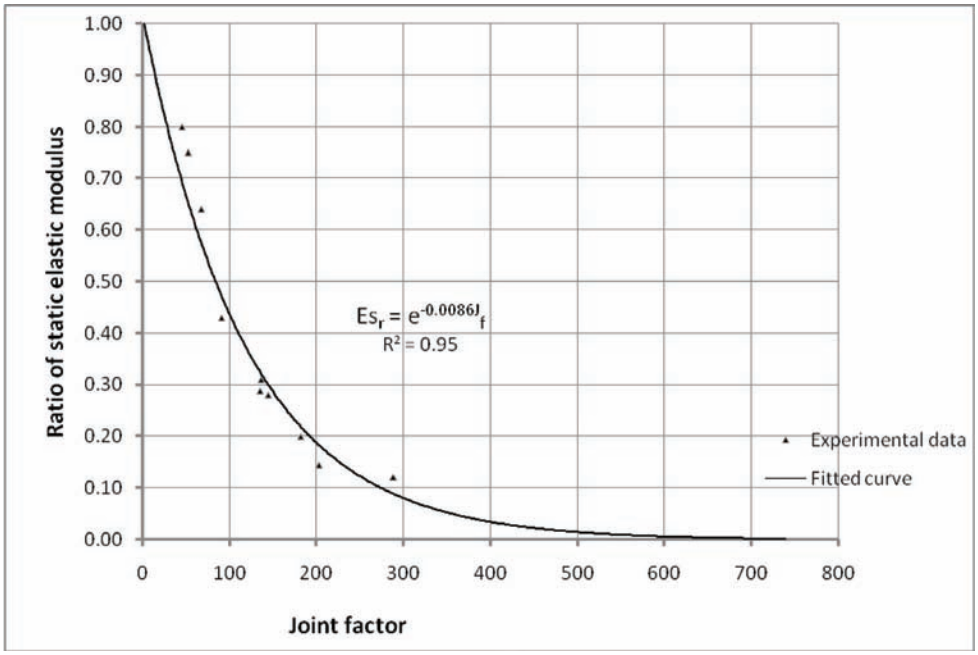

Figure 16. Ratio of dynamic elastic modulus versus joint factor

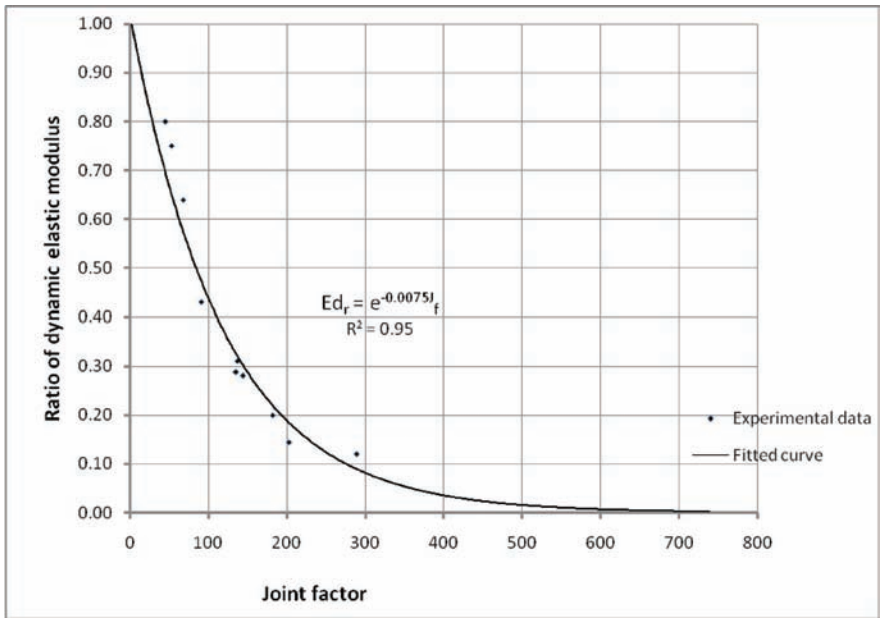

Table 5. Calculated joint factor values with corresponding uniaxial compressive strength ratio for POP with cement mix specimens

Specimen	Joint inclination parameter (n)	Joint strength parameter (r)	Joint frequency (Jn)	Joint factor (Jf)	Uniaxial compressive strength ratio (σr)	Ratio of elastic modulus (Er)	Ratio of dynamic elastic modulus
1J-0^0	0.82	0.4	13	49.63	0.84	0.426	0.64
1J-50^0	0.3	0.4	13	108	0.309	0.258	0.29
1J-70^0	0.64	0.4	13	50.78	0.645	0.728	0.80
1J-90^0	0.95	0.4	13	34.2	0.621	0.52	-
2J-50^0	0.3	0.4	26	216	0.427	0.41	0.43
2J-70^0	0.64	0.4	26	101.56	0.657	0.554	0.15
2J-90^0	0.95	0.4	26	68.42	0.43	0.51	0.75
3J-90^0	0.95	0.4	39	102.63	0.57	0.309	0.28

cement mix specimens, plotted together with the test results of POP specimen.

It can be seen from Figure 17, the variation in the compressive strength ratio for the POP with cement mix (having unconfined compressive strength indicating different wall strength for jointed specimens) followed the expected trend. Figure 18 shows the experimental values of ratio of elastic modulus versus joint factor for POP with cement mix specimens plotted together with the results of POP specimen. There is a good agreement with the corresponding expression presented in equation 4, with the test results of POP specimens. Figure 19 shows the ratio of dynamic elastic modulus versus joint factor for POP - cement mix specimens plotted together with the results of POP specimen and along with the fitted curve. There is no change in the equation (Figure 19) even with the variations in the strength of specimens and shows a good agreement with the corresponding expression presented in equation 4.

6. COMPARISON WITH RESULTS OF DIFFERENT ROCKS

The consistency of results from the present experimental investigation on POP specimens can be understood from the Figure 20 to Figure 23, where the exponential expressions presented in the previous sections were compared with the experimental data of different jointed rocks presented by Brown and Trollope (1970), Brown (1970), Einstein and Hirschfeld (1973), Yaji (1984), Arora (1987), Singh and Dev (1988), Sharma (1989), Roy (1993), Ramamurthy and Arora (1994). Figure 22 presents the values of uniaxial compressive strength ratio versus joint factor from earlier experimental works.

The corresponding variation of uniaxial compressive strength ratio with joint factor based on the exponential relation established (equation 3) using the present experimental data is also plotted. A good comparison has been observed between the present experimental results and the earlier test data for different rocks. Those earlier experimental data covers a wide range of strength variation from very soft rock like POP to very hard rock like granite. This shows that the present experimental investigation is representative of actual jointed rock mass behaviour and is applicable to all type of rocks. Similarly, Figure 21 presents the values of ratio of elastic modulus in unconfined case versus joint factor from earlier experimental works. The corresponding variation of ratio of elastic modulus with joint factor based

Figure 17. UCS ratio versus joint factor for combined data of POP and POP-cement mix specimens

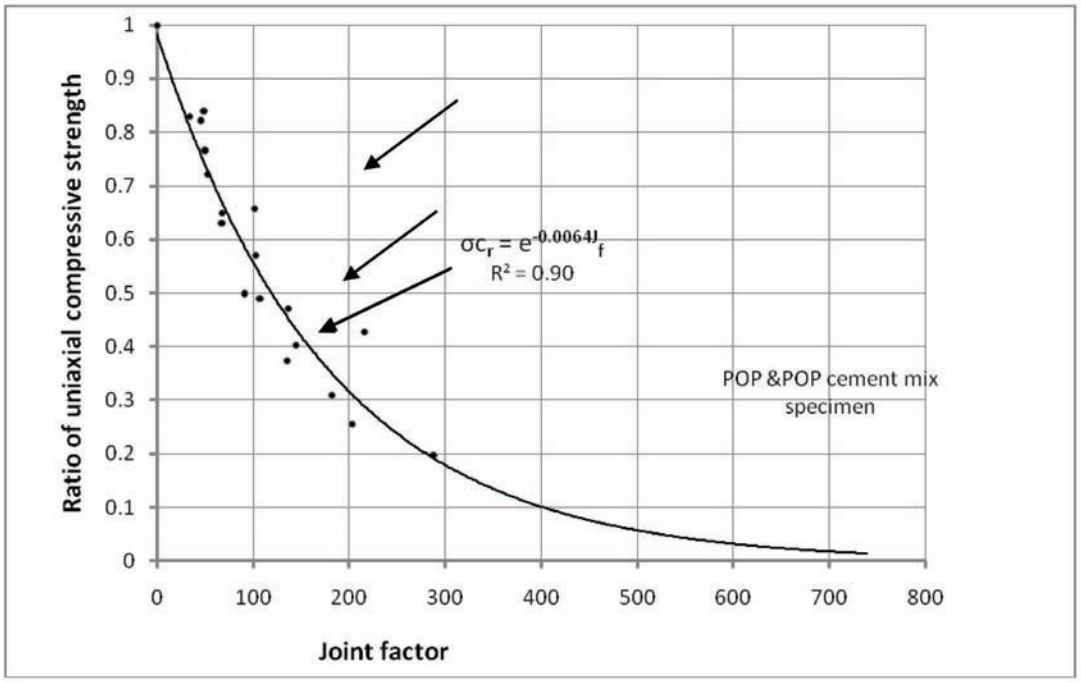

Figure 18. Ratio of elastic modulus versus Joint factor for mixed data of POP and POP-cement mix specimens

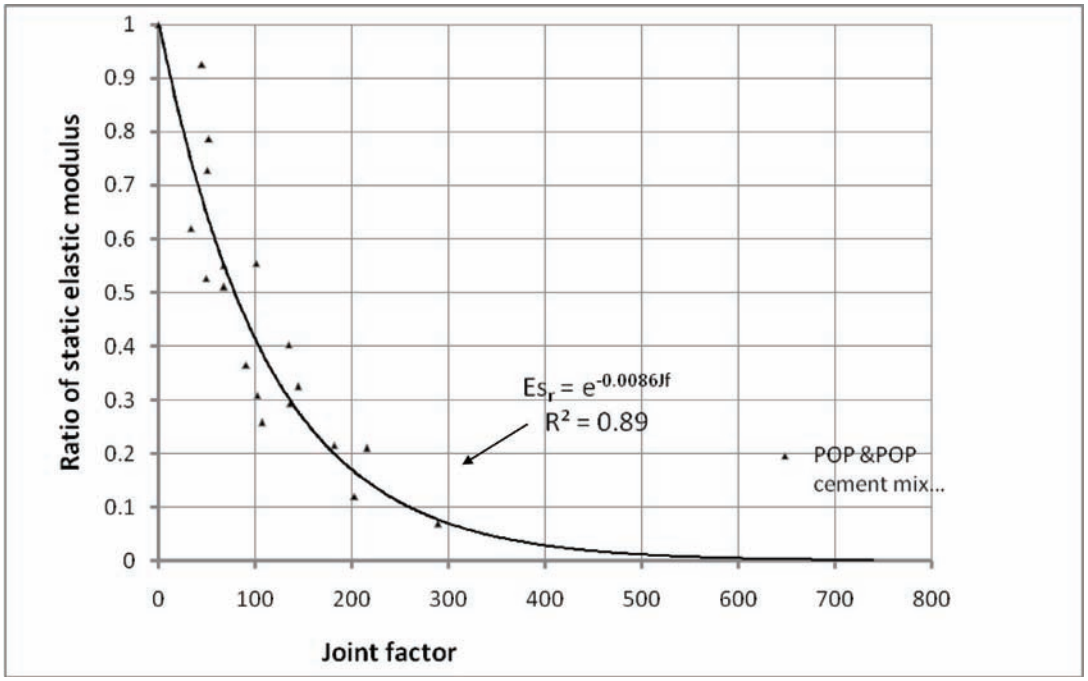

Figure 19. Ratio of dynamic elastic modulus versus Joint factor for mixed data of POP and POP-cement mix specimens

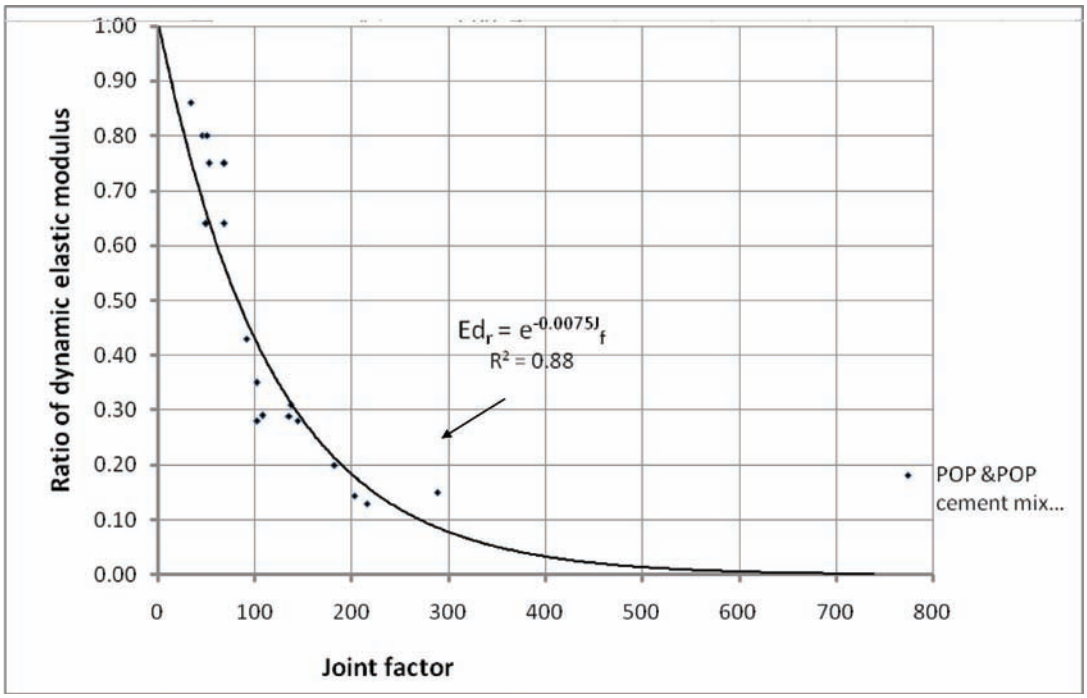

Figures 20. Variation of uniaxial compressive strength ratio with joint factor

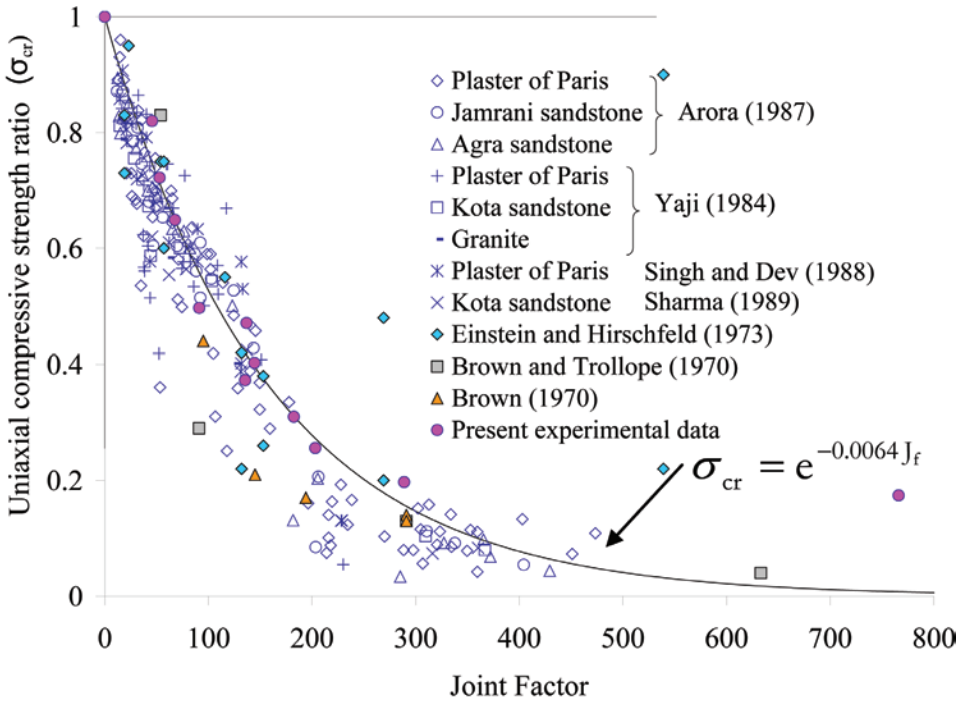

Figures 21. Variation of ratio of elastic modulus for unconfined case with joint factor

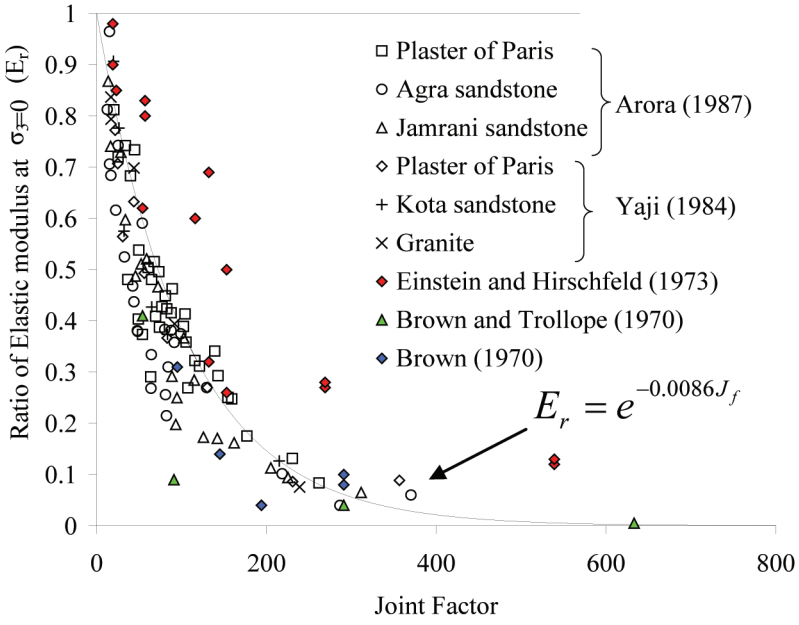

Figures 22. Variation of uniaxial compressive strength ratio with joint factor with comparison of Ramamurthy's equation

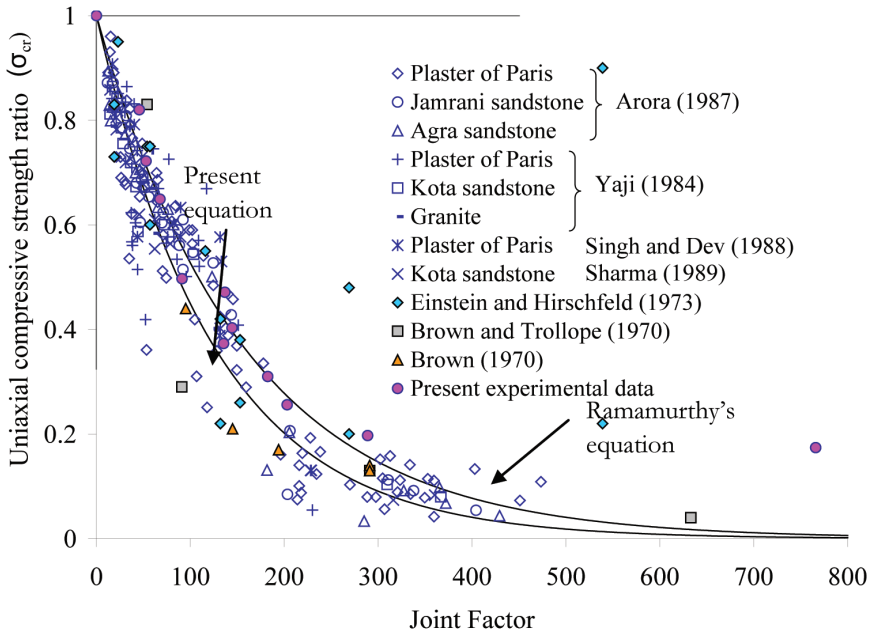

Figures 23. Variation of ratio of elastic modulus for unconfined case with joint factor with comparison of present equation with Ramamurthy's equation

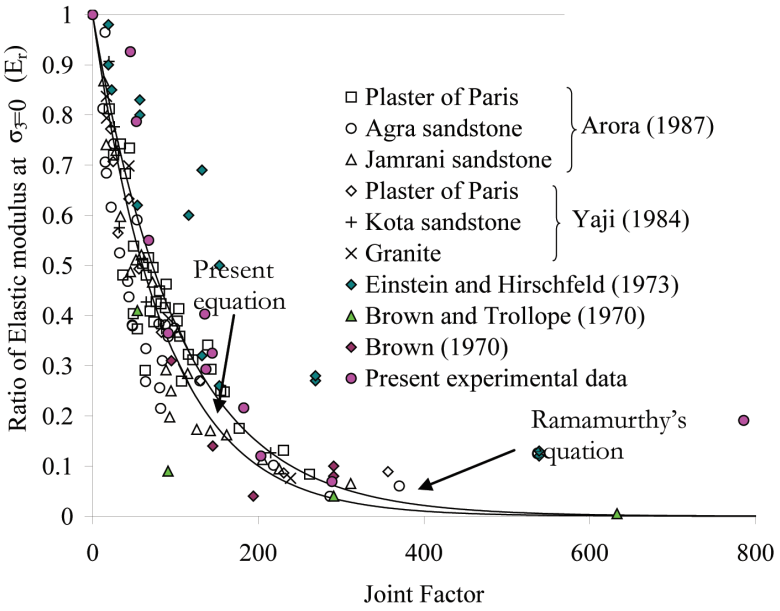

on the exponential relation given in equation 4 using the present experimental data, is also plotted in the same Figure 21.

A good comparison has been observed between the present experimental results and the earlier experimental data for most of the jointed rock types. From these empirical relationships, knowing the intact rock properties and the joint factor, the jointed rock properties can be estimated. These relationships have been used for assessment of the blast induced damage during field experiments, as the modulus of elasticity is essential for calculation of extent of rock mass damage. In Figure 22 and Figure 23, present equations are compared with Ramamurthy's (1993) equation along with experimental data of different rock types where it has been observed that, present equation is in close comparison with earlier expression by Ramamurthy (1993).

7. INFLUENCE OF JOINTS ON STATIC AND DYNAMIC ELASTIC MODULUS

The influence of joints on static and dynamic elastic modulus was investigated based on the data provided in Table 4 and Table 5. Regression analysis was done for the data on ratios of static and dynamic elastic modulus of plaster of Paris (POP) specimen, Plaster of Paris-cement mix specimen and mixed data of plaster of Paris and Plaster of Paris-cement mix specimen. The curves were plotted for the ratio of static elastic modulus and dynamic elastic modulus for all the three groups of data. The plotted curves are shown in Figure 24 to Figure 26. Figure 24 shows the experimental values of ratio of static elastic modulus versus ratio of dynamic elastic modulus for POP specimens. Figure 25 shows the trend of ratio of static elastic modulus versus ratio of dynamic elastic modulus for POP-cement mix specimens. The plot of ratio of static elastic modulus versus ratio of dynamic

Figure 24. Ratio of static elastic modulus versus ratio of dynamic elastic modulus for POP specimens

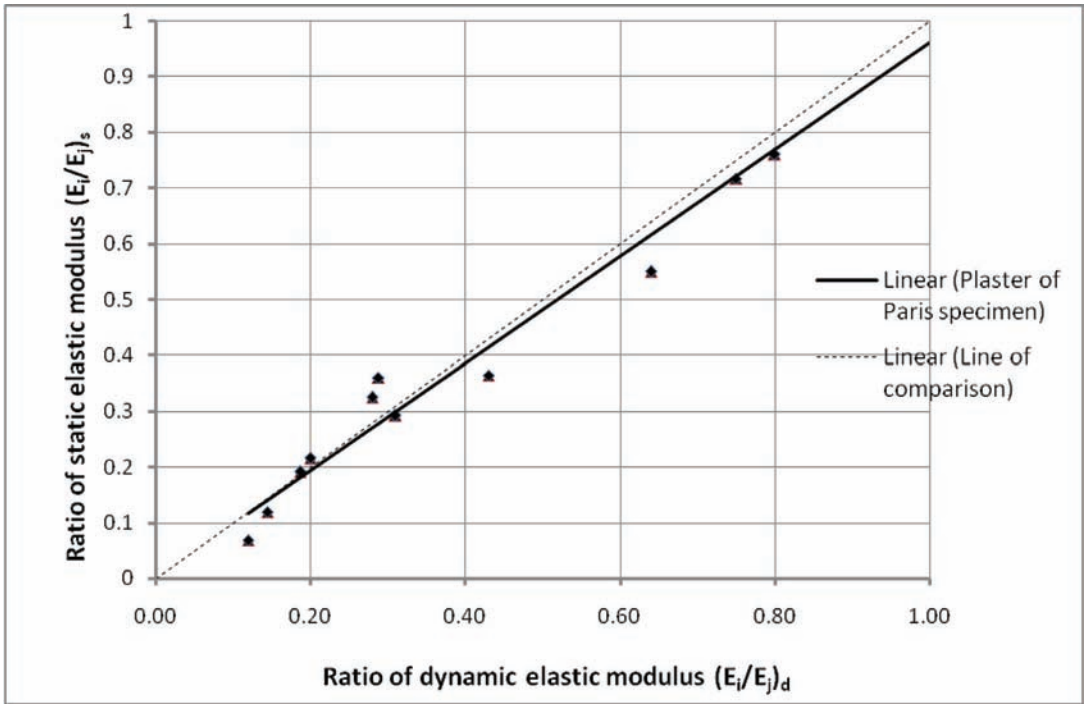

Figure 25. Ratio of static elastic modulus versus ratio of dynamic elastic modulus for POP-cement mix specimens

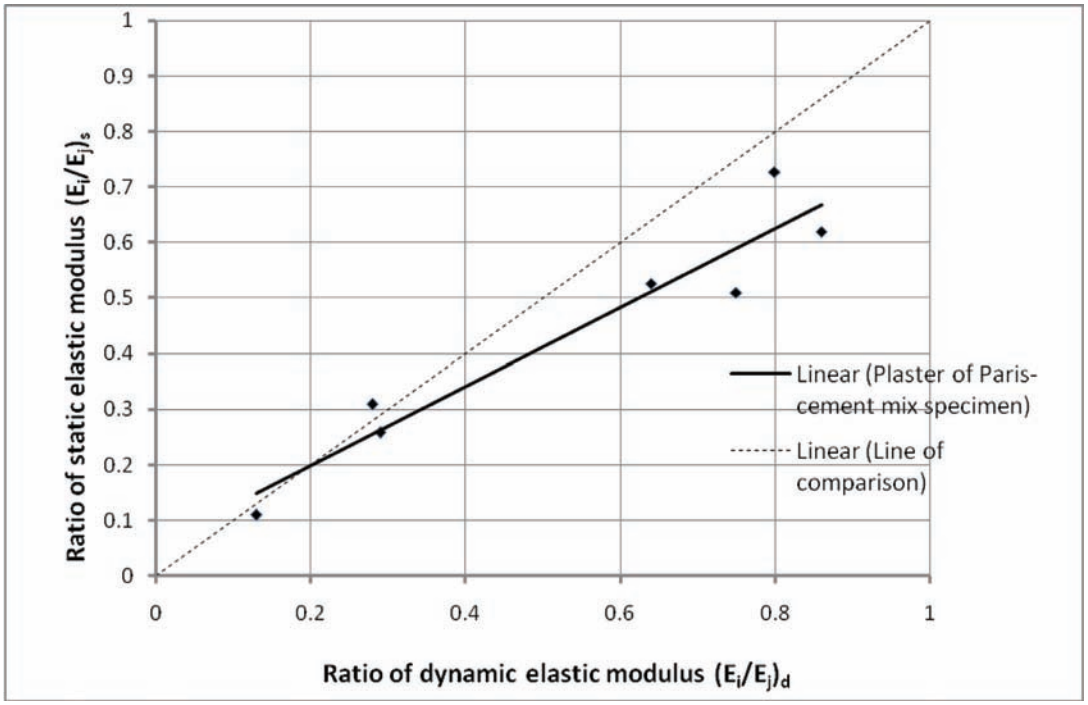

Figure 26. Ratio of static elastic modulus versus ratio of dynamic elastic modulus for POP and POP-cement mix specimens

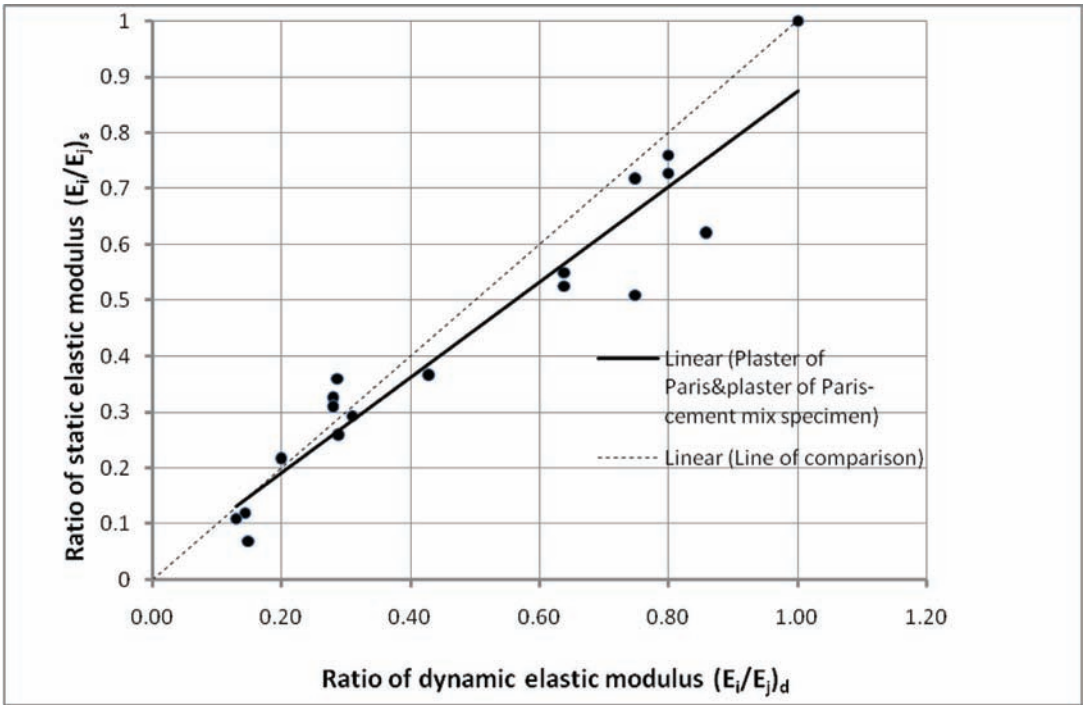

elastic modulus for POP and POP-cement mix specimens together is shown in Figure 26.

It is clear from the analysis shown in Figure 25, Figure 26 and Figure 27 that the trends of ratio of static elastic modulus versus ratio of dynamic elastic modulus for POP specimens and POP-cement mix specimen are always below the line of comparison. This indicates that the anisotropy of the specimen is influencing the dynamic elastic modulus more than the static elastic modulus. The low strain experiments on the POP and POP-cement mix models also indicate that the effect of joints is more predominant for the sample material of higher strength than the lower strength material.

8. CONCLUSION

Uniaxial testing on cylindrical specimens of POP was conducted with different configuration of joints and number of joints to understand the strength and deformational characteristics of jointed rock mass. Cylindrical specimens of POP mixed with Portland cement were also tested to simulate rock of higher strength. The study aims to understand the effect of important joint properties namely joint frequency, joint strength and joint inclination on the response of jointed rocks to loading. The specimens having one to four joints at different inclinations varying from 0^o to 90^o were tested for both static and dynamic properties.

The following conclusions can be drawn from the laboratory experimental study:

1. Exponential correlations were established for the prediction of uniaxial compressive strength ratio/ratio of static and dynamic elastic modulus of rock mass from the intact rock uniaxial compressive strength/elastic modulus and joint factor (Ramamurthy, 1993), which includes joint frequency, joint inclination and joint strength. These relations are useful in characterisation of jointed rock mass by knowing the intact rock properties and the joint factor.
2. Rock mass strength decreases with an increase in the joint frequency and a sharp transition was observed from brittle to ductile behaviour with an increase in the number of joints.
3. The rocks with planar anisotropy exhibit the highest strength in the direction perpendicular to the anisotropy and the lowest at an inclination of 30^o-45^o with the plane of anisotropy in jointed samples. The anisotropy of the specimen influences the dynamic elastic modulus more than the static elastic modulus
4. The low strain experiments on the POP and POP-cement mix models also indicate that the effect of joints is more predominant for the sample material of higher strength than the lower strength material.
5. The anisotropy of the specimen is influencing the dynamic elastic modulus more than the static elastic modulus.

REFERENCES

Arora, V. K. (1987). *Strength and deformation behaviour of jointed rocks*. Unpublished doctoral dissertation, Indian Institute of Technology, Delhi, India.

Brown, E. T. (1970). Strength of Models of Rock with Intermittent joints. *J. Soil Mech. Fdns. Div. Am. Soc. Civ. Engrs.*, *96*(6), 1935–1949.

Brown, E. T., & Trollope, D. H. (1970). Strength of model of jointed rock. *Journal of the Soil Mechanics and Foundations Division*, *96*(2), 685–704.

Ciccitti, M., & Mulargia, F. (2004). Differences between static and dynamic elastic moduli of a typical seismogenic rock. *Int. J. Geophysics*, *157*, 474–477. doi:10.1111/j.1365-246X.2004.02213.x

Einstein, H. H., & Hirschfeld, R. C. (1973). Models studies in mechanics of Jointed Rocks. *Journal of the Soil Mechanics and Foundations Division*, *99*, 229–248.

IS. (1979). *Determination of unconfined compression strength of Rock materials*. New Delhi, India: Bureau of Indian Standards.

ISRM Committee on Laboratory tests. (1977). *Suggested methods for determining Uniaxial compressive strength of Rock Materials* (Document No.1, First Revision). Lisboa, Portugal: ISRM.

Koltonski, & Malecki. (1958). Ultrasonic method for exploration of the properties and structure of mineral layers. *Acustica, 8*, 307-314.

Krautkrammer, J., & Krautkrammer, H. (1993). *Ultrasonic testing of materials*. New Delhi, India: Narosa Publishing House.

Ramamurthy, T. (1993). Strength and modulus responses of anisotropic rocks. In Hudson, J. A. (Ed.), *Comprehensive rock engineering* (*Vol. 1*, pp. 313–329). Oxford, UK: Pergamon Press.

Ramamurthy, T., & Arora, V. K. (1994). Strength prediction for jointed rocks in confined and unconfined states. *International Journal of Rock Mechanics and Mining Sciences & Geomechanics Abstracts*, *31*(1), 9–22. doi:10.1016/0148-9062(94)92311-6

Roy, N. (1993). *Engineering behaviour of rock masses through study of jointed models*. Unpublished doctoral dissertation, Indian Institute of Technology, Delhi, India.

Sharma, V. K. (1989). *Strength properties of jointed rocks*. Unpublished master's thesis, R. E. C. Kurukshetra, India.

Singh, R. K., & Dev, C. (1988). *Strength and modulus tests on jointed specimens of plaster of Paris*. M. Tech Thesis, IIT-Delhi, India.

Yaji, R. K. (1984). *Shear strength and deformation of jointed rocks*. Unpublished doctoral dissertation, Indian Institute of Technology, New Delhi, India.

This work was previously published in International Journal of Geotechnical Earthquake Engineering, Volume 1, Issue 2, edited by T.G. Sitharam, pp. 89-112, copyright 2010 by IGI Publishing (an imprint of IGI Global).

Section 2

Chapter 8
Blast Induced Damage Due to Repeated Vibrations in Jointed Gneiss Rock Formation

M. Ramulu
Central Institute of Mining & Fuel Research, India

T. G. Sitharam
Indian Institute of Science, India

ABSTRACT

Blasting is the most common method of rock excavation technique in mining and civil construction and infrastructure projects. Rock blasting produces seismic waves similar to those produced by earthquakes, but with relatively high frequency and low amplitude. General blast induced damage was extensively studied by researchers globally, but the studies on damage due to repeated blast vibrations is not yet reported, quantitatively, on underground openings. This paper deals with the research work carried on the effect of repeated dynamic loading imparted on the jointed rock mass from subsequent blasts in the vicinity, on the jointed rock mass at Lohari Nag Pala Hydroelectric Power Construction Project. The blast induced damage was monitored by borehole extensometers, borehole camera inspection surveys and triaxial geophones installed at three test sites of different joint orientations at the Main Access Tunnel of power house. The study reveals that there was extra damage of 60%, exclusively due to repeated blast vibrations. The results of the study indicate that repeated dynamic loading, resulted in damage even at 33% of the conventional damage threshold vibrations (V_c) in case of favorable joint orientations and 23% of V_c in case of unfavorable joints. The paper concludes in quantification of effect of repeated blast loading and the orientation of joints on the extension of damage zone in jointed rock mass of underground excavations.

DOI: 10.4018/978-1-4666-0915-0.ch008

1. INTRODUCTION

Blasting produces seismic waves similar to those produced by earthquakes, but with relatively high frequency and low amplitude which can create damage to surrounding structures. The degree of structural damage depends on the total energy of explosion, distance from the source, and the characteristics of the medium. Extensive experimental investigation in this regard was carried out by Thoenen and Windes (1942) of United States Bureau of Mines (USBM), Leet (1946) and Crandell (1949). Based on the experimental results the USBM recommended that no structural damage occurs if the acceleration of vibration is less than 0.1 times the gravity (g) and 0.1 to 1g is caution range; and the acceleration greater than 1g is danger zone. Leet (1946) prefers to limit the size of blasts by the displacements that they produce in the structure and the index of damage is a limiting displacement of 0.03 inches. Crandell (1949) proposes to limit the size of the explosion by limiting the kinetic energy delivered to the ground, which is proportional to the quantity of the explosive. A number of studies attempted to correlate ground-motion levels with observed damage to structures. It is generally agreed that the amount of blast damage correlates best to the peak particle velocity (V_{max}). The blasting criteria for residential structures is generally less than 5 cm/s and for massive concrete structures is generally less than 25 cm/s (Charlie, 1985). Oriard (1989) observed that V_{max} of 8-10 ips normally and not damage the structure, because of the very high frequencies and the rapid, localized attenuation. Tart (1980) observed that at high frequencies the vibration levels of 275 ips generate minor cracks in old concrete. Rock mass damage in underground openings occurs mainly due to blast induced forces, stress redistribution and weathering. As underground excavations are carried out, the in-situ stresses redistribute around the boundary of the openings, leading to high stresses on the backs and corners of the excavations and the blasting activity creates initiation and extension of fractures in the surrounding rock mass. Blast damage is defined as either creation or extension of new fracture surfaces or opening of pre-existing geological discontinuities or both in the rock mass (Law et al, 2001). Blast induced damage weakens a rock mass, potentially leading to stability problems in the underground excavations. The stability of the underground structure is very much dependent upon the integrity of rock immediately surrounding the excavation. The blast damage can easily extend few meters into the rock and the loosened rock can give rise to serious safety and stability problems to the surrounding rock mass of the underground openings. The blast damage problem is more severe and vulnerable for the jointed rock mass in underground excavations (Singh and Xavier, 2005). In spite of recognition of the importance of duration of ground motion on the dynamic response, current engineering practice correlates damage to peak ground motion during an episode of dynamic loading, since it can be related directly to peak transient stress in the ground wave, and the second power of velocity is related to dynamic strain energy (McGarr, 1983). Unfortunately, there are no specific safety guidelines available for the blasted tunnels with regards to the threshold limits of vibrations caused by repeated blasting activity in the close proximity. Many efforts have been made to study blast induced cracking and framing of safety guidelines in residential structures (Langefors and Kihlstroam, 1963; Dowding, 1985; Scott, 1996; Anon, 1997), but less attention was found to study blast induced damage to rock mass in underground openings (Persson et al., 1994). Studies on blast induced damage on underground openings are well documented by many researchers globally (Langefors & Kihlstrom, 1963; Hendron, 1977; Holmberg, 1993; Singh, 1993; Paventi et al, 1996; Yu & Vongpaisal, 1996; Chakraborty et al., 1998; Zhang & Chang, 1999). In a series of experiments the Swedish Detonic Foundation has investigated the extent of cracking emanating from blastholes

in controlled conditions (Olsson & Bergqvist, 1996; Ouchterlony, 1993; Ouchterlony, 1997). Joint orientation with respect to perimeter line of underground opening is one of the influencing parameters of blast induced damage (Connigham & Goetzsche, 1996). Singh and Xavier (2005) observed largest overbreak for the joint orientations of 45^0 and minimum overbreak for parallel and perpendicular joint orientations. Similar results were also obtained by Lewandowski (1996) in his trial blasts on influence of discontinuities for effective pre-splitting. In view of the large amount of underground excavations like tunnels and caverns it is imperative to develop threshold limits of ground vibrations induced by blasting within or outside the underground opening. In this paper, it was aimed at prediction and assessment of blast induced damage and deterioration due to repeated dynamic loading produced by adjacent tunnel blasting.

2. REVIEW OF LITERATURE ON ROCK MASS DAMAGE DUE TO REPEATED BLASTING

The rock mass damage problem will be manifold if the blast loading is applied for repeated number of times, in contrast to the conventional single episode blast loading. Repeated blast loading causes progressive accumulation of damage in joints, which may lead to achievement of residual strength state in joints, with resultant large displacement at the joint surface (Brady, 1990). The effect of repeated blast loading on jointed rock mass was qualitatively studied by many researchers globally (Atchison & Pugliese, 1964; Oriard, 1989; Otuonye, 1997; Law et al., 2001; Villaescusa, 2004). Brady (1990) states that, substantial progress has not been attained in the study of repeated exposures of dynamic loading on jointed rock mass in comparison to conventional blasting with single episode of loading. Brown and Hudson (1974) states that rock mass damage by blast loading is predominantly due to joint motion, which is consistent with the experimental observation that joints decrease in shear strength under cyclic shear loading. Model studies of excavations in jointed rock under cyclic loading by Barton and Hansteen (1979) confirmed that excavation failure occurred by accumulation of shear displacements at joints. On the basis of these findings, St. John and Zahrah (1987) stated that, under dynamic loading, it is the number of excursions of joint motion into the plastic range that determines damage to an excavation. Wagner (1984) provided an indication of the general inadequacy of dynamic design based on V_{max} of single blast round. A possible conclusion with regards to dynamic behavior under a range of V_{max} is that repeated dynamic loading may amplify problems of dynamic instability in jointed rock mass in the underground openings like, multiple excavations, tunnels and caverns.

Although far-field damage is not a severe problem at the excavation sites where the blasting faces moves away and vibration gets attenuated substantially, the authors observed that it is an acute problem when the rock mass is subjected to repeated vibrations due to multiple excavations in the vicinity as in the case of multiple tunnels and caverns. In view of the above arguments it was decided to go for the investigation of both near field and far field damage assessments at the Lohari Nag Pala Hydroelectric Power Project (LNPHPP).

3. SITE DESCRIPTION

3.1 General

LNPHPP is located in the Central Crystalline of Higher Himalayan Zone and situated in Uttarkashi District of Uttaranchal State about 230 km from Rishikesh on National Highway No.108. The Project of 600MW capacity is located on the right bank of Bhagirathi River. The location of

Figure 1. Location of the LNPHPP site on Bhagirathi River, Uttaranchal, India

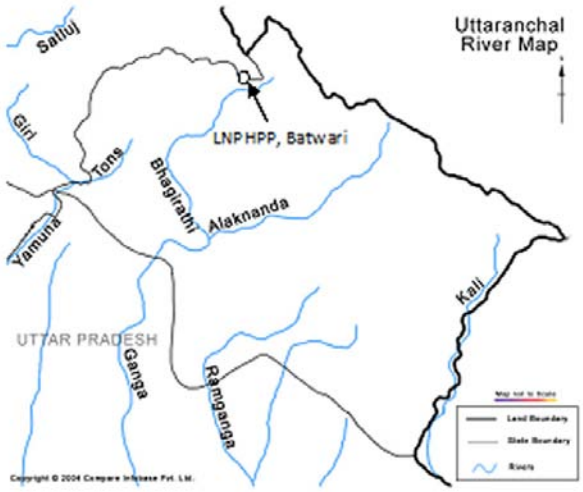

the site falls at a Longitude of 78.53^{0}E and Latitude of 30.25^{0}N and is shown in Figure 1. This infrastructural project comprises of construction of 73.40 m wide Barrage across river Bhagirathi. The major underground structures under excavation include Head Race Tunnel (HRT), Power House and Tail Race Tunnel (TRT). The HRT is of 14 km long and 6.0 m diameter with horse-shoe shape on the right bank of river meant for water transmission to the Underground Power House. The dimensions of underground Power House to be excavated are 155 m X 22 m X 47 m. Water from the Power House is discharged back in to the Bhagirathi River through a 350 m long Tail Race Tunnel (TRT) with 7.5 m diameter (horse-shoe shape) tunnel. The Powerhouse is proposed to house four units of 150 MW each totaling 600 MW. The construction of 14000 m Head Race Tunnel will be accessed from three numbers of intermediate construction adits, apart from inlet and outlet ends, which will facilitate the excavation of HRT from eight faces. The power house is accessed with TRT, Main Access Tunnel (MAT) of 8m diameter (D-shape) and a Cable &Ventilation Tunnel (CVT) of 6m diameter (D-shape). There is also another adit to access the TRT. All these tunnels around powerhouse are called power house complex, which is shown in Figure 2. As there was repeated number of blast loadings on the underground openings, the experimentation was designed to determine the effect of repeated vibrations on rock mass damage, on the basis of previous experience of the authors (Ramulu, 2009). The damage assessment was carried out at both the side walls of the tunnel as the joint orientation with respect to tunnel perimeter line was making acute angle at the Left-side and obtuse angle at the Right-side of the tunnel. The damage assessment was also carried out at Crown rock mass of the tunnel where the joint orientation with respect to tunnel perimeter line was making 180^0 angle. The objective of damage assessment at three different locations is to know the effect of joint orientation with respect to the perimeter line of the tunnel. The tunnel profile where the experimentation was carried out is shown in Figure 3.

3.2 Geological and Geotechnical Information of Experimental Site

The LNPHPP falls in the Uttrakhand Himalayas and is located on the River Bhagirathii upstream

Figure 2. Plan view of various tunnels near the power house complex, LNPHPP

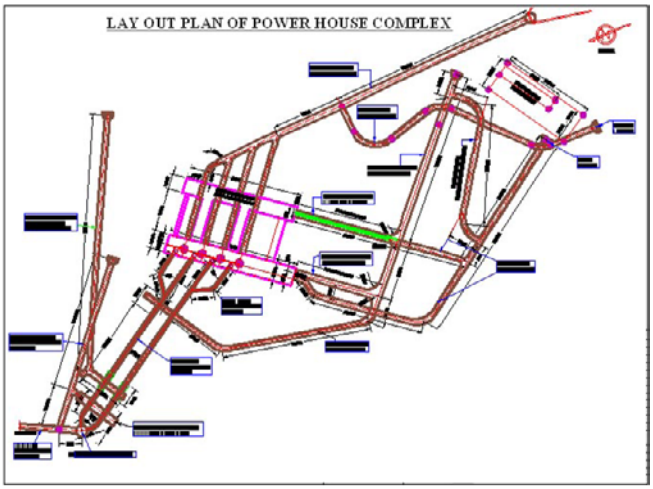

Figure 3. Experimentation tunnel with varying joint orientations at both Left and Right-sides

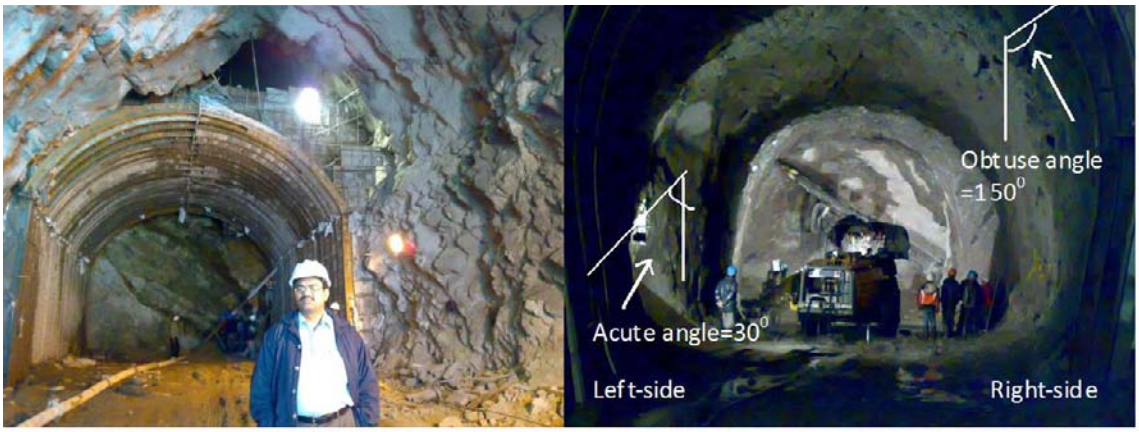

(a) Tunnel portal (b) Excavated tunnel profile

of Uttarkashi district. The Uttarkahsi region is made up of two main tectonic units namely the Himalayan Central Crystallines and the Lesser Himalayan Formation. The slab of the Central Crystallines has been thrusted southward along the Main Central Thrust (MCT) over the quartzite and volcanic of Berinag Formation of the Lesser Himalayas or rock belonging to Garhwal Group. The Garhwal Group towards north is followed by the Central Crystallines which have been divided into three zones i.e. Upper Crystallines, Middle Crystallines and Lower Crystallines. Garhwal Group towards north is followed by the Central Crystallines which have been divided into three zones i.e. Upper Crystallines, Middle Crystallines and Lower Crystallines. The main rock type of powerhouse complex is schistose gneiss and augen gneiss with abundance of mica and geotechnically the rock mass is negotiating in "Fair Category" and it's having three prominent joint sets. The main

Table 1. General geological information

Location	Crown to Spring level (Both Sides)	Below Spring level(Left-side)	Below Spring level (Right-side)
Rock type	Schistose/Augen gneiss with alternative bands of mica & quartz	Mica schist with alternative bands of quartz	Schistose/Augan gneiss with bands of mica and quartz
Critical joint angle	$50^0/52^0$, $210^0/50^0$	$095^0/55^0$, $175^0/45^0$	$095^0/55^0$, $175^0/45^0$
Seepage	Moderate	Continuous	Occasional
Wedge portion	Crown	None	Walls
Spacing	6-20, 20-60cm	6-20, 20-60cm	<6, 6-20cm
Opening	0.25-2.5mm	0.25-2.5mm	0.25-2.5mm
Joint Roughness	Rough, Planar& Undulating	Rough, Undulating	Smooth, Undulating
Joint Alteration	Altered joint, highly staining	Moderately altered walls	Moderately altered walls
Type of Filling	Mica, Quartz	Mica, Quartz	Quartz
Rock Strength	Weak-Medium strong (25-50MPa)	Weak-Medium strong (25-50MPa)	Weak (5-25 MPa)
Nos. of Joint Sets	Three joint sets + Random	Three joint sets + Random	Three joint sets + Random
Degree of Weathering	Slightly Weathered Rock	Moderately-Highly Weathered	Moderately Weathered
Water Inflow	Dripping (Low)	Damp	Seepage at places
Rock mass Quality (Q)	1.53-3.04 Poor rock	0.86-1.14, Poor rock	1.15-3.04, Poor rock
Rock mass Rating (RMR)	46-49, Class III, Fair	37-44, Class IV, Poor	52-57, Class III, Fair

two joint sets intersecting at right angle which makes wedge continuously. Some weak zone/ clay filling, altered rock, sheared rock mass and excessive flow of water at places makes the rock poor. In maximum area it is found that the regional trend of foliation is perpendicular to the tunnel alignment, another joint which is intersecting the foliation at right angle and creates wedge on roof. The strike of the foliation is going through along the tunnel alignment which is geologically not favorable because of probabilities of plane failure and wedge failure in presence of heavy joint planes. The detailed geological information is given in the Table 1. Core samples were collected from both the monitoring locations by underground coring machine. Engineering properties like Rock Quality Designation (RQD) compressive strength, tensile strength, density and compressional wave velocity (Vp) were determined from the core samples. In-situ compressive strengths were also determined by using Schmidt hammer rebound testing. The average intact rock properties of the Schistose/ Augan gneiss at two different experimental locations are given in Table 2.

4. DETAILS OF THE BLASTING AND INSTRUMENTATION

The tunnel was excavated with heading and benching simultaneously by using drilling and blasting method. Rocket boomer was used for drilling of blast holes of 45 mm diameter. Wedge cut blasting pattern was adopted with a maximum hole depth of 3.5m for the tunnels of $32m^2$ area of cross section. The blast pattern practiced for the full face tunnel blasting at powerhouse complex is shown in Figure 4. The specific charge was varied depend-

Table 2. Average intact rock properties of the Schistose/Augan gneiss

Location	Rock type	Mass Density, kg/m^3	Tensile strength, MPa	Young's modulus, GPa	P-wave velocity, m/s
Right-side wall	Schistose/Augan gneiss with acute joint orientation	2450	3.5	21.5	2958
Left-side wall	Schistose/Augan gneiss with obtuse joint orientation	2445	3.1	19.25	2610
Crown	Schistose/Augan gneiss with obtuse joint orientation	2420	3.3	20.18	2830

ing on the static and dynamic properties of rock. The explosive used was cartriged emulsion with 80% strength. The in-hole velocity of detonation (VOD) of the explosive was determined as 3000-3100 m/s by using VOD monitoring instrument called SuperTrap (M/s MREL Inc., Canada). Long delay detonators from 1 to 10 were used to fire various rows in different delays. The maximum charge per delay used in the blast round was 32 kg in the bottom holes and total charge per round was 169kg. Total number of holes used was 87 which include 13 dummy holes at the Crown periphery of the tunnel line. The specific charge used for Schistose/Augen gneiss was 1.75 kg/m^3. The progress per round with this blast pattern was observed as 2.5 to 2.75m out of 3m effective depth of blast round.

Instrumentation carried out in this study include, triaxial geophones for vibration monitoring, borehole camera survey for observing crack extension, loosening of joints and borehole extensometers for measurement of plastic deformations. It has become common practice, recently, to use peak particle velocity (V_{max}) as an indicator of the potential for rock mass damage, as the V_{max} is directly proportional to the dynamic strain (Jaeger & Cook, 1979). Numerous authors used V_{max} as criteria for blast damage in rock mass (Langefors and Kihlstrom, 1963; Kutter and Fairhurst, 1971; Holmberg and Persson, 1978; Holmberg and Persson, 1980; Oriard, 1982; Singh, 1993; Yu and Vongpaisal, 1996; Villaescusa et all, 2004). Application of borehole extensometers for blast damage inspections was reported by many authors globally (Niklasson, 1985; Stacey et al, 1990; Kim, et al, 1990; Villaescusa et al, 2004). Application of borehole camera for blast damage inspections was reported by many authors globally (Niklasson, 1985; Beyer and Jacobs, 1986; Stacey et al, 1990; Rocque et al, 1992; Singh, 1993; Andrieux et al, 1994; Doucet et al, 1996; Liu et al, 1998). A room of 0.5 m^3 inside the wall of MAT was made for installation of geophones to capture the blast vibrations from the surrounding excavations and for the installation of borehole extensometers. The damage monitoring stations were located at the Chainage of 45m inside the MAT, which was exposed to the vibrations from face blasting of MAT, CVT as well as TRT adit (Figure 6). A typical damage monitoring set-up at the tunnel wall is shown in Figure 5, where the geophones, borehole extensometers and borehole camera survey holes are shown. The location of borehole extensometers and geophones and blasting location is schematically shown in Figure 6. The details of installation of instrumentation are given in the following sections.

4.1 Installation of Geophones

It was required to measure the blast vibrations in the near-field as well as far-field zones with respect to blast site to assess the rock mass damage. Therefore a room of about 0.5 m^3 (1m x 1m x0.5m) was excavated inside the sidewall for installation

Figure 4. Blast design at power house complex, LNPHPP

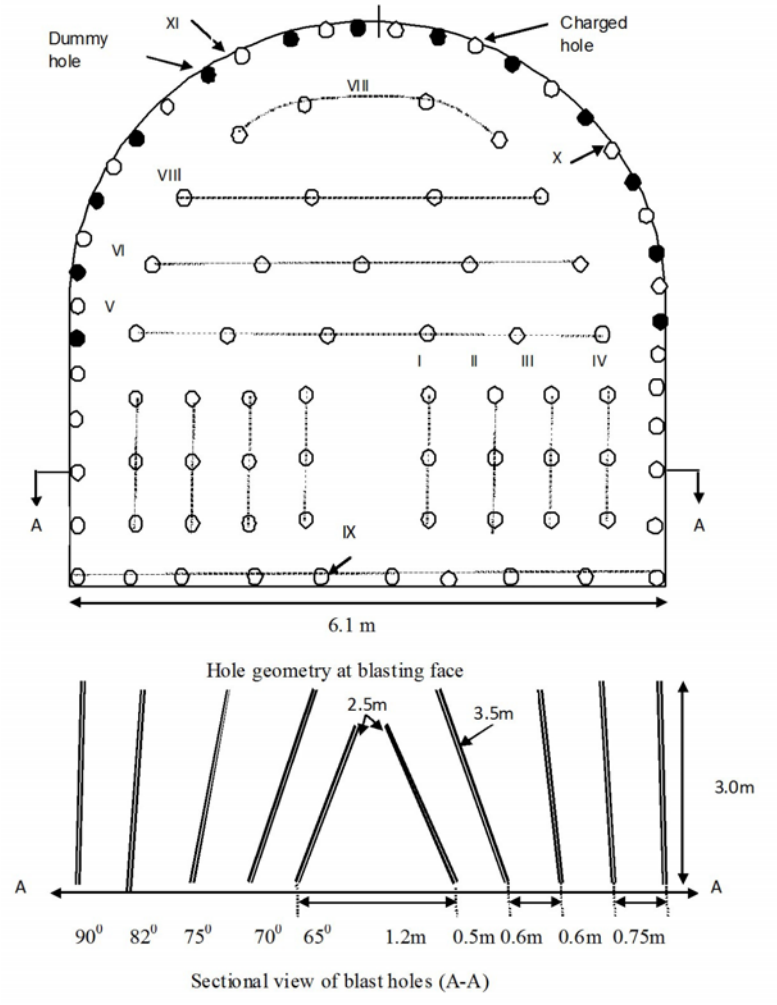

(The numbers in Roman letters denote delay numbers)

of geophones at a height of 1m from the bottom. The geophone room excavation was carried out by controlled blasting by using mild explosive charges to avoid disturbance to surrounding rock mass. The geophone room was located at about 5m from the initial blasting face and the vibration monitoring was carried out continuously, while the blasting face receded away up to a distance of 45-50m. The geophone sensors of higher frequency and recording equipment with faster sampling rates were used for near-field monitoring and ordinary low frequency geophone sensors were used for far-field vibrations monitoring. Both the seismographs used for vibration monitoring are shown Figure 7.

4.2 Installation of Borehole Extensometers

Holes were drilled across the joint planes and foliations of the rock mass in the tunnel wall to install borehole extensometers. Conventional

Figure 5. Schematic of installation locations of geophones, borehole extensometers and borehole camera inspection holes

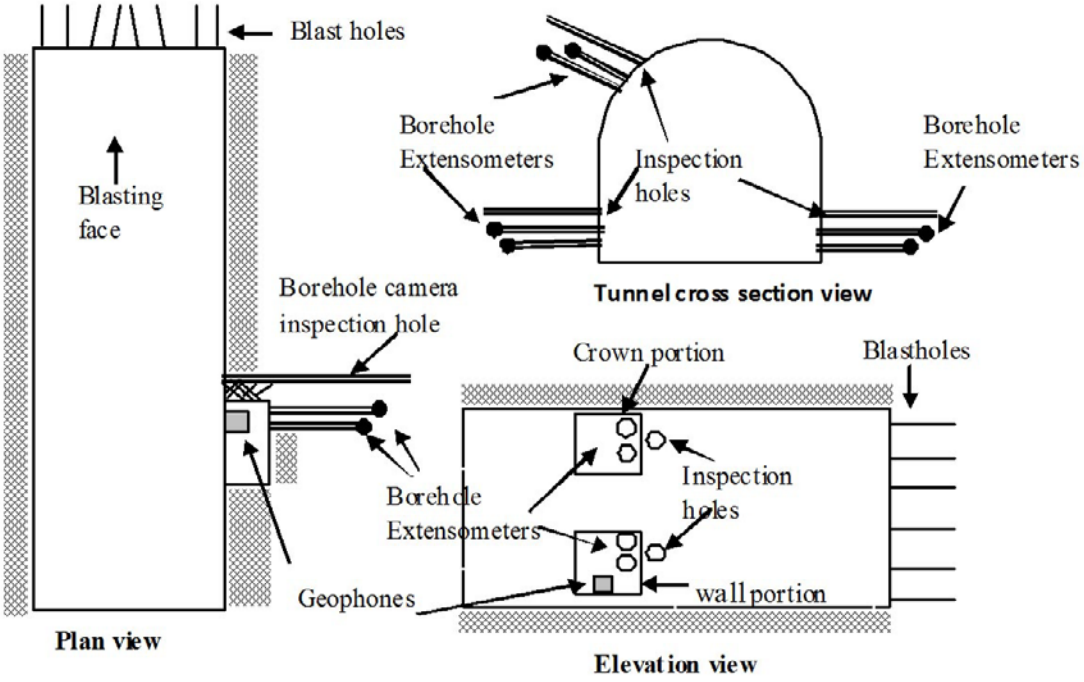

Figure 6. Schematic view of vibration and damage monitoring stations with respect to blasting location

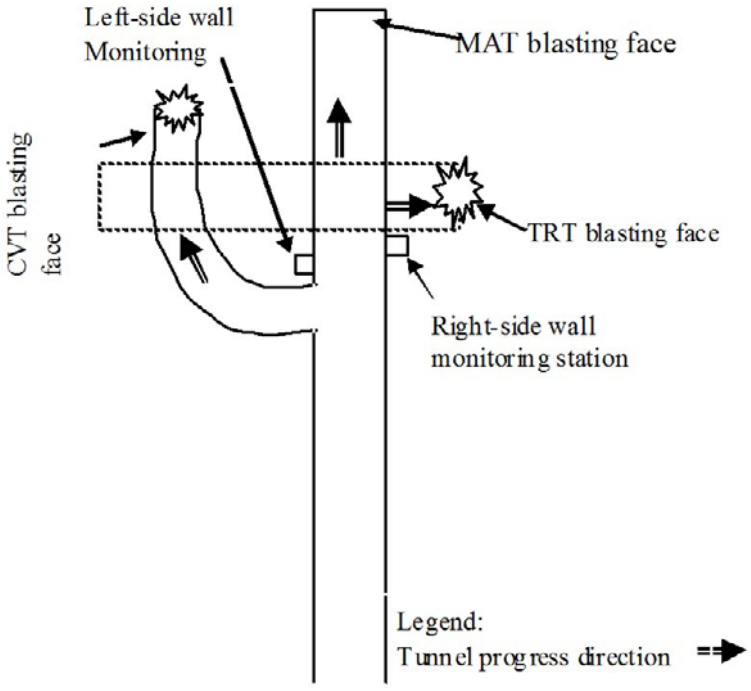

Figure 7. The installation of (i) borehole extensometer and (ii) geophones

borehole extensometers available in the market were used for measurement of plastic deformations. Two borehole extensometers were installed at the Left-side and two more were installed at the Right-side of the tunnel wall, at a height of 1.5m from ground level. Each extensometer consists of two extension rods with varying lengths inserted into the borehole and installed as per the norms prescribed by ISRM (1992). Digital gauges were used to measure the positive or negative extension values of the extensometer at the free end in the mouth piece of extensometer. The lengths of borehole extension rods were 3 and 4m at the Left-side and 3.5 and 4.5m at the Right-side of the tunnel wall. The installation of borehole extensometer and geophones are shown in Figure 7.

4.3 Installation of Borehole Camera

Borehole camera inspection holes of 36mm diameter and 5m depth were drilled across the joint planes of the rock mass in the sidewall, approximately 0.5m away from the geophone location as well as extensometer (Figure 5). The location and direction of holes were made such that it can intersect maximum joint planes so that the joint displacements and possible new cracks can be detected by borehole cameras. The camera observation holes were made at the close proximity of geophone holes, so that the possible rock mass damage levels can be correlated with the measured peak particle velocity (V_{max}). The monitoring program consisted of surveying the inspection hole before and after each blasting event. The borehole camera used in this study was a robust unit with semi-rigid fiberglass signal cable. This camera contains a standard video output and can be connected with any TV or video-recording system with VCR input. Borehole surveys were made by using a front view lens attachments, which could capture images from all the sides of the hole. This gave a clearer picture of the borehole wall, before and after blasting. All surveys were recorded in a computer, attached to the camera and analysed on surface to determine the frequency of cracks and crack extensions before and after every blast.

5. EXPERIMENTATION ON THE EFFECT OF REPEATED BLAST LOADING

5.1 Near-Field Blast Damage Assessment

The near-field damage to the rock mass at the experimental site occurred due to the production blast rounds conducted within the tunnel. The near-field damage was assessed by the Holmberg-Persson model (1978) as well as borehole camera survey. The principle of Holmberg-Persson Equation, is to add the contribution of every small portion of the explosives column along the full charge length to derive the peak particle velocity (V_{max}) at a fixed sensor location. More details about the Holmberg-Persson (H-P) model can be known from the sited references (Andrieux et al., 1994; LeBlanc, 1995; McKenzie et al., 1995; Meyer & Dunn, 1996; Liu & Proulx, 1996).

The Holmberg-Persson Equation can be simplified to,

$$V_{\max} = K\left[a\right]^{\alpha} \quad (1)$$

where, *a* is here defined as the Holmberg–Persson term and K and α are the rock mass and explosive specific attenuation constants. K and α can be obtained by linear regression from experimental data vibration and distance. The mean values of K and α show the general trend of vibration attenuation in the rock mass. In this study, The Holmberg–Persson approach was applied to determine the site specific constants K and α to model peak particle velocity attenuation across rock mass. Same type of explosive and design parameters were used for all the experiments and analysis of the results are presented in the following paras.

Near-field peak particle velocity (V_{max}) measurements were grouped and analysed separately for two experimental sites. Typical log–log plot of the measured V_{max} values obtained in this study against the Holmberg–Persson term. The V_{max} amplitudes were being experienced at similar distances and for the same design parameters. This plot is used to determine the K and **α** constants by fitting the linear relationship of the form, $Log(V_{max})= \boldsymbol{\alpha}\ Log(a)+Log(K)$. Results of the analysis are summarized in Table 3. The calculated K and α constants were slightly different for different test sites of the tunnel where the monitoring stations were set up. After determining the site specific attenuation constants, preliminary predictions of the extent of blast damage into wall-rock were made by applying the Holmberg–Persson model and by considering a site specific critical V_{max} or damage threshold (V_{cr})given by the following relationship (Persson et al,1994),

$$V_{cr} = \frac{\sigma_T V_p}{E} \quad (2)$$

where,

V_{cr} = Critical peak particle velocity before tensile failure (mm/s);

σ_T = Uniaxial tensile strength of rock (Pa);

V_p = Compressional wave velocity in rock mass (mm/s);

E = Young's Modulus of rock (Pa).

From the properties described in Section 4 (Table 2) and by adopting the above relationship (equation 2), the value of damage threshold peak particle velocities (V_{cr}) calculated were 353, 427 and 407mm/s for the Left-side, Right-side and Crown rock mass, respectively. These threshold values were used to compare the extent of damage caused by the near-field blast rounds, which obviously generated maximum peak particle velocity. The near-field damage analysis was carried out by using H-P model is shown in Figure 8. The

Table 3. Extent of predicted rock mass damage into the tunnel wall

Location	Rock type	K	α	V_{cr} from H-P model	Damage from H-P model	Damage from Borehole camera survey
Left-side wall	Schistose/Augan gneiss with obtuse joint orientation	671	0.75	353 mm/s	1.40 m	1.59 m
Right-side wall	Schistose/Augan gneiss with acute joint orientation	697	0.99	427 mm/s	1.30 m	1.74 m
Crown rock mass	Schistose/Augan gneiss with right angle joint orientation	687	0.90	407 mm/s	1.35 m	1.53 m

above analysis indicates that on average the extent of blast induced damage was 1.40m, 1.30m and 1.35m at Left-side, Right-side and Crown rock mass, respectively. The damage levels assessed by H-P model were cross checked by borehole camera survey before and after each blast round. An initial pre-blasting survey was performed in each hole to take pictures of pre-existing structural features for comparison with post blast surveys. A total of three borehole camera surveys were taken, one each at Left-side, Right-side and Crown rock of tunnel. All the pictures were sorted out first by editing and matching the same images before and after each blast. Consequently, the pictures, which showed differences in fracture existence, were identified by their position coordinates. The images of inspection holes captured by borehole camera clearly indicated that the near-field damage due to production blasts extended up to 1.59m, 1.74m, and 1.53m at Left-side, Right-side and Crown rock mass, respectively. Near-field damage observations of both the methods are given in Table 3. The borehole camera inspection survey results shows contrasting results in comparison to the H-P model analysis. According to the tensile failure criteria the there should be lesser damage to the Right-side wall as it is relatively sound. But the actual damage survey indicates more damage to Right-side wall in comparison to Left-side wall. This might be due to the dominant role of joint orientation over the soundness of the rock. Investigations were further carried out to establish the role of joint orientation in the blast induced damage.

5.2 Far-Field Blast Damage Due to Repeated Vibrations

The multiple rounds of blasting activity were carried out at the power house complex as shown in Figure 6. In order to monitor the effect of repeated blasting due to multiple rounds the peak particle velocity of vibrations and plastic deformations were measured continuously by geophones and borehole extensometers respectively. Far-field rock mass damage observations were also carried out by using borehole camera by regular inspection of observation holes. In order to correlate the far field damage with the vibrations, the V_{max} levels were recorded for every blast round uptill the vibration intensity attenuated to about 45mm/s. All the damage observation systems were monitored for 60 rounds of blasts at all the three monitoring locations of MAT i.e. Right-side wall, Left-side wall and Crown rock. As the blast site is moving away from the monitoring point the vibration intensity, obviously, reduced gradually below critical peak particle velocity. The effect of these reduced vibration levels with the repeated number of exposures on the extent of further damage was studied thoroughly by all the three instruments. The blast damage assessment at Left-side, Right-side and Crown rocks of the MAT tunnel is discussed in the following sections separately.

Figure 8. Results of the analysis by using H-P model

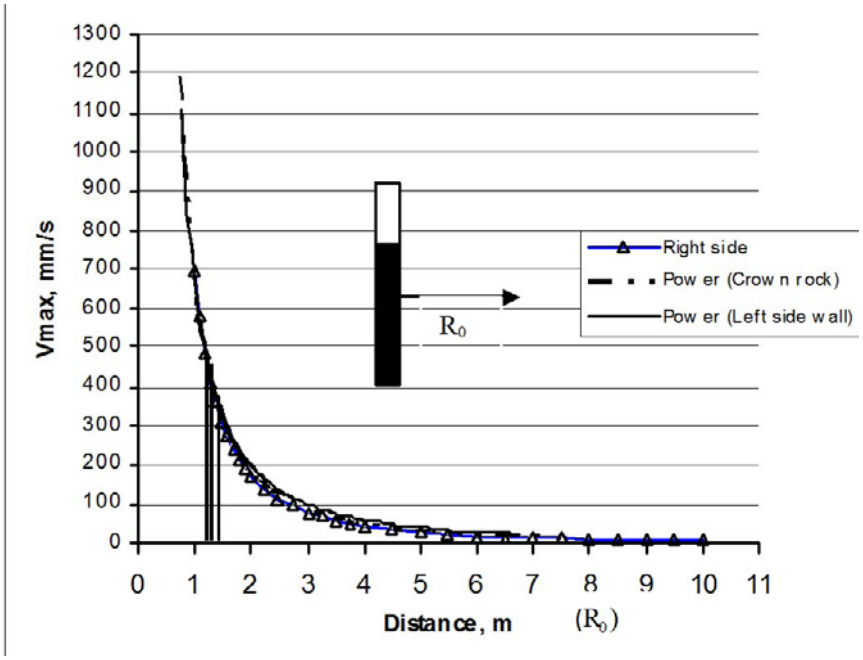

5.2 .1 Damage Assessment of Left-Side Rock Mass at MAT

Peak particle velocities versus no. of occurrences of dynamic loading at gneiss rock mass with acute angle joint orientation is shown in Figure 9. The vibration intensity recorded was ranging from 40 to 1753 mm/s at the monitoring location. A typical near-field vibration event history recorded during the study is shown in Figure 10. The displacements of extensometer rods of 3 and 4m depth at the Left-side tunnel wall were proportional to the V_{max} for few near-field blast rounds of MAT face blasts, where the V_{max} is above V_{cr} (Figure 11). There was no considerable change in the extensometer readings of both 3 and 4m rods for all the V_{max} levels below V_{cr} (353mm/s) for the MAT and CVT face blasts. After 40 blast rounds, the displacements were again observed for TRT face blasts, even at the vibration levels 233.6 mm/s, which is below the V_{cr}. There were no displacements observed below the V_{max} level of 116mm/s. This effect gives an inference that the damage zone was below 3m from the tunnel perimeter. The exact depth of damage zone inside the tunnel walls could not be found with extensometers. Therefore, borehole camera observations were used for determination of exact depth of damage as well as extent of crack network and fracture frequency. As the range of damage extension was already assessed by means of extensometer, the inspection of exact extension of damage by borehole camera had become much easier. Images were captured by an interval of 5cm, within the range of probable damage extension for precise inspection of rock mass damage. The images of borehole sections which contain the interface of intact and disturbed rock mass of tunnel wall are shown in Figure 12. The damage depth measured by the borehole camera inspection survey at the Left-side wall with acute joint orientation was 2.70m.

Figure 9. Peak particle velocities versus no. of dynamic loading cycles at gneiss rock mass with acute joint orientation

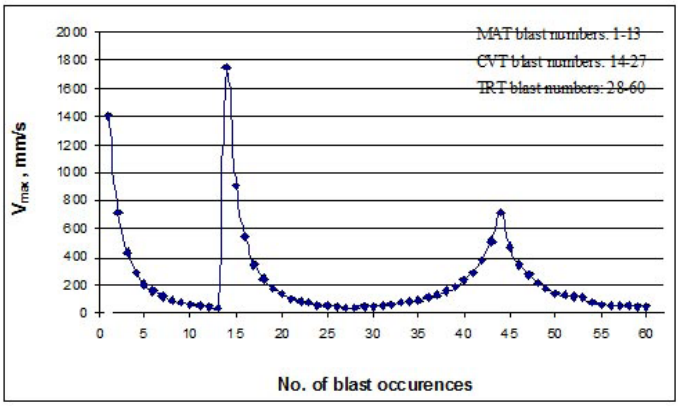

5.2.2 Damage Assessment of Right-Side Rock Mass at MAT

Peak particle velocities versus no. of occurrences of dynamic loading at Right-side of the tunnel is shown in Figure 13. The vibration intensity recorded at the monitoring location was ranging from 42 to 1644 mm/s. The displacements indicated by the extensometer rod of 3m depth at the Right-side wall were proportional to the V_{max} for few blast rounds at the MAT whose V_{max} were above V_{cr} (427mm/s), as shown in Figure 14. After 16 blast rounds it was observed that the displacements suddenly dropped to negligible levels even though the V_{max} recorded was above V_{cr}. This effect gives an inference that the damage zone reached the anchor point of the 3.0m extensometer rod after few close field blast loadings. This might be the reason why the 3.0m extensometer rod did not respond to even the vibrations levels which were greater than the critical vibration levels. There were substantial displacements observed to the 4.0m extensometer rod (Figure 14) for the V_{max} levels above V_{cr} for the MAT and CVT blast rounds and no displacements (>1mm) was observed for the V_{max} levels below V_{cr} for the blast rounds of same locations. After 40 rounds of blast occurrences, the displacements were again observed at the vibration level, 254 mm/s, which is much below the V_{cr}. There were no displacements observed below the V_{max} level of 98 mm/s. This result gives an inference that the anchor point of 4.0m rod was in elastic zone and the damage zone was within 4m from the tunnel perimeter. The borehole inspection survey was conducted to cross check the damage assessment by extensometers and for exact damage measurement. The images of borehole sections which contain the interface of intact and disturbed rock mass are shown in Figure 15. The maximum damage depth measured by the borehole camera survey with obtuse joint angle orientation was 3.6m. This was the reason for the roof failure occurred near the test site. The roof failure due to extension of fractures beyond 3m due to repeated blast induced damage is shown in Figure 16. The maximum length of roof bolts designed for that rock mass was also 3m.

5.2.3 Damage Assessment of Crown Rock Mass at MAT

Peak particle velocities versus no. of occurrences of dynamic loading at Right-side of the tunnel is shown in Figure 17. The vibration intensity recorded at the monitoring location was ranging from 43.44 to 1602 mm/s. The displacements

Figure 10. Near-field vibration event history recorded during the experimentation

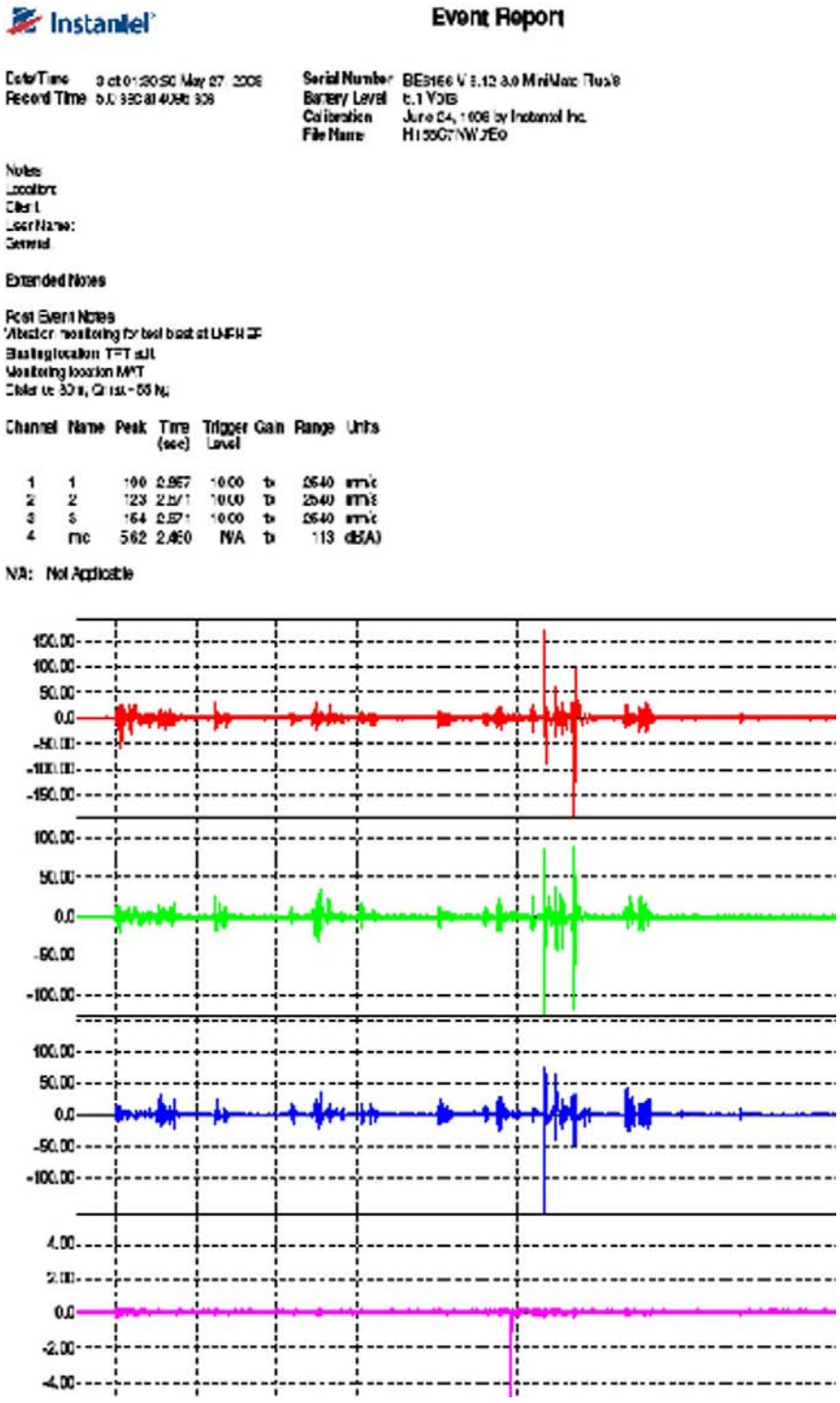

Figure 11. Plastic deformations of extensometer rods at Gneiss rock mass with acute joint orientation

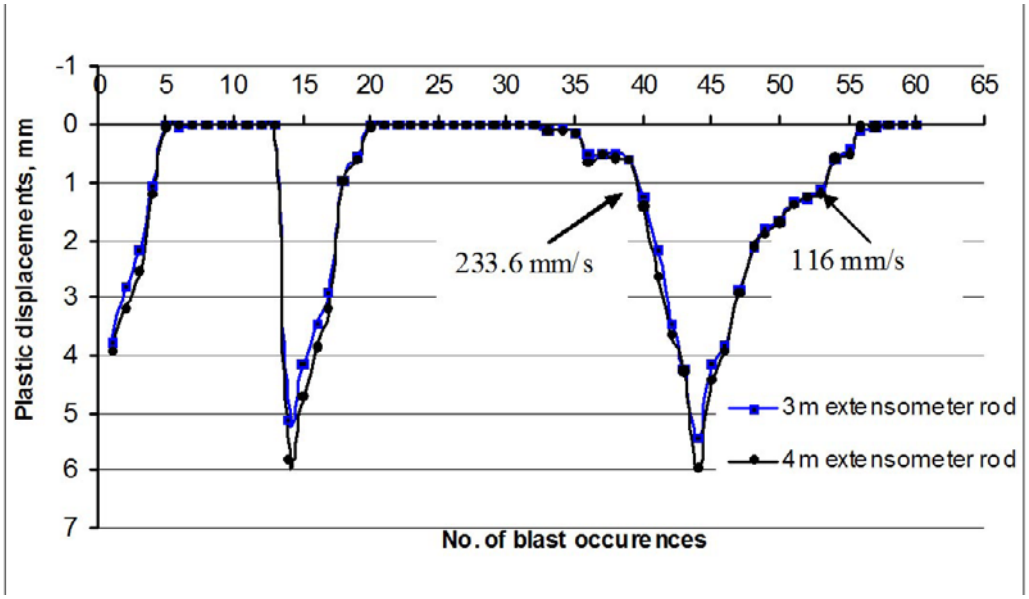

Figure 12. Images of pre-blast and post-blast inspection surveys of rock mass with acute joint orientations captured by borehole camera

indicated by the extensometer rod of 3m depth at the Right-side wall were proportional to the V_{max} for few blast rounds at the MAT whose V_{max} were above V_{cr} (407mm/s), as shown in Figure 18. After 42 blast rounds it was observed that there were no displacements observed even though the V_{max} recorded was above V_{cr}. This effect gives an inference that the damage zone extended beyond the anchor point of the 3.0m extensometer rod after the exposure of 42 close field and far-field blast loadings. This might be the reason why the 3.0m extensometer rod did not respond to higher vibrations levels than the V_{cr}. There were substantial displacements observed to the 4.0m extensometer rod (Figure 18) for the V_{max} levels above V_{cr} for the MAT and CVT blast rounds and no displacements (>1mm) was observed for the V_{max} levels below V_{cr} for the blast rounds of same

Figure 13. Peak particle velocities versus no. of occurrences of dynamic loading at Gneiss rock mass with obtuse joint orientation

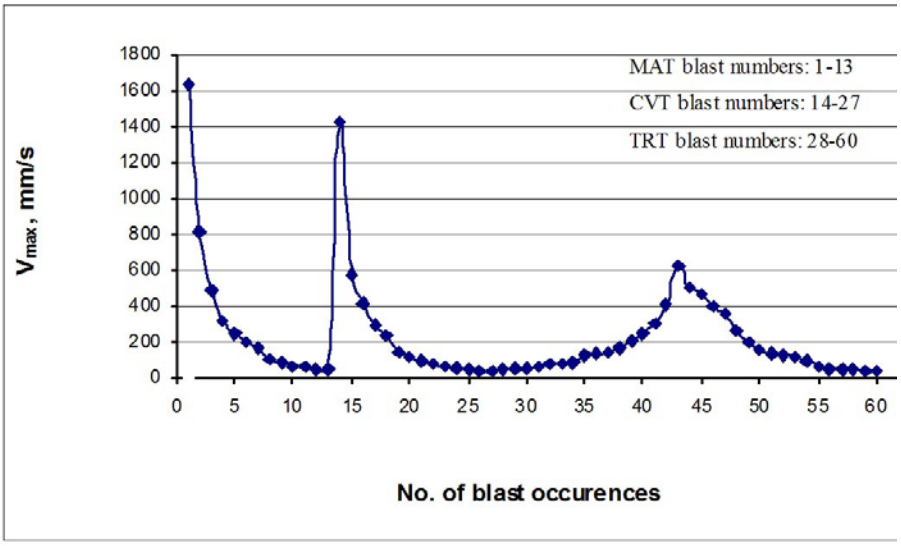

Figure 14. Plastic deformations of extensometer rods at Gneiss rock mass with obtuse joint orientation

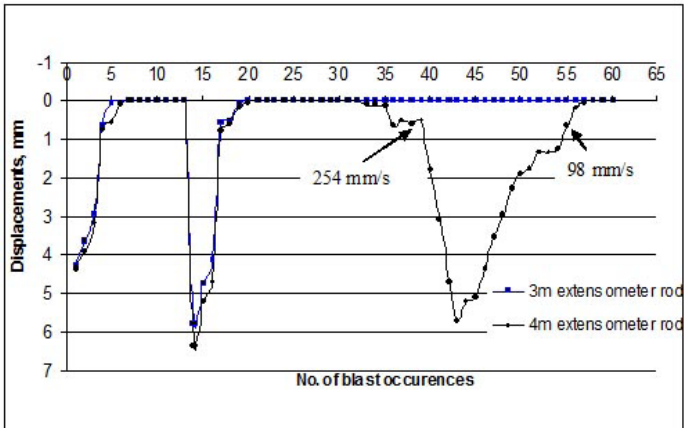

locations. After 39 rounds of blast occurrences, the displacements were again observed at the vibration level, 268 mm/s, which is much below the V_{cr}. There were no displacements observed below the V_{max} level of 112 mm/s. This phenomena gives an inference that the anchor point of 4.0m rod of the extensometers was in elastic zone and the damage zone was within 4m from the tunnel perimeter.

The borehole inspection survey was conducted for capturing the damaged rock strata due to repeated blasting at Crown of tunnel. The images of borehole sections which contain the interface of intact and disturbed rock mass are shown in Figure 19. The maximum damage depth measured by the borehole camera survey with joint angle parallel to the tunnel profile was 3.21m, but

Figure 15. Images of intact and disturbed rock mass with obtuse joint orientations captured by borehole camera

Figure 16. Roof failure due to extension of fractures due to repeated blast induced damage

the maximum length of roof bolts designed for that rock mass was only 3m. This inadequate length of roof bolts led to roof failure due to extension of fractures beyond 3m due to repeated blast induced damage is shown in Figure 20. The far-field damage due to repeated loading at the three monitoring locations is given in Table 4.

6. RESULTS AND DISCUSSIONS

The near field blast loading due to main tunnel excavations, could generate displacements in the rock mass, only when the peak particle velocity exceeded the critical vibration levels (V_{cr}). After repeated exposures of vibrations due to blast rounds at MAT, CVT and TRT, plastic displacements observed even at lower levels of vibrations than the V_{cr}. The extra damage due to repeated

Figure 17. Peak particle velocities versus no. of occurrences of dynamic loading at Gneiss rock mass with obtuse joint orientation

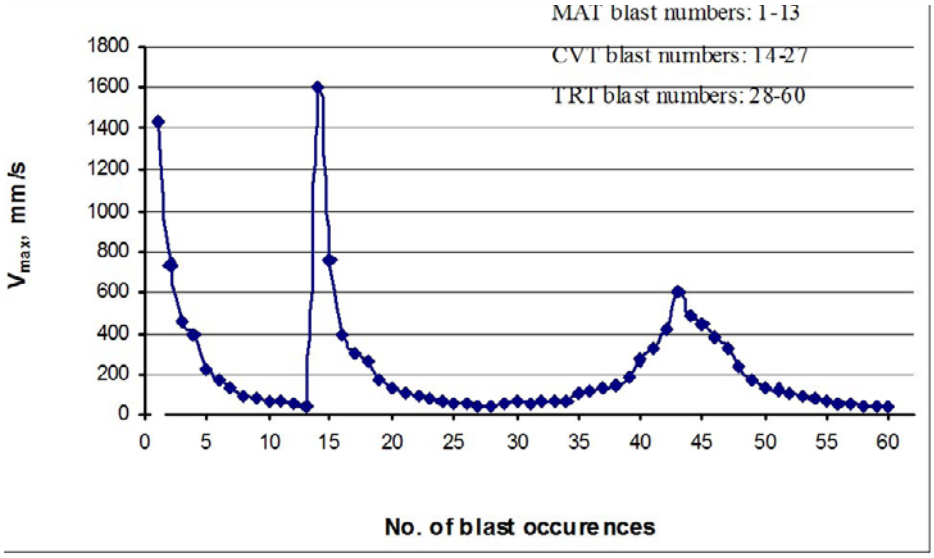

Figure 18. Plastic deformations of extensometer rods at Gneiss rock mass with obtuse angle joint orientation

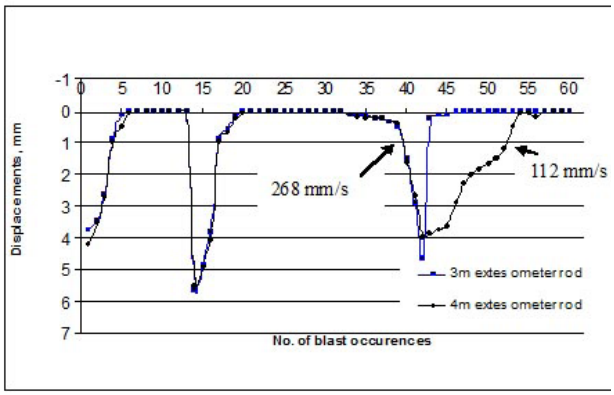

blast loading was 1.11m, 1.86m and 1.68m at the Left-side, Right-side and Crown portions of the tunnel respectively.

After the occurrences of 53 numbers of blast rounds with the V_{max} levels ranging from 40-1753 mm/s, considerable displacements observed in the extensometer even at the V_{max} level of 116 mm/s, which is approximately 33% of V_{cr} in the Gneiss rock mass with acute joint orientation. The displacements observed at the V_{max} level of 98 mm/s i.e. at approximately 23% of V_{cr} in the Gneiss rock mass with obtuse joint orientation, after 54 numbers of occurrences of blast loading. Similarly, displacements observed at the V_{max} level of 112 mm/s i.e. at approximately 27.5% of V_{cr} in the Crown rock mass with parallel joint orientation, after 52 numbers of blast occurrences. These results are well in line with the observations of

Figure 19. Borehole camera images of intact and disturbed rock mass with obtuse angle joint orientations

Figure 20. Roof failure due to extension of fractures beyond 3m due to repeated blast induced damage

Table 4. Far-field damage due to repeated loading at both the sides of tunnel wall

Location	Rock type	No of cycles of blast loading	Threshold vibration limits, mm/s	Maximum Extent of damage, m
Left-side wall	Schistose/Augan gneiss with obtuse joint orientation	53	116	2.70
Right-side wall	Schistose/Augan gneiss with acute joint orientation	52	98	3.60
Crown rock	Schistose/Augan gneiss with obtuse joint orientation	54	112	3.21

Dowding & Rosen (1978). The threshold vibration limits with number of cycles of repeated loading for two different rock mass are given in Table 4. The study also reveals that the overall damage was about 33% and 19% more at Right-side and Crown rock mass respectively, in comparison to the Left-side rock mass. The observations also indicate that the repeated dynamic loading resulted in the damage at the vibration levels even at 23% of V_{cr} when the unfavorable joints exist. These observations were almost similar to the findings of Adamson and Scherpenisse (1998), which says that of threshold vibration level falls down to 25% of V_{cr} in repeated loading conditions. The findings of the study clearly indicate that the phenomena of repeated blasting with respect to number of cycles of loading should be taken in to consideration for proper assessment of comprehensive blast induced damage.

7. CONCLUSION

A comprehensive blast monitoring program aimed at the investigation on the effect of repeated blast induced damage due to near-field and far-field vibrations was conducted in a Gneiss rock mass. The damage levels predicted for near-field blast loading by Holmberg-Persson model were 1.40m, 1.30m and 1.35m for the Left-side, Right-side and Crown rock mass, respectively. The damage levels measured for the same rock mass by borehole camera was 1.59m, 1.74m and 1.53m for the Left-side, Right-side and Crown rock mass, respectively. Estimates of the maximum extent of rock mass damage made through the application of the Holmberg-Persson model compared well with measured results for Left-side wall and Crown rock mass, although the former one was at lower side of damage. The damage results of Holmberg-Persson model were deviating with the measured results for Right-side wall. This might be because of the additional effect of joint orientations, playing a dominant role at Right-side wall rock mass. Although there are deviations, the modelling approaches like Holmberg-Persson model are very useful for the project engineers for preliminary assessment and estimation of the damage and for practical methods to model peak particle velocity attenuation.

The study also found that repeated dynamic loading imparted on the exposed tunnel from subsequent blasts in the vicinity is going to contribute to rock mass weakening and preconditioning. After 53 repeated blast rounds, the threshold vibration level for the Gneiss at Left-side wall was found to be 116 mm/s. The dynamic loading due to repeated blasts resulted in 70%, 107% and 110%of extra damage, in addition to the near-field damage, at Left-side, Right-side and Crown rock mass, respectively. The repeated dynamic loading also resulted in reduced threshold peak particle velocity to 33%, 23% and 28% of critical peak particle velocity at Left-side, Right-side and Crown rock mass, respectively. The study also revealed that the overall damage was about 75% more at tunnel wall with obtuse angle joint orientation in comparison to the acute angle joint orientation. The findings of the study clearly indicate that the repeated blast loading extends damage to a substantially dangerous levels and the effect is severe in case of unfavorable joint orientations. Therefore the phenomena of repeated blasting with respect to number of cycles of loading is an important aspect to be considered for proper assessment of blast induced damage and for planning of safety measures of underground openings.

ACKNOWLEDGMENT

The research work presented in this paper is a part of PhD degree of the first author from Indian Institute of Science and it is also part of CSIR sponsored project No. 70 (0058)/06/ EMR-II-CSIR for which the authors are grateful to CSIR. The authors express their sincere thanks to the Director, CMRI for permitting to publish this

paper. The authors express their sense of gratitude to Mr. P.B. Choudhury, Dr. John Loui P., Dr. A.K. Raina, Dr. M.R.Saharan and Mr.B.K.Jha for their cordial help during the field studies. The authors express their sincere thanks to the Director, CIMFR (CMRI) for permitting to publish this paper. The authors also express their sincere thanks to all the scientists of CIMFR regional centre, Nagpur for their valuable assistance during the field work. The authors are also thankful to the executives of M/s Patel Engineering Ltd. and NTPC for their cooperation during the field studies.

REFERENCES

Adamson, W. R., & Scherpenisse, C. R. (1998, February 2-5). The measurement and control of blast induced damage of final pit walls in open pit mining. In *Proceedings of 24th Annual Conf. on Explosives and Blasting Research* (p. 539), New Orleans, LA.

Andrieux, P., McKenzie, C., Heilig, J., & Drolet, A. (1994). The impact of blasting on excavation design – A geomechanics approach. In *Proceedings of the 10th Symposium on Explosives and Blasting Research ISEE* (pp. 107–119), Austin, USA.

Anon. (1997). DGMS, India, S&T circular number 7 on *Criteria for safe vibration limits on structures* (pp. 1-8).

Atchison, T. C., & Pugliese, J. M. (1964). Comparative Studies of Explosives in Limestone. *BuMines Rept. of Inv. 6395* (p. 25).

Barton, N., & Hansteen, H. (1979). Very large span openings at shallow depth: deformation magnitudes from jointed models and finite element analysis. In *proceedings of the 4th rapid Excavation & Tunneling conference*, (Vol. 2) (pp. 1331-1353), Atlanta,GA.

Beyer, R.R., & Jacobs, A.M. (1986). Borehole television for geotechnical investigations. *Water Power and Dam construction, 38*(9), 16-28.

Brady, B. H. (1990). Dynamic performance and design of underground excavations in jointed rock. In Brummer (Ed.), *Static and dynamic considerations of Rock Engineering* (pp.1-10), Balkema, Rotterdam.

Brown, E. T., & Hudson, J. A. (1974). Fatigue failure characteristics of some models of jointed rock. *Earthquake Engineering & Structural Dynamics*, *2*, 379–386. doi:10.1002/eqe.4290020407

Chakraborty, A.K., Raina, A.K., Ramulu, M., Jethwa, J.L., & Gupta, R.N. (1998, November). Lake Tap at Koyna, *World Tunnel. Subsurface Exc.* (pp. 456-460).

Charlie, W. A., Veyera, G. E., Doehring, D. O., & Abt, S. R. (1985 October 15). *Blast induced liquefaction potential and transient porewater pressure response of saturated sands*. Final Report to Air Force Office of Scientific Research, Grant No. AFOSR-80-0260.

Connigham, C. V. B., & Goetzsche, A. F. (1996). The specification of blast damage limitations in tunneling contracts. *Tunnelling and Underground Space Technology*, *5*(3), 23–27.

Crandell, F. J. (1949). Ground Vibrations Due to Blasting and Its Effect Upon Structures. *Journal of the Boston Society of Civil Engineers* (pp. 222-245).

Doucet, C., Cameron, A., & Lizotte, Y. (1996, February 4-8). The effects of rock mass characteristics on fragmentation in controlled blasting experiments in small development headings. *ISEE's 22nd Annual Conference* (pp.1-11), Orlando, FL.

Dowding, C. H. (1985). *Blast Vibration monitoring*. Englewood Cliffs NJ: Prentice Hall.

Dowding, C. H., & Rozen, A. (1978). Damage to rock tunnels from earthquake loading. *J. Geotech. Eng. Div. ASCE*, *104*(GT2), 175–191.

Hendron, A. J. (1977). Engineering of Rock Blasting on Civil Projects. In W.J. Hall (Ed.) *Structural and Geotechnical Mechanics*. Prentice-Hall, Inc.

Holmberg, R. (1993). *Recent developments in control rock damage.* In A.A. Balkema & Rossamanith (Ed.), *Rock Fragmentation by Blasting* (pp. 197-198). Rotterdam.

Holmberg, R., & Persson, P. A. (1978, February 1-3). The Swedish Approach to Contour Blasting. *Conference on Explosives and Blasting Technique*. Society of Explosives Engineers, New Orleans, Louisiana, USA.

Holmberg, R., & Persson, P. A. (1980). Design of Tunnel Perimeter Blast Hole Patterns to Prevent Rock Damage. *Transactions of the Institution of Mining and Metallurgy*, *89*, A37–A40.

ISRM. (1992). Commission on Testing methods. *Suggested methods for installation of borehole extensometer*. International Society for Rock Mechanics.

Jaeger, J. C., & Cook, N. G. W. (1979). *Fundementals of rock mechanics* (3rd ed.). London, UK: Chapman & Hall.

Kim, H.-Y., Lee, K.-W., Mizuta, Y., & Lee, H.-K. (1990). A study on determination of the relaxed zone around an excavated tunnel. In Brummer (Ed.), *Static and dynamic considerations of Rock Engineering,* Rotterdam: Balkema (pp. 177-182).

Kutter, H. K., & Fairhurst, C. (1971). On the Fracture Process in Blasting. *International Journal of Rock Mechanics and Mining Sciences*, *8*, 181–202. doi:10.1016/0148-9062(71)90018-0

Langefors, U., & Kihlstrom, B. (1963). *The modern techniques of rock blasting*. New York: J. Wiley and Sons, Inc.

Law, T. M., May, J., Spathis, A. T., Du Plessis, A. T., & Palmer, A. M. (2001). Blast damage and blast dilution control: The applicaton of bulk emulsion systems at the WMC St Ives junction mine. *J. Rock Fragmentation by Blasting (Fragblast)*, *5*(1-2), 1–20.

LeBlanc, T., Heilig, J., & Ryan, J. (1995). Predicting the Envelope of Damage from the Detonation of a Confined Charge. In *Proceedings of the Sixth High-Tech Seminar on the State of the Art in Blasting Technology Instrumentation and Explosives Applications* (pp. 225–291), Massachusetts, USA.

Leet, L. D. (1946) *Vibrations from Blasting* (p. 34). Wilmington, DE: Hercules Powder Co.

Lewandowski, T., Luan Mai, V. K., & Danell, R. (1996, August). Influence of discontinuities on presplitting effectiveness. In *Proceedings of 5th Int. Symposium on Rock Fragmentation by Blasting* (pp. 217-225), Montrial, Canada.

Liu, Q., Tran, H., Counter, D., & Andrieux, P. (1998). A case study of blast damage evaluation in open stope mining at Kidd Creek mines. In the *24th Annual Conference on Explosives and Blasting Research* (pp. 323-336), New Orleans, LA.

McGarr, A. (1983). Estimating ground motion for small nearby earthquakes. *Seismic design of embankments and caverns* (pp. 113-127), New York, ASCE.

McKenzie, C., Scherpenisse, C., Arriagada, J., & Jones, J. (1995). Application of Computer Assisted Modelling to Final Wall Blast Design. In *Proceedings of the EXPLO'95 – A Conference Exploring the Role of Rock Breakage in Mining and Quarrying* (pp. 285–292), Brisbane, Australia.

Meyer, T., & Dunn, P. G. (1996). Fragmentation and Rock mass Damage Assessment – Sunburst Excavator and Drill and Blast. In *Proceedings of the NARMS 1996 – Rock Mechanics Tools and Techniques* (pp. 609–617).

Niklasson, B. (1985). Vertical crater retreat mining at the Luossavaara research mine, Swedish Detonic Research Foundation. In *11th Annual Conference on Explosives and Blasting Research* (pp.46-61), San Diego, CA.

Olson, M., & Bergqvist, I. (1996). Crack lengths from explosives in small diameter boreholes. In Rossamanith (Ed.), *Rock Fragmentation by Blasting*. Rotterdam: A.A. Balkema (pp. 193-198).

Oriard, L. L. (1989, February 5-10). The Scale of Effects in Evaluating Vibration Damage Potential. In *Proceedings of the 15th Annual Conference on Explosives and Blasting Research, International Society of Explosives Engineers* (pp.161-176), New Orleans, LA.

Oriord, L. L. (1982). Blasting effects and their control. *Underground Mining Methods Handbook*, SME of AIME (pp. 1590-1603), Littleton, Colorado.

Otuonye, F. O. (1997). Dynamic response of a fully grouted resin roof bolt to blast loading. In *Proceedings of Annual Conferance on Explosives and Blasting Research,* Explosives Reference Database on CD-ROM. Int. Society of Explosive Engineers, Ohio, USA.

Ouchterlony, F. (1997). Prediction of crack lengths in rock after cautious blasting with zero interholedelay. *Int. J. Rock Fragmentation by Blasting*, *1*, 417–444.

Ouchterlony, F., Sjoberg, C., & Jonsson, B. A. (1993). Blast damage prediction from vibration measurements at the SKB underground laboratories at ÄSPÖ in Sweden. *Intl. Soc. Explosive Engg*. (pp. 189-197), San Diego, CA.

Paventi, M., Lizotte, Y., Scoble, M., & Mohanty, B. (1996). Measuring rock mass damage in drifting. In Mohanty (Ed.), *Rock Fragmentation by Blasting* (pp. 131-138).

Persson, P. A., Holmberg, R., & Lee, J. (1994). *Rock Blasting and Explosives Engineering* (p. 540), Boca Raton, FL: CRC press Inc.

Ramulu, M., Chakraborty, A. K., & Sitharam, T. G. (2009). Damage assessment of basaltic rock mass due to repeated blasting in a railway tunnelling project – a case study. *Tunnelling and Underground Space Technology*, *24*, 208–221. doi:10.1016/j.tust.2008.08.002

Rocque, P. (1992). Techniques utilized for the detection and characterization of blast induced damage. Unpublished M. Sc. Eng. Thesis. Ontario, Canada: Queen's University at Kingston.

Scott, A., Cocker, A. N., Djordjevic, N., Higgins, M., La Rosa, D., Sarma, K. S., & Wedmaier, R. (1996). *Open Pit Blast Design, Analysis and optimization* (p. 338). Julius Kruttschnitt Mineral Research Centre, The University of Queensland.

Singh, S. P. (1993, February). Damage causing potential of different explosives. In *Proceedings of the 9th annual symposium on Explosives and Blasting Research* (pp. 325-337), San Diego, CA.

Singh, S. P., & Xavier, P. (2005). Causes, impact and control of overbreak in underground excavations. *Tunnelling and Underground Space Technology*, *20*, 63–71. doi:10.1016/j.tust.2004.05.004

St. John, C. M., & Zahrah, T. F. (1987). A seismic design of underground structures. *Tunnelling and Underground Space Technology*, *2*(2), 165–197. doi:10.1016/0886-7798(87)90011-3

Stacey, T. R. Cameron-Clarke, & Mival, K. (1990). Stabilisation of old workings by blasting: Case study of a failed experiment. In Brummer (Ed.), *Static and dynamic considerations of Rock Engineering*, Balkema, Rotterdam, pp.317-324.

Tart, R. J., Oriard, L. L., & Plump, J. H. (1980). Blast Damage Criteria for a Massive Concrete Structure. In T.S. Vinson (Ed.), *Minimizing Detrimental Construction Vibrations*. Special Technical Publication (pp. 125-140), New York: ASCE.

Thoenen, J. R., & Windes, S. L. (1942). Seismic Effects of Quarry Blasting. *Bureau of Mines*. *Bull.*, *442*, 83.

Villaescusa, E., Onederra, I., & Scott, C. (2004). Blast Induced Damage and Dynamic Behaviour of Hangingwalls in Bench Stoping. *J. Rock fragmentation by blasting*. *Fragblast*, *8*(1), 23–40. doi:10.1080/13855140512331389614

Wagner, H. (1984). Support requirements for rockburst conditions. *Rockbursts and seismicity in mines* (pp. 209-218). S. Africa Inst. Mining & Metallurgy, Johannesbug.

Yu & Vongpaisal. (1996). New blast damage criteria for underground blasting. *CIM Bulletin*, *89*(998), 139–145.

Zhang, J. C., & Chang, C. (1999, August 8-10). On damage mechanism of micro crack zone in Rock blasting and its measurements. In *Proceedings of the 6th Int. Symposium of Rock fragmentation by blasting* (pp. 358-363), The South African Ist. of Mining and Metal. Johansburg.

This work was previously published in International Journal of Geotechnical Earthquake Engineering, Volume 1, Issue 1, edited by T.G. Sitharam, pp. 110-134, copyright 2010 by IGI Publishing (an imprint of IGI Global).

Chapter 9
Production Blast-Induced Vibrations in Longhole Open Stoping: A Case Study

John Henning
Goldcorp Inc., Canada

Hani Mitri
McGill University, Canada

ABSTRACT

This paper examines stope design approaches employed at a metal mining operation in Canada for extraction of transverse primary, transverse secondary, and longitudinal stopes. Variations in stope and slot design, blast design, and blast vibration attenuation are presented in detail. It is shown that the type of blasthole stoping technique employed varies according to stope sequence and ore zone width. Within this range of stopes, blasting design practices have been standardized in terms of drillhole diameter, powder factor, and the type and pattern of the explosives used.

1. DESCRIPTION OF OREBODY

The case study ore deposit is a lens of massive sulphide and associated disseminated breccia and stringer sulphides, located in the Abitibi region of the province of Quebec, Canada. The orebody is hosted within a series of volcanic rocks, primarily schists of varying quality. The main massive pyrite lens extends from 180 m below the surface and is open at depth.

The mine property is situated in the Abitibi Greenstone Belt in the Superior Province of the Canadian Shield. The orebody follows an east-west regional structural trend, dipping steeply south in a tabular form, and is accessed by a shaft, driven

DOI: 10.4018/978-1-4666-0915-0.ch009

to a depth of 1250 m on the footwall side of the orebody. Shaft stations located at 120 m intervals access the main levels of the mine. Rock mass conditions are controlled extensively by the geology, with the dominant schistose fabric controlling the behaviour of wall rocks in all underground excavations. The host rock is strongly schistose, quartz-mica schist.

The schistocity contains sericite and acts as a dominant low friction angle weakness plane in the rock mass. These weakness planes form platy blocks up to 50 mm in thickness. The lenticular shaped massive pyrite orebody, with thickness up to 20 m has lateral and vertical dimensions of 300 m and 1500 m respectively.

2. MINING METHOD

The case study describes a trackless bulk-mining operation, with production levels connected by an internal ramp. Production from below the 1200 m level is hauled by a 40-ton capacity truck up from the 1380 m level, to be dumped in ore and waste bins located on the 1230m level. The mined rock is crushed to minus 150 mm and then hoisted to the surface in skips. Production rates are approximately 1800 tonnes per day. An internal ramp connects the main production levels with three sublevels which are developed at 30 m intervals between the main levels. Footwall haulage drifts, running parallel to the orebody, with 50 m long draw-point cross cuts provide direct access for removing the ore bearing rock from the stopes. The open stope mining with delayed backfill method is used at the mine to take advantage of steeply dipping tabular orebody geometry, and to optimize production rates and recovery. Primary stopes are mined one lift at a time and backfilled with cemented rockfill. Secondary stopes, mined between two primary stopes as indicated in Figure 1, are filled with non-cemented rockfill.

3. STOPE DESIGN

In ore widths exceeding 4 m, stopes are mined transversely. The main ore zone is divided into a grid of 15 m wide stopes with sublevels located at 30 m vertical intervals. Stope widths are up to

Figure 1. Longitudinal sketch of transverse primary and secondary stoping sequence

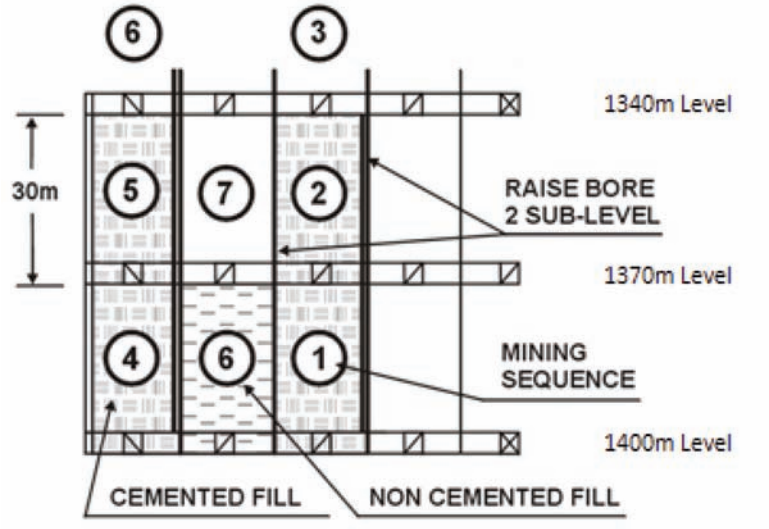

Figure 2. Primary stope schematic drilling pattern

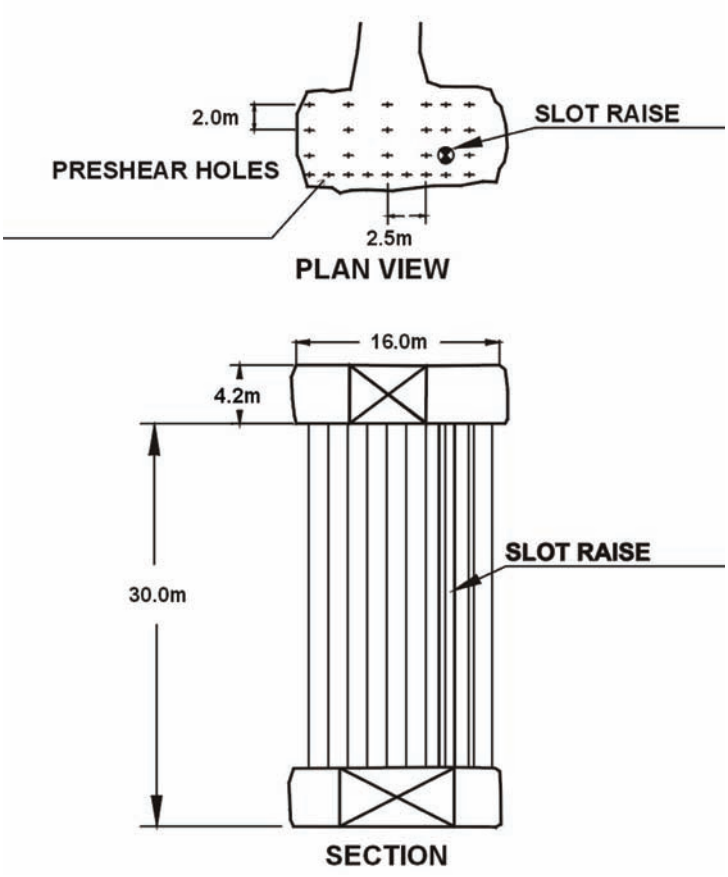

20 m. When mined, primary stope strike lengths are 15 to 17 m, strike lengths for secondary stopes are 13 to 15 m. Stope production sizes are typically 10,000 to 15,000 tonnes. At the lateral fringes of the ore zone, where the ore width is less than 4 m, stopes are mined longitudinally. Strike lengths range from 10 to 15 m, depending on the rock mass quality. Stope sizes range from 4,000 to 6,000 tonnes.

3.1 Primary Transverse Stopes

In the transverse open stope mining method, an expansion slot is developed by enlarging a 1.07 or 1.30 m diameter slot raise to the width of the stope, using parallel hole blasting. Ore is fragmented in the stope using long parallel (primary stopes) or ring-drilled (secondary stopes), and mucked from a drift, orientated perpendicular to the stope strike, at the base of the stope. Stope production drilling is performed by Tamrock Data Solo drills. The top sill of the primary transverse stopes are excavated to the full stope strike length to permit drilling of parallel 100 mm diameter blastholes, typically on a 2.5 m burden and 2.0 m spacing, with an off-center 1.07 or 1.30 m diameter raise-bore slot. Typical schematic primary stope drilling pattern is shown in Figure 2.

3.2 Secondary Transverse Stopes

Observations from blast vibration monitoring and hanging-wall instrumentation, (Henning & Mitri, 1999), and from modelling of rock mass

Figure 3. Secondary stope schematic drilling pattern

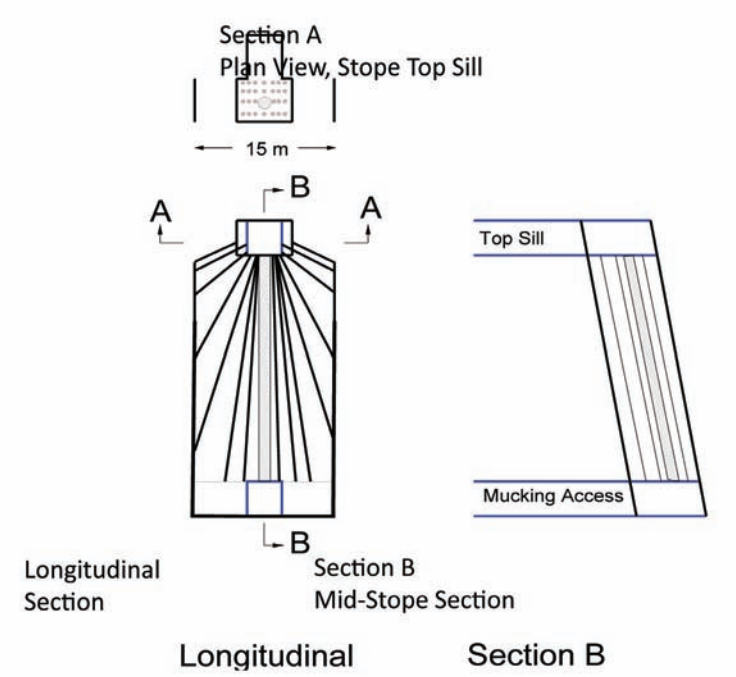

pre-conditioning (Henning et al., 2001), suggest that mining of secondary transverse stopes occurs within a lower stress (stress relieved) environment. This stress reduction is reflected in a reduced requirement for re-drilling of production blastholes and fewer accounts of working ground. In the secondary stopes, 100 mm diameter blastholes are usually drilled in a fan-pattern from a narrow, (5 m wide), top sill access, with a central 1.2 m diameter raisebore slot. Stope production drilling is performed by Tamrock Data Solo drills. Typical secondary stope drilling pattern is shown in Figure 3.

3.3 Longitudinal Stopes

Longitudinal stoping has the following benefits: (1) Improved wall stability and dilution control, as strike length can be reduced to compensate for low quality hanging-wall or footwall conditions, (2) Reduced pre-production development, and (3) Selective mining – by re-slotting, zones of subgrade material are left in place. The disadvantages of longitudinal mining include: (1) Reduced productivity, due to long haulage distances and the smaller stope size, and (2) Reduced mining rate, since pillarless longitudinal stoping allows fewer active stope blocks than transverse open stoping.

With longitudinal mining described in this case study, normally only the first stope in the longitudinal stoping sequence requires a 1.07m diameter raise bore slot. In a variation of common longitudinal, stoping practices, subsequent stope slots are generated from slot blasting against a Styrofoam core suspended against the previous stope end wall prior to backfilling with cemented rockfill. Using this technique, referred to locally as the Eureka mining method (Trahan, 1995), the Styrofoam provides the void for slot blasting (Figure 4). Stope production drilling is performed by Tamrock Data Solo drills. The top sills of the longitudinal stopes are excavated to the full stope strike width to permit drilling of parallel 100 mm diameter blastholes, typically at a staggered 2 m

Figure 4. Eureka mining method (after Trahan, 1995)

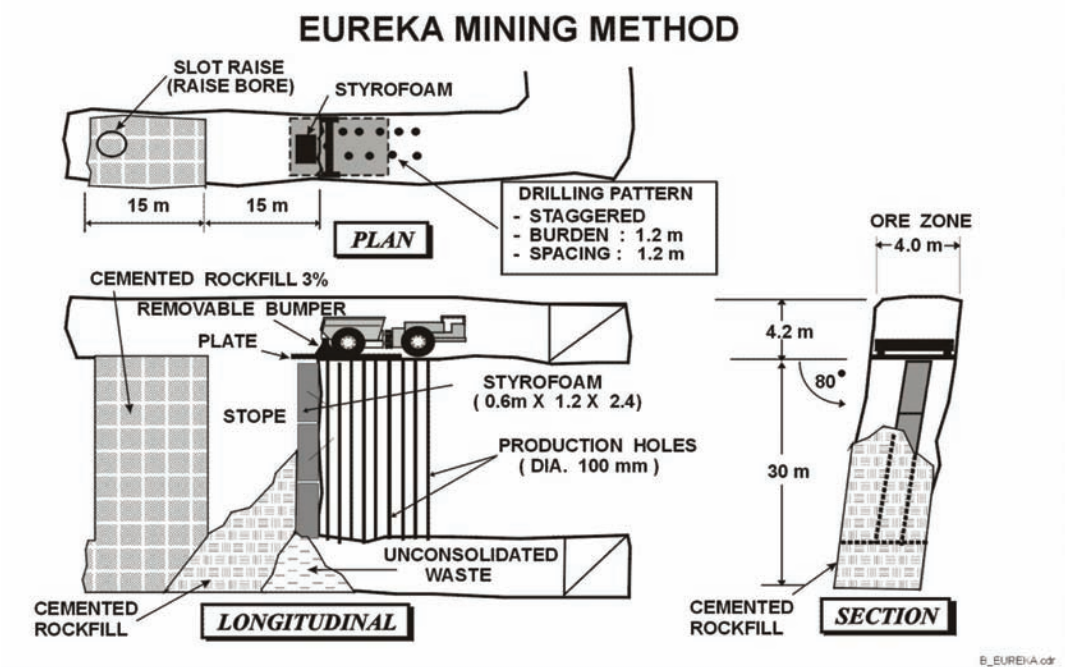

burden and 2 m spacing pattern, as illustrated in Figure 5 and Figure 6.

4. BLASTING PRACTICES

Production blasting of the transverse and longitudinal stopes is performed with AN-FO (AMEX) explosives in mid-stope blastholes. Lower density AN-FO explosives (AMEX K40) are used in the footwall blastholes. Low energy cartridge explosives (Powersplit) are used in the blastholes located closest to the hanging-wall to minimize hanging-wall blast vibration damage. An example of transverse stope loading practice is illustrated in Figure 7. Blast design parameters for slot and production blasting of both transverse and longitudinal stopes are listed in Table 1. Loading procedures for both AN-FO (AMEX and AMEX K40) and the cartridge explosives are illustrated schematically in Figure 8.

4.1 Transverse Stopes

Transverse stopes are normally mined in three blasts, as illustrated in Figure 9. In primary stopes, the first two blasts widen the slot area to the full stope thickness in 10 to 14 m lifts. For the stope final blast, the remaining blastholes are loaded full column, to a maximum charge per delay of 175 kg, and fired into the open slot. Typically, the first two 'slot' blasts represent approximately 5% and 20%, respectively, of the total stope volume. The remaining 75% is broken in the third and final blast.

With the secondary stopes, the lower half in the stope is excavated by the first two blasts. For the final blast, the remaining blasthole rings are fired inwards, towards the central slot. The combination of a fan-drilling pattern with a lower stress environment, permit the blasting of larger volumes at the initial stages of secondary stope extraction. Usually, the first two 'slot' blasts represent approximately 20% and 38%, respec-

Figure 5. Longitudinal (Eureka) drilling pattern

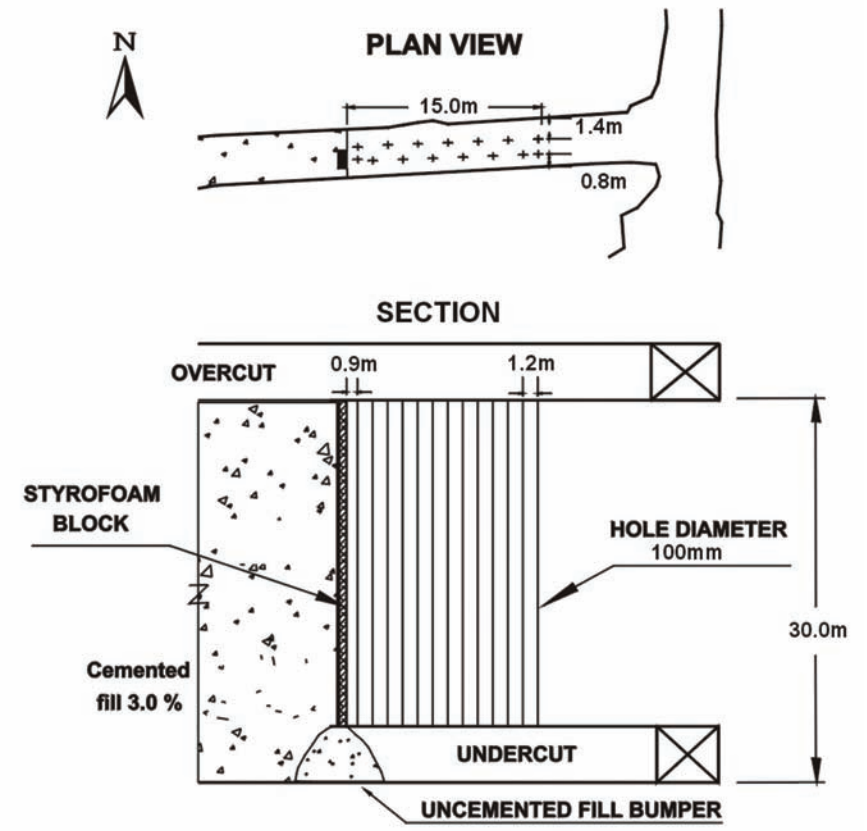

Figure 6. Plan of longitudinal stope drilling and loading practice

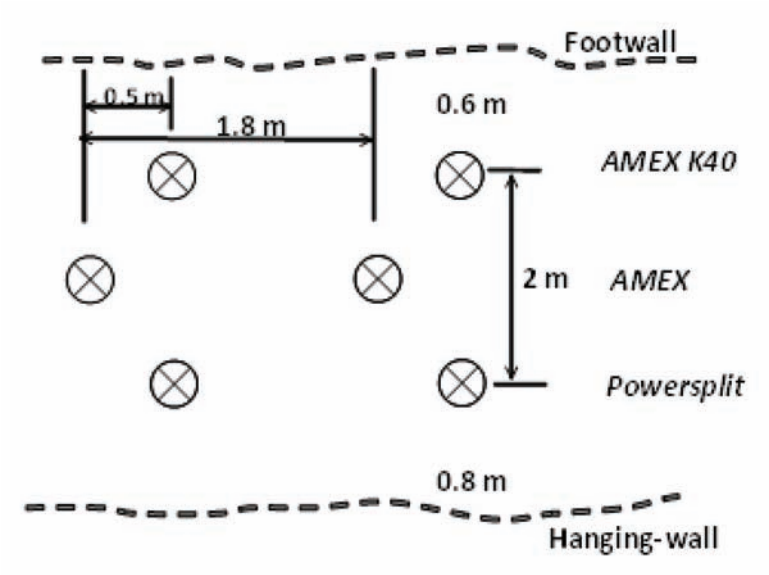

Figure 7. Plan of transverse (primary) loading practice

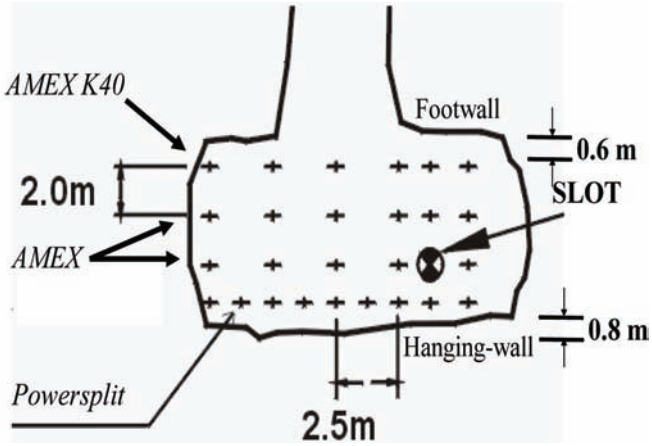

Table 1. Stope blast parameters

	Transverse (Primary and Secondary)		Longitudinal	
	Slot	Square	Slot	Square
Pattern (m)	0.8	2.0 x 2.5	0.9	2.2
Powder Factor (kg/t)	0.85	0.4 – 0.7	1.1	0.7
Maximum charge per delay (kg/ delay)	120	175	85	120 - 175

tively, of the total stope volume. The remaining 42% is broken in the third and final blast.

4.2 Longitudinal Stopes

Longitudinal stopes are mined in three or four blasts, depending on the type of slot used, as indicated in Figure 10. A stope with a drilled slot is mined in three blasts, in a manner similar to the primary transverse stopes. The first two blasts widen the slot area to the full stope thickness in 14 m lifts. For the stope final blast, the remaining blastholes are loaded full column, to a maximum charge per delay of 160 kg, and fired into the open slot. Typically, the first two 'slot' blasts represent approximately 15% and 20%, respectively, of the total stope volume. The remaining 65% is broken in the third and final blast.

Longitudinal stopes utilizing a Styrofoam slot, (Eureka mining method), are mined in four blasts. A small initial blast, representing roughly 4% of the stope volume creates a narrow, 10 m high excavation along the cavity against consolidated backfill of the previous stope. The second and third blasts, representing approximately 12% and 24%, respectively, of the stope volume, complete the 'slot' blasting. The remaining 60% of the stope volume is broken in the fourth blast.

4.3 Blast Vibration

The severity of production blast vibrations within the transverse primary and secondary stope hanging-walls was monitored using triaxial geophones installed onto a solid, competent wall surface. Hanging-wall vibration data was compiled using the peak vector sum velocities of individual blast holes. Non-distinct or overlapping waveforms were omitted from the database, as were blast vibration values likely influenced by air gaps between the blasthole and the geophone. The vibration data was statistically analyzed using scaled distance relationships (Atlas, 1987), to determine the site constants used in the following equation:

Figure 8. Schematic diagrams of blasthole charging procedure

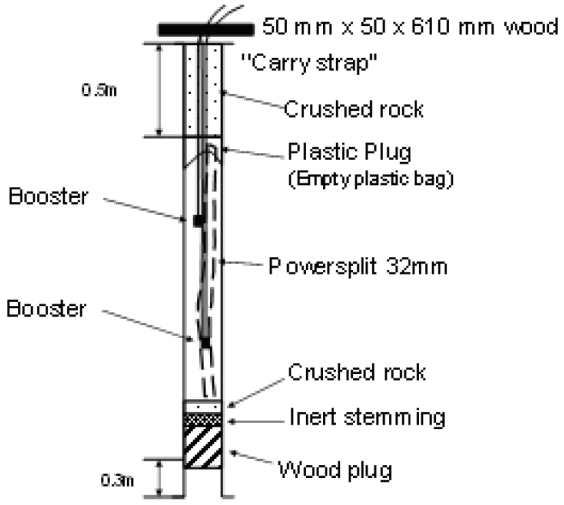

(a) Cartridge explosive (Powersplit)

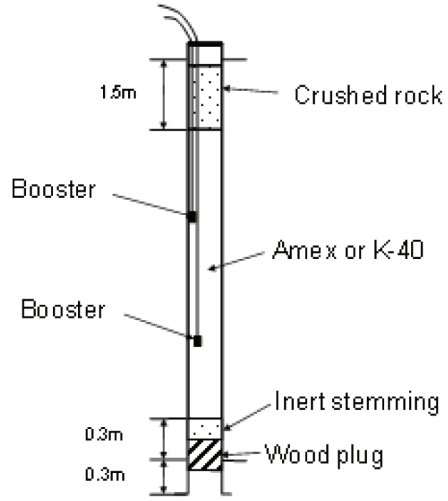

(b) AN-FO (AMEX and AMEX K40)

$$PPV = K (R / W^{0.5})^{-a} \quad (1)$$

Where:

PPV = peak particle velocity (mm/s);
R = radial distance from blast center (m); and
W = explosive charge per delay (kg)

Figure 9. Blast sequence for primary and secondary transverse stopes

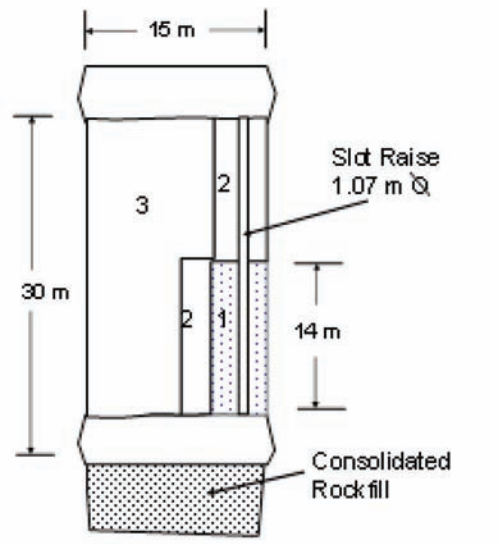

(a) Primary stope

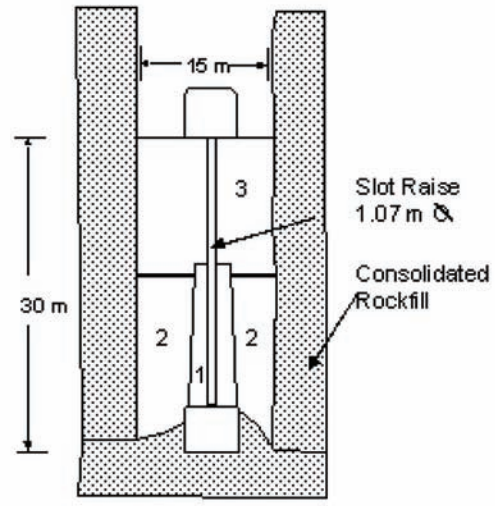

(b) Secondary stope

The site constants "K" and "a" are the functions of the effect of local rock characteristics on ground motion. Constant "K" applies to amplitude whereas "a" indicates vibration attenuation. The calculated site constants are listed in Table 2. The lower site constants for the secondary stope indicate that a lower amplitude vibration reached

Figure 10. Example of blast sequence for longitudinal stopes

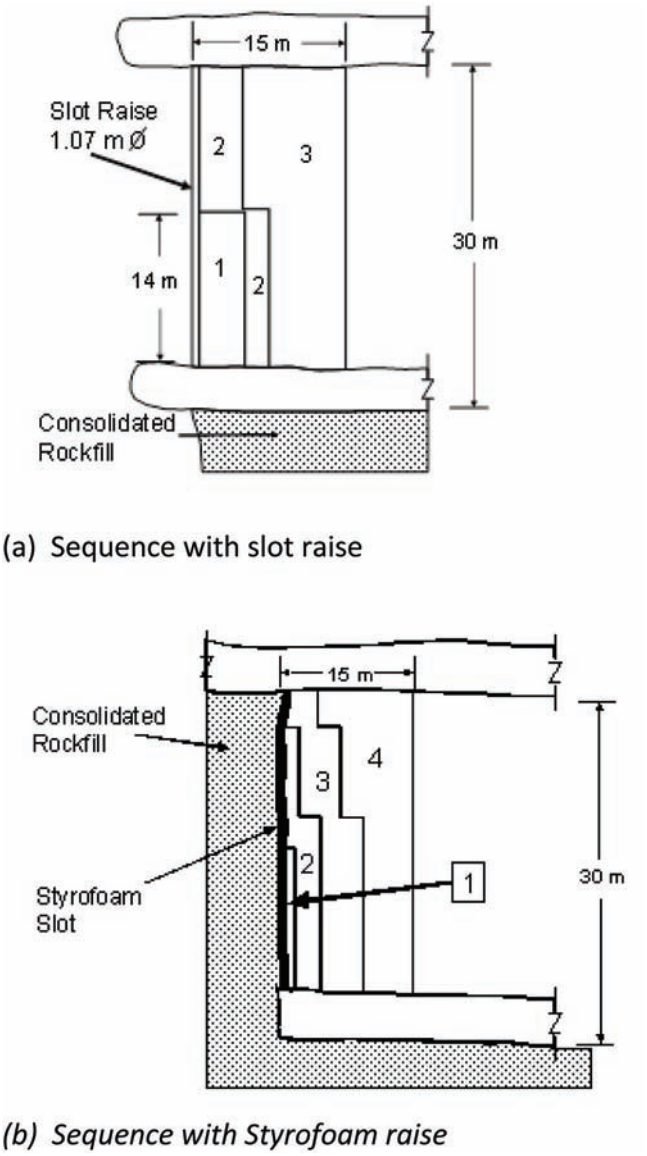

the geophones, due to increased hanging-wall vibration attenuation from the blast source.

To predict the impact of individual blastholes on the hanging-wall, explosive-specific site constants were calculated from the vibrations generated by individual explosive types. AN-FO loaded 100 mm diameter blastholes, representing 48% and 40% of the total blast populations. Vibration attenuation plots for a typical blasthole, located at 2.5 m from the stope hanging-wall boundary, and loaded with 100 kg AN-FO, provided in Figure 11, show estimated hanging-wall vibration levels within five meters of the stope boundary.

In their review of rock fracturing with explosive energy, Saharan et al. (2006) suggest that damage to intact rock is likely to occur when the peak particle velocity exceeds 1000 mm/s. In the

Table 2. Calculated blast vibration site constants

	Primary Transverse Stope		Secondary Transverse Stope	
	K	a	K	a
Total Blast Population	498	1.19	126	0.70
AN-FO Blast Population	283	0.58	141	1.20

Figure 11. Hanging-wall blast vibration attenuation. AN-FO explosive population: 100 kg charge, located in blastholes 2.5 m from hanging-wall contact

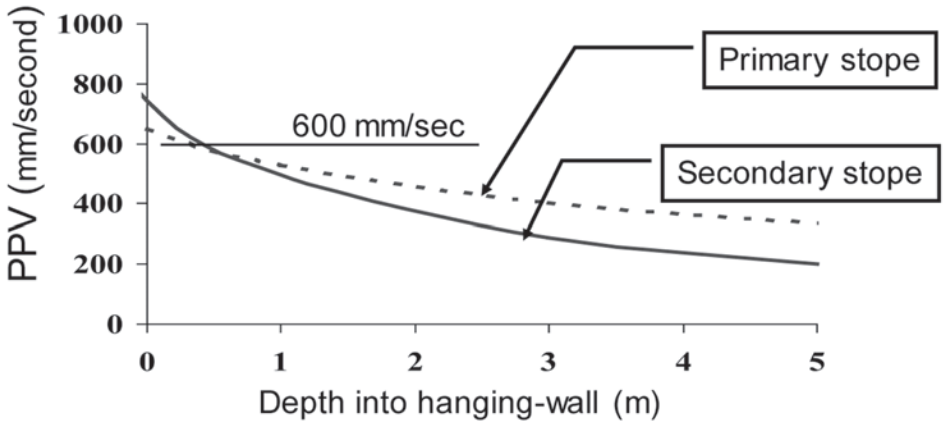

current study, a blast vibration level of 600 mm/s was selected from published damage criteria, CANMET (1993), as a typical threshold limit for vibration induced blast damage. Using this vibration threshold, Figure 11 indicates that existing blasting techniques negatively influence the hanging-walls of both primary and secondary transverse stopes, to a distance of approximately one meter from the stope/hanging-wall contact. The severity of blast vibration damage diminishes away from the stope boundary. Mid-stope blastholes, typically located at a distance of 2.5 m from the hanging-wall contact, generated significant peak vibrations into the hanging-wall. Lower vibration levels recorded during mining of the secondary stope were associated with observed de-lamination of schistocity parallel to the stope wall.

5. CONCLUSION

The type of blasthole stoping technique presented in this case study mine varies according to stope sequence and ore zone width. For each type of stope, blasting design practices have been standardized in terms of drilled hole diameter, range of powder factor, and the type and pattern of the explosives used.

REFERENCES

Atlas Powder Company. (1987). *Explosives and Rock Blasting*. ISBN 0-9616284-0-5

CANMET. (1993). *The development of new blast damage criteria for blasthole mining operations* (DSS file 014sq.23440-1-9050).

Clark, L. M., & Pakalnis, R. C. (1997). An empirical design approach for estimating unplanned dilution from open stope hanging-walls and footwalls. In *Proceedings of the 99th CIM Annual General Meeting*, Vancouver, Canada.

Henning, J. G., Kaiser, P. K., & Mitri, H. S. (2001, July). Evaluation of stress influences on ore dilution: a case study. In *Proceedings of the 38th U.S. Rock Mechanics Symposium*, Washington, DC.

Henning, J. G., & Mitri, H. S. (1999). Examination of hanging-wall stability in a weak rock mass. *CIM Bulletin*, *92*(1032).

Miller, F., Potvin, Y., & Jacob, D. (1992). Laser measurement of open stope dilution. *CIM Bulletin*, *85*(962).

Saharan, M. R., Mitri, H. S., & Jethwa, J. L. (2006). Rock fracturing by explosive energy: Review of state-of-the-art. *Fragblast*, *10*(1-2), 61–81. doi:10.1080/13855140600858792

Trahan, M. (1995). Méthode de minage "Eureka". In *Proceedings of the 10th AMQ colloque en contrôle de terrain*, Val d'Or, Québec, Canada.

This work was previously published in International Journal of Geotechnical Earthquake Engineering, Volume 1, Issue 2, edited by T.G. Sitharam, pp. 1-11, copyright 2010 by IGI Publishing (an imprint of IGI Global).

Chapter 10
Development of a New Blast Vibration Prediction Model Incorporating Burden Variations in Surface Blasting

M. Ramulu
Central Institute of Mining & Fuel Research, India

ABSTRACT

The globally followed common vibration predictor model includes distance from source to vibration monitoring location and quantity of explosive charge per delay without giving much consideration to blast design parameters. Though there are qualitative assertions on the influence of burden on the vibration intensity by many researchers, no work on quantification of influence of burden has been reported. This paper deals with the development of a predictor model incorporating burden deviations in the existing predictor equation. The influence of burden on the vibration was viewed from the angle of detonation and rock fracturing during blasting. The new predictor equation is based on existing models developed by other researchers on the influence of burden on the blasthole pressure and vibration intensity as well as on some logical assumptions. The influence of burden on vibration was examined in two independent phases of blasting, and the net effect was calculated by adding the influence in both the phases. The study provides a quantitative explanation for the common observations of increased vibration levels produced by the blast rounds with excess burden and/or misfired shots.

DOI: 10.4018/978-1-4666-0915-0.ch010

1. INTRODUCTION

Most of the explosive energy, in rock blasting process, is used for generation of seismic waves and airblast (Rollins, 1980; Berta, 1990). Blast vibration and air blast are the common source of annoyance for the nearby people as the open pit mining and habitats are approaching each other due to expansion at both the ends. Vibration and airblast monitoring is an essential part of blast monitoring from the point of structural damage, blast design and human response. Most of the existing structural damage criteria are prescribed in terms of peak particle velocity of vibrations (v_{max}) measured on the ground near the structures, since it can be related directly to peak transient stress in the ground wave, and the second power of velocity is related to dynamic strain energy (McGarr, 1983). Therefore, vibration prediction is an important aspect to arrive at safe blast design and to reduce the human annoyance. The most widely accepted single measurement of ground vibration considered potentially damaging to structures is the peak particle velocity, defined as the highest speed at which an individual earth particle moves or vibrates as the waves pass a particular site. The first measurement of vibrations from a blast was made by Rockwell in 1919 but it was reported in 1927 (Rockwell, 1927). A number of investigators, have since then, made further contributions in developing predictor equations.

Efforts were made to find out a safe level of vibration for buildings and other structures (Thoenen & Windes, 1942; Crandel, 1949). It is very difficult to predict the magnitude, frequency and duration of ground vibrations as they are affected by many variables. Earlier research in the area states that, the level of ground vibration will depend on the maximum explosive charge in any particular delay interval and the distance between the blast and measurement point. But other variables, such as rock type, topography, design parameters, coupling of the explosive in the blast hole may significantly influence the characteristics of the ground vibrations generated. Although it is not possible, in common blasting situations, to take into account all these factors, the influence of design parameters specially burden, cannot be ignored as it can dictate the confinement in some particular occasions.

Many investigators have studied ground vibrations generated from blasting and they have developed different relationships to predict the vibrations at distances from the source. Almost all the models are based on scaled distance concept. The scaled distance is defined as the actual distance (D) of the measuring point from blasting face divided by some power of the maximum explosives weight per delay (Q_{max}). Different researchers have suggested different values of the exponent.

The existing vibration prediction models were developed based on the amount of explosive energy and the attenuation characteristics of rock medium. The general form of vibration prediction model consists of charge weight and distance with a power function as shown in the equation (1) (Devine et al., 1966).

$$v_{\max} = K\left(\frac{D}{Q^{\alpha}}\right)^{-\beta} \qquad (1)$$

where,

v_{max} is the peak particle velocity in mm/s,
D is the distance of the monitoring point from the blast in meters and
Q is the charge weight per delay in kg. K, α and β are constants based on site characteristics.

Ambraseys and Hendron (1968) found that the value of α is 1/2 for all surface blast vibration attenuations. The value of β can be adjusted as 1.6 as it satisfies the attenuation characteristics of most of the rock types (McKenzie, 1993; Konya,

1995). Incorporating the values of α and β in the equation 1 becomes,

$$v_{\max} = K\left(\frac{D}{Q^{1/2}}\right)^{-1.6} \quad (2)$$

The above mentioned prediction model assumes that same quantity of explosive energy is used for generation of vibrations for all the cases of blast configuration. But in actual the explosive energy imparted for generation of vibrations and air blast depends on the energy used for rock fracturing and fragmentation. There is very high range of explosive energy utilisation for blast vibrations, which is complementary to energy used for creation of fractures from optimum blast to worst blast due to change in the blast configurations related to confinement (Wallace, 1996). The confinement in the blasting process is mainly taken care of by delay alignment between the different charge weights and burden distance. Extensive research was carried out to quantify the effect of delay between the successive charges but the influence of burden on vibrations has not yet been quantified. This paper deals with the influence of burden on the intensity of ground vibrations, as the burden is one of the key design parameters and which deviates frequently in the field conditions.

The equation (2) can be written as the ratios of vibrations and charge weight as shown below:

$$\frac{v_2}{v_1} = K\left(\frac{Q_2}{Q_1}\right)^{0.8} \quad (3)$$

2. INFLUENCE OF BURDEN ON VIBRATION – A REVIEW

Though the effect of blast design parameters was broadly considered by many researchers (Siskind et al., 1980; du Pont, 1977) in deriving the vibration predictor equation relevant weight was not assigned to other blast design parameters like burden, spacing and bench height. It is a recognized fact that burden has got its own contribution in influencing blast vibrations (Ramulu, 1998; Raina et al., 2004). Researchers from the then USBM also suggested that more studies are required to firmly establish the effect of blast design parameters like burden, on the intensity of the v_{max} of vibrations (Crum, 1997). Controlling blast vibrations through blast design modification, especially blast geometry which includes burden and spacing, was studied by Anderson et al. (1985) and Wiss (1978).

According to Jimeno (1995), if the confinement or burden is excessive, the energy from the explosion has too much resistance to effectively fracture and displace the rock. In this case, part of the energy becomes seismic and intensifies the vibrations more than when free face conditions in a blast round exist. Avoiding too much burden has become one of the measures to reduce the ground vibrations (Scott, 1996; Persson, 1994). Sames (1999) reveals that, design parameters like delay time, burden, initiation sequence and decoupling charges considerably alter dispersion of the seismic energy. The effect of burden on vibrations was indicated in a number of research works globally (Siskind et al., 1980; Gordon et al., 1997; Crum, 1997). It is interesting to note that the effect of blast design parameters on vibrations was predominant in near-field observations and at farther distances the geological features control the amplitude of vibrations (Nutting, 1997). Ramulu et al. (2001) experienced that ground vibrations and air over-pressure are very sensitive to burden upon which the confinement of charge depends. Some times there exists excess burden due to faulty drilling and due to collapse of one or more drill holes before charging.

According to Floyd (1997) the major cause of elevated ground vibrations is the overconfinement of explosive energy when the blasthole detonates. Along with lack of free faces and insufficient delay

interval between rows, excess blasthole burden and large toe burden are the major causes of over-confinement. This over-confinement causes a large portion of the energy to be absorbed by the rockmass instead of being utilized for fragmentation and muckpile displacement. The excess energy absorbed by rock mass results in enhanced ground vibrations. Anderson (1985) found that, at the same recording location, a totally confined single-charge shot will produce about twice the peak particle velocity in comparison to the single-charge shot with free-face. Dick (1983) reveals that a charge with a properly designed burden will produce less vibration per pound of explosive than a charge with too much burden. An excessive amount of sub-drilling, which results in an extremely heavy confinement of the explosive charge, will also cause higher levels of ground vibration, particularly if the primer is placed in the sub-drilling. In multiple row blasts, there is a tendency for the later rows to become over-confined. To avoid this, it is often advisable to use either longer delay periods or lesser burdens between these later rows to give better relief.

According to Ghosh (1983), if the burden is too large, it is difficult for gases, produced due to detonation of the explosive charge, to properly fragment and move rock forward. The gases will be bottled up within the hole for more than the optimum time. The energy of the explosive not utilized in fragmentation and throw will cause an increase in ground vibration. Sen (1984) conducted small scale experiments on the influence of burden and concluded that the intensity of ground vibration increases with increase in burden up to a critical burden, beyond which it remains constant. According to Dowding (1985), excess burden which involves much greater confinement, tend to produce greater particle velocity than a normal burden in a production blast, monitored at the same scaled distance. This is the reason why a pre-split shot produces much greater vibration than the normal production blast. Heiling's (1997) findings also show that confined and choked blasts produce more vibration than the unconfined blasts. Rustan (1987) also conducted field experiments with various burden and states that, in case of excess burdens (more than critical), little energy is used for rock movement and cracking and more energy is used in the form of vibrations and quasi-static borehole pressure. Scott (1996) and Persson (1994) also suggest to avoid too much burden for reducing ground vibrations.

Blair and Armstrong (2001) reported that there is no influence of either burden or choked face confinement on the intensity of vibrations and it is the condition of rock mass surrounding blasthole which affects the vibrations. Results of model experiments conducted by Blair and Armstrong (2001) revealed that the vibration can never increase by more than a factor of 2 due to burden. They conducted field experiments with single blastholes and the results indicated that maximum vibration intensity for the blastholes with higher burdens in the lower scaled distance range. Where as the higher scaled distance range showed no effect of burden. In one of the graphs, they showed that larger burden gives lower vibration but in this case too early peak (the arrival of the P-wave) of the vibration was read by ignoring the maximum value which was shown later. Ramulu et al. (2002) conducted an extensive experimental study in a limestone quarry to find out the effect of burden on the intensity of ground vibrations and revealed that the vibration intensity is directly proportional to the excessive burden. Ramulu et al. (2004) also conducted a detailed study in open pit bench blasting and found that there is a substantial effect of burden on the vibration intensity.

It is very clear from the above literature review that the effect of burden on ground vibrations was addressed more qualitatively by many publications but quantitative studies were not reported. Therefore it is required to quantify the effect of burden on ground vibrations to predict the realistic vibration intensity to assess the possible damage

Figure 1. Plan view of blast hole and free face showing direct and indirect phases of vibrations (modified after Atchison, 1972)

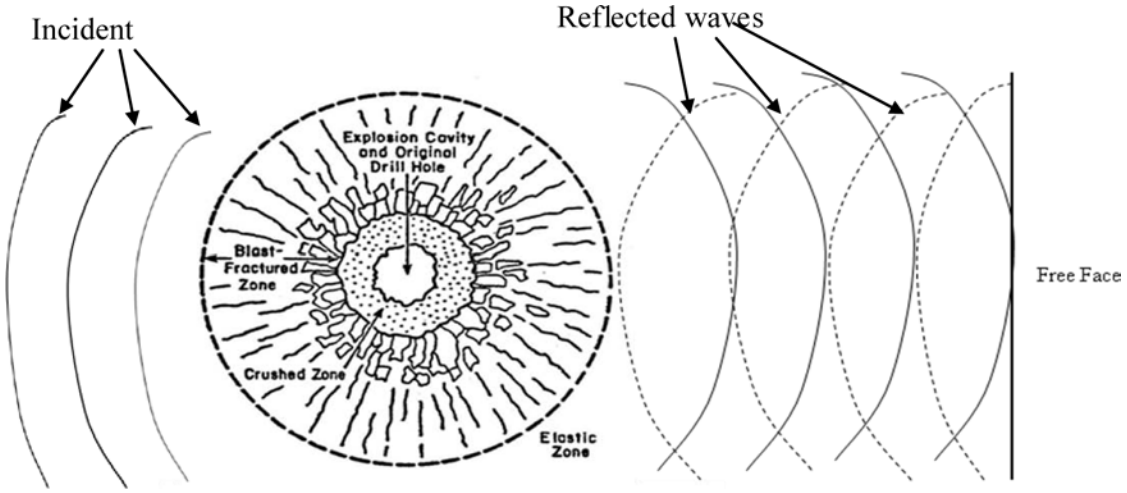

to nearby structures. This paper attempts to fill the gap and incorporate the burden in the existing vibration prediction model.

3. QUANTIFICATION OF BURDEN ON BLAST INDUCED VIBRATION

In order to find out the influence of burden on the vibrations, it is required to go into the process of generation of vibrations. When an explosive charge is detonated in a blast hole very rapid decomposition of the charge takes place and forms gases at very high temperature and pressure within a few microseconds. This process results in generation of shock waves and causes the surrounding rock to crush, fracture and vibrate. The shock waves, thus generated, crush the surrounding rock of blast holes up to about two blasthole diameters (Rustan, 1998). High tangential stresses and strains are developed beyond this zone, resulting in radial cracks propagating away from the blast hole. This causes permanent fracture and distortion of the rock up to several drill hole radii (Langefors & Kihlstrom, 1967; Atchison, 1972; Siskind et al., 1973; du Pont, 1977). The intensity of the shock wave attenuates very rapidly as a large amount of energy is utilized in crushing and producing cracks. At some distance from the hole, the intensity drops to a level such that there will be no permanent deformation. The remaining energy goes directly into the surrounding rock as seismic waves which propagate elastically in all directions.

If the surrounding rock contains a free face, the shock waves travelling towards the free face are reflected back which result in fracturing and spalling of rock. In general rock-blasting pattern, a free face is provided to each blast hole before detonation for maximum utilization of explosive energy. The minimum distance from blasthole to the free face is known as the blasthole burden. If the distance from the blast hole to free face is more than a critical limit (optimum burden), the shock wave energy cannot be used fully for rock breaking and a part of the energy is transmitted as seismic energy. If the distance from blasthole to free face is more than or less than the optimum burden, it is called deviated burden. Therefore, it can be noted that the overall seismic energy is the result of both incident shock waves, directly emitted from blastholes and reflected shock waves from free face. Therefore, it can be noted that the

Table 1. Blasthole pressures for different burdens (adapted from Mortazavi & Katsabanis, 2001)

Burden (B), m	Blast hole chamber pressure (p), GPa	B_2/B_1	p_2/p_1
1.5	0.26	1.00	1.00
2.0	0.32	1.33	1.23
2.5	0.38	1.67	1.46
3.0	0.43	2.00	1.65
3.5	0.45	2.33	1.73
4.0	0.46	2.67	1.77

Figure 2. Plot of pressure ratios versus burden ratios (Mortazavi & Katsabanis, 2001)

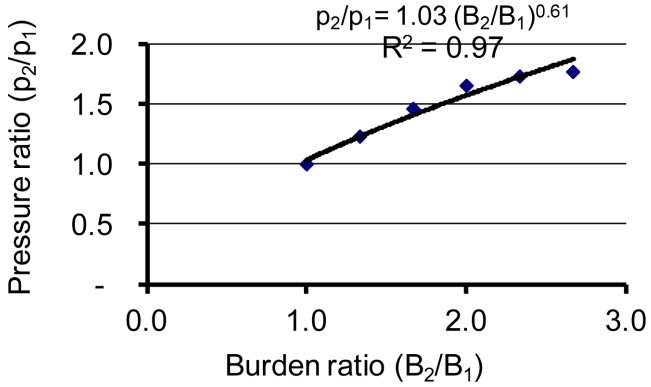

overall seismic energy is the result of both incident shock waves, directly emitted from blastholes and reflected shock waves from free face. The phase of vibration generation due to direct wave system can be called here as direct phase and the phase of vibration generation due to reflected wave system could be called as indirect phase. The influence of burden on the characteristics of ground vibrations can be viewed through these two independent phases as shown in Figure 1.

3.1 Influence of Burden on Vibrations During Direct Phase

The effect of variation of burden on the blasthole chamber pressure was studied by Mortazavi and Katsabanis (2001) by means of a dynamic blasthole expansion model, which was a numerical study. The data of blast hole chamber pressure recorded by the above authors for various burden distances by using discontinuous deformation analysis code is given in Table 1. For comparison, the least burden was assumed as the optimum burden (B_1) and the least pressure as the optimum pressure (p_1). The ratio of burdens and corresponding ratios of pressures are calculated by dividing various burden and pressure values by B_1 and p_1, respectively. The burden ratios and pressure ratios, thus calculated are given in Table 1. Regression analysis of the data of burden ratios and chamber pressure ratios is shown in Figure 2.

The regression equation developed for burden ratios and pressure ratios is given in the following sections:

$$\frac{P_2}{P_1} = 1.03\left(\frac{B_2}{B_1}\right)^{0.61} \quad (4)$$

Figure 3. Vibration vs. specific charge for small-scale quarry blasts (adapted from du Pont, 1977)

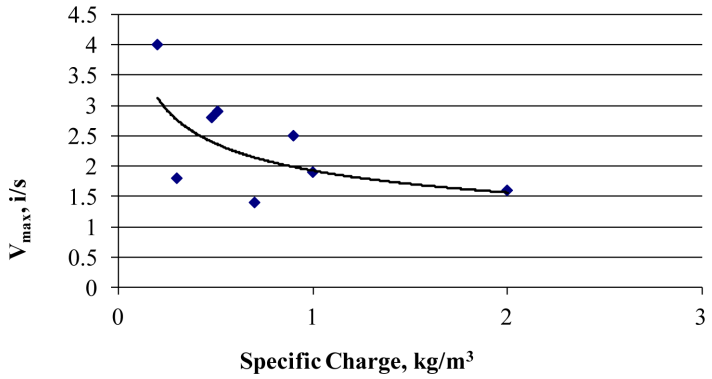

or approximately,

$$\frac{P_2}{P_1} = \left(\frac{B_2}{B_1}\right)^{0.6} \tag{5}$$

As the blast hole chamber pressure is directly proportional to vibration, the chamber pressure ratio in equation (5) can be replaced by the vibration ratio.

$$\frac{v_2}{v_1} = \left(\frac{B_2}{B_1}\right)^{0.6} \tag{6}$$

Therefore, the relation between burden and vibration during the direct phase in model studies was expressed as equation (6).

3.2 Influence of Burden during Indirect Phase

An insufficient specific charge (weight of explosive per unit rock volume broken) can increase vibration by delaying and reducing the effect of reflected tensile waves from free faces (du Pont Handbook, 1977). Excessive specific charge will increase throw and flyrock and may increase air overpressure. The substantial increase of vibration that can occur from insufficient specific charge is difficult to counteract by other measures such as reducing the charge per delay and increasing the delay interval (Andrews, 1981). For surface mining, the specific charge varies from 0.15 to 1.5 kg/m^3 while 0.3 to 0.6 kg/m^3 being the most common (Ash, 1990). Jimeno et al. (1995) observed that when the specific charge was reduced by 20 per cent from the optimum, the vibration levels were two to three times higher as a consequence of poor rock breakage. Wathen et al. (1996) carried out blasting in limestone with low specific charge so as to protect nearby equipment from fly rock. He monitored vibrations while increasing the distance between the equipment and the blast site, as well as the specific charge. Experiments of du Pont (1977) and Andrews (1981) reveals that decrease in specific charge resulted in an increase of vibration levels, which is shown in Figure 3 and Figure 4. It is clear from the above discussion that an increase in the burden to more than the optimum level reduces specific charge, which results in adverse fragmentation and an increase in the vibration levels. Therefore, it is assumed that the portion of energy, which could not be utilised for rock fracturing, would be used for increasing the intensity of vibrations. Here, the minor increase/decrease in the levels of airblast and throw are neglected.

Therefore it is clear from the above discussions that the explosive energy, which could not be used for fragmentation, manifests in the form of vibra-

Figure 4. Vibration versus specific charge for full-scale mine blasts (adapted from Andrews, 1981)

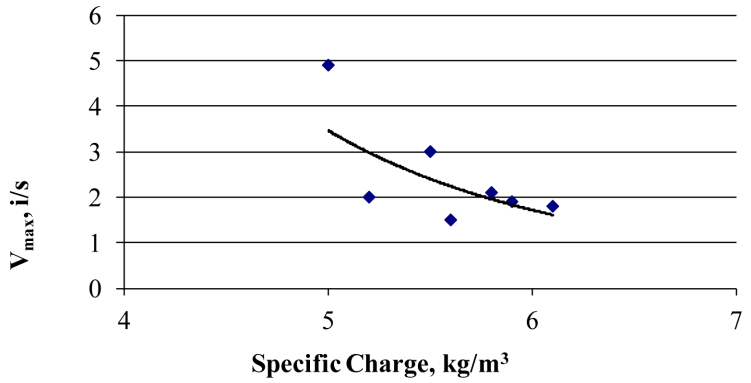

Table 2. Explosive energy per kg of rock broken for different burdens (adapted from Rustan, 1983)

Blast No.	**Burden (m)**	**Explosive energy per kg of rock broken (kcal/kg)**	**B_2/B_1**	**E_2/E_1**	v_2/v_1
1	1	0.432	1	1.00	1.00
2	2.1	0.123	2.1	0.28	1.54
3	3	0.095	3	0.22	1.59
4	4.2	0.049	4.2	0.11	1.66

tions. This energy is the complementary of the energy that is used for the fragmentation and it can be represented in the form of useful energy (E) in the equation (3).

$$\frac{v_2}{v_1} = \left(1 + \left(1 - \frac{B_2}{B_1}\right)\right)^{0.8} \quad (7)$$

Studies similar to those carried out by Rustan (1983) with small-scale experiments in single-hole blasts at limestone quarries were considered for comparison of explosive energy utilisation for different burdens. The explosive energy per kg of rock broken for different burdens is given in Table 2. The data is further analysed for calculation of vibrations corresponding to various burdens. The vibration intensities corresponding to each round of experiment were calculated using the equation (7). The least burden in Table 2 is assumed as the optimum burden (B_1) and the other burdens are considered as excess burdens. The ratios of E_2/E_1 and v_2/v_1 for corresponding B_2/B_1 are given in Table 2. Curve drawn by regression analysis of B_2/B_1 and v_2/v_1 is shown in Figure 5.

The equation thus derived is given below:

$$\frac{v_2}{v_1} = 1.05\left(\frac{B_2}{B_1}\right)^{0.36} \text{ with R2= 0.88} \quad (8)$$

Equation (8) can be simplified as,

$$\frac{v_2}{v_1} = \left(\frac{B_2}{B_1}\right)^{0.4} \quad (9)$$

3.3 Combined Effect of Burden on Vibrations

In order to combine the effects of two different phases, it is required to find out the phase difference in terms of time as the minimum delay

Figure 5. Plot of vibration ratios versus burden ratios

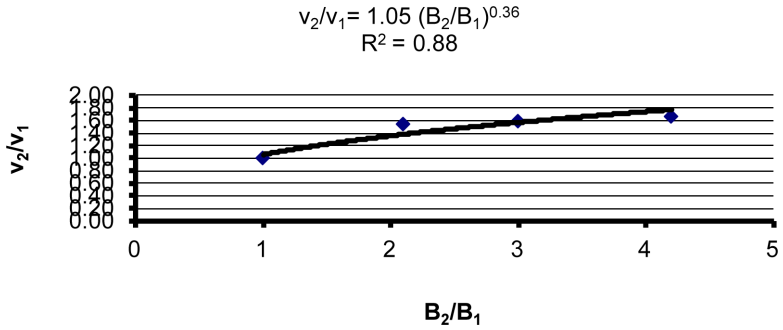

Figure 6. Seismic wave recorded at 8 m from a blast hole in a copper mine in India (Ramulu et al., 2004)

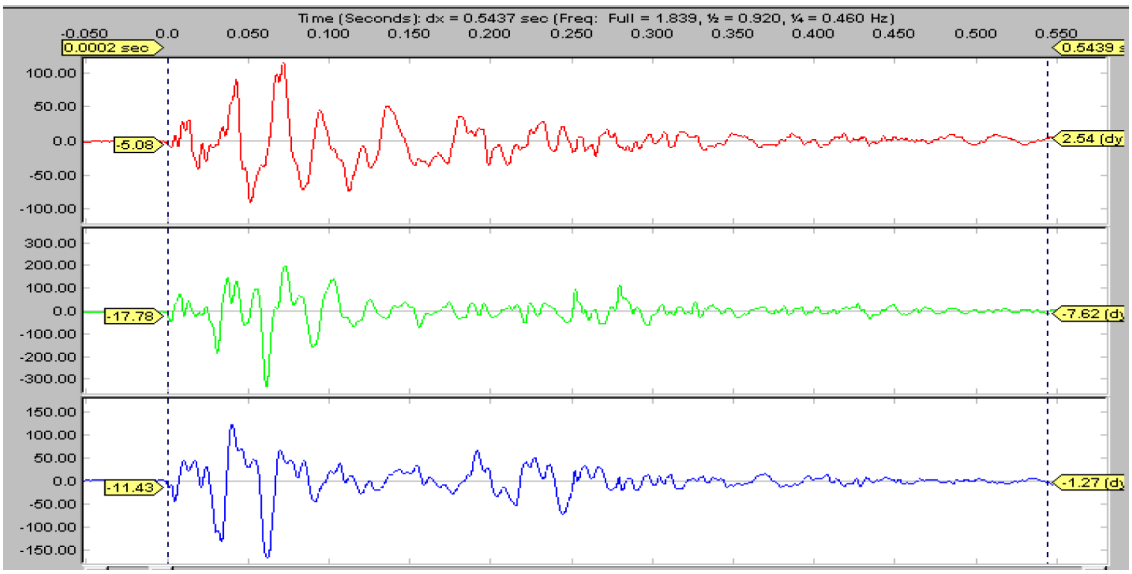

interval required to avoid constructive interference is 8 ms (Duvall et al., 1968). The phase difference between the direct and indirect phases can be calculated by means of the some established values. Considering the seismic wave velocity (P-wave) of rock medium as 2000 to 3000 m/s and burden up to 15 m, the phase difference in two different phases would be 3-6 ms, which is considered as the same delay from vibration point of view (Anderson, 1989). In fact the peak cycle of the particle vibration in the near field condition of a typical bench blast takes around 15 to 25 ms as shown in the Figure 6 (Ramulu et al., 2004). Therefore, the phase difference of 3-6 ms cannot be treated as a separate delay and the two effects can be added together to get the net effect. The increase in vibration due to both the phases can be calculated by adding the increase in vibration in individual phases.

Therefore the overall increase in vibration (v_i) due to both the effects can be

$$v_i = v_{1i} + v_{2i} \tag{10}$$

Substituting the values of v_{1i} and v_{2i} from the equations (6) and (9),

$$v_i = v_1\left(\left(\frac{B_2}{B_1}\right)^{0.6} - 1\right) + v_1\left(\left(\frac{B_2}{B_1}\right)^{0.4} - 1\right) \quad (11)$$

The equation (11) can be simplified as,

$$v_i = v_1\left[\left(\frac{B_2}{B_1}\right)^{0.6} + \left(\frac{B_2}{B_1}\right)^{0.4} - 2\right] \quad (12)$$

The addition of $\left(\frac{B_2}{B_1}\right)^{0.6} + \left(\frac{B_2}{B_1}\right)^{0.4}$ gives $2\left(\frac{B_2}{B_1}\right)^{0.5}$ for the burden ratios ranging from 0.1 to 100 which can cover all the practical burden deviations. Therefore the equation (12) can be simplified as below:

$$v_i = 2v_1\left[\left(\frac{B_2}{B_1}\right)^{0.5} - 1\right] \quad (13)$$

Total vibration received at a particular point due to deviated burden (V_2) is the sum of actual vibration due to optimum burden and the increase/ decrease in vibration due to deviated burden.

$$v_i = 2v_1\left[\left(\frac{B_2}{B_1}\right)^{0.5} - 1\right] + v_1$$

or (14)

$$v_i = v_1\left[2\left(\frac{B_2}{B_1}\right)^{0.5} - 1\right]$$

Assigning back the original notation as under, we get:-

$$v_d = v_0\left[2\left(\frac{B_d}{B_0}\right)^{0.5} - 1\right] \text{ or } v_d = v_0\left[2(B)^{0.5} - 1\right] \quad (15)$$

where,

v_d - Vibration due to deviated burden,
v_0 - Vibration due to optimum burden,
B_d – Deviated burden and
B_0 – Optimum burden
B - Ratio of deviated burden to optimum burden

Therefore, the final prediction model incorporating burden, gets a simple form as expressed in equation (15).

Considering the dual effects of burden on vibrations, the overall increase in vibration for different values of burdens ranging from 1 to 2 times the optimum burden is calculated and is given in Table 3. The tabulated values of percentage increase in burden and percentage increase in vibration are shown in graphical form in the Figure 7.

4. EXPERIMENTAL VALIDATION OF BURDEN BASED PREDICTION MODEL

The burden based prediction model was tested for validation in field conditions. Field tests were conducted in sandstone formations at two different Indian coal mines of Singareni Collieries Company Ltd. (SCCL), and Western Coalfields Ltd. (WCL). The experiments and the results of the field studies are explained separately for different test sites.

4.1 Validation Tests at SCCL, India

Seven trial blasts were conducted at an open pit coal mine of SCCL with burdens ranging from 6 to 13.5 m i.e. with the burden ratios varying between 1 to 2.25. The vibration was recorded by seismograph stationed at a fixed location for all the trials to minimise effect of medium change. The data generated during the experimentation included burden, distance of vibration measurement, charge per delay and corresponding vibration, which is provided in Table 4. The regression analysis of the burden ratios and vibration for all

Table 3. Percentage increase in vibration for different increments of burden

Percentage increase in burden	Percentage increase in vibration
5	5
10	10
20	19
30	28
40	37
50	45
60	53
70	61
80	68
90	76
100	83

the observations are provided in Figure 8. Based on the vibration generated with optimum burden and the prediction model given in equation (15) the vibrations for various burdens were calculated and given in Table 4. The regression analysis of the burden ratios and predicted vibration levels was carried out and provided in Figure 8. The trends of curves drawn for measured and predicted vibrations are almost same. Some deviations in both the curves may be due to possible variations in the medium due to progression of blast location at a particular bench.

4.2 Validation Tests at WCL Coal Mine, India

Seven trial blasts were conducted at WCL coal mine for validation of the burden based prediction model. The design parameters at WCL coal mine are given in Table 5.

Five of 7 trial blasts were conducted with optimum burden and vibration was recorded by seismographs stationed at 4 to 5 locations. The seismograph stations were fixed for all the trials to minimise the change of medium. One trial blast was conducted with a burden of 12 m and another trial was with 16 m. The data generated during the experimentation included burden, distance of vibration measurement, charge per delay and corresponding vibration, which is provided in Table 6. The regression analysis of the scaled distance (SD) and vibration for all the 3 sets of burdens i.e., optimum (OB), 2OB and 1.5OB) was carried out and the curves are provided in Figure 9.

The prediction equation with optimum burden:

$$v = 501\ (D/\sqrt{Q})^{-1.27} \text{ with } R^2 = 0.97 \qquad (16)$$

The prediction equation with 1.5 times the optimum burden:

$$v = 782\ (D/\sqrt{Q})^{-1.33} \text{ with } R^2 = 0.93 \qquad (17)$$

Figure 7. Percentage increase in vibration versus percentage increase in burden

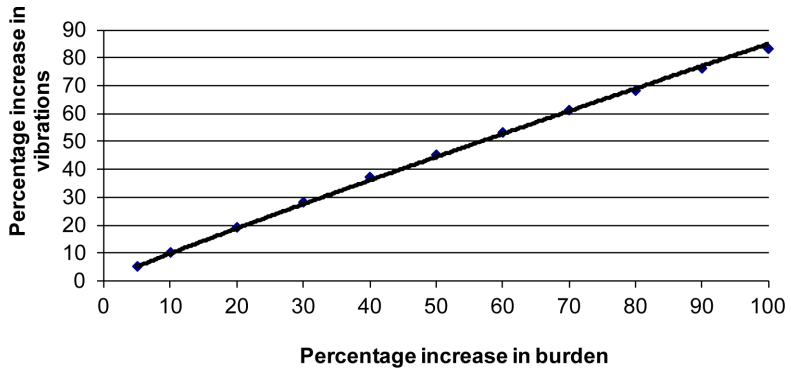

Table 4. Data generated during validation tests at SCCL Coal mine

Blast No.	B_2/B_1 (Optimum B=6m)	Scaled distance, (D/√Q), m/ $kg^{0.5}$	$v_{meas.}$ mm/s	$v_{pred.}$ mm/s
1	1.0	9.6	15.1	15.1
2	1.1	9.4	13.7	16.3
3	1.3	9.3	18.4	19.8
4	1.4	9.3	19.6	20.9
5	1.8	9.6	24.8	24.9
6	2.0	9.5	27.8	27.6
7	2.3	9.8	33.4	30.2

$v_{meas.}$-Measured peak particle velocity; $v_{prid.}$ Predicted peak particle velocity

Table 5. Design details of trial blasts conducted at WCL mine

1.	Blasthole burden	8-16 m; (Optimum burden =8m)
2.	Hole spacing	8 m
3.	No. of holes per delay	1
4.	No. of holes per round	60
5.	No. of rows in a round	6
6.	Initiation system	Detonating fuse
7.	Hole diameter	250 mm
8.	Bench height	30 m
9.	Explosive used	Site Mixed Emulsion
10.	Designed specific charge	0.6 kg/m^3

Figure 8. Predicted and measured vibration versus burden ratios at SCCL coal mine

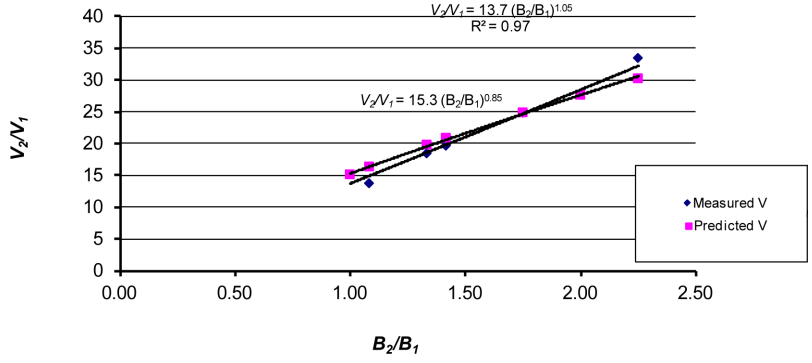

Figure 9. Measured vibrations versus scaled distance at WCL coal mine

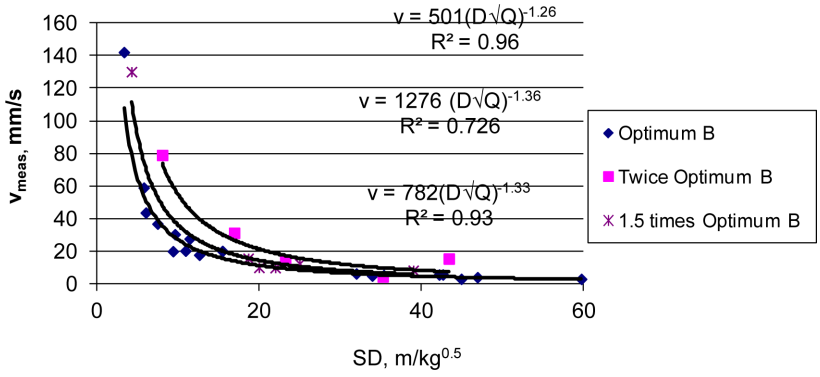

The prediction equation with 2 times the optimum burden:

$$v = 1276\ (D/\sqrt{Q})^{-1.37} \text{ with } R^2 = 0.73 \quad (18)$$

Figure 10. Measured and predicted vibrations versus scaled distance with increased burden by one and half times the optimum burden at WCL coal mine

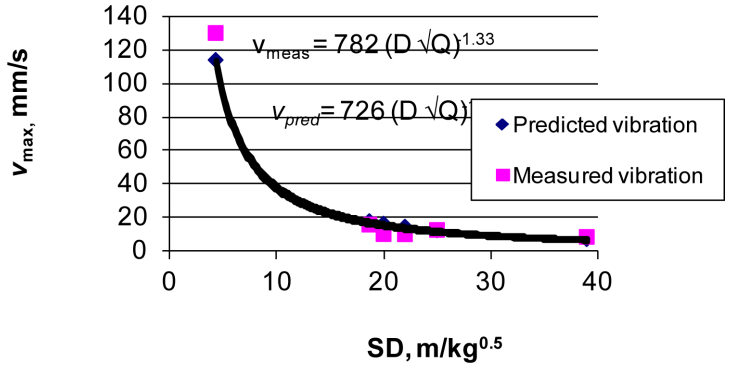

Figure 11. Measured and predicted vibrations versus scaled distance with increased burden by twice the optimum burden at WCL coal mine

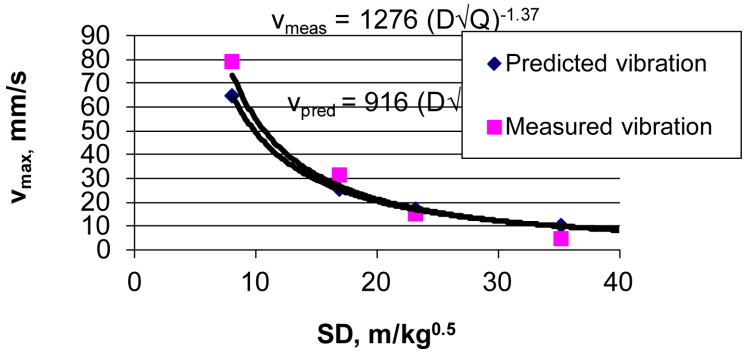

Both the coefficient and the negative power (slope) of the curves are increasing gradually from optimum burden to double the optimum burden.

The vibration for the blasts of excess burden was calculated by using the burden based predictor equation (15), $v_2 = v_1(2B^{0.5} - 1)$. The general optimum vibration level (v_1) for different blasts is calculated by substituting the corresponding scaled distance in the in the equation (16), which was derived for the blast rounds with optimum burden (OB). The v_1 so calculated is multiplied by the quantity ($2B^{0.5} - 1$) to get the predicted vibration with excess burden (v_2) for each blast. The predicted vibrations calculated for different scaled distances for each blast are given Table 6. Relationships are drawn for scaled distance versus predicted vibration (v_{pred}) as well as measured vibration (v_{meas}) for both the excess burdens i.e., one and half times the optimum burden and twice the optimum are shown in Figure 10 and Figure 11.

The trendlines drawn in Figure 10 and Figure 11 show that the predicted vibration levels calculated on the basis of the burden based predication model are almost in line with the measured vibration levels in both the trial blasts with excess burdens. These results confirm the experimental validation of the burden based predication model.

Table 6. Data generated during the experimentation for validation tests at WCL mine

Sl No.	Blast No.	B_2/B_1, (Optimum B=8m)	Scaled distance, (D/√Q), m/kg$^{0.5}$	$v_{meas.}$, mm/s	$v_{pred.}$ mm/s (For excess burden)
1	1	1	5.8	58.9	58.9
2	1	1	11.5	27.6	27.6
3	1	1	7.5	36.8	36.8
4	1	1	12.6	17.7	17.7
5	1	1	33.9	4.9	4.94
6	2	1	3.4	142.0	142
7	2	1	6.1	43.6	43.6
8	2	1	10.9	20.2	20.22
9	2	1	9.4	19.9	19.9
10	2	1	35.4	5.3	5.3
11	3	1	44.9	2.98	2.98
12	3	1	42.2	5.59	5.59
13	3	1	15.5	20.07	20.07
14	3	1	9.6	30.3	30.3
15	4	1	32.0	6.24	6.24
16	4	1	42.6	5.64	5.64
17	4	1	46.9	3.98	3.98
18	4	1	59.7	2.94	2.94
19	5	1.5	25.0	12.4	12.18
20	5	1.5	20.0	9.94	16.17
21	5	1.5	22.0	9.81	14.33
22	5	1.5	18.7	15.6	17.65
23	5	1.5	4.3	130	113.91
24	5	1.5	39.0	8.24	6.92
25	6	2	8.1	78.9	64.48
26	6	2	16.9	31.2	25.17
27	6	2	23.2	14.8	16.86
28	6	2	35.25	4.41	9.93
29	6	2	43.39	15.4	7.63

$v_{meas.}$-Measured peak particle velocity; $v_{prid.}$ Predicted peak particle velocity

5. CONCLUSION

The following conclusions can be drawn from the results of the model and experimental studies:

1. The models developed for prediction of peak particle velocity of vibration fall short of incorporating the burden, which is the most important blast design parameter.
2. This study provides a burden based vibration prediction model to calculate the peak particle velocity with various practical burden values.
3. The influence of burden on vibration was studied in detail and it was confirmed by

experimental and model studies that the burden influences the vibration directly and indirectly.

4. Burden has significant influence on the resultant ground vibrations. The increase due to excess burden can be estimated by inserting a factor which consists of ratio of excess burden to optimum burden.
5. The net vibration due to deviated burden is a function of vibration with optimum burden and ratio of excess burden to optimum burden. [$v_2=v_1(2B^{0.5}-1)$].
6. The new prediction model was tested in the field conditions and validated successfully for the burden varying from optimum burden to 2.25 times the optimum burden.
7. The new predictor equation can be used for estimation of vibration levels when there is deviation of burden due to choking of holes and misfires, which result in increased vibration intensity. This is useful for adopting safety measures for sensitive structures in the vicinity of the blast zone.

ACKNOWLEDGMENT

The author is indebted to the valuable advises of late Dr. A. K Chakaborty in guiding this research work. The author expresses his sincere gratitude to Dr. A. K. Soni, Dr. A. K. Raina and Mr. P. B. Choudhury for their help during the field experiments. The permission of Director, Central Institute of Mining and Fuel Research to publish the paper is acknowledged thankfully.

REFERENCES

Ambraseys, N. R., & Hendron, A. J. (1968). *Dynamic behavior of rock masses in rock mechanics in engineering practice* (K. G. Stagg & O. C. Zienkievicz, Eds.). New York: John Wiley and Sons.

Anderson, D. A., Ritter, A. P., Winzer, S. R., & Reil, J. W. (1985). A method for site specific prediction and control of ground vibration from blasting. In *Proceedings of the E Firstt Mini-Symposium on Explosives and Blasting Research*, San Diego, CA (pp. 28-43).

Andrews, A. B. (1981, January 19-23). Design criteria for sequential blasting. In *Proceedings of the Seventh Conf. on Explosives and Blasting Technique*, Phoenix, AZ (pp. 173-192). Montville, OH: Society of Explosives Engineers.

Ash, R. L. (1990). *Design of blasting rounds, Int. Surface Mining* (2nd ed., pp. 565–583). New York: AIME.

Atchison, T. C. (1972). Fragmentation Principles (Chapter 7.2). In *Proceedings of Surface Mining* (pp. 355-372). New York: AIME.

Bauer, A., & Crosby, W. A. (1990). *Blasting; Surface Mining* (2nd ed., pp. 552–554). Littleton, CO: Metallurgy and Exploration, Inc.

Berta, G. (1990). *Explosives: An Engineering Tool*. Milano, Italy: ltalesplosivi.

Birch, W. J., & Chaffer, R. (1983). Prediction of ground vibrations from blasting on opencast sites, Trans. Instn. Min. Metall., Section A. *Mineral Industry*, *92*, A102–A107.

Blair, D. P., & Armstrong, L. W. (2001). The influence of burden on blast vibration. Rock Fragmention by Blasting. *Fragblast*, *5*(1-2), 108–129. doi:10.1076/frag.5.1.108.3315doi:10.1076/frag.5.1.108.3315

Crandell, F. J. (1949). Ground Vibrations Due to Blasting and Its Effect upon Structures. *Journal of the Boston Society of Civil Engineers*, 222-245.

Crum, S. V., Siskind, D. E., & Eltschlager, K. (1997). Blast vibration measurements at far distances and design influences on ground vibrations. In *Proceedings of Annual conference on Explosives and blasting research, explosives reference database on CD-ROM*. Montville, OH: International society of explosive engineers.

Devine, J. F., Beck, R. H., Meyer, A. V. C., & Duvall, W. I. (1966). Effect of charge weight on vibration levels from quarry blasting. In *Proceedings of USBM (RI-6774)* (pp. 37-38).

Dick, R. A., Larry, R., Fletcher, D., & Andrea, V. D. (1983). *Explosives and Blasting Procedures Manual*. Bureau of Mines.

Dowding, C. H. (1995). *Blast vibration monitoring and control*. Upper Saddle River, NJ: Prentice Hall.

du Pont, E. I. (1977). *Blasters Hand book* (175th Anniversary ed.). Wilmington, DE: E. I. du Pont de Nemours, Inc.

Duvall, I. W., & Devine, J. F. (1968). *Avoiding damage by air blasts and ground vibrations from blasting, Surface mining*. New York: AIMMPE Inc.

Floyd, J. L., & Conn, D. B. (1997). PhotoSeis-an advanced method for vibration analysis and control. In *Proceedings of Annual conference on Explosives and blasting research, explosives reference database on CD-ROM*. Montville, OH: International society of explosive engineers.

Ghosh, A. A., & Daemen, J. J. K. (1983). *A new analytical predictor of ground vibrations induced by blasting, Volume IV* (Rep. to the office of surface mining).

Gordon, G., & Nies, D. (1997). Small Borehole Blasting In High Liability Locations. In *Proceedings of Annual conference on Explosives and blasting research, explosives reference database on CD-ROM*. Montville, OH: International society of explosive engineers.

Heiling, J., Zeitsas, A., & Cox, N. (1997). Free face blasting is it the best for quarrying. In *Proceedings of the 41st Annual Conf*. (pp. 33-44). Australia: Institute of Quarrying.

Jimeno, C. L., Jimeno, E. L., & Carcedo, F. J. A. (1995). *Drilling and Blasting of Rocks* (pp. 183–184). Rotterdam, The Netherlands: A. A. Balkema.

Konya, C. J. (1995). *Airblast monitoring and control blast design*. Montville, OH: Int. Development Corporation.

McGarr, A. (1983). Estimating ground motion for small nearby earthquakes. In *seismic design of embankments and caverns* (pp. 113-127). New York: ASCE.

Mckenzie, C. K. (1993). Methods of improving blasting operations. In J. A. Hudson (Ed.), *Comprehensive Rock Engineering* (*Vol. 4*, pp. 71–94). Oxford, UK: Pergamon Press.

Mortazavi, A., & Katsabanis, P. D. (2001). Modelling burden size and strata dip effects on the surface blasting process. *International Journal of Rock Mechanics and Mining Sciences*, *38*, 481–498. doi:10.1016/S1365-1609(01)00015-6doi:10.1016/S1365-1609(01)00015-6

Nutting, M. J., & Froedge, D. T. (1997). The Mapping Of Vibration Patterns Around A Blast. In *Proceedings of Annual conference on Explosives and blasting research, explosives reference database on CD-ROM*. Montville, OH: International society of explosive engineers.

Persson, P. A., Holmberg, R., & Lee, J. (1994). *Rock Blasting and Explosives Engineering*. Boca Raton, FL: CRC.

Raina, A. K., Ramulu, M., Chakraborty, A. K., Choudhury, P. B., & Bandopadhay, C. (2004). *Monitoring and control of blast vibrations in dragline bench of Sasti OCP, WCL* (pp. 2-10). Unpublished CMRI internal Report.

Ramulu, M., Chakraborty, A. K., & Raina, A. K. (2004). *Blast optimization and Ground Vibration Monitoring at Malanzkhand Copper Project, Malanzkhand* (pp. 15-25). Unpublished CMRI internal Report.

Ramulu, M., Chakraborty, A. K., Raina, A. K., Choudhury, P. B., Jethwa, J. L., & Singh, T. N. (1998). *Blast Induced Ground Vibration Monitoring at Lakshmi Cement Limestone mines, Rajasthan* (pp. 12-17). Unpublished CMRI internal Report.

Ramulu, M., Chakraborty, A. K., Raina, A. K., & Reddy, A. H. (2004). Influence of burden on the intensity of ground vibrations and air overpressure in opencast bench blasting. In *Proceedings of the ISEE's 30th Annual Conference on Explosives and Blasting Techniques*, New Orleans, LA (pp. 465-478).

Ramulu, M., Raina, A. K., Chakraborty, A. K., Reddy, A. H., & Jethwa, J. L. (2002). Influence of burden on the intensity of ground vibrations in a limestone quarry. In *Proceedings of the International Conference fragmentation and blasting, Fragblast* (pp. 617-624).

Rockwell, E. H. (1927). Vibrations caused by quarry blasting and their effect on structures. *Rock Products*, *30*, 58–61.

Rollins. (1980). *Energy partitioning* (Tech. Rep.). Rolla, Missouri: University of Missouri Rolla, Rock mechanics and explosive research center.

Rustan, A. (1998). *Rock blasting terms and symbols*. Rotterdam, The Netherlands: A. A. Balkema.

Rustan, A., & Lin, N. S. (1983). New method to test the rock breaking properties of explosives in full scale. In *Proceedings of the First International Symposium on Rock Fragmentation by Blasting*, Lulea, Sweden (pp. 36-47).

Sames, F. (1999). The influence of blast parameters on vibration and air overpressure. In *Proceedings of the 6th Int. Symposium on Rock Fragmentation by Blasting (FRAGBLAST-6)*, Johansberg, South Africa (pp. 149-154).

Scott, A., Cokker, A., Djordjevic, N., Higgins, M., La Rosa, D., Sarma, K. S., & Wedmaier, R. (1996). Open Pit Blast Design Analysis and Optimisation. *JKMRC*, 266-280.

Sen, G. C., & Silitonga, M. (1984). Effect of confinement on ground vibrations due to blasting. In *Proceedings of the Australian, Inst. of Min. Metall* (pp. 213-215).

Siskind, D. E., Stagg, M. S., Kopp, J. W., & Dowding, C. H. (1980). *Structure Response and Damage Produced by Ground Vibration From Surface Mine Blasting*. U. S. Bureau of Mines.

Thoenen, J. R., & Windes, S. L. (1942). Seismic effects of quarry blasting. *Bureau of Mines Bulletin*, *442*, 83.

Wallace, J. (1996). What a gas: blasting under pressure. In *Proceedings of the 22nd Ann. Conf. on Explosives and Blasting Techniques* (pp. 140-150).

Wathen, D., & Thomas, M. E. (1996). Blasting with a light touch. In *Proceedings of the 22nd Ann. Conf. on Exp. and Blasting tech* (pp. 152-161).

Wiss, J. F., & Linehan, P. W. (1978). *Control of vibrations and blast noise from surface coal mining* (Volumes I-IV, Report to U.S. Bureau of Mines). Bureau of Mines.

This work was previously published in International Journal of Geotechnical Earthquake Engineering, Volume 1, Issue 2, edited by T.G. Sitharam, pp. 72-88, copyright 2010 by IGI Publishing (an imprint of IGI Global).

Chapter 11
Dynamic Tensile Test of Coal, Shale and Sandstone Using Split Hopkinson Pressure Bar: A Tool for Blast and Impact Assessment

Kaiwen Xia
University of Toronto, Canada

Sheng Huang
University of Toronto, Canada

Ajay Kumar Jha
Indian Institute of Technology, India

ABSTRACT

The dynamic tensile strength plays a pivotal role in rock fragmentation affecting the overall economics under the present 'Mine to Mill Concept'. In this paper, a modified SHPB technique and Brazilian test method is presented to test the dynamic tensile strength of coal, shale and sandstone rock samples collected from three opencast mines of Coal India Limited and is compared with the static strength value. The dynamic tensile strength of coal and rock is much higher than static strength and tensile strength of coal and rock samples increase with loading rate. The result shows that the dynamic strength of the coal sample is 1.5 times higher than static strength and the dynamic strength of the sandstone sample is 3 times higher than the static strength.

DOI: 10.4018/978-1-4666-0915-0.ch011

1. INTRODUCTION

In India, coal accounts for the prime source of energy consumption (>50%) and has been considered as major energy source. A growing demand of coal has put a higher pressure to augment the production particularly from opencast mines in India. The dynamic tensile strength of coal or rock plays pivotal role in rock fragmentation under blast induced loading. The mechanical properties of coal and host rocks are vital factors for the blast efficiency in terms of achieving optimum rock fragmentation and overall economics under 'Mine to Mill concept'. Coal and Coal bearing formations show high sample-to-sample scatter in strength.

The test methods for determining dynamic tensile strength that are successful in comparatively homogeneous rock types cannot be used for coal. The dynamic tensile strength of Indian coal has never been investigated.

2. REVIEW OF DYNAMIC TESTS CARRIED ON COAL, SANDSTONE AND SHALE SAMPLES

Recently, Okubo et al. developed an alternative test method for anthracite coal samples by subjecting the samples to alternating slow and fast strain rates within the quasi-static loading range (Okubo et al., 2006). Shan et al. (2006) extended the alternative test method procedure to the dynamic loading range. Wang et al. (2007) carried out the compression mechanical properties of coal with the confinement of 8.06MPa, and their experiments can also be done with a Hopkinson bar to investigate the dynamic properties with

Table 1. Strength of various coals

Study	coals	Testing method	Strength (MPa)	Strain rate (s^{-1})
Okubo et al.(2006)	Beijing Coal	Uniaxial Compression	50 (X)*	10^{-6}~10^{-5}
			25(Y)	
			22(Z)	
		Uniaxial tension	0.42(X)	
			1.04(Y)	
			0.57(Z)	
		Indirect tension	2.1(Y/Z)**	
			1.9(Z/Y)	
			3.7(X/Z)	
			2.8(Z/X)	
			3.2(Y/Z)	
			3.0(Z/Y)	
Wang et al. (2007)	Jingyuan coal	Compression With 8.06MPa confinement	23.6	-
Shan et al.(2006)	Yunjialing coal	Hopkinson bar (Compression)	9.2/6.1**	24
			13.5/7.1	44
			12.0/8.4	66
			21.0/16.7	118

*Loading direction

**Boring direction/ Loading direction

Table 2. Compressive and tensile strength of sandstones

Study	sandstone	Testing method	Strength (MPa)	Strain rate (s-1)
Chen et al. (2007)	Dry Wuhan sandstone	MTS (Compression)	82.3	10^{-5}
			126.6	10^{-4}
			141.6	10^{-3}
	Saturated Wuhan sandstone	MTS (Compression)	70.5	10^{-5}
			108.3	10-^{4}
			124.1	10^{-3}
Okubo and Fukui (1996)	Kimachi sandstone	MTS (Tension)	3.5	1.50×10^{-3}
		MTS (Compression)	32	1.50×10^{-3}
	Tako sandstone	MTS (Tension)	3.0	1.50×10^{-3}
		MTS (Compression)	32	1.50×10^{-3}
Hobbs (1970)	Lea Hall sandstone	-	47	-
Kubota et al. (2008)	Kimachi sandstone	underwater shock waves (Tension)	17.4	40.0
			16.4	42.1
			13.8	30.0
			12.0	15.9
			11.7	13.9
Li et al. (2000)	Sandstone	SHPB (Compression)	~60	10
				31
				45

confinement. The test results from the above referred literature are summarized in Table 1.

Most of the existing experimental studies for sandstone are carried out under static loading conditions. Chen et al. (2007) performed laboratory experiments on dry and saturated Wuhan sandstones. Kubota et al. (2008) carried out a series of dynamic tests on Kimachi sandstone to measure its dynamic tensile strength using underwater shock waves but the shock waves experiment is too expensive. Li et al. (2000) investigated the dynamic mechanical properties of sandstone using the split Hopkinson pressure bar (SHPB). From Table 2 it can be concluded that dynamic tensile strength at strain rate close to that in explosion (~ 100 /s) is about an order of magnitude higher than the static strength.

It is evident from test results listed in Table 3 that for hard sandstone the higher the strain rate, the higher the strength. This is generally true for soft rocks as evidenced from some experimental investigations. Tests on oil shale were performed by Grady and Kipp (1980) for strain rates between 100 and 10^4 l/s. Linear relationships were established among uniaxial compressive strength, organic volume, and logarithmic strain rate.

3. EXPERIMENTAL SETUP

In this paper, a modified SHPB technique and Brazilian test method is presented to test the dynamic tensile strength of coal, shale and sandstone rock samples. Totally four different kinds of loading rate were tested to investigate the relationship between tensile strength and dynamic loading. Static test results are also presented for the comparison.

Table 3. Strength for various shales

Study	shale	Testing method	Strength (MPa)	Strain rate (s^{-1})
Swan et al. (1989)	Kimmeridge Bay shale	Static compression with confinement (Undrained loading series)	140.2	4.00E+0
			130	3.33E+0
			43.9 /28.3*	1.67E-1
			104.1/103.5	1.67E-1
			118.4/110.6	1.67E-1
			131.1/137.3	1.67E-1
			100.8/96.3	8.33E-2
			86.1/84.5	1.67E-2
			74.6/72.2	1.67E-3
			76.9/70.2	1.67E-4
			79.2/69.4	1.67E-5
			32.8/16.8	1.67E-6
			71.7/64.0	1.67E-6
			110.3/91.6	1.67E-6
		Static compression with confinement (Drained undrained loading series)	131.5/115.5	1.67E-1
			130.2/112.5	8.33E-2
			126.0/119.9	1.67E-2
			113.2/110.1	1.67E-3
			112.3/107.7	1.67E-4
			124.9/119.0	1.67E-5
Hobbs (1970)	Hucknau shale	-	58.7	-
Cai et al. (2007)	Meuse/Haute-Marne argillite	Hopkinson bar (compression) Perpendicular to bedding	44.3	699
			43.8	690
			81.5	720
			63.8	805
			62.7	1072
			68.2	1071
			57.3	799
			67.2	975
			72.6	1179
		Hopkinson bar (compression) Parallel to bedding	60	526
			69.1	744
			61.6	1056
			68.5	932
			70.9	859
			62.1	1165

continued on following page

Table 3. Continued

Cai et al. (2007)	Meuse/Haute-Marne argillite	Hopkinson bar (Brazilian)	8.1	6.98
			9.5	8.22
			8.4	7.64
			10	5.36
			10.1	12.79
			12.8	18.42
			11.6	11.35
			5.5	10.93
			9.7	4.25
			5.2	2.76
			10.6	8.23
			6.9	5.48
			11.5	5.99
			9.7	11.34
			5.5	2.82
			8.7	5.92
			11.6	11.25

* strength/ confined pressure

SHPB system is used to conduct the dynamic tensile test of coal (Figure 1) and rock. As a standard facility for dynamic testing, SHPB is composed of a striker bar, an incident bar and a transmitted bar (Figure 2). The specimen is sandwiched between the incident bar and the transmitted bar. The dynamic load is generated by the impact of the impact bar on the incident bar, and the striker bar is launched by a low speed gas gun. The impacting of the striker bar on the free end of the incident bar generates a longitudinal compressive wave propagating in the incident bar as incident wave ε_i. When the incident wave reaches the bar-specimen interface, part of the wave is reflected back as reflected wave ε_r, and the remainder passes through the specimen and then enters the transmitted bar as transmitted wave ε_t. These waves are measured using strain gauges and used to infer the dynamic response of the material (i.e., stress-strain curve) subsequently.

Using these 3 waves, the forces P_1 and P_2 which add on the specimen can be calculated.

$$P_1(t) = EA[\varepsilon_I(t) + \varepsilon_R(t)] \tag{1}$$

$$P_2(t) = EA\varepsilon_T(t) \tag{2}$$

where E and A are Young's modulus and cross-section of the bars, separately.

The tensile strength is then calculated using following relation (Bieniawski & Hawkes, 1978):

$$\sigma_t = \frac{2P_{\max}}{\pi DB} \tag{3}$$

where σ_t is the tensile strength, $P_{\max}$ is the maximum value of loading force P_2, D is the diameter of the specimen, and B is the thickness of the disc specimen.

The striker bar, incident bar and transmitted bar of conventional SHPB system are made by steel. For low impedance materials like coal, the impedance mismatch of bars and samples has to be considered. Some tests for ultra soft materials test with Aluminum bar were carried out, whose

Figure 1. Schematics of SHPB system

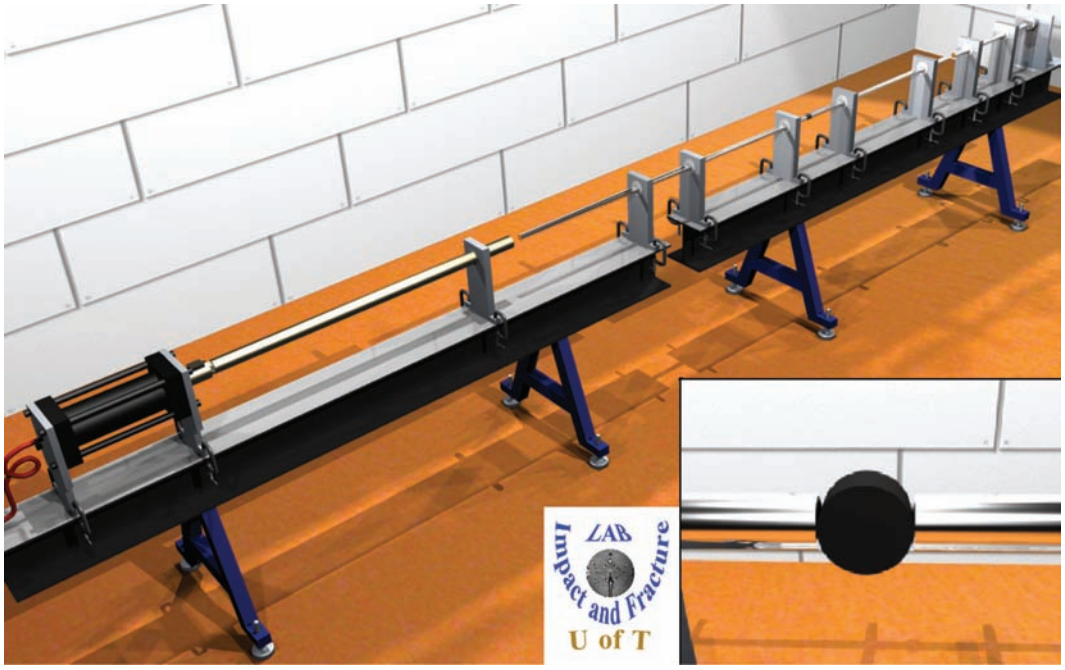

Figure 2. Typical configuration of SHPB

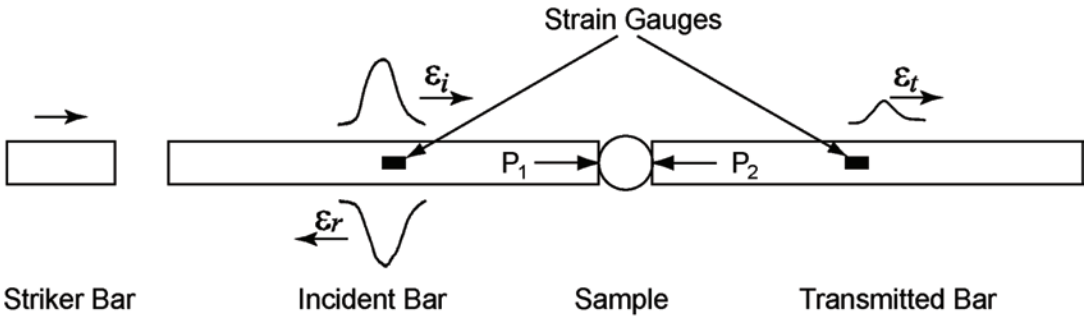

impedance is much lower than that of steel bar (Chen et al., 2009). In this paper, a 25 mm Aluminum SHPB system was modified to test the tensile strength of coal. The bars are made of 7075 Aluminum alloy, with a yield strength of 455 MPa. The length of the striker bar is 300 mm. The incident bar is 2000 mm long and the transmitted bar is 1500 mm long. A 25 mm steel SHPB system is used to test the tensile strength of the rock. The bars are made of maraging steel, with a yield strength of 2.5 GPa. The length of the striker bar is 200 mm. The incident bar is 1500 mm long and the transmitted bar is 1000 mm long.

A pulse shaping technique of SHPB method is utilized for all dynamic tests. The pulse shaping technique in SHPB is especially useful for investigating dynamic response of brittle materials such as rocks (Frew et al., 2001; Frew et al., 2002). Without proper pulse shaping, it is difficult to reach dynamic stress equilibrium in such materials because the sample may fail immediately from its end when it is impacted by the incident

bar. In the modified SHPB test, we use the C1100 copper disc as the main shaper to transform the incident wave from a rectangular shape to a ramped shape. In addition, a small rubber disc is placed in front of the copper shaper to further reduce the slope of the pulse to a desired value. During tests, the striker impacts the pulse shapers before the incident bar, thus generating a non-dispersive ramp pulse propagating into the incident bar and thus facilitating the dynamic force balance for the specimen (Frew et al., 2001; Frew et al., 2002).

The static tests were done by a Digital Tritest machine, manufactured by ELE International Company with Model Number 79167. The Loading speed is 0.1 mm/sec.

4. RESULTS AND DISCUSSIONS

4.1 Dynamic Equilibrium

In order to guarantee a quasi-static state in the dynamic Brazilian test, pulse shaping technique is employed for all our dynamic tests. The dynamic force balance on the two loading ends of the sample is critically assessed. Figure 3 shows the forces on both ends of the specimen in a typical test. From Eq. 1 and 2, the dynamic force on one side of the specimen P1 is proportional to the sum of the incident (In) and reflected (Re) stress waves, and the dynamic force on the other side P2 is proportional to the transmitted (Tr). It can be seen from Figure 3 that the dynamic forces on both sides of the specimens are almost identical during the whole dynamic loading period. The

Figure 3. Dynamic force balance check for a typical dynamic Brazilian test with pulse shaping

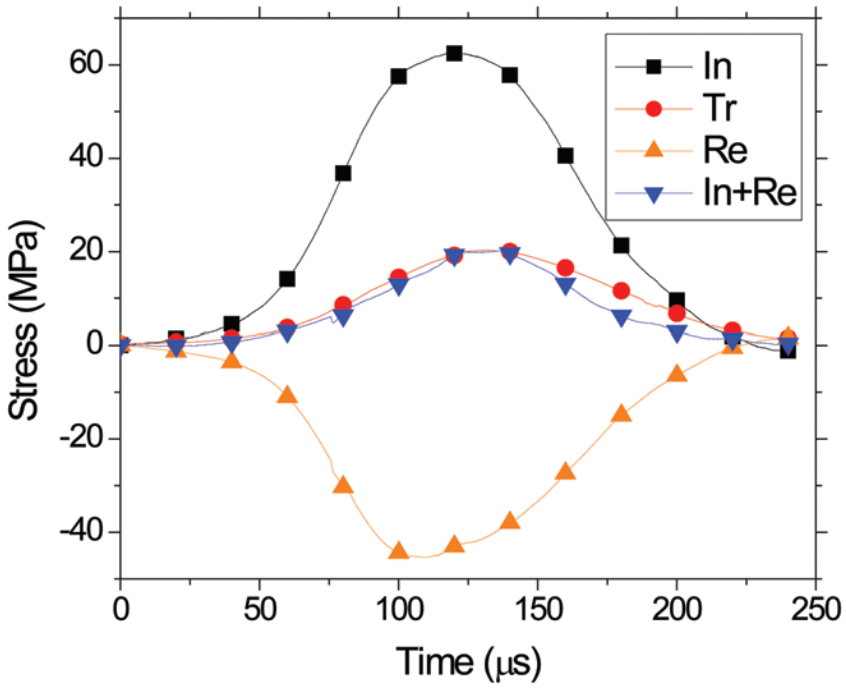

Figure 4. Typical stress-time curve for determining loading rate

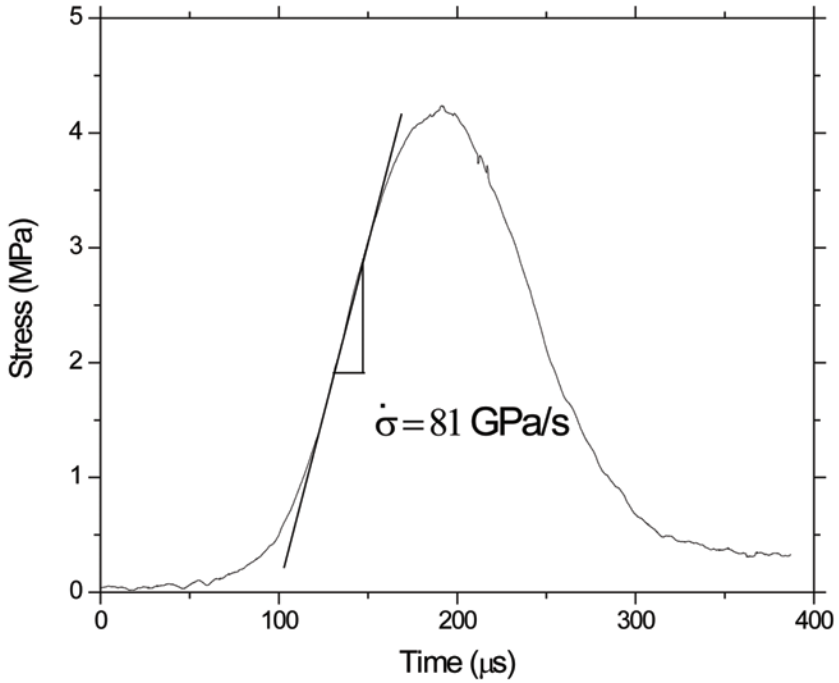

inertial effects are thus eliminated because there is no global force difference in the specimen to induce inertial force. Thus we can use the static tensile strength formula (Eq. 3) to analyse the dynamic results.

4.2 Determination of Loading Rate

The loading rate has a considerable effect on the tensile strength of coal and rock under dynamic loading. The loading rate is characterized with $\dot{\sigma}$ obtained from the time evolution of loading stress. Figure 4 shows loading and unloading in terms of stress (P_1) in a typical test. There exits a regime of approximately linear variation of stress with time from 125 μs to 175 μs. The slope of this region is determined from a least squares fit, shown as a line in the figure and this slope is used as the loading rate.

4.3 Tensile Strength of Coal

Figure 5 shows typical virgin and tested coal samples. The average diameter and thickness of test sample are 52 mm and 22 mm, respectively. After test, the sample was split into halves from the center.

A Photron SA-1 high speed camera was used to illustrate qualitatively these representative instants (Figure 6). This camera record around 180,000 photos/s i.e. the interval time of two photos is 5.34 μs. Each frame contains 125 × 125 pixels. At instant A, the loading started. The crack initiated at instant B; at the same time, the forces add on the sample also was the maximum value. The coal completed fracture at instant C.

Three types of coal sample collected from mines of Coal India Limited, coded as 1-B, 2-C and 3-C, were tested and are presented in this paper, with one static test of 1-B sample (shown in Table 4 and Figure 7).

Figure 5. Typical virgin and tested coal samples (under 237 GPa/s loading rate)

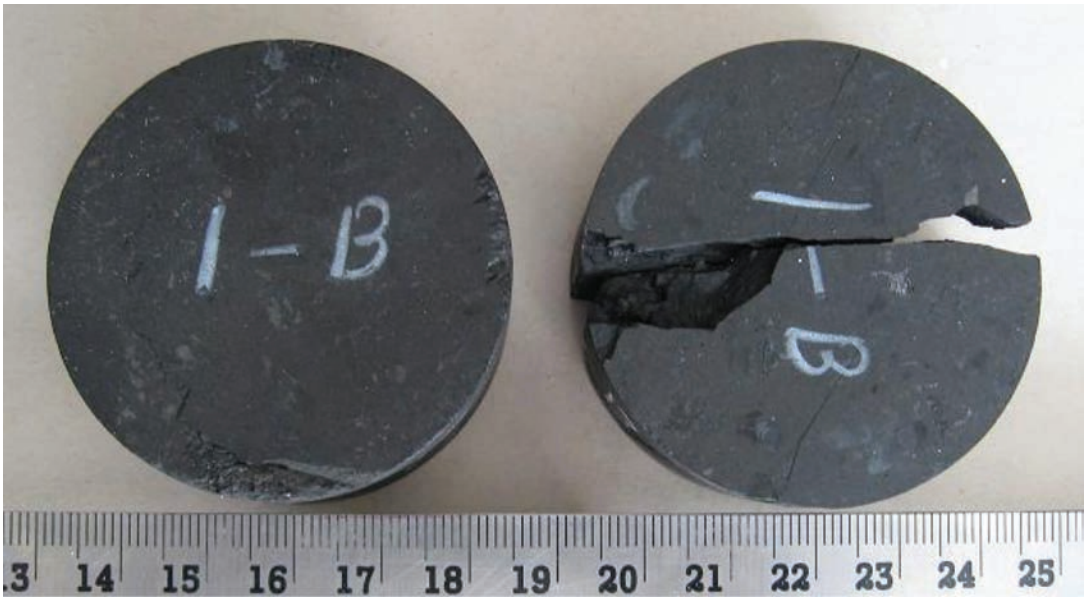

Figure 6. High speed camera snapshots of a dynamic coal test

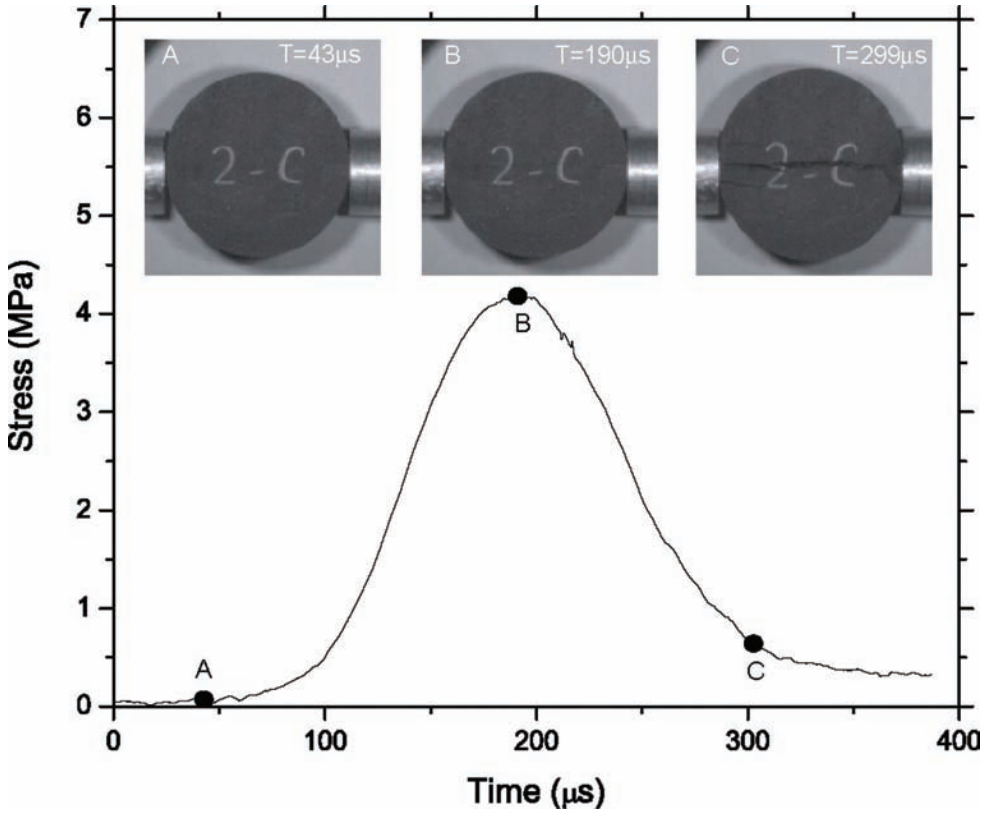

Table 4. The tensile strength of 3 kinds of coal sample

Sample Number	Loading rate (GPa/s)	Tensile strength (MPa)
1-B #1	0.01	2.9
1-B #2	237	4.08
1-B #3	266	4.99
1-B #4	319	4.54
1-B #5	460	6.85
2-C #1	193	4.18
2-C #2	300	4.51
2-C #3	342	5.24
3-C #1	176	3.4
3-C #2	273	5.42
3-C #3	297	5.19
3-C #4	391	6.39
3-C #5	446	5.17
3-C #6	470	6.88
3-C #7	475	5.56
3-C #8	490	7.42

Figure 7. The tensile strength of 3 different types of coal with different loading rate

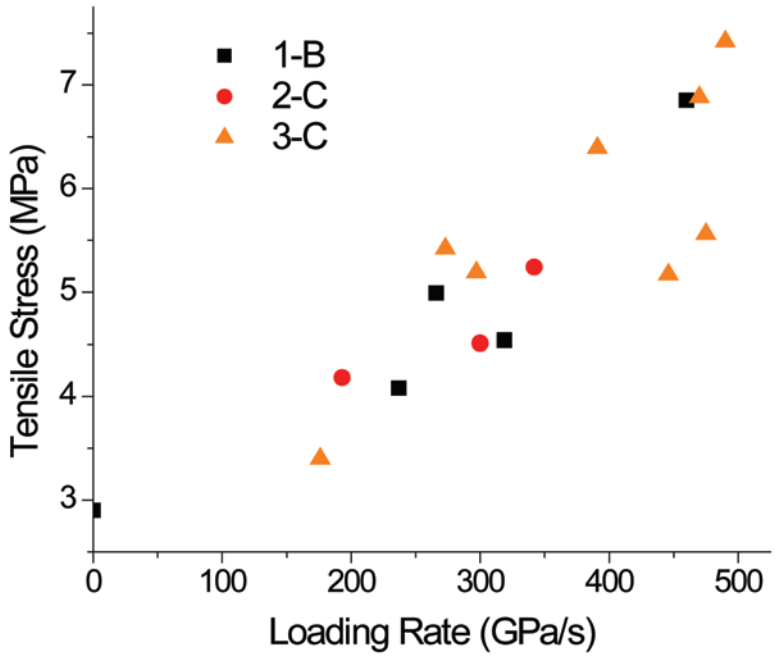

Figure 8. 1-B coal sample results

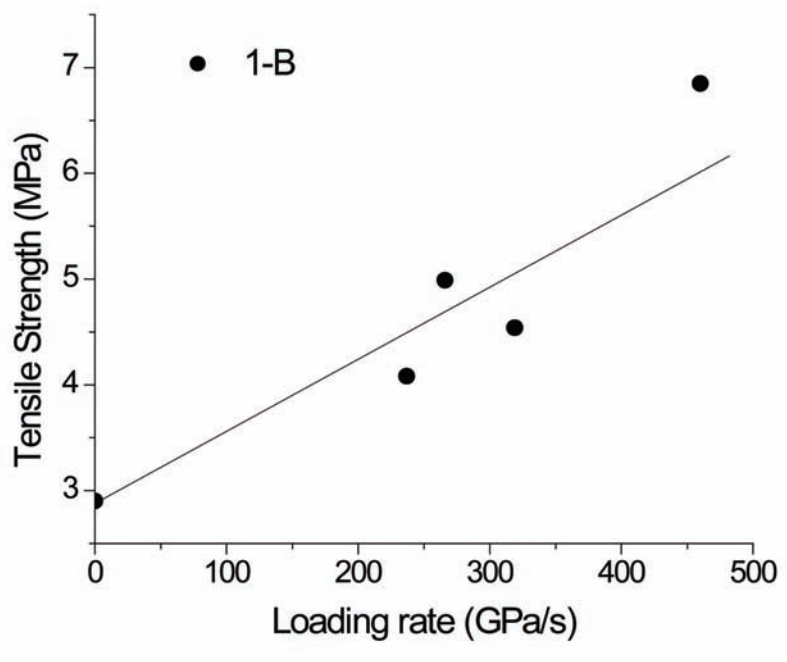

Figure 9. Typical virgin and tested rock samples (under 0.01 GPa/s loading)

The results show the strength of these three types of coal sample which increases with loading rate. It is evident from result that the dynamic tensile strength of coal is much higher as compared to the static tensile strength of coal. The static tensile strength of 1-B coal sample is 2.9 MPa; when the loading rate rises to around 300 GPa/s, the tensile strength is 4.54 MPa, 1.5 times higher than static strength (Figure 8).

4.4 Tensile Strength of Rock

The average diameter and thickness of rock samples are 52 mm and 22 mm, respectively (Figure 9). The crack is straight through the center of the sample.

Three kinds of rock sample of sandstone, 1-A, 2-A and 3-A, were tested and is presented in this paper, with two static tests of 1-A and 2-A samples

Table 5. The tensile strength of three types of rock sample

Sample Number	Loading rate (GPa/s)	Tensile strength (MPa)
1-A #1	0.01	0.83
1-A #2	81.5	2.63
1-A #3	116.32	3
1-A #4	104	2.65
1-A #5	248	3.02
2-A #1	0.01	1.27
2-A #2	126.5	3.92
2-A #3	165	4.1
2-A #4	183.9	3.23
2-A #5	220.6	3.42
2-A #6	365	5.08
3-A #1	1746	24.9
3-A #2	2980	31.4
3-A #3	3221	31.8
3-A #4	3466	28.8
3-A #5	3606	34.8

Figure 10. The tensile strength of two types of sandstone with different loading rate

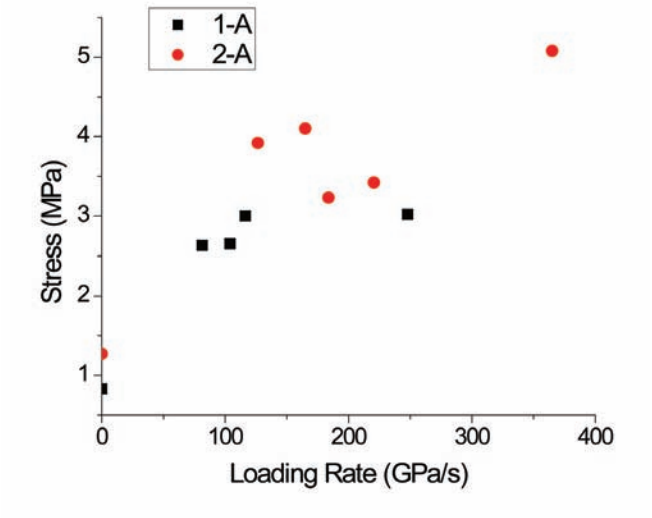

Figure 11. The tensile strength of 3-A rock with different loading rate

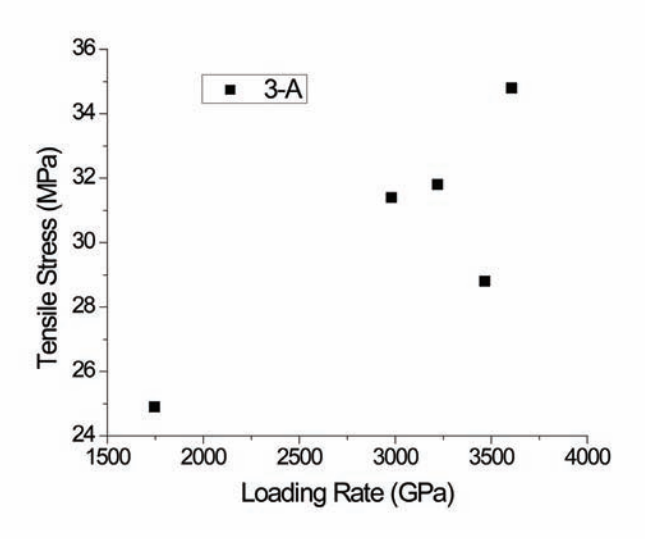

(shown in Table 5, Figure 10, and Figure 11). The dynamic tensile strength of rock is at least 3 times higher than static one (0.83 MPa compared with 2.63 MPa for 1-A, 1.27 MPa compared with 3.92 MPa for 2-A). It is evident from the test results that the tensile strength increases with loading rate.

From Table 5, it is obvious that the rock type. 1-A and 2-A are soft sandstone rock, whose tensile strength is lower than 5 MPa. 3-A rock is hard rock, whose tensile strength is higher than 20 MPa under dynamic loading condition.

5. CONCLUSION

Steel and aluminum SHPB systems may be used to measure the dynamic tensile strength of sandstone/shale (rock) and coal samples, respectively. The dynamic tensile strength of coal and rock is much higher than static strength. The tensile strength of coal and rock sample increases with loading rate. The result shows that the dynamic strength of coal sample is 1.5 times higher than static strength and the dynamic strength of sandstone sample is 3 times higher than the static strength. It may be concluded that under blast induced dynamic loading the dynamic tensile strength should be considered for determining the rock fragmentation.

REFERENCES

Barla, G. (1974). Rock anisotropy: Theory and laboratory testing. In Muller, L. (Ed.), *Rock Mechanics*. New York: Springer Verlag.

Berenbaum, R., & Brodie, I. (1959). The tensile strength of coal. *Journal of the Institute of Fuel*, *32*, 320–327.

Bieniawski, Z. T., & Hawkes, I. (1978). Suggested methods for determining tensile strength of rock materials. *International Journal of Rock Mechanics and Mining Sciences*, *15*, 99–103. doi:10.1016/0148-9062(78)90003-7

Cai, M., Kaiser, P. K., Suorineni, F., & Su, K. (2007). A study on the dynamic behavior of the Meuse/Haute-Marne argillite. *Physics and Chemistry of the Earth*, *32*, 907–916.

Chen, C. S., Pan, E., & Amadei, B. (1998). Determination of deformability and tensile strength of anisotropic rock using Brazilian tests. *International Journal of Rock Mechanics and Mining Sciences*, *35*, 43–61. doi:10.1016/S0148-9062(97)00329-X

Chen, R., Huang, S., Xia, K., & Lu, F. (2009). A modified Kolsky bar system for testing ultrasoft materials under intermediate strain rates. *The Review of Scientific Instruments*, 80.

Chen, Y. P., Wang, S. J., & Wang, E. Z. (2007). Strength and elastic properties of sandstone under different testing conditions. *Journal of Central South University of Technology*, *14*, 210–215. doi:10.1007/s11771-007-0042-z

Coviello, A., Lagioia, R., & Nova, R. (2005). On the measurement of the tensile strength of soft rocks. *Rock Mechanics and Rock Engineering*, *38*, 251–273. doi:10.1007/s00603-005-0054-7

Evans, I. (1961). The tensile strength of coal. *Colliery Engineering*, *38*, 428–434.

Frew, D. J., Forrestal, M. J., & Chen, W. (2001). A split Hopkinson pressure bar technique to determine compressive stress-strain data for rock materials. *Experimental Mechanics*, *41*, 40–46. doi:10.1007/BF02323102

Frew, D. J., Forrestal, M. J., & Chen, W. (2002). Pulse shaping techniques for testing brittle materials with a split Hopkinson pressure bar. *Experimental Mechanics*, *42*, 93–106. doi:10.1007/BF02411056

Grady, D. E., & Kipp, M. E. (1980). Continuum Modeling of Explosive Fracture in Oil-Shale. *International Journal of Rock Mechanics and Mining Sciences*, *17*, 147–157. doi:10.1016/0148-9062(80)91361-3

Hobbs, D. W. (1964). The strength and the stress strain characteristics of coal in triaxial compression. *The Journal of Geology*, *72*, 214–231. doi:10.1086/626977

Hobbs, D. W. (1970). Stress-Strain-Time Behaviour of a Number of Coal Measure Rocks. *International Journal of Rock Mechanics and Mining Sciences*, *7*, 149. doi:10.1016/0148-9062(70)90009-4

Hudson, J. A. (1969). Tensile strength and ring test. *International Journal of Rock Mechanics and Mining Sciences*, *6*, 91–97. doi:10.1016/0148-9062(69)90029-1

Hudson, J. A., Rummel, F., & Brown, E. T. (1972). The controlled failure of rock disks and rings loaded in diametral compression. *International Journal of Rock Mechanics and Mining Sciences*, *9*, 241–248. doi:10.1016/0148-9062(72)90025-3

Kubota, S., Ogata, Y., Wada, Y., Simangunsong, G., Shimada, H., & Matsui, K. (2008). Estimation of dynamic tensile strength of sandstone. *International Journal of Rock Mechanics and Mining Sciences*, *45*, 397–406. doi:10.1016/j.ijrmms.2007.07.003

Mclamore, R., & Gray, K. E. (1967). Mechanical behavior of anisotropic sedimentary rocks. *Journal of Engineering for Industry*, *89*, 62–67.

Mellor, M., & Hawkes, I. (1971). Measurement of tensile strength by diametral compression of discs and annuli. *Engineering Geology*, *5*, 173–225. doi:10.1016/0013-7952(71)90001-9

Okubo, S., & Fukui, K. (1996). Complete stress-strain curves for various rock types in uniaxial tension. *International Journal of Rock Mechanics and Mining Sciences & Geomechanics Abstracts*, *33*, 549–556. doi:10.1016/0148-9062(96)00024-1

Okubo, S., Fukui, K., & Qi, Q. X. (2006). Uniaxial compression and tension tests of anthracite and loading rate dependence of peak strength. *International Journal of Coal Geology*, *68*, 196–204. doi:10.1016/j.coal.2006.02.004

Ross, C. A., Tedesco, J. W., & Kuennen, S. T. (1995). Effects of Strain-Rate on Concrete Strength. *Aci Materials Journal*, *92*, 37–47.

Ross, C. A., Thompson, P. Y., & Tedesco, J. W. (1989). Split-Hopkinson Pressure-Bar Tests on Concrete and Mortar in Tension and Compression. *Aci Materials Journal*, *86*, 475–481.

Shan, R., Cheng, R., & Gao, W. (2006). Study on dynamic constitutive model of anthracite of Yunjialing coal mine. *Chinese Journal of Rock Mechanics and Engineering*, *25*, 2258–2263.

Swan, G., Cook, J., Bruce, S., & Meehan, R. (1989). Strain Rate Effects in Kimmeridge Bay Shale. *International Journal of Rock Mechanics and Mining Sciences & Geomechanics Abstracts*, *26*, 135–149. doi:10.1016/0148-9062(89)90002-8

Wang, G., Wang, Z. T., Rudolph, V., Massarotto, P., & Finley, R. J. (2007). An analytical model of the mechanical properties of bulk coal under confined stress. *Fuel*, *86*, 1873–1884. doi:10.1016/j.fuel.2007.01.002

This work was previously published in International Journal of Geotechnical Earthquake Engineering, Volume 1, Issue 2, edited by T.G. Sitharam, pp. 24-37, copyright 2010 by IGI Publishing (an imprint of IGI Global).

Chapter 12
A Numerical Approach for Simulation of Rock Fracturing in Engineering Blasting

Mani Ram Saharan
Central Institute of Mining & Fuel Research (CIMFR), India

Hani S. Mitri
McGill University, Canada

ABSTRACT

An approach for simulation of rock fracturing as a result of engineering blasting is presented in this paper. The approach uses element elimination technique within the framework of finite element method to capture the physics of engineering blasting. The approach does not require pre-placement of fracture paths which is the severe drawback of the other existing methodologies and approaches. Results of plane stress modelling for isotropic brittle rock behaviour are presented in this paper and these results are in good agreement with the existing knowledge base. The authors also review the existing approaches of numerical modelling to compare the efficacy of the element elimination technique. It is anticipated that the further developments with this approach can prove to be good experimental tool to improve engineering blasting operations.

1. INTRODUCTION

Rock fracturing by blasting can be best studied by understanding rock failure due to stresses under low confinement. Tensile failure (or extensile failure) is the primary mode of rock failure (Batzle et al., 1980; Blair & Cook, 1998; Kranz, 1983) whether stress loading is static or transient dynamic. In the case of rock failure by blasting, the violation to rock's tensile strength near the blasthole periphery is overwhelming which lead to a crushing zone at the periphery of the blasthole and beyond the crushing zone, the violation results in discrete fracture network. The stress

DOI: 10.4018/978-1-4666-0915-0.ch012

Figure 1. Stress created by an explosion pressure (adapted from Timoshenko & Goodyear, 1969)

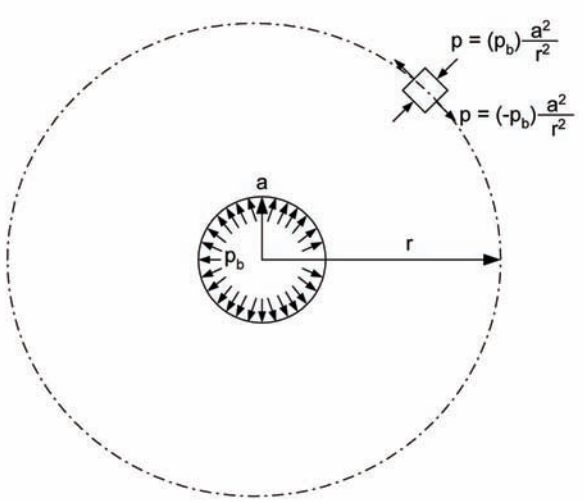

anisotropy, which is created by heterogeneity in rock properties and also the fracturing process are responsible for formation of the discrete fracture network. Stresses set out by the transient dynamic loading in a homogeneous rock mass can be understood from Figure 1. As per Figure 1, at any point in the rock mass, stress generated due to the transient loading from the circular blasthole will result in an equal amount of circumferential tensile and radial compressive stresses. Since the tensile strength of a rock is always much smaller than the compressive strength, fracturing at any point (whether in the form of crushing or discrete fracturing) can be understood from comparison of the tensile strength and the tensile stress values. Discrete fracturing takes place where the stress anisotropy has magnitude lower than the compressive strength but higher than the tensile strength.

Researchers still have wide differences in explaining fundamental operative mechanisms responsible for the rock fracturing by explosive energy despite its prevalent use at global scale and enormous experimental efforts made in the last half century. It can be seen from Table 1 that various theories are propounded in order to explain the failure mechanisms and there is no existence of a unified theory. The differences stem from observational difficulties associated with the prevalent experimental techniques. This is due to an extremely short duration of the explosive load on the rock (in the order of few micro-seconds), a very fast fracturing process covered under the explosive gaseous products, and rock debris (crack speed up to one third of the primary waves speed in rock) apart from the heterogeneous nature of natural materials like rock. Moreover, the prevalent experimental techniques can not have the complete control on the experiments. Continuous efforts are being made to evolve better experimental techniques in order to understand the fundamental operative mechanisms. Such an improvement will be a great aid in an effective application of explosive energy, development of better explosive products as well as safer and more economical mineral extraction procedures from mines.

Rapid advances made with numerical modelling tools and availability of faster computational resources at affordable costs make the numerical simulation as the most promising experimental method to study the dynamic rock fracturing processes. Use of the numerical simulation for dynamic rock fracturing is appealing, essential and most suitable due to a large number

Table 1(a). Continuum approach for numerical simulation of blasting

Explosive Loading	Rock material model	Numerical tool	Key input parameters and fracture representation	Reference work	Key results	Remarks
Static	Elastic	Finite element code	2 GPa static borehole pressure (radius = 50 mm) applied to elastic rock (E = 40 GPa, ν = 0.15, ρ = 2.5 t/m^3). Tensile stresses represented fracture extent calculations.	Khosrou and Mohanty (1996)	Burden to spacing ratio from 0.8 to 1.2 is appropriate for wall-control blasting. Weak planes act as free faces and its position determine amount of back break.	2D static analysis is done for 3D dynamic phenomena. Elastic material model, static modelling and continuous modelling presented overly conservative solutions for rock fracturing.
Dynamic	Elastic	Finite element code	2 GPa dynamic concentrated load applied for 0.1 ms on 100 mm blasthole diameter to an elastic rock (E=28.3 GPa, ν = 0.27 and ρ = 2817 kg/m^3) in 2D plain strain idealization of a 3D problem. The problem solved using implicit finite element procedure using Newmark method. Tensile stresses used for fractures extent identification.	Sunu et al. (1988)	Optimum burden distance depends on elastic modulus and density of rock material. Effect on Poisson's ratio is negligible for such a case.	2D plain strain model assumed in wrong plane for a 3D dynamic problem. Material models were elastic. It is inferred from the publication that the blast source function was a constant concentrated force for a period of 0.1 ms which doesn't reflect a real case.
	plastic	Finite element code	Dynamic load applied using JWL equation of state for 2D axisymmetric models having 100 mm blasthole diameter in elasto-plastic rock obeying metal plasticity rules. Volumetric strain (scalar quantity) apportioned by statistical fracture mech principals used for fractures representation.	Liu (1997) and Liu and Katsabanis (1997)	Results are qualitatively matched with a crater blasting experiment	Associated flow rule used to obey a metal plasticity rule for rock like material. Also, sweeping assumptions made to homogenization of fractures due to demand of the continuous damage modelling. 4GPa is applied as input for shear modulus for a rock with 52 GPa elastic modulus and 0.33 Poisson's ratio.

of complex variables are involved to deal with. This paper presents results of numerical modelling simulations, which are obtained from a newly developed numerical procedure for simulating dynamic fracturing by rock blasting (Saharan & Mitri, 2008; Saharan & Mitri, 2009). A critical review of the previous attempts of the numerical modelling of blasting is also presented in order to understand the difficulties faced by the previous researchers. These reported experience greatly facilitated in understanding complexity of the problem as well as developing the new procedure. Prerequisites for numerical modelling of blasting are enumerated before the review.

2. PREREQUISITES OF NUMERICAL MODELLING OF BLASTING

There are certain prerequisites to start with the numerical simulation of blasting. Parts of the prerequisites are needed to successfully transform a physical phenomenon in a numerical one. This part requires a sound understanding of the transient

Table 1(b). Discontinuum approach for numerical simulation of blasting

Static	elastic	Boundary element code	500 MPa static pressure is applied to rock (properties not provided) representing at depth of 2700m. Fractures were pre-placed in the model and extended.	Toper, 1995	Fracture network grows in σ_1 direction and stress field after blasting changed in magnitude as well as direction (90^0)	2D elasto-static analysis results are contrived with pre-placed fractures. Also, static pressure used (500 MPa) is nowhere near to dynamic pressure in 93 mm diameter holes.
Dynamic	elastic	Discontinuous deformation analysis code (DDA)	1GPa and 2.5 GPa dynamic pressure applied to 100 mm borehole diameter for elastic blocks stacked together with zero cohesion and tension. Separation of distinct blocks represented for fractures.	Mortazavi and Katsabanis (2001)	-	Unrealistic material input data are accompanied with gross wrong assumption of plain strain modelling for a 3D problem.
	elastic	Finite element code	1 GPa dynamic pressure applied to 508 mm diameter blastholes in granitic rock (E = 60 GPa, $\nu = 0.25$, $\rho = 2800$ kg/m^3, $K_{ID} = 1.65$ MPa. m$^{0.5}$, $K_{IID} = 1.03$ MPa. m$^{0.5}$. Fracture mech. rules used for extension of pre-placed fractures.	Lima et al. (2002)	-	Pre-placed fractures grows radially surrounding the boreholes but their growth is inhibited by the presence of already developed fractures from previously blasted surrounding blastholes. Numerical difficulties prevented fracture growth in time and in directions.
	plastic	Finite element code	500 MPa dynamic pressure applied to 100 mm diamter blasthole in a rock having E = 56.4 GPa, $\nu = 0.25$, $\rho = 2700$ kg/m^3, $G_f = 300$ Pa.m. Fracture path deermined by fracture mech. rules using node release technique.	Cho et al. (2003)	Qualitatively show effect of pressure-pulse on fracturing	Far-field boundaries were placed only at 2-3 m away from the blasthole. Peak pressure of only 500 MPa was used. Results do not confirm failure behaviour from free faces by reflected pressure waves.
	plastic	Distinct element code	1GPa dynamic pressure with gaussian distribution to 50mm diameter blasthole in a 1m x 1m model size representing very hard rock (E=100 GPa, $\nu = 0.09$, r = 2950 kg/m^3, UCS = 340 MPa, Tensile strength = 60 MPa .). Separation of cohesive circular discs and plates represented the fractures.	Donze et al. (1997)	Qualitatively shown that high frequency detonation lead to more crushing with shorter crack length and low frequency detonation to less crushing with longer cracks length. Also, it is shown that cracks aligns into the principal stress direction	Numerical model boundaries placed only at 0.5m away from the explosion source and fractures reaches to those boundary representing a very hard material. This is despite the fact that no artificial damping was used and material consisted very high self-damping characteristics. Also, source function of detonation not carry any physical meaning.

loading characteristics as well as the knowledge of rock failure processes. Apart from the needed transformation, one need to take care of numerical challenges arises due to the transient loading process and wave propagation phenomena during solution time of the numerical modelling. This part requires a good knowledge of the numerical modelling tool adopted for the purpose. The following is a list of the prerequisites (not necessarily in the order and complete) needed for such a simulation task.

A. **Characteristics of the transient load in the blasthole:** Typically, an explosion pressure in a borehole dies down to a stand-off pressure within a few milliseconds. The stand-off pressure is much below to the tensile strength of the most of rocks. The rise time of an explosion pressure to its peak is very short and varies primarily according to the explosive characteristics and secondarily according to the blasthole diameter, blasthole confinement, rock strength, etc. Generally, the rise time for emulsion type explosives for small diameter blastholes are around 25 micro seconds and 100 micro seconds for ANFO type explosives. The subsequent decay in the peak blasthole pressure up to the stand-off pressure is steep in the case of emulsion type explosives and gentle for ANFO type explosives. The pressure-time profile described here is in the good agreement with the observed profiles by Frantzos (1989), Jung et al. (2001), and Daniel (2003).

B. **Rock failure model incorporating physical tensile failure mode:**. Figure 2 depicts a typical stress-strain curve for any brittle material failure. It is evident from Figure 1 and Figure 2 that rocks fail due to the tensile stresses exceeding the rock's tensile strength during the transient dynamic load of blasting as it is much lower than the compressive strength whereas the stress wave of blasting produces the tensile stress and the compressive stress in equal magnitudes. Therefore, a failure criterion which incorporates inelastic strains up to the final failure point due to only tensile stresses is a sufficient requirement to simulate blasting. Further, the fracture initiation is Mode-I category (tensile failure) as per the fracture mechanics principles but subsequent behaviour also include Mode-II behaviour (shear failure). These considerations should be incorporated in the chosen rock failure criterion for the numerical modelling. Also, in numerical modelling parlance, plastic flow of rock like material is non-associated. This characteristic should also be a part of the chosen material model.

C. **Representation of fractures to incorporate stress anisotropy:** Numerically it is critical to consider an appropriate representation of the fractures and this representation should result into stress anisotropy. This stress anisotropy is essential for the fractures propagation. Rocks are heterogeneous in nature and a fracture created by blasting enhances this heterogeneity, which ultimately contributes in the fractures propagation.

D. **Numerical model characteristics for wave propagation:** Numerical models act as high pass band filters, i.e., they filter out critical low frequency loads. These low frequency loads generally control the accuracy of the solution. Also, numerical modelling (particularly the finite element method) is based on deformation produced at nodes due to the applied load. Calculated deformations are used for the calculation of strains and stresses. Hence the accuracy of the modelling depends on the element size chosen (bigger elements give a stiffer response and smaller elements results in a softer response). So, a mesh convergence analysis is first required to find out an appropriate element size. Then the element size should be adjusted to get response from the low frequency loads.

Figure 2. A schematic diagram of brittle material failure

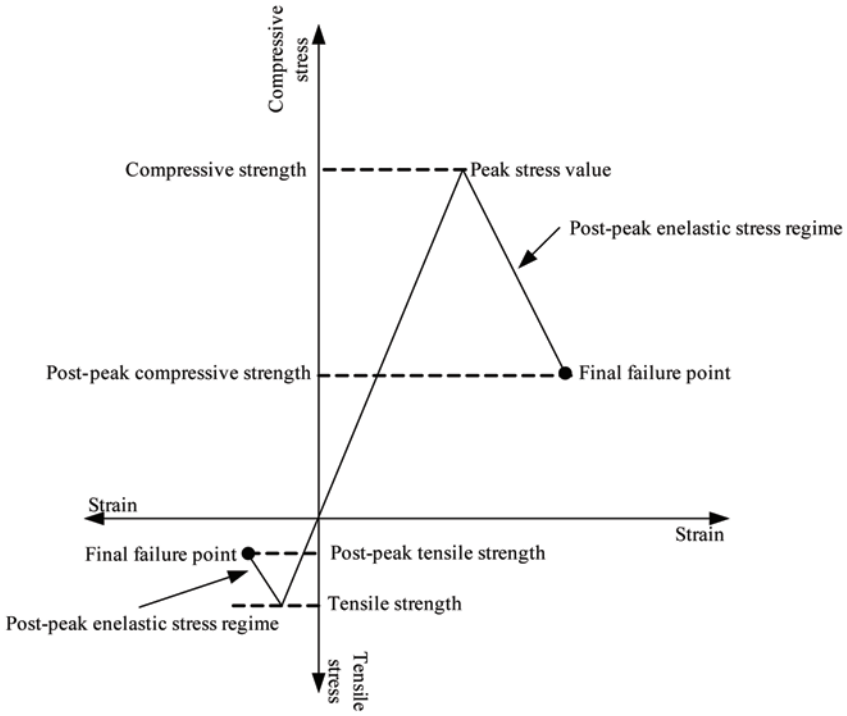

E. **Boundary conditions to represent far-field boundaries:** One of the serious concerns from any numerical modelling exercise involving wave propagation is the spurious reflection of impending waves from the model boundaries. Suitable measures are needed to address this issue.

F. **Distribution of high transient load in the model to avoid numerical singularities:** Application of a high transient dynamic load (in the order of GPa in few microseconds) is generally responsible for unrealistic results from the dynamic numerical modelling. Often a numerical modelling code does not accept such a load rate and it shows errors related to numerical singularity. Proper load distribution (smearing in the numerical parlance) is required to avoid the numerical singularity. The numerical code should be able to smear the high load rate.

G. **Damping of wave propagation in the numerical model:** Rock is inherently a good damper. Further, damping is provided by the energy consumed in fracturing process (numerically, in the plasticity) after blasting. The numerical model should reflect such typical damping characteristics. Also, damping in natural material is hysteretic, so monotonic damping should be avoided to negate the possibility of over damping of critical load frequencies (low modes).

H. **Stability of the solutions:** Blasting in rocks result in fracturing in the vicinity of blastholes, which is completed within a few milliseconds. But blast vibrations last longer without causing further damage and they are transmitted to a longer distance. The system, Earth, gets stabilized after initial fracturing process is completed. The numerical simulations should reflect similar behaviour in representing the unbounded rock medium.

3. REVIEW OF NUMERICAL SIMULATION OF ROCK BLASTING

Numerical simulation of rock fracturing by blasting is approached by two broad methodologies, namely, continuum approach and discontinuum approach. The continuum approach assumes continuity with the fractures representation, while individual cracks are tracked in the discontinuum approach. The primary aim of the continuum approach is to estimate the extent of the weakening in the material around the source; they do not characterize the very local fracture growths.

The popular continuum approach, continuous damage modelling (CDM), either treats rock material as perfectly elastic or fracturing is treated as a continuous accrual of damage in tension. A scalar damage variable represents fractures in the CDM technique and strains larger than the threshold strains represent fracturing phenomena. The scalar damage variable can take values from 0 (corresponding to the undamaged material property) to 1 (corresponding to completely damaged material property).

Khoshrou and Mohanty (1996) used the 2D linear elastic finite element analysis technique to evaluate effects of weak planes on the extent of rock fracturing for smooth-wall blasting. Tensile stresses were used to delineate the fracturing region in their study. Also, blasthole pressure was applied as a static force rather than the dynamic pressure-pulse. This study is one of the few that carefully selected an appropriate approximation of the modelling plane. The study however suffers from the obvious shortcomings of any static elastic analysis as an approximation of the dynamic phenomenon. The linear elastic analyses are always over-conservative and static analyses inherently represent higher damage levels (unless otherwise load scaling studies are done). No study was presented to establish a requisite equivalent dynamic load for the static analyses. Fourney et al. (1993) and Szuladzinski (1993) used a similar approach (static 2D linear elastic finite element models) but with pre-placed fractures. The displacement magnitudes were used as indicators of the fracturing extent. Lima et al. (2002) and Sunu et al. (1988) report the use of an implicit algorithm for dynamic pressure application with 2D elastic material models for their continuum modelling. The fracture energy concept (J-integral) was used to extend the pre-placed fractures in the models by Lima et al. (2002) and the principle stress contours were examined by Sunu et al. (1988). Sunu et al. (1988) adopted an inappropriate plane in the process of idealizing a 3D problem for 2D numerical analysis. The results of the other studies referred above are biased due to pre-placed fractures in the modelling domain.

Contrary to the static modelling approach, blast source functions have also been applied and attempted to solve with time using the equations of motion in continuum elastic or with the CDM techniques. Ryu (2002) reports that the application of exact blast source functions for continuum models (he referred to FLAC, a finite difference code by ITASCA) either results in an unrealistic ground response or in a numerical instability. Donze et al. (2002) reported similar difficulties with a distinct element code and therefore they adopted a Gaussian function to represent the dynamic load profile. The Gaussian function used does not match the pressure-pulse characteristics of a blast load profile. In the popular technique of the CDM, damage evolution is tracked by a scalar damage variable associated either with the Poisson's ratio (Taylor et al., 1986) or the volumetric strain (Yang et al., 1996; Liu & Katsabanis, 1997; Hao et al., 1998, 2002) or the modulus (Curran et al., 1987; Thorne et al., 1990) or global energy (Grady & Kipp, 1993). Studies done by Liu and Katsabanis (1997) are considered noteworthy as they investigated fundamentals of air-deck blasting using the CDM technique. However, the CDM theories of fractures and fragmentation suffer from obvious shortcomings. The discrete nature of cracks is lost in these theories. In homogenizing a cracked solid, sweeping assumptions must

necessarily be made regarding the distribution and geometry of cracks, which at best are described by a few set of variables and their interactions (Repetto et al., 2000). The determination of the effective properties of a cracked solid under dynamic conditions presents additional difficulties, which are stemming from the finite speed at which signals propagate between cracks (Freund, 1990). However, perhaps the most fundamental objection to the CDM theories is that the failure of a brittle specimen is frequently governed by the growth of a few single dominant cracks, a situation that is not amenable to homogenisation (Repetto et al., 2000).

Numerical simulation of blasting is also attempted with the discontinuum approach by using distinct element method (DEM) or discontinuous deformation analysis (DDA) (Hart, 1993; Donze et al., 1997, 2002; Mortazavi & Katsabanis, 2001), boundary element codes (Toper, 1995) and finite element codes (Cho et al., 2003; Jung et al., 2001). Donze et al. (1997, 2002) reported results from distinct element codes, which appear to be overly affected by boundary value problems. The fracturing zone diameter extends to a distance of 1m (which is the model boundary) in the case of 2D modelling (Donze et al., 1997) for an extremely hard rock (tensile strength of 60 MPa) to 7 m subgrade or 10 m radially (again the model boundary) for 3D modelling (Donze et al., 2002). The source function used by Donze et al. (1997, 2002) is a Gaussian function which was probably employed to avoid the numerical singularity associated with the high load rate of transient blast loads. Mortazavi and Katsabanis (2001) employed a discontinuous deformation analysis code and provided zero cohesion and zero tension as the material parameters for the selected material model. Regrettably, their results are affected from the gross misrepresentation of a 3D problem by 2D plain strain idealization. Their analysis also lacks practical significance due to the limitations associated with the discrete element modelling codes. Unrealistic results from the distinct element codes (including discrete elements (DEM) and discontinuous deformation analysis (DDA) approach) are due to the fact that they need unrealistic material input properties (Hazzard et al., 2000). Ryu (2002) points out that the results are not only affected by how interaction of distinct blocks are characterized (stiffness and damping) but also by the algorithm used to solve the equations of motion (implicit and explicit). Errors also emanate from the lacking of suitable boundary conditions and damping characteristics with these numerical procedures. Distinct element codes with spherical elements (used by Donze et al., 1997, 2002) also suffer from poor numerical accuracy due to the high pore volume (Malan & Napier, 1995). Toper (1995) presents post-blast fracture network from simulations of a 500 MPa blasthole pressure in a 93 mm borehole using the static linear elastic boundary element method involving pre-placed fractures in the model. Napier et al. (1997) reported that results obtained by pre-placed fractures carry no practical meaning. Results obtained with the static linear elastic modelling are also affected with the shortcomings of static linear elastic analyses as mentioned above. Further, Toper (1995) incorporated bedding planes in his models with zero cohesion. Cho et al. (2003) used a continuum code (finite element method) and simulated discrete fracture network using a node release technique. Their analyses use the pressure-pulse similar to the measured blasting pulse but with the reduced peak pressure of 500 MPa to avoid numerical instability associated with the high transient load. Results by Cho et al. (2003) appear to be affected by the boundary value problems, as failure at the free face by reflected pressure-pulse does not confirm observed field behaviour of slabbing. Further, Cho et al. (2003) needed the rock strength variation through a statistical distribution function to introduce the stress anisotropy. Studies presented by Jung et al. (2001) only showed a close resemblance with the reported field behaviour. Their modelling involved both the peak-pressure magnitude (about 1GPa for

an 8 mm diameter borehole) and the pressure-time profile similar to the observed values. Further, their procedure needed dynamic compressive and tensile strength values, which were 4.5 times the static strength values, as judgement standard for fractures generation. The publication neither provides the procedure for the fractures initiation/ propagation nor discusses the stability of the results (results are shown only up to few microseconds).

The above numerical experiments are summarized with the Table 1(a) and 1(b). It is evident that a proper numerical procedure is lacking that takes in account the above mentioned prerequisites in order to successfully transform a physical phenomenon in a numerical one. The successful transformation of this physical phenomenon onto the numerical platform is still elusive. This encouraged the authors to develop a new procedure for rock blasting problems. The detailed procedure is explained elsewhere (Saharan & Mitri, 2009) and the key features are summarized in the succeeding section.

Results of 2D plane stress simulations are presented using the new procedure in this publication. The 2D plane stress modelling is performed because the core research topic for which the procedure is developed was a plane stress problem (Saharan & Mitri, 2009). Also, plane stress modelling provides a convenient mean to undertake and understand fundamental studies for the dynamic rock fracturing processes. In past, the laboratory scale studies were undertaken using this plane stress concept (e.g., see Kutter & Fairhurst, 1971; Fourney et al., 1993). The extension of the developed procedure for 3D problems is not difficult but will involve enormous computational resources.

4. KEY FEATURES OF THE NEW PROCEDURE FOR NUMERICAL SIMULATION OF ROCK BLASTING

The new procedure is developed using a general purpose finite element code, ABAQUS (Abaqus, 2003). The prerequisites for the successful transformation of the physical phenomenon in numerical one are achieved as per the followings.

A. **Characteristics of the transient load in the blastholes:** A simplified approach, termed as an optimized pressure profile, is developed to construct pressure-time profile for the transient load. The optimized profile is developed on the basis of knowledge gathered from in-blasthole pressure-time profile measurements (Frantzos, 1989; Jung et al., 2001; Daniel, 2003). The peak pressure of the optimized profile is obtained by using a widely employed equation developed using the equations of state (Clark, 1987). This peak blasthole pressure is applied in its full magnitude (increasing from zero at the time equals to zero second) at a point of time which is consistent with the measured time values for different types of explosives characteristics in different diameter blastholes. Then the peak pressure magnitude is reduced to 90 per cent, 99 per cent and 99.9 per cent values in comparison to the peak magnitude over a time period that is consistent with the two types of explosive characteristics, namely, shock type loading of emulsion type explosives (also termed as ideal detonation) and quasi-static type loading of the ANFO type explosives (also termed as non-ideal detonation). In this manner, the constructed profile encompasses both the shock wave effect and the quasi-static loading by shock wave–gas pressure combination. The optimized pressure-pulse for the two types of explosives is shown in Figure 3.

B. **Rock failure model incorporating physical tensile failure mode:** ABAQUS provides a brittle cracking model to simulate brittle rock failure processes (Abaqus, 2003). This material model is selected for the developed procedure as it fulfills the tensile failure rep-

resentation requirements as desired above. The brittle cracking model is intended for applications in which the rocklike brittle material behaviour is dominated by tensile cracking and where compressive failure is not important (the material model ignores hardening and subsequent softening characteristics of compressive failure). The model includes consideration of the anisotropy induced by cracking. In compression, the model assumes elastic behaviour. The brittle cracking model is a smeared crack model in which individual "macro" cracks are not tracked but constitutive calculations are performed independently at each material point of the finite element model. The presence of cracks enters into these calculations by the way in which the cracks affect the stress and material stiffness associated with the material point. A simple Rankine criterion is used to detect crack initiation. This states that a crack forms when the maximum principal tensile stress exceeds the tensile strength of the brittle material (Figure 4). Although crack detection is based purely on Mode I fracture considerations, ensuing cracked behaviour includes both Mode I (tension softening) and Mode II (shear softening/retention) behaviour. The brittle cracking model is characterized by a stress-displacement response rather than a stress-strain response. This characterization is based on Hilleborg et al.'s (1976) fracture energy proposal to avoid unreasonable mesh sensitive results. Typical input parameters for the material model used for the results shown in this publication are shown in Table 2.

C. **Representation of fractures to incorporate stress anisotropy:** An element elimination technique (EET) is used to represent formation of the fractures. Failed elements, as indicated by the post-peak tensile strength and corresponding the ultimate crack opening displacement, are removed from the calculations by adjusting their Young's modulus to zero. The failed elements represent discrete fractures in the developed procedure. This loss of the homogeneity results in the stress anisotropy and ultimately contributes in the propagation of the discrete fracture network. Thus no statistical variation in strength is required to enforce the stress anisotropy. Further, nodes of the removed elements don't participate in the transferring nodal loads and hence impact of gas pressure in fractures propagation is also indirectly simulated by exerting pressure through the elements attached to the failed elements. The application of the optimized pressure-profile in conjunction with the EET thus obviates need of considering fluid flow to simulate the gas-pressure effect in the fractures propagation.

D. **Numerical model characteristics for wave propagation:** A mesh convergence analysis is done to establish the requisite element size (Figure 5). It may be noted that the selected domain size with elements population more than 4500 elements results into no further change in deformation value at the central hole. This benchmark element population results from element size at the blasthole periphery with a 4.59 mm face size. This element size is then evaluated for its suitability to transmit critical low mode frequency of the intended transient dynamic load of the optimized pressure profile using a nomogram presented by Valliapan et al. (1983). It is also stated that at least ten nodes should exist within the stress wave's wavelength for its effective transmission during the numerical simulation (Abaqus, 2003; Ramshaw et al., 1998). The element size obtained with the mesh convergence analysis is found suitable to both the criteria mentioned above. The element size is kept nearly constant for a zone expecting fractures and beyond this

zone, the element size is gradually increased with distance away from the blasthole in order to obtain a better numerical efficiency. Further, constant stress triangular elements are chosen as they behave superiorly than the isoparameteric elements for the EET (Kikuchi, 1983). Removal of the failed triangular shaped elements also helps in creating a stochastic fracture pattern.

E. **Boundary conditions to represent far-field boundaries:** A review was made to find out a suitable boundary condition for the developed procedure, which can absorb 100 per cent of the primary, secondary and Rayleigh waves of the transient dynamic load at the boundary (Saharan & Mitri, 2009), but no suitable arrangement was found to represent an unbounded medium of rock for the dynamic simulations. Therefore, prevalent roller boundaries (zero orthogonal displacements conditions) are used in the new procedure and these boundaries are kept away at least 250 times the blasthole size from the blasthole. Also, full model domains are used to preclude any possibility of the wave reflection phenomenon. These arrangements not only helped in avoiding the spurious wave reflection but also provided enough time for the fractures propagation.

F. **Distribution of high transient load in the model to avoid numerical singularities:** ABAQUS (Abaqus, 2003) have provisions for bulk viscosity (linear and quadratic, both forms) to prevent numerical oscillations due to high magnitude transient loads. In the numerical parlance, such a provision is helpful in stress smearing. Provisions of bulk viscosity are used in the procedure with the suggested default values by ABAQUS (Abaqus, 2003).

G. **Damping of wave propagation in the numerical model:** It is found that suitable provisions are lacking in numerical modelling codes for an appropriate damping for the material with hysteretic damping characteristics (Saharan & Mitri, 2009). Further, it is suggested that no damping should be used if plasticity is incorporated in the material behaviour (Abaqus, 2003). It is reported (Abaqus, 2003) that the energy absorbed by plasticity is significantly higher than it can be absorbed by any artificial damping method like Rayleigh damping. The developed procedure aims to capture rock fracturing (results of plasticity) on a real time frame (using the optimized pressure-time profile and solving its impact with a 2nd order central difference explicit integration scheme) so no artificial damping is considered.

The prepared model for the developed numerical procedure validation tests is shown in Figure 6. The model is the plane stress idealization of a 3D problem. It uses 4,560 triangular elements and 2,312 nodes. One more model with 10,276 elements and 5,275 nodes is prepared to illustrate the effect of a free face on the rock fracturing process. In this case, a 38mm diameter blasthole is kept 0.5m away from a free boundary (face) and emulsion type explosive pulse is used to provide the dynamic load. Rest of the model conditions remains the same as earlier.

5. FEW IMPORTANT RESULTS OUT OF THE NEW DEVELOPED PROCEDURE VALIDATION TESTS

Few important results of the developed numerical procedure validation tests are shown through Figure 7, Figure 8, Figure 9, and Figure 10. Figure 11 presents the effect of a free face on the rock fracturing process. The results presented in Figures 7 to 11 are in line with many established and important phenomena associated with rock fracturing by explosive energy. Results obtained are unique and first of their kind. Some significant results are discussed in the following sub-sections.

Figure 3. An optimized pressure-pulse for the transient dynamic load

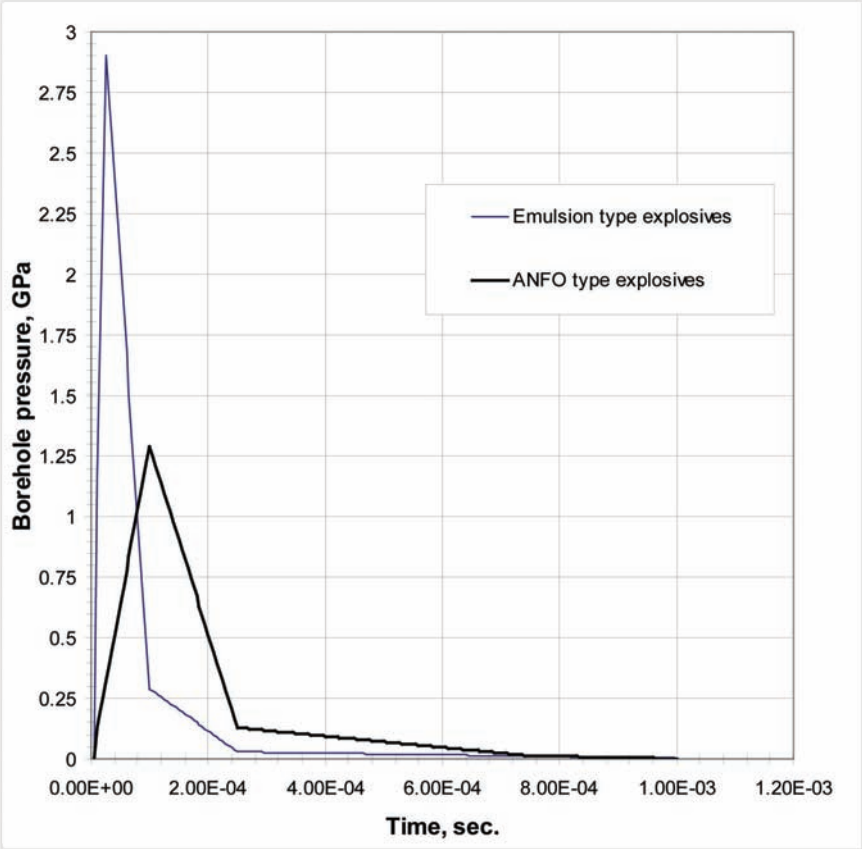

Figure 4. The Rankine failure criterion in the plane stress space

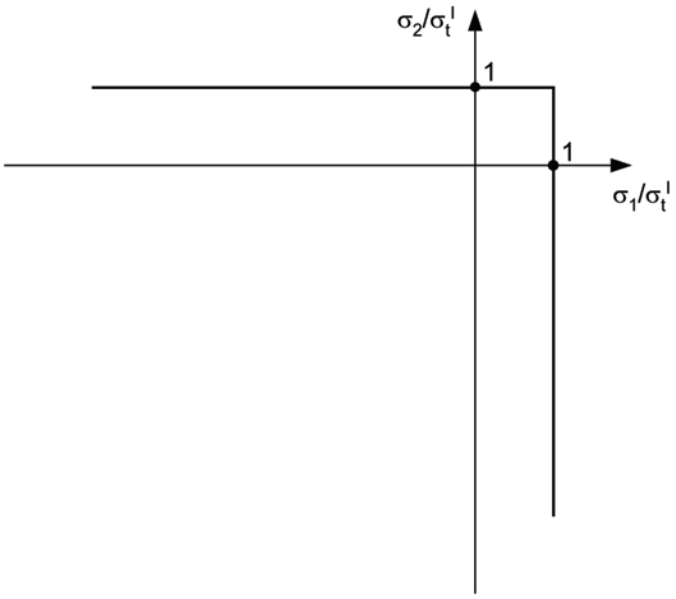

Figure 5. The mesh convergence analysis results

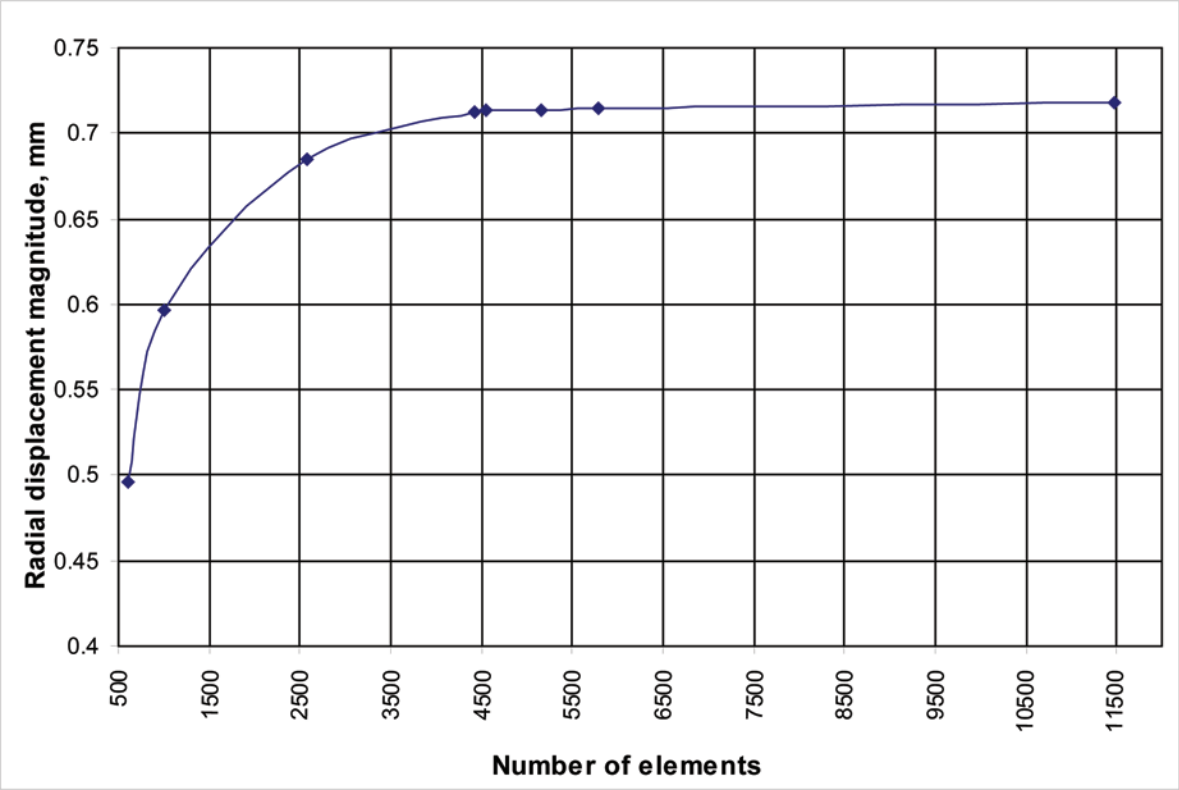

A. **Strain rate dependant rock response:** It can be observed from Figure 7 that the stress required to open the first crack with a high shock load of the emulsion type explosive characteristics is equivalent to 600 MPa while only 159 MPa is required to open up the first crack in the case of the ANFO type explosive characteristics, having quasi-static loading characteristics.

Several researchers have argued in favour of strain rate dependant rock properties (e.g., Prasad et al., 2000). They advise that the material model used for dynamic numerical modelling should contain provisions for strain rate dependant material properties. It is noteworthy that neither the material behaviour, which remains essentially elastic throughout the calculations nor the brittle failure law using element elimination is rate dependant. The element elimination technique in conjunction with inertia, endows the material with a characteristic or intrinsic time scale, an attribute that ultimately accounts for the ability to accurately capture the rate effects.

B. **Characteristics of fracturing zone**: It has been well observed and documented that the emulsion type explosives lead to more crushing around the borehole which follows large numbers of short length radial cracks (e.g., McHugh & Keough, 1982). In contrast to this, the ANFO type explosives result in a smaller crushing zone followed by a few long radial cracks. Similar results are obtained by the numerical modelling as showed in Figure 8 and Figure 9. The results shown in these figures demonstrate a good agreement with the published literature.

Figure 6. Mesh of the model prepared for the validation tests of the developed procedure

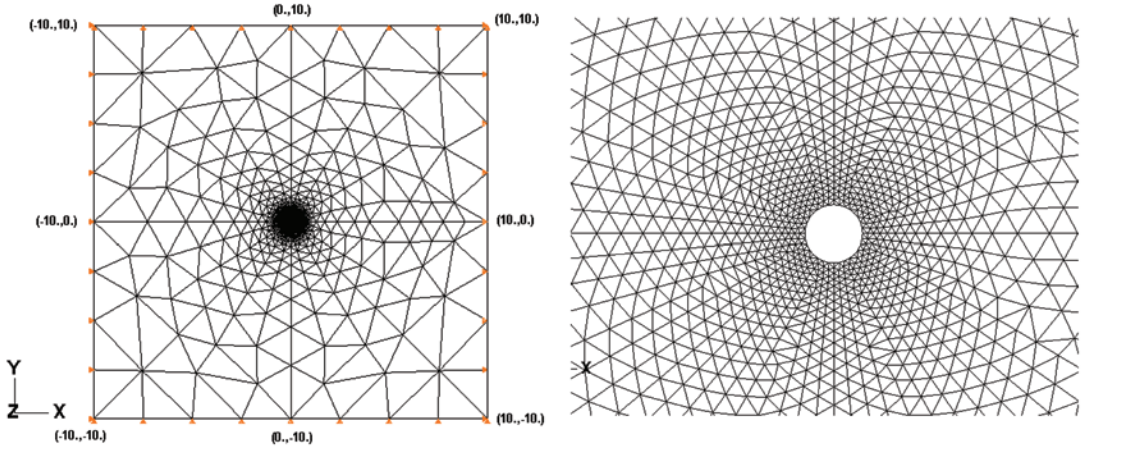

(a) FE mesh and model boundary conditions

(b) Zoom-in view of the model mesh central zone showing 38 mm diameter blasthole

Table 2. Typical granite rock properties used for the numerical modelling

Rock property	Value	Source reference	Remarks
Density (ρ), kg/m^3	2650.0	Diederichs (1999)	Tested and compiled representative values
Young's modulus (E), GPa	60.0		
Poisson's ratio (μ)	0.24		
Tensile strength (UTS), MPa	15.0		
Ultimate crack opening displacement (COD), m	1 x 10^{-5}	Dawding et al. (1985)	Tested value

C. **Extent of the fracturing zone:** Figure 9 presents the extent of such zones predicted by the numerical modelling procedure for the emulsion type and the ANFO type explosives, respectively.

Mosinets and Gorbacheva (1972) and Kexin (1995) provide empirical relations to predict the extent of the crushing and fracturing zone. Numerical results presented herewith are in remarkably good agreement with the empirical predictions. It is noteworthy to mention here that it is out of purview for other numerical tools or techniques, except continuous damage plasticity models capable of tracking failure both in compression and tension (not the continuous damage models based on statistical fracture mechanics), to distinctly reproduce this phenomenon in the first place and accurately simulate in the second place.

D. **Damping of the wave energy:** Peak particle velocity (PPV) plots presented in Figure 10 illustrate that the material model chosen aptly represents the damping characteristics associated with the natural material. The plots showed in Figure 10 are in good resemblance with the routine field PPV measurements where they show a reduction in magnitude with the increase of time. This reduction comes from damping of the wave energy by the earth. It is noteworthy that no artificial damping was considered in the newly developed procedure. Also, the material model showed enough potential to

Figure 7. Fractures initiation load magnitude

(a) Fractures initiation load magnitude for emulsion types explosive= approx. 600 MPa

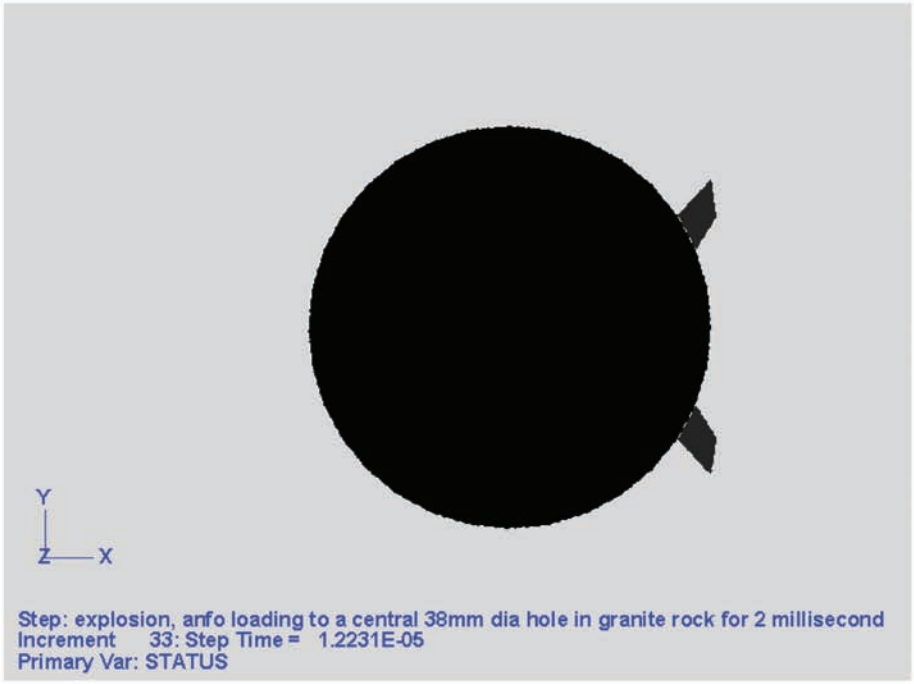

(b) Fractures initiation load magnitude for ANFO types explosive = approx. 159 MPa

Figure 8. Final fracture pattern

(a) Emulsion types explosive, time = 1 millisecond

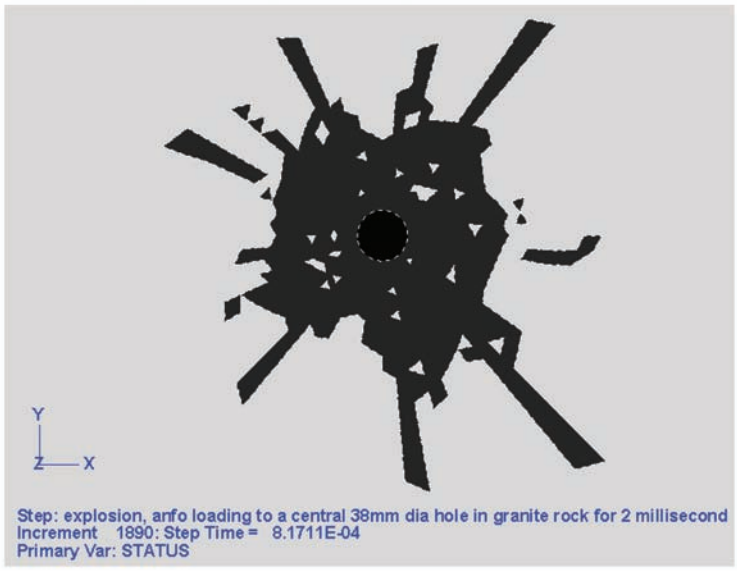

(b) ANFO types explosive, time = 817 microsecond

accurately represent two distinct fracturing characteristics, crushing and cracking, with the single parameter of element elimination.

E. **Model boundary conditions:** Roller boundaries were selected in the new procedure to represent unbounded rock medium. Stable fracture networks and PPV plots presented through Figures 7 to 10 bring out that the results are nowhere affected by spurious wave reflection from the artificial boundaries. Also, the results demonstrate that enough time was provided to capture the fracturing by primary waves only. Hence, the selection of roller boundaries in the present modelling procedure is justified.

Figure 9. The fracture pattern at the end of the calculations (2 milliseconds)

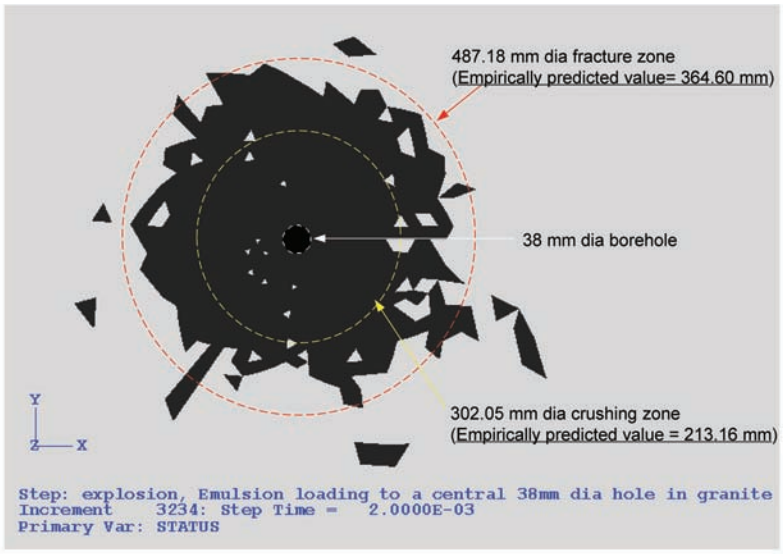

(a) Emulsion types explosive

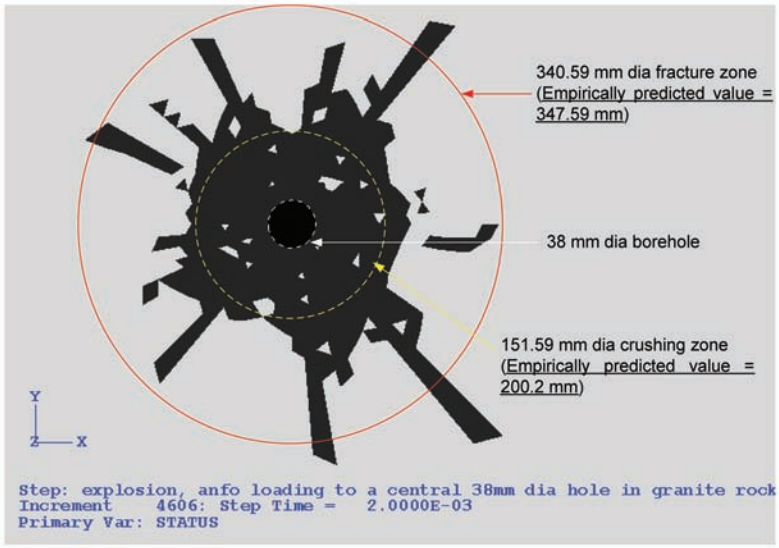

(b) ANFO types explosive

F. **Stability of the solution:** Comparison of Figure 9 with Figure 8 show that fracturing occur only immediately after detonation. There is no change in fracturing pattern once the process is complete. Though Figure 10 indicates continued particles vibration for a longer duration. These results confirm stability of the solution. The results also demonstrate the fact that a sufficient time is provided for the fracturing process.

G. **Effect of a free face on fracturing**: Figure 11 predicts slabbing process due to a free face near the blasthole. Fracturing starts at 6.6 micro seconds, similar to blasting without the free face. The primary wave (calculated wave velocity = 5165.92 m/s) travels to 0.5

Figure 10. Peak particle velocity plots (PPV in the X-axis direction)

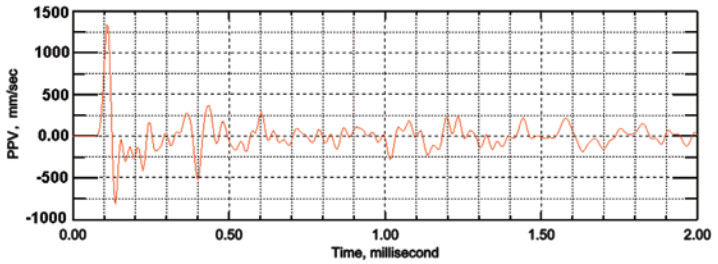

(a) Emulsion types explosive, PPV at 0.5 m from the borehole (point coordinates = 0.5,0.0)

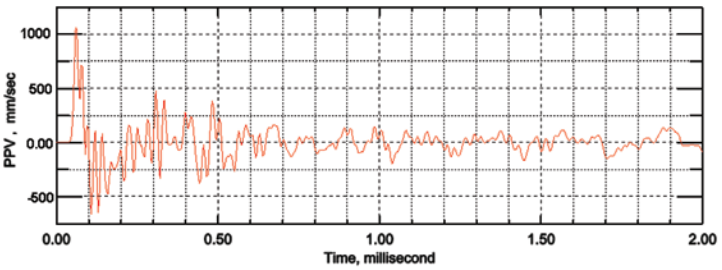

(b) ANFO types explosive, PPV at 0.25m from the borehole (point coordinates = 0.25,0.0)

Figure 11. Effect of free face on rock fracturing by blasting with emulsion type explosives

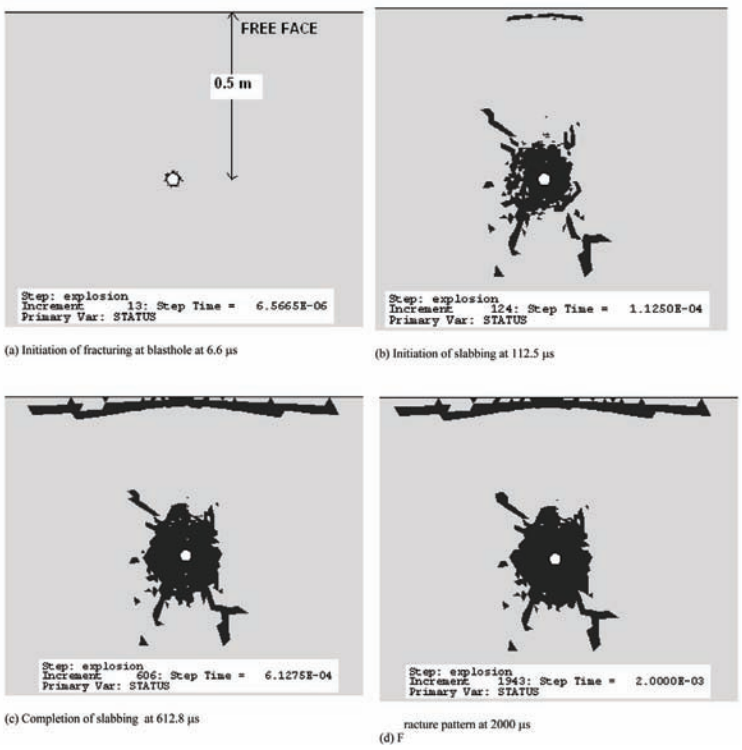

(a) Initiation of fracturing at blasthole at 6.6 μs

(b) Initiation of slabbing at 112.5 μs

(c) Completion of slabbing at 612.8 μs

(d) F racture pattern at 2000 μs

m distance in 96.8 microseconds and returns as a tensile wave. The slabbing starts at 112.5 microseconds. The slabbing process completes at 612.8 microseconds with a slab of 948.7 mm and the fracturing pattern remains the same till the solution time completes. Due to the impact of the reflected waves, the crushing zone and fracture network try to align towards the free face. Further, the fractures zone diameter is 577.4 mm, which is considerably larger than the empirical predictions due the effect of reflected waves. The process demonstrated by the simulation is in well agreement with the field behaviour documented by Bhandari (1979). However, these results bring forth one limitation of the procedure. The procedure simulates discontinuities (fractures) using a continuum approach (the FEM) in which the domain essentially remains a continuum. Only a slab forms due to this continuum. Several slabs are expected to form and detach in the reality.

6. CONCLUSION

A critical analysis of the numerical modelling of rock fracturing by blasting is presented, which elaborated a need to develop a new simulation procedure. A new procedure is developed to simulate the rock fracturing which neither pre-places fractures nor pre-specifies fracturing paths. Results obtained through the procedure are unique and first of their kind. A good conformity with the established knowledge related with fracturing by rock blasting is demonstrated by the new procedure. The presented procedure is, however, can not be applied for the studies involving rock fragmentation as it is evident from Figure 11. This is due to the fact that the procedure does not permit separation of elements and further subdivision into elements size that may arose from interaction of fragments.

ACKNOWLEDGMENT

The work presented in the paper is a part of research work done for PhD thesis of the first author. The research work is financially supported by several organisations and institutes, most notably, Central Institute of Mining & Fuel Research, Dhanbad, India (CIMFR, Erstwhile CMRI-India); Natural Sciences and Engineering Research Council of Canada, Canada (NSERC-Canada) and J.W. McConnel Foundation, McGill University, Canada. The authors are grateful for their generous financial support. Views presented in this paper are personal views of the authors and should not be construed as the views of the organizations they belong. The authors also express gratitude to the valuable comments by the reviewer which helped in improving the text.

REFERENCES

Abaqus. (2003). *Abaqus 6.3-1 user's manuals*. Pawtucket, RI: Abaqus Inc.

Batzle, M. L., Simmons, G., & Siegfried, R. W. (1980). Microcrack closure under stress: direct observation. *Journal of Geophysical Research*, *85*, 7072–7090. doi:10.1029/JB085iB12p-07072doi:10.1029/JB085iB12p07072

Bhandari, S. (1979). On the role of stress waves and quasi-static gas pressure in rock fragmentation by blasting. *Acta Astronautica*, *6*, 365–383. doi:10.1016/0094-5765(79)90104-8doi:10.1016/0094-5765(79)90104-8

Blair, S. C., & Cook, N. G. W. (1998). Analysis of compressive fracture in rock using statistical techniques: Part-I. A non-linear rule-based model. *International Journal of Rock Mechanics and Mining Sciences*, *35*, 837–848. doi:10.1016/S0148-9062(98)00008-4doi:10.1016/S0148-9062(98)00008-4

Cho, S. H., Miyake, H., Kimura, T., & Kaneko, K. (2003). Effect of the waveform of applied pressure on rock fracture process in one free-face. *J. Sc. Tech. Energetic Mat.*, *64*(3), 116–125.

Clark, G. B. (1987). *Principles of rock fragmentation*. London: John Wiley & Sons Inc.

Curran, D. R., Seaman, L., & Shockey, D. A. (1987). Dynamic failure of solids. *Physics Reports*, *147*, 253–388. doi:10.1016/0370-1573(87)90049-4doi:10.1016/0370-1573(87)90049-4

Daniel, R. (2003). Pressure-time history of emulsion explosives. *Personal communications*.

Dawding, C., Labuz, J. F., & Shah, S. P. (1985). Experimental analysis of crack propagation in granite. *International Journal of Rock Mechanics and Mining Sciences*, *22*(2), 85–99. doi:10.1016/0148-9062(85)92330-7doi:10.1016/0148-9062(85)92330-7

Diederichs, M. S. (1999). *Instability of hard rock masses: The role of tensile damage and relaxation*. Unpublished doctoral dissertation, University of Waterloo, Canada

Donze, F. V., Bouchez, J., & Magnier, S. A. (1997). Modelling fractures in rock blasting. *International Journal of Rock Mechanics and Mining Sciences*, *34*(8), 1153–1163. doi:10.1016/S1365-1609(97)80068-8doi:10.1016/S1365-1609(97)80068-8

Donze, F. V., Hotiet, N., & Bernasconi, P. (2002). Optimization of the blasting patterns in shaft sinking. In R. Hammah, W. Bawden, J. Curran, & M. Telesnicki (Eds.), *Proceedings of the 5th North American Rock Mech. Symp. (NARMS-TAC 2002)* (pp. 999-1005). Toronto, Canada: University of Toronto press.

Fourney, W. L., Dick, R. D., Wang, X. J., & Wei, Y. (1993). Fragmentation mechanism in crater blasting. *International Journal of Rock Mechanics and Mining Sciences & Geomechanics Abstracts*, *30*(4), 413–429. doi:10.1016/0148-9062(93)91723-Vdoi:10.1016/0148-9062(93)91723-V

Frantzos, D. C. (1989). *Finite element analysis of radial cracking mechanism around blastholes using measured pressure-time curves for low density ammonium nitrate/fuel oil*. Unpublished doctoral dissertation, Queen's University, Canada.

Freund, L. B. (1990). *Dynamic fracture mechanics*. Cambridge, UK: Cambridge University Press. doi:10.1017/CBO9780511546761doi:10.1017/CBO9780511546761

Grady, D. E., & Kipp, M. E. (1993). Dynamic fracture and fragmentation. In J. R. Asay & M. Shahinpoor (Eds.), *High-pressure shock compression of solids* (pp. 265–322). New York: Springer.

Hao, H., Ma, G. W., & Zhau, Y. X. (1998). Numerical simulation of underground explosions. *Int. J. Blasting by Fragmentation (Fragblast)*, *2*, 383–395.

Hao, H., Wu, C., & Zhou, Y. (2002). Numerical analysis of blast-induced stress waves in a rock mass with anisotropic continuum damage models, Part I: equivalent material property approach. *Rock Mechanics and Rock Engineering*, *35*(2), 79–94. doi:10.1007/s006030200012doi:10.1007/s006030200012

Hart, R. D. (1993). An introduction to distinct element modelling for rock engineering. In J. A. Hudson (Ed.), *Comprehensive rock engineering* (*Vol. 2*, pp. 245–261). Oxford, UK: Pergamon Press.

Hazzard, J. F., Young, R. P., & Maxwell, S. C. (2000). Micromechanical modeling of cracking and failure in brittle rocks. *Journal of Geophysical Research*, *105*(B7), 16683–16697. doi:10.1029/2000JB900085doi:10.1029/2000JB900085

Hilleborg, A., Modeer, M., & Petersson, P. E. (1976). Analysis of Crack Formation and Crack Growth in Concrete by Means of Fracture Mechanics and Finite Elements. *Cement and Concrete Research*, *6*, 773–782. doi:10.1016/0008-8846(76)90007-7doi:10.1016/0008-8846(76)90007-7

Jung, W. J., Utagava, M., Ogata, Y., Seto, M., Katsuyama, K., Miyake, A., & Ogava, T. (2001). Effects of rock pressure on crack generation during tunnel blasting. *Jl. Japan Explosives Soc.*, *62*(3), 138–146.

Kexin, D. (1995). Maintenance of roadways in soft rock by roadway-rib destress blasting. *China Coal Society*, *20*(3), 311–316.

Khosrou, S. H., & Mohanty, B. (1996). Role of discontinuity on stress-field in wall control blasting. In B. Mohanty (Ed.), *Proceedings of the 5th int. sym. rock fragmentation by blasting (FRAGBLAST5)*, Montreal, Canada (pp. 207-216). Rotterdam, The Netherlands: Balkema.

Kikuchi, N. (1983). Remarks on 4CST elements for incompressible materials. *Computer Methods in Applied Mechanics and Engineering*, *37*, 109–123. doi:10.1016/0045-7825(83)90144-5doi:10.1016/0045-7825(83)90144-5

Kranz, R. I. (1983). Microcracks in rocks: a review. *Tectonophysics*, *100*, 449–480. doi:10.1016/0040-1951(83)90198-1doi:10.1016/0040-1951(83)90198-1

Kutter, H. K., & Fairhurst, C. (1971). On the fracture process in blasting. *International Journal of Rock Mechanics and Mining Sciences*, *8*, 181–202. doi:10.1016/0148-9062(71)90018-0doi:10.1016/0148-9062(71)90018-0

Lima, A. D. R., Romanel, C., Roehl, D. M., & Araujo, T. D. (2002). An adaptive strategy for the dynamic analysis of rock fracturing by blasting. In *Proceedings of the Int. Conf. Computational Eng. & Sci*. (ICES'02), Reno, NV.

Liu, L. (1997). *Continuum modelling of rock fragmentation by blasting*. Unpublished doctoral dissertation, Queen's university, Canada.

Liu, L., & Katsabanis, P. D. (1997). Development of a continuum damage model for blasting analysis. *International Journal of Rock Mechanics and Mining Sciences*, *34*(2), 217–231. doi:10.1016/S0148-9062(96)00041-1doi:10.1016/S0148-9062(96)00041-1

Malan, D. F., & Napier, J. A. L. (1995). Computer modelling of granular material microfracturing. *Tectonophysics*, *248*, 21–37. doi:10.1016/0040-1951(95)00019-Jdoi:10.1016/0040-1951(95)00019-J

McHugh, S., & Keough, D. (1982). Use of laboratory derived data to predict fracture and permeability enhancement in explosive pulse tailored field tests. In *Proceedings of the US Symp. Rock Mech., Issues in Rock Mech* (pp. 504-514).

Mortazavi, A., & Katsabanis, P. D. (2001). Modelling burden size and strata dip effects on the surface blasting process. *International Journal of Rock Mechanics and Mining Sciences*, *38*, 481–498. doi:10.1016/S1365-1609(01)00015-6doi:10.1016/S1365-1609(01)00015-6

Mosinets, V. N., & Gorbacheva, N. P. (1972). A seismological method of determining the parameters of the zones of deformation of rock by blasting. *Soviet Mining Science*, *8*(6), 640–647. doi:10.1007/BF02497586doi:10.1007/BF02497586

Napier, J. A. L., Daehnke, A., Dede, T., Hildyard, M. W., Kujipers, J. S., & Malan, D. (1997). Quantification of stope fracture zone behaviour in deep level gold mines. *J. SAIMM*, *97*, 119–134.

Prasad, U., Mohanty, B., & Nemes, J. A. (2000). Dynamic Fragmentation of Selected Rocks Under Impact Loading. In *Proceedings of the 4th North American Rock Mech. Symp.*, Seattle, WA (pp. 577-581).

Ramshaw, C. L., Selby, A. R., & Bettess, P. (1998). Computation of the transmission of waves from pile driving. In B. O. Skipp (Ed.), *ground dynamics and man made processes* (pp. 115–128). London: T. Telford Pub.

Repetto, E. A., Radovitzky, R., & Ortiz, M. (2000). Finite element simulation of dynamic fracture and fragmentation of glass rods. *Computer Methods in Applied Mechanics and Engineering*, *183*, 3–14. doi:10.1016/S0045-7825(99)00208-Xdoi:10.1016/S0045-7825(99)00208-X

Ryu, C. H. (2002). Computer modeling of dynamic ground motion due to explosive blasting and review of some modeling problems. *J. Japan Explosives Society*, *63*(5), 217–222.

Saharan, M. R., & Mitri, H. S. (2008). Numerical Procedure for Dynamic Simulation of Discrete Fractures due to Blasting. *Rock Mechanics and Rock Engineering*, *41*(5), 641–670. doi:10.1007/s00603-007-0136-9doi:10.1007/s00603-007-0136-9

Saharan, M. R., & Mitri, H. S. (2009). *Numerical Simulation for Rock Fracturing by Destress Blasting- As Applied to Hard Rock Mining Conditions*. Berlin: VDM Verlag. ISBN 978-3-639-11064-7

Sunu, M. Z., Reed, S. M., & Singh, R. N. (1988). Evaluating of rock parameters on surface mine blasting by finite element analysis. *Int. J. surface mining and reclamation, 2*, 209-15.

Szuladzinski, G. (1993). Response of rock medium to explosive cavity pressure. In H. P. Rossmanith (Ed.), *Proceedings of the 4th Int. Symp. Rock Fragmentation by Blasting (FRAGBLAST IV)*, Vienna, Austria (pp. 17-23). Rotterdam, The Netherlands: Balekma.

Taylor, L. M., Chen, E. P., & Kuszmaul, J. S. (1986). Micro-crack induced damage accumulation in brittle rock under dynamic loading. *Computer Methods in Applied Mechanics and Engineering*, *55*, 301–320. doi:10.1016/0045-7825(86)90057-5doi:10.1016/0045-7825(86)90057-5

Thorne, B. J., Hommert, P. J., & Brown, B. (1990). Experimental and computational investigation of the fundamental mechanisms of cratering. In *Proceedings of the 3rd Int. Symp. Rock fragmentation by Blasting (FRAGBLAST 3)*, Brisbane, Australia (pp. 412-23).

Timoshenko, S. P., & Goodier, J. N. (1969). *Theory of elasticity*. New York: McGraw Hill.

Toper, A. Z. (1995). Numerical modelling to investigate the effects of blasting in confined rock simulation of a field study. In J. K. Daeman & R. A. Schultz (Eds.), *Proceedings of the 35th U.S. Symposium on Rock Mechanics*, Reno, NV (pp. 541-546). Rotterdam, The Netherlands: Balkema.

Valliapan, S., Lee, I. K., Murti, V., Ang, K. K., & Ross, A. H. (1983). Numerical modelling of rock fragmentation. In R. Holmberg & A. Rustan (Eds.), *Proceedings of the 1st Int. Symp. Rock Frag. By Blasting (FRAGBLAST 1)* (pp. 375-90). Rotterdam, The Netherlands: Balkema.

Yang, R., Bawden, W. F., & Katsabanis, P. D. (1996). A new constitutive model for blast damage. *International Journal of Rock Mechanics and Mining Sciences & Geomechanics Abstracts*, *33*, 245–254. doi:10.1016/0148-9062(95)00064-Xdoi:10.1016/0148-9062(95)00064-X

This work was previously published in International Journal of Geotechnical Earthquake Engineering, Volume 1, Issue 2, edited by T.G. Sitharam, pp. 38-58, copyright 2010 by IGI Publishing (an imprint of IGI Global).

Chapter 13
Numerical Prediction of Rock Fracturing During the Process of Excavation

Zhangtao Zhou
Sichuan University, China

Zheming Zhu
Sichuan University, China

XinXing Jin
Sichuan University, China

Hao Tang
Sichuan University, China

ABSTRACT

During the process of excavation, blasting can induce cracking inside the surrounding rock. Considering the effects of material properties and loading conditions, a rock blasting excavation model with two successive excavation steps was developed through the use of AUTODYN code. Four kinds of equation of state (EOS), linear, shock, JWL, and compaction were applied to the materials employed in this numerical model. A modified principal stress failure criterion was applied to determining material statuses, and TNT explosive and a relatively homogeneous igneous rock, diorite, were used in this numerical model. By using this numerical model, rock fracturing process during blasting excavation was simulated, and rock fracturing process during two successive excavations is presented.

DOI: 10.4018/978-1-4666-0915-0.ch013

1. INTRODUCTION

Fragmentation of rock by blasting is widely used in mining, quarrying and civil construction excavations. The design of blasts requires the knowledge of the detonation properties of the explosive and the responses of the rock. However, our understanding of the blasting process and blasting mechanism is far from complete, as both commercial explosives and rocks are complex materials. Usually blasting can release a large amount of energy within microseconds. Under such circumstances, the target rock undergoes high pressures in the giga Pascals and thermodynamic influences (Gebbeken & Greulich, 2006), and the short duration of blasting loads often exhibits strong spatial and time variations, resulting in sharp stress gradients in the rock and a varying strain rate (Krauthammer, 1999). Therefore, the study on the response of rock under blasting loading is very difficult and hence, it is essential to implement both experimental studies and numerical studies. Experimental studies can generate an experimental database while numerical studies can simulate the processes of rock fracturing to obtain a better understanding of the dominant parameters that control rock fracturing.

During the process of tunnel excavation, two types of loading operate on the surrounding rock: stress wave (or shock wave) loading and explosion gas pressure loading. The stress wave loading arises out of detonation of the explosive charge. For typical commercial explosives, the detonation pressure exerted on the surrounding rock at the moment of initiation could easily exceed 10GPa. This high pressure on the surrounding rock sets off a shock wave in the adjacent rock, but it soon decays to a high amplitude stress wave that propagates in the rock at the velocity of longitudinal wave. It is immediately followed, albeit at a much reduced velocity, by the longer duration gas pressure loading. This loading due to gas expansion continues long after the stress wave has dissipated, as its expansion rate is considerably lower than that of the propagating stress wave (Brinkman & Separating, 1989; Paine & Please, 1994; Zhu et al., 2007). The former initiates cracks or damage zones, and the latter penetrates into these cracks and causes their further extension and propagation, and in more severe case may result in rock burst from excavation surface (Zhou & Hong, 1995; Stewart et al., 2001; Zhan & Wang, 2007).

In rock blasting, three basic fracture zones, i.e., crushed zone, severely fractured zone and incipiently cracked zone as well as the circumferential spalling cracks will occur around the borehole. The fracturing mechanism under blasting loading has been analyzed, and the factors that affect rock fracturing have been discussed in Zhu et al. (2007, 2008). During tunnel blasting, a blast-induced damaged zone immediately around the tunnel boundary is developed. Generally, this zone is characterized by the reduction in its strength and stiffness and the perceived implications are clear, in that they relate mainly to construction and maintenance costs, safety and the long-term performance of the tunnel (Saiang & Nordlund, 2009). The original properties of rock around the tunnel boundary are changed due to blasting impact, resulting in a change in stress distribution and the mechanical properties of rock mass, such as strength, deformability, and in particular permeability through a network of cracks (Golshani & Oda, 2007; Zhu & Bruhns, 2008; Kwon et al., 2008). The characteristic fracture patterns after perimeter blasting of a granite block and rock mass condition around a tunnel boundary excavated by drilling and blasting were showed in literature (Olsson & Bergqvist, 1995; Saiang & Nordlund, 2009). Such a complex physical state of the blasting-induced damage to the rock can significantly influence the mechanical response of the damaged rock mass and, consequently, the overall rock mass around the fractured zone.

Numerical studies have been conducted by a number of researchers using various numerical codes and models to simulate the process of fracturing and fragmentation in blasting for rock

materials (Donez et al., 1997; Chen & Zhao, 1998; Ma et al., 1998; Ma & An, 2008; Wang et al., 2008; Xiao et al., 2008; Zhu & Bruhns, 2008; Zhu, 2009; Wang et al., 2009). Although many significant results have been published, it is far from complete for the study of rack fracturing under blasting loads.

In this paper, in order to investigate the rock fracturing during the process of excavation, a rock blasting excavation model with two successive excavation steps is developed using AUTODYN code and rock fracturing process during blasting is simulated.

2. NUMERICAL MODEL

Figure 1 shows the configuration of the numerical model, in which a cylindrical rock dynamic model with two excavation steps is prepared. The explosive and air are simulated by using Euler processor and the rock is simulated by using Lagrange processor. The whole domain, including rock, air and explosive, is assumed to be x-axis symmetric. As shown in this figure, the cylindrical rock measures 8.0 m in diameter and 10.0 m in length. The borehole is 1500 mm in length and 60 mm in diameter. The explosive column length is 1000 mm and the stemming length is 500 mm. The time period selected for each excavation step is 10 ms since detonation. After 10 ms, the fragmented rock mass were removed and new-formed tunnel was filled with air, then the subsequence excavation will be started to execute. Except for the surface of excavation, all the surfaces of the model are treated by transmitting boundary, in which the stress wave is not allowed to reflect back, which essentially is an analog of an infinitely large rock body. The axial cross section of cylindrical rock is selected as the 2D model.

The diorite rock, which is relatively homogeneous, was employed in this simulation. According to Zhu et al. (2007, 2008), the properties of diorite are: density is 3.16; p-wave velocity is 5.77 km/s; dynamic tensile strength is 112.8 MPa; shear modulus is 39.6 GPa; and dynamic shear strength is 265 MPa. In the following simulations, the properties are the same unless specified otherwise.

2.1 Equation of State (EOS)

In this simulation, three kinds of equation of state, linear, shock, JWL, and Compaction are applied.

The dimension of shock wave propagation is about three to seven times the radius of the explosive charge (Dai, 2002); therefore, for the rock in the immediate vicinity of the explosive charge, shock EOS is applied, which can be expressed as

$$U_S = C_0 + S_1 U_p + S_2 U_p^2 \tag{1}$$

where C_0, S_1 and S_2 are constants which can be determined by experiments, U_s is the shock wave velocity, and U_p is the particle velocity. Currently, for diorite, the parameters C_0, S_1 and S_2 are not available, however, for a similar material, gabbro, the constants are: C_0 = 3.5 km/s, S_1 = 1.32 and S_2 = 0. For the rock material which is far from the explosive charge, linear EOS is employed, which is suitable for small deformation dynamic problem. The linear EOS can be expressed as

$$P = k\left(\rho/\rho_0 - 1\right) = k\mu \tag{2}$$

where P is the pressure, k is the bulk modulus, ρ/ρ_0 is the ratio of the density of current state to initial state.

The JWL (Johns-Wilkins-Lee) equation of state (EOS), which is suited for hydrodynamic of explosive detonation products, is employed as the EOS of TNT explosive in this study. The JWL EOS can be expressed as

Figure 1. Sketch of a rock blasting excavation model with two excavation steps

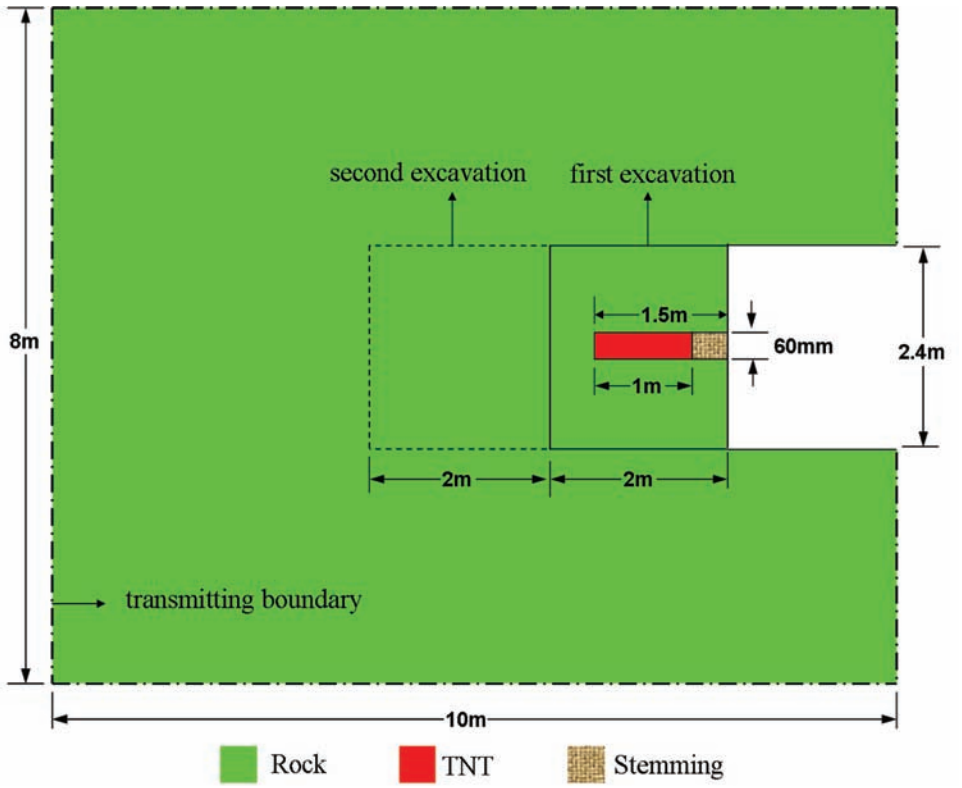

$$P = A(1-\frac{\omega}{R_1 V})e^{-R_1 V} + B(1-\frac{\omega}{R_2 V})e^{-R_2 V} + \frac{\omega \cdot E}{V} \quad (3)$$

where P is hydrostatic pressure, V is specific volume, E is specific internal energy, A, B, R_1,R_2 and ω are constants obtained from dynamic experiments, and for TNT explosive, A = 373.77 GPa, B = 3.747 GPa, R_1 = 4.15, R_2 = 0.9, ω = 0.35.

For the TNT explosive, there is no strength model and failure model applied because after detonation, the TNT explosive is designed to convert to ideal gas which is strengthless and will never fail (Table 1).

For sand as the stemming material, a compaction EOS was applied which is more suitable for porous materials. The relation between pressure and material density was obtained from the experimental results of Laine and Sandvik (2001).

2.2. Failure Criterion of Rock

During the process of stress wave propagation, tensile stresses or shear stresses do occur and cause rock material to fail in tension or in shear. Therefore, a modified principal stress failure criterion is applied to determining material status, which is suitable for describing material tensile failure or shear failure. The modified principal stress failure criterion dictates that when the major principal stress or the maximum shear stress in an element exceeds material tensile or shear strength, the element fails. After an element has failed, it will not be able to sustain any tensile and shear loadings, but it is still able to sustain compressive loading. The normal compressive stresses, σ_x and σ_y, of a failed element must be identical, i.e., $\sigma_x = \sigma_y$. This is because the failed element cannot sustain any

Table 1. Properties of the explosive used in this model

Properties	Value
Reference density (mg/mm^3)	1.63
C-J Detonation velocity (m/s)	3960
C-J Energy / unit volume (kJ/m^3)	6.0×10^6
C-J Pressure (GPa)	210
Parameter A (GPa)	373.7
Parameter B (GPa)	3.75
Parameter R1	4.15
Parameter R2	0.9
Parameter W	0.35
Auto-convert to Ideal Gas	Yes

shear stress (i.e., $\tau = 0$), the corresponding Mohr circle will become a point.

2.3 Erosion Criteria

Erosion criteria that allow removing an element from calculation if a pre-defined strain (instantaneous, incremental geometric strain or effective plastic strain) exceeds. When an element is eroded, the mass of the cell can either be discarded or retained at the four corner nodes of the element. If the mass is retained, conservation of inertia and spatial continuity of inertia are maintained during the erosion process. It is important to understand that although the word seems to imply it, erosion is not truly a physical phenomenon. It is a numerical technique introduced to overcome the problems associated with the mesh distortions caused by gross motions of a Lagrange grid (Century Dynamic Inc, 2003).

3. SIMULATIONS RESULTS

In order to investigate some of the key aspects of fracturing in the surrounding rock during blasting, numerical simulations were carried out using the above numerical model with two excavation steps, the equation of state, the failure criterion, and the related properties. For each excavation, the simulation results of material statuses are presented. Five target points are selected in order to analyze rock fracturing mechanism later.

3.1 Rock Fracturing Process during the First Excavation

In order to investigate the fracturing process of surrounding rock under blast loading, the calculation results of material statuses as a function of time after initiation of TNT explosive are presented in Figure 2. It can be seen that an intense crushed zone is developed near the borehole. The curves of dynamic stresses (σ_1 , σ_2 and τ_{12}) versus time for target 1 in Figure 2 ($x = 7.29m, y = 0.381m$), which is near the borehole, are shown in Figure 3. It can be seen that as the stress wave reaches target 1 at 0.0587 ms, the principal stresses σ_1 and σ_2, and the maximum shear stress τ_{12} start to increase rapidly. At 0.1186 ms, the maximum shear stress is 266.6 MPa which is greater than the rock shear strength 265 MPa, thus, the element containing target 1 fails in shear.

Beyond the shear failure zones, there are tensile failure zones caused by tensile stresses, which can be generally grouped into two distinct types, circumferential tensile failure zones and radial crack zones.

Following the crushed zone, circumferential tensile failure zones with gray color in Figure 2 occur. This failure zones consist of just one surface of a crack. This crack could occur in any axial cross section planes around the tunnel axis and it is caused by the circumferential stress σ_θ. Figure 4 shows the curves of dynamic stresses (σ_1, σ_2, τ_{12} and σ_θ) versus time for the element containing target 2 ($x = 6.81m, y = 0.849m$). It can be seen that the stress wave reaches the element containing target 2 at 0.162 ms and the element fail at 0.353 ms. During this time interval, from 0.162 ms to 0.353 ms, the major principal stress σ_1 reaches its maximum value 55.5 MPa at 0.298 ms. The maximum shear stress τ_{12} reaches its

Figure 2. Material statuses of numerical model during first excavation, air and part of TNT production are not presented. Five targets are selected to record the local stress histories.

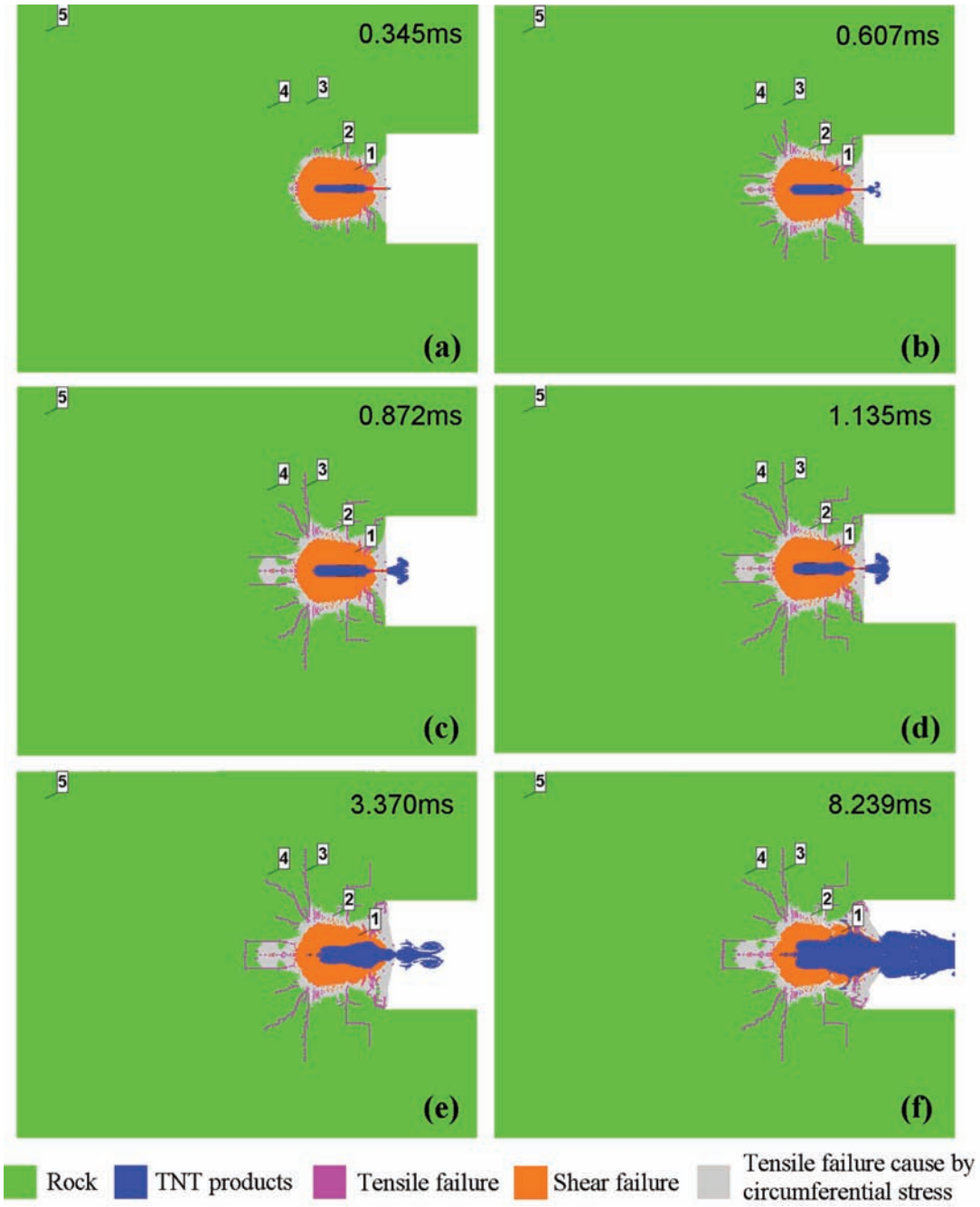

maximum value 140.2 MPa at 0.315 ms. They all do not reach the rock dynamic strengths. However, at 0.353 ms, the circumferential stress is 114.09 MPa which is larger than the rock tensile strength 112.8 MPa. So the element containing target 2 fails in circumferential tensile stress.

After an element has failed, it loses the capability of carrying shear stress, but is still able to

Figure 3. Dynamic stresses (σ_1, σ_2 and τ_{12}) versus time for the element containing target 1

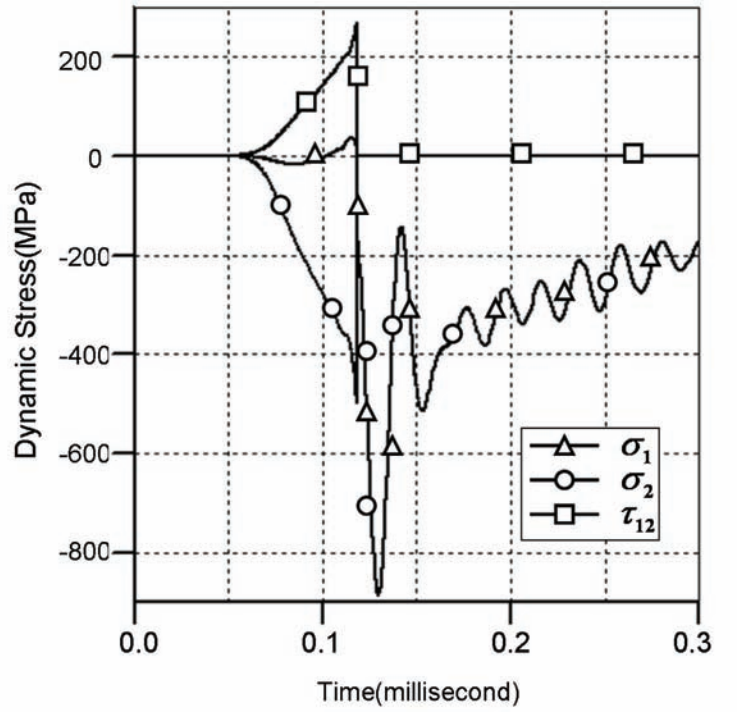

Figure 4. Dynamic stresses (σ_1, σ_2, τ_{12} and σ_θ) versus time for the element containing target 2

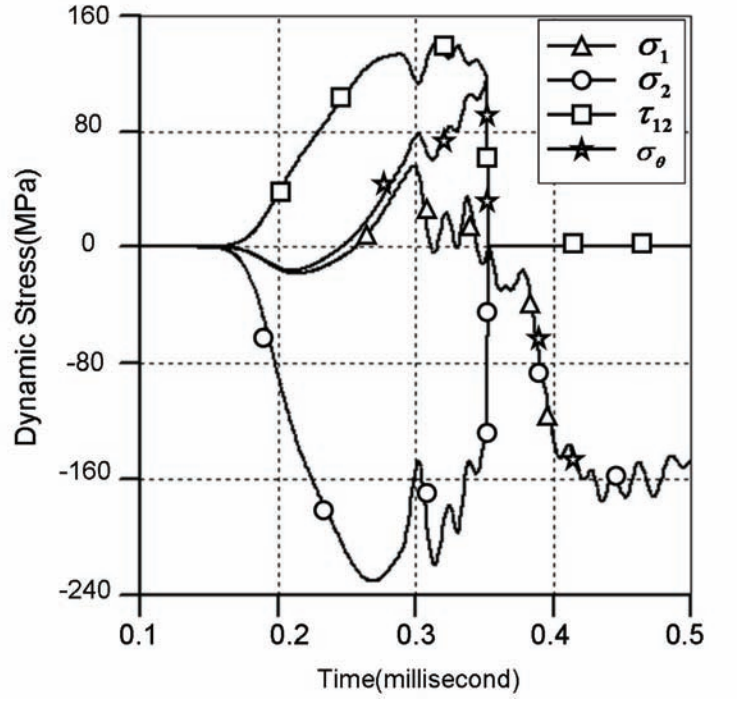

Figure 5. Dynamic stresses (σ_x, σ_y and σ_1) versus time for the element containing target 3

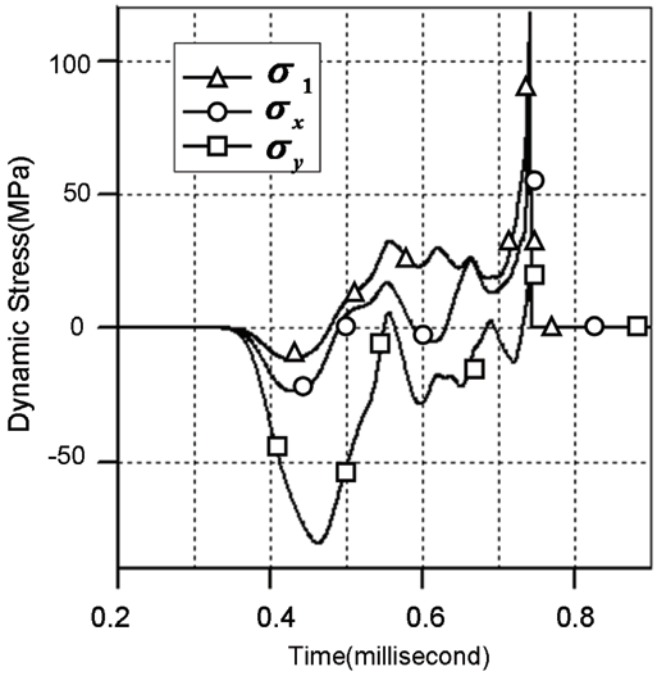

sustain the compressive loads according to the failure criterion utilized in this numerical model. Therefore, after the elements are failed, the shear stresses in Figure 3 and Figure 4 become zero and the normal stresses (σ_1, σ_2 and σ_θ in Figure 4) become identical and compressive.

Near the circumferential tensile failure zones, the radial crack zones with red colour in Figure 2 occur. Figure 5 shows the curve of dynamic stresses versus time for the element containing target 3 ($x = 6.26m, y = 1.84m$). The principal stress σ_1 reaches its maximum value 117.4 MPa at 0.741 ms, which is greater than the rock dynamic tensile strength, thus, the element containing target 3 fails in tension, resulting in a crack passing through this element.

With the dissipation of stress waves, the expanding explosion products start to penetrate into the radial cracks and exert a high quasi-static pressure on the crack surfaces. From Figure 2 (e-f), it can be seen that the borehole expands significantly resulting from the pressure of the explosive products. Beyond the fractured zone, the magnitude of stress waves attenuates and becomes too weak to damage the rock any more.

3.2. Rock Fracturing during the Second Excavation

In order to illustrate the fracturing mechanics during the subsequent excavation, the second excavation after the first excavation shown in Figure 2 is implemented. In mining practices, before an excavation starts, the stress waves produced in the previous excavation have completely vanished. In order to simulate the real mining operations, the second excavation starts after 10 ms of the first detonation, when the stress waves have fully dissipated. At 10 ms, the fragmented rock mass produced by the first excavation is removed and a new-formed tunnel is filled with air, then the subsequent excavation is started to execute. The calculation results of material statuses as a func-

Figure 6. Material statuses during second excavation; air and part of TNT production are not presented

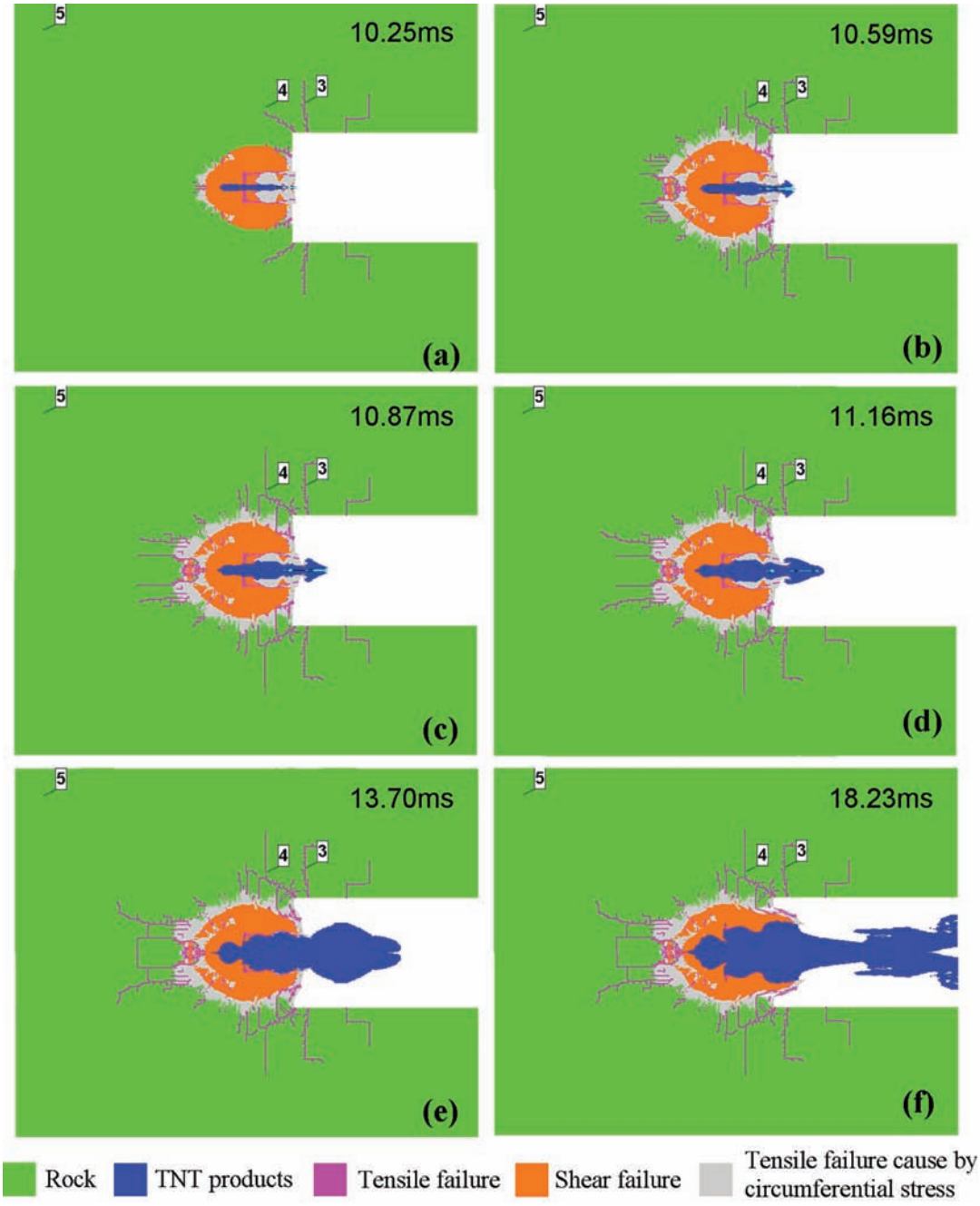

tion of time after initiation of the explosive are presented in Figure 6.

Target 5 ($x = 0.400m, y = 3.600m$) is far away from the borehole in the surrounding rock mass. Figure 7 shows the particle absolute velocity magnitude versus time for the element containing target 5. It can be seen that at both excavations, particle velocity increases drastically as the stress wave reaches target 5, and then it dissipates gradually. At 9.999 ms, just before the second

Figure 7. Absolute velocity versus time for the element containing target 5

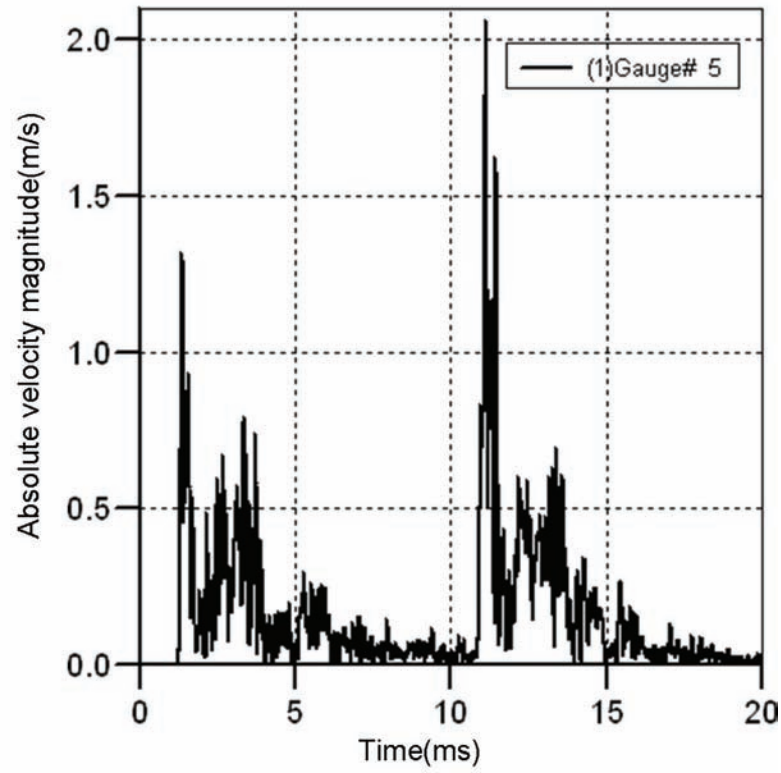

blasting starts, the particle velocity is only 1.69 percent of the maximum value of that produced in the second excavation, thus, the influence of the stress wave induced by the first excavation on the second excavation is very small.

Figure 6 displays material statuses during the second excavation. The damage pattern is similar to those in the first excavation. Some cracks in the surrounding rock produced in the first excavation continue to extend, branch significantly and some even coalesce. In Figure 6 (a-b), the crack passing through the element containing target 3 produced at the first excavation shown in Figure 2 continues to propagate and finally form a kinking crack which is parallel to the tunnel axis. The cracks caused by the first blasting may be very small, however, the small cracks may extend and become large after subsequent blasts.

The curves of the dynamic stresses σ_x, σ_y and σ_1 versus time for the element containing target 4 ($x = 5.41m, y = 1.74m$) during the second excavation is shown in Figure 8. All the stresses are compressive at the initial stage, and later, σ_x and σ_1 change from compression to tension. At 10.426 ms, stress σ_x is 109.83 MPa, and the major principal stress σ_1 reaches its maximum value 113.8 MPa which is greater than the dynamic tensile strength 112.8 MPa, resulting in the element failure. Consequently, the crack near target 4 developed during the first blasting is extended progressively and passes through target 4.

Because the erosion technique was adopted in the simulation of the successive blasting excavation, it should be noted that the simulation results of the second excavation may not be as accurate as those of the first excavation, although it still

Figure 8. Dynamic stresses (σ_x, σ_y and σ_1) versus time for the element containing target 4

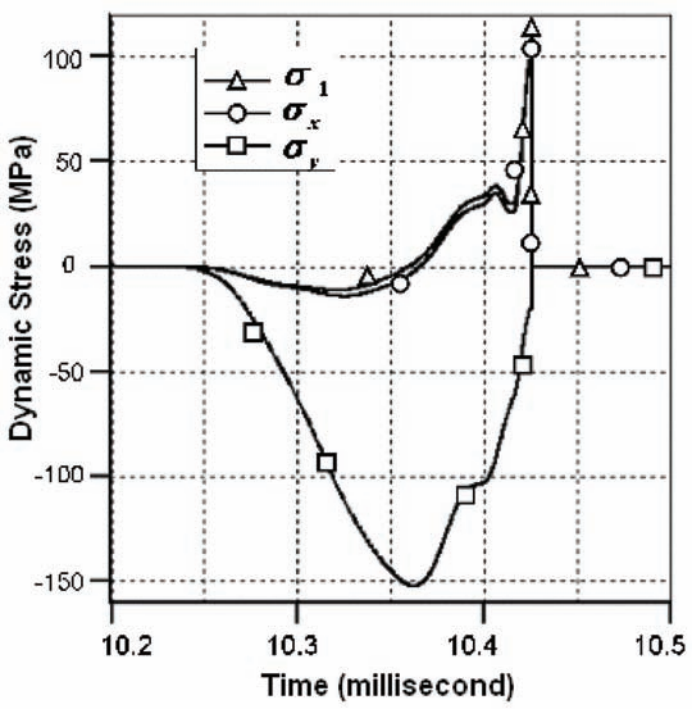

gives correct prediction of the fracturing process due to the second excavation.

4. CONCLUSION

The numerical simulation using AUTODYN code to understand rock fracturing with two successive excavations by blasting and to study rock fracturing processes revealed three distinct zones, which were formed around the blasthole. These zones were termed as crushed zone, circumferential tensile failure zone and radial crack zone; the relations of stress versus time at the targets in these three failure zones were established. It was found that the cracks in the surrounding rock produced by the previous blast would be affected by the subsequent blast. As a result, these cracks continue to extend, branch and some even coalesce and the cumulative damage would be much more for repeated blast loading.

ACKNOWLEDGMENT

This work has been funded in part by the Major State Basic Research Project, Grant No. 2010CB732005; the Funding of Science and Technology of Sichuan province 2008JY0041; the Project of SRF for ROCS, SEM 2008890-19-19; the National Natural Science Foundation of China 50639100.

REFERENCES

Brinkman, J. R. (1989, August). Separating shock waves and gas expansion breakage mechanisms. In *Proceedings of the 2nd international symposium on rock fragmentation by blasting*, Keystone, CO.

Century Dynamic Inc. (2003). *Autodyn theory manual* (Version 6.1).

Chen, S. G., & Zhao, J. (1998). A study of UEDC modeling for blasting wave propagation in joint rock mass. *International Journal of Rock Mechanics and Mining Sciences*, *35*, 93–99. doi:10.1016/S0148-9062(97)00322-7

Dai, J. (2002). *Dynamic Behaviors and Blasting Theory of Rock* (pp. 80–81). Beijing, China: Metallurgical Press.

Donze, F. V., Bouchez, J., & Magnier, S. A. (1997). Modeling fractures in rock blasting. *International Journal of Rock Mechanics and Mining Sciences*, *34*, 1153–1163. doi:10.1016/S1365-1609(97)80068-8

Gebbeken, N., & Greulich, S. (2006). Hugoniot propreties for concrete determined by full-scall detonation experiments and flyer-plate-impact tests. *International Journal of Impact Engineering*, *32*, 2017–2031. doi:10.1016/j.ijimpeng.2005.08.003

Golshani, A., & Oda, M. (2007). Numerical simulation of the excavation damaged zone around an opening in brittle rock. *International Journal of Rock Mechanics and Mining Sciences*, *44*, 835–845. doi:10.1016/j.ijrmms.2006.12.005

Krauthammer, T. (1999). Blat-resistant structural concrete and steel connection. *International Journal of Impact Engineering*, *22*, 887–910. doi:10.1016/S0734-743X(99)00009-3

Kwon, S., Lee, C. S., Cho, S. J., Jeon, S. W., & Cho, W. J. (2009). An investigation of the excavation damaged zone at the KAERI underground research tunnel. *Tunnelling and Underground Space Technology*, *24*, 1–13. doi:10.1016/j.tust.2008.01.004

Laine, L., & Sandvik, A. (2001, November). Derivation of mechanical properties for sand. In T. S. Lok (Ed.), *Proceedings of the fourth Asia-Pacific conference on shock & impact loads on structures*, Singapore (pp. 361-368).

Ma, G. W., & An, X. M. (2008). Numerical simulation of blasting-induced rock fractures. *International Journal of Rock Mechanics and Mining Sciences*, *45*, 966–975. doi:10.1016/j.ijrmms.2007.12.002

Ma, G. W., Hao, H., & Zhou, Y. X. (1998). Modeling of wave propagation induced by underground explosion. *Computers and Geotechnics*, *22*, 283–303. doi:10.1016/S0266-352X(98)00011-1

Olsson, M., & Bergqvist, I. (1995). *Crack propagation in rock from multiple hole blasting* (Part 1, SveBeFo Rep. No. 18). Stockholm, Sweden: Swedish Rock Engineering Research. Paine, A. S., & Please, C. P. (9994). An improved model of fracture propagation by gas during rock blasting-some analytical results. *International Journal of Rock Mechanics and Mining Sciences*, *31*, 699–706.

Saiang, D., & Nordlund, E. (2009). Numerical Analyses of the Influence of Blast-Induced Damaged Rock Around Shallow Tunnels in Brittle Rock. *Rock Mechanics and Rock Engineering*, *42*, 421–448. doi:10.1007/s00603-008-0013-1

Stewart, R. A., Reimold, W. U., Charlesworth, E. G., & Ortlepp, W. D. (2001). The nature of a deformation zone and fault rock related to a recent rockburst at Western Deep Levels Gold Mine, Witwatersabnd Basin, South Africa. *Tectonophysics*, *337*, 173–190. doi:10.1016/S0040-1951(01)00028-2

Wang, Y., Zhu, Z., Zhou, Z., & Xie, H. (2009, June). Numerical investigation of blasting-induced damage in concrete slabs. In *Proceedings of the Symposium on Computational Structrual Engineering*, Shanghai, China (pp. 655-668).

Wang, Z. L., Lia, Y. C., & Wang, J. G. (2008). Numerical analysis of blast-induced wave propagation and spalling damage in a rock plate. *International Journal of Rock Mechanics and Mining Sciences*, *45*, 600–608. doi:10.1016/j.ijrmms.2007.08.002

Xiao, J. Q., Ding, D. X., Xu, G., & Jiang, F. L. (2008). Waveform effect on quasi-dynamic loading condition and the mechanical properties of brittle materials. *International Journal of Rock Mechanics and Mining Sciences*, *45*, 621–626. doi:10.1016/j.ijrmms.2007.07.025

Zhan, X., & Wang, J. (2007). Research on the mechanism and prevention of rockburst at Yinxin Gold Mine. *Journal of China University of Mining & Technology*, *17*(4), 541–545. doi:10.1016/S1006-1266(07)60142-4

Zhou, P., & Hong, K. (1995). The rockburst features of Taipingyi tunnel and the prevention methods. *Chinese Journal of Rock Mechanics and Engineering*, *14*(2), 171–178.

Zhu, W. C., & Bruhns, O. T. (2008). Simulating excavation damaged zone around a circular opening under hydromechanical conditions. *International Journal of Rock Mechanics and Mining Sciences*, *45*, 815–830. doi:10.1016/j.ijrmms.2007.09.007

Zhu, Z. (2009). Numerical prediction of crater blasting and bench blasting. *International Journal of Rock Mechanics and Mining Sciences*, *46*, 1088–1096. doi:10.1016/j.ijrmms.2009.05.009

Zhu, Z., Mohanty, B., & Xie, H. (2007). Numerical investigation of blasting-induced crack initiation and propagation in rocks. *International Journal of Rock Mechanics and Mining Sciences*, *44*, 412–424. doi:10.1016/j.ijrmms.2006.09.002

Zhu, Z., Xie, H., & Mohanty, B. (2008). Numerical investigation of blasting-induced damage in cylindrical rocks. *International Journal of Rock Mechanics and Mining Sciences*, *45*, 111–121. doi:10.1016/j.ijrmms.2007.04.012

This work was previously published in International Journal of Geotechnical Earthquake Engineering, Volume 1, Issue 2, edited by T.G. Sitharam, pp. 12-23, copyright 2010 by IGI Publishing (an imprint of IGI Global).

Chapter 14
Investigations on Impact of Blasting in Tunnels

Kaushik Dey
Indian School of Mines, India

V. M. S. R. Murthy
Indian School of Mines, India

ABSTRACT

Blasting with longer advance per round leaves an impact both visible (in the form of overbreak) and invisible (cracks) in the surrounding rockmass, however, a number of controlled-blasting techniques, that is line drilling, pre-splitting, and smooth blasting, have been developed to minimise this problem. These techniques require additional drilling, controlled charging, and detonation, and thus, are not preferred in regular development activities. Investigations have been carried out in five different horizontal development drivages of metal mines to assess the blasting impact using burn cut and arrive at the blast-induced rock damage (BIRD) model. Vibration monitoring close to the blast was carried out using accelerometers for the first time in India to develop vibration predictors and overbreak threshold levels for individual sites. This paper reports the development of the overbreak predictive model (BIRD) for burn cut blasting in hard rock drivages by combining the relevant rock, blast design, and explosive parameters. A multivariate statistical model has been developed and validated and the same can find ready application in tunnels and mines for exercising suitable engineering controls both in blast design and explosive selection for reduced basting impacts.

DOI: 10.4018/978-1-4666-0915-0.ch014

1. INTRODUCTION

Blasting is the most popular means of excavation for tunnels despite the rapid developments in the mechanical excavators, namely, tunnel boring machines, road headers, continuous miners. Faster drivage rates are possible with the recent developments in explosives (emulsion), initiating systems (NONEL, electronic detonator) and drilling (automation) systems. However, longer pulls, associated with high concentration of explosives, often lead to overbreak due to excess ground vibrations. Overbreak can become an expensive phenomenon in terms of extra concrete backfilling and may also give rise to additional mucking time. Most of the existing controlled blasting techniques, to reduce the blast-induced overbreak, need extra drilling, in turn, adding to drilling and blasting cost and time. Blasting in tunnels aims at the following objectives:

(i) Longer pulls
(ii) Reduced overbreak and rock damage
(iii) Optimized drilling and blasting cost.
(iv) Low cycle time

Thus, it is rational to assess blast-induced overbreak in production blasting and control the same by modifying the blast design.

2. PREVIOUS WORK

Overbreak is largely affected by a host of rock, blast design and explosive parameters. Several researchers have attempted to study overbreak/ blast-induced rock damage either based on experimental studies or relating some of the above influencing parameters. A brief discussion on the previous works is provided in the following section.

(i) Mcknown (1984) and Singh (1992) used half cast factor as a measure of blast-induced overbreak. Half cast factor is the ratio of total visible drill mark length in the wall and roof after blast and the total drilling length and is given by,

$$HCF = \frac{\sum_{i=1}^{n} L_i}{\sum_{r=1}^{n} L_r} \quad (1)$$

Where,

HCF = Half cast factor
L_i = Post-blast drill mark length visible (m)
L_r = Pre-blast drilled length (m)

(ii) Graddy and Kipp (1987) used a scalar, D, to describe the rock damage. The value D lies between 0 (intact rock) and 1 (complete failure). This can also be used to estimate the rock modulus E_d, of the damaged rock, so that

$$E_d = E (1 - D) \quad (2)$$

Where,

E, E_d = Modulus of the intact rock and damaged rock respectively

(iii) A method proposed by JKMRC (Australia, 1990) included the frequency, surface condition and density of discontinuities as a descriptor of damage.
(iv) Forsyth and Moss (1990) devised a method of quantifying blast - induced damage. Their proposed Drift Condition Rating (DCR) comprised two components: firstly, the drift back condition (related to the rockmass integrity and the percentage of half cast visible); and secondly, the amount of overbreak. This empirical rating varied from 0 to 9.

(v) Paventi (1995) reviewed the development of a field procedure for damage monitoring through an empirical blast induced damage index, D_M given by,

$$D_M = I * II*III * IV*(V_A + V_B) \quad (3)$$

Where,

I: considers the reduction in intact rock strength due to micro-fracturing.
II: evaluates the extent of the exposed excavation surface area remaining in place using the post scaling half cast factor.
III: determines the drift condition by assessing the drumminess of the back with a scaling bar.
IV: accounts for the amount of scaling arising from damage.
V_A and V_B: considers the direction of structure with respect to drift direction to account for the anisotropy potentially caused by structural features at meso- and macro- scale.

(vi) Yu and Vongpaisal (1996) proposed a new blast damage criteria based on dynamic tensile strength, compressional wave velocity (P-wave), density of rockmass and peak particle velocity of the blast. The proposed damage criterion is as follows:

$$BDI = \frac{v \times \acute{A}_r \times C_p}{K_r \times DTS} \quad (4)$$

Where,

BDI = Blast Damage Index
v = Vector sum of peak particle velocity (m/s)
ρ_r = Density of rock (g/cc)
C_p = Compressional wave velocity (km/s)
K_r = Site Quality constant (0 – 1.0)
= (RMR – Ground support adjustment)/100.

Table 1. Blast damage index and damage type (after Yu and Vongpaisal, 1996)

BDI	Type of damage
≤0.125	No damage to underground excavation
0.25	No noticeable damage
0.5	Minor and discrete scabbing effect
0.75	Moderate and discontinuous scabbing damage
1.0	Major and continuous scabbing failure
1.5	Severe damage
≥ 2.0	Major caving

DTS = Dynamic tensile strength (MPa)

Based on the blast damage index the rock may be categorized as given in Table 1.

(vii) Singh (2000) studied the roof damage in underground due to surface blasting. Based on underground instrumentation and far-field vibration monitoring, it was found that the BDI value of less than 1 referred to no damage condition and BDI value of more than two referred to severe damage condition, whereas BDI value in between 1 to 2 referred to a minor damage condition.

(viii) Ibarra et al. (1996) proposed perimeter charge factor (PCF) as the controlling parameter for the blast induced rock damage. Perimeter charge factor is defined as the ratio of weight of explosives in the perimeter blast holes and the next row, divided by the volume of rock within this annulus, ignoring the lifters in the invert'. Analysis of the blast data of Aquamilpa Hydroelectric Project, Diversion Tunnel No.2, revealed a relationship between Overbreak/Underbreak with log of Barton's Q index. A linear relationship between the underbreak/overbreak and PCF has been established. An increase in PCF indicates an increase in overbreak and a decrease in underbreak. A composite relationship includ-

ing both PCF and Q value for the prediction of overbreak/underbreak was established. Although, these relations are site-specific, it is easy to establish using multiple regression analysis.

$$\text{Overbreak (\%)} = -K_{o1} + K_{o2} \times \text{PCF} - K_{o3} \times \log(Q)$$
$$\text{Underbreak (\%)} = K_{u1} - K_{u2} \times \text{PCF} + K_{u3} \times \log(Q) \quad (5)$$

Where,

K_{o1}, K_{o2} = Site-specific characteristic constants for overbreak

K_{u1}, K_{u2} = Site-specific characteristic constants for underbreak

The above review clearly brings out that the damage models suggested relate the damage/ overbreak with either a single or a couple of influencing factors. It was felt that the inclusion of predominant factors of representing rock, blast design and explosive could lead to a more rational overbreak predictive model. The major contributing parameters identified are given below:

(i) Rock parameters: Dynamic tensile strength, rock density, Poison's ratio and threshold level of Peak Particle Velocity (PPV) for overbreak.
(ii) Blast design parameters: Confinement and advance factor
(iii) Explosive charge parameters: Perimeter charge factor

3. DESIGN OF EXPERIMENTAL BLASTS

Experimental blasts have been designed such that adequate data on the above-mentioned rock, blast design and explosive charge parameters could be generated. The details of experimental blasts are described in the following sections.

Figure 1. Telescopic overbreak measuring rod

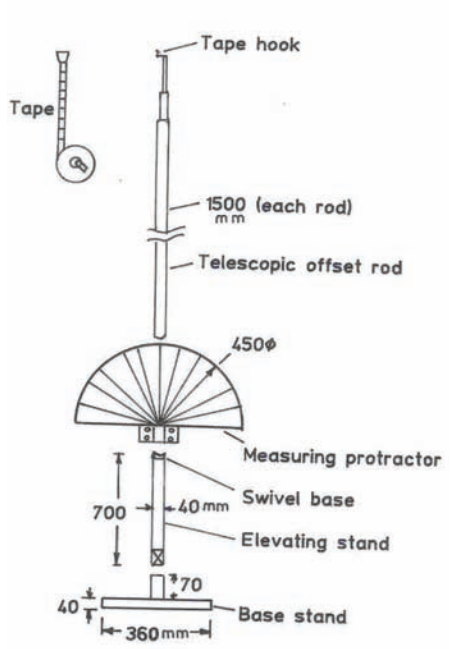

The rock and rockmass properties were determined from the field and laboratory investigations. Poisson's ratio was computed from the measured P-wave and S-wave velocities in the laboratory. Post-blast drivage cross sectional area was measured using telescopic overbreak measuring rod (Figure 1) which had been designed and fabricated at Indian School of Mines, Dhanbad, under the supervision of the authors. Overbreaks were computed using Planimeter after plotting telescopic offset measurements on a graph paper. The overbreaks are expressed in percentage of drivage area. Peak particle velocities and accelerations were monitored as near as to the blast face possible using accelerometer and triaxial geophone based seismographs (Minimate Plus and Minimate 077 of Instantel Inc. Canada). The fixing arrangement of the accelerometer sensors has been shown in Figure 2. The sensors used in the study with their broad specifications are mentioned in Table 2. The measured accelerations are integrated to obtain PPV. Vibration predictor equations between PPV and cube root scaled distance (Eqn. 6) as proposed

Figure 2. Fixing of sensors of the accelerometer

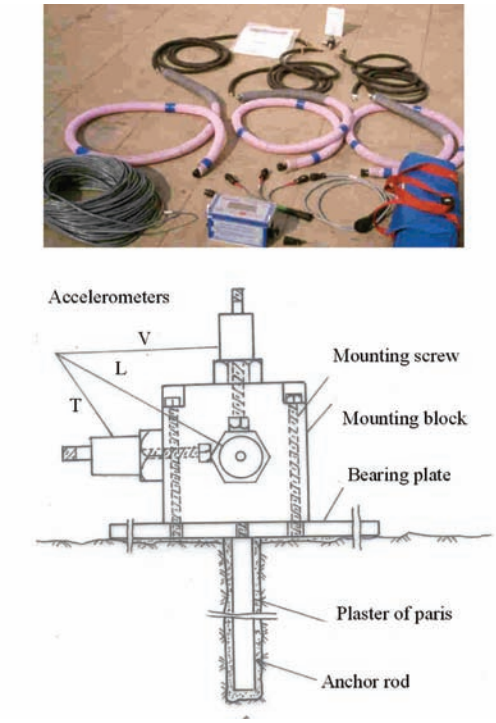

by the Ambraseys and Hendron (1968) were developed for each site. To arrive at the overbreak threshold levels of PPV, the established predictor equations were extrapolated upto the overbreak distances (Murthy and Dey, 2003).

$$SD = R/(W)^{1/3} \quad (6)$$

Where,

SD = Scaled distanceR = Distance from the blast location to monitoring point (m)

W = Maximum charge per delay (kg)Dynamic tensile strength has been estimated using the following equation proposed by Tezuka et al. (1997).

$$\sigma_{td} = (\rho \times c \times v)/960.4 \quad (7)$$

Where,

Table 2. Major specifications of seismic sensors used in the study

Parameters	Accelerometer	High frequency geophone	Triaxial geophone
Frequency range	1 Hz to 3 kHz	1Hz to 2 kHz	2 to 300 HZ
Acceleration range	Upto 500 g (4903 m/s^2)	Geophone natural frequency: 28Hz	Upto 254 mm/s

σ_{td} = Dynamic tensile stress (MPa)ρ = Rock density (g/cm^3)c = P - wave velocity (m/ s) v = PPV (m/s)

In the above equation, substituting the 'v' with threshold level of PPV, dynamic tensile strength of rock is estimated. Confinement, the ratio of drilling depth and tunnel area, has been measured for every blast, because it has a significant impact on the overbreak (Dey, 2004). Similarly, Advance factor, the advancement achieved per unit drilling in a blast round i.e., the ratio of advance and drilling depth, has also been computed.

4. FIELD INVESTIGATIONS

Field investigations have been carried out in five horizontal drivages through hard metamorphic rocks representing different geotechnical conditions. The blasts investigated are the regular production blasts with burn cut carried out in development drivages referred as Site-1 through Site-5. The details of rock properties and experimental blasts are provided in Table 3(a) and Table 3(b). Near-field vibrations were monitored to establish ground vibration predictor equation for each site. The predictor equation has been extrapolated upto the overbreak distance to estimate the threshold level of PPV for overbreak. The predictor equations and estimated vibration threshold levels for overbreak are shown in Figures 3-7.

Table 3(a). Rock properties of the five investigating sites

Parameters	Site-1	Site-2	Site-3	Site-4	Site-5
Dynamic tensile strength (MPa)	34.87	41.46	49.44	42.47	65.16
Threshold level of PPV (mm/s)	2380	2725	2665	2502	3300
Rock density (g/cc) (intact rock)	2.78	2.87	3.24	2.98	3.35
P-wave velocity (km/s) (intact rock)	5.06	5.10	5.50	5.47	5.66
S-wave velocity (km/s) (intact rock)	2.86	2.82	3.32	3.43	3.41
Poisson's ratio	0.266	0.280	0.213	0.242	0.215

5. DEVELOPMENT OF OVERBREAK PREDICTIVE MODEL

A predictive model has been developed for estimation of overbreak from rock parameters, blast design parameters and explosive charge parameters (Dey, 2004). Dynamic tensile strength (DTS), Poisson's ratio (μ), rock density (ρ) and threshold level of PPV (PPV) have been taken as the rock descriptors. Perimeter charge factor (PCF) has been taken as the charge descriptor. Here, to determine the PCF, the perimeter holes are only considered. Advance factor (AF) and confinement (Cn) are considered as blast design descriptors. Advance factor is the advance achieve per unit hole depth and also termed as hole utilization factor. Whereas, confinement is the ratio of hole length and tunnel cross sectional area. As the confinement increases, the higher vibration is observed.

The proposed model considers rock, blast design and charge parameters. The explosive characteristics have been kept the constant for all the cases. The composite model developed, named as BIRD, is given below:

$$\mathrm{OB} = 27.91 + 0.97 \times \mathrm{PCF} - 1.53 \times \frac{(\sigma_{td} \times \mu)}{(\mathrm{DPPV} \times \rho)} - 1.89 \times \frac{\mathrm{AF}}{\mathrm{Cn}} \quad (8)$$

Where,

OB = Overbreak (%)
PCF = Perimeter charge factor (kg/m^3)
DPPV = Threshold level of PPV for damage (m/s)
σ_{td} = Dynamic tensile strength
μ = Poisson's ratio
ρ = Rock density (g/cm^3)
AF = Advance factor (m/m)
Cn = Confinement (m/m^2)

Another overbreak predictive model has also been developed considering the influence of overbreak causative factors namely, perimeter specific charge, measured ground vibration, dominant frequency of the measured vibration, advance factor, P-wave velocity of rock and percentage free face provided in the cut area. The developed model after linear multivariate analysis is given below:

$$A_O = 30.05 + 2.776\ \mathrm{PCF} + 0.068\ v - 0.011\ f_{do} - 0.235\ c_p - 0.030\ F_f - 20.459\ A_F \quad (9)$$

Where,

A_O = overbreak (%)
PCF = perimeter specific charge (kg/m^3)
v = measured PPV (mm/s)
f_{do} = dominant frequency of the measured vibration (Hz)
c_p = P-wave velocity in (km/s)
F_f = free face provided in the cut area (%) = Free face area/First cut area
AF = advance factor (m/m)

The related data pertaining to each site has been statistically analysed using multivariate

Table 3(b). Details of experimental blast results

Sl No.	Drill depth (m)	Perimeter charge factor (kg/m³)	Overbreak (%)	Advance (m)	Face area (m²)	Advance factor (m/m)	Confinement (m/m²)
Site-1							
1	3.2	N.A.	14.24	2.6	14.4	0.81	0.22
2	3.2	1.34	5.83	2.8	14.4	0.88	0.22
3	3.2	1.22	17.01	2.0	14.4	0.63	0.22
4	3.2	1.34	18.8	2.0	14.4	0.63	0.22
5	3.2	1.19	18.43	2.0	16.0	0.63	0.20
6	3.2	N.A.	14.24	2.4	14.4	0.75	0.22
7	3.2	1.03	26.55	1.8	16.0	0.56	0.20
Site-2							
1	1.3	2.31	3.99	1.2	12.0	0.92	0.11
2	3.2	1.16	24.17	2.1	16.0	0.66	0.20
3	3.2	1.25	19.66	2.5	16.0	0.78	0.20
4	1.5	1.59	17.9	1.2	12.0	0.80	0.13
5	1.5	1.32	18.2	1.2	12.0	0.80	0.13
6	1.5	2.14	16.55	1.25	12.0	0.83	0.13
7	1.5	1.62	7.78	1.3	12.0	0.87	0.13
8	1.7	1.74	17.69	1.4	12.0	0.82	0.14
9	1.3	1.31	10.75	1.18	12.0	0.91	0.11
10	1.7	1.36	14.73	1.5	12.0	0.88	0.14
11	3.2	1.13	22.2	2.4	16.0	0.75	0.2
Site-3							
1	1.6	1.41	18.44	1.2	6.25	0.75	0.26
2	1.6	1.34	15.42	1.4	6.25	0.88	0.26
3	1.6	1.40	18.38	1.3	6.25	0.81	0.26
4	1.6	1.24	22.36	1.25	6.25	0.78	0.26
5	1.6	1.44	21.48	1.25	6.25	0.78	0.26
Site-4							
1	1.6	1.31	18.99	1.3	6.25	0.81	0.26
2	1.6	1.48	12.21	1.35	6.25	0.84	0.26
3	1.6	1.48	29.97	0.9	6.25	0.56	0.26
4	1.6	1.31	27.22	0.9	6.25	0.56	0.26
5	1.6	1.41	24.45	1.2	6.25	0.75	0.26
Site-5							
1	1.6	1.41	21.15	1.2	6.25	0.75	0.26
2	1.6	1.17	17.92	1.35	6.25	0.84	0.26
3	1.6	1.32	22.91	1.2	6.25	0.75	0.26
4	1.6	1.45	22.93	1.2	6.25	0.75	0.26

Figure 3. PPV predictor for Site-1 and extrapolation upto overbreak distance

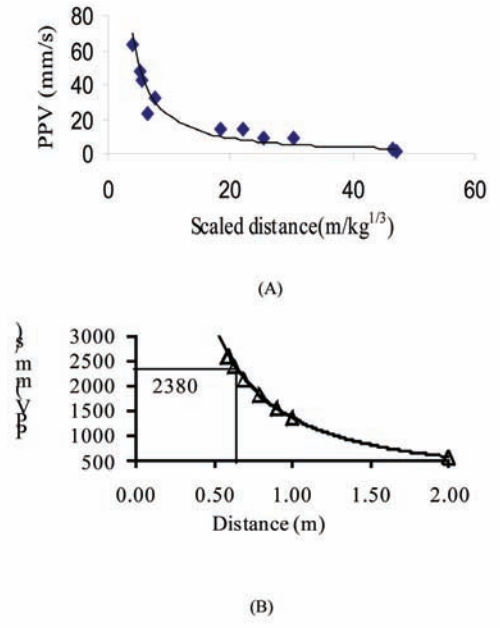

Figure 4. PPV predictor for Site-2 and extrapolation upto overbreak distance

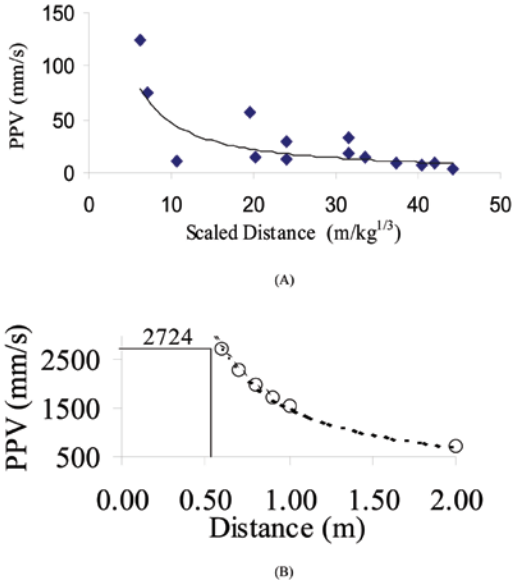

Figure 5. PPV predictor for Site-3 and extrapolation upto overbreak distance

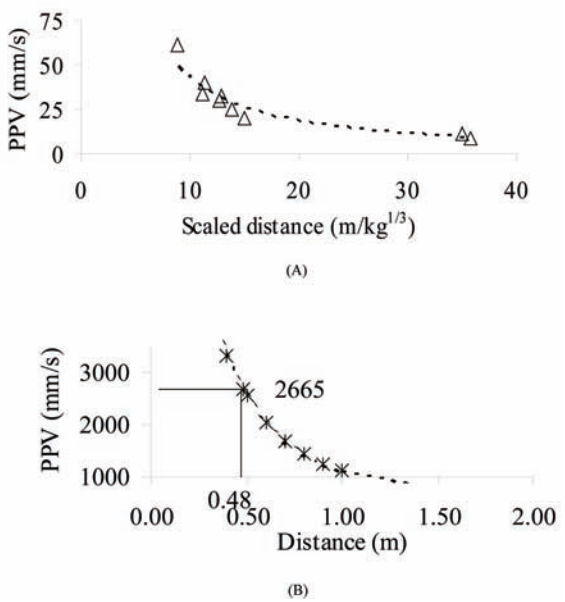

Figure 6. PPV predictor for Site-4 and extrapolation upto overbreak distance

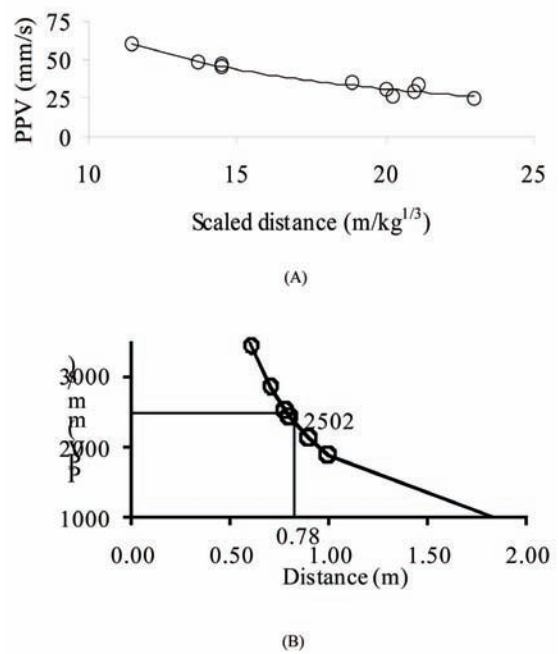

Figure 7. (v) PPV predictor for Site-5 and extrapolation upto overbreak distance

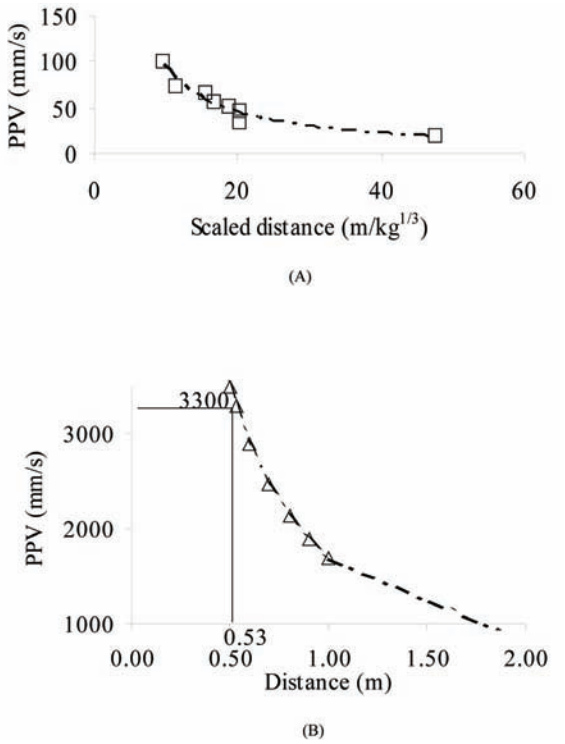

statistical software (SPSS ver 6.0) in order to test the significance of the relationship. For the statistical validation of the model, due to low index of determination, 't' test and 'F' test have been conducted. The results are given in Table 4.

For the validation of the model 't' test has been conducted to test the significance of r (correlation coefficient). The null hypothesis (H_0) is that the r is not significant and as opposed to alternate hypothesis (H_1), where r is significant. The calculated t-value ($t_{calculated}$), which is a function of r, n (no of samples) was found to be 3.21, and is larger than t-value (t_{table}) at 5% significance level (i.e. 2.228 from student t-table). Thus, it can be concluded that the alternate hypothesis (H_1) is valid. It means r is significant. F-test has also been done to test the variances of regression and residuals whether they were alike or not. The calculated F ($F_{calculated}$) is to be 2.763, which is lesser than the F-table (F_{table}) value at 5% significance with 3 and 8 degrees of freedom. In this case, the null hypothesis is valid. In other words, there is no significant difference between variances of regression and residual. Thus, the model proposed is considered valid and applicable.

Accuracy of BIRD model has been tested for 4 blasts, which were kept aside for testing and not used in the development of the predictive model itself. The results are given in Table 5. From the table, it is clear that the percentage error in the prediction varied between 3 and 9 and is considered to be within acceptable limits of prediction. Thus, the BIRD model is validated.

6. CONCLUSION

Blast-induced overbreak has been investigated from the experimental blasts and ground vibration monitoring using state-of-the-art seismographs and analysis modules. The overbreak measurements have been utilized to establish peak particle velocity thresholds. An overbreak predictive model (BIRD) has been developed considering the rock parameters (dynamic tensile strength, Poisson's ratio, estimated damage threshold levels in terms of PPV, density of rock), blast design parameters (advance factor and confinement) and an explosive parameter (perimeter charge factor). Other influencing parameters viz. orientation of joint planes, roughness of joint plane, water inflow characteristics, insitu stress conditions etc. are not considered in these models to make the models simple.

It has been observed that the overbreak threshold levels decrease (from 3300 to 2500 mm/s) with the increase in advance factor (from 0.4 to 0.9). An increase in the confinement (from 0.1 to 0.25) resulted in increase in the overbreak. With the increase in the perimeter charge factor (from 1 to 3.5 kg/m^3)) the percentage overbreak increased from 6 to 30.

The composite overbreak model, namely, BIRD developed is found to be statistically

Table 4. Statistical validation of the proposed overbreak prediction model (BIRD)

Dependent variable	Independent variable	r	$t_{calculated}$	t_{table} (5% Sig.)	$F_{calculated}$	F_{table} (5% Sig.)
Overbreak (%)	Rock descriptor Design descriptor Charge descriptor	0.713	3.21	2.228	2.763	4.07

Table 5. Comparison of the observed and predicted overbreak using BIRD model

INPUT	Blast-1	Blast-2	Blast-3	Blast-4
Perimeter charge factor (kg/m^3)	1.49	1.46	1.32	1.58
Dynamic tensile strength (MPa)	41.46	41.46	41.46	41.46
Poisson's ratio	0.28	0.28	0.28	0.28
Density (g/cm^3)	2.87	2.87	2.87	2.87
Threshold level of PPV for overbreak (mm/s)	2725	2725	2725	2725
Pull (m)	1.6	1.5	2.0	1.4
Face size (m^2)	14.40	14.40	14.40	14.40
Drill depth (m)	3.2	3.2	3.2	3.2
OUTPUT				
Actual overbreak (%)	24.73	23.60	19.97	24.91
Predicted overbreak (%)	22.83	22.93	21.32	23.45
Percentage error (±)	7.68	2.83	6.78	5.86

significant for the cases investigated and could predict overbreak within a percentage error of 10 (Table 4). It can, thus, be concluded that the proposed overbreak prediction model, BIRD, is adequately representative and rational predicting and reducing blasting impacts in tunnels and mines as it considers the critical rock, design and charge parameters influencing overbreak. The model can be refined further by incorporating varied data from different sites.

REFERENCES

Ambraseys, N. R., & Hendron, A. J. (1968). Dynamic behaviour of rockmasses. In Stagg, K. G., & Zienkiewiez, O. C. (Eds.), *Rock Mechanics in Engineering Practices* (pp. 203–207). London: John Willey and Sons.

Anon. (1990). *Advanced blasting technology* (Final Research Rep. No. AMIRA P93D). Brisbane, Australia: JKRMC.

Dey, K. (2004). *Investigation of blast-induced rock damage and development of predictive model in horizontal drivages* (pp. 45-103). Unpublished doctoral dissertation, Indian School of Mines, Dhanbad, India.

Forsyth, W. W., & Moss, A. E. (1990). Observations of blasting and damage around development openings. In *Proceedings of the 92nd Canadian Institute Mining and Metallurgy, Annual General Meeting*, Ottawa, Canada (pp. 245-251).

Grady, D. E., & Kipp, M. E. (1987). *Dynamic rock fragmentation. Fracture mechanics of rock* (pp. 34–46). London: Atkinson B. K.

Ibarra, J. A., Maerz, N. H., & Franklin, J. A. (1996). Overbreak and underbreak in underground openings Part 2: causes and implications. *Geotechnical and Geological Engineering*, *14*(3), 325–340. doi:10.1007/BF00421947

McKown, A. (1984). Some aspects of design and evaluation of perimeter controlled blasting in fractured and weathered rock. In *Proceedings of the 10th Conference on explosive and blasting techniques* (pp. 261-269).

Murthy, V. M. S. R., & Dey, K. (2003, September). Predicting Overbreak From Blast Vibration Monitoring In Lake Tap Tunnel – A Success Story. In. *Proceedings of FRAGBLAST*, *7*(3), 149–166. doi:10.1076/frag.7.3.149.16787

Paventi, M., Lizotte, Y., Scoble, M., & Mohanty, B. (1995, August 23-24). Measuring rockmass damage in drifting. In *Proceedings of Rock fragmentation by blasting, FRAGBLAST-5*, Montreal, Canada (pp. 131-138).

Singh, P. K. (2000). *Evaluation of damages to underground coal mines caused by surface blasting vis-à-vis establishment of blast vibration threshold* (Project No GAP/III/BLASTING/MOC/1996, pp. 1-50). CMRI Coal S & T.

Singh, S. P. (1992, December). Mining Industry and Blast Damage. *Journal of Mines, Metals & Fuels*, 465-472.

Tezuka, M., Kudo, Y., Matsuda, H., Hasui, A., & Nakagawa, K. (1997). Study on estimate of damage zone caused by blasting. In Y. Lee & C. Lee (Eds.), *Proceedings Asian Rock Mechanics Symposium, Environmental and safety concerns in underground construction* (pp. 101-106).

Yu, T. R., & Vongpaisal, S. (1996). New blast damage criteria for underground blasting. *CIM Bulletin*, *89*(2), 139–145.

This work was previously published in International Journal of Geotechnical Earthquake Engineering, Volume 1, Issue 2, edited by T.G. Sitharam, pp. 59-71, copyright 2010 by IGI Publishing (an imprint of IGI Global).

Compilation of References

Abaqus. (2003). *Abaqus 6.3-1 user's manuals*. Pawtucket, RI: Abaqus Inc.

Adamson, W. R., & Scherpenisse, C. R. (1998, February 2-5). The measurement and control of blast induced damage of final pit walls in open pit mining. In *Proceedings of 24th Annual Conf. on Explosives and Blasting Research* (p. 539), New Orleans, LA.

Agrawal, P. K., & Pandey, O. P. (2004). Unusual lithospheric structure and evolutionary pattern of the cratonic segments of the South Indian shield. *Earth, Planets, and Space*, *56*, 139–150.

Ambraseys, N. R., & Hendron, A. J. (1968). *Dynamic behavior of rock masses in rock mechanics in engineering practice* (K. G. Stagg & O. C. Zienkievicz, Eds.). New York: John Wiley and Sons.

Ambraseys, N. R., & Hendron, A. J. (1968). Dynamic behaviour of rockmasses. In Stagg, K. G., & Zienkiewiez, O. C. (Eds.), *Rock Mechanics in Engineering Practices* (pp. 203–207). London: John Willey and Sons.

Anbazhagan, P., Vinod, J. S., & Sitharam, T. G. (2009). Probabilistic seismic hazard Analysis for Bangalore. *J Nat. Haz.*, *48*, 145–166. doi:10.1007/s11069-008-9253-3

Anderson, D. A., Ritter, A. P., Winzer, S. R., & Reil, J. W. (1985). A method for site specific prediction and control of ground vibration from blasting. In *Proceedings of the E Firstt Mini-Symposium on Explosives and Blasting Research*, San Diego, CA (pp. 28-43).

Andrews, A. B. (1981, January 19-23). Design criteria for sequential blasting. In *Proceedings of the Seventh Conf. on Explosives and Blasting Technique*, Phoenix, AZ (pp. 173-192). Montville, OH: Society of Explosives Engineers.

Andrews, D. C. A., & Martin, G. R. (2000). Criteria for liquefaction of silty soils. In *Proceedings of the 12th WCEE 2000 Conferance*, Auckland, NZ.

Andrews, D. J. (1986). Objective determination of source parameters and similarity of earthquakes of different size in Earthquake Source Mechanics. In S. Das, J. Boatwright, & C.H. Scholz (Eds.), *American Geophysical Union* (pp. 259-268). Washington D.C.

Andrieux, P., McKenzie, C., Heilig, J., & Drolet, A. (1994). The impact of blasting on excavation design – A geomechanics approach. In *Proceedings of the 10th Symposium on Explosives and Blasting Research ISEE* (pp. 107–119), Austin, USA.

Annie, O. K., & Stewart, J. P. (2006). Evaluation of the Effectiveness of Theoretical 1D Amplification Factors for Earthquake Ground-Motion Prediction. *Bulletin of the Seismological Society of America*, *96*(4A), 1422–1436. doi:10.1785/0120040196

Anon. (1990). *Advanced blasting technology* (Final Research Rep. No. AMIRA P93D). Brisbane, Australia: JKRMC.

Anon. (1997). DGMS, India, S&T circular number 7 on *Criteria for safe vibration limits on structures* (pp. 1-8).

Arduino, P., Miller, G. R., & Ogurinde, A. (2002). Live modeling of 1-D wave propagation in layered soil media. *Computer Applications in Engineering Education*, *9*(4), 248–258. doi:10.1002/cae.10003

Arora, V. K. (1987). *Strength and deformation behaviour of jointed rocks*. Unpublished doctoral dissertation, Indian Institute of Technology, Delhi, India.

Ash, R. L. (1990). *Design of blasting rounds, Int. Surface Mining* (2nd ed., pp. 565–583). New York: AIME.

Ashby, M. F. (1992). *Materials selection in mechanical design.* London: Pergamon Press.

ASTM standard D 4428-M (2007). *Standard test methods for seismic cross hole testing.* ASTM International, West Conshohocken, PA, 2003, DOI: 10.1520/D4428_D4428M-07.

Atchison, T. C. (1972). Fragmentation Principles (Chapter 7.2). In *Proceedings of Surface Mining* (pp. 355-372). New York: AIME.

Atchison, T. C., & Pugliese, J. M. (1964). Comparative Studies of Explosives in Limestone. *BuMines Rept. of Inv. 6395* (p. 25).

Atkinson, G. M., & Boore, D. M. (2006). Earthquake Ground-Motion Prediction Equations for Eastern North America. *Bulletin of the Seismological Society of America*, *96*(6), 2181–2205. doi:10.1785/0120050245

Atlas Powder Company. (1987). *Explosives and Rock Blasting*. ISBN 0-9616284-0-5

Barla, G. (1974). Rock anisotropy: Theory and laboratory testing. In Muller, L. (Ed.), *Rock Mechanics*. New York: Springer Verlag.

Barton, N., & Hansteen, H. (1979). Very large span openings at shallow depth: deformation magnitudes from jointed models and finite element analysis. In *proceedings of the 4th rapid Excavation & Tunneling conference*, (Vol. 2) (pp. 1331-1353), Atlanta,GA.

Basha, B. M. (2009). *Optimum design of retaining structures under static and seismic loading: A reliability based approach.* Unpublished doctoral dissertation, Indian Institute of Science, Bangaluru, Karnataka, India.

Basha, B. M., & Babu, G. L. S. (2008). Seismic passive earth pressure coefficients by pseudo-dynamic method using composite failure mechanism. *In Geosustainability and Geohazard Mitigation, ASCE Geotechnical Special Publication, 178*, 343 - 350.

Basha, B. M., & Babu, G. L. S. (2009). Computation of sliding displacements of bridge abutments by pseudo-dynamic method. *Soil Dynamics and Earthquake Engineering*, *29*(1), 103–120. doi:10.1016/j.soildyn.2008.01.006

Batzle, M. L., Simmons, G., & Siegfried, R. W. (1980). Microcrack closure under stress: direct observation. *Journal of Geophysical Research*, *85*, 7072–7090. doi:10.1029/JB085iB12p07072doi:10.1029/JB085iB12p07072

Bauer, A., & Crosby, W. A. (1990). *Blasting; Surface Mining* (2nd ed., pp. 552–554). Littleton, CO: Metallurgy and Exploration, Inc.

Berenbaum, R., & Brodie, I. (1959). The tensile strength of coal. *Journal of the Institute of Fuel*, *32*, 320–327.

Berta, G. (1990). *Explosives: An Engineering Tool*. Milano, Italy: ltalesplosivi.

Beyer, R.R., & Jacobs, A.M. (1986). Borehole television for geotechnical investigations. *Water Power and Dam construction, 38*(9), 16-28.

Bhandari, S. (1979). On the role of stress waves and quasi-static gas pressure in rock fragmentation by blasting. *Acta Astronautica*, *6*, 365–383. doi:10.1016/0094-5765(79)90104-8doi:10.1016/0094-5765(79)90104-8

Bieniawski, Z. T., & Hawkes, I. (1978). Suggested methods for determining tensile strength of rock materials. *International Journal of Rock Mechanics and Mining Sciences*, *15*, 99–103. doi:10.1016/0148-9062(78)90003-7

Birch, W. J., & Chaffer, R. (1983). Prediction of ground vibrations from blasting on opencast sites, Trans. Instn. Min. Metall., Section A. *Mineral Industry*, *92*, A102–A107.

BIS-1893. (2002). Indian Standard Criteria for Earthquake Resistant Design of Structures, Part 1 - General Provisions and Buildings. *Bureau of Indian Standards*, New Delhi.

Biswas, S. K. (1987). Regional tectonic framework, structure and evolution of western marginal basins of India. *Tectonophysics*, *135*, 305–327. doi:10.1016/0040-1951(87)90115-6

Blair, D. P., & Armstrong, L. W. (2001). The influence of burden on blast vibration. Rock Fragmention by Blasting. *Fragblast*, *5*(1-2), 108–129. doi:10.1076/frag.5.1.108.3315doi:10.1076/frag.5.1.108.3315

Blair, S. C., & Cook, N. G. W. (1998). Analysis of compressive fracture in rock using statistical techniques: Part-I. A non-linear rule-based model. *International Journal of Rock Mechanics and Mining Sciences*, *35*, 837–848. doi:10.1016/S0148-9062(98)00008-4doi:10.1016/S0148-9062(98)00008-4

Bommer, J., Scherbaum, F., Bungum, H., Cotton, F., Sabetta, F., & Abrahamson, N. A. (2005). On the use of logic trees for ground-motion prediction equations in seismic hazard analysis. *Bulletin of the Seismological Society of America*, *95*, 377–389. doi:10.1785/0120040073

Boominathan, A. (2004). Seismic site characterization for nuclear structures and power plants. *Current Science*, *87*(10), 1388–1397.

Boominathan, A., Dodagoudar, G. R., Suganthi, A., & Uma Maheshwari, R. (2008). Seismic hazard assessment of Chennai city considering local site effects. *Journal of Earth System Science*, *117*(S2), 853–863. doi:10.1007/s12040-008-0072-4

Boore, D. M. (1983). Stochastic simulation of high-frequency ground motions based on seismological models of the radiated spectra. *Bulletin of the Seismological Society of America*, *237*(6), 68–78.

Boore, D. M. (2004). Estimating Vs(30) (or NEHRP Site Classes) from Shallow Velocity Models (Depths < 30 m). *Bulletin of the Seismological Society of America*, *94*(2), 591–597. doi:10.1785/0120030105

Borcherdt, R. D. (1996). Preliminary amplification estimates inferred from strong ground motion recordings of the Northridge earthquake of January 17, 1994. In *Proc. Int. Workshop on Site Response Subjected to Strong Ground Motion* (Vol. 1), Port and Harbor Research Institute, Yokosuka, Japan.

Borcherdt, R. D., & Glassmoyer, G. (1994). Influences of local geology on strong and weak ground motions recorded in the San Francisco Bay region and their implications for site-specific building-code provisions The Loma Prieta, California Earthquake of October 17, 1989-Strong Ground Motion. *U.S. Geol. Surv. Profess. Pap., 1551- A*, A77-A108

Borcherdt, R. D. (1994). Estimates of site-dependent response spectra for design (methodology and justification). *Earthquake Spectra*, *10*, 617–653. doi:10.1193/1.1585791

Borcherdt, R. D. (2002). Empirical evidence for acceleration-dependent amplification factors. *Bulletin of the Seismological Society of America*, *92*, 761–782. doi:10.1785/0120010170

Brady, B. H. (1990). Dynamic performance and design of underground excavations in jointed rock. In Brummer (Ed.), *Static and dynamic considerations of Rock Engineering* (pp.1-10), Balkema, Rotterdam.

Brinkman, J. R. (1989, August). Separating shock waves and gas expansion breakage mechanisms. In *Proceedings of the 2nd international symposium on rock fragmentation by blasting*, Keystone, CO.

Brown, E. T. (1970). Strength of Models of Rock with Intermittent joints. *J. Soil Mech. Fdns. Div. Am. Soc. Civ. Engrs.*, *96*(6), 1935–1949.

Brown, E. T., & Hudson, J. A. (1974). Fatigue failure characteristics of some models of jointed rock. *Earthquake Engineering & Structural Dynamics*, *2*, 379–386. doi:10.1002/eqe.4290020407

Brown, E. T., & Trollope, D. H. (1970). Strength of model of jointed rock. *Journal of the Soil Mechanics and Foundations Division*, *96*(2), 685–704.

BSSC. (2001). NEHRP recommended provisions for seismic regulations for new buildings and other structures 2000 edition, part 1: Provisions. *Report no. FEMA 368, Building seismic safety council for the federal emergency management agency*, Washington, D.C., USA.

Budhu, M. (2002). Virtual laboratories for engineering education. In *Proceedings of the International Conferance on Engineering Education* (CD-ROM), Manchester, U.K., International Network for Engineering Education and Research (INEER), Arlington, Va.

Budnitz, R. J., Apostolakis, G., Boore, D. M., Cluff, L. S., Coppersmith, K. J., Cornell, C. A., & Morris, P. A. (1997). Recommendations for probabilistic seismic hazard analysis: guidance on uncertainty and use of experts. *U.S. Nuclear Regulatory Commission Report* NUREG/CR- 6372.

Cai, M., Kaiser, P. K., Suorineni, F., & Su, K. (2007). A study on the dynamic behavior of the Meuse/Haute-Marne argillite. *Physics and Chemistry of the Earth*, *32*, 907–916.

Campbell, K. W. (1981). Near source attenuation of peak horizontal acceleration. *Bulletin of the Seismological Society of America*, *71*, 2039–2070.

CANMET. (1993). *The development of new blast damage criteria for blasthole mining operations* (DSS file 014sq.23440-1-9050).

Carlos, S. O., Antoni, R., & Xavier, G. (2006). *Assessing and managing earthquake risk.* Springer.

Century Dynamic Inc. (2003). *Autodyn theory manual* (Version 6.1).

Chakraborty, A.K., Raina, A.K., Ramulu, M., Jethwa, J.L., & Gupta, R.N. (1998, November). Lake Tap at Koyna, *World Tunnel. Subsurface Exc.* (pp. 456-460).

Chan, A. H. C. (1988). *User manual for DIANA SWANDYNE-II*. Department of civil engineering, University of Glasgow, UK.

Chang, F.K., & Krinitzsky, E.L. (1977). *Duration, spectral content and predominant period of strong motion earthquake records from Western United States*. Miscellaneous paper 5-73-1, U.S. Army Corps Engineers Waterways Experiment Station Vicksburg, Missipppi.

Chang, N. Y. (1990). *Influence of fines content and plasticity on earthquake-induced soil liquefaction*. contract No. DACW3988-C-0078, US Army WES, MS.

Chantawarungal, K. (1993). *Numerical simulations of three dimensional granular assemblies*. Ph.D. thesis, University of waterloo, waterloo, Ontario, Canada.

Charlie, W. A., Veyera, G. E., Doehring, D. O., & Abt, S. R. (1985 October 15). *Blast induced liquefaction potential and transient porewater pressure response of saturated sands*. Final Report to Air Force Office of Scientific Research, Grant No. AFOSR-80-0260.

Chen, C. S., Pan, E., & Amadei, B. (1998). Determination of deformability and tensile strength of anisotropic rock using Brazilian tests. *International Journal of Rock Mechanics and Mining Sciences*, *35*, 43–61. doi:10.1016/S0148-9062(97)00329-X

Chen, R., Huang, S., Xia, K., & Lu, F. (2009). A modified Kolsky bar system for testing ultrasoft materials under intermediate strain rates. *The Review of Scientific Instruments*, 80.

Chen, S. G., & Zhao, J. (1998). A study of UEDC modeling for blasting wave propagation in joint rock mass. *International Journal of Rock Mechanics and Mining Sciences*, *35*, 93–99. doi:10.1016/S0148-9062(97)00322-7

Chen, Y. P., Wang, S. J., & Wang, E. Z. (2007). Strength and elastic properties of sandstone under different testing conditions. *Journal of Central South University of Technology*, *14*, 210–215. doi:10.1007/s11771-007-0042-z

Cho, S. H., Miyake, H., Kimura, T., & Kaneko, K. (2003). Effect of the waveform of applied pressure on rock fracture process in one free-face. *J. Sc. Tech. Energetic Mat.*, *64*(3), 116–125.

Choudhury, D., & Nimbalkar, S. (2005). Seismic passive resistance by pseudo-dynamic method. *Geotechnique*, *55*(9), 699–702. doi:10.1680/geot.2005.55.9.699

Choudhury, D., & Nimbalkar, S. (2007). Seismic rotational displacement of gravity walls by pseudo-dynamic method: passive case. *Soil Dynamics and Earthquake Engineering*, *27*, 242–249. doi:10.1016/j.soildyn.2006.06.009

Ciccitti, M., & Mulargia, F. (2004). Differences between static and dynamic elastic moduli of a typical seismogenic rock. *Int. J. Geophysics*, *157*, 474–477. doi:10.1111/j.1365-246X.2004.02213.x

Clark, G. B. (1987). *Principles of rock fragmentation*. London: John Wiley & Sons Inc.

Clark, L. M., & Pakalnis, R. C. (1997). An empirical design approach for estimating unplanned dilution from open stope hanging-walls and footwalls. In *Proceedings of the 99th CIM Annual General Meeting*, Vancouver, Canada.

Coduto, D. P. (1999). *Geotechnical.* Upper Saddle River, NJ: Prentice Hall, Inc.

Coelho, P.A.L.F., Haigh, S.K., Madabhushi, S.P.G., & O'Brien, A.S. (2007). Post-earthquake behaviour of footings when using densification as a liquefaction resistance measure. *Ground Improvement Journal – Special Issue on Ground Improvement techniques, 11*(1), 45-53.

Connigham, C. V. B., & Goetzsche, A. F. (1996). The specification of blast damage limitations in tunneling contracts. *Tunnelling and Underground Space Technology*, *5*(3), 23–27.

Cornell, C. A. (1968). Engineering seismic risk analysis. *Bulletin of the Seismological Society of America*, *58*, 1583–1606.

Coviello, A., Lagioia, R., & Nova, R. (2005). On the measurement of the tensile strength of soft rocks. *Rock Mechanics and Rock Engineering*, *38*, 251–273. doi:10.1007/s00603-005-0054-7

Cramer, C.H., & Wheeler, R.L. (2001). The 2001 Gujarat, India earthquake and seismic hazard in central and Eastern North America. *Abstract in Seismological Research Letters, 72*, 396.

Cramer, C. H., & Kumar, A. (2003). 2001 Bhuj, India, earthquake engineering seismoscope recordings and Eastern North America ground motion attenuation relations. *Bulletin of the Seismological Society of America*, *93*, 1390–1394. doi:10.1785/0120020194

Crandell, F. J. (1949). Ground Vibrations Due to Blasting and Its Effect Upon Structures. *Journal of the Boston Society of Civil Engineers* (pp. 222-245).

Crum, S. V., Siskind, D. E., & Eltschlager, K. (1997). Blast vibration measurements at far distances and design influences on ground vibrations. In *Proceedings of Annual conference on Explosives and blasting research, explosives reference database on CD-ROM*. Montville, OH: International society of explosive engineers.

Cundall, P. A., & Strack, O. D. L. (1979). A discrete numerical model for granular assemblies. *Geotechnique*, *29*(1), 47–65. doi:10.1680/geot.1979.29.1.47

Curran, D. R., Seaman, L., & Shockey, D. A. (1987). Dynamic failure of solids. *Physics Reports*, *147*, 253–388. doi:10.1016/0370-1573(87)90049-4doi:10.1016/0370-1573(87)90049-4

Dai, J. (2002). *Dynamic Behaviors and Blasting Theory of Rock* (pp. 80–81). Beijing, China: Metallurgical Press.

Daniel, R. (2003). Pressure-time history of emulsion explosives. *Personal communications*.

Dawding, C., Labuz, J. F., & Shah, S. P. (1985). Experimental analysis of crack propagation in granite. *International Journal of Rock Mechanics and Mining Sciences*, *22*(2), 85–99. doi:10.1016/0148-9062(85)92330-7doi:10.1016/0148-9062(85)92330-7

Devine, J. F., Beck, R. H., Meyer, A. V. C., & Duvall, W. I. (1966). Effect of charge weight on vibration levels from quarry blasting. In *Proceedings of USBM (RI-6774)* (pp. 37-38).

Dey, K. (2004). *Investigation of blast-induced rock damage and development of predictive model in horizontal drivages* (pp. 45-103). Unpublished doctoral dissertation, Indian School of Mines, Dhanbad, India.

Dick, R. A., Larry, R., Fletcher, D., & Andrea, V. D. (1983). *Explosives and Blasting Procedures Manual*. Bureau of Mines.

Diederichs, M. S. (1999). *Instability of hard rockmasses: The role of tensile damage and relaxation*. Unpublished doctoral dissertation, University of Waterloo, Canada

Donze, F. V., Bouchez, J., & Magnier, S. A. (1997). Modelling fractures in rock blasting. *International Journal of Rock Mechanics and Mining Sciences*, *34*(8), 1153–1163. doi:10.1016/S1365-1609(97)80068-8doi:10.1016/S1365-1609(97)80068-8

Donze, F. V., Hotiet, N., & Bernasconi, P. (2002). Optimization of the blasting patterns in shaft sinking. In R. Hammah, W. Bawden, J. Curran, & M. Telesnicki (Eds.), *Proceedings of the 5th North American Rock Mech. Symp. (NARMS-TAC 2002)* (pp. 999-1005). Toronto, Canada: University of Toronto press.

Donze, F. V., Bouchez, J., & Magnier, S. A. (1997). Modeling fractures in rock blasting. *International Journal of Rock Mechanics and Mining Sciences*, *34*, 1153–1163. doi:10.1016/S1365-1609(97)80068-8

Doucet, C., Cameron, A., & Lizotte, Y. (1996, February 4-8). The effects of rock mass characteristics on fragmentation in controlled blasting experiments in small development headings. *ISEE's 22nd Annual Conference* (pp.1-11), Orlando, FL.

Dowding, C. H. (1985). *Blast Vibration monitoring*. Englewood Cliffs NJ: Prentice Hall.

Dowding, C. H. (1995). *Blast vibration monitoring and control*. Upper Saddle River, NJ: Prentice Hall.

Dowding, C. H., & Rozen, A. (1978). Damage to rock tunnels from earthquake loading. *J. Geotech. Eng. Div. ASCE*, *104*(GT2), 175–191.

du Pont, E. I. (1977). *Blasters Hand book* (175th Anniversary ed.). Wilmington, DE: E. I. du Pont de Nemours, Inc.

Duncan, J. M., & Mokwa, R. L. (2001). Passive earth pressures: theories and tests. *Journal of Geotechnical and Geoenvironmental Engineering*, *127*(3), 248–257. doi:10.1061/(ASCE)1090-0241(2001)127:3(248)

Duvall, I. W., & Devine, J. F. (1968). *Avoiding damage by air blasts and ground vibrations from blasting, Surface mining*. New York: AIMMPE Inc.

Einstein, H. H., & Hirschfeld, R. C. (1973). Models studies in mechanics of Jointed Rocks. *Journal of the Soil Mechanics and Foundations Division*, *99*, 229–248.

El Hosri, M. S., Biarez, J., & Hicher, P. Y. (1984). Liquefaction characteristics of silty clay. In *Proceedings of the 8th World Conference Earthquake Eng.* (Vol. 3) (pp. 277-84), San Francisco, CA.

EL Shamy, U. (2006). DEM Based computational Lab for Geotechnical Engineering Education. *GeoDenver*, GSP 166.

Elgamal, A., Fraser, M., & McMartin, F. (2005). Online educational shake table experiments. *Journal of Professional Issues in Engineering Education and Practice*, *131*(1), 41–49. doi:10.1061/(ASCE)1052-3928(2005)131:1(41)

Eurocode-8 (2005) BS-EN 1998-1, Design of structures for earthquake resistance – part 1: General rules, seismic actions and rules for buildings. *European committee for standardization*, Brussels.

Evans, I. (1961). The tensile strength of coal. *Colliery Engineering*, *38*, 428–434.

Fang, Y. S., Chen, T. J., & Wu, B. F. (1994). Passive earth pressures with various wall movements. *Journal of Geotechnical Engineering*, *120*(8), 1307–1323. doi:10.1061/(ASCE)0733-9410(1994)120:8(1307)

Field, E. H. (2000). A modified ground motion attenuation relationship for southern California that accounts for detailed site classification and a basin depth effect. *Bulletin of the Seismological Society of America*, *90*, S209–S221. doi:10.1785/0120000507

Field, E. H., & Jacob, K. H. (1993). The theoretical response of sedimentary layers to ambient seismic noise. *Geophysical Research Letters*, *20*, 2925–2928. doi:10.1029/93GL03054

Floyd, J. L., & Conn, D. B. (1997). PhotoSeis- an advanced method for vibration analysis and control. In *Proceedings of Annual conference on Explosives and blasting research, explosives reference database on CD-ROM*. Montville, OH: International society of explosive engineers.

Forsyth, W. W., & Moss, A. E. (1990). Observations of blasting and damage around development openings. In *Proceedings of the 92nd Canadian Institute Mining and Metallurgy, Annual General Meeting*, Ottawa, Canada (pp. 245-251).

Fourney, W. L., Dick, R. D., Wang, X. J., & Wei, Y. (1993). Fragmentation mechanism in crater blasting. *International Journal of Rock Mechanics and Mining Sciences & Geomechanics Abstracts*, *30*(4), 413–429. doi:10.1016/0148-9062(93)91723-Vdoi:10.1016/0148-9062(93)91723-V

Frankel, A. (1995). Mapping seismic hazard in the Central Eastern United States. *Seismological Research Letters*, *66*(4), 8–21.

Frankel, A., Mueller, C., Barnhard, T., Perkins, D., Leyendecker, E. V., & Dickman, N. (1996). National seismic hazard maps: documentation June 1996. *U.S. Geological Survey Open-file Report*, 96–532.

Frank, S., Bommer, J. J., Bungum, H., Cotton, F., & Abrahamson, N. A. (2005). Composite Ground-Motion Models and Logic Trees: Methodology, Sensitivities, and Uncertainties. *Bulletin of the Seismological Society of America*, *95*(5), 1575–1593. doi:10.1785/0120040229

Frantzos, D. C. (1989). *Finite element analysis of radial cracking mechanism around blastholes using measured pressure-time curves for low density ammonium nitrate/fuel oil*. Unpublished doctoral dissertation, Queen's University, Canada.

Free, M., May, R., & Teymur, B. (2003). Geological and Geotechnical Aspects, The Kocaeli, Turkey Earthquake of 17 August 1999. In D'Ayala & Free (Ed.), *A field report by EEFIT* (pp. 81-121). London, UK: Institute of Structural Engineers.

Freund, L. B. (1990). *Dynamic fracture mechanics*. Cambridge, UK: Cambridge University Press. doi:10.1017/CBO9780511546761doi:10.1017/CBO9780511546761

Frew, D. J., Forrestal, M. J., & Chen, W. (2001). A split Hopkinson pressure bar technique to determine compressive stress-strain data for rock materials. *Experimental Mechanics*, *41*, 40–46. doi:10.1007/BF02323102

Frew, D. J., Forrestal, M. J., & Chen, W. (2002). Pulse shaping techniques for testing brittle materials with a split Hopkinson pressure bar. *Experimental Mechanics*, *42*, 93–106. doi:10.1007/BF02411056

Gebbeken, N., & Greulich, S. (2006). Hugoniot propreties for concrete determined by full-scall detonation experiments and flyer-plate-impact tests. *International Journal of Impact Engineering*, *32*, 2017–2031. doi:10.1016/j.ijimpeng.2005.08.003

Georgiannou, V. N., Burland, J. B., & Hight, D. W. (1990). The undrained behaviour of clayey sands in triaxial compression and extension. *Geotechnique*, *40*(3), 431–449. doi:10.1680/geot.1990.40.3.431

Georgiannou, V. N., Hight, D. W., & Burland, J. B. (1991). Undrained behaviour of natural and model clayey sands. *Soil and Foundation*, *31*(3), 17–29.

Ghosh, A. A., & Daemen, J. J. K. (1983). *A new analytical predictor of ground vibrations induced by blasting, Volume IV* (Rep. to the office of surface mining).

Golshani, A., & Oda, M. (2007). Numerical simulation of the excavation damaged zone around an opening in brittle rock. *International Journal of Rock Mechanics and Mining Sciences*, *44*, 835–845. doi:10.1016/j.ijrmms.2006.12.005

Gordon, G., & Nies, D. (1997). Small Borehole Blasting In High Liability Locations. In *Proceedings of Annual conference on Explosives and blasting research, explosives reference database on CD-ROM*. Montville, OH: International society of explosive engineers.

Grady, D. E., & Kipp, M. E. (1993). Dynamic fracture and fragmentation. In J. R. Asay & M. Shahinpoor (Eds.), *High-pressure shock compression of solids* (pp. 265–322). New York: Springer.

Grady, D. E., & Kipp, M. E. (1980). Continuum Modeling of Explosive Fracture in Oil-Shale. *International Journal of Rock Mechanics and Mining Sciences*, *17*, 147–157. doi:10.1016/0148-9062(80)91361-3

Grady, D. E., & Kipp, M. E. (1987). *Dynamic rock fragmentation. Fracture mechanics of rock* (pp. 34–46). London: Atkinson B. K.

GSI. (2000). *Seismotechnic Atlas of India*. New Delhi: Geology Society of India.

Guo, T., & Prakash, S. (2000). Liquefaction of silt-clay mixtures. In *Proceedings of the 12th World Conferance Earthq. Eng.*, New Zealand.

Hanumantharao, C., & Ramana, G. V. (2008). Dynamic soil properties for microzonation of Delhi India. *Journal of Earth System Science*, *117*(S2), 719–730. doi:10.1007/s12040-008-0066-2

Hao, H., Ma, G. W., & Zhau, Y. X. (1998). Numerical simulation of underground explosions. *Int. J. Blasting by Fragmentation (Fragblast)*, *2*, 383–395.

Hao, H., Wu, C., & Zhou, Y. (2002). Numerical analysis of blast-induced stress waves in a rock mass with anisotropic continuum damage models, Part I: equivalent material property approach. *Rock Mechanics and Rock Engineering*, *35*(2), 79–94. doi:10.1007/s006030200012doi:10.1007/s006030200012

Hart, R. D. (1993). An introduction to distinct element modelling for rock engineering. In J. A. Hudson (Ed.), *Comprehensive rock engineering* (*Vol. 2*, pp. 245–261). Oxford, UK: Pergamon Press.

Hartzell, S. A., Carver, D., Cranswick, E., & Frankel, A. (2000). Variability of site response in Seattle, Washington. *Bulletin of the Seismological Society of America*, *90*, 1237–1250. doi:10.1785/0120000022

Hazarika, H., & Boominathan, A. (2009, June15-18). Liquefaction and ground failures during the 2001 Bhuj Earthquake India. In *Proceedings of International Conference on Performance-Based Design in Earthquake Geotechnical Engineering from case history to practice*, Tokyo, Japan, Chapter 13, (in CD ROM).

Hazzard, J. F., Young, R. P., & Maxwell, S. C. (2000). Micromechanical modeling of cracking and failure in brittle rocks. *Journal of Geophysical Research*, *105*(B7), 16683–16697. doi:10.1029/2000JB900085doi:10.1029/2000JB900085

Heiling, J., Zeitsas, A., & Cox, N. (1997). Free face blasting is it the best for quarrying. In *Proceedings of the 41st Annual Conf.* (pp. 33-44). Australia: Institute of Quarrying.

Hendron, A. J. (1977). Engineering of Rock Blasting on Civil Projects. In W.J. Hall (Ed.) *Structural and Geotechnical Mechanics*. Prentice-Hall, Inc.

Henning, J. G., Kaiser, P. K., & Mitri, H. S. (2001, July). Evaluation of stress influences on ore dilution: a case study. In *Proceedings of the 38th U.S. Rock Mechanics Symposium*, Washington, DC.

Henning, J. G., & Mitri, H. S. (1999). Examination of hanging-wall stability in a weak rock mass. *CIM Bulletin*, *92*(1032).

Hilleborg, A., Modeer, M., & Petersson, P. E. (1976). Analysis of Crack Formation and Crack Growth in Concrete by Means of Fracture Mechanics and Finite Elements. *Cement and Concrete Research*, *6*, 773–782. doi:10.1016/0008-8846(76)90007-7doi:10.1016/0008-8846(76)90007-7

Hobbs, D. W. (1964). The strength and the stress strain characteristics of coal in triaxial compression. *The Journal of Geology*, *72*, 214–231. doi:10.1086/626977

Hobbs, D. W. (1970). Stress-Strain-Time Behaviour of a Number of Coal Measure Rocks. *International Journal of Rock Mechanics and Mining Sciences*, *7*, 149. doi:10.1016/0148-9062(70)90009-4

Holmberg, R. (1993). *Recent developments in control rock damage.* In A.A. Balkema & Rossamanith (Ed.), *Rock Fragmentation by Blasting* (pp. 197-198). Rotterdam.

Holmberg, R., & Persson, P. A. (1978, February 1-3). The Swedish Approach to Contour Blasting. *Conference on Explosives and Blasting Technique*. Society of Explosives Engineers, New Orleans, Louisiana, USA.

Holmberg, R., & Persson, P. A. (1980). Design of Tunnel Perimeter Blast Hole Patterns to Prevent Rock Damage. *Transactions of the Institution of Mining and Metallurgy*, *89*, A37–A40.

Housner, G. W., & Theil, C. C. (1995). The continuing challenge: report on the performance of the state bridges in the Northridge earthquake. *Earthquake Spectra*, *11*(4), 569–615. doi:10.1193/1.1585829

Hudson, J. A. (1969). Tensile strength and ring test. *International Journal of Rock Mechanics and Mining Sciences*, *6*, 91–97. doi:10.1016/0148-9062(69)90029-1

Hudson, J. A., Rummel, F., & Brown, E. T. (1972). The controlled failure of rock disks and rings loaded in diametral compression. *International Journal of Rock Mechanics and Mining Sciences*, *9*, 241–248. doi:10.1016/0148-9062(72)90025-3

Hunt, R. E. (2005). *Geotechnical Investigation Handbook* (2nd ed.). Boca Raton, FL: Taylor & Francis.

Ibarra, J. A., Maerz, N. H., & Franklin, J. A. (1996). Overbreak and underbreak in underground openings Part 2: causes and implications. *Geotechnical and Geological Engineering*, *14*(3), 325–340. doi:10.1007/BF00421947

Idriss, I. M., & Sun, J. I. (1992). *SHAKE91: A computer program for conducting equivalent linear seismic response analyses of horizontally layered soil deposits*. Center for Geotechnical Modeling, Department of Civil and Environmental Engineering, University of California, Davis, 130.

IS 1893 (Part 1). 2002 *Indian Standard Criteria for Earthquake Resistant Design of structures: Part 1 General Provisions and Buildings* (5th Revision).

IS. (1979). *Determination of unconfined compression strength of Rock materials*. New Delhi, India: Bureau of Indian Standards.

Ishihara, K. (1993). Liquefaction and flow failure during earthquakes. *Geotechnique*, *43*(3), 351–41. doi:10.1680/geot.1993.43.3.351

Ishihara, K., & Yoshimine, M. (1992, March). Evaluation of settlements in sand deposits following liquefaction during earthquakes. *Soil and Foundation*, *32*(1), 173–188.

ISRM Committee on Laboratory tests. (1977). *Suggested methods for determining Uniaxial compressive strength of Rock Materials* (Document No.1, First Revision). Lisboa, Portugal: ISRM.

ISRM. (1992). Commission on Testing methods. *Suggested methods for installation of borehole extensometer*. International Society for Rock Mechanics.

Jaeger, J. C., & Cook, N. G. W. (1979). *Fundementals of rock mechanics* (3rd ed.). London, UK: Chapman & Hall.

Jimeno, C. L., Jimeno, E. L., & Carcedo, F. J. A. (1995). *Drilling and Blasting of Rocks* (pp. 183–184). Rotterdam, The Netherlands: A. A. Balkema.

Jung, W. J., Utagava, M., Ogata, Y., Seto, M., Katsuyama, K., Miyake, A., & Ogava, T. (2001). Effects of rock pressure on crack generation during tunnel blasting. *Jl. Japan Explosives Soc.*, *62*(3), 138–146.

Kaila, K. L., Krishna, V. G., & Mall, D. M. (1981). Crustal structure along Mehmedabad-Billimora profile in the Cambay basin, India, from deep seismic sounding. *Tectonophysics*, *76*, 99–130. doi:10.1016/0040-1951(81)90255-9

Kaila, K. L., Tewari, H. C., Krishna, V. G., Dixit, M. M., Sarkar, D., & Reddy, M. S. (1990). Deep seismic sounding studies in the north Cambay and Sanchor basins, India. *Geophysical Journal International*, *103*, 621–637. doi:10.1111/j.1365-246X.1990.tb05676.x

Kanagalingam, T., & Thevanayagam, S. (2006). Energy dissipation and liquefaction assessment in sands and silty soils. ASCE. In D. J. DeGroot et al. (Eds.), *Geotechnical Engineering in the Information Age*, I0-7844-0803-3.

Kexin, D. (1995). Maintenance of roadways in soft rock by roadway-rib destress blasting. *China Coal Society*, *20*(3), 311–316.

Khosrou, S. H., & Mohanty, B. (1996). Role of discontinuity on stress-field in wall control blasting. In B. Mohanty (Ed.), *Proceedings of the 5th int. sym. rock fragmentation by blasting (FRAGBLAST5)*, Montreal, Canada (pp. 207-216). Rotterdam, The Netherlands: Balkema.

Kijko, A., & Graham, G. (1998). Parametric-historic procedure for probabilistic seismic hazard analysis, Part I: Estimation of maximum regional magnitude Mmax. *Pure and Applied Geophysics*, *152*, 413–442. doi:10.1007/s000240050161

Kikuchi, N. (1983). Remarks on 4CST elements for incompressible materials. *Computer Methods in Applied Mechanics and Engineering*, *37*, 109–123. doi:10.1016/0045-7825(83)90144-5doi:10.1016/0045-7825(83)90144-5

Kim, H.-Y., Lee, K.-W., Mizuta, Y., & Lee, H.-K. (1990). A study on determination of the relaxed zone around an excavated tunnel. In Brummer (Ed.), *Static and dynamic considerations of Rock Engineering,* Rotterdam: Balkema (pp. 177-182).

Koester, J. P. (1994). The influence of fines type and conent on cyclic strength. In Proceedings of the ASCE Conv., Atlanta. *Geotech. Spec. Pub. 44*, 17-32.

Koltonski, & Malecki. (1958). Ultrasonic method for exploration of the properties and structure of mineral layers. *Acustica, 8*, 307-314.

Konya, C. J. (1995). *Airblast monitoring and control blast design*. Montville, OH: Int. Development Corporation.

Kramer, S. L. (1996) *Geotechnical earthquake engineering*. New York: Prentice Hall.

Kramer, S. L., & Stewart, J. P. (2004). *Geotechnical aspects of seismic hazards; In Earthquake Engineering from Engineering Seismology to Performance Based Engineering.* CRC press.

Kranz, R. I. (1983). Microcracks in rocks: a review. *Tectonophysics*, *100*, 449–480. doi:10.1016/0040-1951(83)90198-1doi:10.1016/0040-1951(83)90198-1

Krauthammer, T. (1999). Blat-resistant structural concrete and steel connection. *International Journal of Impact Engineering*, *22*, 887–910. doi:10.1016/S0734-743X(99)00009-3

Krautkrammer, J., & Krautkrammer, H. (1993). *Ultrasonic testing of materials*. New Delhi, India: Narosa Publishing House.

Krinitzsky, E. L. (2002). How to obtain earthquake ground motions for engineering design. *Engineering Geology*, *65*, 1–16. doi:10.1016/S0013-7952(01)00098-9

Krinitzsky, E. L. (2003). How to combine deterministic and probabilistic methods for assessing earthquake hazards. *Engineering Geology*, *70*, 157–163. doi:10.1016/S0013-7952(02)00269-7

Kubota, S., Ogata, Y., Wada, Y., Simangunsong, G., Shimada, H., & Matsui, K. (2008). Estimation of dynamic tensile strength of sandstone. *International Journal of Rock Mechanics and Mining Sciences*, *45*, 397–406. doi:10.1016/j.ijrmms.2007.07.003

Kumar, J. (2001). Seismic passive earth pressure coefficients for sands. *Canadian Geotechnical Journal*, *38*, 876–881. doi:10.1139/cgj-38-4-876

Kumar, J., & Subba Rao, K. S. (1997). Passive pressure coefficients, critical failure surface and its kinematic admissibility. *Geotechnique*, *47*(1), 185–192. doi:10.1680/geot.1997.47.1.185

Kutter, H. K., & Fairhurst, C. (1971). On the fracture process in blasting. *International Journal of Rock Mechanics and Mining Sciences*, *8*, 181–202. doi:10.1016/0148-9062(71)90018-0doi:10.1016/0148-9062(71)90018-0

Kutter, H. K., & Fairhurst, C. (1971). On the Fracture Process in Blasting. *International Journal of Rock Mechanics and Mining Sciences*, *8*, 181–202. doi:10.1016/0148-9062(71)90018-0

Kwon, S., Lee, C. S., Cho, S. J., Jeon, S. W., & Cho, W. J. (2009). An investigation of the excavation damaged zone at the KAERI underground research tunnel. *Tunnelling and Underground Space Technology*, *24*, 1–13. doi:10.1016/j.tust.2008.01.004

Laine, L., & Sandvik, A. (2001, November). Derivation of mechanical properties for sand. In T. S. Lok (Ed.), *Proceedings of the fourth Asia-Pacific conference on shock & impact loads on structures*, Singapore (pp. 361-368).

Langefors, U., & Kihlstrom, B. (1963). *The modern techniques of rock blasting*. New York: J. Wiley and Sons, Inc.

Law, T. M., May, J., Spathis, A. T., Du Plessis, A. T., & Palmer, A. M. (2001). Blast damage and blast dilution control: The applicaton of bulk emulsion systems at the WMC St Ives junction mine. *J. Rock Fragmentation by Blasting (Fragblast)*, *5*(1-2), 1–20.

LeBlanc, T., Heilig, J., & Ryan, J. (1995). Predicting the Envelope of Damage from the Detonation of a Confined Charge. In *Proceedings of the Sixth High-Tech Seminar on the State of the Art in Blasting Technology Instrumentation and Explosives Applications* (pp. 225–291), Massachusetts, USA.

Lee, K.L., & Albaisa, A. (1974). Earthquake induced settlements in saturated sands. *J. Geotech. Eng. Div., ASCE, 100*(4), 387-406.

Leet, L. D. (1946) *Vibrations from Blasting* (p. 34). Wilmington, DE: Hercules Powder Co.

Lee, Y., & Anderson, J. G. (2000). A custom southern California ground motion relationship based on analysis of residuals. *Bulletin of the Seismological Society of America*, *90*, S170–S187. doi:10.1785/0120000509

Lew (2001). *The Seismic Design Handbook.* Kluwer academic publishers.

Lewandowski, T., Luan Mai, V. K., & Danell, R. (1996, August). Influence of discontinuities on presplitting effectiveness. In *Proceedings of 5th Int. Symposium on Rock Fragmentation by Blasting* (pp. 217-225), Montrial, Canada.

Lima, A. D. R., Romanel, C., Roehl, D. M., & Araujo, T. D. (2002). An adaptive strategy for the dynamic analysis of rock fracturing by blasting. In *Proceedings of the Int. Conf. Computational Eng. & Sci*. (ICES'02), Reno, NV.

Liu, L. (1997). *Continuum modelling of rock fragmentation by blasting*. Unpublished doctoral dissertation, Queen's university, Canada.

Liu, L., & Katsabanis, P. D. (1997). Development of a continuum damage model for blasting analysis. *International Journal of Rock Mechanics and Mining Sciences*, *34*(2), 217–231. doi:10.1016/S0148-9062(96)00041-1doi:10.1016/S0148-9062(96)00041-1

Liu, Q., Tran, H., Counter, D., & Andrieux, P. (1998). A case study of blast damage evaluation in open stope mining at Kidd Creek mines. In the *24th Annual Conference on Explosives and Blasting Research* (pp. 323-336), New Orleans, LA.

Lobo-Guerrero, S., & Vallejo, L. E. (2006, February 26-March 1). DEM as an educational tool in geotechnical engineering. In *Proceedinhgs of the Geocongress 2006*, Atlanta, GA.

Lunne, T., Robertson, P. K., & Powell, J. J. M. (1997). Cone Penetration Testing in Geotechnical Practice. *Blackie Academic & Professional,* London.

Luong, M. P., & Sidaner, J. F. (1981). Undrained behaviour of cohesionless soils under cyclic and transient loading. In *Proceedings of the Int. Conf. Rec. Advances in Geotechnical Earthquake engineering and soil dynamics* (Vol. 1.) (pp. 215-220), St Louis, MI.

Madabhushi, S. P. G. (2007). Geotechnical Aspects of the 921 Ji-Ji earthquake of Taiwan. *EEFIT Report* (pp. 14-38). London, UK: Institution of Structural Engineers.

Madabhushi, S. P. G., & Zeng, X. (1993). An analysis of the seismic behaviour of quay walls. In K. Arulanandan & R.F. Scott (Ed.), *Proceedings Verification of Liquefaction Analyses by Centrifuge studies*, (VELACS), (Vol. 2), Davis, California.

Madabhushi, S. P. G., Knappett, J. A., & Haigh, S. K. (2009). *Design of pile foundations in liquefiable soils*. Imperial College Press. ISBN 978-1-84816-362-1.

Madabhushi, S. P. G., Patel, D., & Haigh, S. K. (2005). Geotechnical Aspects of the Bhuj Earthquake. *EEFIT Report*. London, UK, Institution of Structural Engineers. ISBN 0901297 372.

Madabhushi, S. P. G., & Zeng, X. (1998). Behaviour of gravity quay walls subjected to earthquake loading. Part II: Numerical Modelling. *Journal of Geotechnical Engineering. American Society of Civil Eng.*, *124*(5), 418–428.

Madabhushi, S. P. G., & Zeng, X. (2006). Seismic Response of Flexible Cantilever Retaining Walls with Dry Backfill, *Geomechanics and Geoengineering. International Journal (Toronto, Ont.)*, *1*(4), 275–290.

Madabhushi, S. P. G., & Zeng, X. (2007). Simulating Seismic Response of Cantilever Retaining Walls with Saturated Backfill. *ASCE Journal of Geotechnical and GeoEnv. Engineering*, *133*(5), 539–549.

Ma, G. W., & An, X. M. (2008). Numerical simulation of blasting-induced rock fractures. *International Journal of Rock Mechanics and Mining Sciences*, *45*, 966–975. doi:10.1016/j.ijrmms.2007.12.002

Ma, G. W., Hao, H., & Zhou, Y. X. (1998). Modeling of wave propagation induced by underground explosion. *Computers and Geotechnics*, *22*, 283–303. doi:10.1016/S0266-352X(98)00011-1

Makdisi, F. I., & Seed, H. B. (1978). Simplified procedure for estimating dam and embankment earthquake induced deformations. *Journal of Geotechnical Engineering*, *104*(7), 1427–1434.

Malan, D. F., & Napier, J. A. L. (1995). Computer modelling of granular material microfracturing. *Tectonophysics*, *248*, 21–37. doi:10.1016/0040-1951(95)00019-Jdoi:10.1016/0040-1951(95)00019-J

McGarr, A. (1983). Estimating ground motion for small nearby earthquakes. In *seismic design of embankments and caverns* (pp. 113-127). New York: ASCE.

McHugh, S., & Keough, D. (1982). Use of laboratory derived data to predict fracture and permeability enhancement in explosive pulse tailored field tests. In *Proceedings of the US Symp. Rock Mech., Issues in Rock Mech* (pp. 504-514).

Mckenzie, C. K. (1993). Methods of improving blasting operations. In J. A. Hudson (Ed.), *Comprehensive Rock Engineering* (*Vol. 4*, pp. 71–94). Oxford, UK: Pergamon Press.

McKenzie, C., Scherpenisse, C., Arriagada, J., & Jones, J. (1995). Application of Computer Assisted Modelling to Final Wall Blast Design. In *Proceedings of the EXPLO'95 – A Conference Exploring the Role of Rock Breakage in Mining and Quarrying* (pp. 285–292), Brisbane, Australia.

McKown, A. (1984). Some aspects of design and evaluation of perimeter controlled blasting in fractured and weathered rock. In *Proceedings of the 10th Conference on explosive and blasting techniques* (pp. 261-269).

Mclamore, R., & Gray, K. E. (1967). Mechanical behavior of anisotropic sedimentary rocks. *Journal of Engineering for Industry*, *89*, 62–67.

Mellor, M., & Hawkes, I. (1971). Measurement of tensile strength by diametral compression of discs and annuli. *Engineering Geology*, *5*, 173–225. doi:10.1016/0013-7952(71)90001-9

Meyer, T., & Dunn, P. G. (1996). Fragmentation and Rock mass Damage Assessment – Sunburst Excavator and Drill and Blast. In *Proceedings of the NARMS 1996 – Rock Mechanics Tools and Techniques* (pp. 609–617).

Miller, F., Potvin, Y., & Jacob, D. (1992). Laser measurement of open stope dilution. *CIM Bulletin*, *85*(962).

Morrison, E. E., & Ebeling, R. M. (1995). Limit equilibrium computation of dynamic passive earth pressure. *Canadian Geotechnical Journal*, *32*, 481–487.

Mortazavi, A., & Katsabanis, P. D. (2001). Modelling burden size and strata dip effects on the surface blasting process. *International Journal of Rock Mechanics and Mining Sciences*, *38*, 481–498. doi:10.1016/S1365-1609(01)00015-6doi:10.1016/S1365-1609(01)00015-6

Mosinets, V. N., & Gorbacheva, N. P. (1972). A seismological method of determining the parameters of the zones of deformation of rock by blasting. *Soviet Mining Science*, *8*(6), 640–647. doi:10.1007/BF02497586doi:10.1007/BF02497586

Murthy, V. M. S. R., & Dey, K. (2003, September). Predicting Overbreak From Blast Vibration Monitoring In Lake Tap Tunnel – A Success Story. In. *Proceedings of FRAGBLAST*, *7*(3), 149–166. doi:10.1076/frag.7.3.149.16787

Nadim, F., & Whitman, R. V. (1983). Seismically induced movement of retaining walls. *Journal of Geotechnical Engineering*, *109*(7), 915–931. doi:10.1061/(ASCE)0733-9410(1983)109:7(915)

Nakamura, Y. (1989). A method for dynamic characteristics estimation of subsurface using microtremor on the ground surface. *Quarterly Report of the Railway Technical Research Institute*, *30*(1), 25–33.

Napier, J. A. L., Daehnke, A., Dede, T., Hildyard, M. W., Kujipers, J. S., & Malan, D. (1997). Quantification of stope fracture zone behaviour in deep level gold mines. *J. SAIMM*, *97*, 119–134.

Nashed, R., Thevanayagam, S., & Martin, G. R. (2009). Densification and Liquefaction Mitigation of Saturated Silty Soils by Dynamic Compaction – Design. *Ground Improvement Journal*, Institute of Civil Engineers, UK.

Nazarian, S., & Stokoe, K.H. (1983). *Use of spectral analysis of surface waves for determination of moduli and thicknesses of pavement systems*. Transportation Research Record No. 954.

Neelima Satyam, D., & Rao, K. S. (2009). Dynamic site characterization in Delhi region using MASW testing. *International Journal of Earth Sciences and Engineering*, *2*(1), 32–42.

Newmark, N. M. (1965). Effects of earthquakes on dams and embankments. *Geotechnique*, *15*(2), 139–160. doi:10.1680/geot.1965.15.2.139

Niklasson, B. (1985). Vertical crater retreat mining at the Luossavaara research mine, Swedish Detonic Research Foundation. In *11th Annual Conference on Explosives and Blasting Research* (pp.46-61), San Diego, CA.

Nimbalkar, S. S., & Choudhury, D. (2008). Effects of body waves and soil amplification on seismic earth pressures. *Journal of Earthquake and Tsunami*, *2*(1), 33–52. doi:10.1142/S1793431108000256

Ni, Q., Tan, T. S., Dasari, G. R., & Hight, D. W. (2004). Contribution of fines to the compressive strength of mixed soils. *Geotechnique*, *54*(9), 561–569.

Nutting, M. J., & Froedge, D. T. (1997). The Mapping Of Vibration Patterns Around A Blast. In *Proceedings of Annual conference on Explosives and blasting research, explosives reference database on CD-ROM*. Montville, OH: International society of explosive engineers.

Okubo, S., & Fukui, K. (1996). Complete stress-strain curves for various rock types in uniaxial tension. *International Journal of Rock Mechanics and Mining Sciences & Geomechanics Abstracts*, *33*, 549–556. doi:10.1016/0148-9062(96)00024-1

Okubo, S., Fukui, K., & Qi, Q. X. (2006). Uniaxial compression and tension tests of anthracite and loading rate dependence of peak strength. *International Journal of Coal Geology*, *68*, 196–204. doi:10.1016/j.coal.2006.02.004

Olson, M., & Bergqvist, I. (1996). Crack lengths from explosives in small diameter boreholes. In Rossamanith (Ed.), *Rock Fragmentation by Blasting*. Rotterdam: A.A. Balkema (pp. 193-198).

Olsson, M., & Bergqvist, I. (1995). *Crack propagation in rock from multiple hole blasting* (Part 1, SveBeFo Rep. No. 18). Stockholm, Sweden: Swedish Rock Engineering Research. Paine, A. S., & Please, C. P. (9994). An improved model of fracture propagation by gas during rock blasting-some analytical results. *International Journal of Rock Mechanics and Mining Sciences*, *31*, 699–706.

Oriard, L. L. (1989, February 5-10). The Scale of Effects in Evaluating Vibration Damage Potential. In *Proceedings of the 15th Annual Conference on Explosives and Blasting Research, International Society of Explosives Engineers* (pp.161-176), New Orleans, LA.

Oriord, L. L. (1982). Blasting effects and their control. *Underground Mining Methods Handbook*, SME of AIME (pp. 1590-1603), Littleton, Colorado.

Otuonye, F. O. (1997). Dynamic response of a fully grouted resin roof bolt to blast loading. In *Proceedings of Annual Conferance on Explosives and Blasting Research,* Explosives Reference Database on CD-ROM. Int. Society of Explosive Engineers, Ohio, USA.

Ouchterlony, F., Sjoberg, C., & Jonsson, B. A. (1993). Blast damage prediction from vibration measurements at the SKB underground laboratories at ÄSPÖ in Sweden. *Intl. Soc. Explosive Engg*. (pp. 189-197), San Diego, CA.

Ouchterlony, F. (1997). Prediction of crack lengths in rock after cautious blasting with zero interholedelay. *Int. J. Rock Fragmentation by Blasting*, *1*, 417–444.

Paventi, M., Lizotte, Y., Scoble, M., & Mohanty, B. (1995, August 23-24). Measuring rockmass damage in drifting. In *Proceedings of Rock fragmentation by blasting, FRAGBLAST-5*, Montreal, Canada (pp. 131-138).

Paventi, M., Lizotte, Y., Scoble, M., & Mohanty, B. (1996). Measuring rock mass damage in drifting. In Mohanty (Ed.), *Rock Fragmentation by Blasting* (pp. 131-138).

Persson, P. A., Holmberg, R., & Lee, J. (1994). *Rock Blasting and Explosives Engineering* (p. 540), Boca Raton, FL: CRC press Inc.

Petersen, M. D., Rastogi, B. K., Schweig, E. S., Harmsen, S. C., & Gomberg, J. S. (2004). *Sensitivity analysis of seismic hazard for the northwestern portion of the state of Gujarat, India.*

Pitman, T. D., Robertson, P. K., & Sego, D. C. (1994). Influence of fines on the collapse of loose sands. *Canadian Geotechnical Journal*, *31*, 728–739. doi:10.1139/t94-084

Prasad, U., Mohanty, B., & Nemes, J. A. (2000). Dynamic Fragmentation of Selected Rocks Under Impact Loading. In *Proceedings of the 4th North American Rock Mech. Symp.*, Seattle, WA (pp. 577-581).

Pyke, R., Seed, H. B., & Chan, C. K. (1975). Settlement of sands under multi directional shaking. *Journal of the Geotechnical Engineering Division*, *101*(4), 379–397.

Raghu Kanth, S. T. G., & Iyengar, R. N. (2006). Seismic hazard estimation for Mumbai city. *Current Science*, *91*(11), 1486–1494.

Raghu Kanth, S. T. G., & Iyengar, R. N. (2007). Estimation of Seismic Spectral Acceleration in Peninsular India. *Journal of Earth System Science*, *116*(3), 199–214. doi:10.1007/s12040-007-0020-8

Raina, A. K., Ramulu, M., Chakraborty, A. K., Choudhury, P. B., & Bandopadhay, C. (2004). *Monitoring and control of blast vibrations in dragline bench of Sasti OCP, WCL* (pp. 2-10). Unpublished CMRI internal Report.

Ramamurthy, T. (1993). Strength and modulus responses of anisotropic rocks. In Hudson, J. A. (Ed.), *Comprehensive rock engineering* (*Vol. 1*, pp. 313–329). Oxford, UK: Pergamon Press.

Ramamurthy, T., & Arora, V. K. (1994). Strength prediction for jointed rocks in confined and unconfined states. *International Journal of Rock Mechanics and Mining Sciences & Geomechanics Abstracts*, *31*(1), 9–22. doi:10.1016/0148-9062(94)92311-6

Ramshaw, C. L., Selby, A. R., & Bettess, P. (1998). Computation of the transmission of waves from pile driving. In B. O. Skipp (Ed.), *ground dynamics and man made processes* (pp. 115–128). London: T. Telford Pub.

Ramulu, M., Chakraborty, A. K., & Raina, A. K. (2004). *Blast optimization and Ground Vibration Monitoring at Malanzkhand Copper Project, Malanzkhand* (pp. 15-25). Unpublished CMRI internal Report.

Ramulu, M., Chakraborty, A. K., Raina, A. K., & Reddy, A. H. (2004). Influence of burden on the intensity of ground vibrations and air overpressure in opencast bench blasting. In *Proceedings of the ISEE's 30th Annual Conference on Explosives and Blasting Techniques*, New Orleans, LA (pp. 465-478).

Ramulu, M., Chakraborty, A. K., Raina, A. K., Choudhury, P. B., Jethwa, J. L., & Singh, T. N. (1998). *Blast Induced Ground Vibration Monitoring at Lakshmi Cement Limestone mines, Rajasthan* (pp. 12-17). Unpublished CMRI internal Report.

Ramulu, M., Chakraborty, A. K., & Sitharam, T. G. (2009). Damage assessment of basaltic rock mass due to repeated blasting in a railway tunnelling project – a case study. *Tunnelling and Underground Space Technology*, *24*, 208–221. doi:10.1016/j.tust.2008.08.002

Rastogi, B. K. (2001). Ground deformation study of Mw 7.7 Bhuj earthquake of 2001. *Episodes*, *24*, 160–165.

Regulatory Guide 1.165 (1997). *Identification and characterization of seismic sources and determination of safe shutdown earthquake ground motion*. Published by U.S. Nuclear Regulatory Commission.

Reiter, L. (1990). *Earthquake hazard analysis – Issues and Insights*. New York: Columbia University Press.

Repetto, E. A., Radovitzky, R., & Ortiz, M. (2000). Finite element simulation of dynamic fracture and fragmentation of glass rods. *Computer Methods in Applied Mechanics and Engineering*, *183*, 3–14. doi:10.1016/S0045-7825(99)00208-Xdoi:10.1016/S0045-7825(99)00208-X

Richards, R., & Elms, D. G. (1979). Seismic behavior of gravity retaining walls. *Journal of the Geotechnical Engineering Division*, *105*(4), 449–464.

Richards, R., Elms, D. G., & Budhu, M. (1990). Dynamic fluidization of soils. *Journal of Geotechnical Engineering*, *116*(5), 740–759. doi:10.1061/(ASCE)0733-9410(1990)116:5(740)

Rockwell, E. H. (1927). Vibrations caused by quarry blasting and their effect on structures. *Rock Products*, *30*, 58–61.

Rocque, P. (1992). Techniques utilized for the detection and characterization of blast induced damage. Unpublished M. Sc. Eng. Thesis. Ontario, Canada: Queen's University at Kingston.

Rodriguez-Marek, A., Bray, J. D., & Abrahamson, N. A. (2001). An empirical geotechnical seismic site response procedure. *Earthquake Spectra*, *17*(1), 65–87. doi:10.1193/1.1586167

Rollins. (1980). *Energy partitioning* (Tech. Rep.). Rolla, Missouri: University of Missouri Rolla, Rock mechanics and explosive research center.

Ross, C. A., Tedesco, J. W., & Kuennen, S. T. (1995). Effects of Strain-Rate on Concrete Strength. *Aci Materials Journal*, *92*, 37–47.

Ross, C. A., Thompson, P. Y., & Tedesco, J. W. (1989). Split-Hopkinson Pressure-Bar Tests on Concrete and Mortar in Tension and Compression. *Aci Materials Journal*, *86*, 475–481.

Roy, N. (1993). *Engineering behaviour of rock masses through study of jointed models*. Unpublished doctoral dissertation, Indian Institute of Technology, Delhi, India.

Rustan, A. (1998). *Rock blasting terms and symbols*. Rotterdam, The Netherlands: A. A. Balkema.

Rustan, A., & Lin, N. S. (1983). New method to test the rock breaking properties of explosives in full scale. In *Proceedings of the First International Symposium on Rock Fragmentation by Blasting*, Lulea, Sweden (pp. 36-47).

Ryu, C. H. (2002). Computer modeling of dynamic ground motion due to explosive blasting and review of some modeling problems. *J. Japan Explosives Society*, *63*(5), 217–222.

Saharan, M. R., & Mitri, H. S. (2008). Numerical Procedure for Dynamic Simulation of Discrete Fractures due to Blasting. *Rock Mechanics and Rock Engineering*, *41*(5), 641–670. doi:10.1007/s00603-007-0136-9doi:10.1007/s00603-007-0136-9

Saharan, M. R., & Mitri, H. S. (2009). *Numerical Simulation for Rock Fracturing by Destress Blasting- As Applied to Hard Rock Mining Conditions*. Berlin: VDM Verlag. ISBN 978-3-639-11064-7

Saharan, M. R., Mitri, H. S., & Jethwa, J. L. (2006). Rock fracturing by explosive energy: Review of state-of-the-art. *Fragblast*, *10*(1-2), 61–81. doi:10.1080/13855140600858792

Saiang, D., & Nordlund, E. (2009). Numerical Analyses of the Influence of Blast-Induced Damaged Rock Around Shallow Tunnels in Brittle Rock. *Rock Mechanics and Rock Engineering*, *42*, 421–448. doi:10.1007/s00603-008-0013-1

Sames, F. (1999). The influence of blast parameters on vibration and air overpressure. In *Proceedings of the 6th Int. Symposium on Rock Fragmentation by Blasting (FRAGBLAST-6)*, Johansberg, South Africa (pp. 149-154).

Schnabel, P. M., Lysmer, J., & Seed, H. B. (1972). *SHAKE: A computer program for earthquake response analysis of horizontally layered sites*. Report No. EERC 72/12, Earthquake Engineering Research Centre, University of California, Berkley.

Schofield, A. N. (1981), Dynamic and earthquake geotechnical modelling, *Proc. Int. Conf. Rec. Advances in Geotechnical Earthquake engineering and soil dynamics*, St Louis, Vol.3., pp 1081-1100.

Scott, A., Cocker, A. N., Djordjevic, N., Higgins, M., La Rosa, D., Sarma, K. S., & Wedmaier, R. (1996). *Open Pit Blast Design, Analysis and optimization* (p. 338). Julius Kruttschnitt Mineral Research Centre, The University of Queensland.

Seeber, L., Armbruster, J. G., & Jacob, K. H. (1999). Probabilistic Assessment of Seismic Hazard for Maharashtra, *Govt. of Maharashtra*. Unpublished Report.

Seed, H. B., & Idriss, I. M. (1970). *Soil modules and damping factors for dynamic response analyses*. Report EERC 70–10, Earthquake Engineering Research Center, University of California, Berkeley.

Seed, H. B., & Idriss, I. M. (1982). *Ground motions and soil liquefaction during earthquakes" Monograph Series* (Vol. 5). Earthquake Engineering Research Institute.

Seed, H. B., & Whitman, R. V. (1970). Design of earth retaining structures for dynamic loads. *Lateral stresses in the ground and design of earth retaining structures, ASCE*, New York, (pp. 103–147).

Seed, H.B, Martin, P.P., & Lysmer, J. (1976). Pore water pressure change during soil liquefaction. *J. Geotech. Eng. Div., ASCE, 102*(4), 323-346.

Seed, H.B., Idriss, I.M., & Arango, I. (1983). Evaluation of liquefaction potential using field performance data. *J. Geot.. Eng. Div., ASCE, 109*(3), 458-482.

SEISAT. (2000). Seismotectonic Atlas of India. published by *Geological Survey of India*.

Sen, G. C., & Silitonga, M. (1984). Effect of confinement on ground vibrations due to blasting. In *Proceedings of the Australian, Inst. of Min. Metall* (pp. 213-215).

SHAKE. 2000 (2000). *A computer program for conducting equivalent-linear seismic response analyses for horizontally layered soil deposits*. A modified PC version of the original SHAKE program published in 1972 by Schnabel, Lysmer and Seed (modifications made by Idriss IM, Sum JI). EERI, University of California, Berkley.

Shan, R., Cheng, R., & Gao, W. (2006). Study on dynamic constitutive model of anthracite of Yunjialing coal mine. *Chinese Journal of Rock Mechanics and Engineering*, *25*, 2258–2263.

Sharma, V. K. (1989). *Strength properties of jointed rocks*. Unpublished master's thesis, R. E. C. Kurukshetra, India.

Shenthan, T. (2001). *Factors affecting liquefaction mitigation in silty soils using stone columns.* MS Thesis, Department of Civi, Structural and Environ. Eng., University at Buffalo, NY, USA.

Sidle, R. C., Kamai, T., & Trandafir, A. C. (2005). Evaluating landslide damage during the 2004 Chuetsu earthquake, Niigata, Japan. *Eos, Transactions, American Geophysical Union*, *86*(13), 133–136. doi:10.1029/2005EO130001

Silver, M. L., & Seed, H. B. (1971a). Deformation characteristics of sands under cyclic loading. *Journal of the Soil Mechanics and Foundations Division*, *97*(SM8), 1081–1098.

Silver, M. L., & Seed, H. B. (1971b). Volume changes in sands during cyclic loading. *Journal of the Soil Mechanics and Foundations Division*, *97*(SM9), 1171–1182.

Singh, P. K. (2000). *Evaluation of damages to underground coal mines caused by surface blasting vis-à-vis establishment of blast vibration threshold* (Project No GAP/III/BLASTING/MOC/1996, pp. 1-50). CMRI Coal S & T.

Singh, R. K., & Dev, C. (1988). *Strength and modulus tests on jointed specimens of plaster of Paris*. M. Tech Thesis, IIT-Delhi, India.

Singh, S. (1994). Liquefaction characteristics of silts. Ground failures under seismic conditions. In S. Prakash & P. Dakoulas (Eds.), *Proceedings ASCE Convention, GSP. 44, ASCE,* (pp. 105-116).

Singh, S. P. (1992, December). Mining Industry and Blast Damage. *Journal of Mines, Metals & Fuels*, 465-472.

Singh, S. P. (1993, February). Damage causing potential of different explosives. In *Proceedings of the 9th annual symposium on Explosives and Blasting Research* (pp. 325-337), San Diego, CA.

Singh, S. P., & Xavier, P. (2005). Causes, impact and control of overbreak in underground excavations. *Tunnelling and Underground Space Technology*, *20*, 63–71. doi:10.1016/j.tust.2004.05.004

Siskind, D. E., Stagg, M. S., Kopp, J. W., & Dowding, C. H. (1980). *Structure Response and Damage Produced by Ground Vibration From Surface Mine Blasting*. U. S. Bureau of Mines.

Sitharam, T. G., Vinod, J. S., & Ravishankar, B. V. (2009). Post liquefaction undrained monotonic behaviour of sands: Experiments and DEM simulations. *Geotechnique*.

Sitharam, T. G., Vinod, J. S., & Rothenburg, L. (2005). *Shear behavior of glass beads, International conference micromechanics of granular media. Powder and Grains* (pp. 257-260), University of Stuttgart, Germany.

Sitharam, T.G., & Anbazhagan, P. (2007). Seismic hazard analysis for Bangalore region. *Journal of natural hazards, 40*, 261-278.

Sitharam, T. G. (2003). Discrete element modeling of cyclic behaviour of granular materials. *Geotechnical and Geological Engineering*, *21*, 297–329. doi:10.1023/B:GEGE.0000006036.00597.0b

Sitharam, T. G., Dinesh, S. V., & Shimizu, N. (2002). Micromechanical modeling of monotonic shear behaviour of granular media using three dimensional DEM. *International Journal for Numerical and Analytical Methods in Geomechanics*, *26*, 1167–1189. doi:10.1002/nag.240

Sitharam, T. G., & Vinod, J. S. (2008). Numerical simulation of liquefaction and pore pressure generation in granular materials using DEM. *International Journal of Geotechnical Engineering*, *2*(2), 103–113. doi:10.3328/IJGE.2008.02.02.103-113

Sitharam, T. G., & Vinod, J. S. (2009). Critical state behaviour of Granular materials from isotropic compression and rebound paths: DEM simulations. *Granular Matter*, *11*(1), 33–42. doi:10.1007/s10035-008-0113-3

Sitharam, T.G., & GovindaRaju, L. (2004). Geotechnical aspects and ground response studies in Bhuj earthquake, India. *Geotechnical and Geological Engineering*, *22*, 439–455. doi:10.1023/B:GEGE.0000025045.90576.d3

Soh, C. K., & Gupta, A. (2000). Intelligent interactive tutoring system engineering mechanics. *Journal of Professional Issues in Engineering Education and Practice*, *126*(4), 166–173. doi:10.1061/(ASCE)1052-3928(2000)126:4(166)

Sokolov, Y. V., Loh, C. H., & Wen, K. L. (2001). Empirical models for site- and region-dependent ground motion parameters in the Taepei area: A unified approach. *Earthquake Spectra*, *17*(2), 313–332. doi:10.1193/1.1586177

Soubra, A. H. (2000). Static and seismic passive earth pressure coefficients on rigid retaining structures. *Canadian Geotechnical Journal*, *37*, 463–478. doi:10.1139/cgj-37-2-463

Soubra, A. H., & Macuh, B. (2002). Active and passive earth pressure coefficients by a kinematical approach. In *Proceedings of Institution of Civil Engineers*. *Geotechnical Engineering*, *155*(2), 119–131.

Soydemir, C. (1994, October). Earthquake-induced settlements in silty sands for New England seismicity. Ground failures under seismic conditions. In S. Prakash & P. Dakoulas (Eds.), *Proceedings of the ASCE Convention, GSP. 44, ASCE* (pp. 77-90), Atlanta, GA.

St. John, C. M., & Zahrah, T. F. (1987). A seismic design of underground structures. *Tunnelling and Underground Space Technology*, *2*(2), 165–197. doi:10.1016/0886-7798(87)90011-3

Stacey, T. R. Cameron-Clarke, & Mival, K. (1990). Stabilisation of old workings by blasting: Case study of a failed experiment. In Brummer (Ed.), *Static and dynamic considerations of Rock Engineering*, Balkema, Rotterdam, pp.317-324.

Steedman, R. S., & Zeng, X. (1990). The influence of phase on the calculation of pseudo-static earth pressure on a retaining wall. *Geotechnique*, *40*(1), 103–112. doi:10.1680/geot.1990.40.1.103

Steidl, J. H. (2000). Site response in southern California for probabilistic seismic hazard analysis. *Bulletin of the Seismological Society of America*, *90*, S149–S169. doi:10.1785/0120000504

Stepp, J. C., Wong, I., Whitney, J., Quittemeyer, R., Abrahamson, N., & Toro, G. (2001). Yucca Mountain PSHA Project Members, Probabilistic seismic hazard analyses for ground motions and fault displacements at Yucca Mountain, Nevada. *Earthquake Spectra*, *17*, 113–151. doi:10.1193/1.1586169

Stewart, J. P., Liu, A. H., & Choi, Y. (2003). Amplification Factors for Spectral Acceleration in Tectonically Active Regions. *Bulletin of the Seismological Society of America*, *93*(1), 332–352. doi:10.1785/0120020049

Stewart, R. A., Reimold, W. U., Charlesworth, E. G., & Ortlepp, W. D. (2001). The nature of a deformation zone and fault rock related to a recent rockburst at Western Deep Levels Gold Mine, Witwatersabnd Basin, South Africa. *Tectonophysics*, *337*, 173–190. doi:10.1016/S0040-1951(01)00028-2

Subba Rao, K. S., & Choudhury, D. (2005). Seismic passive earth pressures in soils. *Journal of Geotechnical and Geoenvironmental Engineering*, *131*(1), 131–135. doi:10.1061/(ASCE)1090-0241(2005)131:1(131)

Sun, J. I., Golesorkhi, R., & Seed, H. B. (1988). *Dynamic moduli and damping ratios for cohesive soils.* EERC 88-15, University of California, Berkeley.

Sunu, M. Z., Reed, S. M., & Singh, R. N. (1988). Evaluating of rock parameters on surface mine blasting by finite element analysis. *Int. J. surface mining and reclamation, 2*, 209-15.

Suto, K. (2007). Multichannel analysis of surface waves (MASW) for investigation of ground competence: an introduction in Engineering Advances in Earthworks. In *Proceedings of the Sydney Chapter 2007 Symposium* (pp. 71-81). Australian Geomechanics Society.

Swan, G., Cook, J., Bruce, S., & Meehan, R. (1989). Strain Rate Effects in Kimmeridge Bay Shale. *International Journal of Rock Mechanics and Mining Sciences & Geomechanics Abstracts*, *26*, 135–149. doi:10.1016/0148-9062(89)90002-8

Szuladzinski, G. (1993). Response of rock medium to explosive cavity pressure. In H. P. Rossmanith (Ed.), *Proceedings of the 4th Int. Symp. Rock Fragmentation by Blasting (FRAGBLAST IV)*, Vienna, Austria (pp. 17-23). Rotterdam, The Netherlands: Balekma.

Tart, R. J., Oriard, L. L., & Plump, J. H. (1980). Blast Damage Criteria for a Massive Concrete Structure. In T.S. Vinson (Ed.), *Minimizing Detrimental Construction Vibrations*. Special Technical Publication (pp. 125-140), New York: ASCE.

Tatsuoka, F., Sasaki, T., & Yamada, S. (1984). Settlement in saturated sand induced by cyclic undrained simple shear. In Proc. 8th World Conf. Earthq. Eng., San Francisco, CA, V3, 95-102.

Taylor, L. M., Chen, E. P., & Kuszmaul, J. S. (1986). Micro-crack induced damage accumulation in brittle rock under dynamic loading. *Computer Methods in Applied Mechanics and Engineering*, *55*, 301–320. doi:10.1016/0045-7825(86)90057-5doi:10.1016/0045-7825(86)90057-5

Terzaghi, K., Peck, R. B., & Mesri, G. (1996). *Soil mechanics in engineering practice* (3rd ed). New York: John Wiley and Sons.

Tewari, H. C., Dixit, M. M., Sarkar, D., & Kaila, K. L. (1991). A crustal density model across Cambay basin, India and its relationship with the Aravallis. *Tectonophysics*, *194*, 123. doi:10.1016/0040-1951(91)90276-X

Tezuka, M., Kudo, Y., Matsuda, H., Hasui, A., & Nakagawa, K. (1997). Study on estimate of damage zone caused by blasting. In Y. Lee & C. Lee (Eds.), *Proceedings Asian Rock Mechanics Symposium, Environmental and safety concerns in underground construction* (pp. 101-106).

Thevanayagam, S. (2000). Liquefaction potential and undrained fragility of silty soils. In the *Proceedings of the12th World Conf. Earthq. Eng*., New Zealand.

Thevanayagam, S., & Ecemis, N. (2008). Effects of permeability on liquefaction resistance and cone resistance. *ASCE Geotechnical Special Publication 181, Geotechnical Earthquake Engineering and Soil Dynamics* (p. 11).

Thevanayagam, S., Fiorillo, M., & Liang, J. (2000). Effect of non-plastic fines on undrained cyclic strength of silty sands. In R.Y.S. Pak & J. Yamamura (Eds.), *ASCE Geotech Spec. Publ. 107*, (pp. 77-91).

Thevanayagam, S., Liang, J., & Shenthan, T. (2000). Contact index and liquefaction potential of silty and gravely soils. In the *Proceedings of the 14th ASCE Eng. Mech. Conference,* Austin, Texas.

Thevanayagam, S., Martin, G. R., Shenthan, T., & Liang, J. (2001). Post-liquefaction pore pressure dissipation and densification in silty soils. In *Proceedings of the 4th Intl. Conf. Soil Dynamics & Earthq. Eng.,* San Diego, CA.

Thevanayagam, S. (2007a). Intergrain contact density indices for granular mixes I - Framework. J. *Earthquake Engineering and Engineering Vibrations*, *6*(2), 123–134. doi:10.1007/s11803-007-0705-7

Thevanayagam, S. (2007b). Intergrain contact density indices for granular mixes- II: Liquefaction resistance. *J. Earthquake Engineering and Engineering Vibrations*, *6*(2), 135–146. doi:10.1007/s11803-007-0706-6

Thevanayagam, S., & Martin, G. R. (2002). Liquefaction in silty soils: screening and remediation issues. *J. Soil Dyn. & Eq. Eng.*, *22*, 1035–1042. doi:10.1016/S0267-7261(02)00128-8

Thevanayagam, S., Shenthan, T., Mohan, S., & Liang, J. (2002). Undrained fragility of sands, silty sands and silt. *ASCE. Journal of Geotechnical and Geoenvironmental Engineering*, *128*(10), 849–859. doi:10.1061/(ASCE)1090-0241(2002)128:10(849)

Thoenen, J. R., & Windes, S. L. (1942). Seismic effects of quarry blasting. *Bureau of Mines Bulletin*, *442*, 83.

Thoenen, J. R., & Windes, S. L. (1942). Seismic Effects of Quarry Blasting. *Bureau of Mines. Bull.*, *442*, 83.

Thorne, B. J., Hommert, P. J., & Brown, B. (1990). Experimental and computational investigation of the fundamental mechanisms of cratering. In *Proceedings of the 3rd Int. Symp. Rock fragmentation by Blasting (FRAGBLAST 3)*, Brisbane, Australia (pp. 412-23).

Timoshenko, S. P., & Goodier, J. N. (1969). *Theory of elasticity*. New York: McGraw Hill.

Tokimatsu, K., & Seed, H. B. (1984). *Simplified procedures for the evaluation of settlements in sands due to earthquake shaking*. Report No. UCB/EERC-84/16, Univ. of Calif., Berkeley, CA.

Tokimatsu, K., & Seed, H.B. (1987). Evaluation of settlements in sands due to earthquake shaking. *J. Geotech. Eng. Div., ASCE, 113*(8), 861-78.

Toper, A. Z. (1995). Numerical modelling to investigate the effects of blasting in confined rock simulation of a field study. In J. K. Daeman & R. A. Schultz (Eds.), *Proceedings of the 35th U.S. Symposium on Rock Mechanics*, Reno, NV (pp. 541-546). Rotterdam, The Netherlands: Balkema.

Toro, G. N., Abrahamson, N., & Schneider, J. (1997). Model of strong ground motions from earthquakes in central and eastern North America: Best estimates and uncertainties. *Seismological Research Letters*, *68*, 41–57.

Trahan, M. (1995). Méthode de minage "Eureka". In *Proceedings of the 10th AMQ colloque en contrôle de terrain*, Val d'Or, Québec, Canada.

Uma Maheshwari, R., Boominathan, A., & Dodagoudar, G. R. (2008). Development of empirical correltation between shear wave velocity and standard penetration resistance in soils of Chennai. In *Proceedings of 14th World Conference on Earthquake Engineering*, Beijing, Paper No: 04-01-0090.

Vaid, Y. P. (1994). Liquefaction of silty soils. *ASCE Conv. Geotech. Spec. Publ.*, *44*, 1–16.

Valliapan, S., Lee, I. K., Murti, V., Ang, K. K., & Ross, A. H. (1983). Numerical modelling of rock fragmentation. In R. Holmberg & A. Rustan (Eds.), *Proceedings of the 1st Int. Symp. Rock Frag. By Blasting (FRAGBLAST 1)* (pp. 375-90). Rotterdam, The Netherlands: Balkema.

Villaescusa, E., Onederra, I., & Scott, C. (2004). Blast Induced Damage and Dynamic Behaviour of Hangingwalls in Bench Stoping. *J. Rock fragmentation by blasting. Fragblast*, *8*(1), 23–40. doi:10.1080/1385514 0512331389614

Vinod, J. S. (2006). *Liquefaction and dynamic properties of granular materials: A DEM approach.* Ph.D. thesis, submitted to Indian Institute of science, Bangalore, India

Vipin, K. S., Anbazhagan, P., & Sitharam, T. G. (2009). Estimation of peak ground acceleration and spectral acceleration for South India with local site effects: probabilistic approach. *Natural Hazards and Earth System Sciences*, *9*, 865–878.

Wagner, H. (1984). Support requirements for rockburst conditions. *Rockbursts and seismicity in mines* (pp. 209-218). S. Africa Inst. Mining & Metallurgy, Johannesbug.

Wallace, J. (1996). What a gas: blasting under pressure. In *Proceedings of the 22nd Ann. Conf. on Explosives and Blasting Techniques* (pp. 140-150).

Wang, W. (1990). *Bounding surface hypoplasticity model for granular soils and its applications*. University of California, Davis.

Wang, Y., Zhu, Z., Zhou, Z., & Xie, H. (2009, June). Numerical investigation of blasting-induced damage in concrete slabs. In *Proceedings of the Symposium on Computational Structrual Engineering*, Shanghai, China (pp. 655-668).

Wang, G., Wang, Z. T., Rudolph, V., Massarotto, P., & Finley, R. J. (2007). An analytical model of the mechanical properties of bulk coal under confined stress. *Fuel*, *86*, 1873–1884. doi:10.1016/j.fuel.2007.01.002

Wang, Z. L., Lia, Y. C., & Wang, J. G. (2008). Numerical analysis of blast-induced wave propagation and spalling damage in a rock plate. *International Journal of Rock Mechanics and Mining Sciences*, *45*, 600–608. doi:10.1016/j.ijrmms.2007.08.002

Wathen, D., & Thomas, M. E. (1996). Blasting with a light touch. In *Proceedings of the 22nd Ann. Conf. on Exp. and Blasting tech* (pp. 152-161).

Wiss, J. F., & Linehan, P. W. (1978). *Control of vibrations and blast noise from surface coal mining* (Volumes I-IV, Report to U.S. Bureau of Mines). Bureau of Mines.

Xiao, J. Q., Ding, D. X., Xu, G., & Jiang, F. L. (2008). Waveform effect on quasi-dynamic loading condition and the mechanical properties of brittle materials. *International Journal of Rock Mechanics and Mining Sciences*, *45*, 621–626. doi:10.1016/j.ijrmms.2007.07.025

Yaji, R. K. (1984). *Shear strength and deformation of jointed rocks*. Unpublished doctoral dissertation, Indian Institute of Technology, New Delhi, India.

Yamamuro, J.A., & Lade, P.V. (1998). Steady-state concepts and static liquefaction of silty sands. *J. Geotech. and Geoenv. Engrg. Div., ASCE, 124*(9), 868-877.

Yang, R., Bawden, W. F., & Katsabanis, P. D. (1996). A new constitutive model for blast damage. *International Journal of Rock Mechanics and Mining Sciences & Geomechanics Abstracts*, *33*, 245–254. doi:10.1016/0148-9062(95)00064-Xdoi:10.1016/0148-9062(95)00064-X

Yang, S. L., Sandven, R., & Grande, L. (2006). Instability of sand–silt mixtures. *Soil Dynamics and Earthquake Engineering*, *26*(2-4), 183–190. doi:10.1016/j.soildyn.2004.11.027

Yoshimi, Y., Kuwabara, F., & Tokimatsu, K. (1975). One-dimensional volume change characteristics of sands under low confining stresses. *Soil and Foundation*, *15*(3), 51–60.

You, Z. (2005, June 1-3). Introduction to discrete element method - a numerical method to engineering graduate students. In *Proceedings of the McMat2005, Joint ASME/ASCE/SES Conference on Mechanics and Materials*, Baton Rouge, LA.

Youd, T. L., Idriss, I. M., Andrus, R. D., Arango, I., Castro, G., & Christian, J. T. (2001). Liquefaction Resistance of Soils: Summary Report from the 1996 NCEER and 1998 NCEER/NSF Workshops on Evaluation of Liquefaction Resistance of Soils. *ASCE J. of Geotech. and Geoenv. Eng.*, *127*(10), 817–833. doi:10.1061/(ASCE)1090-0241(2001)127:10(817)

Yu & Vongpaisal. (1996). New blast damage criteria for underground blasting. *CIM Bulletin*, *89*(998), 139–145.

Yu, T. R., & Vongpaisal, S. (1996). New blast damage criteria for underground blasting. *CIM Bulletin*, *89*(2), 139–145.

Zeng, X., & Steedman, R. S. (1993). On the behavior of quay walls in earthquakes. *Geotechnique*, *43*(3), 417–431. doi:10.1680/geot.1993.43.3.417

Zeng, X., & Steedman, R. S. (2000). Rotating block method for seismic displacement of gravity walls. *Journal of Geotechnical and Geoenvironmental Engineering*, *126*(8), 709–717. doi:10.1061/(ASCE)1090-0241(2000)126:8(709)

Zhang, J. C., & Chang, C. (1999, August 8-10). On damage mechanism of micro crack zone in Rock blasting and its measurements. In *Proceedings of the 6th Int. Symposium of Rock fragmentation by blasting* (pp. 358-363), The South African Ist. of Mining and Metal. Johansburg.

Zhan, X., & Wang, J. (2007). Research on the mechanism and prevention of rockburst at Yinxin Gold Mine. *Journal of China University of Mining & Technology*, *17*(4), 541–545. doi:10.1016/S1006-1266(07)60142-4

Zhou, P., & Hong, K. (1995). The rockburst features of Taipingyi tunnel and the prevention methods. *Chinese Journal of Rock Mechanics and Engineering*, *14*(2), 171–178.

Zhu, D. Y., & Qian, Q. (2000). Determination of passive earth pressure coefficients by the method of triangular slices. *Canadian Geotechnical Journal*, *37*, 485–491. doi:10.1139/cgj-37-2-485

Zhu, W. C., & Bruhns, O. T. (2008). Simulating excavation damaged zone around a circular opening under hydromechanical conditions. *International Journal of Rock Mechanics and Mining Sciences*, *45*, 815–830. doi:10.1016/j.ijrmms.2007.09.007

Zhu, Z. (2009). Numerical prediction of crater blasting and bench blasting. *International Journal of Rock Mechanics and Mining Sciences*, *46*, 1088–1096. doi:10.1016/j.ijrmms.2009.05.009

Zhu, Z., Mohanty, B., & Xie, H. (2007). Numerical investigation of blasting-induced crack initiation and propagation in rocks. *International Journal of Rock Mechanics and Mining Sciences*, *44*, 412–424. doi:10.1016/j.ijrmms.2006.09.002

Zhu, Z., Xie, H., & Mohanty, B. (2008). Numerical investigation of blasting-induced damage in cylindrical rocks. *International Journal of Rock Mechanics and Mining Sciences*, *45*, 111–121. doi:10.1016/j.ijrmms.2007.04.012

About the Contributors

T. G. Sitharam is a Professor in the Department of Civil Engineering at Indian Institute of Science (Bangalore, India) and Chairman, Centre for Infrastructure, Sustainable Transportation, and Urban Planning (CiSTUP), Indian Institute of Science, Bangalore. He obtained his Bachelor's from University of Mysore, Master's degree in Geotechnical Engineering from Indian Institute of Science (Bangalore, India) in 1986 and a PhD in Civil Engineering from University of Waterloo (Waterloo, Ontario, Canada) in 1991. Further, he worked as a post doctoral researcher at Center for Earth Sciences and Engineering (CESE), University of Texas at Austin (Texas, USA) until 1994. He has served as a visiting Professor in Dalhousie University, University of Waterloo (Canada) and Yamaguchi University (Japan), William Mong Fellow in Hong Kong and visiting scientist to several other universities in the world. His research interests are in the areas of earth science and engineering, and in particular geotechnical engineering, soil dynamics, geotechnical earthquake engineering, and rock mechanics. He is convener and member of working group of experts of geotechnical engineers in geohazards program of National Disaster Management Authority (NDMA), Govt. of India. He has developed guidelines for geotechnical and geophysical investigations for seismic microzonation projects. He is also member of Programme Advisory and Monitoring Committee (PAMC) for the nationally coordinated programme on Seismicity by Ministry of Earth Sciences (MoES) and Department of Science and Technology (DST) DST, Govt. of India. He was a member of TC 29 Laboratory Stress Strain Strength Testing of Geomaterials, International Society of Soil Mechanics and Geotechnical Engineering (ISSMGE) for the year 2001-2005. Professor Sitharam has guided sixteen PhD students, three MSc(Engg) students, and several ME project students. Currently he has twelve Doctoral students working with him for their PhD degrees. He has written four textbooks, and also guest edited volumes on geotechnics and earthquake hazards for *Current Science* and seismic microzonation for *Journal of Earth System Science*. He has more than 300 publications to his credit in journal and conferences. He is also editorial board member of *Geotechnique Letters* and *Electronic Journal of Geotechnical Engineering* (EJGE), USA. He was the associate editor of *Journal of Civil Engineering Materials*, ASCE, USA and he is presently the chief Editor of *The International Journal of Geotechnical Earthquake Engineering* (IJGEE).

* * *

G. L. Sivakumr Babu is an Associate professor in the Department of Civil Engineering at Indian Institute of Science (Bangalore, India). He obtained M.E degree in Geotechnical Engineering from Anna University (Chennai, India) in 1987 and a PhD in Civil Engineering from Indian Institute of Science (Bangalore, India) in 1991. Further he was a visiting scholar at Purdue University, Lafayette, USA during

1995 - 1996. He was a Alexander von Humboldt Fellow and served as a visiting scientist in Germany during 1999 - 2000. His research interests are in the area of risk and reliability applications in geotechnical engineering, geosynthetics and reinforced soil structures, Environmental geotechnology, fibers in geotechnical engineering, earthquake geotechnical engineering and geotechnics for disaster mitigation. He is also a editorial board member and guest editor for the International Journal of GEORISK - Assessment and Management of Risk for Engineered Systems and Geohazards, Taylor & Francis Group. He is a secretary for the International Technical Committee (TC-40) on forensic geotechnical engineering (FGE), a body of International Society for Soil Mechanics and Geotechnical Engineering (ISSMGE). Prof. Sivakumar Babu has guided 5 Ph.D students, two MSc(Engg) students and several ME project students. He has written one text book on introduction to soil reinforcement and geosynthetics, and also edited proceedings on the risk assessment in site characterization and geotechnical design, (GEORISK 2004) and case studies in geotechnical engineering, (GEOPRACTICE 2005).

B. Munwar Basha obtained his PhD in Civil Engineering (Specialization, Geotechnical Engineering) from the Indian Institute of Science Bangalore, Karnataka (India) in 2009. He is working as a Research Associate at the Indian Institute of Science Bangalore. He obtained M.Tech degree in Geotechnical Engineering from Indian Institute of Technology (Kanpur, India) in 2004 and a B.Tech degree in Civil Engineering from Jawaharlal Nehru Technological University (Anantapur, Andhra Pradesh, India) in 2001. He was recipient of a University Gold Medal for the first rank in B.Tech, in the entire University. His research interests focus on the seismic design of retaining structures and optimum design of retaining structures under static and seismic loading using reliability based design optimization (RBDO). He has publications in Canadian Geotechnical Journal, Computers and Geotechnics, International Journal of Geomechanics ASCE, Soil Dynamics and Earthquake Engineering, Geosynthetics International and Indian Geotechnical Journals. He published 8 international journal referred publications, 3 ASCE geotechnical special publications and 9 National and International conference papers.

A. Boominathan is Professor of Geotechnical Engineering, at the Department of Civil Engineering, Indian Institute of Technology Madras (IITM) India. He specializes in soil dynamics, geotechnical earthquake engineering, site characterization, microzonation, pile foundation analysis and dynamic soil-structure interaction. His research has been mainly sponsored by Indira Gandhi Centre for Atomic Research (IGCAR) Kalpakkam, Department of Science and Technology (DST) New Delhi, and Ministry of Earth Sciences (MoES) of Government of India. He has authored and co-authored over 95 scientific papers and has served as Reviewer for over 10 Journals. He received IGS-Shri M.S. Jain biennial prize for the best paper on Innovations in Piling and Other Construction Techniques for the paper "Behavior of Pile Walls in Liquefying Soil Layers" for the year 2003-2004. He is a graduate of the Russian University of Moscow (1980) and received his Ph.D. in 1986 from Moscow Civil Engineering Institute of Russia.

Stuart Haigh is a University Lecturer at the Cambridge University Engineering Department and a Fellow of Trinity College, Cambridge. He obtained his undergraduate degree in Engineering from the University of Cambridge following which he remained at Cambridge to conduct research into the behaviour of pile foundations in laterally spreading soils for his PhD.Over the last seven years he has carried out

Post-doctoral research in the UK and Canada, focusing mainly on the physical and numerical modelling of soil dynamics and earthquake engineering, before being appointed as a University Lecturer in 2008. He has recently co-authored a book on 'Design of Pile Foundations in Liquefiable Soils' together with Dr Madabhushi and Dr Knappett (University of Dundee).

Gopal Madabhushi is a Reader in Geotechnical Engineering at the Cambridge University Engineering Department. He is the Asst Director of Schofield Centre and a Fellow of Girton College, Cambridge. He obtained his PhD from University of Cambridge in 1992. He is a Life Fellow of the Cambridge Commonwealth Society and Cambridge Philosophical Society. Dr Madabhushi's expertise lies in dynamic centrifuge modelling and finite element analysis of problem in earthquake engineering. He has published to date 80 technical papers in various International Journals and authored over 200 papers at International Conferences and Workshops. He won the TK Hsieh prize in 2005 awarded by the ICE, London for his work on the pile foundations in liquefiable soils. He was awarded the Shamsher Prakash Research Award in 2006 for his contributions in the field of Earthquake Geotechnical Engineering. He has recently co-authored books on 'Design of Pile Foundations in Liquefiable Soils' and 'Seismic Design of Buildings to Eurocode 8'.

More Ramulu is working as Senior Scientist in Central Institute of Mining & Fuel Research, Regional Centre, Nagpur, under the aegis of Council of Scientific and Industrial Research, New Delhi, India. He has got 12 years of research experience in Rock Mechanics and Blasting engineering. His main research area of specialisation is Controlled blasting and rock mass damage. He passed out his Bachelors in Mining Engineering from Osmania University, Hyderabad in the year 1995 with three University Gold medals. He did his M.Tech in Blasting Engineering from Visveswaraya National Institute of Technology with A-grade distinction. He was also awarded MGMI gold medal for excellent academic track record. He is pursuing his PhD in Blasting & Geotechnical Engineering from Indian Institute of Science (IISc), Bangalore under the guidance of Prof.T.G.Sitharam. Mr. Ramulu published 10 technical papers in various International Journals and more than 20 papers in national Journals. He also filed 5 patents on Blasting and Societal mission related devices, which include both Indian and US patents.

T. Shenthan is a senior engineer at Advanced Earth Sciences, Inc., California. He earned his MS and PhD degrees in geotechnical engineering from University at Buffalo, State University of New York. Dr. Shenthan conducts research and consulting work in geotechnical earthquake engineering in the area of soil liquefaction, ground improvement for liquefaction mitigation, and numerical simulations of ground improvement process using vibratory stone columns. His work was published in a number of geotechnical engineering and earthquake engineering journals, conference publications, and workshops.

S. Thevanayagam is an associate professor of geotechnical engineering at University at Buffalo, State University of New York.Prof. Thevanayagam conducts active research in geotechnical earthquake engineering in the area of soil liquefaction, ground improvement for liquefaction mitigation, large scale physical simulation of earthquake effects on soils and foundations, and numerical simulations. His work was published in a number of geotechnical engineering, earthquake engineering, and applied physics journals, conference publications, workshops, and books.

J. S. Vinod is currently a lecturer at University of Wollongong, Australia. He received his Doctorate degree from Indian Institute of Science, Bangalore, in the area of Geotechnical Engineering. He has worked as a research fellow in one of the Australian Research Council (ARC) Linkage project on chemical stabilisation at the University of Wollongong. Vinod is a member/life member of many professional societies. His research interests are in the area of numerical modelling of granular materials, soil dynamics, and earthquake engineering. He has published over 26 publications, including 10 peer-reviewed journal articles, one edited proceeding and book chapter, and 15 referred conference papers, three of where were keynote papers.

K. S. Vipin is a research scholar in the Department of Civil Engineering at Indian Institute of Science, Bangalore. He obtained his MTech degree in traffic engineering and transportation planning from the National Institute of Technology, Calicut in 2001. He graduated from Kerala University in the field of civil engineering in the year 1998. His research interests include probabilistic and deterministic seismic hazard analysis, probabilistic liquefaction evaluation, earthquake geotechnical engineering and engineering seismology.

Index

F

G

H

I

J

K

L

M

N

O

P

Q

R

S

T

U

V

W